Ibrahim Dincer · Adnan Midilli
Haydar Kucuk *Editors*

Progress in Sustainable Energy Technologies Vol II

Creating Sustainable Development

Springer

Progress in Sustainable Energy Technologies Vol II

Ibrahim Dincer • Adnan Midilli • Haydar Kucuk
Editors

Progress in Sustainable Energy Technologies Vol II

Creating Sustainable Development

Springer

Editors
Ibrahim Dincer
Department of Mechanical Engineering
University of Ontario Institute of Technology
Oshawa, ON, Canada

Adnan Midilli
Department of Mechanical Engineering
Recep Tayyip Erdoğan University
Rize, Turkey

Haydar Kucuk
Department of Mechanical Engineering
Faculty of Engineering
Recep Tayyip Erdoğan University
Rize, Turkey

ISBN 978-3-319-07976-9 ISBN 978-3-319-07977-6 (eBook)
DOI 10.1007/978-3-319-07977-6
Springer Cham Heidelberg New York Dordrecht London

Library of Congress Control Number: 2014941874

Printed on acid-free paper

Springer is part of Springer Science+Business Media (www.springer.com)

Preface

A secure supply of energy resources is generally agreed to be a necessary but not sufficient requirement for development within a society. Furthermore, sustainable development demands a sustainable supply of energy resources. The implications of these statements are numerous, and depend on how "sustainable" is defined. One important implication of these statements is that sustainable development within a society requires a supply of energy resources that, in the long term, is readily and sustainably available at reasonable cost and can be utilized for all required tasks without causing negative societal impacts.

Energy sources and their utilization are intimately related to sustainable development. For societies to attain or try to attain sustainable development, much effort must be devoted not only to discovering sustainable energy sources but also to increasing the energy efficiencies of processes utilizing these resources. By increasing the energy efficiencies, society maximizes the benefits it derives from utilizing its energy resources, while minimizing the negative impacts associated with their use. This implication acknowledges that all energy resources are to some degree finite, so that greater efficiency in utilization allows such resources to contribute to development over a long period of time, i.e., to make development more sustainable.

Since sustainable energy technologies appear to be a primary path for sustainable development, it is a critical area where the conference series on Sustainable Energy Technologies was initiated and focused. The conference, since 2002, has been running successfully under the title of "International Conference on Sustainable Energy technologies (SET)." The conference has a multidisciplinary nature and aims to provide a forum for researchers, scientists, engineers, and practitioners from all over the world to exchange information, to present high-quality research results and new developments in the wide domain covered by sustainable energy technologies, and discuss the future direction and priorities in the field.

This unique volume contains, in addition to some invited contributions, selected papers from the 11th International Conference on Sustainable Energy technologies (SET-2012), September 2–5, 2012, Vancouver, Canada. The primary theme of the

book is sustainable development depending on sustainable energy technologies. It covers a broad range of topics on sustainable energy, sustainable environment, sustainable buildings, sustainable development, energy and exergy analysis, entropy generation, energy strategy, energy savings, waste management, hydrogen production, fuel cells, heat pumps, heat and mass transfer applications, low energy buildings, etc.

In conclusion, the editors of this volume gratefully acknowledge the assistance provided by Dr. Ugur Akbulut in reviewing and revising several chapters, checking for consistency and finalizing them for publication. The editors also register their sincere appreciation to the authors for their contributions which have made this unique book possible. Furthermore, Dr. Dincer acknowledges the support provided by the Turkish Academy of Sciences in Ankara, Turkey.

Oshawa, ON, Canada — Ibrahim Dincer
Rize, Turkey — Adnan Midilli
Rize, Turkey — Haydar Kucuk

Contents

Chapter 1
Energy and Exergy Analyses of an Active Magnetic Refrigerator

Hadi Ganjehsarabi, Ibrahim Dincer, and Ali Gungor

Abstract In this paper, a thermodynamic model for predicting the performance of active magnetic refrigerator (AMR) is developed using energy and exergy analyses. Through this model, the cooling power, total power consumption, as well as the coefficient of performance (COP), exergy efficiency and exergy destruction rates of an AMR are determined. The effects of increasing mass flow rate on the COP, exergy efficiency and exergy destruction rates of the system are investigated. The results are presented to show that when mass flow rate increases, the COP and exergy efficiency curves reach their maximum values and then slightly decreases with increasing mass flow rate. The rate of exergy destruction increases with increasing mass flow rate due to the pump power requirements. The numerical results show that in order to reach optimal performance, mass flow rate must be adjusted carefully regarding to different operating conditions.

Keywords Active magnetic refrigerator • Energy • Exergy efficiency • Porous medium

1.1 Introduction

As energy-related environmental concerns, such as acid precipitation, pollution, stratospheric ozone depletion, and global climate change became major issue in 1980s, interest in magnetic refrigeration, as a new solid state cooling technology competitive with conventional vapor compression refrigeration system, has been increasing. This will also address the increasing energy demand [1]. Barclay and Steyert [2] suggested the concept of an Active Magnetic Regenerator (AMR) which presents the highly improved performance characteristics of system by utilizing the

H. Ganjehsarabi • A. Gungor
Faculty of Engineering, Department of Mechanical Engineering, Ege University, TR-35100 Bornova, Izmir, Turkey

I. Dincer (✉)
Faculty of Engineering and Applied Science, University of Ontario Institute of Technology, 2000 Simcoe Street North, Oshawa, ON, Canada L1H 7K4
e-mail: Ibrahim.Dincer@uoit.ca

I. Dincer et al. (eds.), *Progress in Sustainable Energy Technologies Vol II: Creating Sustainable Development*, DOI 10.1007/978-3-319-07977-6_1

refrigerant itself as an active regenerator in the refrigeration cycle. Brown [3] developed a reciprocating magnetic refrigerator near room temperature based on the Ericsson cycle. Aprea et al. [4] developed a dimensionless numerical model in order to predict the general behavior of the AMR system. Apera et al. [5] carried out a practical model for predicting the performance of a cascade AMR system. Tagliafico et al. [6] performed a 1-D dynamic model of an active reciprocating magnetic regenerator and a parametric analysis of its behavior. Yu et al. [7] reviewed research on magnetic refrigerator and heat pump prototypes constructed before 2010. Moreover, worthwhile operational data of the prototype AMR have been reported [8–11].

In this paper, a comprehensively model of a magnetic refrigeration system is created using a MATLAB software. The studied literature survey shows the lack of available studies on exergy analysis of magnetic refrigeration systems. In order to achieve this objective, the following specific analyses are conducted:

- To model and simulate an active magnetic regenerator refrigeration.
- To perform energy and exergy analyses of the system.
- To conduct a parametric study by changing important design parameter and investigating its effect on the system performance.

1.2 Actıve Magnetıc Regeneratıve Refrıgerator

The schematic of AMRR system is shown in Fig. 1.1, which comprises four main processes. In the magnetization stage, the magnetic field in the bed is applied to the magnetic material with no fluid flow which caused each particle of bed to warm up. In the isofield cooling process, the fluid is blown from the cold end to the hot end while maintaining the magnetic field, absorbs heat from the bed and rejects heat to the surrounding in the hot heat exchanger. Next in the adiabatic demagnetization process, the regenerator bed is cooled by the demagnetization effect. Finally, in the isofield heating stage, the fluid moved through the bed from the hot end to the cold end and it is cooled by the bed, emerging at a temperature lower then cold end and removes heat from the cold end [12].

1.3 Analysis

1.3.1 Heat Transfer Modeling

1.3.1.1 Modeling of Magnetization and Demagnetization Processes

A homogeneous ferromagnetic material model has been used in order to characterize the thermal and magnetic behaviours. The entropy balance equation for the

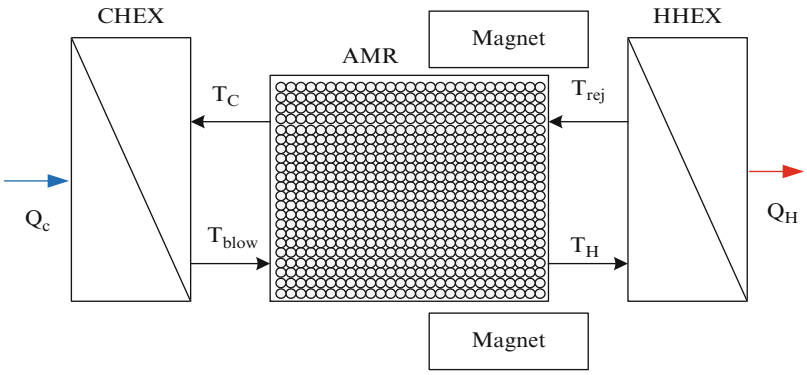

Fig. 1.1 Schematic of an AMRR system (HHEX: hot heat exchanger, AMR: active magnetic regenerator, CHEX: cold heat exchanger) [13]

magnetocaloric solid refrigerant and the entrained fluid in the porous matrix is given as follow:

$$ds = m_s \frac{c_s}{T_s} dT_s + \nu_s m_s \left(\frac{\partial M}{\partial T_s}\right)_H dH + m_f ds_f \tag{1.1}$$

In order to study the transient behaviour, the mass of the entrapped fluid compared with the mass of the magnetic material is ignored. Therefore, the bed temperature distribution can be calculated by integrating the following differential equation:

$$\left(\frac{\partial T_s}{\partial t}\right) = -\frac{T_s}{c_s} \nu_s \left(\frac{\partial M}{\partial T_s}\right)_H \frac{dH}{dt} \tag{1.2}$$

1.3.2 Governing equations

The mechanism of heat and mass transfer in a AMR bed is complicated; hence, some assumptions must be made in order to establish the governing equations. The several assumptions made in this study are (1) the effect of viscous dissipation on the energy balance of the fluid flow throughout the bed is neglected; (2) the heat transfer fluid is incompressible ($\rho_f = \text{constant}$); (3) the temperature and velocity profile of heat transfer fluid are uniform during the period of flow blowing; (4) the axial heat conduction in the regenerator is neglected; (5) heat loss to the environment in the regenerator is negligible; (6) the properties of magnetic material (except for the specific heat) are constant in the regenerator.

Based on the above assumptions, the energy-balance expression of the heat transfer fluid (f) and the magnetic material (s) can be written as

$$\varepsilon\rho_f c_f A_c \frac{\partial T_f}{\partial t} + \rho_f c_f u A_c \frac{\partial T_f}{\partial x} = h a_{sf} A_c (T_s - T_f) \tag{1.3}$$

$$(1-\varepsilon)\rho_s c_s A_c \frac{\partial T_s}{\partial t} = h A_c a_{sf} (T_f - T_s) \tag{1.4}$$

here the subscripts f and s refer to fluid and solid, respectively. Here, ε is porosity, A_c is the cross-sectional area of the regenerator, c is the specific heat and a_{sf} is the specific surface area. The heat transfer coefficient is calculated by using a correlation given by Rohsenow et al. [14]:

$$Nu_f = 2 + 1.1 Re_p^{0.6} Pr_f^{1/3} \tag{1.5}$$

here Re_p is the particle Reynolds number for a packed sphere regenerator calculated using particle diameter in a packed sphere and the free flow velocity and *Pr* is the Prandtl number of the heat transfer fluid.

1.3.3 Solution Procedure

The set of equations governing the four processes in the regenerator are highly nonlinear and coupled. In order to solve the governing equations, the equations are discretized in time and the space. An iterative resolution of the Eqs. (1.2–1.4) provides the regime solution utilizing a tentative profile temperature of the bed. Before the time step was increased, an inner iteration was performed until the following convergence criterion was satisfied:

$$\delta = \mathrm{Max}\left(|T_s(0,x) - T_{s_l}(t_1 + t_2 + t_3 + t_4, x)| \prec 10^{-6}\right. \tag{1.6}$$

1.3.4 Thermodynamic Analyses

In this study, it is aimed to conduct a comprehensive exergy analysis and an exergetic performance assessment of an active magnetic refrigerator. In order to accomplish this, the governing equations and numerical procedures used by MATLAB must be outlined in order to obtain sufficient data for the thermodynamic assessment. Finally, these procedures are utilized to gain insights on the effectiveness of the AMR refrigeration system through energy and exergy analyses.

1.3.4.1 Energy Analysis

The cooling capacity, heat rejection and the rate of magnetic work performed on the regenerator during cyclic steady-state operation are the basic outputs of this model.

The cooling power and heat rejection to the surroundings are numerically computed through the integrals as follows:

$$Q_C = \int_{t_1+t_2+t_3}^{t_1+t_2+t_3+t_4} \dot{m}(t) c_f (T_C - T_{f_{II}}(t,0)) dt \tag{1.7}$$

$$Q_H = \int_{t_1}^{t_1+t_2} \dot{m}(t) c_f (T_f(t,L) - T_H) dt \tag{1.8}$$

The pressure drop in the heat transfer fluid flow can be calculated by using the Ergun correlation [15]:

$$\frac{\partial P}{\partial x} = 180 \left(\frac{1-\varepsilon}{\varepsilon}\right)^2 \frac{\mu_f}{d_p} u + 1.8 \left(\frac{1-\varepsilon}{\varepsilon}\right) \frac{\rho_f}{d_p} u \tag{1.9}$$

The power required for moving the heat transfer fluid through the regenerator is written as

$$W_p = \frac{\dot{m}(t)(\Delta P_C + \Delta P_H)}{\eta_p \rho_f} (t_2 + t_4) \tag{1.10}$$

The coefficient of performance (COP) of the system can be found as

$$COP = \frac{\dot{Q}_C}{\dot{W}_P + \dot{W}_M} \tag{1.11}$$

1.3.4.2 Exergy Analysis

For overall system, the total exergy destruction rate of the system can be written as follows [16]:

$$\dot{E}x_{des} = \dot{E}x_{in} - \dot{E}x_{out} + \dot{W}_M + \dot{W}_P - \dot{E}x_q \tag{1.12}$$

here $\dot{E}x_q$ is the exergetic cooling power as

$$\dot{E}x_q = \dot{Q}_c \left(\frac{T_H}{T_c} - 1\right) \tag{1.13}$$

The exergy efficiency of the system can be calculated as

$$\eta_{ex} = \frac{\dot{E}x_q}{\dot{W}_P + \dot{W}_M} \tag{1.14}$$

1.4 Results and Discussion

In this present study, a thermodynamic analysis of an active magnetic refrigerator is conducted by using energy and exergy analyses. In this regard, COP and exergy efficiency of the system are examined for performance assessment. The parametric studies considering variation of significant parameters for designing regenerator with cooling power, heat rejection, COP, exergy efficiency and exergy destruction rate are presented accordingly. The parameters reported in Table 1.1 are used to carry out the simulation.

The effect on cooling power and exergetic cooling power output of varying mass flow rate is shown in Fig. 1.2. It is evident that an increase in mass flow rate leads to an increase in cooling power. However, a further increase in the mass flow rate (>0.2 kg/s) leads to a reduction in the cooling power. It is due to the increase in mass flow rate which overwhelms the magnetocaloric effect exhibited by the regenerator bed and, thereafter, the cooling power is decreased. Similarly, the exergetic cooling power initially increases at lower mass flow rates until it attains its maximum value and eventually decreases with an increase of fluid mass flow rate.

Variations in heat rejection to the surrounding with respect to mass flow rate is plotted in Fig. 1.3. It can be observed that as mass flow rate increases the heat rejection increases up to 495.2 W at 0.25 kg/s and then slightly decreases.

Figure 1.4 shows the effect of mass flow rate on pump work. It is shown that, an increase in mass flow rate results in increase in pump work.

Figure 1.5 shows the effect of varying mass flow rate on COP. The result shows in Fig. 1.5. demonstrate that a higher mass flow rate results in a higher pumping work which leads to a reduction of COP. It is mainly due to the higher viscous losses.

Figure 1.6 presents the effect of the mass flow rate on the overall system performance. As it is shown, an increase in mass flow rate leads to a decrease in system exergy efficiency. This is due to the fact that the higher mass flow rate, the higher pumping work which leads to a reduction of exergy efficiency. On the other side, an increase in mass flow rate while fixing other design parameters, lead to an increase in the exergy destruction rate as a result of required pumping power.

Table 1.1 Model parameters

Characteristics	Values	Dimensions
d_p	600	μm
L	0.2	m
ε	25 %	–
D	0.01	m
m_{bd}	115	g
$\dot{m}_f$	0.025	$kg\ s^{-1}$
H_{low}	0	T
H_{high}	1.5	T
$t_1 = t_3$	0.2	s
$t_2 = t_4$	0.5	s
T_H	295	K
T_C	275	K

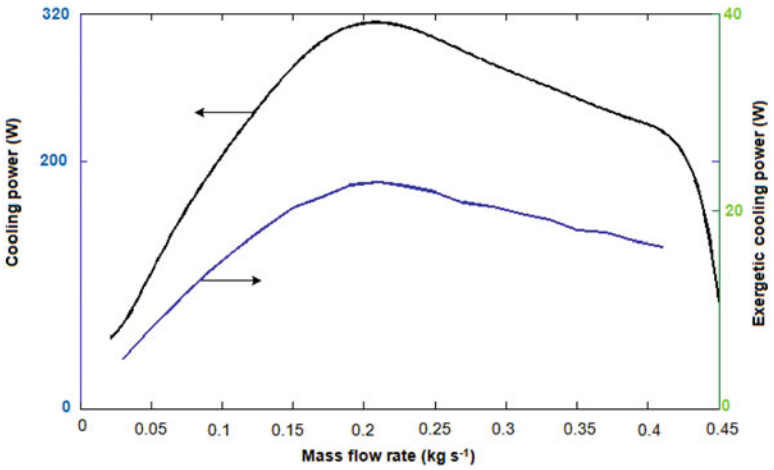

Fig. 1.2 Effect of mass flow rate on cooling power and exergetic cooling power

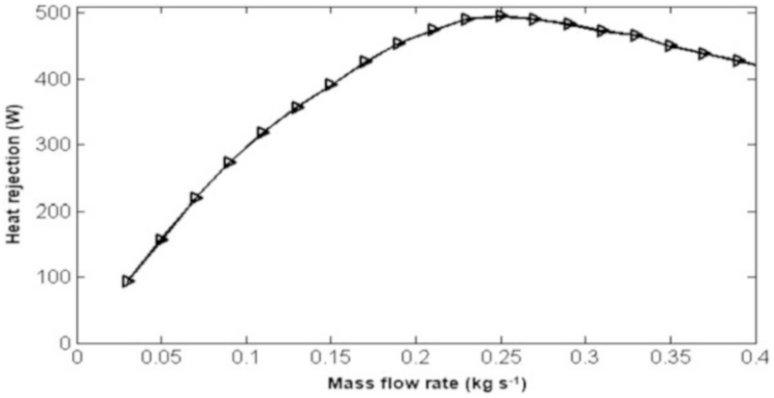

Fig. 1.3 Effect of mass flow rate on heat rejection

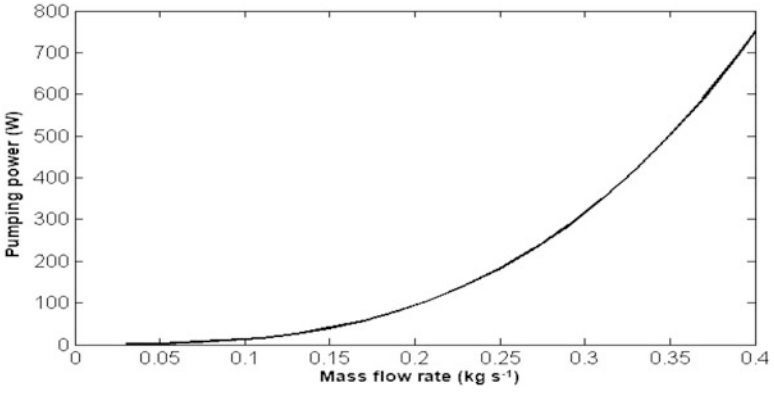

Fig. 1.4 Effect of mass flow rate on the work of pump

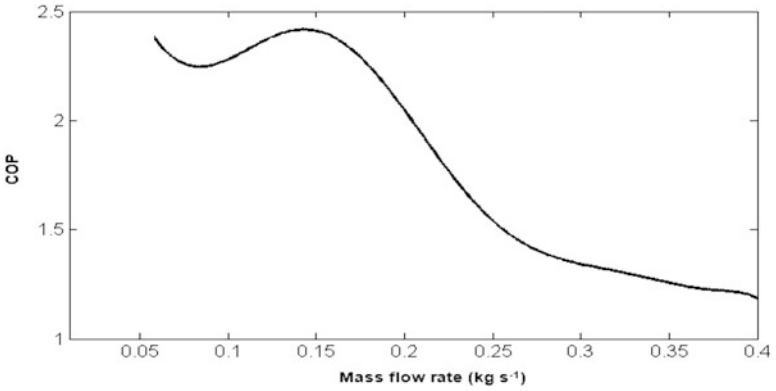

Fig. 1.5 Effect of mass flow rate on COP of the system

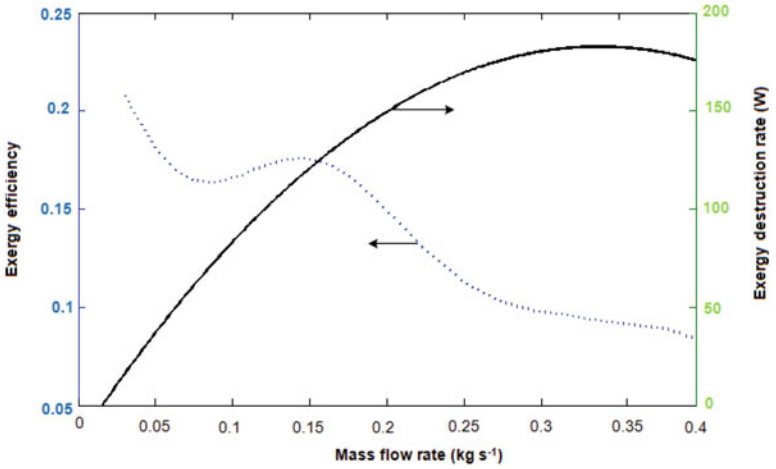

Fig. 1.6 Effect of mass flow rate on system exergy efficiency and total exergy destruction rate of the system

In order to yield optimal performance, the numerical results demonstrate that the mass flow rate must be carefully adjusted with respect to various operating conditions.

1.5 Conclusions

In this paper we have sought to determine how design parameter such as mass flow rate affect the COP, exergy efficiency and exergy destruction rate of the AMR cycle. An increase in mass flow rate increases the exergy efficiency until pick and then decrease slightly. An increase in mass flow rate increases the exergy

destruction rate as a result of pumping power requirements. In order to yield optimal performance, the numerical results show that the mass flow rate must be adjusted carefully with respect to various operating conditions.

Nomenclature

Ac	Cross-sectional area m^2
a_{sf}	Specific surface area m^2/m^3
c	Specific heat J kg K^{-1}
COP	Coefficient of performance
D	Diameter of the regenerator section m
d_P	Diameter of the particles μm
$\dot{E}x$	Exergy flow rate (W)
h	Convection coefficient (W m^{-2} K^{-1})
H	Magnetic field A m^{-1}
H_{max}	Maximum magnetic field A m^{-1}
k	Thermal conductivity W m^{-1} K^{-1}
L	Length of the regenerator m
m	Mass kg
$\dot{m}$	Mass flow rate kg s^{-1}
M	Magnetic intensity A m^{-1}
Nu	Nusselt number
Pr	Prandtl number
$\dot{Q}$	Heat transfer rate, W
Re	Reynolds number dimensionless
s	Specific entropy (J kg^{-1} K^{-1})
t	Time coordinate s
t_1	Magnetization time step (s)
t_2	Isofield cooling time step (s)
t_3	Demagnetization time step (s)
t_4	Isofield heating time step (s)
T	Temperature K
u	Local velocity m/s
V	Volume L
X	Axial position m
$\dot{W}$	Work kJ s^{-1}
ΔP	Pressure drop Pa

Greek Letters

ε	Porosity of the regenerator bed
μ_0	Permeability of free space (m kg s^{-2} A^{-2})
ρ	Density kg m^{-3}
η	Efficiency (−)

Subscripts

ad Adiabatic
C Cooling
D Demagnetization
des Destruction
ex Exergy
f Fluid
H Rejection
M Magnetic
P Pump
s Solid

References

1. Ganjehsarabi H, Dincer I, Gungor A (2013) Thermodynamic analysis and performance assessment of a cascade active magnetic regenerative refrigeration system. Int J Air Cond Ref 21(3):1350016.1–1350016.10
2. Barclay JA, Steyert WA (1982) Active magnetic regenerator. US patent No. 4332135, 1982
3. Brown GV (1976) Magnetic heat pumping near temperature. J Appl Phys 47:3673–3680
4. Aprea C, Greco A, Maiorino A (2013) A dimensionless numerical analysis for the optimization of an active magnetic regenerative refrigerant cycle. Int J Energy Res 37:1475–1487
5. Aprea C, Greco A, Maiorino A (2011) A numerical analysis of an active magnetic regenerative cascade system. Int J Energy Res 35:177–188
6. Tagliafico G, Scarpa F, Tagliafico LA (2010) A dynamic 1-D model for a reciprocating active magnetic regenerator; influence of the main working parameters. Int J Refrig 33(2):286–293
7. Yu B, Liu M, Egolf PW, Kitanovski A (2010) A review of magnetic refrigerator and heat pump prototypes built before 2010. Int J Refrig 33(6):1029–1060
8. Arnold DS, Tura A, Ruebsaat-Trott A, Rowe A (2014) Design improvements of a permanent magnet active magnetic refrigerator. Int J Refrig 37:99–105
9. Lozano JA, Engelbrecht K, Bahl CRH, Nielsen KK, Eriksen D, Barbosa JR, Smith A, Prata AT, Pryds N, Olsen UL (2013) Performance analysis of a rotary active magnetic refrigerator. Appl Energy 111:669–680
10. Zimm C, Boeder A, Chell J, Sternberg A, Fujita A, Fujieda S, Fukamichi K (2006) Design and performance of a permanent-magnet rotary refrigerator. Int J Refrig 29:1302–1306
11. Okamura T, Yamada K, Hirano N, Nagaya S (2006) Performance of a room temperature rotary magnetic refrigerator. Int J Refrig 29:1327–1331
12. Hall JL, Reid CE, Spearing IG, Barclay JA (1996) Thermodynamic considerations for the design of active magnetic regenerative refrigerators. Adv Cryogenic Eng 41:1653–1663
13. Rosario L, Rahman M (2010) Analysis of a magnetic refrigerator. Appl Therm Eng 31:1082–1090
14. Rohsenow WM, Hartnett JP, Ganic ENI (1985) Handbook of heat transfer, vol 6. McGraw-Hill, New York, NY, pp 10–11
15. Kaviany M (1995) Principles of heat transfer in porous media. Springer, New York, NY
16. Ganjehsarabi H, Dincer I, Gungor A (2014) Exergoeconomic analysis of a cascade active magnetic regenerative refrigeration system. Progress in exergy, energy, and the environment. 69–80

Chapter 2
Evaluation of Sustainable Energy Options for Non-residential Buildings

Behnaz Rezaie, Ibrahim Dincer, and Ebrahim Esmailzadeh

Abstract The building sector, as the major energy consumers, demands most of the energy research to assess different energy suppliers from various aspects. In this study, two non-residential buildings, one being commercial and the other industrial, are chosen as case studies. For these case studies, two different renewable energy technologies and one hybrid system are considered for a specified size. The environmental impact indices, renewable energy indices, and the renewable exergy indices have been evaluated for every energy options. The results obtained indicate that the hybrid system (without considering the economics factors) is superior since having top indices. The importance of the energy consumption patterns in buildings were proven by the indices. Utilization of the non-fossil fuels is one part of the solution to environmental hazards while energy conservation being the other. It is shown that the re-design of the energy resources would be achievable for buildings.

Keywords Sustainability • Exergy • Renewable energy • Energy • Industrial building • Environmental impact

2.1 Introduction

Population growth, as well as, modern life style increases the energy demand. Energy supply and environmental impact are major issues of increasing energy consumption. Therefore, other sources of energy, which are sustainable, are favorable energy resources in our era and due to this reason renewable energy is receiving much attention. Meanwhile, smart use of energy improves the overall situation. Knowing the energy consumption of each sector is beneficial to tackle the sector with highest energy consumption. Global energy consumption in 2010 is depicted in Fig. 2.1, which shows that building sector allocated the highest energy consumption. Therefore, an insight to the energy consumption in building sector is

B. Rezaie • I. Dincer (✉) • E. Esmailzadeh
Faculty of Engineering and Applied Science, University of Ontario Institute of Technology, 2000 Simcoe Street North, Oshawa, ON, Canada L1H 7K4
e-mail: Behnaz.Rezaie@uoit.ca; Ibrahim.Dincer@uoit.ca; ezadeh@uoit.ca

I. Dincer et al. (eds.), *Progress in Sustainable Energy Technologies Vol II: Creating Sustainable Development*, DOI 10.1007/978-3-319-07977-6_2

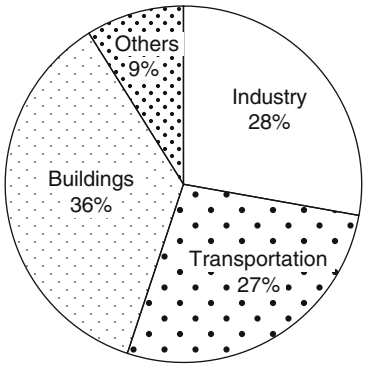

Fig. 2.1 Global energy consumption in 2010 (Data from IEA)

beneficial to unravel the energy issue. Many researches were performed on the subject of energy consumption in buildings [1–3].

A trigeneration system with the goal of improving energy utilization efficiency of buildings was suggested by Huang et al. [4]. Sustainable operations as well as efficient design were reported as important strategies for buildings [5]. Three factors to have the environmental friendly buildings, namely, energy efficiency, energy conservation, and renewable energy were stated by Zaki et al. [6].

Energy efficient buildings also make use of conventional energy sources and rely mostly on fossil fuels. Over and above the major savings in the energy usage, and also cutting down on the greenhouse gases GHG, one can say that much attention has recently been paid on the measurement of energy consumption of buildings. In this regard, Balta et al. [3] have stated that the energy consumption of a building is a function of many variables, such as, the building type, construction materials, occupancy behavior, climatologic conditions, heating and cooling equipment, domestic hot water, and the lighting. As for buildings, Vivancos et al. [7] presented the research results for the thermal characterization of brick, and Drochytka [8] illustrated the role of design for the building envelope to enhance the energy efficiency. Also, Wan et al. [9] showed the trends of energy consumption for future buildings under different climates. Balta et al. [10] stated that exergy analysis is essential for energy system improvement and should be used as a potential tool for sustainable buildings design. The flows of energy in the building systems are more tangible if exergy analysis is considered [11, 12]. Thus, exergy analysis shows possibility of more efficient design by dropping inefficiencies in the system [13]. Environmental advantages and economics of energy can be detected easier by an exergy analysis [10]. Furthermore, energy and exergy ratios are defined and utilized in building sectors for recognizing the building's energy option benefits [14–18].

The present study is based on a previous research, which sizing various energy options for different buildings [19]. The focus is placed on the non-residential buildings while the thermodynamic analysis could be extended to the exergy investigation. Moreover, the energy considerations and the exergy aspects with various energy options for several case studies will be analyzed beyond the

efficiency analysis. The study covers the environmental aspects of different possibilities of energy. Parallel with the present study, another study is performed with emphasis on residential buildings [20]. Two non-residential buildings are selected, one a commercial building and the other an industrial building. For every case study the energy, exergy and the environmental impacts of these renewable energy options have been assessed. Some indices are proposed in this work as a useful tool for comparing several energy options from different aspects, including the energy, exergy, and the environmental impact in a peek period.

2.2 Methodology

Different methods of sizing various energy options, namely, environmental impact, energy, and exergy aspects will be defined in this section. Furthermore, these methods will be applied to the previously mentioned case studies.

2.2.1 Sizing Methods

The sizing methods were discussed in detail in the previous study performed by Rezaie et al. [19]. Here, the proposed methodologies for sizing the solar electricity and solar thermal system are used respectively.

2.2.2 Environmental Impact Assessment Method

One of the major reasons to use the non-fossil fuel energy supplier is to protect the environment against the undesirable greenhouse gases (GHGs). To show the performance of each technology, initially, the emitted CO_2 by the conventional fuel for each case study has been estimated. Then the "environmental impact index" is calculated for each design. The environmental impact index is expressed as

$$I_E = 100\,(R_{CO2})/E_{CO2} \tag{2.1}$$

where I_E represents the environmental impact index, R_{CO2} stands for the reduced CO_2 by the design, and E_{CO2} is the emitted CO_2 by the conventional design, respectively. Note that I_E is a dimensionless factor.

It is worth mentioning that the method of estimation of CO_2 for electricity generation should be explained prior to the calculation of the environmental impact index. Electricity is generated in different plants through using different fuels. In Canada, these resources are namely, the hydro, thermal, nuclear, combustion engine, and very limited renewable energies. The resulting pollution due to the

electricity generation varies depending on the fuel resources. In a report titled "Power Generation in Canada", published by the Canadian Electricity Association, the electricity generation configuration in the Province of Ontario was [21]:

- 37 TWh from hydro,
- 45 TWh from thermal (mainly coal-based power plants),
- 63 TWh from nuclear and
- 6.7 TWh from combustion engine sources.

When visiting the website "Plug into Green Canada" [22] it offers a calculator, which considers the combination of the above-mentioned sources and presents the total generated amount of CO_2. Alternatively, this calculator can be utilized to estimate the amount of CO_2 from the electricity generation.

To obtain the amount of CO_2 from the burning of natural gas, one has to refer to the report published by the Natural Gas Association [23]. It clearly states that to obtain 1 GJ of energy by burning natural gas, one would generate the unwanted amount of 50.3 kg of CO_2.

2.2.3 Energy Method

The energy demand for each case is important enough to be measured by having the index of the estimated renewable energy. The index of renewable energy is defines as:

$$I_{RE} = 100\ (RE)/TE \tag{2.2}$$

where, I_{RE} represents the renewable energy index, RE refers to the renewable energy, and TE stands for the total energy demand. One should note that I_{RE} is a dimensionless parameter.

2.2.4 Exergy Method

Exergy is defined as a tool to appraise and develop energy systems, by giving more meaningful and valuable information than the more conventional energy analysis [24]. Exergy analysis particularly recognizes the actual thermodynamic losses and efficiencies. Hence, exergy analysis can help in reducing the thermodynamic losses in thermal systems. Exergy with the definition of the *available energy* can be computed for the two case studies. The exergy for commercial case study and industrial case study consists of the exergy from the natural gas and the exergy form the electricity, respectively. Hence, the exergy for electricity determines as [25]:

$$\mathrm{Ex} = \mathrm{E} \times \mathrm{R} \tag{2.3}$$

where Ex stands for the exergy, E is for the energy, and R stands for the energy grade function. It can be said that R has different values for various kinds of energy, e.g., for the electricity R = 1.0, and for the natural gas R = 0.913.

The exergy of the solar energy is calculated by:

$$\mathrm{Ex} = \left(1 - \frac{T_0}{T_s}\right)\mathrm{E}$$

where $T_0 = 20°\mathrm{C}$ (environment temperature) and $T_s = 5{,}000\ °\mathrm{C}$.

Then, the renewable exergy index can be calculated and the index of the renewable exergy can be defines as

$$\mathrm{I_{REx}} = 100\ (\mathrm{REx})/\mathrm{TEx} \tag{2.4}$$

where $\mathrm{I_{REx}}$ represents the renewable exergy index, REx is the renewable exergy, and TEx stands for the total exergy demand. Also, note that $\mathrm{I_{REx}}$ is a dimensionless factor.

2.3 Energy Options Considered

Different energy options for non-residential buildings are tested in this study. Here, the commercial and industrial buildings are categorized as non-residential buildings. In the following, one institutional building and one industrial building have been considered as case studies to assess their energy options.

Ground source energy system, as a source of renewable energy with high performance (the average coefficient of performance (COP) of a ground source energy system is 4), is an interesting source of renewable energy. Geothermal system cost effectively provides energy for heating and cooling of a building. This system can be a reasonable source of energy for heating and cooling of a commercial building due to case studies circumstances.

2.3.1 Commercial Building

The commercial case study here is the central public library in Brampton (in Ontario), having latitude 43.536, and longitude −79.556. In the commercial buildings, there is a demand for electricity to run several computers, lights and appliances, and also furnaces to activate the heating systems as well as providing hot water, and running the air-conditioning system to generate cool air in the summer. Typically, natural gas is used for heating space and providing hot water

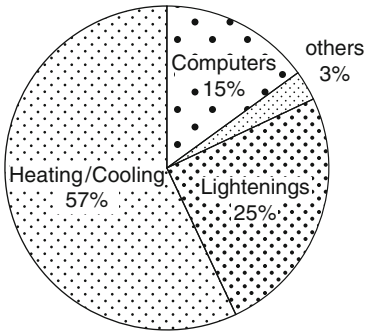

Fig. 2.2 Electricity usage distribution in commercial building case study (Brampton Library)

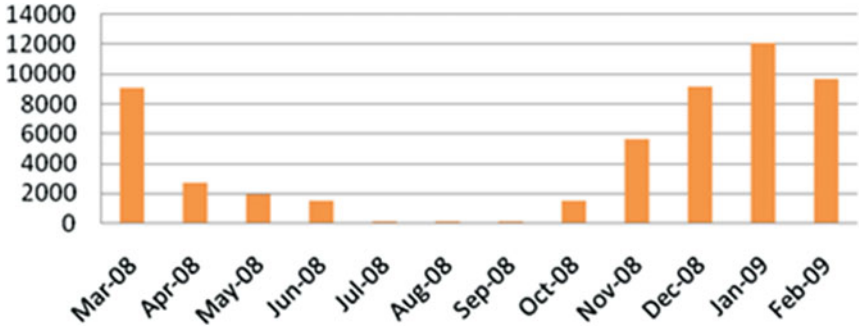

Fig. 2.3 Natural gas Consumption (m^3) in Brampton Library, commercial building case study

in commercial buildings. This library is a two-storey building with the residential area being approximately 1,352 m^2, in both stories. There are many lights in the library, and computers for the use of public and staff. In this case, lightening and computers consume a considerable portion of energy. Figure 2.2 shows the distribution of energy consumption in the commercial case study and illustrates the electricity consumption percentage in the central library. The annual natural gas consumption in this library is 72,748 m^3, and the average monthly consumption is 6,062.3 m^3. Figure 2.3 illustrates the distribution of the natural gas consumption in the central library. Electricity consumption in this library is 765,765.00 kWh (765.8 MWh) per year, and the daily consumption is 2,098.00 kWh for this commercial building.

2.3.1.1 Option 1

Solar water heaters can be employed for this building to heat the space as well as provide hot water. The main demand is for heating the space rather than heating the water, since it is a commercial building. Moreover, there is a large space at the back of the building and wide roof available for installing the solar collectors' panels.

Fig. 2.4 Layout of energy resources for commercial case study when using solar thermal energy

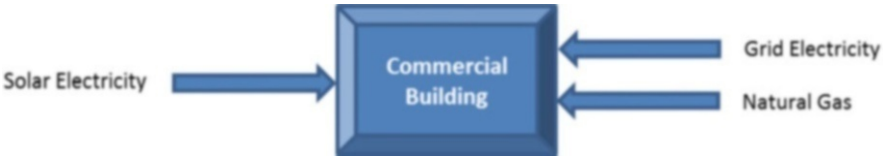

Fig. 2.5 Layout of energy resources for commercial case study when using solar electricity

Figure 2.4 shows the layout of the energy resources for commercial case study. Solar thermal is the renewable source of energy together with two conventional sources of energy—a) grid electricity and b) natural gas. Using the solar thermal energy will reduce the natural gas consumption considerably.

Energy is calculated by using the calculator available in the WSE technology [26]; the engine of this calculation is based on deducting the heat loss of the building by considering the isolation rate as well as the desired temperature, from the heat resulting from the solar collectors. According to this calculator, for the desired temperature of 22 °C throughout the heating space of 1,352 m^2, there is a need of 58 solar collectors WSE58, which should be installed.

The energy generated by 58 solar collectors WSE58 is $58 \times 2{,}741{,}310 = 156$ MJ/h. By considering 7 h of sun per day as the average for all days in the year, the energy produced by these solar panels is: $156 \times 7 = 1{,}092$ MJ/day

Assuming that there are 300 days of sun per year in Ontario, Canada; the energy produced by the solar collectors is 327600 MJ per year. This energy can be released from the use of 8,798.4 m^3 natural gas (201,600 MJ /37,233,949 J = 8798.4). In other words, the gas consumption is reduced by 8,798.4 m^3 every year. In the 25 years life-span of the solar panels, this saving would become as 219,960.5 m^3 natural gas.

2.3.1.2 Option 2

The PV panels are the best technology for the commercial case study in order to generate electricity because this building is located in an urban area, downtown Brampton.

Figure 2.5 illustrates the layout of resources of energy for the commercial case study. Solar electricity through PV panels will generate electricity, which reduces the grid electricity consumption. Grid electricity in smaller amounts and natural gas

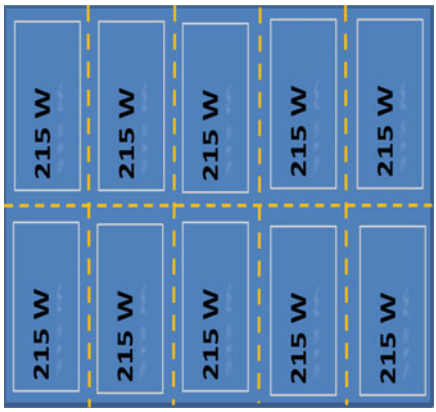

Fig. 2.6 Placing 10 modules in one mount

are both conventional sources of energy for the commercial case study in this design.

The average daily electricity consumption in the commercial case study is 2,098 kWh, and the average insulation coefficient 3.53 kWh/m^2/d in Toronto area, the electricity consumption by the sun hours per day would be 2,098/3.53 = 594 kW = 594,000 W (AC).

Hence, 594,000/(CEC = 194) = 3061 W, and 3,061/(CEC = 0.94) = 3257, hence, 3257 is the number of PV panels; PV panels are 210 W each. Before going further for the arrangement of the array, the availability of the installation space should be assessed.

The area of each panel is $0.9 \times 1.7 = 1.53$ m^3. Roof of the building is the installation area and the available area on the roof is $13 \times 22 = 286$ m^3. For the ease of maintenance, every 10 panels in the form of 2×5 places on one mount. Figure 2.5 shows the configuration of 10 modules in one mount.

Then the area of each mount, which contains 10 PV modules, would be $5 \times 3.4 = 17$ m^2. From each side 0.2 m will be added for maintenance purposes, and then the area of each mount comes to $5.4 \times 3.8 = 20.52$ m^2. Figure 2.6 illustrates a mount dimension and surrounded area.

On the roof with the dimensions of 13 m by 22 m, 10 mounts can be installed, and each mount contain 10 PV panels. Then $10 \times 10 = 100$ PV modules 215 W will generate electricity for the library. The layout for the roof design is depicted in Fig. 2.7.

2.3.1.3 Option 3

The "hybrid system" can be considered by the solar technologies through combining the PV panels for generating electricity and the solar water heaters for heating the space. In hybrid system electricity and natural gas consumption will be reduced and the reduction will be calculated in the following paragraphs. This hybrid system

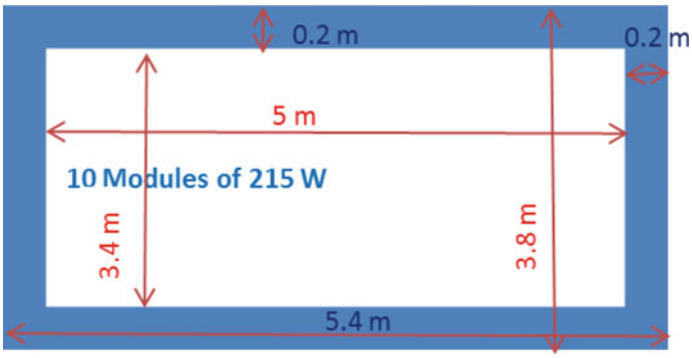

Fig. 2.7 Dimensions on a mount. Blue area is considered for maintenance needs

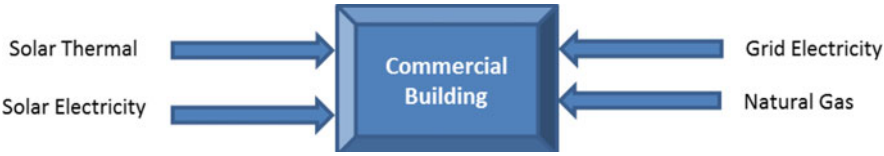

Fig. 2.8 Layout of energy resources for commercial building case study, when using hybrid system

would be directly dependent on the solar energy. In hybrid system, still grid electricity and natural gas are in the system as a backup system for the time there is not quite enough sun in the sky. Figure 2.8 depicts the layout of energy sources in the commercial building case study.

Hybrid system consists of the solar water heaters (Solar Thermal) and PV panels (Solar Electricity). Solar water heaters and PV modules were computed in earlier sections. Based on the previous assessment, the hybrid system is including 58 panels of WSE58 as solar thermal energy for converting the solar energy to 156 MJ/h, plus 100 panels of PV modules 215 W to generate 68.3 kW per day. The configuration of PV modules and the angles of panels are described in the previous section.

2.3.2 Industrial Building

Industrial building case study is a plastic injection company in Mississauga, having latitude 43.640 and longitude −79.622. This building can be categorized as an industrial building and one of the specifications of industrial buildings is having high energy consumption. Industrial buildings are high in using electricity over running the machines and production equipment. These machines produce some heat as well. There is not a great demand for having hot water running; however there is great need for heating the building and working space.

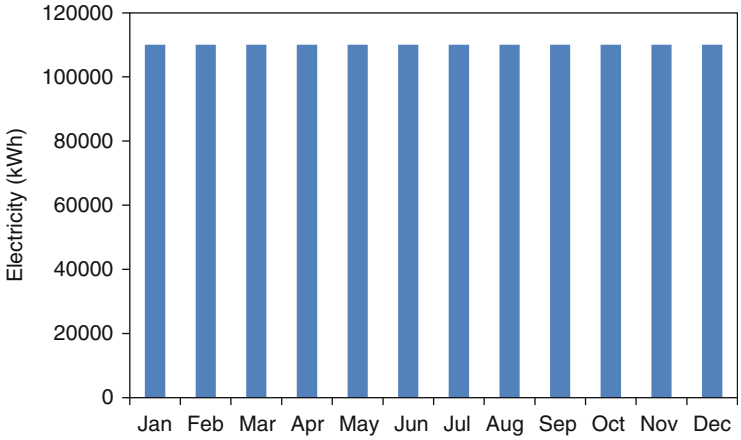

Fig. 2.9 Electricity consumption (kWh) in injection plastic company, Industrial building case study (from the actual monthly bills)

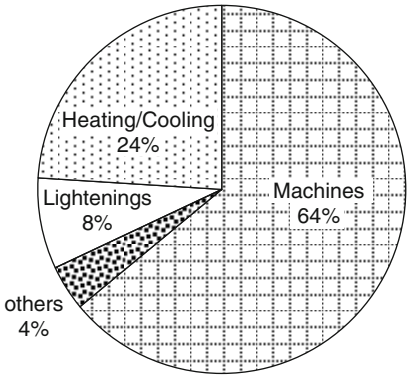

Fig. 2.10 Electricity usage distribution for industrial building case study (Industrial building case study information)

The area of this industrial unit is 1,900 m^2 (30 × 63.3); there are 100 employees, some working on shop-floor and some are in office space, they are working 5 days per week and each day for 16 h. 24 computers are running all the time, and average load of each computer is 200 W. Lighting load is 10 W/m^2, for 100 h/W. For the 12 months electricity usage was 1320 MWh, and then the monthly average electricity consumption comes down to 110 MWh. Figure 2.9 shows the electricity usage in this company in each month of year. Since the major electricity users are machines and the company runs with the same schedule, the electricity consumption would almost be the same in each month.

As the industrial company case study is an industrial building, the energy consumption pattern is totally different from the prior cases. In this case machines including computers have the highest portion of electricity consumption. Figure 2.10 illustrates energy distribution in the industrial building case study. Also, the natural gas consumption in the last 12 months was 43,000 m^3. The information for monthly usage of natural gas is not available.

Fig. 2.11 Layout of energy resources for industrial building case study, when using solar thermal energy

2.3.2.1 Option 1

Solar water heater can be used for this industrial building to heat the space as well as providing hot water. There is a big space on the back of the building and also big roof available for installing the solar collectors' panels. Figure 2.11 shows the layout of the energy resources for industrial building case study. Solar thermal is the renewable source of energy beside two conventional sources of energy, i.e., the grid electricity and the natural gas. Solar thermal caused reduction of the natural gas consumption.

By using the calculator available in the WSE technology website; for heating the spaces of this company with the area of 1,900 m^2 and for the desired temperature of 22 °C, one would know that 75 solar collectors WSE58 are needed.

The Energy generated by 75 solar collectors WSE58 is $75 \times 2{,}741{,}310 = 205.6$ MJ/h. By considering 7 h of sun per day as average for all days in the year, the energy produced by these solar panels would be: $205.6 \times 7 = 1{,}439.2$ MJ/day.

The assumption is that there are 300 days of sun per year in Ontario, Canada. Then, the energy produced by the solar collectors is 431,760 MJ per year. This energy can be released from 11,606 m^3 natural gas (431,760 MJ / 37,233,949 J = 11606.4), in other word the gas consumption is reduced by 11,606 m^3 every year. In 25 years life-span of the solar panels this saving is 290,161 m^3 natural gas.

2.3.2.2 Option 2

For the PV the average electricity consumption in industrial building case study is 110,000 kWh, generating this much electricity with the average insulation coefficient of 3.53 kWh/m^2/d for Toronto area resulted in having thousands of PV modules, which is not a reasonable decision. Because, that many PV panels demand huge area to stand, this area is not suitable for the injection company. Moreover, the maintenance of so many PV panels is very costly. Maintenance of the PV modules includes adjusting the angle of incident towards sun four times per year, plus cleaning the snow of the panels during the long Canadian winter, though PV modules will be chosen based on the available space on the roof of the building.

Fig. 2.12 Layout of energy resources for industrial building case study, when using solar electricity energy

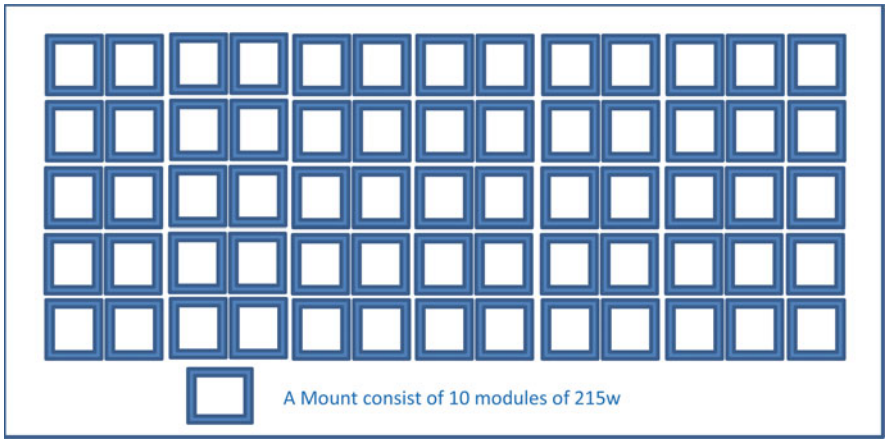

Fig. 2.13 Configuration of PV modules on the roof of injection plastic company, industrial building case study

Figure 2.12 illustrates the layout of resources of energy for the industrial building case study. Solar electricity through PV panels generates electricity, which reduces the grid electricity consumption. Grid electricity in a smaller amount and natural gas are the conventional sources of energy for the industrial building case study in this design.

The area on the roof of this injection company is 30 m × 63.3 m. The actual available area for PV panels is $30 \times 50 = 1{,}500\ m^2$. In this scenario, the sizing of the PV panels is based on the vacant space on the roof.

Every 10 PV panels are placed together on a mount with a dimension of 5 m × 3.8 m; considering 0.2 m from each side for maintenance, the actual space for each mount is 5.4 m × 3.8 m. Figure 2.13 depicts a sketch of a mount containing 10 PV panels. The best arrangement of the mounts on the roof is 5 × 13, which results into a total of 65 mounts, with each mount containing 10 panels. The total 650 PV panels would then generate electricity for the injection company. The electricity generating from 650 modules 215 W is roughly $215 \times 650 \times 90\ \% \times 3.53 = 443{,}985.8$ W/day = 444 kW/day. Figure 2.13 depicts the configuration of 650 modules on the roof of the injection plastic company.

Fig. 2.14 Layout of energy resources for industrial building case study when using hybrid system

The photovoltaic panels should have the right angle towards sun for getting the maximum amount of solar energy. The angle for each season is then:

Fall/Spring: Angle = Latitude = 43.6°
Summer: Angle = Latitude − 15 = 43.6 −15 = 28.6°
Winter: Angle = Latitude + 15 = 43.6 + 15 = 58.6°

As the seasons change, it is strongly recommended that the angle of PV modules be changed in order to obtain maximum energy from the sun.

2.3.2.3 Option 3

The second hybrid system is defined by the solar technologies through combining PV panels for generating the electricity and solar water heaters for heating the space. In the hybrid system, electricity and natural gas consumption is reduced. The reduction is calculated in the following paragraphs. This hybrid system is directly dependent on the solar energy. In hybrid system, the grid electricity and natural gas are still in the system as a backup for the time that there would not be enough sunshine. Figure 2.14 depicts the layout of energy sources in the industrial building case study. The hybrid system consists of the solar water heaters (solar thermal) and PV panels (solar electricity). Solar water heaters and PV modules are discussed in previous sections. Based on the previous assessments, hybrid system includes 72 panels of WSE58 as the solar thermal energy source to convert the solar energy to 205.6 MJ/h, plus 650 panels of PV modules of 215 W to generate 444 kW per day. The configuration of the PV modules and the angles of the panels are described in earlier section.

2.4 Analysis

The energy options are sized technologically in the previous section. Different aspects of each option have been assessed in this section. When considering the importance of environment, one major aspect of the analysis is the environmental impact of energy as the main purpose of the options. Different design proposals will be measured individually for each option within every case study. Also, energy

analysis for each technology options will be performed to show the share of the renewable energy in the proposed design. Following that exergy, as the quality of energy for each energy technology will be examined. It can be another tool to measure capability of different design proposals. The overall analysis of energy options provides insight for the designers and researchers.

2.4.1 Environmental Impact

It has been explained in the introduction that environment issues are very serious matters for human being. The main aspect of any design should be the consideration of the environmental effects of the new design/product/system on the society. To quantify the environment impact, two case studies as explained in Sect. 2.3, with varieties of technology options are chosen. As mentioned, one case study is a commercial building and the other one is an industrial building. The impacts of the environmental issues on every single energy technology, proposed in the previous section, for both case studies are examined in the following paragraphs.

2.4.1.1 Commercial Case Study

When the residential building of commercial case study is running with the conventional energy, say the natural gas and electricity, the volume of the emitted CO_2 is the sum of the emitted CO_2 to generate 765,765 kWh of electricity and the burning of 72,748 m^3 of natural gas. By using the available calculator given in reference [12], one could find that 2,688.7 tons of CO_2 has been emitted to the environment when 765,765 kWh of electricity has been generated. According to the report published in reference [27], the energy contained in every cubic meter of natural gas is 36,116.7 kJ. Therefore, the total energy resulted from the natural gas for the commercial case study is:

$$\begin{aligned} 72,748\ \left(\mathrm{m}^3/\mathrm{year}\right) \times 36,116.7\ (\mathrm{kJ}) &= 2,627,417,691.6\ \mathrm{kJ/year} \\ &= 2,627.4\ \mathrm{GJ/year}. \end{aligned}$$

It has been mentioned before that the energy of 1 GJ from burning of the natural gas is equivalent to the generating of 50.3 kg of CO_2, hence:

$$\begin{aligned} 2,627.4\ (\mathrm{GJ/year}) \times 50.3\ (\mathrm{kg\ of\ CO_2}) &= 132,159.1\,\mathrm{kg\ of\ CO_2 per\ year} \\ &= 132.2\ \mathrm{ton/year}. \end{aligned}$$

Therefore, the total amount of CO_2 emitted to the environment, when for the commercial case study the conventional fuel was used, is:

$$2,688.7\ (\text{ton of } CO_2/\text{year}) + 132.2\ (\text{ton of } CO_2/\text{year}) = 2,820.9\ \text{ton of } CO_2 \text{ per year.}$$

Option 1

As mentioned before, by releasing energy of 1,054,350 kJ from natural gas, the mass of 58 kg CO_2 emits into the atmosphere. Therefore, by releasing 327,600 MJ of natural gas, 16.5 Ton of CO_2 is emitted into the atmosphere. In other words, 58 panels prevent emitting 16.5 tons of CO_2 into the air each year; this is 412.5 tons of CO_2 in the 25 years of the panels' life. Figure 2.14 shows the environmental impact index.

Option 2

Following the previous section the PV panels will generate 2,083 kWh per month in accordance with the calculator available in the "Plug into Green Canada" website. In order to generate 2,083 kWh electricity per month, the mass of 7,312 kg CO_2 per year will be emitted into the atmosphere in Ontario. Figure 2.14 depicts the environmental impact index for Option 2 energy.

Option 3

With a similar logic, the emission reduction for hybrid system is equal to the emission reduction by 58 panels of WSE58 which was calculated along with the emission reduction by 100 PV modules. Then, the quantity of emission reduction by hybrid system is defined as

$$16.5 + 7.3 = 23.8\ \text{tons of } CO_2/\text{year}$$

The environmental impact index has been demonstrated in Fig. 2.15.

2.4.1.2 Industrial Case Study

For every day of running of the house, for industrial case study with the conventional energy system being the natural gas and electricity, the volume of the emitted CO_2 can be estimated as the total emitted CO_2 for generating 1,320 MWh of electricity plus the burning of 43,000 m^3 of the natural gas. In order to generate 1.320 MWh of electricity it would produce 4,634,664.8 kg of CO_2 annually according to the reports published [26].

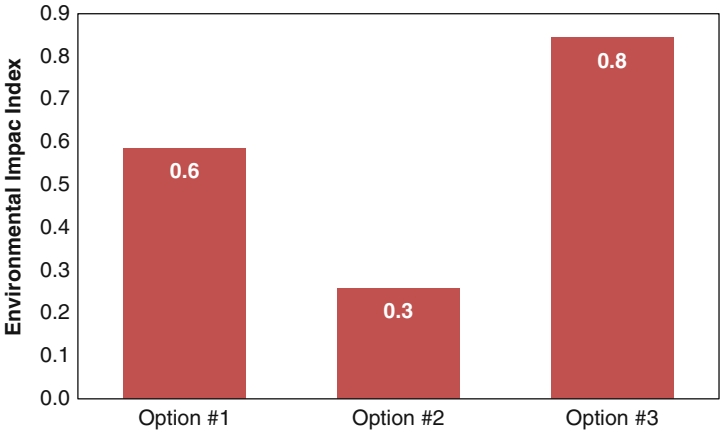

Fig. 2.15 Environmental impact index for commercial building case study

Therefore, the consumed natural gas would contain [27]:

$$43,000\ (\mathrm{m}^3/\mathrm{year}) \times 36,116.7\ (\mathrm{kJ}) = 1,553,018,100\ \mathrm{kJ/year} = 1,553\ \mathrm{GJ\ per\ year}$$

$$1,553\ (\mathrm{GJ/year}) \times 50.3\ (\mathrm{kg\ of\ CO_2}) = 78,116.8\ \mathrm{kg\ of\ CO_2\ per\ year}$$

And the total amount of CO_2 emitted for the Industrial case study with the conventional fuel is:

$$4,634,664.8\ (\mathrm{kg\ of\ CO_2/year}) + 78,116.8\ (\mathrm{kg\ of\ CO_2/year}) = 4,712,781.6\ \mathrm{kg\ of\ CO_2\ per\ year} = 4,712.8\ \mathrm{ton/year}$$

Option 1

As mentioned earlier, by releasing 1,054,350 kJ of energy from natural gas, the mass of 53 kg CO_2 emits into the atmosphere. Then, by receiving 431,760 MJ of energy from the natural gas, the mass of 21.7 tons of CO_2 emits into the atmosphere. Figure 2.15 depicts the environmental impact index for Option 1 energy.

Option 2

The energy generated by 650 modules is 13.5 MW/month. This means that the injection company uses the amount of 13.5 MW less electricity in each month. These PV modules save the environment from 47,391 kg of CO_2 per year, in accordance with the calculator in the website of "Plug into Green Canada". Figure 2.15 depicts the environmental impact index for Option 2 energy.

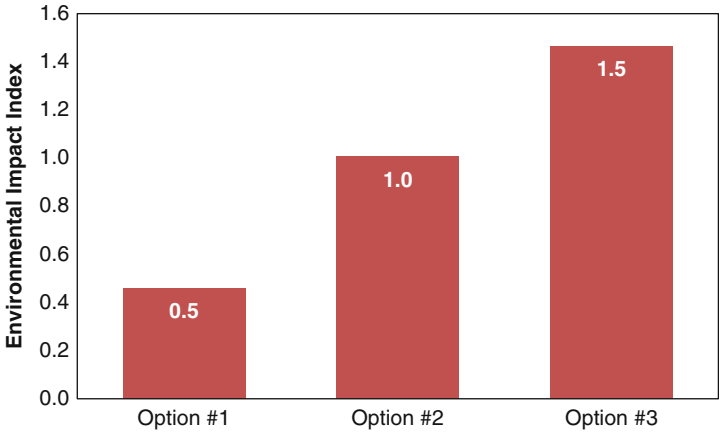

Fig. 2.16 Environmental impact index for energy options of industrial building case study

Option 3

Emission reduction for the hybrid system is equal to the emission reduction by 72 panels of WSE58, plus emission reduction by 650 PV modules. Hence, the quantity of emission reduction by the hybrid system is:

$$21.7 + 47.4 = 69.1 \text{ Ton } CO_2/\text{year}$$

Figure 2.16 depicts the environmental impact index for Option 3 energy.

2.4.2 Energy Aspect

2.4.2.1 Commercial Case Study: Energy Demand

The annual energy requirement of commercial case study is the sum of the natural gas and the electricity consumptions. The energy value of the natural gas used by the commercial case study (72,748 m^3) was calculated for 2,627.4 GJ per year. Also, the energy value of 765,765 kWh per year can be estimated as:

$$\begin{aligned} 765,765 \text{ (kWh/year)} \times 3.6 \text{ (MJ/kWh)} &= 2,756,754 \text{ MJ/year} \\ &= 2,756.8 \text{ GJ per year} \end{aligned}$$

Then the total energy demand for commercial case study is calculated as

$$2,627.4 \text{ (GJ/year)} + 2,756.8 \text{ (GJ/year)} = 5,384.2 \text{ GJ per year}$$

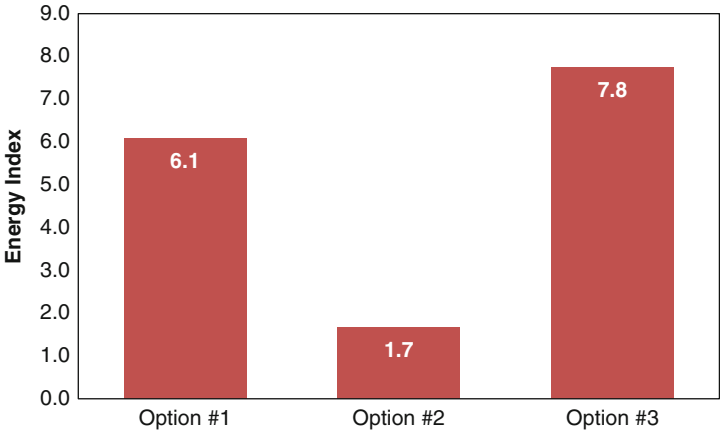

Fig. 2.17 Energy impact index for commercial building case study

The energy value of each technology is already defined in the design of Sect. 2.5. The summary of the energy index are in illustrated in Fig. 2.17. The energy of each design is presented in Table 2.1.

2.4.2.2 Industrial Case Study: Energy demand

The energy demand for the industrial case study is the total sum of the natural gas and the electricity consumptions. The energy value of the natural gas, used by industrial case study (43,000 m^3), was determined in Sect. 2.4 as 1,553 GJ per year. The energy value of 1,320 MWh per year can be computed from:

$$1,320 \times 10^3 (\text{kWh/year}) \times 3.6\ (\text{MJ/kWh}) = 4,752\ \text{X}\,10^3 \text{MJ per year} = 4,752\ \text{GJ per year}$$

Therefore, the total energy demand for Industrial case study would be:

$$1,553\ (\text{GJ/year}) + 4,752\ (\text{GJ/year}) = 6,305\ \text{GJ per year}$$

Initially, the different technology options were examined and then the energy value of every technology has been adapted. Hence, the renewable energy index of every design option is calculated accordingly. The results of the energy for the industrial case study are summarized in Fig. 2.18. The energy of each design is listed in Table 2.1.

Table 2.1 Summary of energy, exergy and CO_2 reduction of each energy options for both cases

		Commercial building case study				Industrial building case study			
		Renewable technology	Energy (MJ)	Energy (MJ)	CO_2 Reduction (tons)	Renewable technology	Energy (MJ)	Energy (MJ)	CO_2 Reduction (tons)
Option 1	Solar Thermal	58 WSE58	327.6	307.9	16.5	75 WSE58	431.8	405.9	21.7
Option 2	Solar Elec.	100 × 215 W	90	84.6	7.3	650 × 215 W	583.2	548.2	47.4
Option 3	Hybrid	58 WSE58 + 100 × 215 W	417.6	392.5	23.8	75 WSE58 + 650 × 215 W	1015	954.1	69.1

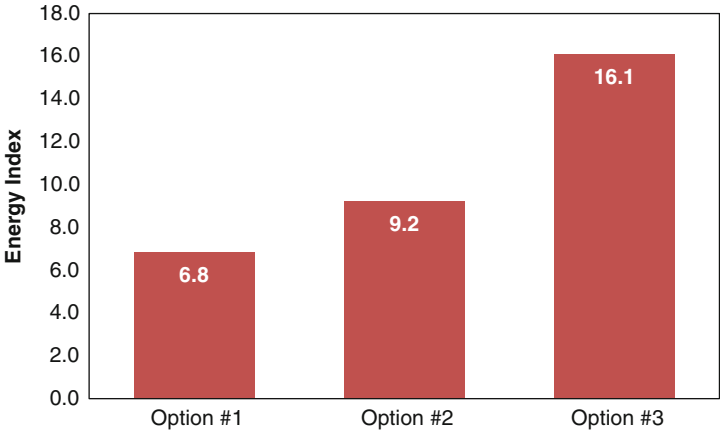

Fig. 2.18 Energy impact index for energy options of industrial building case study

2.4.3 Exergy Aspect

2.4.3.1 Commercial Case Study

The exergy for the commercial case study can be estimated by using Eq. (2.3). Hence, the exergy for electricity can be determined as:

$$\text{Exergy of electricity} = 2,756.8\ (\text{GJ}) \times 1 = 2,756.8\ \text{GJ per year}$$

and the exergy of the natural gas can be calculated as:

$$\text{Exergy of natural gas} = 2,627\ (\text{GJ}) \times 0.913 = 2,398.5\ \text{GJ per year}$$

Then the total exergy for the commercial case study would be:

$$2,756.8\ (\text{GJ}) + 2,398.5\ (\text{GJ}) = 5,155.3\ \text{GJ per year}$$

The renewable exergy index for various technology options considered for the commercial case study can be calculated by using Eq. (2.4). The calculated results are presented in Fig. 2.19 and Table 2.1.

2.4.3.2 Industrial Case Study

The exergy for the industrial case study can be estimated using Eq. (2.3). Hence, the exergy for the electricity can be evaluated as:

$$\text{Exergy of electricity} = 6,305\ (\text{GJ}) \times 1 = 6,305\ \text{GJ per year}$$

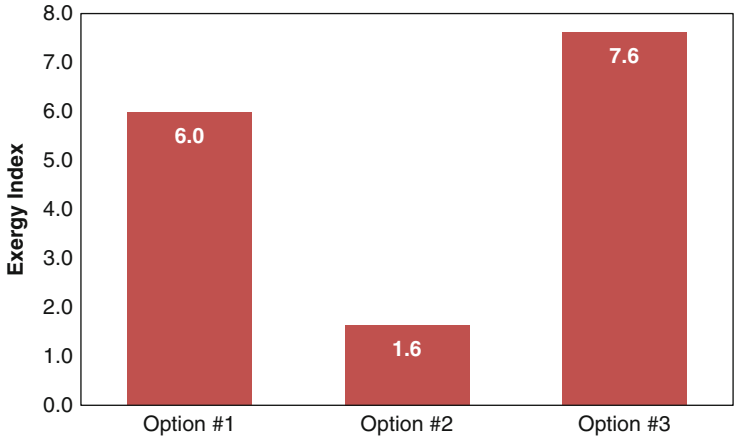

Fig. 2.19 Exergy impact index for commercial building case study

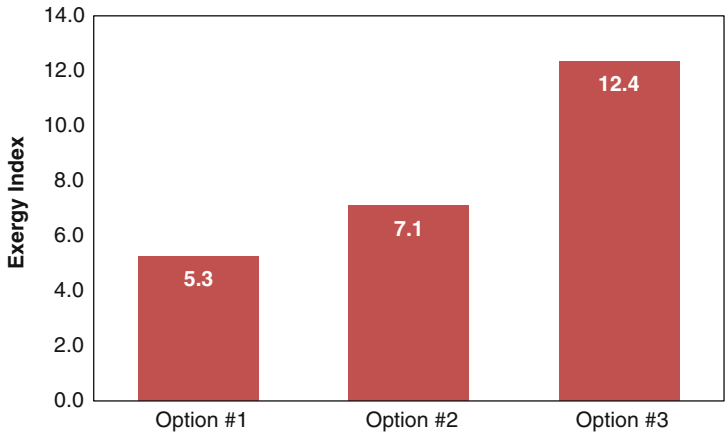

Fig. 2.20 Exergy impact index for energy options of industrial building case study

and the exergy of the natural gas can be calculated as:

$$\text{Exergy of natural gas} = 1,553\ (\text{GJ}) \times 0.913 = 1,417.9\ \text{GJ per year}$$

Then the total exergy for the industrial case study would be the sum of them as:

$$6,305\ (\text{GJ}) + 1,417.9\ (\text{GJ}) = 7,722.9\ \text{GJ per year}$$

Equation (2.4) is the renewable exergy index for different technology options, which has been used to compute for the industrial case study. The computed results of exergy calculations for the industrial case study have been summarized in Fig. 2.20 and Table 2.1.

2.5 Results and Discussion

In comparing different renewable energy design options for the commercial and industrial buildings, the environmental impact, energy, and the exergy, as well as, the environmental impact indices, renewable energy and the exergy indices have been computed. Results of those calculations are presented in Figs. 2.14, through 2.19 for the case studies. Comparisons of various options in this study are based on the environmental impact, energy and the exergy approaches. For the final choice decision, these various options must be considered depending on the management priority cost factor.

In analyzing the commercial case study, the hybrid system has the highest environmental index as illustrated in Fig. 2.14. Since the hybrid systems are formed as the combination of two renewable technologies, the ranking of the hybrid systems as the top priority is a sensible choice. Following the hybrid system, solar heater and PV panels are ranked second and third choices by considering the environmental index, energy and exergy indices. This prioritization is for this particular case study (Brampton library). Depending on the project and its specific situations the design of different energy sources will vary; apparently prioritizations would vary too.

For assessing the industrial case study, the hybrid system has the highest environmental index as depicted in Fig. 2.15. For this case study the PV panels stand as the second choice and the solar heater is the last choice, based on the environmental, energy and exergy indices. As explained earlier, this prioritization is only for this specific building with its own stand-alone situation.

The study of proportions shows the importance of energy resources available in buildings. Using the non-fossil fuels is one part of the solution to the environmental issues and the energy conservation is another part of the resolution. Re-design of energy resources model is effective and achievable for buildings. Whenever equipment is available to use the non-fossil fuel in a building, then the change of energy resources would greatly beneficial in reducing the environmental impact of the building.

2.6 Conclusions

Two non-residential buildings were chosen to consider different energy options. Each building was treated as an independent case study, and various renewable energy and hybrids systems were designed and sized for every one of them. The environmental impact and the energy and exergy aspects of each design were fully assessed through the analysis of the environmental impact index, the renewable energy index and the exergy index. The following important results are obtained from the computer simulation runs and by evaluating the results for both cases:

- The highest environmental impact index belongs to the hybrid system, being 0.8 for the commercial case study and 1.5 for the industrial case study, respectively. Therefore, it indicates that the hybrid system is a far better option.

- The renewable energy indices demonstrate that the hybrid system has a superior technology by achieving the highest energy index of 7.8 for the commercial case study and 16.1 for the industrial case study.
- The upmost renewable exergy index fits well into the hybrid system, being 7.6 for the commercial case study and 12.4 for the industrial case study. This reiterates that the hybrid system is an outstanding design choice.
- Hybrid systems are ranked as top choices with higher indices since they are made with the combination of two technologies and hence, exhibit the advantages of both technologies.

The results presented here are only based on the environmental, energy and the exergy aspects without considering any economic factors. For having a thorough prioritization, it is recommended that one should also consider carefully the initial capital costs, annual maintenance fees, and other financial aspects of every design in order to arrive at an optimum decision. However, if the financial factors taken into consideration then one could say that hybrid systems would be the most expensive technologies since they are made of the combination of two renewable technologies.

Nomenclature

CEC	California Energy Commission
COP	Coefficient of Performance
E	Energy
I_E	Environmental Impact Indices
R_{CO2}	Reduced CO_2
E_{CO2}	Emitted CO_2
Ex	Exergy
R	Energy grade function
RE	Renewable Energy
I_{RE}	Renewable Energy Index
REx	Renewable Exergy
I_{REx}	Renewable Exergy Index
TE	Total Energy
TEx	Total Exergy demand.

References

1. Rezaie B, Rosen MA (2012) District heating and cooling: review of technology and potential enhancements. Appl Energy 93:2–10
2. Pérez-Lombard L, Ortiz J, Pout C (2008) A review on buildings energy consumption information. Energy Build 40(3):394–398

3. Balta MT, Dincer I, Hepbasli A (2011) Development of sustainable energy options for buildings in a sustainable society. Sustainable Cities Society 1(2):72–80
4. Huang Y, Wang Y, Rezvani S, McIlveen-Wright D, Anderson M, Hewitt N (2011) Biomass fuelled trigeneration system in selected buildings. Energy Convers Manag 52(6):2448–2454
5. Chua K, Chou S (2011) A performance-based method for energy efficiency improvement of buildings. Energy Convers Manag 52(4):1829–1839
6. Zaki WRM, Nawawi AH, Ahmad SS (2010) Economic assessment of operational energy reduction options in a house using marginal benefit and marginal cost: a case in bangi, malaysia. Energy Convers Manag 51(3):538–545
7. Vivancos J, Soto J, Perez I, Ros-Lis JV, Martínez-Máñez R (2009) A new model based on experimental results for the thermal characterization of bricks. Build Environ 44(5):1047–1052
8. Drochytka R, Zach J, Korjenic A, Hroudová J (2013) Improving the energy efficiency in buildings while reducing the waste using autoclaved aerated concrete made from power industry waste. Energy Build 58:319–323
9. Wan KK, Li DH, Liu D, Lam JC (2011) Future trends of building heating and cooling loads and energy consumption in different climates. Build Environ 46(1):223–234
10. Balta MT, Dincer I, Hepbasli A (2010) Performance and sustainability assessment of energy options for building HVAC applications. Energy Build 42(8):1320–1328
11. Tolga Balta M, Kalinci Y, Hepbasli A (2008) Evaluating a low exergy heating system from the power plant through the heat pump to the building envelope. Energy Build 40(10):1799–1804
12. Schmidt D (2004) Design of low exergy buildings-method and a pre-design tool. Int J Low Energy Sustainable Build 3(2004):1–47
13. Rosen MA, Dincer I (1999) Exergy analysis of waste emissions. Int J Energy Res 23 (13):1153–1163
14. Coskun C, Oktay Z, Dincer I (2011) Estimation of monthly solar radiation distribution for solar energy system analysis. Energy 36(2):1319–1323
15. Coskun C, Oktay Z, Dincer I (2009) New energy and exergy parameters for geothermal district heating systems. Appl Therm Eng 29(11):2235–2242
16. Coskun C, Oktay Z, Dincer I (2012) Thermodynamic analyses and case studies of geothermal based multi-generation systems. J Clean Prod 32:71–80
17. Oktay Z, Coskun C, Dincer I (2008) Energetic and exergetic performance investigation of the bigadic geothermal district heating system in turkey. Energy Build 40(5):702–709
18. Oktay Z, Dincer I (2008) Energetic, exergetic and environmental assessments of the edremit geothermal district heating system. ASHRAE Trans 114(1):118–127
19. Rezaie B, Esmailzadeh E, Dincer I (2011) Renewable energy options for buildings: Case studies. Energy Build 43(1):56–65
20. Rezaie B, Dincer I, Esmailzadeh E (2013) Energy options for residential buildings assessment. Energy Convers Manag 65:637–646
21. Canadian Electricity Association (2004) Power generation in canada. June 10, 2012
22. Plug into Green Canada. Available: www.plugintogreencanada.com. doi: www.plugintogreencanada.com
23. Natural Gas and Environment. http://www.naturalgas.org/overview/background.asp. doi: http://www.naturalgas.org/overview/background.asp. Available 10 June 2010
24. Rosen MA, Dincer I, Kanoglu M (2008) Role of exergy in increasing efficiency and sustainability and reducing environmental impact. Energy Policy 36(1):128–137
25. Hevert HW, Hevert SC (1980) Second law analysis: an alternative indicator of system efficiency. Energy 5(8):865–873
26. WSE Technology (2009) doi: www.wsetech.com.

Chapter 3
Exergoeconomic and Enviroeconomic Analyses of Hybrid Electric Vehicle Thermal Management Systems

H.S. Hamut, I. Dincer, and G.F. Naterer

Abstract Thermal management systems (TMSs) are one of the key components of hybrid electric vehicles in terms of their impact on vehicle efficiency, as well as the vehicle's overall cost and environmental footprint. In this paper, exergoeconomic and enviroeconomic (environmental cost) analyses of hybrid electric vehicle thermal management systems are conducted with respect to various system parameters as well as operating conditions. In the exergy analysis, balance equations are applied to each system component of the TMS, in order to determine exergy destruction rates and calculate the exergy efficiencies of the system and its individual components. In the economic analysis, investment cost rates are calculated with respect to equipment costs, which are determined by cost correlations for each system component, and capital recovery factors. Thus, by combining the two analyses, an exergoeconomic model is created whereby the exergy streams are identified, fuel and productsare defined and cost equations are allocated for each component. The costs from the economic analysis are used to determine the unit cost of exergy, cost rate of exergy destruction as well as other useful exergoeconomic variables for each component. Moreover, an enviroeconomical (environment cost) analysis is also conducted based on the established carbon price associated with the released CO_2 to the environment, corresponding to the indirect emissions from the electricity used in the TMS under varying carbon prices and electricity generation mixes.

Keywords Exergy • Exergoeconomics • Enviroeconomics • Hybrid electric vehicle • Thermal management

H.S. Hamut • I. Dincer (✉)
Faculty of Engineering and Applied Science, University of Ontario Institute of Technology (UOIT), 2000 Simcoe St. North, Oshawa, ON, Canada L1H 7K4
e-mail: Halil.Hamut@uoit.ca; Ibrahim.Dincer@uoit.ca

G.F. Naterer
Faculty of Engineering and Applied Science, Memorial University of Newfoundland, 240 Prince Phillip Drive, St. John's, NL, Canada A1B 3X5
e-mail: gnaterer@mun.ca

I. Dincer et al. (eds.), *Progress in Sustainable Energy Technologies Vol II: Creating Sustainable Development*, DOI 10.1007/978-3-319-07977-6_3

3.1 Introduction

Thermodynamic analyses of hybrid electric vehicles are essential to improve energy systems in terms of their efficiencies and performance under various system parameters and operating conditions. Among these methods, exergy analysis is an valuable tool to better understand the intrinsic efficiencies of the thermal management system components by determining the irreversibilities in each cycle, as well as the overall system and how nearly the respective performances approach ideal conditions. By analyzing both the quality (usefulness) and quantity of the energy, the true magnitude of losses, and their causes and locations are identified by investigating the sites of exergy destruction in order to make improvements on the individual components and overall system [1, 2].

Even though exergy analysis can be used to improve the efficiencies of the components and corresponding systems, the feasibility of applying these improvements is generally constrained by the limitation of financial resources. Moreover, in many cases, the approaches taken by purely scientific means may not always be cost effective. Thus, in order to achieve the optimum design for energy systems, techniques combining scientific disciplines (mainly thermodynamics) with economic disciplines (mainly cost accounting) should be utilized. In this paper, a SPECO method, especially by the CGAM problem [3], will be used to conduct exergoeconomic analysis of a hybrid electric vehicle TMS.

Exergoeconomics is a branch of Applied Thermodynamics that deals with second law based process synthesis that can provide information that is useful to the design and operation of a cost-effective system which cannot be obtained by conventional energy, exergy or economic analyses [4, 5]. During the past several decades, exergoeconomic analysis have been carried out for various applications by many researchers [1, 6–12].

Even though exergoeconomics have been widely used in past literature, there are still very limited studies available for air conditioning applications. Wall [13] presented an application of thermoeconomics to the optimization of a heat-pump. The author chose the efficiencies of the compressor, condenser, evaporator and electric motor as the variable to be optimized, created cost relations in terms of their efficiencies and conducted parametric studies based on the price of electricity and the temperature of the heat input. D'Accadia and Rossi [14] applied thermoeconomic optimization to a conventional refrigeration plant in order to minimize the overall operation and amortization costs. The authors used a theory of exergetic unit costs to evaluate the economic cost of all internal flows and products. They presented a case study where the overall operation and amortization costs were reduced 1.8 % with respect to the base case and concluded that a design configuration not far from the real global optimum can be obtained my means of sequential, local optimization of the system. This would have acceptable accuracy when compared to conventional and more complex optimization methods.

Al-Otaibi et al. [15] studied thermoeconomic optimization of vapor compression refrigeration systems and verified their model with an illustrative example for an

actual system using R134a as a refrigerant. The authors concluded that increasing the refrigerant flow rate requires more compressor work input and therefore increases the corresponding overall cost. Sanaye and Malekmohammadi [16] presented a thermal and economic optimum design of an air conditioning unit with a vapour compression refrigeration system that includes a compressor, condenser, and evaporator along with centrifugal and axial fans. The authors chose heat exchanger temperatures, their heating surface areas as well as fan and compressor powers among the design variables and studied the performance of the system under various situations, then implemented an optimization procedure. The authors selected the objective function for optimization as the total cost per unit cooling load of the system including capital investment for components as well as the required electricity cost. Sayyaadi and Nejatolahi [17] analyzed a cooling tower assisted vapor compression refrigeration machine based on two objective functions including the total exergy destruction of the system (as a thermodynamic criterion) and the total product cost of the system (as an economic criterion), simultaneously. The authors obtained three optimized systems (namely single objective thermodynamic, single objective economic, and multi-objective systems) based on the objective functions and compared the correspondingresults. Although exergoeconomic analysis was used in various air conditioning applications, to our knowledge, there have been no models developed in past literature to analyze hybrid electric vehicle thermal management systems with respect to exergoeconomics.

Moreover, an enviroeconomic (environmental cost) analysis will also be conducted in order to evaluate the system's impact on the environment in terms of the amount of carbon dioxide released through the electricity consumptionand its associated cost based on theinternational carbon price (or CO_2 emission price). By assigning a cost to the greenhouse gas emissions, the corresponding economic impact of the generated CO_2 emissions could be tracked and later used as a part of the exergoeconomic evaluation, which in term can provide incentives to lower the emissions by altering the design and/or cost structure of the thermal management system.

3.2 Energy and Exergy Analyses

A thermal management system of an electric vehicle with liquid battery cooling will be analyzed in this study. The system is composed of a refrigerant loop to provide air conditioning for the cabin and a battery coolant loop to keep the electric battery operating in its ideal temperature range. A description of the system and its associated components can be found in [18].

The TMS system is initially studied with respect to exergy analysis. Exergy (also called available energy or availability) of a system is the "maximum shaft work that can be done by the composite of the system and a specified reference environment" [19]. It is based on both the first and second laws of thermodynamics. Thus, the

thermal management system is examined with respect to exergy analysis in order to better understand the true efficiencies of the components by finding the irreversibilities in each component, as well as the overall system and how nearly the respective performance approaches ideal conditions.

In the first step of the exergy analysis, the mass, energy, entropy and exergy balances are used in order to determine the heat input, rate of entropy generation and exergy destruction rates as well as the energy and exergy efficiencies. In general, a balance equation for a quantity in a system may be written as follows;

$$Input + Generation - Output - Consumption = Accumulation \tag{3.1}$$

where input and output terms refer to quantities entering and exiting through the system, respectively, whereas generation and consumption terms refer to quantities produced or consumed within the system. The accumulation term refers to a potential accumulation of the quantity within the system [20].

In steady-state conditions, however, all properties are uniform with time and therefore, all the accumulation terms become zero. Thus, under the steady-state assumption, the balance equations for mass, energy, entropy and exergy can be written as follows;

$$\Sigma_i \dot{m}_i = \Sigma_e \dot{m}_e \tag{3.2a}$$

$$\Sigma_i \dot{m}_i h_i + \dot{Q} + \dot{W} = \Sigma_e \dot{m}_e h_e \tag{3.2b}$$

$$\Sigma_i \dot{m}_i s_i + \dot{S}_{gen} = \Sigma_e \dot{m}_e s_e \tag{3.2c}$$

$$\Sigma_i \dot{m}_i ex_i + \dot{E}x_Q + \dot{W} = \Sigma_e \dot{m}_e ex_e + \dot{E}x_D \tag{3.2d}$$

where

$$\dot{E}x_Q = \Sigma\left(1 - \frac{T_0}{T}\right)\dot{Q} \tag{3.2e}$$

In the first two equations above, $\dot{m}$ and $\dot{E}$ are associated with the mass flow rate and energy transfer rate. They show that the respective total rates in/out across the boundary are conserved (neglecting reactions). In the third equation, $\dot{S}$ is the entropy flow or generation rate. The amount transferred out across the boundary must exceed the rate in which entropy enters, while the difference is the rate of entropy generation within the boundary due to associated irreversibilities. Similarly, in Eq. (3.2d), $\dot{E}x$ is the exergy flow rate and it shows that exergy transferred across the boundary must be less than the rate inwhich exergy enters. The difference is the rate of exergy destruction (or lost work) within the boundary due to associated irreversibilities [20]. In addition $\dot{E}x_Q$ is the exergy transfer by heat at a given temperature (T). In addition, the specific flow exergy associated with the coolant medium, for a system at rest, relative to the environment where kinetic and potential terms can be ignored, is shown below.

Table 3.1 Exergy efficiencies and exergy destruction rates associated with each system component

Component	Exergy efficiency	Exergy destruction rate
Compressor	$\dot{E}x_{2,act} - \dot{E}x_1)/\dot{W}_{comp}$	$\dot{E}x_{D,comp} = T_0\dot{m}_r(s_2 - s_1)$
Condenser	$\dot{E}x_{\dot{Q}_H}/(\dot{E}x_2 - \dot{E}x_3)$	$\dot{E}x_{D,cond} = T_0[\dot{m}_c(s_{14} - s_{13}) - \dot{m}_r(s_2 - s_3)]$
Evaporator	$\dot{E}x_{\dot{Q}_L}/(\dot{E}x_4 - \dot{E}x_{1'})$	$\dot{E}x_{D,evap} = T_0[\dot{m}_e(s_9) - \dot{m}_{r1}(s_4 - s_1)]$
Chiller	$\dot{E}x_{\dot{Q}_{ch}}/(\dot{E}x_5 - \dot{E}x_{1''})$	$\dot{E}x_{D,ch} = T_0\left[\dot{m}_{cool}\left(C_{wg}\ln(T_6/T_7)\right) - \dot{m}_{r2}(s_5 - s_1)\right]$
Evaporator TXV	$\dot{E}x_4/\dot{E}x_{3'}$	$\dot{E}x_{D,evap,TXV} = T_0\dot{m}_{r1}(s_4 - s_3)$
Chiller TXV	$\dot{E}x_5/\dot{E}x_{3'}$	$\dot{E}x_{D,ch,TXV} = T_0\dot{m}_{r2}(s_5 - s_3)$
Pump	$(\dot{E}x_{8,act} - \dot{E}x_7)/\dot{W}_{pump}$	$\dot{E}x_{D,pump} = T_0\dot{m}_{cool}\left(C_{wg}\ln(T_6/T_0)\right)$
Battery	$\dot{E}x_{\dot{Q}_{bat}}/(\dot{E}x_6 - \dot{E}x_8)$	$\dot{E}x_{D,bat} = T_0\dot{m}_{cool}\left(C_{wg}\ln(T_6/T_8)\right)$

$$ex_{coolant} = (h - h_0) - T_0(s - s_0) \tag{3.3}$$

The exergy rate is determined as

$$\dot{E}x = \dot{m}ex \tag{3.4}$$

Based on the above balance equations,the energetic coefficient of performance (COP) for the entire cooling system becomes

$$COP_{en,system} = \frac{\dot{Q}_{evap} + \dot{Q}_{ch}}{\dot{W}_{comp} + \dot{W}_{pump}} \tag{3.5}$$

Actual cooling systems are less efficient than the ideal energy models due to irreversibilities in the actual systems. Thus, the aim of the exergy analysis is to determine the system irreversibilities by calculating the exergy destruction rates in each component and to calculate the associated exergy efficiencies. This methodology helps to focus on the parts where the greatest impact can be achieved on the system since the components with larger exergy destruction rates also have more potential for improvement [18]. The exergy efficiency and exergy destruction rate calculations for each component can be observed in Table 3.1.

Based on the work input to the system (in terms of the compressor and pump) and the associated cooling load (with regards to the evaporator and the chiller) under the defined boundary conditions, the exergy efficiency of the TMS is also determined as

$$\psi_{system} = \frac{\dot{Ex}_{\dot{Q}_{evap}} + \dot{Ex}_{\dot{Q}_{ch}}}{\dot{W}_{comp} + \dot{W}_{pump}} \tag{3.6}$$

3.3 Exergoeconomic Analysis

3.3.1 Exergoeconomic Model

Design of various thermal management systems is normally performed by conventional methods based on scientific analyses, experimental data and practical experience. Most of these systems are often operating outside of their optimum parameters which results in inefficient use of resources, increasing production costs and adverse environmental impact. The objective of exergoeconomic analysis is to determine the inefficiencies in the system and calculate the associated costs. In this section,an exergy costing method (SPECO method) is used for the analysis [21, 22].

In order to conduct an exergoeconomic analysis, a flow cost rate, $\dot{C}(\$/h)$, is defined for each flow in a system, and a cost balance is written for each component to provide exergy costing asfollows,

$$\dot{C}_{q,k} + \sum_i \dot{C}_{i,k} + \dot{Z}_k = \sum_e \dot{C}_{e,k} + \dot{C}_{w,k} \tag{3.7}$$

where

$$\dot{C}_j = c_j \dot{E}x_j \tag{3.8}$$

Exergy transfer by entering and exiting streams as well as by power and heat transfer rates are written respectively as follows;

$$\dot{C}_i = c_i \dot{E}x_i = c_i \dot{m}_i ex_i \tag{3.9a}$$

$$\dot{C}_e = c_e \dot{E}x_e = c_e \dot{m}_e ex_e \tag{3.9b}$$

$$\dot{C}_w = c_w \dot{W} \tag{3.9c}$$

$$\dot{C}_q = c_q \dot{E}x_q \tag{3.9d}$$

However, before the analysis can be conducted, the fuel and product exergies need to be defined for each component. The product exergy is defined according to the purpose of owning and operating a component under consideration, while the fuel represents the resources consumed in generating the product, where both are expressed in terms of exergy [11]. The fuel and products for each component can be seen in Table 3.2.

By combining exergy and exergoeconomic balance equations, the following equation can be obtained;

$$\dot{E}x_{F,k} = \dot{E}x_{P,k} + \dot{E}x_{D,k} \tag{3.10}$$

The cost rate of exergy destruction is defined as follows:

Table 3.2 Fuel and product definitions with respect to the system

Component	Fuel	Product
Compressor	$\dot{W}_{comp}$	$\dot{E}x_2 - \dot{E}x_1$
Condenser	$\dot{E}x_2 - \dot{E}x_3$	$\dot{E}x_{14} - \dot{E}x_{13}$
Evaporator TXV	$\dot{E}x_3$	$\dot{E}x_4$
Chiller TXV	$\dot{E}x_3$	$\dot{E}x_5$
Evaporator	$\dot{E}x_4 - \dot{E}x_1$	$\dot{E}x_9$
Chiller	$\dot{E}x_1 - \dot{E}x_5$	$\dot{E}x_7 - \dot{E}x_6$
Pump	$\dot{W}_{pump}$	$\dot{E}x_8 - \dot{E}x_7$
Battery	$\dot{E}x_6 - \dot{E}x_8$	$\dot{W}_{bat}$

$$\dot{C}_{D,k} = c_{F,k}\dot{E}x_{D,k} \tag{3.11}$$

Here, the component exergy destruction costs are determined by evaluating the exergy destruction rates associated with each component $\left(\dot{E}x_{D,k}\right)$ with respect to the exergy balance equations shown in Table 3.1. Moreover, from Eq. (3.7), the steady state form of te control volume cost balance can be written as shown below. The cost balances are generally written so that all terms are positive.

$$\sum_e \left(c_e\dot{E}x_e\right)_k + c_{w,k}\dot{W}_k = c_{q,k}\dot{E}x_{q,k} + \sum_i \left(c_i\dot{E}x_i\right)_k + \dot{Z}_k \tag{3.12}$$

The above equation states that the total cost of the exiting exergy streams equals the total expenditure to obtain them, namely the cost of the entering exergy streams plus the capital and other costs [23, 24]. In general, there are "n_e" exergy streams exiting the component, "n_e" unknowns and only one equation, the cost balance. Thus, "$n_e - 1$" auxiliary equations need to be formulated using F and P rules.

The F rule (fuel rule) refers to the removal of exergy from an exergy stream within the considered component when exergy differences between the inlet and outlet are considered in the fuel definition for this stream. Thus, this rule states that the specific cost (cost per exergy unit) associated with this fuel stream exergy removal must be equal to the average specific cost at which the removed exergy was supplied to the same stream in upstream components. This provides an auxiliary equation for each removal of exergy, which equals the number of exiting exergy streams and "$n_{e,F}$" that are associated with the definition of the fuel for each component. The P rule (product rule) refers to the supply of exergy to an exergy stream within the component and states that each exergy unit is applied to any stream associated with the product at the same average cost. Since this corresponds to an exiting stream, the number of auxiliary equations provided by this rule always equals $n_{e,P} - 1$ where $n_{e,P}$ is the number of exiting exergy streams that are included in the product definition. Thus, since each exiting stream is defined as either fuel or product, the total number of exiting streams is equal to "$n_{e,F} + n_{e,P}$", which provides "$n_e - 1$" auxiliary equations [22].

On the economic side, the capital investment can be calculated with respect to the purchase costof equipment and capital recovery as well as maintenance factor over the number of operation hours per year as shown below;

$$\dot{Z}_k = \frac{Z_k \cdot CRF \cdot \varphi}{N} \tag{3.13}$$

where N is the annual number of operation hours for the unit and φ is the maintenance factor, generally taken as 1.06 [11]. CRF is the capital recovery factor which depends on the interest rate i) and equipment life-time in years (n) as shown below;

$$CRF = \frac{i \times (1+i)^n}{(1+i)^n - 1} \tag{3.14}$$

Here Z_k is the purchase equipment cost of the thermal management system components that should be written in terms of design parameters. The correlations for each component are shown below;

$$Z_{comp} = \left(\frac{573\dot{m}_{ref}}{0.8996 - \eta_s}\right)\left(\frac{P_{cond}}{P_{evap}}\right)\ln\left(\frac{P_{cond}}{P_{evap}}\right) \tag{3.15a}$$

where

$$\eta_s = 0.85 - 0.046667\left(\frac{P_{cond}}{P_{evap}}\right) \tag{3.15b}$$

Here $\dot{m}_{ref}$ is the refrigerant mass flow rate (kg/s) and η_s is the isentropic efficiency of a scroll compressor [25],

$$Z_{cond} = 516.621A_{cond} + 216.45 \tag{3.16}$$

$$Z_{evap} = 309.143A_{evap} + 231.195 \tag{3.17}$$

where A_{cond} and A_{evap} are the heat transfer areas associated with the condenser and evaporator respectively [26].

$$Z_{pump} = 308.9\dot{W}_{pump}^{C_{pump}} \tag{3.18a}$$

$$C_{pump} = 0.25 \text{ for } 0.02 \text{ kW} < \dot{W}_{pump} < 0.3 \text{ kW} \tag{3.18b}$$

$$C_{pump} = 0.45 \text{ for } 0.3 \text{ kW} < \dot{W}_{pump} < 20 \text{ kW} \tag{3.18c}$$

$$C_{pump} = 0.84 \text{ for } 20 \text{ kW} < \dot{W}_{pump} < 200 \text{ kW} \tag{3.18d}$$

Here $\dot{W}_{pump}$ is the pumping power in kW and C_{pump} is the pump coefficient with respect to the corresponding pumping power ranges shown below [27],

$$Z_{evap,txv} = a_{txv} k_{txv} \dot{m}_{ref,a} \tag{3.19}$$

$$Z_{ch,txv} = a_{txv} k_{txv} \dot{m}_{ref,b} \tag{3.20}$$

where a_{txv} is the annuity factor for the evaporator which is based on an interest rate of 5 % and depreciation time of 15 years [13] and k_{txv} is the cost per mass flow rate of refrigerant which is taken to be $5,000 [15].

$$Z_{bat} = C_{bat} K_{bat} \tag{3.21}$$

Here C_{bat} is the typical lithium-ion battery pack costs per kilowatt-hour, taken as $500 [28] and K_{bat} is the energy storage capacity of the battery pack in kWh, which is taken as 16 kWh.

3.3.2 Cost Accounting

Cost balances for each component are needed to be solved in order to estimate the cost rate of exergy destruction in each component. In the cost balance equations with more than one inlet or outlet flow, the number of unknown cost parameters exceed the number of cost balances for that component. Thus, auxiliary exergoeconomic equations created by F and P rules are used to equate the number of unknowns with the number of equations [11]. Implementing Eq. (3.12) for each component together with the auxiliary equations form a system of linear equations as follows;

$$\left[\dot{E}x_k\right] \times [c_k] = \left[\dot{Z}_k\right] \tag{3.22}$$

where the equation entails matrixes of exergy rate (from exergy analysis), exergetic cost vector (to be evaluated) and the vector of $\dot{Z}_k$ factors (from economic analysis) respectively [29]. The matrix form of the equation for each equation can be seen below.

$$\begin{bmatrix} 1 & & & & & & & & & & & & & 0 \\ 0 & -1 & 0 & 0 & 0 & 0 & 0 & 0 & 0 & -\dot{W}_{comp} & 0 & 0 & -1 \\ 0 & 1 & -1 & 0 & 0 & 0 & 0 & 0 & 0 & 0 & 0 & 1 & 0 \\ 0 & \dot{E}x_3 & -\dot{E}x_2 & 0 & 0 & 0 & 0 & 0 & 0 & 0 & 0 & 0 & 0 \\ -\dot{E}x_4 & 0 & 1 & -1 & 0 & 0 & 0 & 0 & 0 & 0 & 0 & 0 & 0 \\ 1 & 0 & 0 & \dot{E}x_1 & 0 & 0 & 0 & -1 & 0 & 0 & 0 & 0 & 0 \\ 0 & 0 & 0 & -1 & 0 & 0 & 0 & 0 & 0 & 0 & 0 & 0 & 0 \\ -1 & 0 & 1 & 0 & -1 & 0 & 0 & 0 & 0 & 0 & 0 & 0 & 0 \\ 0 & 0 & 0 & 0 & 1 & 1 & -1 & 0 & 0 & 0 & 0 & 0 & 0 \\ 0 & 0 & 0 & 0 & 0 & 1 & -1 & 0 & 0 & 0 & 0 & 0 & 0 \\ 0 & 0 & 0 & 0 & 0 & 0 & 1 & 0 & 0 & 0 & \dot{W}_{pump} & 0 & 0 \\ 0 & 0 & 0 & 0 & 0 & 0 & 0 & 1 & 0 & -\dot{W}_{bat} & 0 & 0 & 0 \\ 0 & 0 & 0 & 0 & 0 & 0 & 0 & 0 & 0 & 0 & 1 & 0 & 0 \\ 0 & 0 & 0 & 0 & 0 & 0 & 0 & 0 & 0 & 0 & 0 & \dot{W}_{pump} & -\dot{W}_{comp} \\ 0 & 0 & 0 & 0 & 0 & 0 & 0 & 0 & 0 & 0 & 0 & 1 & 0 \\ 0 & & & & & & & & & & & & 0 \end{bmatrix} \times \begin{bmatrix} \dot{C}_1 \\ \dot{C}_2 \\ \dot{C}_3 \\ \dot{C}_4 \\ \dot{C}_5 \\ \dot{C}_6 \\ \dot{C}_7 \\ \dot{C}_8 \\ \dot{C}_9 \\ \dot{C}_{10} \\ \dot{C}_{11} \\ \dot{C}_{12} \\ \dot{C}_{13} \\ \dot{C}_{14} \end{bmatrix} = \begin{bmatrix} -\dot{Z}_{comp} \\ -\dot{Z}_{cond} \\ 0 \\ -\dot{Z}_{etxv} \\ -\dot{Z}_{evap} \\ 0 \\ -\dot{Z}_{ctxv} \\ -\dot{Z}_{chil} \\ 0 \\ -\dot{Z}_{pump} \\ -\dot{Z}_{bat} \\ -0.075\dot{W}_{comp} \\ 0 \\ 0 \end{bmatrix}$$

$$\dot{C}_1 + \dot{Z}_{comp} + \dot{W}_{comp} = \dot{C}_2$$

$$\dot{C}_2 + \dot{C}_{13} + \dot{Z}_{cond} = \dot{C}_3 + \dot{C}_{14}$$

$$\dot{C}_2 \dot{E}x_3 = \dot{C}_3 \dot{E}x_2$$

$$\dot{C}_3 + \dot{Z}_{etxv} = \dot{C}_4$$

$$\dot{C}_4 + \dot{Z}_{evap} = \dot{C}_9 + \dot{C}_1$$

$$\dot{C}_4 \dot{E}x_1 = \dot{C}_1 \dot{E}x_4$$

$$\dot{C}_3 + \dot{Z}_{ctxv} = \dot{C}_5$$

$$\dot{C}_5 + \dot{C}_6 + \dot{Z}_{chil} = \dot{C}_1 + \dot{C}_7$$

$$\dot{C}_6 \dot{E}x_7 = \dot{C}_7 \dot{E}x_6$$

$$\dot{C}_7 + \dot{Z}_{pump} + \dot{W}_{pump} = \dot{C}_8$$

$$\dot{C}_8 + \dot{Z}_{bat} = \dot{C}_6 + \dot{W}_{bat}$$

$$\dot{C}_{11} = c_{elect} \dot{W}_{comp}$$

$$\dot{C}_{11} \dot{W}_{pump} = \dot{C}_{12} \dot{W}_{comp}$$

$$\dot{C}_{13} = 0$$

Here, c_{elect} is the unit cost of electricity, which is taken as $0.075\$/kWh$. By solving these equations, the cost rate of each flow can be calculated, which can be used to determine the cost rate of exergy destruction in each system component.

Moreover, certain additional variables can also provide useful exergoeconomic evaluation. Among these variables, an exergoeconomic factor is an important parameter and provides the contribution of non-exergy related costs to the total cost of a component. It is defined as

$$f_k = \frac{\dot{Z}_k}{\dot{Z}_k + c_{f,k} \dot{E}_{D,k}} \tag{3.23}$$

where $c_{f,k}$ is the unit exergy cost of the fuel of any k component and $\dot{E}_{D,k}$ is the associated exergy destruction. When a component hasa low exergoeconomic factor value, cost savings in the entire system might be achieved by improving the component efficiency even if the capital investment for that component will increase. On the other hand, a high value might suggest a decrease in the investment costs at the expense of its exergetic efficiency [30].

3.4 Enviroeconomic (Environmental Cost) Analysis

Most hybrid electric vehicles (HEVs) use electricity from the grid to power the TMS (thermal management system). The TMS has a significant role in reducing the associated GHG emissions compared to conventional vehicles. Even though these vehicles produce virtually zero GHG emissions in all-electric mode during operation, there may still be indirect emissions associated with the generation of electricity [31]. These emissions, especially under a high carbon derived electricity generation mix, can be significantly high (possibly even higher than conventional vehicles) and therefore the associated CO_2 GHG emissions and corresponding environmental costs should be calculated [18].

For the studied model, various electricity generation mixes are considered from one that mainly utilizes a natural gas combined cycle to less environmentally friendly options that primarily use coal and steam [32]. The associated environmental assessment based on the corresponding CO_2 emissions can be calculated as shown below [33]:

$$x_{\mathrm{CO2}} = \frac{y_{\mathrm{CO2}} \times \dot{W}_{total} \times t_{total}}{10^6} \tag{3.24}$$

where x_{CO2} is the associated CO_2 emissions released in a year (tCO_2/year) and y_{CO2} is the corresponding CO_2emissions for a coal fired electricity generator, $\dot{W}_{total}$ is the total power consumption of the TMS and t_{total} is the total working hours of the system in a year, which is assumed to be 1,460 based on 4 h of daily driving.

In order to conduct an enviroeconomic analysis, a carbon price (or CO_2 emissions price) is needed to be established along with calculating the quantity of the carbon released. The carbon price is an approach imposing a cost on the emission of greenhouse gases which cause global warming. The international carbon price is typically between 13 and 16 \$/tCO_2 based on different carbon scenarios [34]. The enviroeconomic parameter in terms of CO_2 emissions price in a year (\$/year) can be calculated as shown below;

$$C_{\mathrm{CO2}} = (c_{\mathrm{CO2}})(x_{\mathrm{CO2}}) \tag{3.25}$$

where c_{CO2} is the CO_2 emissions price per tCO_2.

3.5 Results and Discussion

Based on the exergy analysis; theexergetic efficiency and exergy destruction rates are calculated for each component in the thermal management system. Among these components, the heat exchangers have the lowest exergy efficiencies with respect to the high temperature differences and phase change which results in more entropy generation between the refrigerant and coolants. In the chiller, the low exergy efficiency occurs as a result of the high exergy destruction from high coolant temperatures causing the refrigerant to pass through a phase change. In the evaporator, the exergy losses are relatively high since (aside from the frictional losses) only part of the heat rejection occurs during the phase change process with large temperature differences between the working fluid in the evaporator and the vehicle cabin. The condenser is calculated to have a lower exergy efficiency than the evaporator and the chiller,mainly due to the relatively higher temperature difference between the condenser exit and ambient air (taken at 35 °C), when compared to the differences between the evaporator exit and vehicle cabin temperature as well as the refrigerant and coolant temperatures. It should be noted that the battery is modeled as a system and thus the internal efficiencies for the batteryare not considered in this analysis. In this regard, the battery has high efficiencies within the target operating temperature range (up to 50 °C). However, the associated efficiency would decrease significantly as the battery is heated up beyond this range. The exergy efficiencies and exergy destruction rates can be seen in Fig. 3.1.

Among the remaining components, the compressor has a relatively low exergy efficiency due to the high compression pressure ratio and change in temperature of the refrigerant passing through the compressor, which contributes to an increase in exergy destruction. On the other hand, the thermal expansion valves have high exergy efficiencies since the processes are isenthalpic and have little or no heat loss. Therefore the exergy losses occur mainly due to a pressure drop in the expansion valves. These exergy losses in the thermal expansion valves can be reduced by lowering (or sub-cooling) the temperature of the refrigerant exiting the condenser even further, which can be achieved by utilizing the refrigerant vapour exiting the evaporator. The coolant pump also has a relatively higher efficiency since there is no significant heat loss from the pump.

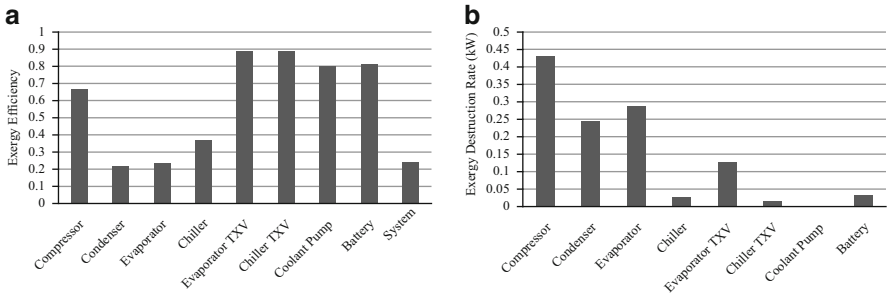

Fig. 3.1 (**a**) Exergy efficiency of TMS and its components. (**b**) Exergy destruction rate of TMS and its components

Table 3.3 Exergy flow rates, cost flow rates and the unit exergy costs associatedwith each state of TMS

State	$\dot{E}x\,(kW)$	$\dot{C}(\$/h)$	$c(\$/kJ)$
1	0.71	0.20	0.14
2	1.58	0.18	0.28
3	1.27	0.18	0.23
4	1.01	0.20	0.20
5	0.12	0.20	0.02
6	0.02	1.05	0.02
7	0.04	1.05	0.04
8	0.04	1.18	0.05
9	0.36	1.75	0.63
10	0.01	0.03	0.88
11	1.30	0.08	0.10
12	<0.01	0.08	<0.01
13	–	–	–
14	0.07	2.64	0.18

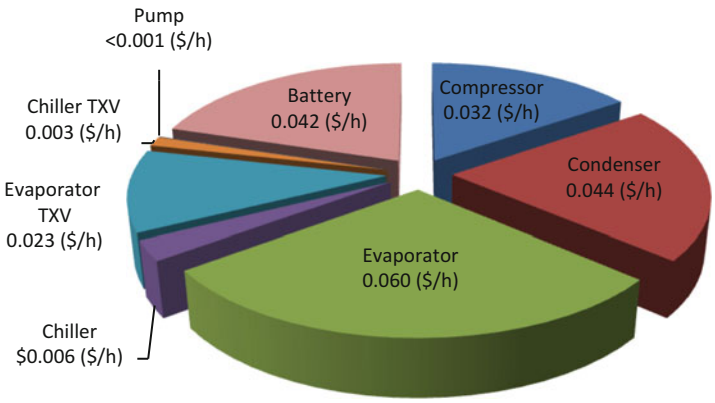

Fig. 3.2 Cost rate of exergy destruction for thermal management system components

In this study, the exergy analysis is provided in order to gain a further understanding of the true efficiencies of each component and corresponding irreversibilities. However, this does not provide any information regarding the economic constraints on improving the efficiency of the components or the associated costs. Thus, an exergoeconomic analysis is also conducted where the cost formation can be determined for the thermal management system. In Table 3.3, It can be seen that the highest cost rate is achieved at state 10, which is the exit state of the electric battery and the lowest cost rate is associated with the pump input. In the table, state 13 has no value, since it is available ambient air entering the condenser.

Based on the calculated costs, the exergy destruction costs are also determined for each component. In Fig. 3.2, it can be seen that the evaporator has the highest cost rate of exergy destruction, followed by the condenser, battery and compressor.

Table 3.4 Cost rate of exergy destruction, exergoeconomic factor, investment cost rate and investment plus exergy destruction cost associated with the TMS components

Component	$\dot{C}_{D,k}$ (\$/*h*)	f (%)	$\dot{Z}_k$ (\$/*h*)	$\dot{Z}_k+\dot{C}_{D,k}$ (\$/*h*)
Compressor	0.03	55.95	0.04	0.07
Condenser	0.04	73.84	0.12	0.17
Evaporator	0.06	57.47	0.08	0.14
Chiller	0.01	59.19	0.01	0.01
Evaporator TXV	0.02	6.28	0.00	0.02
Chiller TXV	<0.01	6.28	<0.01	<0.01
Pump	<0.01	99.69	0.01	0.01
Battery	0.04	95.27	0.85	0.90

The high exergy destruction cost of the battery is mostly associated with the high fuel cost for the battery, while the majority of the exergy destruction cost of the compressor, condenser and evaporator is associated with relatively high exergy destruction rates for these components.

However, before any remarkscan be made regarding design or investment changes, the components should be analyzed with respect to their exergoeconomicsignificance and the impact of improving the component efficiency on the total capital investment costs. From an exergoeconomic viewpoint, the components that have the highest priority are the ones that have the highest sum of total capital investment and exergy destruction cost rate $\left(\dot{Z}+\dot{C}_D\right)$. Among these components, the relationship between the exergy efficiency investment costs of the components is investigated with the help of the exergoeconomic factor. These values for each component are provided in Table 3.4.

When the components are analyzed with respect to $\dot{Z}+\dot{C}_D$, an electric battery by far has the highest cost compared to the rest of the components as shown in the table. Moreover, the battery is also determined to have a significantly high exergoeconomic factor (f), which suggests that the cost effectiveness of the entire system could be improved by reducing the total capital investment for this component. After the battery, the highest sum of total capital investment and cost rate of exergy destruction aredetermined to be the condenser and evaporator, wherethe condenserhas a relatively high exergoeconomic factor value. Therefore, methods of reducing the investment cost on this component should also be investigated at the expense of their exergetic efficiencies. Moreover, for the compressor and chiller, the non-exergy related costs and total cost of a component are divided rather equally, thus the current investment cost for these components are found to be reasonable. Finally, based on the exergoeconomic analysis, the thermal expansion valves and exergy related costs are high, thus improving the component efficiency is suggested even if the capital investment for that component will increase. However, the thermal expansion valves along with the pump are determined to have lowerpriorities for the overall system with respect to the exergoeconomic viewpoint.

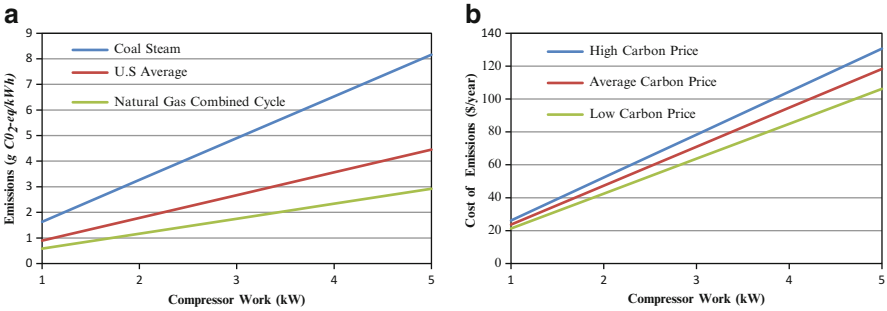

Fig. 3.3 (**a**) Emissions released with respect to varying compressor work under different electricity generation mixes (**b**) Cost of emissions with respect to varying compressor work under different carbon price values

Furthermore, the indirect amount of CO_2 emissions released to the environment as a result of the electricity consumed from the grid are also calculated with respect to various electricity generation mixes, includingone that utilizes a natural gas combined cycle to one that uses primarily coal/steam, with a range of 400 to 1,118 gCO_2eq/kWh including life cycle estimates for electricity production. The associated emissions with respect to various electricity generation mixes can be seen in Fig. 3.3a. In addition, a carbon price is established and the associated cost of corresponding CO_2 emissions are determined accordingly under various carbon price ranges are shown in Fig. 3.3b.

3.6 Conclusions

In this paper, mass, energy, entropy and exergy balance equations are applied to each thermal management system component of hybrid electric vehicles, in order to determine various work and heat terms as well as exergy destructions rates to calculate the associated exergy efficiency of the system and its individual components. In the economic analysis, investment cost rates are calculated with respect to purchase equipment costs, which are determined using cost correlations for each system component, and a capital recovery factor. In the exergoeconomic analysis, the exergy streams are identified, fuel and products are defined for each component and cost equations are allocated. In order to solve the cost equations, auxiliary equations are formulated using fuel and product rules. The costs from the economic analysis are used as inputs in the cost equation matrix to determine the unit cost of exergy, cost rate of exergy destruction as well as other useful exergoeconomic variables includingthe exergoeconomic factor for each component. Moreover, an enviroeconomical (environmental cost) analysis is also conducted based on theestablished carbon price associated with thereleased CO_2 to the environment

with respect to the indirect emissions from the electricity consumed by the system under varying carbon prices and electricity generation mixes.

Based on the analyses, the following concluding remarks can be made.

- The exergetic performance results indicate that the pump and thermal expansion valves have very high exergy efficiencies (0.79 and 0.88 respectively), while the heat exchangers (evaporator, condenser and chiller) have much lower efficiencies in the system (0.22, 0.23 and 0.37 respectively), which can be improved by reducing the mean temperature difference between the working fluids.
- The compressor is calculated to have the highest exergy destruction rate with 0.43 kW and it is determined that small improvements in this component can provide better enhancements in system performance compared to other components in the system.
- The evaporator is determined to have the largest cost rate of exergy destruction in the system with 0.06 $/h.
- Based on the exergoeconomic analysis, the electric battery is determined to have the highest exergoeconomic importance based on the total capital investment and exergy destruction cost rate. Moreover, based on the components exergoeconomic factor calculations, it is determined that the cost effectiveness of the entire system could be improved by reducing the total capital investment for the battery. On the other hand, the pump and thermal expansion valves are determined to have lower priorities with respect to an exergoeconomic viewpoint.
- Enviroeconomics (Environmental cost) is determined to be a useful tool for assigning a cost on the greenhouse gas emissions. The corresponding economic impact of the generated CO_2 emissions are able to be tracked. This approach can later be used as a part of the exergoeconomic evaluation. The cost associated with emissions for the best and worst case scenarios are calculated to be within 9.9 and 155 $/year with respect to the studied parameter ranges.

Acknowledgements Financial support from Automotive Partnerships Canada (APC) and the Natural Sciences and Engineering Research Council of Canada (NSERC) is gratefully acknowledged.

Nomenclature

A	Area (m^2)
C	Cost per unit of exergy ($/kj)
$\dot{C}$	Cost rate associated with exergy ($/h)
C_{CO2}	CO_2emissions price per year ($/year)
D	Diameter (m)
$\dot{E}_X$	Exergy rate (kW)
f	Exergoeconomic factor

h	Specific enthalpy (kJ/kg)
k	Cost per mass flow rate ($s/kg)
K	Energy storage capacity (kW)
$\dot{m}$	Mass flow rate (kg/s or L/min)
N	Annual number of operation hours (h)
P	Pressure (kg/m s^2)
Pr	Prandtl number
$\dot{Q}$	Heat transfer rate (kW)
r	Relative cost difference
Re	Reynolds number
s	Specific entropy (kJ/kg K)
t	Total working hours per year (h/year)
T	Temperature (K or °C)
T_0	Ambient temperature (K or °C)
$\dot{W}$	Work rate or power (kW)
Z	Purchase equipment cost ($)
$\dot{Z}$	Cost rate associated with the sum of capital investment ($/h)

Greek Symbols

Δ	Change in variable
φ	Maintenance factor
ψ	Exergy

Superscripts

n	Equipment lifetime (years)

Subscripts

0	Ambient
act	Actual
bat	Battery
cool	Coolant
c cond	Condenser
ch	Chiller
comp	Compressor
D	Destruction
e	Exit
elect	Electricity
en	Energy
ex	Exergy

evap	Evaporator
F	Fuel
gen	Generation
i	In
k	Component
P	Product
q	Heat
ref	Refrigerant
s	Isentopic
txv	Thermal expansion valve
w	Work
wg	Water/glycol mix

Acronyms

COP	Coefficients of performance
CRF	Capital recovery factor
EV	Electric vehicle
GHG	Greenhouse gas
GWP	Global warming potential
TMS	Thermal management system
TXV	Thermal expansion valve

References

1. Rosen MA, Dincer I (2003) Exergoeconomic analysis of power plants operating on various fuels. Appl Therm Eng 23:643–658
2. Hamut HS, Dincer I, Naterer GF (2013) Performance assessment of thermal management systems for electric and hybrid electric vehicles. Int J Energy Res 31(1):1–12
3. Tsatsaronis G, Pisa J (1994) Exergoeconomic evaluation and optimization of energy system; application to the CGAM problem. Energy 19:287–321
4. Sciubba E (2005) Exergo-economics: thermodynamic foundation for a more rational resource use. Int J Energy Res Res 29:613–636
5. Tsatsaronis G (2007) Definitions and nomenclature in exergy analysis and exergoeconomics. Energy 32:249–253
6. Tribus M, Evans R (1962) The thermoeconomics of seawater conversion UCLA No. 62–63
7. El-Sayed YM, Evans RB (1970) Thermoeconomics and the design of heat systems. Trans ASME J Eng Power 92:27–34
8. Kotas TJ (1985) The exergy method of thermal plant analysis. Anchor Brendon Ltd, Tiptree, Essex, Great Britain
9. Valero A, Lozano MA, Munoz M (1986) A general theory of exergy savings. In: Gaggioli R (ed) Computer-aided engineering of energy systems, AES, vol. 2, American Society of Mechanical Engineers, New York, pp 1–21
10. Tsatsaronis G (1987) A review of exergoeconomic methodologies. In: Moran M, Sciubba E (eds) Second law analysis of thermal systems. American Society of Mechanical Engineers, New York, pp 81–87

11. Bejan A, Tsatsaronis G, Moran M (1986) Thermal design and optimization. Wiley, New York
12. Moran MJ (1999) Engineering thermodynamics, in mechanical engineering handbook. CRC Press LLC, Boca Raton
13. Wall G (1991) Optimization of refrigeration machinery. Int J Refrig 14:336–340
14. D'Accadia MD, de Rossi F (1998) Thermoeconomic optimization of a refrigeration plant. Int J Refrig 21(1):42–54
15. Al-Otabi DA, Dincer I, Kalyon M (2004) Thermoeconomic optimization of vapor-compression refrigeration systems. Int Commun Heat Mass Trans 31:95–107
16. Sanaye S, Malekmohammadi HR (2004) Thermal and economical optimization of air conditioning units with vapor compression refrigeration system. Appl Therm Eng 24:1807–1825
17. Sayyaadi H, Nejatolahi M (2011) Multi-objective optimization of a cooling tower assisted vapor compression refrigeration system. Int J Refrig 34:243–256
18. Hamut HS, Dincer I, Naterer GF (2012) Exergy analysis of a TMS (thermal management system) for range extended EVs (electric vehicles). Energy 46(1):117–125
19. Dincer I, Rosen MA (2007) Exergy: energy, environment and sustainable development. Elsevier, Oxford
20. Dincer I, Kanoglu M (2010) Refrigeration systems and applications, 2nd edn. John Wiley and Sons, West Sussex
21. Tsatsaronis G, Lin L (1990) On exergy costing in exergoeconomics, computer-aided energy systems analysis. Am Soc Mech Eng 21:1–11
22. Lazzaretto A, Tsatsaronis G (2006) SPECO: a systematic and general methodology for calculating efficiencies and costs in thermal systems. Energy 31:1257–1289
23. Abusoglu A, Kanoglu M (2009) Exergetic and thermoeconomic analyses of diesel engine powered cogeneration: Part 1—Formulations. Appl Therm Eng 29:234–241
24. Abusoglu A, Kanoglu M (2009) Exergetic and thermodynamic analyses of diesel engine powered cogeneration: Part 2—Application. Appl Therm Eng 29:242–249
25. Valero A (1994) CGAM problem: definition and conventional solution. Energy 19:268–279
26. Selbaş R, Kizilkan Ö, Şencan A (2006) Thermoeconomic optimization of subcooled and superheated vapor compression refrigeration cycle. Energy 31:2108–2128
27. Sanaye S, Niroomand B (2009) Thermal-economic modeling and optimization of vertical ground-coupled heat pump. Energy Conv Manag 50:1136–1147
28. Hensley R, Newman J, Rogers M (2012) Battery technology charges ahead. McKinsey Quarterly, Detroit, USA
29. Ahmadi P, Dincer I, Rosen MA (2011) Exergy, exergoeconomic and environmental analyses and evolutionary algorithm based multi-objective optimization of combined cycle power plants. Energy 36:5886–5898
30. Sayyaadi H, Sabzaligol T (2009) Exergoeconomic optimization of a 1000MW light water reactor power generation system. Int J Energy Res 33:378–395
31. Samaras C, Meisterling K (2008) Life cycle assessment of greenhouse gas emissions from plug-in hybrid vehicles: implications for policy. Environ Sci Technol 42:3170–3176
32. Yang C, Maccarthy R (2009) Electricity grid: impacts of plug-in electric vehicle charging. Recent Work, Institute of Transportation Studies (UC Davis)
33. Caliskan H, Dincer I, Hepbasli A (2011) Exergoeconomic, enviroeconomic and sustainability analyses of a novel air cooler. International Green Energy Conference, Eskisehir
34. Den Elzen MGJ, Hof AD, Beltran M, Grassi G, Roelfsema M, van Ruijven B et al (2011) The Copenhagen accord: abatement costs and carbon prices resulting from the submissions. Environ Sci Policy 14:28–39

Chapter 4
CFD Analysis of a Shell and Tube Heat Exchanger Linking a Supercritical Water-Cooled Nuclear Reactor and a Copper-Chlorine Hydrogen Production Cycle

Ali H. Abedin, Murat Aydin, and Marc A. Rosen

Abstract Among various hydrogen production methods, such as steam methane reforming and thermochemical water splitting, the copper-chlorine thermochemical cycle is an advanced method to produce hydrogen that can help achieve sustainable development and clean energy systems. The cycle requires large amounts of heat as the main energy input, and using nuclear heat is a promising option for reducing emissions of greenhouse gases and other pollutants. An investigation is reported of an analysis of an intermediate high-pressure shell and tube heat exchanger using FLUENT software. The RNG k-ε turbulence model is adopted for modeling turbulent flow. In this study, the flow field and the characteristics of a shell and tube heat exchanger for heat extraction from supercritical water-cooled nuclear reactors (SCWRs) to the heat transfer fluid that serves as the heating fluid in a hydrogen production process based on the copper-chlorine thermochemical water decomposition cycle are investigated. The results show that the heat transfer is improved by increasing the operating pressure, although higher pressure drops also occur in the heat exchanger in such instances. Also, the effects of using baffles and various baffle arrangements are studied.

Keywords Hydrogen production • Super-critical water-cooled reactor • FLUENT • Computational fluid dynamics

A.H. Abedin (✉)
Golder Associates Ltd, 6925 Century Avenue, Suite #100, Mississauga, ON, Canada, L5N 7K2
e-mail: ali.hajiabedin@gmail.com

M. Aydin
Energy Institute, Istanbul Technical University, 34469 Ayazaga Campus,
Maslak, Istanbul, Turkey
e-mail: murat.aydin@uoit.ca

M.A. Rosen (✉)
Faculty of Engineering and Applied Science, University of Ontario Institute of Technology,
2000 Simcoe Street North, Oshawa, ON, Canada, L1H 7K4
e-mail: marc.rosen@uoit.ca

I. Dincer et al. (eds.), *Progress in Sustainable Energy Technologies Vol II: Creating Sustainable Development*, DOI 10.1007/978-3-319-07977-6_4

4.1 Introduction

A worldwide concern is that societal energy demands are increasing while fossil fuel resources, which dominate most national energy systems, will become scarcer and more expensive in coming years [1, 2]. Furthermore, there are many environmental concerns related to the global energy consumption like climate change and atmospheric pollution. Greenhouse gas (GHG) emissions are considered the main cause of climate change [3]. Therefore, increasing global energy demand and concern regarding environmental problems is fostering the utilization of cleaner and more efficient energy systems and technologies.

Hydrogen is an important alternative energy carrier that can contribute to avoiding environmental problems and increasing the efficiency of energy utilization. Hydrogen has widespread potential applications. Hydrogen is a promising alternative for fossil fuels as an energy carrier because its oxidation does not release GHG emissions, if it is produced from non-carbon based energy sources.

Several thermochemical water splitting cycles, e.g., sulphur-iodine (S-I) and copper-chlorine (Cu-Cl), have been examined [4, 5] and scale-up developments are underway [6–9]. Among various methods of hydrogen production, many consider thermochemical hydrogen production cycles to be promising. These cycles utilize heat as the main energy input to split water. A thermochemical hydrogen production cycle includes some endothermic and exothermic physical and chemical processes. The net result of these processes is the decomposition of water into hydrogen and oxygen. The endothermic processes always require more heat than that can be supplied by exothermic processes, so heat from external heat sources must be supplied. Major processes in the Cu-Cl hydrogen production cycle are shown in Table 4.1 [10].

The focus of this paper is to examine the heat extraction from external heat sources, and to design an appropriate heat exchanger for linking a nuclear reactor and a thermochemical water splitting cycle for hydrogen production. A supercritical water-cooled nuclear reactor (SCWR) is considered as the heat source and the heat requirement of a Cu-Cl hydrogen production cycle is considered as the heat extraction load for the analysis and design. The intermediate heat exchanger for heat extraction from the SCWR is designed using the LMTD method, and the design and operating parameters of the heat exchanger are determined. Also, the flow field and the heat transfer characteristics of a shell and tube heat exchanger are studied with CFD using FLUENT software and the pressure drop and the variation of velocity are investigated here for various heat exchanger layouts and operating pressures.

Table 4.1 Major chemical processes of the copper-chlorine cycle[a]

Step	Process and heat flow	Major reaction
I	Electrolytic hydrogen production	$2CuCl(s) + 2HCl(aq) + V_E = H_2(g) + 2CuCl_2(aq)$ in aqueous solution, at 30 ~ 100 °C
II	Drying of cupric chloride (endothermic)	$CuCl_2(aq) + n_f H_2O(l) + Q = CuCl_2 \bullet nhH_2O(s) + (n_f - n_h) H_2O$, where $n_f > 7.5$, $n_h = 0 \sim 4$, depending on temperature. Below 80 °C, crystallization; at 100-200 °C, spray drying
III	Hydrolysis of cupric chloride (endothermic)	$2CuCl_2 \bullet n_h H_2O(s) + H_2O(g) + Q = CuOCuCl_2(s) + 2HCl(g) + n_h H_2O(g)$, at 400 °C
IV	Oxygen production (endothermic)	$CuOCuCl_2(s) + Q = 2CuCl(molten) + 0.5O_2$ (g), at 530 °C
All	Summation of all steps	$H_2O(l) = H2(g) + ½O_2(g)$ (net reaction)

[a]Symbols: *aq* aqueous, *g* gas, *l* liquid, n_f number of free water, n_h number of hydrated water, *Q* heat, *s* solid, V_E electricity

4.2 Design of the Shell and Tube Heat Exchanger

As stated previously, heat needs to be extracted from an external energy source (here, the nuclear reactor) and transported to the thermochemical hydrogen plant. The operation is expected to utilize a heat transfer fluid and a pipeline between the plants. Solely from a heat transfer perspective, the nuclear reactor coolant can be directly pumped to the hydrogen plant through a pipeline and used as the heating fluid for hydrogen production cycles. However, separation of the plants is often viewed as desirable. So, an intermediate heat exchanger that can transfer heat from the nuclear reactor coolant to another heat transfer fluid is considered here between the nuclear power and hydrogen production plants. Haji Abedin et al. [11] previously studied possible alternatives for heat transfer fluids and demonstrated that, considering various parameters e.g. thermal properties, transportation over long distance in a pipeline, and phase change avoidance over large pressure and temperature ranges, helium is a potentially good option as a heat transfer fluid.

The heat exchanger considered here is an intermediate heat exchanger to recover heat from a process in the Cu-Cl hydrogen production cycle in order to improve the thermal efficiency of the overall cycle shown in Fig. 4.1. The geometry and properties of the heat exchanger are as follows:

- Supercritical water (tube side):
  - Inlet conditions: $T_{t,2} = 640$ °C, $P_{t,2} = 26$ MPa
- Helium (shell side):
  - Inlet conditions: $T_{s,1} = 230$ °C, $P_{s,1} = 2$ MPa

The results of an analysis show that a shell diameter of 0.73 m with 420 tubes is needed to achieve a heat transfer rate of 100 MW_{th} [11].

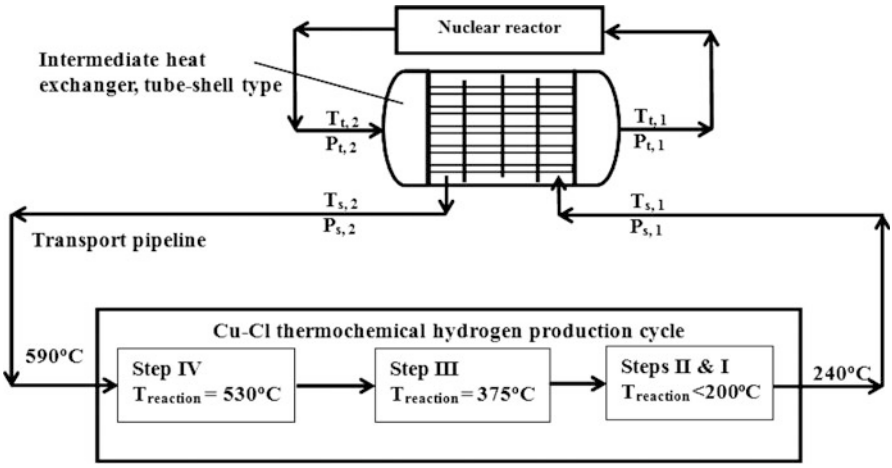

Fig. 4.1 Layout for the heat ows of a nuclear reactor, an intermediate heat exchanger, and a thermochemical Cu-Cl hydrogen production cycle

4.3 Computational Analysis and Results

In order to analyze computationally the system model and investigate the effects of varying design parameters on the flow field, a 2-D grid mesh was generated using the commercial code GAMBIT. The mesh consists of unstructured tetrahedral elements. The commercial code FLUENT based on the Finite Volume Method is employed to simulate the flow. The RNG k-ε turbulence model is used for modeling turbulent flow and heat transfer in the shell side of the model. Also, the effects are investigated of varying selected parameters, e.g. utilizing baffles and the arrangements of baffles in the heat exchanger, and the overall operating pressure.

The helium (shell-side heat transfer fluid) at the inlet is specified to have a temperature of 230 °C and a total operating pressure of 2 MPa. The inlet velocity of the flow is taken as 66 m/s [11]. The shell wall is assumed to be adiabatic. Several significant results are obtained based on the analysis. These are listed and explained below, and the implications of each are given:

- The effect of utilizing baffles on pressure drop of the shell side is studied. Figure 4.2 shows the operating pressure contour when there is no baffle inside the shell. In this case, the pressure drop is 0.01 MPa between the inlet and outlet of the shell. But when using 40 % cut baffles, the operating pressure drops from 2 MPa to 1.97 MPa. Note that baffle cut refers to the cut of the baffle used inside of the shell relative to the total diameter of the shell; a 40 % cut means the baffle height is 40 % of the shell diameter (Fig. 4.3).
- The effect of utilizing baffles on the velocity is investigated. Following a similar format as the previous point, Fig. 4.4 shows the velocity contour when there is no baffle inside the shell and Fig. 4.5 shows the velocity contour when there are

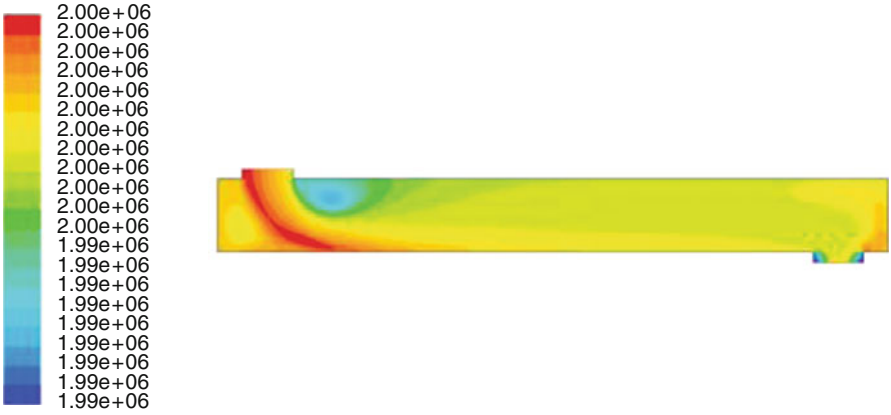

Fig. 4.2 Total pressure (in Pascals) contour with no baffle inside the shell

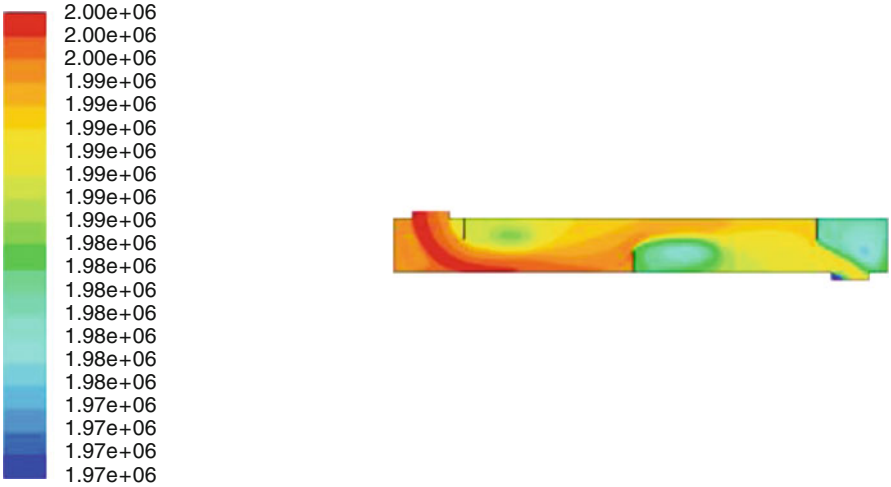

Fig. 4.3 Total pressure (in Pascals) contour with 40 % cut baffles inside the shell

3 baffles with 40 % cut inside the shell. The results show that using baffles increases the velocity at the outlet of the shell.

- Another design parameter examined is baffle cut. In the previous figures, 40 % cut baffles were used. Here, the results are compared to those with 80 % cut baffles. Figures 4.6 and 4.7 show respectively velocity and pressure contours with 80 % cut baffles. The results show that increasing baffle cut increases the velocity at the outlet of the shell and also increases the pressure drop along the shell.

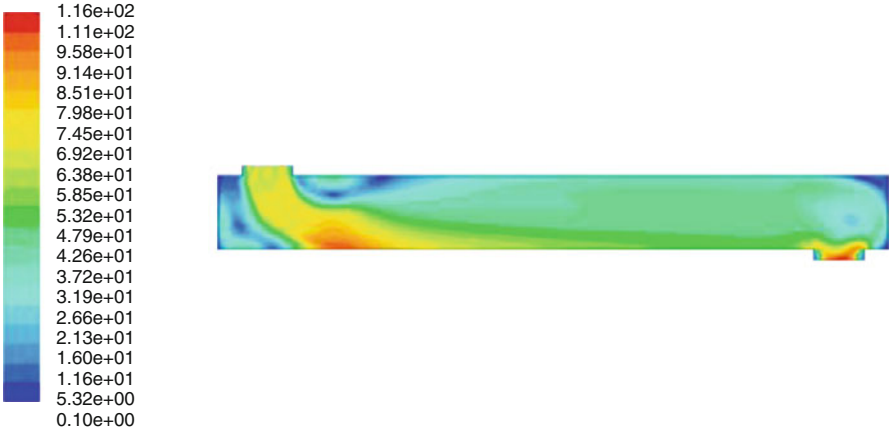

Fig. 4.4 Velocity (in m/s) contour with no baffle

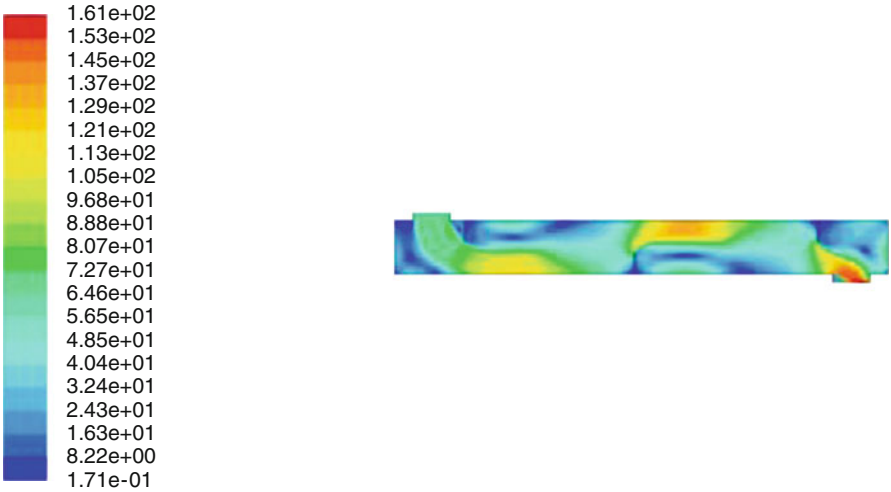

Fig. 4.5 Velocity (in m/s) contour with 40 % cut baffles

4.4 Conclusions

In this study, a 2-D numerical simulation for a shell and tube heat exchanger with various baffle configurations is performed. The major conclusions can be listed as follows:

- Increasing the operating pressure improves heat transfer in the shell and tube heat exchanger, although it increases the pressure drop between the inlet and outlet of the shell side.

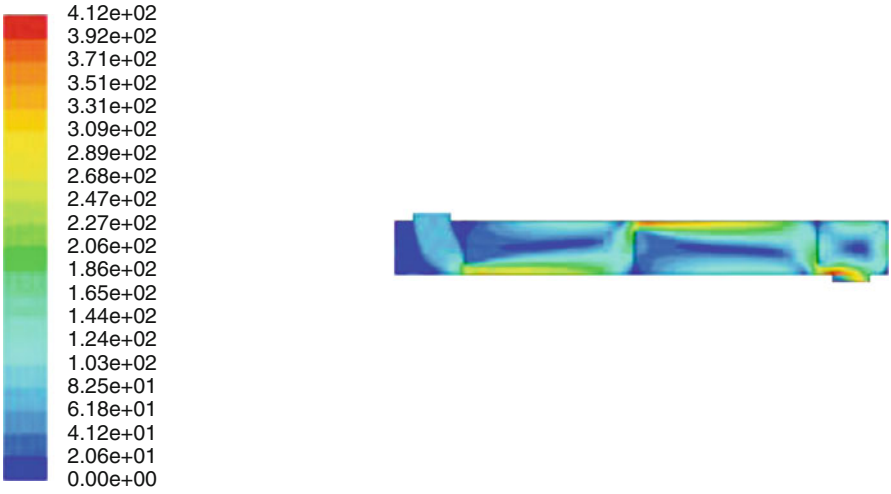

Fig. 4.6 Velocity (in m/s) contour with 80 % cut baffles

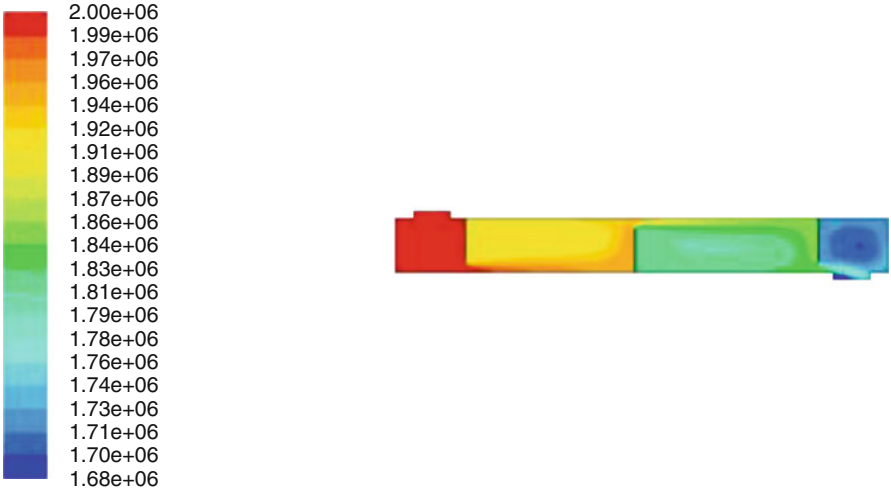

Fig. 4.7 Total pressure (in Pascals) contour with 80 % cut baffles

- Utilizing baffles in the shell side increases the velocity of the flow inside the shell and as a result improves heat transfer, but it also increases the pressure drop in the shell side of the heat exchanger.
- Increasing the baffle cut percentage improves heat transfer in the shell side by increasing the velocity, although it raises the corresponding pressure drop.

Acknowledgement The authors gratefully acknowledge the financial support provided by the Natural Sciences and Engineering Research Council of Canada.

References

1. Rasthal JE, Drennen TE (2007) Pathways to a hydrogen future. Elsevier, London
2. Rahm D (2002) Sustainable energy and the states: essay on politics markets and leadership. McFarland, North Carolina
3. Fuglestvedt JS, Hailemariam K, Stuber N (2005) Alternatives to the global warming potential for comparing climate impacts of emissions of greenhouse gases. Clim Chang 68:281–302
4. Rosen MA, Naterer GF, Chukwu CC, Sadhankar R, Suppiah S (2012) Nuclear-based hydrogen production with a thermochemical copper-chlorine cycle and supercritical water reactor: equipment scale-up and process simulation. Int J Energy Res 36:456–465
5. Terada A, Kubo S, Okuda H, Kasahara S, Tanaka N, Iwatsuki J (2007) Development of hydrogen production technology by thermo-chemical water splitting IS process pilot test plan. J Nucl Sci Technol 44:477–482
6. Naterer GF, Gabriel K, Lu L, Wang ZL, Zhang Y (2009) Recent advances in nuclear based hydrogen production with the thermochemical copper-chlorine cycle. J Eng Gas Turbines Power 34:032905
7. Naterer GF, Gabriel K, Wang ZL, Daggupati VN, Gravelsins R (2008) Thermochemical hydrogen production with copper-chlorine cycle. I: oxygen release from copper oxychloride decomposition. Int J Hydrog Energy 33:5439–5450
8. Wang ZL, Naterer GF, Gabriel K (2008) Multiphase reactor scale-up for Cu-Cl thermochemical hydrogen production. Int J Hydrog Energy 33:6934–6946
9. Wang ZL, Naterer GF, Gabriel K, Gvavelsins R, Daggupati V (2009) New Cu-Cl thermochemical cycle for hydrogen production with reduced excess steam requirements. Int J Green Energy 6:616–626
10. Wang ZL, Naterer GF, Gabriel K (2010) Thermal integration of SCWR nuclear and thermochemical hydrogen plants. Proceedings of the 2nd Canada-China Joint Workshop on Supercritical Water-Cooled Reactors (CCSC-2010), Toronto, Ontario, Canada, April 25–28.
11. Haji Abedin A, Wang ZL, Rosen MA (2011) Heat extraction from supercritical water-cooled nuclear reactors for hydrogen production plants. Proceedings of the International Conference on Hydrogen Production, Thessaloniki, Greece, June 19-21, paper 243THE, pp. 1–10.

Chapter 5
Entropy Generation of Hydrogen Flow in a Curved Annular Duct

Haydar Kucuk, Ugur Akbulut, and Adnan Midilli

Abstract The main objective of this study is to numerically investigate the entropy generation of both hydrodynamically and thermally fully developed laminar flow of hydrogen gas under various operating pressures and temperatures in the concentric curved annular ducts with rectangular cross section. In this regard, the solutions of discretized continuity, momentum and energy equations have been obtained using elliptic Fortran Program based on the SIMPLE algorithm. The solutions have been achieved for (1) Dean numbers ranging from 2.3 to 202.9, (2) Annulus dimension ratios of 5.5, (3) Operating pressures of 0.101325, 1, 10, 40, 70 and 100 MPa, (4) Core wall temperature of 50 and 80 °C, (5) Duct wall temperature of 25 °C. In this regard, overall entropy generation in the whole flow field has been analyzed in detail. Moreover, the effects of Dean number, operating pressure and core wall temperature on entropy generation arising from the flow and heat transfer have been investigated. Accordingly, it is concluded that the effect of volumetric entropy generation that is a result of fluid flow can be neglected as compared with volumetric entropy generation due to heat transfer. When Dean number, operating pressure and core wall temperature increase the total volumetric entropy generation goes up. Thus, it is expected that this study will contribute to develop the energy efficient-hydrogen gas heaters for practical applications including hydrogen exchangers, PEMFC applications, hydrogen gas turbines, chemical mixing processes and hydrogen gas dryers in hydrogen industry.

Keywords Entropy generation • Hydrogen • Curved annular ducts • Laminar flow

5.1 Introduction

Recently, efficiently and effectively use of hydrogen and its technologies has been an important expectation for energy consumers as well as energy producers and distributors in energy sector. The key factor creating this expectation is to ensure a

H. Kucuk (✉) • U. Akbulut • A. Midilli
Department of Mechanical Engineering, Faculty of Engineering,
Recep Tayyip Erdoğan University, 53100 Rize, Turkey
e-mail: haydar.kucuk@erdogan.edu.tr; ugur.akbulut@erdogan.edu.tr;
adnan.midilli@erdogan.edu.tr

I. Dincer et al. (eds.), *Progress in Sustainable Energy Technologies Vol II: Creating Sustainable Development*, DOI 10.1007/978-3-319-07977-6_5

clean and sustainable environment for the future generations by reducing the economical, environmental and social impacts of fossil fuel consumption. If so, may hydrogen as an energy carrier and its technologies be a key tool to achieve this target? In this regard, more and more researchers, investigators and scientists have focused on the efficiently production and utilization of hydrogen and its technologies for better economic sustainability of hydrogen. On the other hand, it is clear that hydrogen has been utilizing in some industrial and commercial applications such as fuel cells, gas turbines, hydrogen burners, internal combustion engines, etc. In these hydrogen systems, it is known that hydrogen gas flows through the pipes and channels whose entropic effects are not first considered. On the other word, because hydrogen has not been a cost effective fuel and energy carrier in our daily life, yet, it may not be quite important or the main objective to determine the thermodynamic behavior of hydrogen gas flowing throughout the pipes and channels whose shapes are different from each other. However, considering the recent developments in hydrogen industry, it is obvious that, in the near future, hydrogen will be used in double-pipe heat exchangers, air conditioning systems, cooling systems, and drying machineries in addition to the above applications. Particularly, for these engineering applications, the curved annular ducts may be preferred because of their contribution to efficiently and effectively heating and/or cooling processes in hydrogen energy systems [1, 2]. Thus, in case hydrogen gas flows in the curved annular ducts, the researchers can face to face an important scientific problem to determine and evaluate thermodynamic behavior of hydrogen gas under various operating temperatures and pressures. In fact, this problem can be assumed to be an industrial, technological and scientific problem by taking into consideration the flow types which are laminar and turbulent flows. Therefore, laminar or turbulent flow of hydrogen gas in the curved annular ducts should be considered for better understanding its behavior in terms of entropy phenomena. If so, is it possible to characterize laminar flow of hydrogen gas in a concentric curved annular channel by the secondary flow created by centrifugal effects in the cross-section? In fact, the nature of this phenomenon depends upon the Dean number, which is the ratio of the Reynolds number to the square root of the dimensionless radius of curvature [1, 2]. Also, it is known that the secondary flows passages originate principally from the interaction between the centrifugal force, the pressure gradient, and the viscous forces [1, 2]. Thus, in case of hydrogen flow in the ducts, the secondary flow motion in the flow field of hydrogen gas may enhance heat transfer to hydrogen gas from the heating element while it may induce pressure drops in flow field, which may be quite important contribution to improve hydrogen flow system for hydrogen based heating applications in the future. In the scope of this work, a detailed literature review has been performed. It is noticed that many works have been mostly concentrated, and numerically and/or experimentally conducted on the heat transfer and fluid flow in curved annular duct with rectangular or circular cross section [1–7]. Second law analysis or entropy generation studies have been studied by many researchers in different shaped-channels in the literature [8–22]. Moreover, in these studies, air has been generally used as fluid. However, in this paper, we focused on entropy generation of both hydrodynamically and thermally fully developed

laminar flow of hydrogen gas under various operating pressures and temperatures in concentric curved annular ducts with rectangular cross section. This lack of information is the motivation for this work. In this regard, the overall entropy generation in the whole flow field has been analyzed. The effects of Dean number and operating pressure and temperatures on entropy generated from fluid flow and heat transfer have been investigated in detail. In terms of the scientific and industrial benefits, this study aims to help

- understand the main concepts and issues about entropic behavior of hydrogen gas in a concentric curved annular ducts with rectangular cross section,
- provide the researchers and scientists some detailed information on entropy generation of hydrogen flow in a concentric curved annular ducts with rectangular cross section due to the irreversibilities caused by fluid flow and heat transfer,
- introduce the effect of operating pressure and temperature on entropy generation through the hydrogen gas flow in a concentric curved annular ducts with rectangular cross section,
- find out the effect of centrifugal force created by curvature on entropy generation resulting from fluid flow and heat transfer.

5.2 Modeling

5.2.1 Problem Statement

The problem undertaken in this study is to numerically investigate the entropy generation of both hydrodynamically and thermally fully developed laminar flow of hydrogen gas under various operating pressures and temperatures in concentric curved annular ducts with rectangular cross section. The physical configuration and the coordinate system of the problem are illustrated in Fig. 5.1.

5.2.1.1 General Assumptions

In order to numerically investigate the entropic behavior of hydrogen gas flow in a concentric curved annular ducts with rectangular cross section the following general assumptions should be taken into consideration.

- Steady-state, hydrodynamically and thermally fully developed, compressible laminar hydrogen gas flow.
- The core wall temperature which is hot ($T_i = T_h$) and the channel wall temperature which is cold ($T_o = T_c$) are constant.
- Radius of curvature (R) is large compared with the channel dimensions ($R + x \approx R$) [1, 2, 23–27].

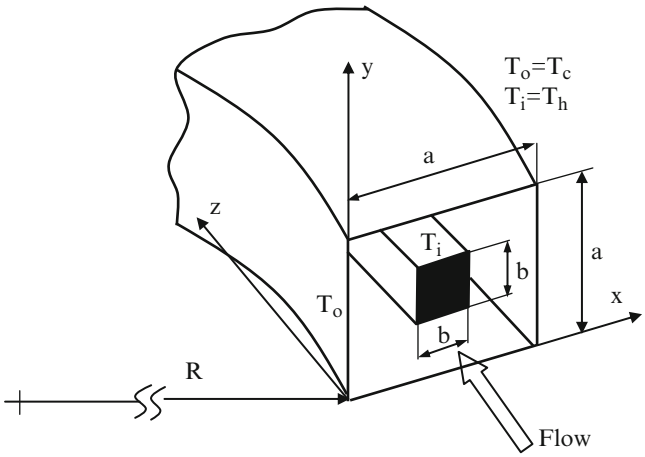

Fig. 5.1 Problem geometry and coordinate system

- By taking into consideration the compressibility factor of hydrogen gas, the physical properties of this gas depending on the operating pressures and temperatures have been computed by taking the data from the Standard Reference Data Program of National Institute of Standards and Technology (NIST).

5.2.1.2 Governing Equations and Boundary Conditions

The governing equations describing the continuity, momentum and energy equations, and the required boundary conditions in a concentric curved annular ducts with rectangular cross section can be concluded as:

Continuity equation describing steady-state, hydrodynamically and thermally fully developed, compressible laminar flow

$$\frac{\partial(\rho u)}{\partial x}+\frac{\partial(\rho v)}{\partial y}+\frac{\rho u}{R+x}=0 \tag{5.1}$$

Momentum equations describing steady-state, hydrodynamically and thermally fully developed, compressible laminar flow

$$\frac{\partial(\rho uu)}{\partial x}+\frac{\partial(\rho vu)}{\partial y}-\frac{\rho w^2}{R+x}=-\frac{\partial p}{\partial x}+\mu\left(\frac{\partial^2 u}{\partial x^2}+\frac{\partial^2 u}{\partial y^2}+\frac{1}{R+x}\frac{\partial u}{\partial x}-\frac{u}{(R+x)^2}\right) \tag{5.2}$$

$$\frac{\partial(\rho uv)}{\partial x}+\frac{\partial(\rho vv)}{\partial y}=-\frac{\partial p}{\partial y}+\mu\left(\frac{\partial^2 v}{\partial x^2}+\frac{\partial^2 v}{\partial y^2}+\frac{1}{R+x}\frac{\partial v}{\partial x}\right) \tag{5.3}$$

$$\frac{\partial(\rho uw)}{\partial x}+\frac{\partial(\rho vw)}{\partial y}-\frac{\rho uv}{R+x}=-\frac{R}{(R+x)}\frac{\partial p}{\partial z}+\mu\left(\frac{\partial^2 w}{\partial x^2}+\frac{\partial^2 w}{\partial y^2}+\frac{1}{R+x}\frac{\partial w}{\partial x}-\frac{w}{(R+x)^2}\right) \tag{5.4}$$

Energy equation describing steady-state, hydrodynamically and thermally fully developed, compressible laminar flow

$$\frac{\partial\left(\rho c_p uT\right)}{\partial x}+\frac{\partial\left(\rho c_p vT\right)}{\partial y}+\frac{R}{(R+x)}\frac{\partial\left(\rho c_p wT\right)}{\partial z}=\left[\frac{\partial^2(kT)}{\partial x^2}+\frac{\partial^2(kT)}{\partial y^2}+\frac{1}{(R+x)}\frac{\partial(kT)}{\partial x}\right] \tag{5.5}$$

The model neglects all terms of the order 1/R and $1/R^2$, with the exception of the centrifugal force term [1, 2, 23–27]. Considering hydrogen gas flow, the equations are subjected to the following boundary conditions at the channel and core walls of the concentric curved annular duct with rectangular cross section:

$$u=v=w=0,\quad T_o=T_c\quad\text{and}\quad T_i=T_h \tag{5.6}$$

In the fully developed hydrogen gas flow, the pressure gradient varies only in the cross-section of the concentric curved annular duct. Therefore, the axial pressure gradient (∂P/∂z) given in Eq. (5.4) remains constant [1, 2, 23, 28, 29, 35, 36]. The axial temperature gradient (∂T/∂z) presented in Eq. (5.5) is assumed to be zero because of thermally fully developed flow under axially and peripherally constant wall temperature boundary condition [30, 31, 35, 36]. In order to perform the numerical solution the physical properties of hydrogen gas under various operating pressures and temperatures in the concentric curved annular duct with rectangular cross section have been computed by using Standard Reference Data Program of National Institute of Standards and Technology (NIST).

5.2.2 Numerical Solution Procedure

The Eqs. (5.1)–(5.5) are approximated with finite difference equations by the control volume-based finite difference method for the dependent variables, u, v, w and T. The convection and diffusion terms are discretized by using the upwind scheme and the central difference scheme, respectively. The finite difference

equations for the dependent variable of interest are solved by ADI (Alternating-Direction Implicit) method [32]. This method uses the Tri-Diagonal Matrix Algorithm, TDMA, making successive sweeps over the computational field. Because the pressure-correction equation is a Poisson equation, Alternating-Direction Implicit solution of the difference equations is replaced by the Stone's solution method [33]. A staggered grid system is employed in this study and the solutions are obtained by an iterative scheme. Iteration is repeated until the residuals in each equation are small enough and the relaxation factor is taken 0.5, 0.5, 1, 0.7 and 0.45 for u, v, w, T and P, respectively. To check the validity of the numerical results, grid-independent study has been performed and a uniform grid system of 100×100 has been chosen for all the cases in this study.

After numerically determining the velocity and the temperature fields during the hydrogen gas flow in the concentric curved annular duct with rectangular cross section, the volumetric entropy generation due to the heat transfer irreversibility (S_T''') and the fluid frictional irreversibility (S_P''') can be calculated by the following equations [8, 9, 14, 34–36]:

$$S_T''' = \frac{k}{T^2}(|\nabla T|)^2 \tag{5.7}$$

$$S_P''' = \frac{\mu}{T}\left(\frac{\partial u}{\partial y} + \frac{\partial v}{\partial x}\right)\frac{\partial u}{\partial y} \tag{5.8}$$

Considering Eqs. (5.7) and (5.8), total volumetric entropy generation of hydrogen gas in the flow field can be obtained to be

$$S_{gen}''' = S_T''' + S_P''' \tag{5.9}$$

According to Bejan [34], the ratio of S_P''' and S_T''' is defined as the irreversibility distribution ratio, ϕ:

$$\phi = \frac{S_P'''}{S_T'''} \tag{5.10}$$

Bejan number (Be) proposed by Paoletti et al. [37] is a parameter that describes the contribution of heat transfer entropy generation on overall entropy generation, which is defined as

$$Be = \frac{S_T'''}{S_{gen}'''} \tag{5.11}$$

The range of Be is from 0 to 1; $Be = 0$ and $Be = 1$ are two limiting cases representing the irreversibility is dominated by fluid friction and heat transfer, respectively.

For evaluation of the entropy generation in whole hydrogen gas flow field in the concentric curved annular duct with rectangular cross section, the average entropy generation rates, $S'''_{P,ave}$, $S'''_{T,ave}$, $S'''_{gen,ave}$, are defined by

$$S'''_{P,ave} = \frac{1}{A}\int\int S'''_P dxdy \tag{5.12}$$

$$S'''_{T,ave} = \frac{1}{A}\int\int S'''_T dxdy \tag{5.13}$$

$$S'''_{gen,ave} = \frac{1}{A}\int\int S'''_{gen} dxdy \tag{5.14}$$

Average irreversibility distribution ratio (ϕ_{ave}) and average Bejan number (Be_{ave}) are defined in Eqs. (5.15) and (5.16) as fallows,

$$\phi_{ave} = \frac{S'''_{P,ave}}{S'''_{T,ave}} \tag{5.15}$$

$$Be_{ave} = \frac{S'''_{T,ave}}{S'''_{gen,ave}} \tag{5.16}$$

The average velocity of hydrogen gas is calculated as

$$w_{ave} = \frac{1}{A}\int\int w dxdy \tag{5.17}$$

The Reynolds number is given as

$$\mathrm{Re} = \frac{\rho \mathrm{w_{ave}} \mathrm{D_h}}{\mu} \tag{5.18}$$

The Dean number is defined as fallows

$$\mathrm{De} = \mathrm{Re}\sqrt{\frac{\mathrm{D_h}}{\mathrm{R}}} \tag{5.19}$$

5.3 Results and Discussion

The entropy generation of hydrodynamically and thermally fully developed hydrogen gas flow in the concentric curved annular duct with rectangular cross section under various operating temperatures and pressures has been numerically studied by taking into consideration the above general assumptions. The numerical solutions whose validation was previously presented in the literature [2, 26] have been

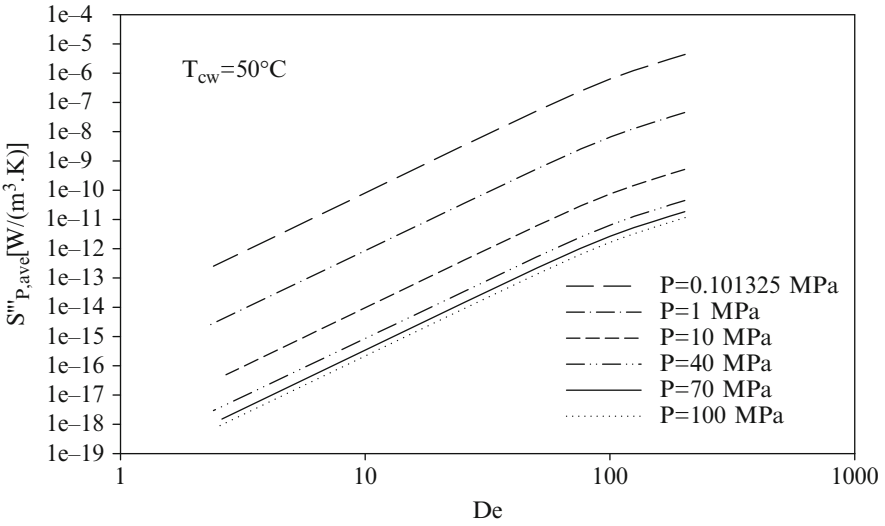

Fig. 5.2 The variation of average volumetric entropy generation due to the fluid flow with Dean number; $T_{cw} = 50\ ^{\circ}C$

applied for hydrogen gas flow in this duct. The solutions for hydrogen gas flow have been performed by taking into account the following parameters: (1) the Dean number ranging from 2.3 to 202.9, (2) the annulus dimension ratio a/b = 5.5, (3) the radius of curvature of R = 10 m, (4) the core wall temperature of 50 and 80 °C, (5) the duct walls temperature of 25 °C.

The variation of average volumetric entropy generation resulting from hydrogen gas flow computed from Eq. (5.12) is given in Figs. 5.2 and 5.3 for 50 °C and 80 °C of core wall temperatures depending on Dean number, respectively. It is seen that the volumetric entropy generation due to hydrogen gas flow is very low in concentric curved annular duct under constant wall temperature boundary condition for laminar flow of hydrogen gas because of very low gradient of u and v velocities (see Eq. (5.8)) occurring on the cross-section. At the lowest Dean number, entropy generation because of hydrogen gas flow is almost zero for each core wall temperature when P = 100 MPa. When Dean number increases the entropy generation resulting from hydrogen gas flow increases because of curvature creating centrifugal force. Centrifugal force causes the secondary flows of hydrogen gas, which are increasing the friction, in the cross-section of the concentric curved annular duct [1]. Also, it is observed that when the operating pressure decreases the volumetric entropy generation due to hydrogen gas flow increases because as operating pressure decreases the density of hydrogen gas decreases and the hydrogen gas molecules rapidly move so the friction increases in the cross-section of the channel. However, when the core wall temperature increases the volumetric entropy generation resulting from hydrogen gas flow slightly increases.

The variations of average volumetric entropy generation caused by heat transfer are shown Figs. 5.4 and 5.5 and distributions of average total volumetric entropy

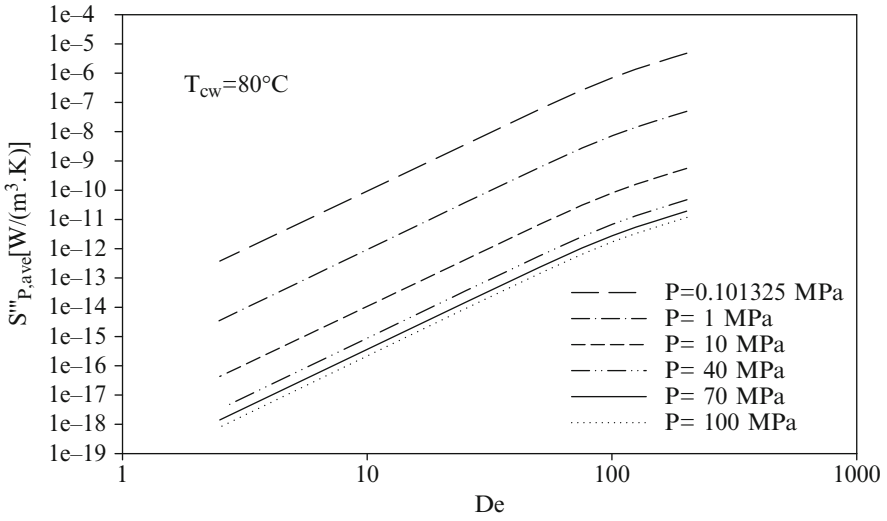

Fig. 5.3 The variation of average volumetric entropy generation due to the fluid flow with Dean number; $T_{cw} = 80$ °C

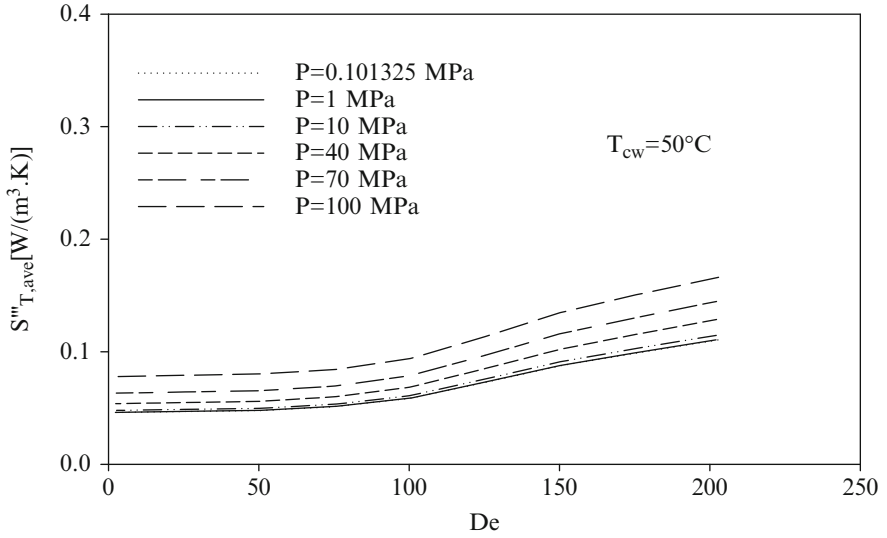

Fig. 5.4 The variation of average volumetric entropy generation due to the heat transfer with Dean number; $T_{cw} = 50$ °C

generation are presented in Figs. 5.6 and 5.7 for 50 °C and 80 °C of core wall temperature, respectively. Total volumetric entropy generation is equal to sum of volumetric entropy generation resulting from hydrogen gas flow and heat transfer (see Eq. (5.9)). As entropy generation due to hydrogen gas flow is too small, the

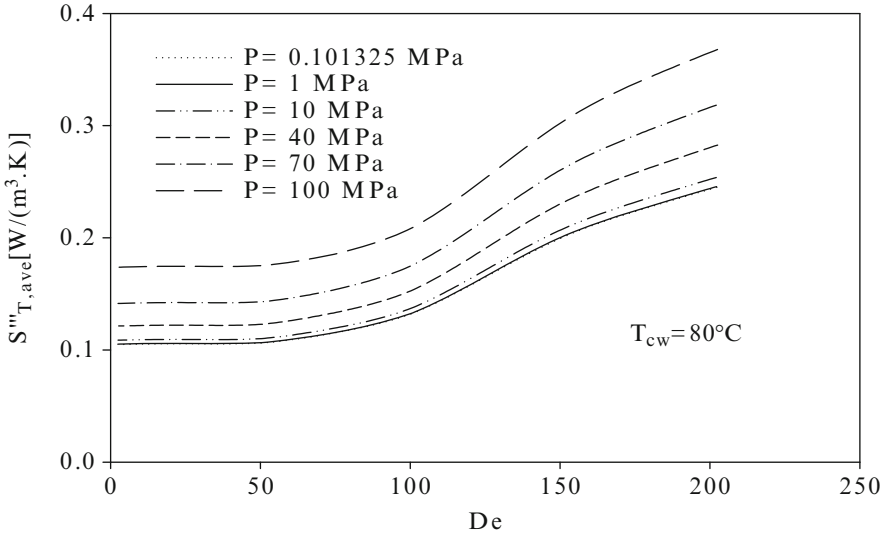

Fig. 5.5 The variation of average volumetric entropy generation due to the heat transfer with Dean number; $T_{cw} = 80\ ^{\circ}C$

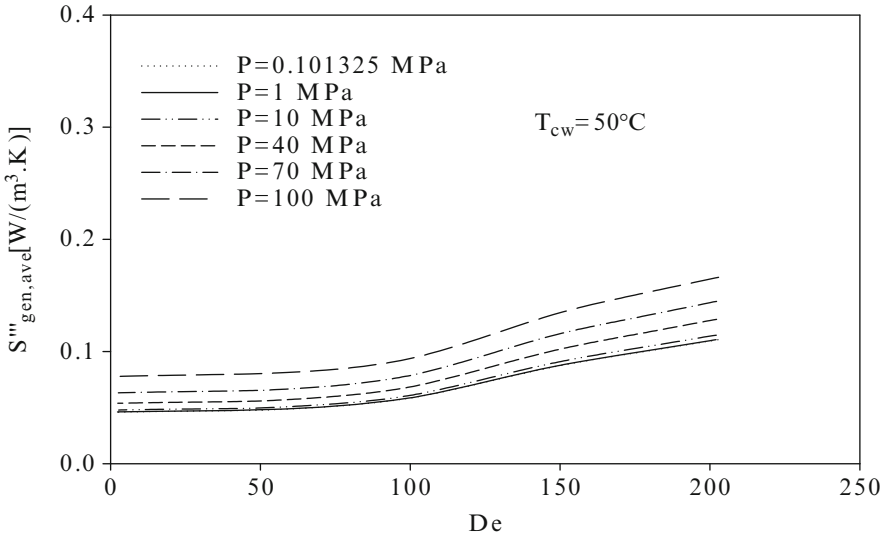

Fig. 5.6 The variation of average total volumetric entropy generation with Dean number; $T_{cw} = 50\ ^{\circ}C$

entropy generation due to heat transfer is almost equal to total entropy generation (see Figs. 5.4, 5.5, 5.6, and 5.7). Because of high temperature gradient, the entropy generation resulting from heat transfer creates all entropy generation in the cross-section of curved annular square channel under constant wall temperature boundary

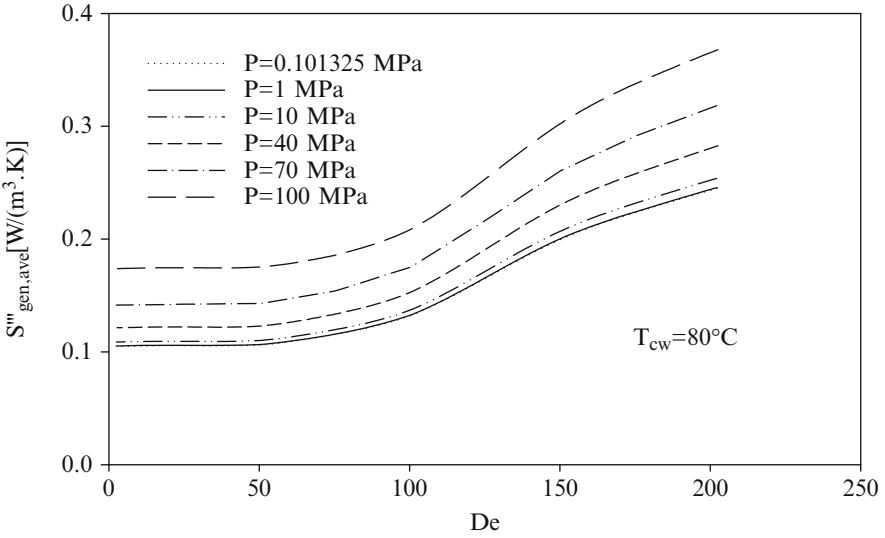

Fig. 5.7 The variation of average total volumetric entropy generation with Dean number; $T_{cw} = 80\ ^{\circ}C$

condition for laminar flow of hydrogen gas. As seen in Figs. 5.4, 5.5, 5.6, and 5.7, both entropy generations increase when Dean number increase because of secondary flows of hydrogen gas. Also, it is seen that when the operating pressure increases total volumetric entropy generation and entropy generation due to heat transfer highly increases because as the operating pressure increases the thermal conductivity of hydrogen gas increases (see Eq. (5.7)). Moreover, it seems that when the temperature of core wall increases the entropy generation due to heat transfer and total entropy generation highly increases because high temperature gradient occurs with increasing of hydrogen gas temperature in the cross-section of curved annular duct.

The variation of average irreversibility distribution ratio is illustrated as in Figs. 5.8 and 5.9 for 50 °C and 80 °C of core wall temperatures, respectively. It is seen that the irreversibility distribution ratio is very low so, the effect of volumetric entropy generation resulting from hydrogen gas flow can be neglected as compared with volumetric entropy generation due to heat transfer in concentric curved annular ducts under constant wall temperature boundary condition for laminar flow of hydrogen gas. Also, it is observed that irreversibility distribution ratio increases when Dean number increases. It can be said that the increase of entropy generation due to hydrogen gas flow is higher than that of entropy generation due to heat transfer when Dean number increases. Moreover, the rise of friction with curvature creating centrifugal force is higher than that of heat transfer in curved annular duct for fully developed laminar flow of hydrogen gas. However, it is seen that when the operating pressure decreases the irreversibility distribution

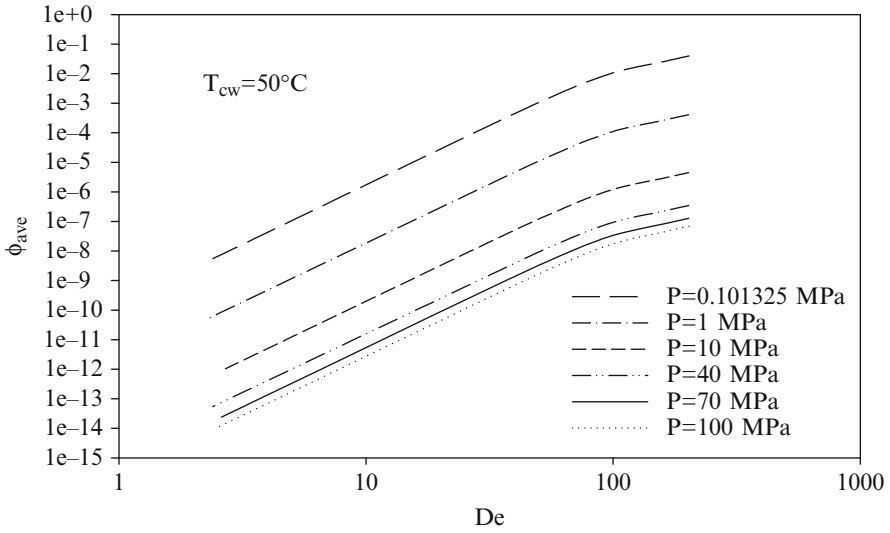

Fig. 5.8 The variation of average irreversibility distribution ratio with Dean number; $T_{cw} = 50\ °C$

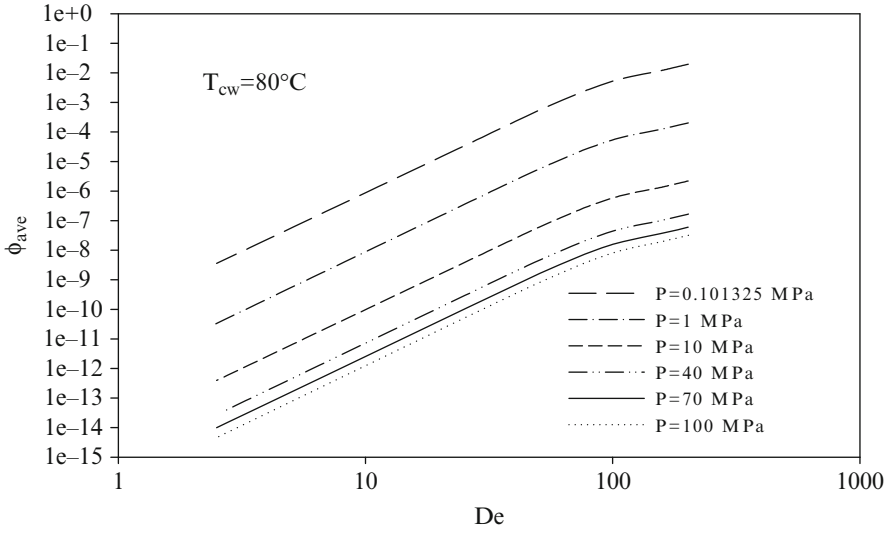

Fig. 5.9 The variation of average irreversibility distribution ratio with Dean number; $T_{cw} = 80\ °C$

ratio highly increases in the curved annular duct cross-section. Also, as the core wall temperature increases the irreversibility distribution ratio slightly decreases.

The average Bejan number given in Eq. (5.16) is almost equal to 1 for all annulus operating pressures and temperatures and Dean numbers. It can be said that the volumetric entropy generation resulting from heat transfer irreversibility of

hydrogen gas is completely dominant on the cross-section of concentric curved annular ducts under constant wall temperature boundary condition for laminar flow of hydrogen gas flow. When Dean number increases and both operating pressure and core wall temperature decrease the Bejan number decreases.

5.4 Conclusions

The entropy generation of hydrogen gas flow for hydrodynamically and thermally fully developed, steady, compressible laminar flow in the concentric curved annular duct was numerically investigated under constant wall temperature boundary condition.

The effect of hydrogen gas frictional irreversibility is highly lower than heat transfer irreversibility of hydrogen gas on volumetric entropy generation.

The effect of volumetric entropy generation resulting from hydrogen gas flow can be neglect as compared with volumetric entropy generation due to heat transfer in concentric curved annular ducts under constant wall temperature boundary condition for laminar flow of hydrogen gas.

When Dean number, operating pressure and core wall temperature increases the total volumetric entropy generation increases. Thus, it is expected that this study will contribute to develop the energy efficient-hydrogen gas heaters for practical applications including hydrogen exchangers, PEMFC applications, hydrogen gas turbines, chemical mixing processes and hydrogen gas dryers in hydrogen industry.

Nomenclature

a	Width or height of the curved channel, m
A	Duct cross section area, m^2
b	Width or height of core, m
Be	Bejan number
dP/dz	Axial pressure gradient, Pa m^{-1}
dT/dz	Axial temperature gradient, K m^{-1}
De	Dean number
D_h	Hydraulic diameter, m
k	Thermal conductivity, W m^{-1} K^{-1}
P	Pressure, Pa
Re	Reynolds number
R	Radius of curvature of a curved channel, m
S_P'''	Volumetric entropy generation rate due to friction, W m^{-3} K^{-1}
S_T'''	Volumetric entropy generation rate due to heat transfer, W m^{-3} K^{-1}
S_{gen}'''	Total volumetric entropy generation rate, W m^{-3} K^{-1}

T Temperature, K
u, v, w Velocity components in x-, y- and z-directions, m s^{-1}
x, y, z Cartesian coordinates, m

Greeks

α Thermal diffusivity, $m^2 s^{-1}$
μ Dynamic viscosity, kg $m^{-1} s^{-1}$
ν Kinematic viscosity, $m^2 s^{-1}$
ρ Density, kg m^{-3}
ϕ Irreversibility distribution ratio

Subscripts

ave Average
c Cold
h Hot
i Inner
o Outer

References

1. Kucuk H, Asan H (2009) A numerical study on heat and fluid flow in concentric curved annular square ducts. Heat Transf Eng 30(5):383–392
2. Kucuk H, Asan H (2009) Forced convection heat transfer in eccentric curved annular square ducts. J Therm Sci Technol 29(1):67–78
3. Choi HK, Park SO (1992) Laminar entrance flow in curved annular ducts. Int J Heat Fluid Flow 13(1):41–49
4. Choi HK, Park SO (1994) Mixed convection flow in curved annular ducts. Int J Heat Mass Transf 37(17):2761–2769
5. Petrakis MA, Karahalios GT (1999) Fluid flow behaviour in a curved annular conduit. Int J Non Linear Mech 34:13–25
6. Garimella S, Richards DE, Christensen RN (1988) Experimental investigation of heat transfer in coiled annular ducts. J Heat Transf 110:329–336
7. Petrakis MA, Karahalios GT (1997) Exponentially decaying flow in a gently curved annular pipe. Int J Non Linear Mech 32(5):823–835
8. Ko TH, Ting K (2006) Entropy generation and optimal analysis for laminar forced convection in curved rectangular ducts: a numerical study. Int J Therm Sci 45(2):138–150
9. Ko TH (2006) Numerical investigation on laminar forced convection and entropy generation in a curved rectangular duct with longitudinal ribs mounted on heated wall. Int J Therm Sci 45 (4):390–404
10. Ko TH, Ting K (2005) Entropy generation and thermodynamic optimization of fully developed laminar convection in a helical coil. Int Commun Heat Mass Transf 32:214–223
11. Ko TH (2006) Thermodynamic analysis of optimal curvature ratio for fully developed laminar forced convection in a helical coiled tube with uniform heat flux. Int J Therm Sci 45 (7):729–737
12. Ko TH, Cheng CS (2007) Numerical investigation on developing laminar forced convection and entropy generation in wavy channel. Int Commun Heat Mass Transf 34:924–933

13. Ko TH (2006) Numerical analysis of entropy generation and optimal Reynolds number for developing laminar forced convection in double-sine ducts with various aspect ratios. Int J Heat Mass Transf 49(3–4):718–726
14. Ko TH (2006) A numerical study on entropy generation and optimization for laminar forced in a rectangular curved duct with longitudinal ribs. Int J Therm Sci 45(11):1113–1125
15. Mahmud S, Fraser RA (2002) Second law analysis of heat transfer and fluid flow inside a cylindrical annular space. Exergy 2:322–329
16. Yari M (2009) Second-law analysis of flow and heat transfer inside a microannulus. Int Commun Heat Mass Transf 36(1):78–87
17. Demirel Y, Kahraman R (2000) Thermodynamic analysis of convective heat transfer in an annular packed bed. Int J Heat Fluid Flow 21(4):442–448
18. Mahmud S, Fraser RA (2003) The second law analysis in fundamental convective heat transfer problems. Int J Therm Sci 42(2):177–186
19. Gorla RSR, Bydr LW, Pratt DM (2007) Second law analysis for microscale flow and heat transfer. Appl Therm Eng 27(8–9):1414–1423
20. Tasnim SH, Mahmud S (2002) Mixed convection and entropy generation in a vertical annular space. Exergy 2:373–379
21. Mahmud S, Fraser RA (2003) Analysis of entropy generation inside concentric cylindrical annuli with relative rotation. Int J Therm Sci 42(5):513–521
22. Chen S (2010) Analysis of entropy generation in counter flow premixed hydrogen air combustion. Int J Hydrogen Energy 35(3):1401–1411
23. Gyves TW, Irvine TF (2000) Laminar conjugated forced convection heat transfer in curved rectangular channels. Int J Heat Mass Transf 43:3953–3964
24. Gyves TW (1997) A numerical solution to conjugated mixed convection heat transfer in curved square channel. Ph.D. Thesis, State University of New York at Stony Brook
25. Kucuk H (2003) Numerical investigation of heat transfer and fluid flow in concentric or eccentric curved annular ducts. Ph.D. Thesis, Karadeniz Technical University
26. Asan H, Kucuk H (2007) A numerical computation of heat and fluid flow in L-shaped curved channels. Heat Transf Eng 28:112–119
27. Gyves TW, Irvine TF, Naraghi MHN (1999) Gravitational and centrifugal buoyancy effects in curved square channels with conjugated boundary conditions. Int J Heat Mass Transf 42:2015–2029
28. Cheng KC, Akiyama M (1970) Laminar forced convection heat transfer in curved rectangular channels. Int J Heat Mass Transf 13:471–490
29. Dong ZF, Ebadian MA (1991) Numerical analysis of laminar flow in curved elliptic ducts. J Fluids Eng 113:555–562
30. Incropera FP, DeWitt DP (1990) Fundamentals of heat and mass transfer, 3rd edn. Wiley, Singapore
31. Çengel YA (2003) Heat transfer: a practical approach, 2nd edn. McGraw-Hill, New York, NY
32. Roache PJ (1982) Computational fluid dynamics, Revisedth edn. Hermosa, Albuquerque, NM
33. Stone HL (1968) Iterative solution of implicit approximations of multi-dimensional partial differential equations. SIAM J Numer Anal 5:530–558
34. Bejan A (1982) Entropy generation through heat and fluid flow, 1st edn. Wiley, New York, NY
35. Kucuk H (2010) Numerical analysis of entropy generation in concentric curved annular ducts. J Mech Sci Technol 24(9):1927–1937
36. Kucuk H (2011) Numerical analysis of entropy generation and minimisation in eccentric curved annular ducts. Int J Exergy 9(1):40–65
37. Paoletti S, Rispoli F, Sciubba E (1989) Calculation of exergetic losses in compact heat exchanger passages. ASME AES 10:21–29

Chapter 6
Influence of Turbine Inlet Temperature on the Efficiency of Externally Fired Gas Turbines

Paulo Eduardo Batista de Mello, Sérgio Scuotto, Fernando dos Santos Ortega, and Gustavo Henrique Bolognesi Donato

Abstract Many researchers have considered externally fired gas turbines (EFGT) as an option for the implementation of biomass-fueled power plants. The EFGT cycle with regeneration or the gas-vapor combined cycle using one EFGT, also known as externally fired combined cycle (EFCC), could lead to significant efficiency improvements if compared to current technology used for power generation from biomass. This work presents one improved numerical model used for the simulation of EFGT cycle. The results were obtained with a numerical model for the EFGT cycle coupled with a model for the high temperature heat exchanger (HTHE) that is necessary for the cycle implementation. The model of the heat exchanger is based in correlations for the Colburn and friction factors, obtained with CFD simulations. In previous work, the model included only laminar regime for the heat exchanger. The present work extends the correlations that describe the behavior of the heat exchanger to turbulent and transitional regimes. The updated model of the EFGT cycle is used to investigate the influence of the turbine inlet temperature over the cycle efficiency. The results obtained confirm that the pressure drop caused by the heat exchanger is one important parameter that influences the cycle efficiency. The feasibility of the EFGT cycle is discussed taking into consideration that the highest temperature in EFGT cycle is not in the turbine inlet, but in the high temperature heat exchanger.

Keywords High temperature heat exchangers • Turbine inlet temperature • EFGT cycle

P.E.B. de Mello (✉) • S. Scuotto • F.d.S. Ortega • G.H.B. Donato
Centro Universitário da FEI, Av. Humberto de Alencar Castelo Branco, 3972,
CEP 09850-901, São Bernardo do Campo, SP, Brazil
e-mail: pmello@fei.edu.br; sscuotto@uol.com.br; ferortega@fei.edu.br; gdonato@fei.edu.br

I. Dincer et al. (eds.), *Progress in Sustainable Energy Technologies Vol II: Creating Sustainable Development*, DOI 10.1007/978-3-319-07977-6_6

6.1 Introduction

Externally fired gas turbines (EFGT) cycle has been considered as an option for the implementation of biomass-fueled power plants. Its implementation, with adequate efficiency, depends on a high temperature heat exchanger. This component is the main obstacle for the implementation of EFGT because other components of the cycle are standard. The components of EFGT cycle can be seen in Fig. 6.1.

The externally fired gas turbine (EFGT cycle) has been implemented experimentally using metallic high temperature heat exchangers [1, 2]. The use of metallic heat exchangers for the implementation of EFGT cycle introduces a serious limitation: the turbine inlet temperature (TIT) must be maintained lower than 750 °C. This temperature limitation has negative impact over the cycle efficiency. Current technology used for manufacturing of metallic high temperature heat exchangers imposes one superior limitation for the maximum temperature, that should not exceed 800 °C. In Fig. 6.1 is possible to observe that the maximum temperature in EFGT is not in the turbine inlet, but after the combustion chamber. As a consequence, the turbine inlet temperature (TIT) should not exceed 750 °C when a metallic heat exchanger is used.

The use of ceramics for the construction of the high temperature heat exchanger has been considered in the past. More recently, the use of plate and fin or OSF (offset strip fin) heat exchangers have been proposed as one alternative [3] for the construction of HTHEs using ceramics. The geometry of these heat exchangers is considerably different than current geometries used for metallic heat exchangers and structural integrity is a concern due to the brittle behavior of ceramics combined to its intrinsic microcracks distribution. The thermal design of heat exchangers depend on correlations for the prediction of heat transfer and pressure

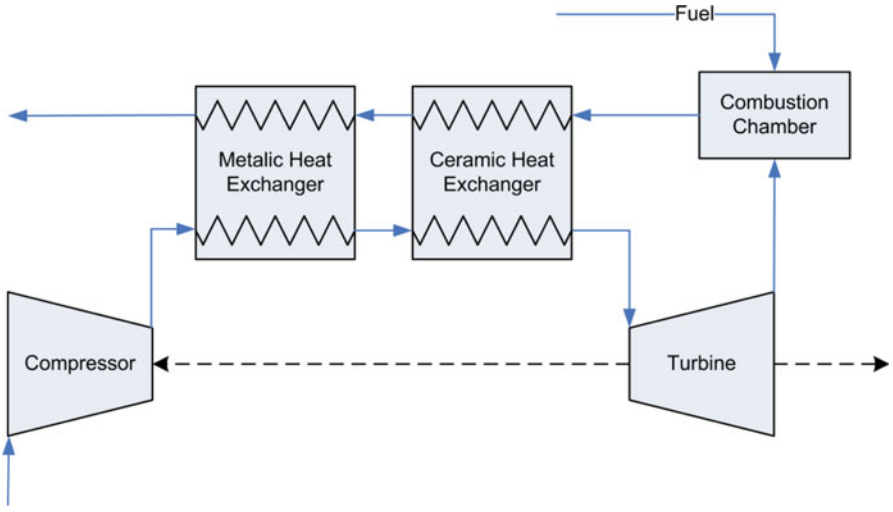

Fig. 6.1 Arrangement of the EFGT components

drop, that are not available for the geometries proposed for ceramic HTHEs. Correlations for the prediction of Colburn and friction factors for one OSF geometry of ceramic heat exchanger have been obtained by Monteiro and de Mello [4] using CFD simulations in the laminar regime.

Numerical models for the simulation of EFGT cycle are capable of investigating the influence of some parameters over cycle performance. Turbine inlet temperature and pressure drop caused by the heat exchanger are investigated numerically by Kautz and Hansen [5] but without considering that these two parameters are coupled, for a given heat exchanger. In a recent work [6], one model that predicts the effectiveness of the heat exchanger and couples it to pressure drop is presented. This kind of model is capable of linking the thermodynamic model of the cycle with the HTHE model and gives one good estimative of the heat exchanger dimensions.

Experimental works related to ceramic heat exchangers are rare. A good review about new technological development in this area is presented by Sommers et al. [7]. Experiments with one heat exchanger composed of plates can be found in Alm et al. [8] but the authors were not particularly interested in high temperature applications. One ceramic heat exchanger for high temperature applications constructed with plates is investigated experimentally by Kee et al. [9] using one geometrical configuration that resembles the geometry considered in current study. However, the dimensions of the fins, channels and the entire heat exchanger are much higher in current work, due to the application considered. The pressure drop imposed by the heat exchanger in one EFGT cycle deserves special attention and requires one geometrical configuration specially developed for the application.

6.2 Objectives

The objective of the present work is to improve a previous HTHE model proposed by this research group for the simulation of externally fired gas turbines (de Mello and Monteiro [6]). The model will be improved extending the correlations that predict heat transfer and pressure drop in the heat exchanger, including the transitional and turbulent regimes. The correlations were obtained using CFD simulations.

The model for the EFGT cycle, with the detailed model for the ceramic heat exchanger, is implemented using EES—Engineering Equation Solver. The results obtained with simulations with the improved model show the influence of turbine inlet temperature (TIT) over the cycle efficiency.

6.3 Thermodynamic Model of the EFGT Cycle

The arrangement of the components considered in the model is presented by Fig. 6.2. The main simplification conducted is that one single ceramic heat exchanger is used in the cycle, in contrary to a slightly more complex configuration presented in Fig. 6.1 that used the ceramic heat exchanger only for the high temperature part of the system. Only the pressure drop caused by the ceramic heat exchanger is included in the model. Air standard assumptions are used in the modeling (air specific heat is not considered as a constant).

Under these assumptions, work consumed by the compressor WC and work produced by the turbine WT can be obtained from Eqs. (6.1) and (6.2). The heat supplied in the combustion chamber is obtained from Eq. (6.3). Enthalpy at the compressor outlet is determined considering its isentropic efficiency, and the same approach is conducted for the turbine.

$$W_C = \dot{m}_{air}(h_2 - h_1) \tag{6.1}$$

$$W_T = \dot{m}_{air}(h_3 - h_4) \tag{6.2}$$

$$Q_{cc} = \dot{m}_{exaust}(h_5 - h_4) \tag{6.3}$$

The net electric efficiency is calculated from Eq. (6.4), including the efficiency of the electric generator.

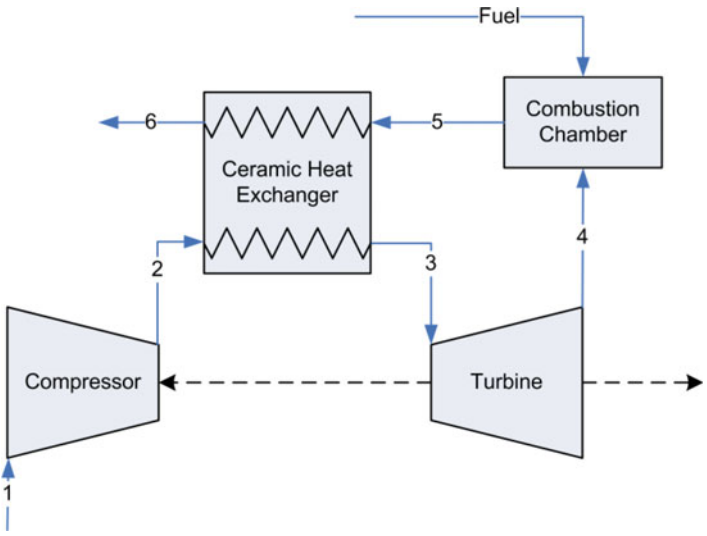

Fig. 6.2 Arrangement of the EFGT components considered in the simulation

$$\eta_{el} = \frac{W_{net}\eta_{EG}}{Q_{cc}} = \frac{\dot{m}_{air}[(h_3 - h_4) - (h_2 - h_1)]\eta_{EG}}{\dot{m}_{exaust}(h_5 - h_4)} \tag{6.4}$$

The ceramic heat exchanger has a strong influence over the EFGT cycle and this influence is considered in the model by the effectiveness and pressure drop in each side. The effectiveness of the heat exchanger is obtained from its dimensions and Colburn correlations, discussed in the next section. With the heat exchanger effectiveness the heat exchanger outlet conditions (temperatures and enthalpies) can be determined using Eq. (6.5), remembering that the mass flow rates are almost equal in each side of the heat exchanger.

$$\varepsilon = \frac{q_{act}}{q_{\max}} = \frac{h_3 - h_2}{h_5 - h_2} \tag{6.5}$$

The heat exchanger correlations for the friction factor are used for the determination of pressure drop in each side of the heat exchanger so that Eqs. (6.6) and (6.7) can be used for the determination of pressure in positions 3 and 5, shown in Fig. 6.2, remembering that position 6 is opened to atmosphere and pressure in position 2 can be determined from the pressure ratio produced by the compressor π_C.

$$\Delta P_{hot} = P_5 - P_6 \tag{6.6}$$

$$\Delta P_{cold} = P_2 - P_3 \tag{6.7}$$

It is important to note that the pressure drop produced by the ceramic heat exchanger has the effect of decreasing the pressure ratio in the turbine, for a given pressure ratio in the compressor. These pressure ratios are defined by Eqs. (6.8) and (6.9).

$$\pi_C = \frac{P_2}{P_1} \tag{6.8}$$

$$\pi_T = \frac{P_3}{P_4} \tag{6.9}$$

Simulations conducted in the current work use data from the commercial micro gas turbine Turbec T100 (ABB/Volvo). The data is available in Kautz and Hansen [5] and is repeated herein in Table 6.1. Pressure ratio shown in Table 6.1 is imposed to the compressor ($\pi_C = 4.5$) while turbine pressure ratio is derived from pressure drop caused by the heat exchanger.

Table 6.1 Design data for Turbec T100 micro gas-turbine, according to [5]

Net electric output	100	kW
Thermal power input	333	kJ/s
Turbine power	282	kW
Compressor power	159	kW
Net electric efficiency	30.0	%
Pressure ratio	4.5	–
Compressor isentropic efficiency	0.768	–
Turbine isentropic efficiency	0.826	–
Gas-temperature turbine inlet (T_3 in Fig. 6.2)	950	°C
Exhaust-gas temperature (T_4 in Fig. 6.2)	650	°C
Gas-temperature after recuperator (T_6 in Fig. 6.2)	270	°C
Mass flow, air	0.7833	kg/s
Mass flow, exhaust-gas	0.79	kg/s

6.4 Model for the High Temperature Heat Exchanger (HTHE)

Due to the lack of experimental data for the ceramic heat exchanger considered in current work, CFD simulations were used to obtain its heat transfer and pressure drop behavior. The configuration is similar to the one proposed by Schulte-Fischedick et al. [3] and is composed by ceramic plates, as shown in Fig. 6.3.

Each plate presents complex geometry, especially considering that it is made of ceramics, and requires appropriate manufacturing processes. The typical geometry of one of the plates if shown in Fig. 6.4 where it is possible to see the many fins used to enhance heat transfer achieving one more compact heat exchanger.

The most appropriate form to characterize the heat exchanger behavior is the use of Colburn and friction factor correlations, as a function of Reynolds number, as proposed by Kays and London [10]. The heat exchanger is not simulated entirely, but only one small part of it. The symmetry of the flow in the finned region of the plate is used to limit the extension of the calculation domain and maintain computational effort at a reasonable level. This approach was used by Monteiro and de Mello [4], who conducted the validation of the CFD simulations comparing the numerical results with experimental data for finned flat tubes geometry that present fluid flow characteristics very similar to the ceramic offset strip fin heat exchanger proposed by Schulte-Fischedick et al. [3] and used in the current work.

Monteiro and de Mello [4] present one detailed discussion about the CFD simulations necessary to characterize the behavior of the ceramic heat exchanger that is not repeated herein. The discussion includes the solution procedure, specification of boundary conditions, the validation simulations using data for finned flat tubes, the grid refinement study and geometrical details about the ceramic heat exchanger. In the present work, the same approach was used, but with the addition

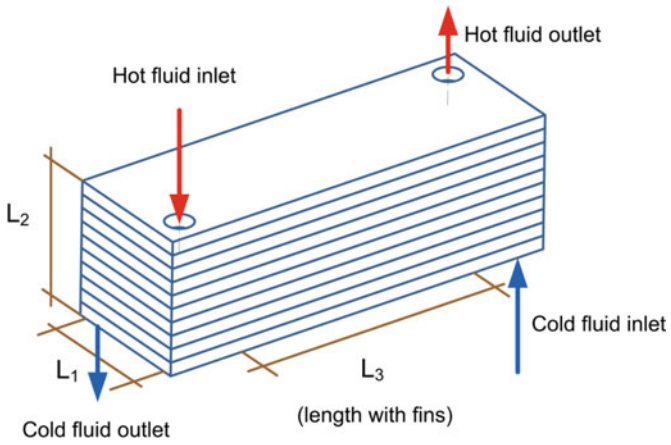

Fig. 6.3 Ceramic heat exchanger composed by plates

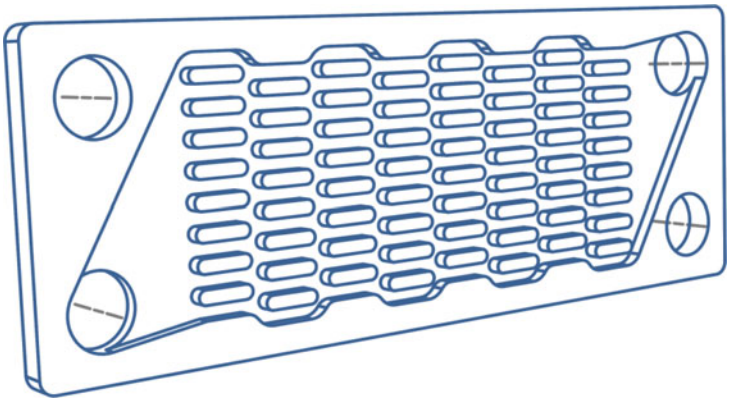

Fig. 6.4 One plate of a ceramic OSF (offset strip fins) heat exchanger

of one transitional model available in CFX 12, to extend the correlations to an increased Reynolds range.

The performance of the transitional model available in CFX 12 was investigated by Abraham et al. [11], where details about the governing equations can be found. The performance of the model was investigated for straight pipe geometry using different boundary conditions: uniform heat flux and uniform wall temperature. After comparing to many different experiment sources, Abraham et al. [11] concluded that the transitional model is capable of predicting the average heat transfer with good accuracy, but presents small deviations from experiments (25 %) only in the local heat transfer of the development region. The transitional model requires 18 % extra computational effort compared to fully turbulent models, for the same domain and grid, but the grids need to be more refined, in order to obtain y+ as close as possible to 1 close to the domain walls.

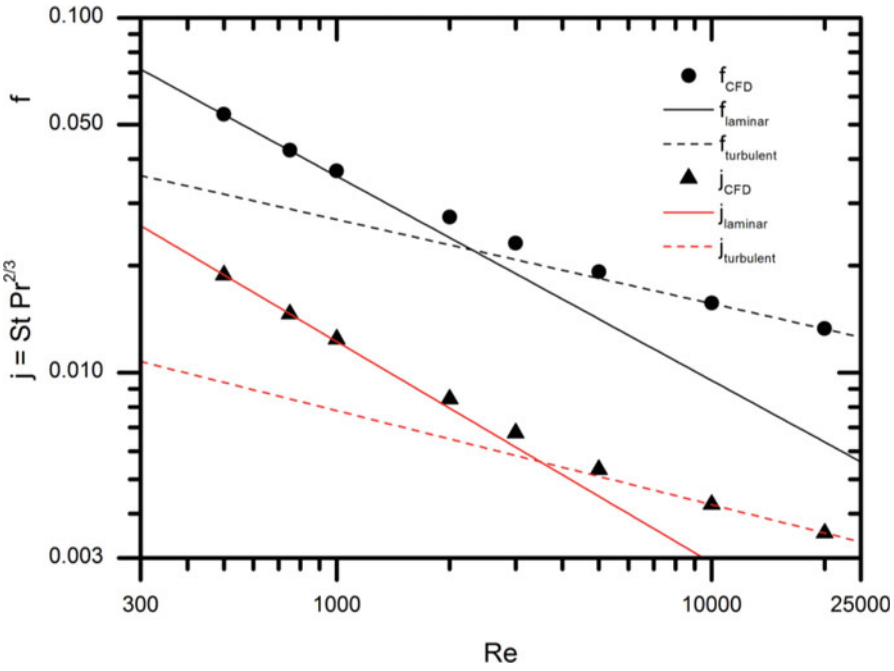

Fig. 6.5 Colburn and friction factor as a function of Reynolds number: correlations obtained for the laminar (Eqs. (6.10) and (6.11)) and turbulent regimes (Eqs. (6.12) and (6.13)) compared to CFD simulations

The numerical results obtained with the transitional model for the ceramic heat exchanger geometry are summarized by Fig. 6.5. In summary, the mass flow rate and wall temperature are imposed as boundary conditions. The results obtained with the CFD simulation are the pressure drop and outlet temperature. The process needed to obtain the Colburn and friction factors from pressure drop and outlet temperature is describe in detail in Monteiro and de Mello [4] and is not repeated here.

The results of Fig. 6.5 show a clear transition of regime for Reynolds number between 2,000 and 3,000. Laminar regime can be well described by Eqs. (6.10) and (6.11), while turbulent regime is well described by Eqs. (6.12) and (6.13). The numerical results obtained for Reynolds 2,000 and 3,000 are not in agreement with the correlations but asymptotically approach the correlations.

$$j_{\text{laminar}} = 0.9109\text{Re}^{-0.624} \tag{6.10}$$

$$f_{\text{laminar}} = 1.9126\text{Re}^{-0.576} \tag{6.11}$$

$$j_{\text{turbulent}} = 0.0487\text{Re}^{-0.265} \tag{6.12}$$

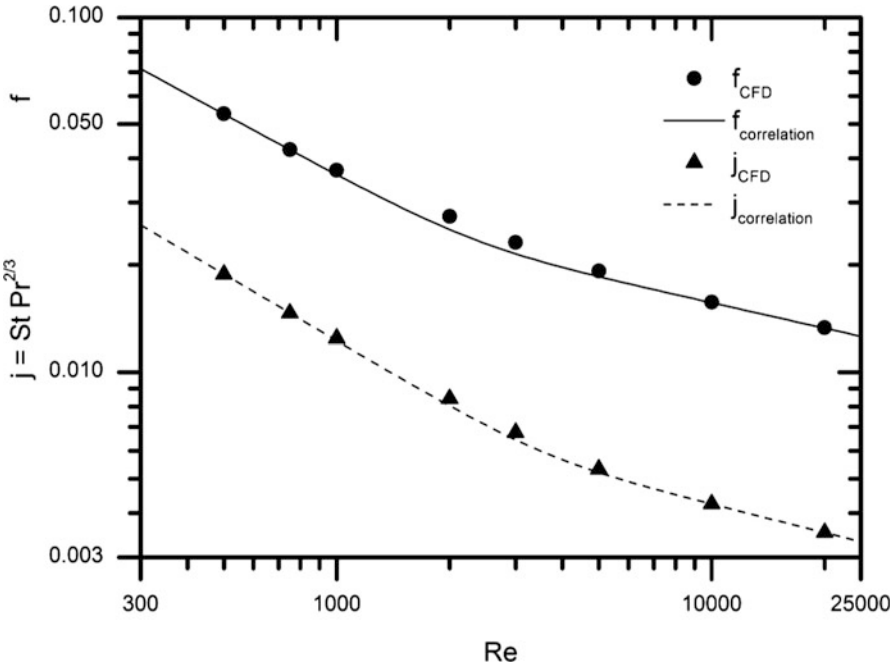

Fig. 6.6 Colburn and friction factor as a function of Reynolds number: correlations (Eqs. (6.14) and (6.15)) valid for the laminar, turbulent and transitional regimes compared to CFD simulations

$$f_{\text{turbulent}} = 0.1388\text{Re}^{-0.237} \tag{6.13}$$

The implementation of the heat exchanger model in the EFGT cycle is easier if one unique correlation for the Colburn and friction factors, valid for any Reynolds regime, is available. The solution for this problem was to use the approach proposed by Manglik and Bergles [12], that solved this problem with good results. The details related to procedure needed to obtain the coefficients of the wider Reynolds range correlation proposed by Manglik and Bergles [12] is not discussed in their work, but can be deduced with some effort.

The correlations given by Eqs. (6.14) and (6.15) are the final correlations valid for any Reynolds regime and the coefficients in these correlations are obtained exclusively from the coefficients of Eqs. (6.10)–(6.13), so that no additional curve fitting is required.

$$j = 0.9109\text{Re}^{-0.624}\left(1 + 1.7 \times 10^{-13}\text{Re}^{3.6}\right)^{0.1} \tag{6.14}$$

$$f = 1.9126\text{Re}^{-0.576}\left(1 + 3.9 \times 10^{-12}\text{Re}^{3.4}\right)^{0.1} \tag{6.15}$$

The graph of Fig. 6.6 shows that the correlations are capable of reproducing the Colburn and friction factors obtained with CFD simulations over the entire

Table 6.2 Data of the ceramic heat exchanger geometry

Flow passage hydraulic diameter ($4r_h$)	4.635	mm
Fin length in flow direction	20.0	mm
Fin width	5.0	mm
Plate spacing (and fin height) (b)	5.0	mm
Plate thickness (a)	5.0	mm
Total heat transfer area/volume between plates	431	m^2/m^3
Fin area/total area	0.424	–
σ	0.125	–
α	108	m^2/m^3

Reynolds range considered. The highest deviation is observed for the friction factor in the transitional regime and is lower than 8 % for Re = 2,000.

Another point to note from the work of Manglik and Bergles [12] is that their correlations include geometrical parameters of the offset strip fins. It was possible to include the geometrical parameters in the correlations because the experimental data related to offset strip fins was abundant. Of course, it is possible to conduct one series of CFD simulations and achieve the same results, but we consider that some experimental validation with the actual ceramic heat exchanger should be performed in order to guarantee the performance of the CFD simulations first.

The correlation for the friction factor is used to obtain the pressure drop in each side of the heat exchanger, using Eq. (6.16).

$$\Delta P = \frac{G^2 v_i}{2}\left[\left(1+\sigma^2\right)\left(\frac{v_o}{v_i}-1\right)+f\frac{\alpha V}{\sigma A_{fr}}\frac{v_m}{v_i}\right] \tag{6.16}$$

Details of the geometry of the fins are needed to obtain parameters α (ratio of total transfer area of one side of exchanger to total exchanger volume) and σ (ratio of free-flow to frontal area of one side of exchanger). The same plate design and fin arrangement is used in both sides of the heat exchanger so that α and σ are equal in both sides. Table 6.2 presents the parameters related to the heat exchanger geometry simulated.

Methodology proposed by Kays and London [10] is used to define Reynolds number (Eq. 6.17) and to conduct all the calculations related to the heat exchanger.

$$\mathrm{Re} = \frac{G D_h}{\mu} = \frac{\dot{m} D_h}{\sigma A_{fr} \mu} \tag{6.17}$$

The effectiveness of the heat exchanger is evaluated in a similar way, from the Colburn factor. In summary, Colburn factor is used to obtain the overall heat transfer coefficient U, including the effects of thermal resistance of the ceramic wall and the fin efficiency. For a given heat transfer area and mass flow rate in the heat exchanger the number of transfer units NTU can be determined.

One appropriate relation, valid for counter-flow configurations, is used to obtain the effectiveness ε from the NTU. The details can be found in de Mello and Monteiro [6].

6.5 Results and Discussion

The highest temperature in EFGT cycle is not in the turbine inlet (position 3, in Fig. 6.2), but in the high temperature heat exchanger, just after the combustion chamber (position 5, in Fig. 6.2). For a given ceramic material used for the construction of the heat exchanger, it is reasonable to consider one maximum temperature that should not be exceeded in order to maintain structural integrity. The first round of simulations considers that T_5, the highest temperature in the heat exchanger, is maintained at 1,100 °C. At the same time, the finned length of the heat exchanger L_3 (shown in Figs. 6.3 and 6.4) is constant and equal to 1.5 m. The graph in Fig. 6.7 shows the influence of the heat exchanger frontal area, determined by L_1 and L_2, over the net electric efficiency of the EFGT cycle and over TIT (T_3). The effectiveness of the heat exchanger increases with its volume (due to higher heat transfer area), resulting in a higher T_3 and higher net electric efficiency.

It is important to note that the increase in efficiency is not produced by higher TIT only. One careful inspection on the turbine pressure ratio π_T reveals that the increase in heat exchanger frontal area reduces pressure drop caused by the heat exchanger. It can be deduced from Fig. 6.8, which shows that the value of turbine pressure ratio π_T approaches $\pi_C = 4.5$ when the heat exchanger volume is increased. It is clear that the pressure drop produced by the heat exchanger has a pronounced negative effect over the net electric work obtained with EFGT. For the conditions simulated, the turbine pressure drop is 4.2 or bellow, when the heat exchanger Reynolds number is higher than 1,300. It is clear that the plate-fin heat exchanger configuration considered for the implementation of EFGT cycle should be used in laminar regime. Otherwise, pressure drop caused by the heat exchanger will compromise EFGT performance.

In EFGT cycle, structural integrity should be a concern for both the ceramic heat exchanger and the turbine. As a result, turbine inlet temperature may be the main limitation in certain cases. The second round of simulations considers that T_3 (TIT) should not be higher than 950 °C, value that corresponds to operational conditions of Turbec T100 micro gas-turbine, as shown in Table 6.1. As a consequence, variations in the heat exchanger effectiveness would result in alteration on the highest temperature in the heat exchanger T_5. Again, the finned length of the heat exchanger L_3 (shown in Figs. 6.3 and 6.4) is constant and equal to 1.5 m.

The results obtained with this second round of simulations are shown in Fig. 6.9. The increase in frontal area of the heat exchanger maintains the flow under laminar regime reduces pressure drop imposed to the flow and increases the heat exchanger effectiveness. The increased heat exchanger effectiveness has the advantage of

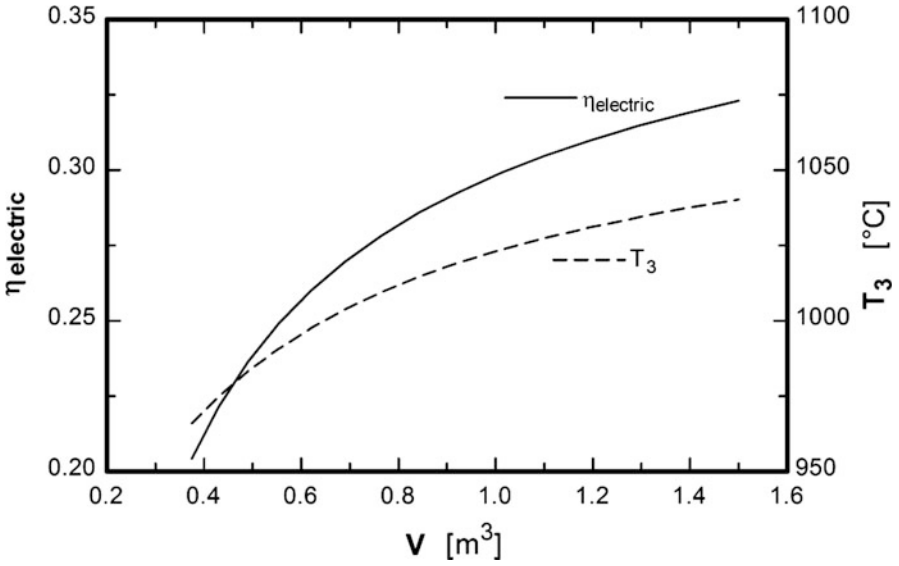

Fig. 6.7 Influence of the HTHE dimensions over net electric efficiency and T_3 (TIT) when T_5 is fixed at 1,100 °C

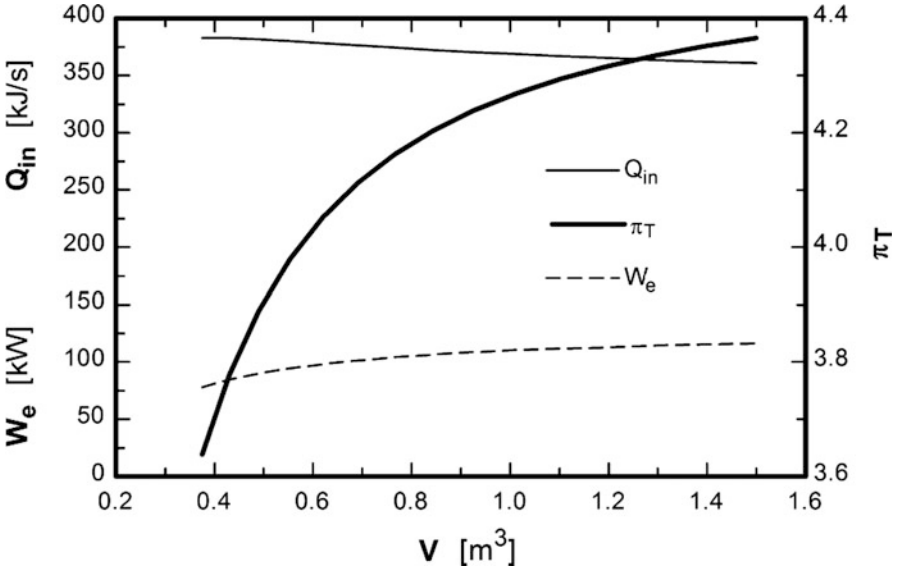

Fig. 6.8 Influence of the HTHE dimensions over turbine pressure ratio π_T, net electric work W_e and heat input Q_{in}, when T_5 is fixed at 1,100 °C

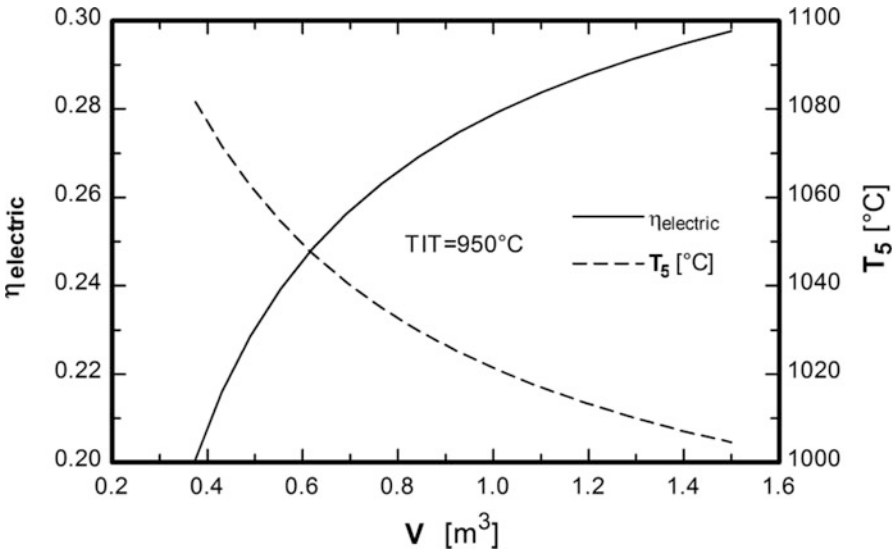

Fig. 6.9 Influence of the HTHE dimensions over net electric efficiency and T_5 when T_3 (TIT) is fixed at 950 °C

reducing the maximum temperature (T_5), which contributes to establish less severe operational conditions.

In previous work, de Mello and Monteiro [6] did not observed significant net electric efficiency reduction due to pressure drop. In that work, the correlations that described the heat exchanger behavior were valid for laminar regime only.

6.6 Final Remarks

In the present work we have extended the Reynolds range for the correlations of friction and Colburn factors for a particular configuration of heat exchanger that could be manufactured with ceramics, including transitional and turbulent regimes. These correlations are essential for the performance prediction of the heat exchanger. The investigation of fins geometry over the performance would be one interesting result that would require the development of new correlations for Colburn and friction factors, including geometrical parameters, as conducted by Manglik and Bergles [12] for offset strip fin configuration. However, there are other issues that should be investigated in parallel: manufacturing, structural integrity, cost, durability, etc.

The next step that will be conducted by our research group is to manufacture one ceramic heat exchanger with the geometry similar to the one shown in Fig. 6.4 and test it. Preliminary investigation related to manufacturing technology of the heat exchanger was conducted using one small plate with fins of 5 mm width, as shown

Fig. 6.10 Ceramic plate constructed with alumina using gelcasting technique

in Fig. 6.10. This plate was produced using the gelcasting technique and was constructed with alumina (Al_2O_3). The tests suggest that careful drying of green plates is critical in order to minimize warping and cracks. Besides, significant improvements were achieved using osmotic drying [13]. The investigation has shown that fins with 5 mm width are feasible and this dimension could be further reduced in order to achieve higher compactness.

After the production of the plates, they must be joined in order to obtain the heat exchanger. For this purpose, the surface of the plates must be firstly ground to reduce their surface roughness and grant a good contact between each pair of plates. The adhesion must seal completely the contact between each plate to avoid gas leakage. This may be achieved by applying a thin layer of amorphous colloidal silica suspension on each plate and heating this arrangement up to 1,200 °C. At this temperature, the silica reacts with alumina to form a layer of mullite, which is completely bonded to both surfaces. As the silica layer is softened with heating, it can relieve small strains by viscous flow, before forming mullite. This minimizes thermomechanical stresses during the heating cycle.

Another serious concern is related to structural integrity against brittle fracture and thermal fatigue. Since engineering ceramics present randomly oriented microcracks, porosity and essentially brittle response, accurate characterization of mechanical properties is mandatory. To better support the HTHE development, a series of tests in the range 20–1,000 °C are planned to obtain elastic moduli and ultimate tensile and compressive strength as a function of temperature. All strength data will be described using Weibull statistics and the weakest link theory, which will guide design activities imposing low failure probability. The modified Coulomb-Mohr failure criteria will be employed to properly investigate structural integrity of the ceramic heat exchangers operating at high temperatures.

The construction of one experimental bench work to test the ceramic heat exchanger operating at high temperature (around 1,000 °C) was already started. Flow rates in each side of the heat exchanger, ranging between 0.001 and 0.01 kg/s, will be measured by turbine flow meters. Simulations indicate that one heat

exchanger with dimensions $120 \times 120 \times 350$ mm will be sufficient to obtain heat transfer of 4,000 kJ/s and effectiveness close to 70 %. The results obtained with the experiments will be used to validate the simulation methodology used during design stage.

As shown by the simulations presented in Sect. 6.5, the heat exchanger needed to implement one 100 kWe EFGT is much bigger than the prototype to be tested in our experimental bench work. We consider that the bench work is one important intermediate step to validate the design methodology.

The viability of EFGT could also be questioned observing that one heat exchanger of 1.5 m^3 is needed for a system of 100 kWe. We consider that it is too soon to attest the viability because the thermal performance of the ceramic heat exchanger could be significantly improved using optimization procedures. In addition, the ceramic heat exchanger is only necessary for temperatures above 800 °C. Due to this, it is possible to use one more compact metallic heat exchanger in parts of the cycle where temperature is bellow this limit, to reduce the size of the ceramic heat exchanger, as shown in Fig. 6.1.

Acknowledgements The authors would like to acknowledge Centro Universitário da FEI and Fundação de Amparo à Pesquisa do Estado de São Paulo (FAPESP) for the research support.

Nomenclature

a	Plate thickness (m)
A_{fr}	Exchanger total frontal area (m^2)
b	Plate spacing (m)
D_h	Hydraulic diameter (m)
f	Friction factor
G	Exchanger flow stream mass velocity (kg/s m^2)
h	Enthalpy (kJ/kg)
j	Colburn factor
L_1	Exchanger external core dimension perpendicular to the flow (m)
L_2	Exchanger external core dimension perpendicular to the flow (m)
L_3	Exchanger external core dimension in the flow direction (m)
m_{air}	Air mass flow (kg/s)
m_{exaust}	Exaust mass flow (kg/s)
NTU	Number of transfer units
P	Pressure (Pa)
q	Heat transferred in recuperator (kJ/kg)
Q_{cc}	Heat supplied in combustion chamber (kJ/s)
Re	Reynolds number
U	Overall heat transfer coefficient (W/m^2 K)
v	Specific volume (m^3/kg)
V	Volume of the heat exchanger (m^3)

W_e Electric net work output (W)
W_{net} Mechanical net work output (W)

Greek Symbols

α Ratio of total transfer area of one side of exchanger to total exchanger volume (m^2/m^3)
β Ratio of total transfer area of one side of exchanger to volume between plates (m^2/m^3)
ε Effectiveness
η_{EG} Efficiency of electric generator
η_{el} Net electric efficiency
μ Dynamic viscosity (kg/m s)
π_C Pressure ration in compressor
π_T Pressure ration in turbine
σ Ratio of free-flow to frontal area of one side of exchanger

Subscript and Superscripts

act Actual
c Cold
f Fin
h Hot
max Maximum
min Minimum

References

1. Traverso A, Massardo A, Scarpellini R (2006) Externally fired micro-gas turbine: modelling and experimental performance. Appl Therm Eng 26(16):1935–1941
2. Al-Attab K, Zainal Z (2010) Performance of high-temperature heat exchangers in biomass fuel powered externally fired gas turbine systems. Renew Energy 35(5):913–920
3. Schulte-Fischedick J, Dreißigacker V, Tamme R (2007) An innovative ceramic high temperature plate-fin heat exchanger for EFCC processes. Appl Therm Eng 27(8–9):1285–1294
4. Monteiro DB, de Mello PEB (2012) Thermal performance and pressure drop in a ceramic heat exchanger evaluated using CFD simulations. Energy 45:489–496
5. Kautz M, Hansen U (2007) The externally-fired gas-turbine (EFGT-cycle) for decentralized use of biomass. Appl Energy 84(7–8):795–805
6. de Mello PEB, Monteiro DB (2012) Thermodynamic study of an EFGT (externally fired gas turbine) cycle with one detailed model for the ceramic heat exchanger. Energy 45:497–502
7. Sommers A, Wang Q, Han X, T'Joen C, Park Y, Jacobi A (2010) Ceramics and ceramic matrix composites for heat exchangers in advanced thermal systems: a review. Appl Therm Eng 30:1277–1291
8. Alm B, Imke U, Knitter R, Schygulla U, Zimmermann S (2008) Testing and simulation of ceramic micro heat exchangers. Chem Eng J 135:S179–S184
9. Kee RJ, Almand BB, Blasi JM, Rosen BL, Hartmann M, Sullivan NP, Zhu H, Manerbino AR, Menzer S, Coors WG, Martin JL (2011) The design, fabrication and evaluation of a ceramic counter-flow microchannel heat exchanger. Appl Therm Eng 31:2004–2012

10. Kays W, London A (1984) Compact heat exchangers. McGraw-Hill, New York
11. Abraham JP, Sparrow EM, Tong JCK (2009) Heat transfer in all pipe flow regimes: laminar, transitional/intermittent, and turbulent. Int J Heat Mass Transf 52:557–563
12. Manglik R, Bergles A (1995) Heat transfer and pressure drop correlations for the rectangular offset strip fin compact heat exchanger. Exp Thermal Fluid Sci 10(2):171–180
13. Trunec M (2011) Osmotic drying of gelcast bodies in liquid desiccant. J Eur Ceram Soc 31:2519–2524

Chapter 7
Exergy and Exergo-Economic Based Analysis of a Gas Turbine Power Generation System

Ali Mousafarash and Pouria Ahmadi

Abstract In this research study, energy, exergy and exergo-economic analysis of Montazer Ghaem gas turbine power plant which is located near Tehran, capital city of Iran is carried out. The results of this study reveal that the highest exergy destruction occurs in the combustion chamber (CC), where the large temperature difference is the major source of the irreversibility. In addition, the effects of the gas turbine load variations and ambient temperature are investigated to see how system performance changes: the gas turbine is significantly affected by the ambient temperature which leads to a decrease in net power output. The results of the load variation of the gas turbine show that a reduction in gas turbine load results in a decrease in the exergy efficiency of the cycle as well as all the components. As was expected, an increase in ambient temperature has a negative effect on the exergy efficiency of the cycle, so this factor could be countered by using gas turbine air inlet cooling methods. In addition, an exergo-economic analysis is conducted to determine the cost of exergy destruction in each component and to determine the cost of fuel. The results show that combustion chamber has the largest cost of exergy destruction, which is in line with the exergy analysis.

Keywords Energy • Exergy • Efficiency • Exergy destruction • Exergoeconomic

7.1 Introduction

Power generation is a fundamental pillar of infrastructure for other industries and for industrial growth and development. Rapid growth in demand for electricity in certain countries is driving heavy investment in new power plants over the short term. Gas turbine power plants present a prime option in the energy mix. Awareness

A. Mousafarash (✉)
Faculty of Mechanical Engineering, Shahid Rajaee Teacher Training University (SRTTU), Lavizan, Tehran, Iran
e-mail: alimoosafarash@gmail.com

P. Ahmadi
Faculty of Engineering and Applied Science, University of Ontario Institute of Technology, 2000 Simcoe Street North, Oshawa, ON, Canada L1H 7K4
e-mail: Pouria.Ahmadi@uoit.ca

I. Dincer et al. (eds.), *Progress in Sustainable Energy Technologies Vol II: Creating Sustainable Development*, DOI 10.1007/978-3-319-07977-6_7

of limited hydro-carbon resources, environmental and economic concerns, and ever-increasing demand for electricity necessitate the design of optimal gas turbine power plants in terms of technical and cost aspects. Exergy analysis is based on the first and second laws of thermodynamics and makes it possible to characterize the optimal analysis technique on energy systems as well as to identify energy levels and thermodynamic adverse processes clearly in a system. This method is used to describe different energy flows and contributes to reductions in several losses that may occur in the system. Thermodynamics have been used for almost a century to model energy systems, including advanced power plants. The first law of thermodynamics is usually used to model a system; it cannot determine the source of irreversibilities in the system under consideration. In energy systems analysis, which is essentially based on the first law of thermodynamics, there is no difference between various energy states. For instance, a thermal energy unit that has been desorbed by a condenser in a steam turbine power plant is equal to one output work unit from a turbine in the same power plant.

As a result, an analysis based on energy equilibrium may be misleading due to its failure to provide information about internal losses in the system. For example, analysis of energy in adiabatic systems like adiabatic compressors, combustion chambers and or thermal converters may lead to a hasty conclusion that there is no energy loss in this equipment. Nevertheless, even without adapting second law techniques, an experienced designer knows that with respect to their capabilities in feeding various processes and capacity for conversion into other forms of energy, they have some different qualities. It is thus obvious that to conduct an efficiency analysis of energy systems performance criteria must be devised for evaluating thermodynamic efficiency. One may refer to the thermal efficiency of power cycles and or yield coefficient of heat exchangers, as examples of performance criteria. However, like energy analysis, such criteria are mainly based on the first law of thermodynamics, where downgrade of energy quality is not considered. Similarly, results obtained by these criteria may be interpreted only within the field of limited processes, and many pieces of equipment and processes lack criteria of this kind. For this reason, it seems that a thermodynamic concept in which the second law of thermodynamics (downgrade of energy quality) is considered could be used without limitation for conducting an effective analysis of all processes of energy conversion.

The potential for conducting useful mechanical work by means of energy consumption is the criterion of the exergy method for numerical evaluation of the quality of different states of energy. A criterion that is formed according to the second law of thermodynamics may be adapted for all energy conversion systems and its result could be interpreted independently of the type of equipment. Exergetic analysis is used to address the magnitude, place, numerical value and the reasons for occurrence of thermodynamic inefficiencies; based on its results the efficiency of the consuming systems and energy converter may be improved. In addition, by adapting this analysis, one may remove the ambiguities that are created due to first law analyses and criteria. In the next section of this paper, we will explain the meaning and provide a history of exergy subjects, and detail their concept and

computation technique. In the following section, exergy analysis and its relationships with the Montazer Ghaem gas turbine power plant are examined. Although exergy is a new term, the primary evaluations on the rate of energy convertibility of a system into work hark back to the time of definition and presentation of the second law of thermodynamics. By publishing a paper in 1824, Sadi Carnot showed that the conversion of thermal energy into mechanical work might be limited in thermal machines. The essay was hailed as the first accurate numerical analysis of the quality of different energy modes and the ability to convert them into each other.

"Work potential" and "Maximum usable work" from a certain amount of energy was examined after the mathematical formulation of the second law in works by Clausius, Thomson, Maxwell and especially Gibbs. For the first time, Gouy and Stodola separately and clearly defined work potential in 1889 and 1898, respectively. During the 1930s, attention was drawn toward the practical dimensions of this concept, and industrial progress ensued. In the same year, by purposing some essays, Bosnjakovic documented techniques of the second law of thermodynamics to analyze energy systems. Subsequently, in 1956, Rant defined the work potential of energy precisely and employed the term "Exergy" for the first time in denoting this quantity. The 1980s and 1990s saw increasing attention and credibility being lent to exergy analysis, and several conferences were held to support and develop this field of applied thermodynamics. The continuum of papers inspired by these conferences led to the documentation of the current forms of exergetic topics.

Many researchers including Kotas [1], Moran and Shapiro [2] conducted exergy analyses for combined cycle power plants and calculated losses in different parts. In an essay, Facchini et al. [3] carried out an exergy analysis of a combined cycle power plant and concluded that the maximum losses occur inside the combustion chamber, because of the great difference between the flame temperature and operating fluid, and concluded that exergy analysis was a helpful concept for comparing performance in gas turbine cycles. Looking at recent studies indicates that they tried to improve efficiency and output power in these power plants. Bassily [4] simulated and reduced losses for a triple pressure combined cycle power plant; he took a recovery boiler with seven pinch points and examined the impact on them of input temperature inside the gas turbine. His aim was to lower the temperature on the pinch points. Sung and Kim [5] carried out an exergy analysis of a gas turbine cycle at different loads and concluded that the chemical reactions that occurred in the combustion chamber as well as different high temperatures between the flame and operating fluid, would cause maximum losses in gas turbine cycles. Javadabadi et al. [6] conducted an exergy analysis of the gas turbine cycle of a 116 MW power plant and concluded that the impact of rising input temperature in gas turbine turbines may improve total exergy efficiency of the gas turbine cycle, and would reduce exergy losses. Similarly, they came to the result that maximum losses will occur in the combustion chamber in a gas-fired power plant. Ahmadi et al. [7] carried out an exergy analysis on a gas turbine power plant with input air as coolant into a compressor (Fog System). Their results showed that although application of a Fog System led to improvement in output power in the gas cycle, but it would increase exergetic losses of the cycle. Thus, the importance of exergy analysis is

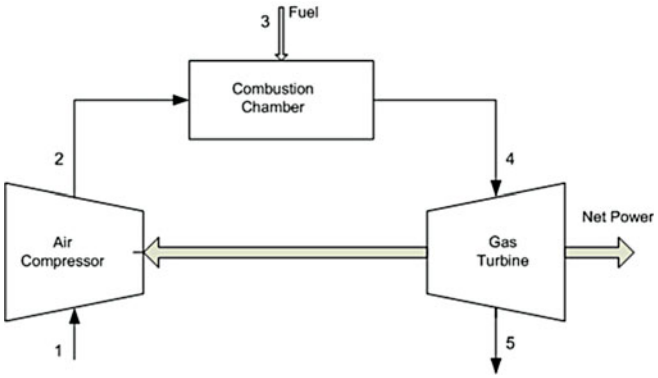

Fig. 7.1 Schematic of the Montazer Ghaem gas turbine power plant

clear in power production cycles. The present study comprised a comparative exergy and exergo-economic analysis of the Montazer Ghaem power plant shown in Fig. 7.1 at different loads and ambient temperatures. In brief, the study consists of the following elements:

- Exergy analysis of a typical GT power plant.
- Analysis of system performance at different ambient temperatures and partial loads.
- Exergo-economic analysis of the gas turbine power plant.

7.2 Exergy Analysis

Exergy is the maximum theoretical useful work that may be received from energy in a system of ideal machines. It is clear that exergy is not stored in a single process, but may be destroyed due to irreversibility. In this method, it is possible to analyse each element of the cycle separately and to obtain the share of each one in total loss of the cycle. Regarding gas turbine power plants, with respect to input fuel or any input flow into the power plant, one may obtain the maximum capacity of the power plant by exergy analysis. The exergy of matter flow may be divided into its major components including kinetic exergy, potential exergy, physical exergy and chemical exergy. In this research paper, due to their dispensable rates, kinetic and potential terms are ignored. Physical exergy is defined as the maximum theoretical useful work obtained as a system interacts with an equilibrium state [8]. Chemical exergy is associated with the departure of the chemical composition of a system from its chemical equilibrium. Chemical exergy is an important part of exergy in the combustion process [9]. Applying the first and second laws of thermodynamics, the following exergy balance is obtained:

$$\dot{E}x_Q + \sum_i \dot{m}_i ex_i = \sum_e \dot{m}_e ex_e + \dot{E}x_W + \dot{E}x_D \tag{7.1}$$

In this formula ex is the total specific exergy and $\dot{E}x_D$ is the exergy destruction rate, other terms in this equation are defined as [10]:

$$\dot{E}x_Q = \left(1 - \frac{T_0}{T_i}\right)\dot{Q}_i \tag{7.2}$$

$$\dot{E}x_W = \dot{W} \tag{7.3}$$

$$ex_{ph} = (h - h_0) - T_0(s - s_0) \tag{7.4}$$

$$\dot{e}x = \dot{e}x_{ph} + \dot{e}x_{ch} \tag{7.5}$$

Where T is the absolute temperature (K) and subscripts i and 0 refer to ambient conditions. The mixture chemical exergy is obtained by following relations [11]:

$$ex_{mix}^{ch} = \left[\sum_{i=1}^{n} X_i ex^{ch_i} + RT_0 \sum_{i=1}^{n} X_i Ln X_i\right] \tag{7.6}$$

The following equation is used to calculate the fuel exergy [12]:

$$\xi = ex_f / LHV_f \tag{7.7}$$

For most of usual gaseous fuels, the ratio of chemical exergy to lower heating value is usually close to 1. Since the main fuel used in power plants is methane, one may write [1]:

$$\xi_{CH_4} = 1.06 \tag{7.8}$$

In this paper, exergy analysis of Montazer Ghaem gas turbine power plant is conducted. Initially, exergy of different points of the cycle, which are characterized in Fig. 7.1, were computed and then, exergetic losses and their exergetic efficiency were calculated by writing down exergetic balance for each element in the gaseous cycle. In Table 7.1, the exergy destruction rate and exergy efficiency equations for plant components are given.

7.3 Exergo-Economic Analysis

The goal of conducting thermo-economic investigations of systems is to minimize the cost of exergy. In exergy costing, a certain cost is determined for each of the exergetic flows. The cost balance may be considered for the total system, and input and output exergies to/from the total system may be priced. A cost balance that is

Table 7.1 The exergy destruction rate and exergy efficiency equations for plant components

Component	Exergy destruction	Exergy efficiency
Compressor	$\dot{E}x_1 + \dot{W}_C = \dot{E}x_2 + \dot{E}x_D$	$\eta_{ex,C} = (\dot{E}x_2 - \dot{E}x_1)/\dot{W}_C$
Combustion chamber	$\dot{E}x_2 + \dot{E}x_3 = \dot{E}x_4 + \dot{E}x_D$	$\eta_{ex,CC} = \dot{E}x_4/(\dot{E}x_2 + \dot{E}x_3)$
Gas turbine	$\dot{E}x_4 = \dot{W}_{GT} + \dot{E}x_5 + \dot{E}x_D$	$\eta_{ex,GT} = \dot{W}_{GT}/(\dot{E}x_4 + \dot{E}x_5)$

recorded for kth element denotes that the sum cost rates in exergies of output flows are equal to the total cost rates of exergies in input flows plus the cost rate of the capital investment, operating and maintenance. For each flow line in the system, a parameter called the flow cost rate ($/s) was defined. Thus, for a system that receives heat and produces work, the exergetic balance may be written as follows [13]:

$$\sum \dot{C}_{e,k} + \dot{C}_{w,k} = \dot{C}_{q,k} + \sum \dot{C}_{i,k} + \dot{Z}_k \tag{7.9}$$

$$\sum \left(c_e \dot{E}_e\right)_k + c_{w,k}\dot{W}_k = c_{q,k}\dot{E}_{q,k} + \sum \left(c_i \dot{E}_i\right)_k + \dot{Z}_k \tag{7.10}$$

$$\dot{C}_j = c_j \dot{E}_j \tag{7.11}$$

The exergy product is the partial of the system and is defined as a target for application of that element in the system. Moreover, the exergy fuel of the system may be defined as those exergies that are consumed to produce the exergy product of the given system components, where we indicate them by $\dot{E}_P, \dot{E}_F$ respectively. Similarly, the cost rates of fuel and product are indicated by $\dot{C}_F, \dot{C}_P$ respectively. In the exergetic balance that is written for an element of a system, there is no term that directly denotes cost of exergy destruction. For this reason, the cost caused by exergy destruction is called the latent cost in the elements of the system. Exergy destruction cost is considered an important parameter in the exergo-economic analysis.

$$\dot{E}_{F,k} = \dot{E}_{P,k} + \dot{E}_{D,k} \tag{7.12}$$

Where $\dot{E}_{F,k}$ represents the fuel exergy rate for kth element, and $\dot{E}_{P,k}$ stands for the product exergy rate of kth element and $\dot{E}_{D,k}$ is the exergy destruction rate of that element due to the irreversibilities, respectively. Assuming that the product $E_{P,k}$ is fixed and that the unit cost of fuel $c_{F,k}$ of the kth component is independent of the exergy destruction, we can define the cost of exergy destruction by the equation [11]:

$$\dot{C}_{D,k} = c_{F,k}\dot{E}_{D,k} \tag{7.13}$$

More details of the exergoeconomic analysis, cost balance equations and exergoeconomic factors are completely discussed in references [12, 14, 15]. Several

methods have been suggested to express the purchase cost of equipment in terms of design parameters in Eq. (7.9) [9, 11, 16]. In this paper we have used the cost functions that are suggested by Ahmadi et al. [17]. To convert the capital investment into cost per unit time one may write:

$$\dot{Z}_k = Z_k.CRF.\varphi/(N \times 3600) \tag{7.14}$$

Where Z_k is the purchase cost of kth component in U.S dollars, N is the annual number of operating hours of the unit, $\varphi = 1.06$ [17] is the maintenance factor and the Capital Recovery Factor (CRF) depends on the interest rate as well as estimated equipment life; CRF is determined using the relation [17]:

$$CRF = \frac{i(1+i)^n}{(1+i)^n - 1} \tag{7.15}$$

Where i is the interest rate and n is the total operating period of the system in years. For each component of the Montazer Ghaem gas turbine power plant, the term $\dot{C}_{D,k} + \dot{Z}_k$ is calculated to give insight into purchase cost and exergy destruction cost.

7.4 Results and Discussion

In this section, results of exergy and exergo-economic analysis are presented. Figures 7.2 and 7.3 show the exergy destruction rate and exergy efficiency of different elements in the gas turbine cycle of the Montazer Ghaem power plant, respectively. These figures signify that the combustion chamber has the maximum rate of exergy destruction and the minimum rate of exergy efficiency among other elements. This is due to the chemical reactions inside the combustion chamber as well as high temperature differences between the operating fluid and flame. At the same time, it is observed that by lowering the irreversibility load, all elements of this cycle are reduced and thus exergy efficiency is improved.

In Figs. 7.4 and 7.5, it is seen that by raising ambient temperature, exergy destruction rate is increased in the compressor since the ratio of pressure in the compressor is the same in three states and with respect to reduction of density of input air, the compressor needs more consuming work and thus the exergy destruction of the compressor is increased. However, the exergy destruction rate of the combustion chamber is reduced by raising the temperature since both discharge of the input fluid reduces and fuel discharge decreases, whereas fuel exergy is tangibly reduced so exergy destruction is lowered overall. At the same time, it is observed that the exergy destruction rate of the turbine is improved by a rise in temperature.

In Figs. 7.6 and 7.7, the exergy efficiency of total gas turbine cycle is given for different loads and ambient temperatures respectively. From these results, it is seen

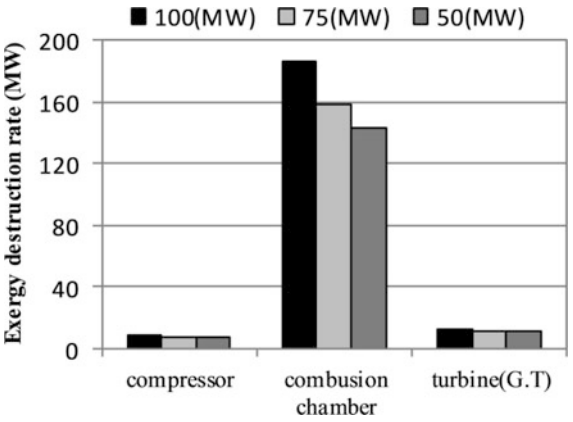

Fig. 7.2 Exergy destruction rates of components of the power plant versus load variations

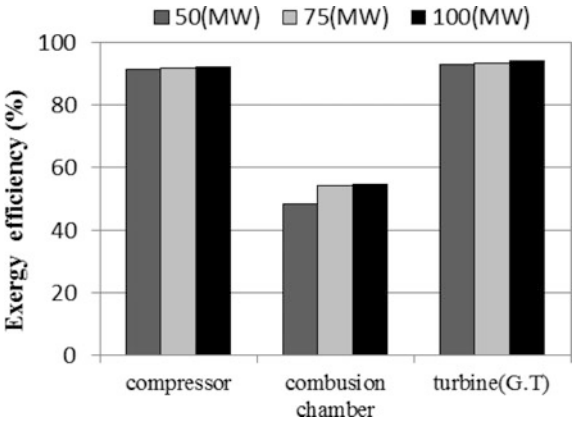

Fig. 7.3 Exergy efficiency rates of components of the power plant versus load variations

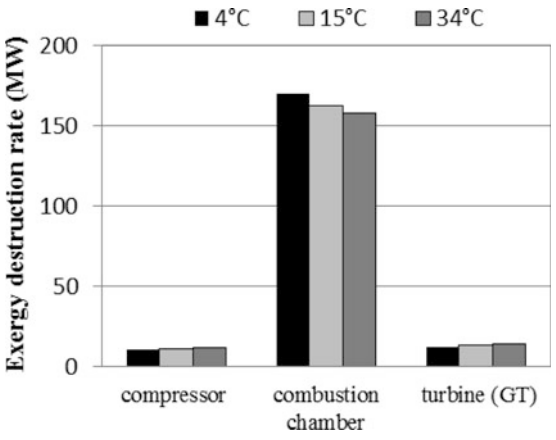

Fig. 7.4 Exergy destruction rates of components of the power plant versus various ambient temperatures

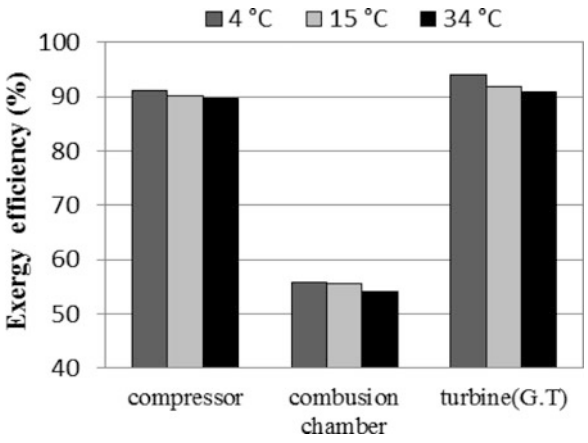

Fig. 7.5 Exergy efficiency rates of components of power plant versus various ambient temperatures

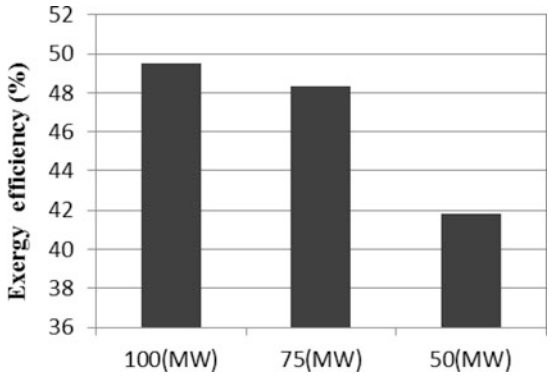

Fig. 7.6 Total power plant exergy efficiency for various loads

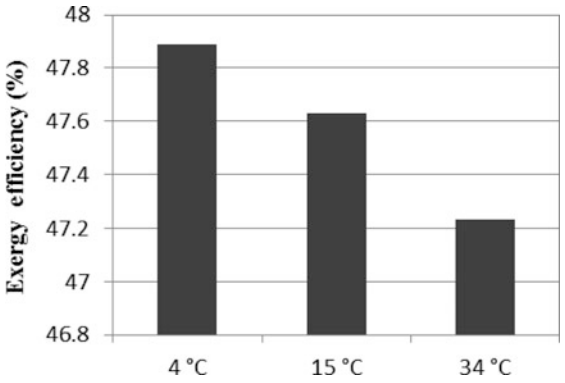

Fig. 7.7 Total power plant exergy efficiency for various ambient temperatures

that the rate of total exergy destruction in the total gas turbine cycle is improved by increasing the load and raising ambient temperature. Table 7.2 shows that in exergo-economic analysis, the combustion chamber is the major component for

Table 7.2 Cost of exergy destruction for each component of the steam power plant

Component	$\dot{C}_{D,k} + \dot{Z}_k$ (\$/h)
Compressor	286.33
Combustion chamber	2,028.517
Gas turbine	355.42

exergy loss, since cost of exergy destruction is also higher in the combustion chamber than in other elements. These results suggest total agreement between the exergy analysis and the exergo-economic analysis.

7.5 Conclusions

In the current paper, exergetic analysis is carried out for a typical gas turbine power plant at different working conditions. For each element in the power plant, exergy efficiency and exergy destruction ratio are computed in three loads of 50, 75 and 100 MW for 4 °C as ambient temperature as well as 85 MW for 4, 15 and 34 °C ambient temperatures. The exergy efficiency of total cycle was obtained in all conditions. Results indicate that the combustion chamber may be considered as the foremost factor for exergy destruction and relatively low efficiency. This is due to higher fuel exergy and chemical reactions of fuel with air, and heat transfer inside the combustion chamber.

The other interesting result is that by reducing the load in all elements, the rate of exergy efficiency is decreased. This point may imply that the power plant achieves maximum efficiency at its nominal load. Rising temperatures have an opposite trend against load increase and may cause reductions in the exergy efficiency of all elements and, hence, the relative efficiency of the whole power plant. Thus, it can be concluded that the best working conditions considered for the power plant are: 100 MW load at 4 °C.

By considering technical conditions, exergo-economic analysis of power plants may play an effective role in informing the management of technical conditions. Similarly, this analysis may reflect the importance of paying attention to the exergy efficiency of power plants and improvements through identifying the price of exergy destruction proportional to the fuel price and the price of purchasing elements. The results of this study indicate that the combustion chamber attracts the maximum cost in terms of exergy destruction and, thus, constitutes the prime target for optimization efforts. It should be noted that the results that were obtained from exergo-economic analysis, comply with the results coming from exergy analysis, and these verify the accuracy and authenticity of both methods.

Nomenclature

$\dot{C}$	Cost per unit of exergy ($/MJ)
$\dot{C}_D$	Cost of exergy destruction ($/h)
CRF	Capital recovery factor
ex	Specific exergy (kJ/kg)
$\dot{e}x$	Specific exergy rate (kW/kg)
$\dot{E}x$	Exergy flow rate (kW)
h	Specific enthalpy (kJ/kg)
LHV	Lower heating value (kJ/kg)
$\dot{m}$	Mass flow rate (kg/s)
P	Pressure (kPa)
$\dot{Q}$	Heat transfer rate (kW)
R	Gas constant (kJ/kg K)
s	Specific entropy (kJ/kg K)
T	Temperature (K)
$\dot{W}$	Work transfer rate (kW)
$\dot{Z}$	Capital cost rate ($/s)
Z_k	Component purchase cost ($)

Greek Symbols

η_{ex}	Exergy efficiency
φ	Maintenance factor
ξ	Coefficient of fuel chemical exergy

Subscript and Superscripts

C	Compressor
CC	Combustion chamber
ch	Chemical
D	Destruction
e	Exit condition
GT	Gas turbine
f	Fuel
i	Inlet Condition
k	Component
ph	Physical
0	Reference ambient condition
$\cdot$	Rate

References

1. Kotas TJ (1985) The exergy method in thermal plant analysis. Butterworths, London
2. Moran MJ, Shapiro HN (2000) Fundamentals of engineering thermodynamics, 4th edn. Wiley, New York
3. Facchini B, Fiaschi D, Manfrida G (2000) Exergy analysis of combined cycles using latest generation gas turbine. ASME J Engrg Gas Turbine Power 122:233–238
4. Bassily AM (2005) Modeling, numerical optimization, and irreversibility reduction of a triple-pressure reheat combined cycle. Int J Energy 32(5):778–794
5. Song TW, Sohn JL, Kim JH, Kim TS, Ro ST (2002) Exergy-based performance analysis of the heavy duty gas turbine in part-load operating condition. Int J Exergy 2:105–112
6. Ebadi MJ, Gorji-Bandpy M (2005) Exergetic analysis of gas turbine plants. Int J Exergy 2 (4):31–39
7. Ahmadi P, Abadi A, Ghaffarizadeh AR, Naghib I (2008) Effect of Fog inlet air cooling method on combined cycle power plant output power. 16th Annual (International) Conference on Mechanical Engineering-ISME. Shahid Bahonar University of Kerman, Iran
8. Dincer I, Rosen MA (1999) Energy environment and sustainable development. Appl Energy 64:427–440
9. Cihan A, Hacıhafızoglu O, Kahveci K (2006) Energy-exergy analysis and modernization suggestions for a combined-cycle power plant. Int J Energy Res 30:115–126
10. Ahmadi P, Rosen MA, Dincer I (2011) Greenhouse gas emission and exergo environmental analyses of a trigeneration energy system. Int J Greenh Gas Control 5:1540–1549
11. Bejan A, Tsatsaronis G, Moran M (1996) Thermal design and optimization. Wiley, New York
12. Ameri M, Ahmadi P, Hamidi A (2009) Energy, exergy and exergoeconomic analysis of a steam power plant (a case study). Int J Energy Res 33:499–512
13. Ameri M, Enadi N (2012) Thermodynamic modeling and second law based performance analysis of a gas turbine power plant (exergy and exergoeconomic analysis). J Power Technol 92(3):183–191
14. Sahoo PK (2008) Exergoeconomic analysis and optimization of a cogeneration system using evolutionary programming. Appl Therm Eng 28(13):1580–1588
15. Ahmadi P, Dincer I (2011) Thermodynamic analysis and thermoeconomic optimization of a dual pressure combined cycle power plant with a supplementary firing unit. Energy Convers Manag 52(5):2296–2308
16. Roosen P, Uhlenbruck S, Lucas K (2003) Pareto optimization of a combined cycle power system as a decision support tool for trading off investment vs. operating costs. Int J Therm Sci 42:553–560
17. Ahmadi P, Barzegar Avval H, Ghaffarizadeh A, Saidi MH (2011) Thermo economic-environmental multi-objective optimization of a gas turbine power plant with preheater using evolutionary algorithm. Int J Energy 35(5):389–403

Chapter 8
Non Repeating Thermal Bridges and the Impact on Overall Heating Energy Consumption in a Typical UK Home

Hasim Altan and Young Ki Kim

Abstract A non-repeating thermal bridge occurs at junctions when building components such as a metal lintel crossing from the buildings' interior to exterior with a little or no intervening insulation, creating a 'bridge' for heat losses through the external wall. In the UK, when considering a domestic building with standards of the building regulation 2006, the proportion of heat losses due to non-repeating thermal bridges is typically 10–15 %. This can rise up to 30 % in highly insulated low energy buildings. Limiting thermal bridging will therefore become increasingly important as more energy efficient buildings are being built due to more stringent requirements by the current and future building regulations, and the endorsements of higher levels by the Code for Sustainable Homes (CfSH) standard. The study has undertaken dynamic computer simulations to calculate the impact on heating energy consumption and to provide both cost and CO_2 benefit analysis for a typical four bedroom terraced house with installation of Glass Reinforced Plastic (GRP) lintels and conventional use of Steel lintels under London climate. Furthermore, two-dimensional temperature and relative humidity distribution study has been carried out to investigate the condensation risks, and the results are presented in this paper based on energy performance where a better insulated home with GRP lintels showed better performance levels in heating energy consumption, CO_2 emissions and overall energy bills. However, the most significant result of the reductions was achieved by improving the building fabric. Moreover, the reduction achieved from installation of GRP lintels has provided a further 10 % energy demand reduction compared with the conventional Steel lintel use in the case study home. With regard to the condensation risk and the two-dimensional study, the paper has shown that the GRP lintel use would reduce non-repeating thermal bridges significantly, particularly around junctions, and at the same time can help keeping dry the area around the junctions. On the other hand, the Steel lintel use would have high risks for condensation and again can cause further health implications with mould growth on surfaces.

H. Altan (✉) • Y.K. Kim
Faculty of Engineering & IT, The British University in Dubai, Dubai International Academic City, P.O. Box 345015, Dubai, United Arab Emirates
e-mail: hasim.altan@buid.ac.ae; kim19021@hanmail.net

I. Dincer et al. (eds.), *Progress in Sustainable Energy Technologies Vol II: Creating Sustainable Development*, DOI 10.1007/978-3-319-07977-6_8

Keywords GRP lintel • Condensation risk • Heat losses • Thermal bridging • Energy efficiency

8.1 Introduction

The Climate Change Act (2008) requires that by 2050 the UK's annual carbon dioxide (CO_2) emissions should be reduced by 80 % compared to 1990 levels. Home energy use is responsible for over a quarter of UK's CO_2 emissions which currently contribute to Climate Change. Therefore, the main aim is to reduce CO_2 emissions from all dwellings by an average of 80 % to help meeting a long term goal [1].

The UK Government has committed for all new homes from 2016 to be net zero carbon emitters which would help cutting down any future CO_2 emissions caused by new build homes. On the other hand, considering the existing housing stock, the government funded energy efficiency schemes in the UK with main objectives to reduce fuel poverty and to minimise heating energy demand by several energy efficiency measures such as cavity wall insulation, loft insulation, draught proofing, and the option to improving a gas central heating system with energy efficiency boiler replacement [2].

In a 2006 Building Regulation compliant dwelling in the UK (i.e. a representative 2006 compliant dwelling), the proportion of heat losses due to non-repeating thermal bridges is typically 10–15 %. This can rise up to 30 % in better and highly insulated low energy buildings [3]. The purpose of this study is to quantify the impact on heating energy consumption when replacing conventional Steel lintels with lass Reinforced Plastic (GRP) lintels within a given case study home, in this case a typical four bedroom terraced house. Moreover, a comparison study has been compiled with the consideration of various building standards such as '2006 Building Regulation', 'Best Practice' and 'Worst Case with No Insulation'. Furthermore, the paper discusses the benefits with regard to energy bill and CO_2 emissions and payback analysis when the case of GRP lintels installed as replacement to the common Steel lintels.

8.2 Energy Efficiency of UK Housing

8.2.1 Current Standards in Existing Dwellings

Figure 8.1 shows the average performance of the existing housing stock which is band E rated (A to G band is based on the Standard Assessment Procedure (SAP) rating score) [4] and there is still a poorly performing housing stock behind. These are either F or G rated dwellings and it is where significant CO_2 emission cuts can be made from the domestic building sector. If the UK Government's saving target

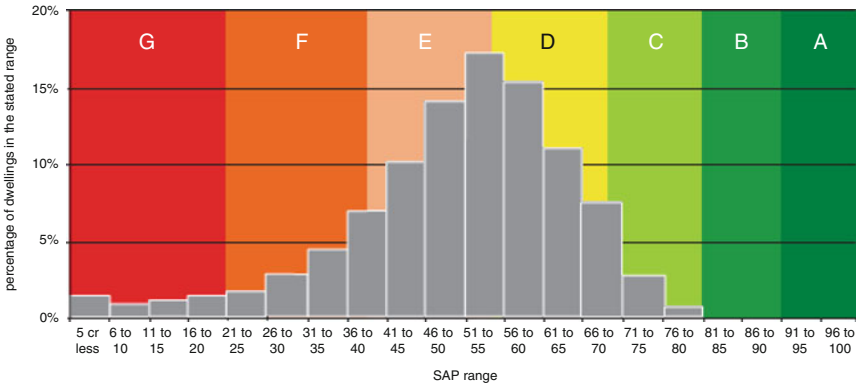

Fig. 8.1 Performance of the UK's existing housing stock [5]

of overall 80 % cut in CO_2 emissions was to be made across the housing stock by 2050, the majority of dwellings will have to be an energy performance rated no worse than band B, where again CO_2 emissions from most existing dwellings would be no more than around 1.5 tonnes per year. This is estimated from an 80 % cut in emissions from 160 million tonnes per year to no more than 32 million tonnes per year, shared by all dwellings that would still be emitting CO_2 in 2050 [4, 5]. In a typical three-bedroom semi-detached house with 88.8 m^2 Total Floor Area (TFA), household consumes 3,423 kWh/year, 3,412 kWh/year, 3,057 kWh/year and 1,314 kWh/year of energy for space heating, hot water, lighting and appliances, and cooking respectively [5, 6].

Improving thermal properties of building fabric and envelope through tightening building regulations has been one of the ways forward for the country when tackling energy efficiency in new build homes in the last 10 years. However, there are still more to be done to improve energy efficiency in the existing housing stock in order to meet the overall CO_2 emission reduction targets.

8.2.2 Thermal Bridging

Thermal bridges or cold bridges are weak points in the building envelope where heat losses are worse than through the main building elements. The reason thermal bridging has become important is very clear today. In the past, thermal bridges were considered as insignificant causes for losses and therefore were not included in the building regulations. Today however (and same applies for the past one decade), by increasing the minimum requirements for the standards of building envelope, i.e. U-value of building fabrics and the level of insulation through new and tightened building regulations; thermal bridging has become more relevant and must be considered. By improving the building fabric's thermal property, the majority of heat losses from buildings through thermal bridging and ventilation

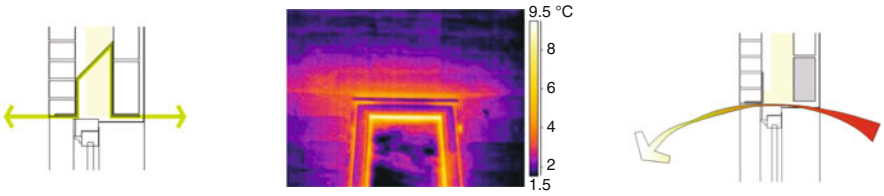

Fig. 8.2 Common thermal bridges and air infiltration at and around lintels

could be minimised. The Approved Document Part L 2010 points out that those thermal bridges can account for more heat losses than all the walls put together [7].

To conserve energy and to prevent cold spots where condensation and mould can form, thermal bridges need to be either completely eliminated or minimised [8]. It is almost impossible to eliminate all thermal bridges, but the effect can be minimised with careful detailing design and construction. Figure 8.2 shows thermal bridging and air infiltration at and around lintels including an Infrared (IR) image of a steel lintel over a window opening.

8.2.3 Airtightness

Air leakage is defined as the flow of air through gaps and cracks in the building fabric. Uncontrolled air leakage increases the amount of heat loss as warm air is displaced through the envelope by colder air from outside [8–10]. Air leakage of warm damp air through the building structure can also lead to condensation within the fabric (interstitial condensation), which reduces insulation performance and causes fabric deterioration. The air permeability of a building can be determined by means of a pressure test. In terms of Building Regulation Part L for new dwellings [11], it is indicated that reasonable provision for airtightness is to achieve a pressure test result of no worse than 10 $m^3/(h\ m^2)$ @ 50 Pa. Current good practice for energy efficient dwellings includes achieving airtightness of 7 $m^3/(h\ m^2)$ @ 50 Pa and best practice is 4 $m^3/(h\ m^2)$ @ 50 Pa with heat recovery unit [11]. Table 8.1 shows the various air permeability standards. In 1998, the Building Research Establishment (BRE) carried out air pressure test to obtain the heating season mean background infiltration rate of a typical UK dwelling and it was 0.65 ach^{-1}. From this study, replacing old leaky windows with modern sealed windows would reduce the background infiltration rate by 0.23 ach^{-1} [12]. Furthermore, replacing windows while simultaneously changing the existing lintels to GRP lintels together with the use of airtight tapes around the openings and the lintels would help to improve airtightness of the dwelling as well as to provide a better thermal envelope.

Table 8.1 Air permeability standards

Building standards	Maximum air permeability [$m^3/(h\ m^2)$ @ 50 Pa]
AD L1A of Building Regulations (2010)	10 (0.5 ach^{-1})
EST (naturally ventilated)	7 (0.35 ach^{-1})
EST (mechanically ventilated with heat recovery unit)	4 (0.2 ach^{-1})
The Netherlands	6 (0.3 ach^{-1})
Germany (air changes per hour at 50 Pa)	1.8 ~ 3.8 (n50 h^{-1})
PassivHaus	<1 (0.1 ach^{-1})
Super E (Canada) (air changes per hour at 50 Pa)	1.5 (0.075 h^{-1})

Note: Energy Saving Trust (EST), Approved Document L1A (AD L1A)

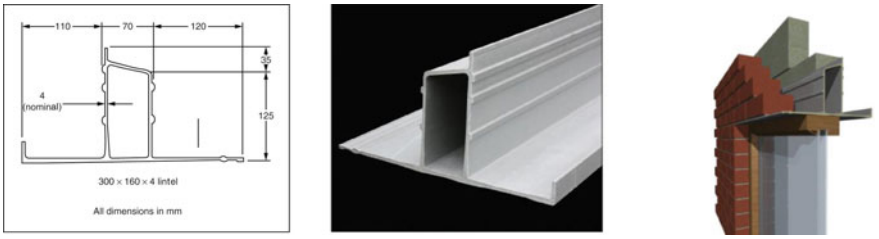

Fig. 8.3 GRP lintel profile and exterior

Table 8.2 Thermal characteristics of a GRP lintel

Lintel type	CO_2 emissions (kg CO_2 per kg)	U-value (W/m^2 K)	Linear thermal bridge Heat loss, Ψ Psi value (W/m K)
Steel Lintel	1.91	2.94[a]	0.287
GRP Lintel	5.5	0.833	0.04

[a]Minimum R-value for the lintel is 0.34 m^2 K/W [13]

8.2.4 GRP Lintel

A GRP lintel is made of glass reinforced plastic which makes it high load bearing yet lightweight and has a profile as shown in Fig. 8.3 and a mass of 5.96 kg/m. It is suitable for use in external or internal walls of 100 mm brick/block work with a 75–100 mm cavity, and clear openings of between 400 and 1,700 mm, to support walls, floors, roofs, or a combination of these structures, above window or door openings [13].

Table 8.2 shows the thermal characteristics of a GRP lintel comparing with a conventional Steel lintel. GRP lintels have a very low heat transmitter rate. Thus, it is possible to reduce the effect of thermal bridging by replacing a conventional Steel

Table 8.3 Adopted building standards (U-value and ach^{-1})

Unit	No insulation	2006 Building regulation	Best practice	Case study home
Wall	2.071	0.35	0.25	0.23
Floor	1.463	0.25	0.15	0.1
Roof	1.54 (flat) 2.93 (pitch)	0.25 (flat) 0.16 (pitch)	0.15	0.14
Window/door	6.121	1.978	1.978	2.26
Air infiltration	1	0.5	0.3	0.5

lintel with a GRP lintel. The thermal profile of a GRP lintel is also adopted further in energy simulation analysis.

8.3 Methodology

8.3.1 Case Study Home and Building Standards

In order to carry out simulation studies, a four bedroom terraced house with a TFA of around 140 m^2 has been modelled within a dynamic computer software package, in this case DesignBuilder [14]. The properties are of timber frame construction and built using off-site manufacturing techniques. The internal panelling consists of a vapour permeable paper based membrane, wrapped and sealed into door and window openings with cellulose fibre insulation also for sound reduction in partitioning wall units. Total external walls are built up to achieve a U-value of 0.21 W/m^2 K and a minimum SAP rating of 100 (B rated) [4].

The case study house was adopted with three different building standards which are as follows: 'No Insulation', '2006 Building Regulation' and 'Best Practice'. Table 8.3 and Fig. 8.4 provide more details on building fabric (thermal characteristics) and floor plans.

8.3.2 Energy Bill and Carbon Dioxide Emissions

As part of the computer simulations studies, the DesignBuilder [14] software has been used for calculations of the heating energy consumption based on a certain geographical location and climatic data, in this case London. In the simulations, both the CO_2 emissions and the energy bills have been calculated with values of unit price and CO_2 emissions rate referenced from SAP 2009 [4] as shown in Table 8.4). From the energy bills calculated, the annual savings have been estimated with simplified payback periods for each by also calculating the installation of GRP lintels through different building standards.

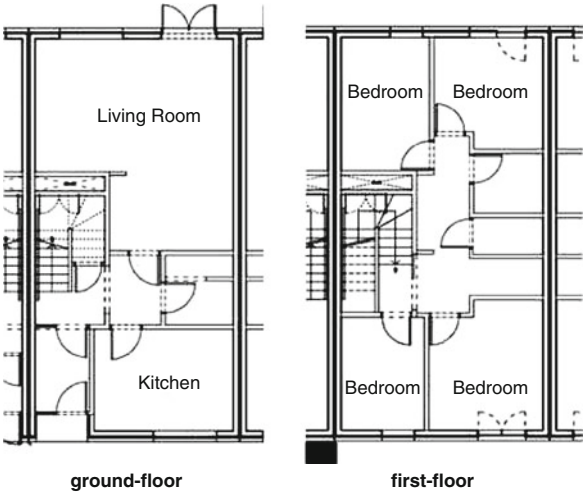

Fig. 8.4 Case study home (four bedroom terraced house) floor plans

Table 8.4 Unit price and CO_2 emissions from energy sources in SAP 2009 [4]

Unit	Unit price (p/kWh)	CO_2 emissions (kg/kWh)
Gas	3.10	0.198

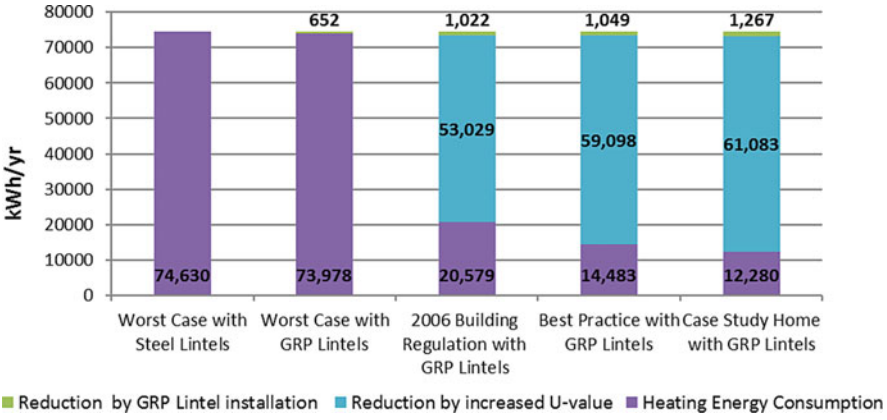

Fig. 8.5 Heating energy consumption and reduction breakdown

8.4 Results and Discussion

8.4.1 Energy Consumption

Figure 8.5 shows the heating energy consumption compared with the worst case scenario with GRP lintels installed through different building standards.

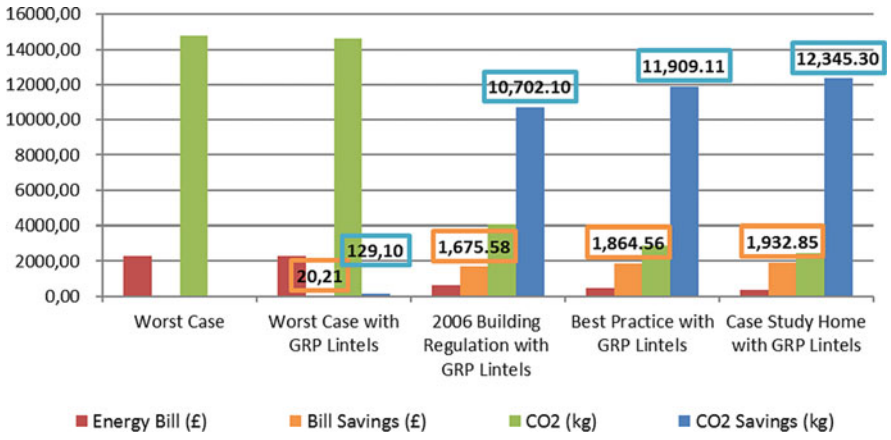

Fig. 8.6 Overall energy bill and CO_2 savings

The simulation results have indicated that a GRP lintel with a high insulation level of building standard shows better performance of heating energy consumption providing better energy efficiency. Using GRP lintels within a non-insulated house due to thermal bridging through building fabric and junctions reduces heating energy consumption by 652 kWh/year. However, introducing insulation into the building fabric would significantly improve the heating energy savings compared with the worst case scenario, and the savings are estimated as 54,052 kWh/year, 60,147 kWh/year and 62,350 kWh/year for different standards as follows: '2006 Building Regulation with GRP Lintels', 'Best Practice with GRP Lintels' and 'Case Study Home with GRP Lintels' respectively. In summary, it can be seen that the majority of the reduction is made by increasing insulation levels in the building fabric. However, the results also show that increasing thermal properties of the building fabric with the use of a GRP lintel helps to further improve the heating energy reduction.

The best case scenario in this case is the 'Case Study Home with the GRP lintels', showing savings of a further 10 % of heating energy consumption, which also provided a clear view on why a highly insulated dwelling should consider reducing its thermal bridges. Well detailed and constructed buildings would therefore result in huge reductions in heating energy consumption with additional reductions obtainable from eliminating thermal bridges.

8.4.2 Cost and Carbon Dioxide Analysis

Figures 8.6 and 8.7 show the overall energy bills by also using the GRP lintels together with CO_2 emissions from heating energy savings. After introducing insulation into the building fabric, there are significant savings in energy bills as

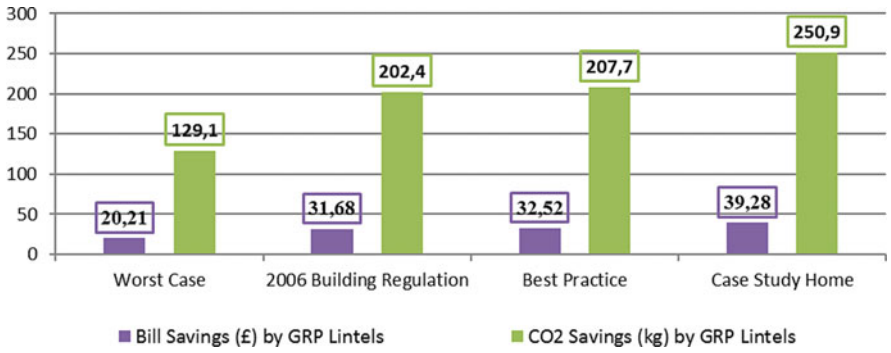

Fig. 8.7 Energy bill and CO_2 savings by GRP lintels

expected that can be made and again reduction in associated CO_2 emissions. As mentioned above, most of the reductions were made by increasing the building fabric's thermal properties and in addition, the GRP lintel installation has contributed to further reduction in heating energy bills and associated CO_2 emissions as shown in Fig. 8.7.

Figure 8.7 shows how the impact of GRP lintels on energy bills and CO_2 emissions through savings using different building standards. Again, the better the insulation levels are with GRP lintels the better the performance results are in terms of overall savings in energy bills and CO_2 emissions. However, the savings between '2006 Building Regulation' and 'Best Practice' cases are almost insignificant, and therefore further studies should be undertaken to investigate the likely reasons behind this.

8.4.3 Payback Analysis

The payback period for the GRP lintel installation has been calculated within the case study home considering various building standards which was also based on heating energy bills as shown in Table 8.5. Total length of GRP lintels within a selected dwelling is about 13.3 m and the unit price of a GRP lintel is provided by the supplier company [13]. The total difference in unit price between the supply of a GRP lintel and a Steel lintel is around £400 per house (the price is excluding labour charge and transportation). Thus, the best payback period is estimated in the case study home with GRP lintels as around 10.2 years and in the worst case scenario as almost 20 years. The payback periods shown in Table 8.5 represents the additional values for installing GRP lintels in new build homes instead of Steel lintels.

Table 8.6 shows typical payback periods for energy efficiency measures in a case study house. Most of these improvements are allowances received through grants from either the UK government or energy suppliers, and as a result, the payback periods are much shorter. However, these measures should not be compared

Table 8.5 Payback periods

Case	Reduction (kWh/year)	Energy bill savings (£/year)[a]	Payback period (year)[b]
Worst case scenario with GRP lintels	652	20.2	19.8
2006 Building regulation with GRP lintels	1022	31.7	12.6
Best practice with GRP lintels	1049	32.5	12.3
Case study home with GRP lintels	1267	39.3	10.2

[a]Unit price is 3.10 p/kWh for gas [4]
[b]Total length of the GRP lintel used is about 13.3 m required for installation in a case study home and the total price for is around £532 [13]

Table 8.6 Typical payback periods in home improvement (as part of energy efficiency)

Improvement	Installation cost[a]	Annual savings	Payback period
Hot water tank insulation	£12	£40	5 months
Hot water pipe insulation	£10	£10	1 year
Loft insulation (270 mm)	£199	£205	Less than 1 year
Suspended timber floor insulation	£90 (DIY)	£50	2 years
Cavity wall insulation	£149	£160	Less than 1 year
Draught proofing	£90 (DIY)	£30	3 years
Solar PVs	£11,700	£1,200	Around 10 years
Solar thermal	£4,000	£650	Around 6 years

[a]Costs are average values based on UK government grants [5]

directly with the GRP lintel installation as lintel is more directly related to construction detailing rather than energy efficiency.

8.4.4 Temperature and Humidity Distribution Analysis

Two-dimensional temperature (°C) and relative humidity (%) profiles through the GRP lintel under winter conditions have been simulated. The boundary conditions are as follows: Temperatures for internal and external conditions are adopted as 20 °C and 5 °C; relative humidity levels for internal and external conditions are adopted as 55 % and 84 % respectively. Figure 8.8 illustrates the results, in this case temperature distribution as shown on the left and relative humidity distribution as shown on the right. From the results (see Fig. 8.8d), it can be concluded that filling the box cavity of a GRP lintel would not be recommended and even a GRP lintel filled with insulation gives a negative impact on the surface temperature distributions, it would have no effect on the reduction of thermal bridging. On the other hand, the Steel lintel shows that heat losses through a Steel lintel are significant and therefore, there is a very high likely risk of condensation around internal surface of window frames and also at the attached internal wall surfaces. This also provides

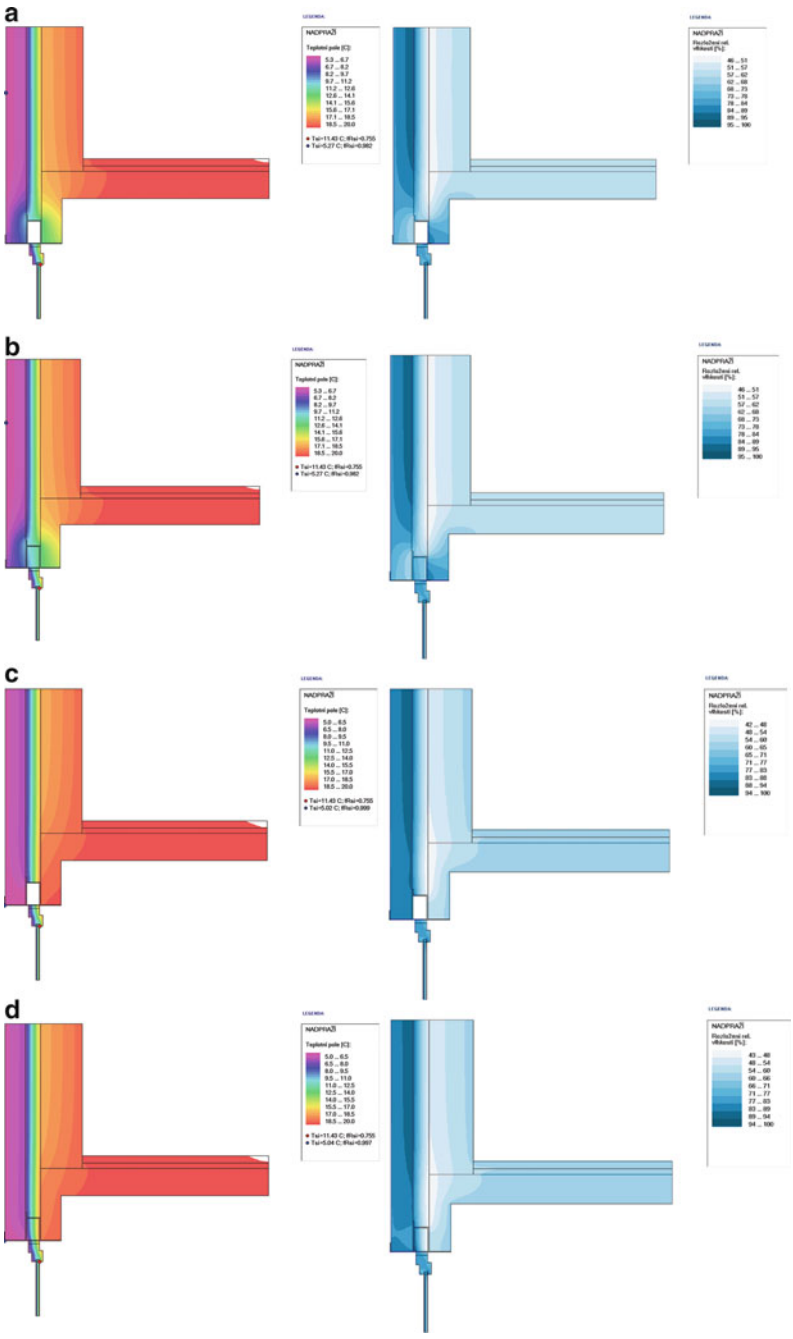

Fig. 8.8 Two-dimensional temperature and humidity distributions. (**a**) Steel lintel, (**b**) steel lintel filled with insulation, (**c**) GRP lintel, (**d**) GRP lintel filled with insulation

further impact on the health of occupants and may likely to cause problems due to mould growth on indoor surfaces.

The red circles show where the thermal bridges occurred and where there are risks of condensation. An especially high risk of condensation could occur between a window frame and a lintel where the surface temperature is around 13 °C and the relative humidity level is over 90 %. On the contrary, the window with a GRP lintel shows better performance as it almost eliminates of thermal bridging. The internal wall surface temperature is almost the same with room temperatures and humidity levels that are within an acceptable range without any condensation problems. To prevent interstitial condensation between the external brick and the cavity insulation layer, vapour barriers should be installed.

8.5 Conclusions

The studies were carried out to investigate the impact of Fulbrook Glass Reinforced Plastic (GRP) lintel [13] on heating energy consumption. In terms of energy consumption, a better insulated home with GRP lintels shows a better performance in terms of heating energy consumption, CO_2 emissions and overall energy bills. However, the most significant result of these reductions would be achieved through the improvement of building fabric's thermal property. Moreover, the reduction achieved from the GRP lintel installation should not be ignored, especially as demonstrated in the best case scenario, i.e. in the case study home with GRP lintels, which gave a further 10 % energy demand reduction compared with the other scenario where there was no GRP lintel installation in the case study home as shown in Fig. 8.9.

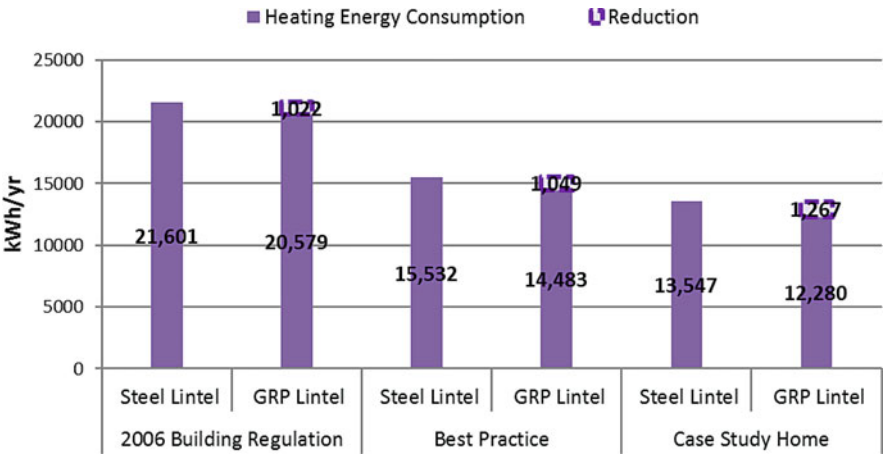

Fig. 8.9 Heating energy savings due to GRP lintel incorporated with different building standards

The two-dimensional temperature and humidity distribution studies showed that the GRP lintel installation could reduce thermal bridges significantly around junctions. In terms of the condensation risk, under typical winter conditions, the Steel lintel installation would have high risks for condensation and again may cause further health implications with mould growth on indoor surfaces. On the other hand, the GRP lintel installation shows better results in terms of minimising heat losses at and around lintel profiles, and at the same time helps keeping dry the area around the junctions. Therefore, the condensation risks would be very low, much lower than a conventional Steel lintel.

The study has undertaken dynamic computer simulations to calculate heating energy consumption and to provide cost and CO_2 analysis for the GRP lintel installation. The results have given some ideas for energy efficiency as well as cost benefit analysis for the GRP lintel use by also considering various different building standards. However, without a post occupancy monitoring of a live project and a case study home with the GRP installation, it is difficult to cross-check the results obtained in the simulations and to also validate them. Therefore, further studies are planned for the near future.

Acknowledgements The authors would like to thank Chris Sullivan (Material Edge Ltd) for providing information about a GRP lintel (The Litel®) and Prof. Dr. Jitka Mohelnikova at Brno University of Technology – Faculty of Civil Engineering (VUT FAST Brno) for her input and advice. The authors would also like to thank the Building Environments Analysis Unit (BEAU) Research Centre (2007–2013) at the University of Sheffield and the British government funding Engineering and Physical Sciences Research Council (EPSRC) for making this research collaboration possible.

References

1. HM Treasury (2006) Pre-budget report 2006, investing in Britain's potential: building our long-term future. HM Treasury, London
2. DECC (2011) Annual report on fuel poverty statistics 2011. National Statistics, Department of Energy & Climate Change (DECC)
3. LSI. Low carbon housing, learning zone, Leeds Metropolitan University, Leeds Sustainability Institute (LSI). http://www.leedsmet.ac.uk/teaching/vsite/low_carbon_housing/thermal_bridging/introduction/index.htm. Accessed on 24 Feb 2012
4. BRE (2010) The government's standard assessment procedure for energy rating of dwellings 2009 edition. Building Research Establishment (BRE), Garston, Watford
5. EST (2010) CE317—Domestic low and zero carbon technologies: technical and practical integration in housing. UK. Energy Saving Trust (EST)
6. CLG (2009) English Housing Condition Survey 2007. Annual report, Communities and Local Government (CLG)
7. NHBC. Approved Document Part L 2010: Special Edition. Technical Extra, September 2011, Issue 03, National House Building Council (NHBC). http://www.nhbc.co.uk/NHBCPublications/LiteratureLibrary/Technical/TechnicalExtra/filedownload,44601,en.pdf. Accessed 24 Feb 2012

8. Government of Ireland (2008) Limiting thermal bridging and air infiltration: acceptable construction details. Report by Department of the Environment, Community and Local Government, HomeBond, Sustainable Energy Ireland (SEI), July 2008
9. EST (2005) Guide GPG224—improving airtightness in dwellings. Energy Saving Trust (EST)
10. BRE (2006) BRE Information Paper IP 1/06—assessing the effects of thermal bridging at junctions and around openings. Building Research Establishment (BRE), Garston, Watford
11. HM Government (2010) The Building Regulation 2010: conservation of fuel and power in new dwellings. Approved Document Part L1A. HM Government, London
12. Stephen RK (1998) Airtightness in UK dwellings: BRE's test results and their significance. BRE Report 359. Building Research Establishment, Garston, Watford
13. Litel. LITEL®. http://litel.co.uk/. Accessed 24 Feb 2012
14. DesignBuilder. DesignBuilder software. DesignBuilder Software Ltd. http://www.designbuilder.co.uk/. Accessed 24 Feb 2012

Chapter 9
An Evaluation of Indoor Environment in Deprived Community Housing in Yorkshire and the Humber Region of England, UK

Hasim Altan and Mohamed Refaee

Abstract This study has been undertaken as part of the BIG Energy Upgrade (BEU) a.k.a. Energy Innovation for Deprived Communities (EIDC) project, which aims to provide a detailed understanding of indoor environment and to deliver a new approach to energy efficiency and renewable energy projects within a minimum of ten of the most deprived communities across six Local Authorities in Yorkshire and the Humber region in the UK. It was important for the success of the BEU/EIDC project that detailed monitoring and post occupancy evaluation is performed on a sample of houses before rolling out wider refurbishment. The data were collected from the indoor monitoring equipment for two houses and statistically analysed to investigate the indoor thermal condition and air quality. Air temperature and relative humidity levels within an indoor environment will vary with the time of year and physical indoor environment. However, increased temperature within a confined space such as an indoor environment can create a more suitable environment for the growth of unwanted bacteria and fungi. With the guidelines, it would be reasonable to maintain a temperature of around 23–25 °C within a house. Also, if levels of humidity become too dry, i.e. below 40 % can have adverse effects, some people susceptible to sore throats due to the dryness of the air. Air temperature, relative humidity and carbon dioxide levels were monitored, and the results have been compared with the accepted standard guidelines such as ASHRAE and CIBSE. The results showed that the indoor thermal environment conditions in the two naturally ventilated homes had a mean air temperature and relative humidity of 20.5 °C and 47 % respectively during autumn season. The mean CO_2 levels were in the range 520–1,400 ppm and followed a pattern rising during morning and evening periods in response to human indoor activity. Detailed analysis of CO_2 at four periods during the day showed that afternoon times contained lower values of CO_2 compared with morning and evening.

H. Altan (✉) • M. Refaee
Faculty of Engineering & IT, The British University in Dubai, Dubai International Academic City, P.O. Box 345015, Dubai, United Arab Emirates
e-mail: hasim.altan@buid.ac.ae; m.refaee@gmail.com

I. Dincer et al. (eds.), *Progress in Sustainable Energy Technologies Vol II: Creating Sustainable Development*, DOI 10.1007/978-3-319-07977-6_9

Keywords Indoor environment • Social housing • Energy innovation • Post occupancy monitoring

9.1 Introduction

In the United Kingdom, buildings contribute about 45 % of its overall annual carbon dioxide (CO_2) emissions, with more than a quarter coming from the existing domestic buildings. For the country to meet its 80 % CO_2 reduction target by 2050 (from the 1990 baseline), it will need extensive refurbishment of existing buildings to improve their energy efficiency [1].

A study on determinants of winter indoor temperatures in low income households in England [2–4] showed that statistical distribution indicated very low and wider variation in indoor temperatures due to the efficiency of the heating systems and insulation. Moreover, the study shows that a clear relationship between temperature and required energy use. In another field study [5], it was found that factors influencing occupant window opening behaviours are the outdoor air temperature i.e. the higher the outdoor temperature is the most likely the window is to be opened by the home residents. In addition, it was illustrated that other factors can motivate opening of windows such as outdoor relative humidity and wind speed.

An investigation was carried out on different cities in China [6], the main aim of the study was to investigate the actual conditions of the residential indoor thermal environment for evaluating thermal comfort and predicting the energy conservation feasibility for space heating and cooling. Some homes in one area showed that the winter indoor thermal conditions was at a stable level and maintaining comfort due to central heating system and relative humidity levels were relatively low. In another city the indoor air temperature was found relatively low and as a result, indoor conditions were uncomfortable during winter period, however in summer, it was found that indoor air temperatures were relatively high.

Indoor thermal condition can be varied within acceptable limits due to casual heat gains from domestic appliances and indoor human activities [3]. Isakssona and Karlsson presented some results from their study of indoor climate in low energy houses by using qualitative and quantitative methods. Their study also indicated that different dwelling topology can affect the heat gains through common walls and floors. The indoor environment is an influential factor to environmental quality [7]. People spend a majority of their time in buildings; the average western person spends up to 85 % of their life in a building, or in a vehicle conveying them from one building to another [8].

Increasing the attention to indoor air quality has contributed to the awareness of poor health associated with a poor indoor environment. Two types of illnesses related to poor indoor air quality have been identified: Sick Building Syndrome (SBS) and Building Related Illness (BRI). While the definition of SBS varies slightly in the literature, SBS can be defined as the discomfort or sickness associated with poor indoor environments with no clear identification of the source

substance. BRI is defined as a specific recognised disease entity caused by some known agents that can be identified clinically [9, 10].

This study has been undertaken as part of the BIG Energy Upgrade (BEU), also known as the Energy Innovation for Deprived Communities (EIDC) project, which aimed at delivering a new approach to energy efficiency and renewable energy projects within a minimum of ten of the most deprived communities across six Local Authorities in Yorkshire and the Humber region in England, UK. The properties have been assessed by energy efficiency experts and then brought up to the modern standards with a range of measures including so-called smart electricity meters, heating system upgrades, boiler replacements, wall and loft insulation, double glazing, insulated cladding, and even solar panels where appropriate. It was important for the success of the BEU/EIDC project that detailed monitoring and post occupancy evaluation was performed on a sample of houses before rolling out a wider refurbishment (i.e. retrofit). The aim of this study was to investigate indoor environments of the two deprived community homes (in this case homes were chosen from Kirklees area in Yorkshire, England UK) before retrofit and to correlate with energy consumption.

9.2 On-Site Measurements and Monitoring

Indoor air temperatures and relative humidity levels were measured at the two selected homes using HOBO U12-012 and U10-003 data loggers [11]. Indoor carbon dioxide levels were also recorded in the two pre-refurbished homes using Telaire 7001 CO_2 meters [12]. Although CO_2 is not toxic it is commonly used as an indicator of air quality. High levels of CO_2 indicate inadequate ventilation in an indoor space. All HOBO U12-012 data loggers and CO_2 meters were placed in the living room in each selected home, specifically in the breathing zone of a person sitting on a sofa (approximately 1.5 m above the floor), and away from open windows. In addition, participants were requested to behave as normal within their homes during the monitoring period in order to obtain realistic data. Again, HOBO U10-003 data loggers were placed in the bedroom in each selected home. This particular HOBO data logger is only used for two channel inputs i.e. measuring two variables, which in this case are indoor air temperature and relative humidity levels.

The objective of monitoring indoor air quality was to gain an insight into conditions within deprived communities, i.e. residents' homes, and to compare indoor environmental conditions i.e. air temperature (°C), relative humidity (RH) and carbon dioxide (CO_2) levels with the accepted standards/guidelines. Average levels of each variable were collected in 15-min intervals over a 24-h period for periods of 2 weeks. Electric energy consumption was collected via installed smart meters. Table 9.1 and Fig. 9.1 describe the type of dwelling, age, tenure, window type, ventilation method, cooker type, and number of occupants, and their ages of the selected houses within Kirklees area, Yorkshire, UK.

Table 9.1 Description of the two selected dwellings

Description	Dwelling K1	Dwelling K2
Type of building	Semi-detached	Semi-detached
Home age (year)	65	65
Dwelling—tenure	Rented	Owned
Window type	Fully double glazed	Fully double glazed
Ventilation	Natural—at least one window open every day	Natural—at least one window open every
Cooker type	Electric	Electric
No. of occupants and ages	4 (67, 65, 38 and 37 years)	3 (60, 57 and 33 years)

Fig. 9.1 Photos of the two semi-detached dwellings (K1 *left* and K2 *right*)

9.3 Results and Discussion

To investigate the indoor thermal condition and air quality in the two selected dwellings, data were collected from the indoor monitoring equipment and then statistically analysed.

The American Society of Heating, Refrigerating and Air Conditioning Engineers (ASHRAE) authority recommends that carbon dioxide levels should not exceed 1,000 ppm (parts per million) inside a space [13]. The reason to use ASHRAE as CO_2 standard guideline is that there are no UK CO_2 standards for indoor air quality. However, CO_2 is not toxic but it is used as a guide to whether or not a space has a sufficient quantity of fresh air. Figure 9.2 shows the percentage of CO_2 levels for 1 week. It can be seen that in home one (K1), the CO_2 reaches a level of 400 ppm of 70 % of the time during the week. Home two (K2) on the other hand, reaches a level of 600 ppm of 60 % of the time during the week. The levels above the recommended value (1,000 ppm) occurred about 30 % of the time.

Figure 9.3 shows the indoor CO_2 levels of the living rooms in two homes for 1 week. As can be seen that the levels are fluctuating around the recommended

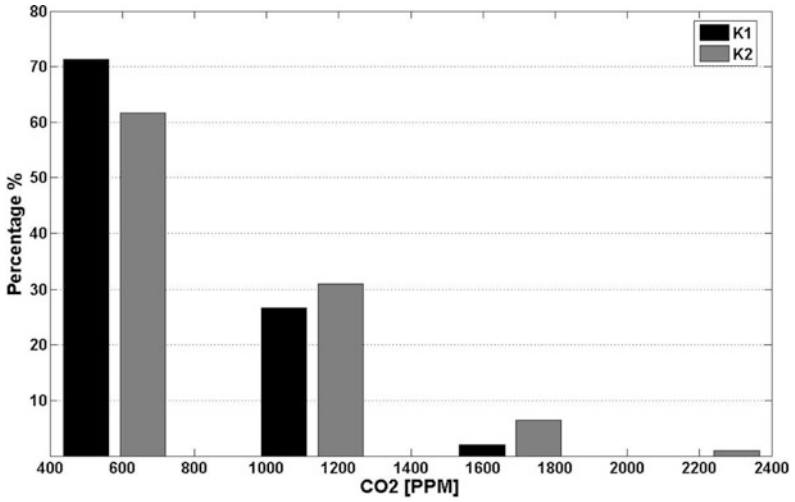

Fig. 9.2 Percentage of CO_2 during 1 week in both selected dwellings

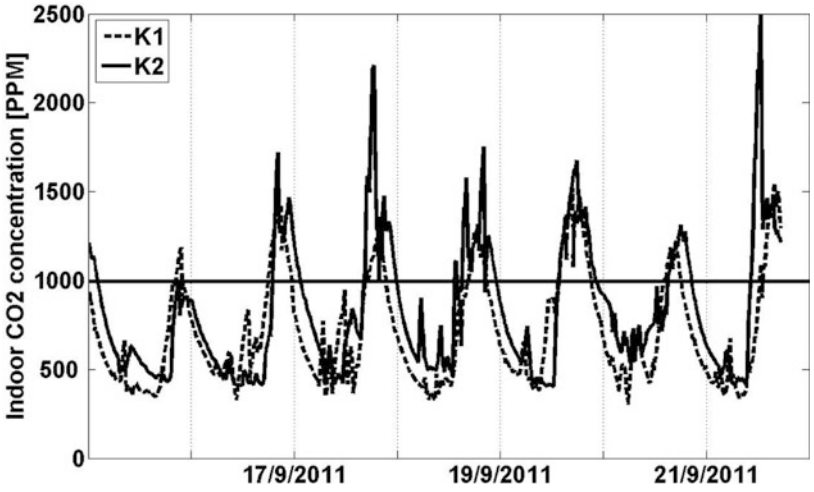

Fig. 9.3 Levels of CO_2 in the two living rooms for 1 week

value (1,000 ppm) for indoor spaces, in this case for the living rooms. A random day was chosen (16th September 2011; 16/9/2011) as a snapshot to plot its CO_2 concentration against time to investigate the behaviour of carbon dioxide during that day.

Figure 9.4 indicates that the indoor CO_2 levels followed a pattern in the two homes where the levels were seen to be less than 1,000 ppm during early morning and throughout day time, later rising at evening and night time due to the increase of

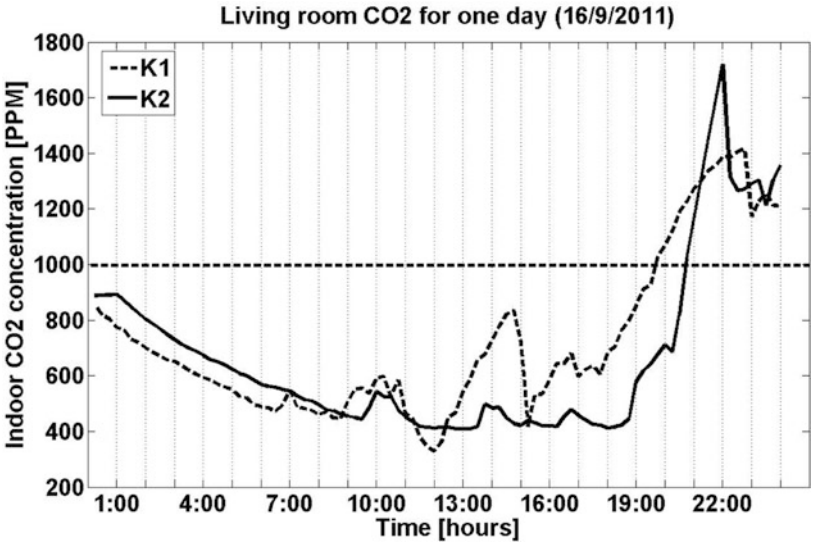

Fig. 9.4 Level of CO_2 in the two living rooms for 1 day

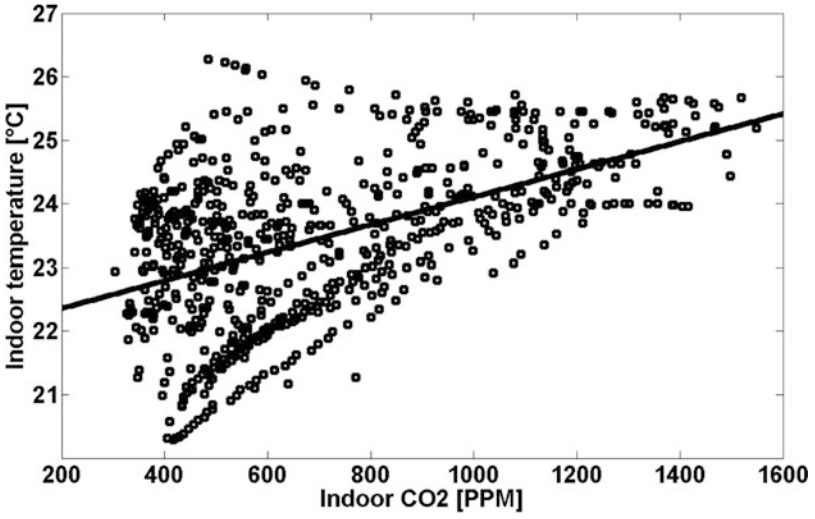

Fig. 9.5 Correlation of daily temperature and daily carbon dioxide levels

human activity and the lack of ventilation i.e. not opening windows during evening and night time.

Daily indoor air temperature and daily CO_2 levels were correlated with statistically significant results ($r = 0.51$, $P = <0.05$). Figure 9.5 shows this direct (positive) relation. The results indicated that the warmer space has lack of air ventilation rates

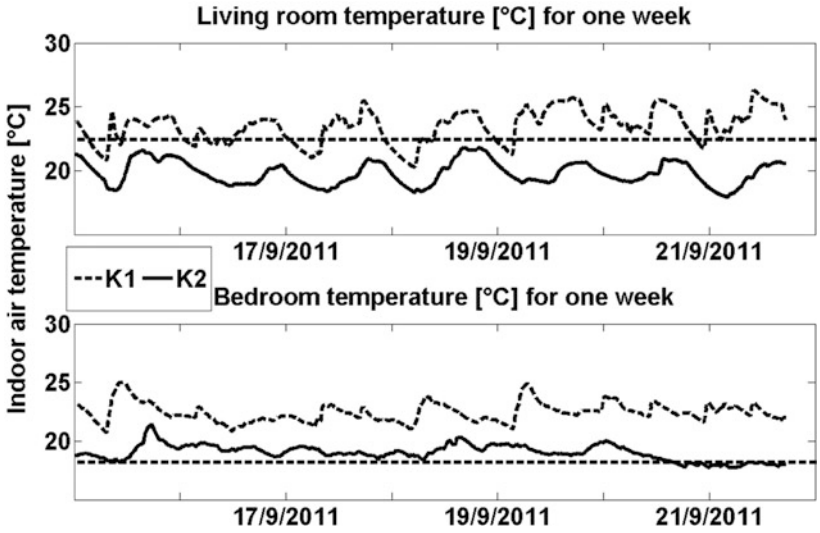

Fig. 9.6 Daily mean indoor temperature profile in the living rooms and the bedrooms of the two selected homes for 1 week

and therefore the CO_2 levels are higher as a result, which also reflected on the dilemma of achieving proper ventilation rates while maintaining indoor thermal comfort.

The indoor temperature pattern should be maintained between 22 and 23 °C within living room space and between 17 and 19 °C within bedroom spaces [14]. The results have been compared with the published standards and guidelines which are also the accepted benchmarks, i.e. can be seen as good practice cases.

Figure 9.6 presents the daily mean indoor air temperature (°C) of the living room and the bedroom in the two selected homes for 1 week (15/9/2011 to 21/9/2011). The dashed line in Fig. 9.6 is the minimum internal air temperature of 22 °C as recommended for living room space and again of 18 °C as recommended for bedroom space. In comparison with the standard guidelines (i.e. the minimum and the maximum levels), it is clear that one home (K2) did not perform accordingly within the CIBSE recommendation for the range of internal temperatures (22–23 °C) in the living room space while the other home (K1) performed accordingly within the limits of acceptability. On the other hand, the standard guideline of internal temperatures (17–19 °C) for the bedroom space has been met within the bedrooms of the two selected homes.

The limits of acceptability has been evaluated and determined by the recommended standards and guidelines which in this case, ASHRAE and CIBSE [13, 14].

Figure 9.7 shows the frequency distribution of different temperature values occurred per week within the living room and the bedroom spaces of the two dwellings. The living rooms of K1 and K2 homes have the value of 19 and 23 °C

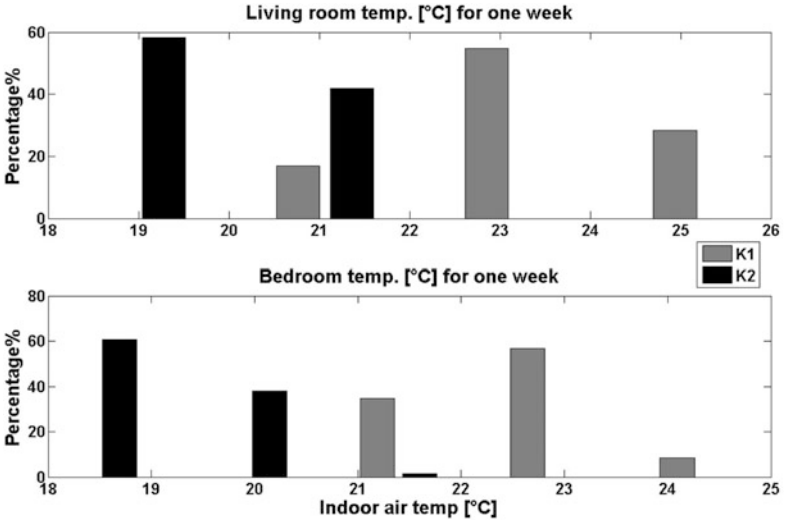

Fig. 9.7 Percentage of indoor temperature for living room and bedroom spaces of the two homes during 1 week

respectively which are the most often occurred values per week. Again, the bedrooms of K1 and K2 homes showed the same results as the two separate living rooms as indicated in Fig. 9.7.

The recommended level of indoor relative humidity should be between 40 and 70 % [13]. If levels of humidity become too dry, i.e. below 40 %, this can have adverse effects, some people susceptible to sore throats due to the dryness of the air.

Figure 9.8 presents the daily mean indoor relative humidity (RH%) of the living room and the bedroom in the two selected homes for 1 week (15/9/2011 to 21/9/2011). The dashed lines in Fig. 9.8 define the comfort zone which is the range of internal relative humidity levels between 40 and 70 % as recommended for indoor spaces. In comparison with the standard guidelines (i.e. the comfort zone), it is clear that both homes (K1 and K2) did perform accordingly within the ASHRAE recommendation for the range of internal relative humidity levels (40–70 %) in both the living room and the bedroom spaces. On the other hand, the standard guideline of internal temperatures (17–19 °C) for the bedroom space has been met within the bedrooms of the two selected homes.

Figure 9.9 shows the frequency distribution of relative humidity values occurred per week within the living room and the bedroom spaces of the two dwellings. The living room of K1 home has the most occurring values ranged from 40 to 50 % while the bedroom of same home ranged from 45 to 55 % respectively which are the most often occurred values per week. On the other hand, the living room and the bedroom of K2 home have values above 60 % as shown in Fig. 9.9.

In summary, the results of the investigation has shown that the measured values of temperature and relative humidity did meet the recommended standards and guidelines except the living room indoor conditions for one of the selected homes

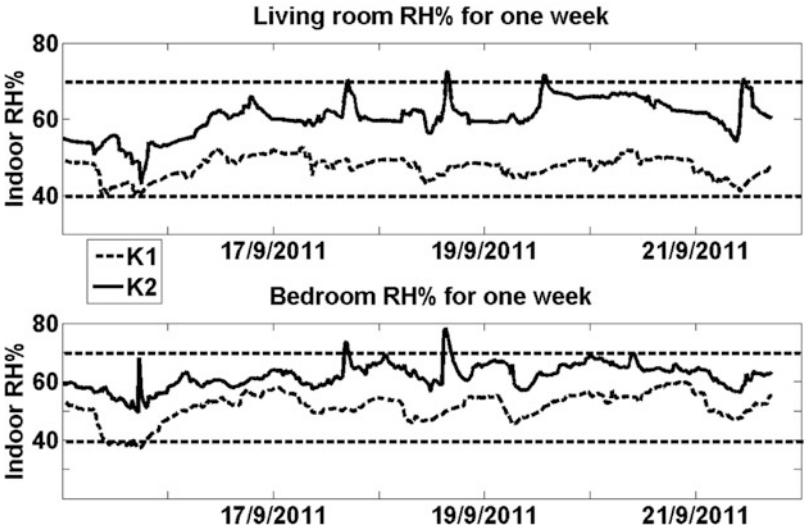

Fig. 9.8 Daily mean indoor relative humidity profile in the living rooms and the bedrooms of the selected homes for 1 week

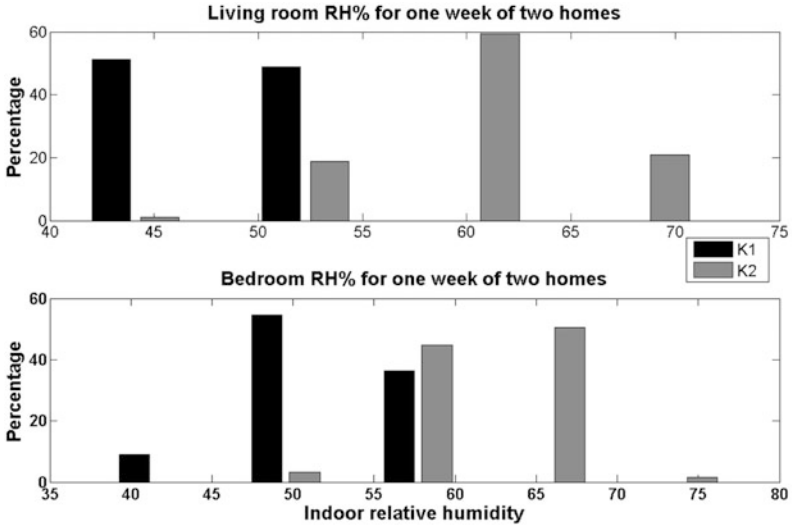

Fig. 9.9 Percentage of indoor relative humidity for living room and bedroom spaces of the two homes during 1 week

where the values of temperature were below that of recommendation levels. In addition, it was found that there was a proportional relation between indoor temperature and carbon dioxide levels which reflected on the dilemma of achieving proper ventilation rates while maintaining indoor thermal comfort. The average

relative humidity on the other hand, for the living room and the bedroom agreed with the standard guidelines for both homes. Moreover, the level of CO_2 is fluctuating around the recommended value of 1,000 ppm for indoor space where the levels were seen to be below this value during early morning and day time, and later rising at evenings and night time due to the increase of human activity and the lack of ventilation indoors.

9.4 Conclusions

This study aimed to investigate indoor environment conditions, particularly air temperature, relative humidity and carbon dioxide levels, in the two case study dwellings as representative homes from within the deprived communities of Yorkshire region, UK before a major refurbishment programme called the BIG Energy Upgrade (BEU). To further generalise the results for the deprived communities across the UK, it would be necessary to do more sampling on a larger population. Although this study is based on a limited number of samples, in this case two homes, it is believed that the results are still representative of the similar dwellings across different regions in the country and therefore it is important to plan ahead bespoke measures and again innovative solutions for mass retrofit/refurbishment of the existing social housing.

Acknowledgements This paper is the result of the work undertaken as part of the BIG Energy Upgrade Programme (BEU). The project has attracted £7 million from the European Regional Development Fund through the Yorkshire and the Humber ERDF Programme 2007–2013. The authors would like to thank the Building Environments Analysis Unit (BEAU) Research Centre (2007–2013) at the University of Sheffield for making this research collaboration possible between both authors.

References

1. NRC. National Refurbishment Centre (NRC). http://www.rethinkingrefurbishment.com/. Accessed 26 Mar 2012
2. Oreszczyn T, Hong S, Ridley I, Wilkinson P (2006) Determinants of winter indoor temperatures in low income households in England. Energy Buildings 38:245–252
3. Altan H, Refaee M, Han L, Noguchi M (2013) Measured home environment and energy consumption compared to accepted standards. Open House Int 38(3):64–71
4. Refaee M, Altan H (2013) Trends of indoor environment and energy consumption incidence by human activities. J Eng Technol 2(2):110–115
5. Zhang Y, Barrett P (2012) Factors influencing the occupants' window opening behaviour in a naturally ventilated office building. Energy Environ 50:125–134
6. Yoshino H, Yoshino Y, Zhang Q, Mochida A, Li N, Miyasaka Z (2006) Indoor thermal environment and energy saving for urban residential buildings in China. Energy Buildings 38:1308–1319

7. Isakssona C, Karlsson F (2006) Indoor climate in low-energy houses—an interdisciplinary investigation. Build Environ 41:1678–1690
8. Saunders T (2002) The boiled frog syndrome: your health and the built environment. Thomas Wiley Academy, West Sussex
9. Molhave L (1987) The sick buildings—a sub-population among the problem buildings. In: Seifert B, Esdorn H, Fischer M (eds) Indoor Air'87, vol 2, Proceedings of the IV international conference on indoor air quality and climate. Institute for Water, Soil and Air Hygiene, Berlin, pp 469–473
10. Burge S, Hedge A, Wilson S (1987) Sick building syndrome: a study of 4373 office workers. Ann Occup Hyg 31:493–504
11. Onset. Onset Hobo Loggers. http://www.onsetcomp.com/products/. Accessed 22 Apr 2014
12. MicroDAQ. Telaire 7001 carbon dioxide monitor. http://www.microdaq.com/telaire/. Accessed 22 Apr 2014
13. ASHRAE (1992) ASHRAE Standard 62: ventilation for acceptable indoor air quality. American Society of Heating, Refrigerating and Air Conditioning Engineers (ASHRAE), Atlanta, GA
14. CIBSE (2006) Environmental design CIBSE guide A. Chartered Institution of Building Service Engineers, London

Chapter 10
The Application of Phase Change Materials to Improve the Climate Resilience of a Low-Energy Prototype House

Lucelia Rodrigues, David Tetlow, Mark Gillott, and Vasileios Sougkakis

Abstract Due to a number of reasons including the effects of climate change and a shift towards a more widespread use of Modern Methods of Construction (MMC) for housing development, overheating issues in British homes has become a greater concern in recent years. Some of the most important advantages of MMC are the reduced use of materials, reduced construction time (particularly on site), reduced weather dependency, reduction of waste production, the possibility of reuse and recycling of components, and the possible lightness of the structure. MMC systems can deliver highly insulated, almost airtight homes, in line with requirements to reduce energy use for heating. However, they will generally have lower thermal mass than traditional construction and hence be less able to passively control temperature swings in warmer periods. This may contribute to uncomfortably high temperatures, which can affect the well-being and health of the occupants.

The Mark Group Research House, a super insulated steel frame home, was designed to test MMC solutions and innovative technologies, and to be highly energy efficient. In previous work done by the authors, a computer model was used to investigate the house's potential for overheating in today's weather as well as in future climate scenarios. The authors have found that the house was generally comfortable but, despite the addition of mitigating strategies, presented a high risk of overheating that was aggravated when the future climate was considered. This risk was partially attributed to the low levels of thermal mass in the house.

The integration of thermal mass, usually obtained through the use of exposed concrete or brick, can be problematical in MMC dwellings. The use of Phase Change Materials (PCM) may present a solution to this issue. PCM has been proven to work in a number of building applications but not much work has been undertaken investigating its applicability in housing. The work presented in this article reports on the integration of PCM in the Mark Group Research House as a solution

L. Rodrigues (✉) • D. Tetlow • M. Gillott • V. Sougkakis
Faculty of Engineering, University of Nottingham, University Park,
Nottingham NG7 2RD, UK
e-mail: Lucelia.Rodrigues@nottingham.ac.uk; David.Tetlow@nottingham.ac.uk;
Mark.Gillott@nottingham.ac.uk; laxvs4@nottingham.ac.uk

I. Dincer et al. (eds.), *Progress in Sustainable Energy Technologies Vol II: Creating Sustainable Development*, DOI 10.1007/978-3-319-07977-6_10

to the overheating problem identified earlier. The results have shown that the PCM helps to regulate the temperatures in the house even when future climate scenarios are considered. However, it is only effective when coupled with an efficient ventilation strategy, which may not be an easy to implement solution because of its dependency on user behaviour.

Keywords Thermal mass • Overheating

10.1 Introduction

Climate change is becoming a serious issue within the UK and many other worldwide developed economies and overheating in housing has been gaining increasing attention from the research community, the industry and policy makers [1–5]. A large proportion of the country's people now live in densely populated urban based environments, this falls in line with the prediction that 60 % world population will be urban residents within two decades [8]. As a result of the impact of climate change, the current set of UK government climate scenarios indicates that increase on the mean daily maximum temperature could reach 9.5 °C on current levels, the highest variation being 12.3 °C [9].

As a result of the high population and the limited amount of land available, house prices in the UK are very high. This has led to an aging housing stock with low energy efficiency, as mass upgrade is uneconomical. Most UK houses rely solely on natural ventilation alone for cooling during summer periods [1]. This is likely to cause problems in the future if the suggested higher temperatures caused by climate change occur.

In order to rapidly deliver financially affordable houses of better quality, the British government is prioritising the modernisation of the house building sector. This will be done through the promotion of Modern Methods of Construction (MMC). A commitment was given in 2007 to increase the rate of house-building by providing 240,000 additional homes a year in order to complete two million dwellings by 2016 [10, 11]. Simultaneously, an ambitious target was set in 2007 to build all new houses to meet zero carbon dioxide emissions (zero carbon) from 2016. This would mitigate climate change and meet the targets set by the Kyoto Protocol that came into force in 2005 [12].

An issue is present in the fact that the rising risk of overheating may be a result of the effort done in previous decades to reduce energy demand for heating. Buildings have been constructed due to changes in the building regulations, that are highly sensitive to alterations in energy input, especially in MMC configurations with low thermal mass [13]. These are thermally responsive in shorter periods of time (i.e. quickly getting too hot or too cold). A review of existing work has qualified this [14–18] and further discussed in work undertaken by the authors [13, 19]. It is likely that more home owners will seek to install air-conditioning to deal with the problem. These systems that are now financially available to occupants, and has

been suggested that the use of this in the UK is rising by 8 % per year [20], a situation that could lead to an additional annual six million tonnes of carbon emissions by 2020.

One technology that has been research extensively to provide lightweight, high density thermal mass is Phase Change Materials (PCMs) [21–25]. PCMs are a unique technology that store energy in latent form as they change phase from solid to liquid. This is a favourable property as theoretically the material can absorbed large quantities of heat in a relatively small magnitude of space, over a small temperature range. The advantage of this property, in a building application context, is that the technology could be placed into small areas (such as building materials or services) and theoretically has beneficial impacts on moderation of temperature. Phase Change Materials have been used widely since the past decade, despite the fact that their use in buildings was considered since the 1980s [6].

PCMs fall into two categories: inorganic and organic, and due to a number of technical and chemical disadvantages, only organic types are currently used in building applications. For the purpose of this report, discussion of these shall not be elaborated on, however details can be found in the supplied references. It should be noted, however, that the majority of current commercial PCM systems, used in static applications, are supplied in microencapsulated form, i.e. microscopic quantities of PCM (6–20 μm) coated in high density polythene (HDPE) [26–28]. This provides a suitable containment medium for the technology, and allows it to be incorporated into building materials. Without microencapsulation, PCMs would leach out of the system when it became liquid. The cost of microencapsulation is high and this is reflected in the materials it is supplied in. A new technology that could resolve this problem is the use of shape stabilization. This technique involves containing the PCM inside a microscopic polymer based lattice structure, which retains the material after melting and prevents leakage. The technology is well documented and commercial building products utilizing it are now available [29].

Research into PCMs has been done on both active and passive systems. In relation to the former, this has been done in both air conditioning systems [30], and central heating systems [31–33]. In the latter, PCMs have been included into wall systems including: brickwork, concrete and plasterboard [23, 34–36]. The main issue with the use of the technology is its cost, and this is a direct result of the manufacturing implications. This, however, has not prevented a number of UK institutions from adopting the technology and monitoring its impact. The most notable of these is the BASF house on the creative Energy Homes site in the University of Nottingham. This building has plasterboard containing PCM and its performance has been well documented [13, 19, 37]. In light of the costs associated with the technology, necessity caused by the effects of climate change could increase demand for its use. Economically, this would reduce its cost as more efficient methods of manufacture could be invented and increase in commercial competition would drive down price.

The previously mentioned Creative Energy Homes (CEH) project on the University of Nottingham campus provides a unique research facility aiming to stimulate sustainable design ideas primarily using MMC and promote new ways of

providing affordable, environmentally sustainable housing [38]. Each CEH dwelling is fully monitored to provide quantitative data on environmental conditions, energy performance characteristics, micro-generation output and occupancy behaviour. Qualitative data has also been collected. The Mark Group Research House is one of seven dwellings in the CEH. It is an innovative home created to address some of the challenges facing the construction industry by achieving high efficiency and fast construction. The construction methods used were steel frame and polystyrene formwork filled with low carbon concrete. Although the house's design may reduce energy consumption for heating when compared with conventionally built homes, it is likely to cause overheating during the summer as the light structure has little thermal mass and the large glazed areas allow high levels of solar gain to enter. Nonetheless, the MMC industry states that "most framing systems both steel and concrete have about the same effect on a building's energy consumption" [39].

This article presents a research effort undertaken on this property by incorporating PCM technology into its existing design and monitoring the impact on internal temperature. This was done through the use of building simulation using EDSL TAS, a commercial product that has recently provided users the option to incorporate PCMs in its facilities. The results in the paper compound previous research that has already been done on the layout of materials incorporated into the building [7]. Research methodology is provided, in addition to presentation of results, discussion, and conclusions.

10.2 House Design

The house is based on a steel frame design that is highly insulated and extremely airtight. It was filled with mineral wool insulation and externally the frame received polystyrene panels with rendering. The roof allows roof-mounted renewable energy systems and is made of structural insulated panels that comprise integral timber rafters fixed to, and stabilised by, a rigid facing board and filled with polyurethane foam which is sprayed in the factory. A major feature of the house is the integrated sunspace that aims to provide free passive solar heating in the winter and high levels of natural daylight. Windows connect the sunspace to the house and allow warm air to be directly delivered to its main circulation. The top of the sunspace has a connection to the heat exchanger so excess heat can be extracted and used for other purposes. The energy to run the technologies and the house's lighting and appliances is provided by an array of photovoltaic panels. The four-bedroom house, constructed over three levels, includes a basement with garage and a roof space. The total floor area is around 230 m^2 (170 m^2 of heated space). The main entrance is located in the sunspace that provides an intermediate area between outdoor and indoor. Figure 10.1 shows the house plans and section.

The house is designed using passive solar design strategies can have south facing glazing comprising 50 % to practically 100 % of the total facade area as long as solar gains are controlled [40]. It presents much larger windows on the south than

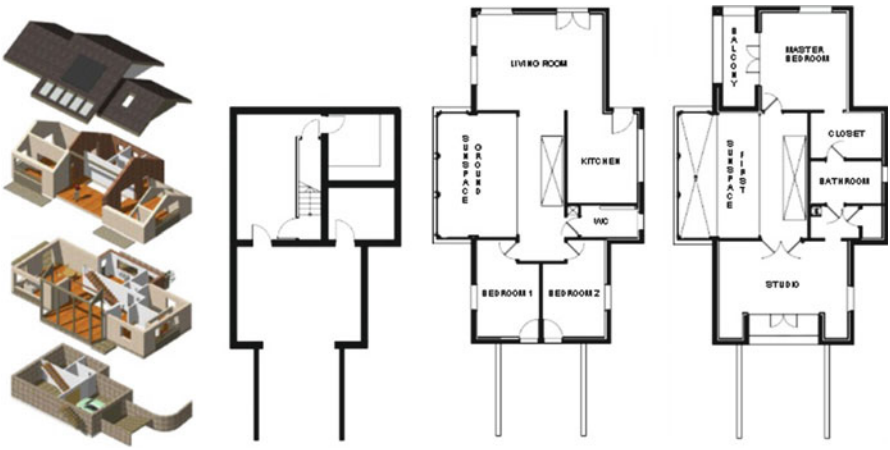

Fig. 10.1 The Mark Group artistic perspective and floor plans (Available at www.creative-energy-homes.co.uk [Accessed on the 10th of August 2009])

any other façade. The windows and external doors (with the exception of those in the sunspace) are made of a composite of timber and aluminium and triple glazed with argon filling with a u-value of 0.71 W/m^2 K. Integrated internal blinds have been incorporated in all the south, southeast and southwest windows to provide controllable solar shading.

Details of the materials the house is constructed from can be found in the following reference [7, 13]. Phase Change Materials (PCM) have been used in an attempt to provide a higher level of thermal mass. In this case, around 100 m^2 of a shape-stabilized PCM board, with an operating temperature between 18 and 22 °C has been used. Every square meter of this board absorbs 730 kJ of heat between the temperatures of 15–35 °C. Shape stabilized PCM board is a new technology and only one company currently markets it within the UK. EDSL TAS has recently included the facility to use this product within its simulation parameters.

The home has a mixed mode hybrid ventilation system which combines natural ventilation, mechanical ventilation and an Earth-Air Heat Exchanger (EAHE). EAHEs, also known as ground pipes, work by using the thermal mass of the earth as a heat sink to condition air that is then delivered to the space. It was installed to provide the sunspace with cooling during summer days and with pre-heated air in winter, which can be further heated up by solar radiation. The system currently installed is made of a single PVC pipe with a diameter of 110 mm and a length of 85 m [41]. The system was buried at a depth of approximately 3 m except when closer to the house where it followed the foundation depth of approximately 2.5 m. The house design envisaged complete monitoring system, which was not installed by the time this work was finished.

10.3 Simulation Model and Methodology

A computer model of the house based on the design was built in EDSL TAS. The materials of the envelope followed those described in the previous section. A series of five dynamic simulations were carried out to analyse the internal conditions of the building in different scenarios and are described in the following section.

Before modifications were made to the materials of the model a base case scenario (Case 1) was run to assess the performance of the house under current UK weather conditions. This included strategies to reduce additional gains, including shading, ventilation, and use of the EAHE. In the subsequent cases the same conditions were applied to the house. The following alterations were then made in the subsequent simulations:

- Case 1: Base case simulation
- Case 2: one layer of PCM board was applied to the ceiling sections of the roof and ground floor section of the sunspace.
- Case 3: As case 2, except two layers of PCM were applied
- Case 4: No PCM was incorporated. Instead all light weight external walls in the house were replaced with insulated precast concrete.
- Case 5: As Case 2, with additional layers of PCM applied to the ceilings of the bedrooms

The assumptions made within the model were as follows:

Weather and Calendar: Data used was the CIBSE Design Summer Year Weather Data (DSY) for Nottingham based on the year 2002. It is assumed that summer is from the 1st of May to the 30th of September and winter is from the 1st of October to the 30th of April.

Internal Gains: The base case simulated the house with ventilation, internal gains, and added the benefit of the EAHE. As no guides are available that provide a suggestion of gains for dwellings [42], the following values were assumed:

Occupants: Four people use the house, a couple in the master bedroom and one in each single. The sensible heat gain for each person was 70 W and the latent was 50 W. Occupancy in circulation spaces was ignored. The sunspace had no occupancy.

Lighting: Provided by low-energy compact florescent bulbs resulting in the following thermal loads when in use: Kitchen: 75 W, Living and dining rooms: 50 W, Bedrooms: 50 W, Circulation: 50 W, Toilet and bathroom: 25 W

Equipment gains: a living room TV was used for 3 h in the evenings producing 150 W. The house's service equipment for heating and hot water is located in the basement causing 10 W for 24 h. In the loft, where the heat exchanger connected to the solar collectors is located, 3 W of gain was applied for 24 h.

Appliances: all items in the kitchen (fridge, cooker, oven, dishwasher and kettle) were simulated with a continuous gain of 10 W.

Infiltration: In all simulations it was placed at 0.2 ACH (atmospheric pressure).

Ventilation: Air movement occurred from outside and within the house (i.e. between the sunspace and circulation zones).

Sunspace external windows (*24 h*): Set to open automatically when the temperature reached 24 °C and fully opened at 28 °C (the design anticipates automation for these windows). They were set to close should the wind reach 2 m/s or the external temperature become warmer than the internal. In winter they were set to open if the circulation zone reached >24 °C.

Sunspace internal windows to circulation (*24 h*): In winter, these would open if the temperature in the sunspace exceeded 18 °C and be fully opened at 21 °C. It would begin to close if the temperature either in the sunspace or in the circulation reached 24 °C. In summer they remained closed. The other windows in the house (living room, kitchen and bedrooms) were set to start opening when temperatures reached 24 °C and fully open (50 % of the area) when it reached 28 °C. They were set to close should the wind reach 2 m/s or the external temperature become warmer than the internal. Those in the bathrooms, walk-in closet and studio were kept closed as these zones were rarely used.

Comfort Temperature Range: The benchmarks suggested by CIBSE, were used. The simulation results are illustrated by means of the number of hours in a year when temperatures in the room go >25 °C, >26 °C and >28 °C.

Heating: Was used during the heating period (1st of October to the 30th of April) for 12 h (from 5 p.m. to 5 a.m.). The thermostat was set to a lower limit of 18 °C and an upper limit of 21 °C and radiators were used as emitters. When this was active the whole house would be heated (except for the sunspace, loft and basement).

Cooling: In all cases the EAHE delivering 1 m^3/s at 10 °C inside the sunspace, approximately 1.2 kg of air per second. As the volume of it is very large (around 140 m^3), this rate is able to provide the space with 25 ACH of fresh air. The temperature of this was chosen based on the previous monitoring.

10.4 Results and Discussion

The results are presented in three formats, percentage of time the internal temperature of each zone exceeds: 25, 26, and 28 °C. These are shown for all cases in Figs. 10.2, 10.3, and 10.4.

In Case 1 (the base case), overheating is highest in the sunspace areas. The temperature in the sunspace is on average >25 °C for 11 % of the time, >26 °C for 8 %, and >28 °C for 4 %. If only the habitable sections of the space are taken into account in the average calculation, these values fall to 8 %, 6 %, and 3 % respectively. In all other areas the impact of overheating is less prevalent. The average value of the bedrooms is >25 °C for 7 %, >26 °C for 6 %, and >26 °C for 2 %. The most affected area of these is the master bedroom. In the remaining areas of the model overheating impact is negligible.

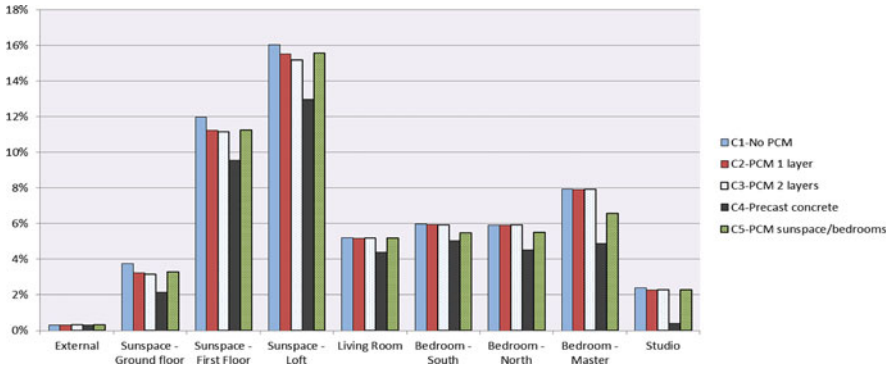

Fig. 10.2 Percentage of time when temperature exceeds 25 °C

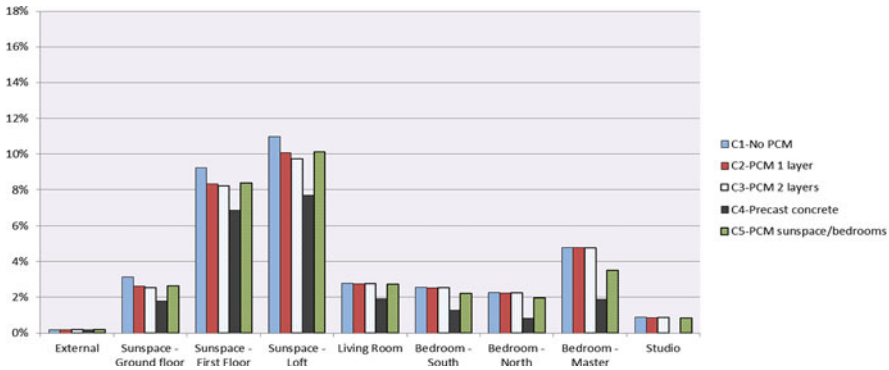

Fig. 10.3 Percentage of time when temperature exceeds 26 °C

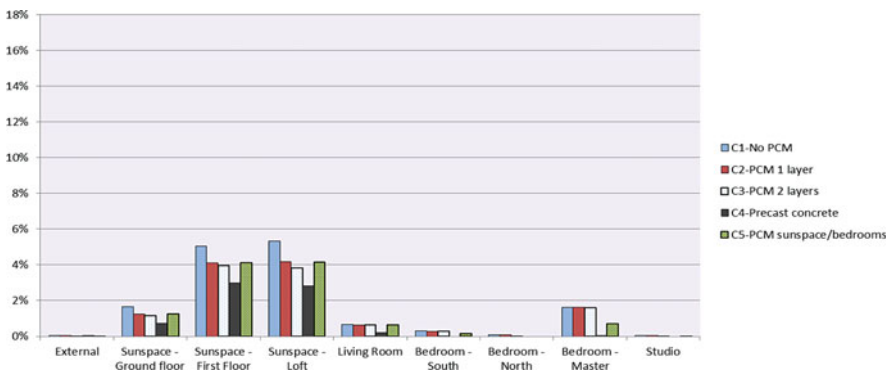

Fig. 10.4 Percentage of time when temperature exceeds 28 °C

10.4.1 Application of PCM

With the application of the PCM board in Case 2 the impact reduces, albeit to a minor extent. The temperature in the sunspace is on average >25 °C for 10 % of the time, >26 °C for 7 %, and >28 °C for 3 %. In the habitable sunspace areas these values reduce to: >25 °C for 7 %, and >26 °C for 5 %, and >28 °C for 3 %.

It would be logical to assume that the addition of a further layer of PCM would enhance the reduction observed in Case 2. However, the results of Case 3 in Figs. 10.2, 10.3, and 10.4 shows this has not happened as visual inspection indicates only minor reduction has occurred. In all other areas in Case 3 the quantity of observable overheating remains the same and there is no improvement over Case 1.

In Case 5, the addition of the PCM board to the bedroom areas has reduced overheating in the sunspace to the same degree as that shown in Case 2. Additionally there has also been a reduction in the bedroom areas. In the two smaller bedrooms in Case 5, overheating >25 °C has reduced from 6 % in Case 1 to 5 %, >26 °C it has reduced from 3 % in Case 1 to 2 %, and it has had minor impact with temperatures >28 °C. In the master bedroom in Case 5 overheating >25 °C has reduced from 8 % in Case 1 to 6.5 %, >26 °C it has reduced from 5 % in Case 1 to 3 %, and >28 °C has reduced from 2 % in Case 1 to around 1 %.

The results of Case 1 show that overheating above the temperatures specified by CIBSE occur in percentages ranging from 3 to 16 % of the total annual simulation time, the size of these depending on the zone location in the simulation. Considering the range of these percentages, the impact the addition of the PCM could have on them was limited. It has been shown that these impacts have ranged between 1 and 2 %. Tables 10.1, 10.2, and 10.3 show the numerical values of these percentages. Additionally, the percentage improvement comparisons over Case 1 have also been included.

When the temperature of the analysis of overheating is increased from 25 to 28 °C, the quantity of the percentage of overheating reduces. For example, in the sunspace ground floor in Case 1, the annual overheating quantity is 3.77 % above 25 °C, and this reduces to 1.66 % when the analysis is above 28 °C.

The addition of PCM in the various cases has reduced overheating, and the columns giving the improvement over Case 1 show the improvements range between 14 and 16 % when analysis is >25 °C, and 24–30 % when the analysis is >28 °C. Logically this shows that the impact of the PCM board inclusion becomes more apparent at higher temperature. However, these improvements should be taken in context as the amount of reduction, over which these improvements are calculated, is over a smaller range at higher temperatures. For example in the sunspace ground floor, when overheating is analysed >25 °C, a reduction of 14 % has occurred as the percentage of overheating time has reduced from 3.77 % in Case 1 to 3.25 % in Case 2. Comparatively, when overheating is analysed >28 °C, a reduction of 24 % has occurred as the percentage of overheating time has reduced from 1.66 % in Case 1 to 1.26 % in Case 2.

Table 10.1 Percentage of time when temperature is above 25 °C and percentage of reduction

	Case 1 (%)	Case 2 (%)	Case 3 (%)	Case 4 (%)	Case 5 (%)	Case 2 reduction over Case 1 (%)	Case 3 reduction over Case 1 (%)	Case 4 reduction over Case 1 (%)	Case 5 reduction over Case 1 (%)
Sunspace GF	3.77	3.25	3.16	2.16	3.26	−14	−16	−43	−13
Sunspace FF	11.96	11.23	11.13	9.55	11.23	−6	−7	−20	−6
Sunspace loft	16.03	15.53	15.16	12.97	15.55	−3	−5	−19	−3
Living room	5.22	5.18	5.17	4.39	5.17	−1	−1	−16	−1
Bedroom—south	5.97	5.95	5.91	5.03	5.46	0	−1	−16	−9
Bedroom—north	5.92	5.92	5.91	4.52	5.51	0	0	−24	−7
Bedroom—master	7.93	7.91	7.91	4.87	6.58	0	0	−39	−17
Studio	2.39	2.28	2.26	0.39	2.27	−4	−5	−84	−5

Table 10.2 Percentage of time when temperature is above 26 °C and percentage of reduction

	Case 1 (%)	Case 2 (%)	Case 3 (%)	Case 4 (%)	Case 5 (%)	Case 2 reduction over Case 1 (%)	Case 3 reduction over Case 1 (%)	Case 4 reduction over Case 1 (%)	Case 5 reduction over Case 1 (%)
Sunspace GF	3.13	2.61	2.55	1.78	2.64	−16	−19	−43	−16
Sunspace FF	9.22	8.34	8.21	6.87	8.36	−10	−11	−25	−9
Sunspace loft	10.98	10.07	9.70	7.71	10.09	−8	−12	−30	−8
Living room	2.77	2.76	2.75	1.93	2.74	0	−1	−30	−1
Bedroom—south	2.57	2.55	2.55	1.28	2.21	−1	−1	−50	−14
Bedroom—north	2.26	2.25	2.25	0.81	1.94	−1	−1	−64	−14
Bedroom—master	4.78	4.77	4.75	1.88	3.49	0	−1	−61	−27
Studio	0.90	0.87	0.86	0.00	0.83	−4	−5	−100	−8

Table 10.3 Percentage of time when temperature is above 28 °C and percentage of reduction

	Case 1 (%)	Case 2 (%)	Case 3 (%)	Case 4 (%)	Case 5 (%)	Case 2 reduction over Case 1 (%)	Case 3 reduction over Case 1 (%)	Case 4 reduction over Case 1 (%)	Case 5 reduction over Case 1 (%)
Sunspace GF	1.66	1.26	1.16	0.73	1.26	−24	−30	−56	−24
Sunspace FF	5.03	4.11	3.96	2.99	4.11	−18	−21	−41	−18
Sunspace loft	5.32	4.18	3.82	2.82	4.16	−21	−28	−47	−22
Living room	0.65	0.64	0.64	0.21	0.64	−2	−2	−68	−2
Bedroom—south	0.30	0.29	0.29	0.00	0.15	−4	−4	−100	−50
Bedroom—north	0.07	0.07	0.07	0.00	0.00	0	0	−100	−100
Bedroom—master	1.63	1.63	1.61	0.05	0.70	0	−1	−97	−57
Studio	0.06	0.06	0.06	0.00	0.06	0	0	−100	0

10.4.2 Application of Concrete

In Case 4 the presence of concrete has had more of an impact than the PCM in all simulated zones. In temperatures >25 °C the maximum percentage drop caused by concrete inclusion as occurred in the Sunspace loft, where 16 % in Case 1 has reduced to around 12.5 %. Significant reductions have also occurred in all other areas, most notably the master bedroom. The impact of these reductions is also noticeable in Figs. 10.3 and 10.4. The percentage improvements can be further analysed in Table 10.3.

As can be seen the improvements in the table are significant and this would be expected. Concrete is a very dense material and therefore has a large thermal mass, and this will have caused the reductions shown in the results. It should be noted that in the wall construction where the concrete was included, 240 m^2 of the material with a thickness of 100 mm was exposed to the internal environment. However, considering the amount of additional thermal mass exposed and the reduction it has caused, the impact of the PCM inclusion has been placed into context.

Relatively comparable reductions can be achieved albeit with lighter materials on a smaller surface area. The thickness of the PCM layer was 12.5 mm, 12.5 % that of the concrete (100 mm), and the surface area exposed was approximately 30 m^2 (compared to 240 m^2 of concrete). This quantity of PCM provided a reduction to overheating that was around a third of that provided by the concrete in the areas of the house it was installed in. However, the results of this study have also shown this effect is limited to small thicknesses of the PCM board, as the results of Case 3 have shown when a thicker layer of PCM was applied.

10.5 Conclusions

This study has analysed the impact of including PCMs into dynamic simulation in a building designed through MMC. The application of the PCM materials was limited to areas where risk of overheating was greater, i.e. the sunspace and bedroom areas. The results of the base case (Case 1) showed that impacts of the inclusion were limited to a small range between 3 and 16 % percentage of annual overheating time. The size of this range was dependant on the zone location within the simulation. The impact of PCM inclusion was most apparent in the zones where it was installed. For example, when overheating was analysed >25 °C, in the sunspace areas reductions of 13–16 % (on the Case 1 values) occurred with PCM inclusion. Comparatively, when overheating was analysed in the bedroom areas with PCM inclusion, reductions in overheating ranging between 9 and 17 % (on the Case 1 values) were achieved. The impact of these reductions increased when temperatures of overheating >26 °C and >28 °C were analysed. However, these results should be taken in context as the overheating percentage in the base case (Case 1) was also reduced.

Inclusion of concrete to the external walls of the building significantly reduced the amount of overheating in all zones analysed within the study. However, the impact of the PCM reduction was comparative with that of the thermal mass of the concrete. Considering the thickness of the PCM layer was 12.5 % that of the concrete and the exposed surface area of the PCM was 10 % that of the concrete, the PCM had a considerable impact on the quantity of overheating when the two materials were directly compared. However, PCM board was not installed in all zones, and overheating in these areas was not mitigated. Therefore additional board would have to installed in these areas if a direct comparison were to be carried out correctly.

This exercise has shown that the inclusion of PCM can be potentially used as a methodology to mitigate overheating in low thermal mass housing. However, considering the magnitude of reduction it is likely to achieve, it would be prudent to use it in conjunction with other methodologies, such as ventilation, as it would unlikely provide a full solution.

Nomenclature

Acronyms

ACH	Air changes per hour
CEH	Creative Energy Homes
DSY	Design summer year
EAHE	Earth-air heat exchanger
FF	First floor
GF	Ground floor
HDPE	High density polythene
MMC	Modern methods of construction
PCM	Phase change materials

References

1. Arup (2008) Your home in a changing climate. Three Regions Climate Change Group, London
2. Zero Carbon Hub (2010) Carbon compliance for tomorrows new homes—topic 3 future climate change. NHBC Foundation, London, Aug 2010. Report No. ZCHD130210
3. Holmes MJ, Hacker JN (2007) Climate change, thermal comfort and energy: meeting the design challenges of the 21st century. Energy Build 39(7):802–814
4. Simon R (2008) Effects of climate change on the built environment. Energy Policy 36 (12):4552–4557
5. Hacker J, Capon R, Mylona A (2009) Use of climate change scenarios for building simulation: the CIBSE future weather years. Chartered Institution of Building Services Engineers (CIBSE), London

6. Sharma A, Tyagi VV, Chen CR, Buddhi D (2009) Review on thermal energy storage with phase change materials and applications. Renew Sustain Energy Rev 13(2):318–345, Pubmed Central PMCID: PCM 03b
7. Rodrigues L, Gillott M, Tetlow D (2013) Summer overheating potential in a low-energy steel frame house in future climate scenarios. J Sustain Cities Soc 7:1–15
8. UN-HABITAT (2008) State of the World's Cities 2008/2009—harmonious cities programme (UNHS, ed.). Earthscan, London
9. Jenkins G, Murphy J, Sexton D, Lowe J, Jones P, Kilsby C (2009) UK climate projections: briefing report. Met Office Hadley Centre, Exeter, UK
10. Department for Communities and Local Government (2007) Homes for the future: more affordable, more sustainable. Communities and Local Government, London, July 2007. Report No.: Contract No.: Cm 7191
11. Department for Communities and Local Government (2009) Code for sustainable homes technical guide. Communities and Local Government Publications, London, p 68
12. Department for Communities and Local Government (2008) Definition of zero carbon homes and non-domestic buildings: consultation. London, 17 Dec 2008. Report No.: Contract No.: 08CCSD05675
13. Rodrigues L (2009) An investigation into the use of thermal mass to improve comfort in British housing. University of Nottingham, Nottingham
14. Orme M, Palmer J (2003) Control of overheating in future housing—design guidance for low energy strategies. DTI Partners in Innovation Programme, St Albans. Contract No.: EBR24763/9/1.2
15. EST (2005) Building energy efficient buildings using modern methods of construction (CE139). Energy Saving Trust and BRE, London, 23 Aug 2005. Report No.: Contract No.: CE139
16. Dunster B (2005) UK housing and climate change: heavyweight vs. lightweight construction. London, Jan 2005. Report No. 116210
17. EST (2005) Avoidance of overheating and airconditioning in urban housing. Energy Saving Trust and BRE, Watford, Mar 2005. Report No.: 221427
18. Hacker JN, Saulles TPD, Minson AJ, Holmes PMJ (2006) Embodied and operational carbon dioxide emissions from housing: a case study on the effects of thermal mass and climate change. Build 40(3):375–384
19. Rodrigues L, Gillott M (eds) (2011) The summer performance of the BASF house. PLEA 2011—27th conference on passive and low energy architecture, 13–15 July 2011. Presses Universitaires de Louvain, Louvain-la-Neuve, Belgium
20. Littlefair P (2005) Avoiding air-conditioning. Constr Future 24:11
21. Agyenim F, Hewitt N, Eames P, Smyth M (2010) A review of materials, heat transfer and phase change problem formulation for latent heat thermal energy storage systems (LHTESS). Renew Sustain Energy Rev 14(2):615–628
22. Arteconi A, Hewitt NJ, Polonara F (2012) State of the art of thermal storage for demand-side management. Appl Energy 93:371–389
23. Baetens R, Jelle BP, Gustavsen A (2010) Phase change materials for building applications: a state-of-the-art review. Energy Build 42(9):1361–1368
24. Farid MM, Khudhair AM, Razack SAK, Al-Hallaj S (2004) A review on phase change energy storage: materials and applications. Energy Convers Manag 45:1597–1615
25. Tyagi VV, Buddhi D (2007) PCM thermal storage in buildings: a state of art. Renew Sustain Energy Rev 11(6):1146–1166, Pubmed Central PMCID: PCM 03a
26. Alkan C, Sarı A, Karaipekli A (2011) Preparation, thermal properties and thermal reliability of microencapsulated n-eicosane as novel phase change material for thermal energy storage. Energy Convers Manag 52(1):687–692
27. Sarı A, Alkan C, Karaipekli A, Uzun O (2009) Microencapsulated n-octacosane as phase change material for thermal energy storage. Sol Energy 83(10):1757–1763

28. Tyagi VV, Kaushik SC, Tyagi SK, Akiyama T (2011) Development of phase change materials based microencapsulated technology for buildings: a review. Renew Sustain Energy Rev 15 (2):1373–1391
29. Zhang YP, Lin KP, Yang R, Di HF, Jiang Y (2006) Preparation, thermal performance and application of shape-stabilized PCM in energy efficient buildings. Energy Build 38(10):1262–1269
30. Darkwa J (2009) Mathematical evaluation of a buried phase change concrete cooling system for buildings. Appl Energy 86(5):706–711
31. Cabeza LF, Ibanez M, Sole C, Roca J, Nogués M (2006) Experimentation with a water tank including a PCM module. Sol Energy Mater Sol Cells 90:1273–1282, Epub x
32. Ibanez M, Cabeza LF, Sole C, Roca J, Nogués M (2006) Modelization of a water tank including a PCM module. Appl Therm Eng 26:1328–1333, Epub s
33. Mehling H, Cabeza LF, Hippeli S, Hiebler S (2003) PCM-module to improve hot water heat stores with stratification. Renew Energy 28:699–711, Epub x
34. Alawadhi EM (2008) Thermal analysis of a building brick containing phase change material. Energy Build 40(3):351–357
35. Darkwa K, O'Callaghan PW, Tetlow D (2006) Phase-change drywalls in a passive-solar building. Appl Energy 83(5):425–435
36. Kuznik F, David D, Johannes K, Roux J-J (2011) A review on phase change materials integrated in building walls. Renew Sustain Energy Rev 15(1):379–391
37. Rodrigues L, Gillott M (2013) The climate resilience of a low-energy prototype house. Proc ICE Eng Sustain 166:337–350
38. Gillott M, Rodrigues LT, Spataru C (2010) Low-carbon housing design informed by research. Proc ICE Eng Sustain 163(2):77–87
39. Gorgolewski M (2007) Framing systems and thermal mass. Mod Steel Constr 47:45–48
40. EST (2005) Reducing overheating—a designer's guide. Energy Saving Trust, London, Mar 2005. Report No.: Contract No.: CE129
41. Kennett S (2005) Domestic bliss. Build Serv J (May 2005):42–45. Pubmed Central PMCID: EAHE 56*
42. CIBSE (2006) Guide A: environmental design, 7th edn. Chartered Institution of Building Services Engineers, London

Chapter 11
Green Jubail Industrial City

Mohammed I.Y. Aleid

Abstract In this study the focus is on reduction of pollution in Jubail Industrial City (J.I.City), but this could be implemented to any industrial city in general. It's a fact that the pollution in J.I.City is caused from many sources. Some of them are:

1. Chemical reactors in petrochemical plants.
2. Use of diesel fuel in boilers in petrochemical plants.
3. Use of diesel fuel and Gasoline in power plants/water desalination plant.
4. Use of diesel trucks to transfer the product to port and city.
5. Use of gasoline fuel in personal automobile.

Population and pollution of gasoline automobile in growing continuously and tremendously in J.I.City since this industrial city has large residential area, J.I.City therefore has lots of individual vehicles. Beside that there is no public transportation system currently available except for schools to transport student.

The research recommends Electric Vehicle (EV) as a solution to reduce the amount of pollution created by internal combustion engine cars which is currently the only available personal transportation means.

The starting point is rules and legislations to be set by the city council (Royal Commission for Jubail) to facilitate the solutions and make them possible and implementable.

The city council will be the starting point for implementation of EV, next stage will be major companies in the area to implement EV, third stage will be schools public transportation system, fourth stage will be to establish a new public transportation system that is operated by EV only. Fifth stage is to establish electric train to move J.I.City products to port and other cities. Last stage is to abandon personal internal combustion engines cars from entering J.I.City. The research is recommending an EV that can be economical and effective for J.I.City environment.

Keywords Pollution • Electric vehicle • Green • Jubail • Industrial city

M.I.Y. Aleid (✉)
Royal Commission for Jubail and Yanbu, Jubail Industrial College, Jubail Industrial City, P O box 10001, Jubail, Eastern Province 31961, KSA
e-mail: eid_mi@jic.edu.sa; mohammedcad@gmail.com

I. Dincer et al. (eds.), *Progress in Sustainable Energy Technologies Vol II: Creating Sustainable Development*, DOI 10.1007/978-3-319-07977-6_11

11.1 Introduction

Jubail Industrial City (J.I.City) like any other Industrial city suffers from the effects of pollution in atmosphere, related to the release of CO, CO_2 and other gases from petrochemical industry, power plants and other industries. Simply all these gases make their way to our environment to pollute air. Human Lungs is the first victim then animals lungs followed by plants and agriculture and therefore the cycle continues. Human will be the worst in the whole cycle of pollution since human breath polluted air, then he eats polluted animals and polluted plants.

Although automobile pollution is part of the problem only but the availability of pollution gases from cars is very close to human breathing unlike factories and plants pollution which occasionally only comes down to the level of human breathing.

In Jubail Industrial city and Saudi Arabia population of environment increase with a direct proportional relation with the population increasing, and in the same time population of vehicles, the ratio of people to vehicles can be as bad as every adult own a car whether old or new i.e. the ratio is one adult to one car (1:1), one important factor also is that there is no public transportation system another one is that 1 l of gasoline cost 0.92 Saudi Riyal that is equivalent to 0.25 US dollar which is effectively cheaper than 1 l of canned water, all the said factors made getting internal combustion engine car for transportation a matter can't be avoided.

11.2 Methodology

1. Questionnaire to check community awareness.
2. Interview with officials in city council.
3. Analysis of Air Quality Reading Log installed in Jubail Industrial City.
4. Calculation of pollution because of car toxic gases in J.I. City.
5. Possible saving of city council if using Electric Vehicle (EV).
6. Comparison of market EV.

11.3 Questionnaire

Questionnaire was prepared to know the community awareness of environmental pollution and check the acceptance of community to the Electric Vehicle (EV).

Questionnaire consisted from 13 questions (Appendix) and 318 people participated in the questionnaire.

Age of participants 44 % range from 20 to 30 years, 42 % those ranging from 31 to 50 years and 14 % was the percentage of people aged more than 51 years (Fig. 11.1).

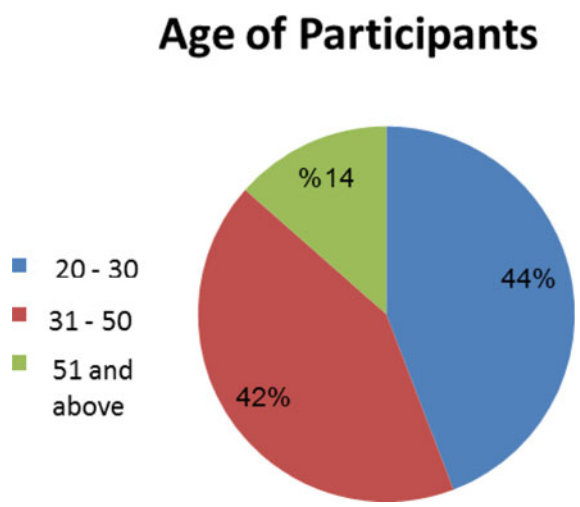

Fig. 11.1 Age of questionnaire participants

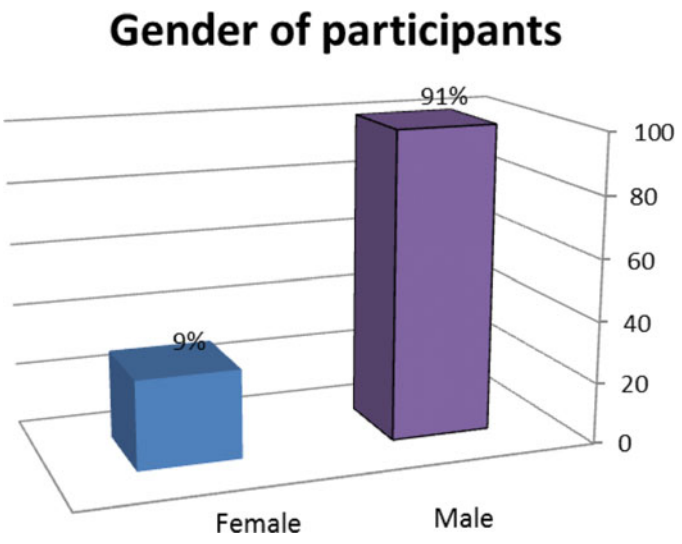

Fig. 11.2 Gender of questionnarie participants

Gender of participants mainly was male participants, with 9 % female participation (Fig. 11.2).

The highest Percentage of participants was faculty staff members 53 %, followed by student participation 33.5 % finally 7.2 % of admin staff participation, 2.8 % engineers and 2.8 % technicians see Fig. 11.3.

When we asked whether it's known that our environment is contaminated by other than industrial pollution 91.5 % said yes (Fig. 11.4).

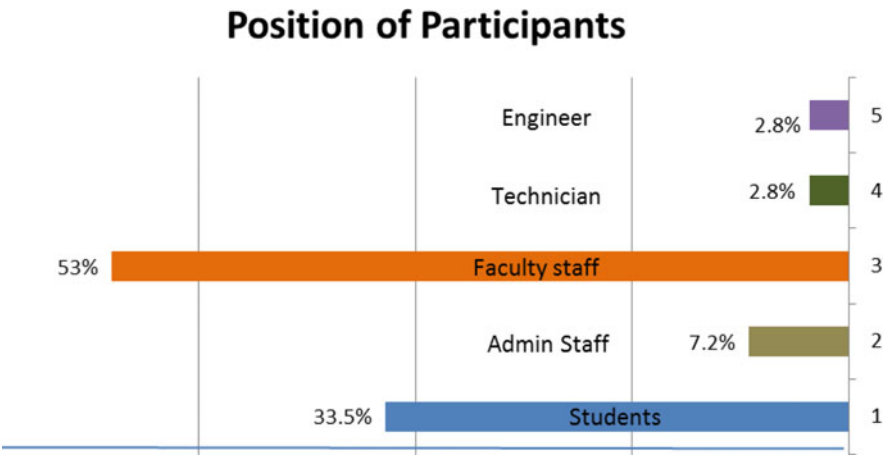

Fig. 11.3 The career of participants

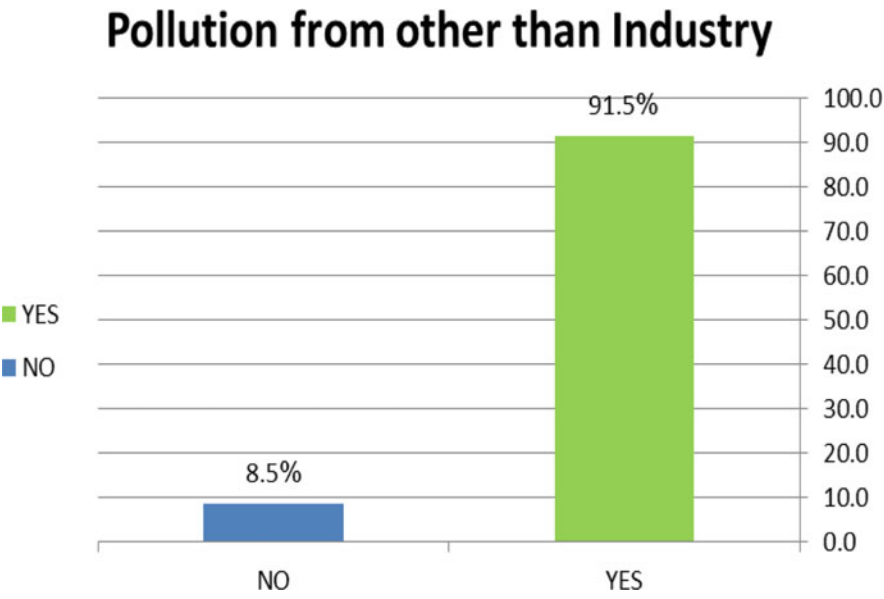

Fig. 11.4 Pollution come from source other than industry

When people were asked whether they know that gasoline and diesels produce sound pollution 89 % of people said yes see Fig. 11.5.

Ninety-six percent of people know that their car pollute environment see Fig. 11.6.

Eighty-three percent of questionnaire sample know that Electric Vehicle has no sound and toxic gas pollution see Fig. 11.7.

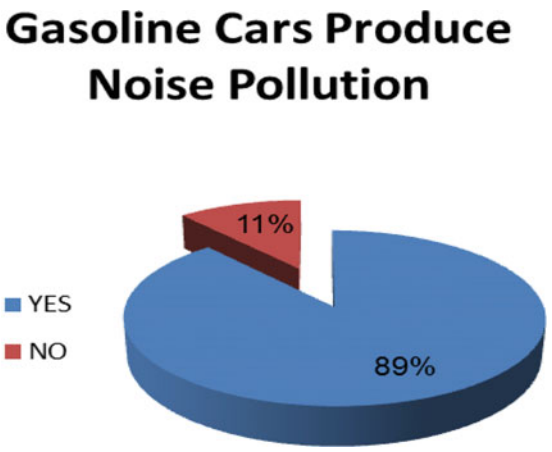

Fig. 11.5 Majority of people agreed that Engines produce noise pollution

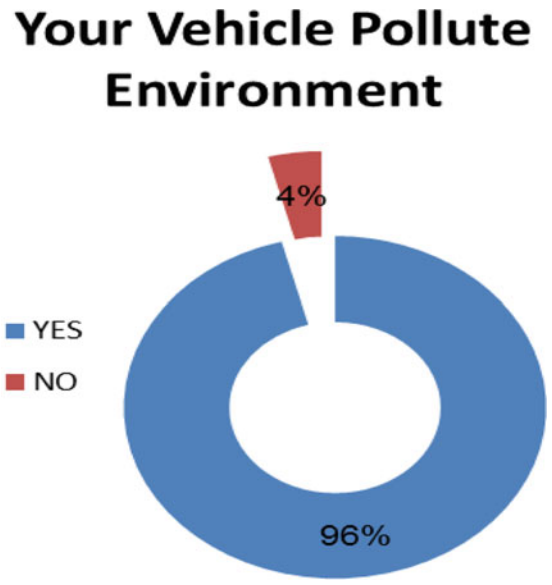

Fig. 11.6 People that are not aware that their car pollute environment were 4 %

Thirty-five percent of people are not aware that natural gas operated engine has a very low pollution effect (Fig. 11.8).

When people were asked if they support electric or gas public transportation, 87 % agreed (Fig. 11.9).

Nearly 60 % of people agreed to stop every 200 km to charge EV (Fig. 11.10).

Sixty-two percent of community is ready to change their gasoline or diesel car to EV or gas powered car (Fig. 11.11).

When questionnaire participants were asked, if they are to chose to change their car what would they chose. Forty-four percent chosen EV and gasoline powered car, 32 % chosen EV, 17 % chose EV and Gas powered finally only 7 % their choice was Gas-powered car (Fig. 11.12).

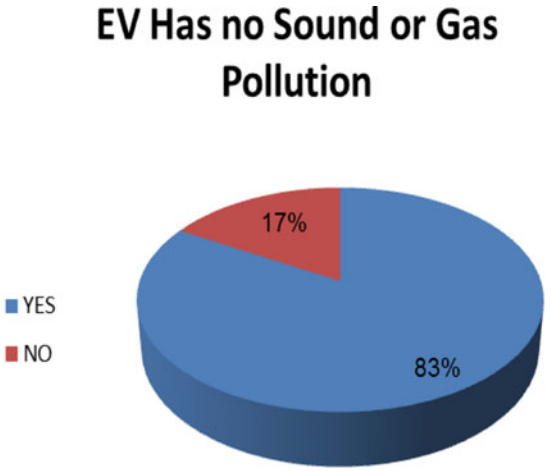

Fig. 11.7 Awareness of Electric Vehicle

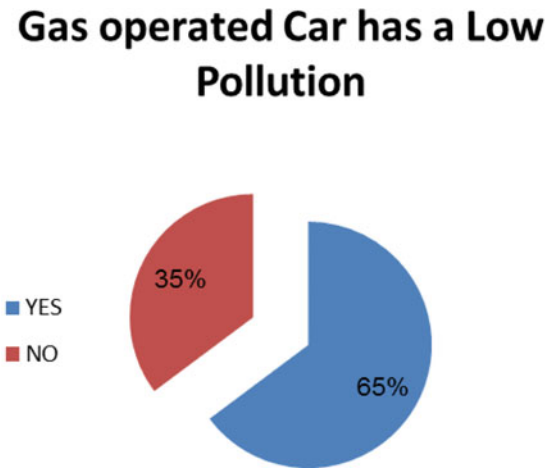

Fig. 11.8 Awareness of community about Gas Cars

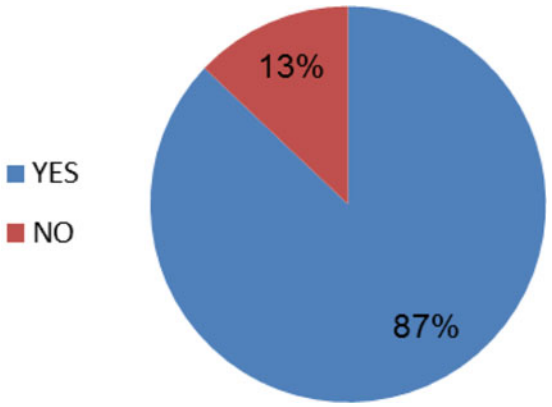

Fig. 11.9 Support for electrical or gas operated public transportation

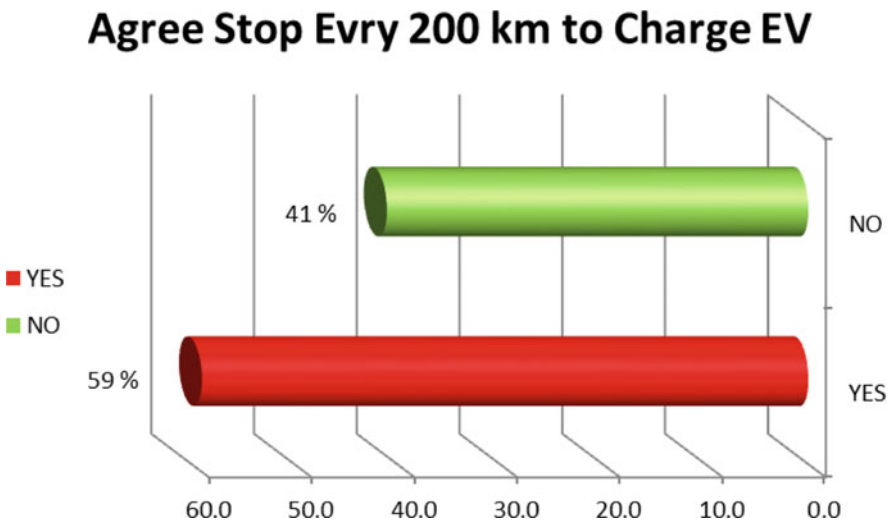

Fig. 11.10 Acceptance of people to EV charging every 200 km

Fig. 11.11 Percentage of people ready to change their diesel or gasoline car to EV

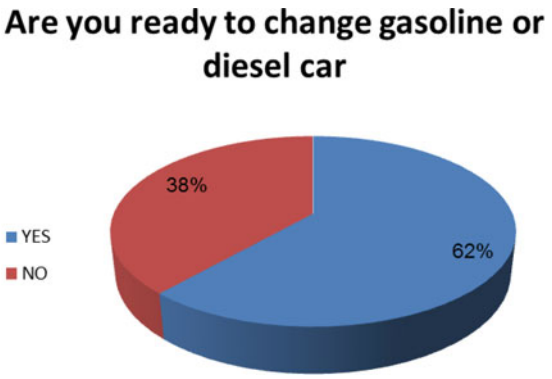

11.4 Pollution in J. I. City

Whatever the pollution volume in J. I. CITY our target to decrease this pollution, to do that we need to prove that there is more pollution because of vehicle emissions.

As shown in Fig. 11.13 there are total nine air quality analyzer units spread around inside and outside Jubail Industrial city, monitored by environment department of city council (Royal Commission for Jubail). Results of these units are monitored and maintained by environment department, we met Mr. Ali Abdullah Mubarak and he provided details about positions of the units and also provided us with 1 week 24 h readings for the whole 9 units.

Typical Engine Combustion [1]:

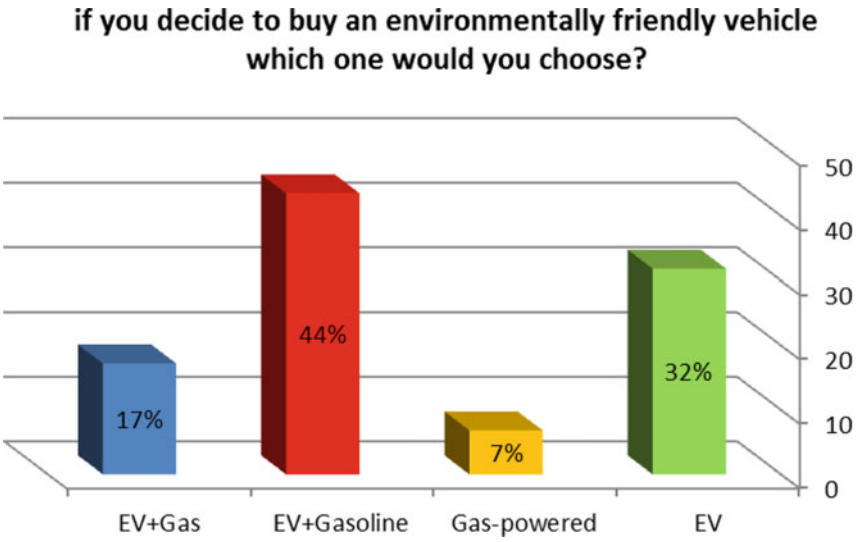

Fig. 11.12 In case people decide to change their car which one they would choose

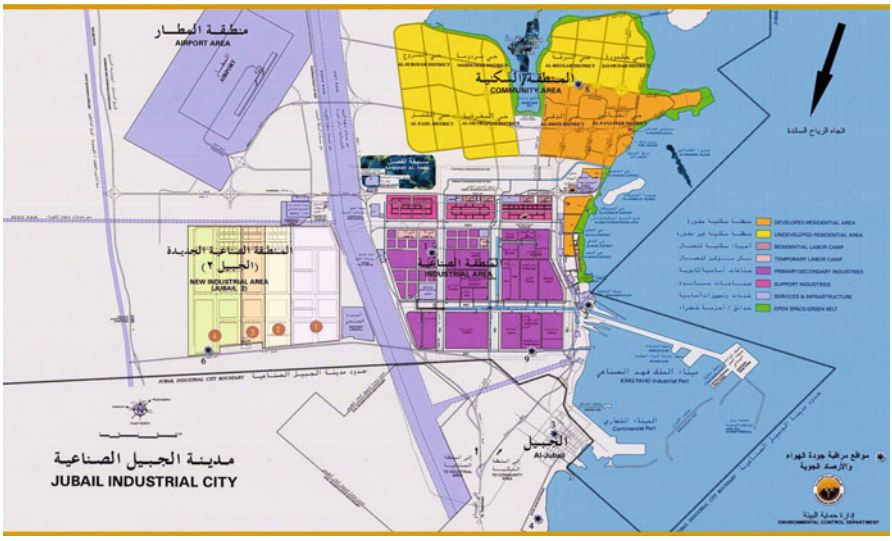

Fig. 11.13 Total nine air quality analyzer units spread around inside and outside J. I. City

$$\text{Fuel} + \text{Air} \Rightarrow \text{Hydrocarbons} + \text{Nitrogen Oxides} + \text{Carbon Dioxide} + \text{Carbon Monoxide} + \text{water}$$

We will concentrate here on CO gas emissions

Figure 11.14 show reading of air quality in Jubail town as provided to us from EPCD department in city council in Jubail, we will notice a peak in reading of CO

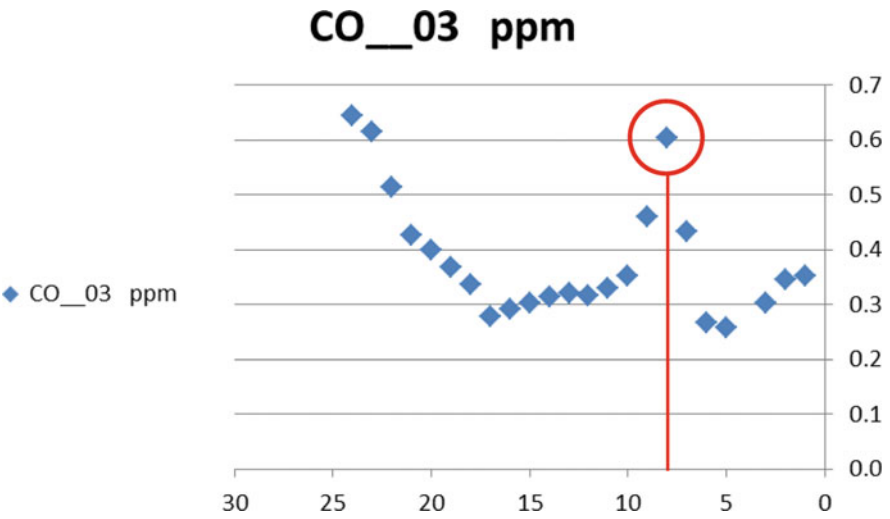

Fig. 11.14 Reading of CO gas at Jubail Town on Saturday during 24 h

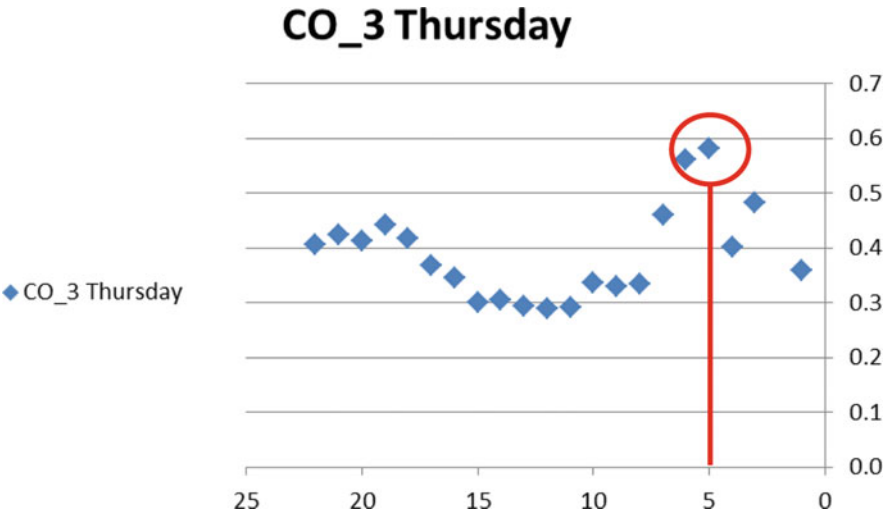

Fig. 11.15 CO level in Jubail town during weekend

gas at 8:00 a.m. which is just after the morning rush hour during week day Fig. 11.14.

As shown in Fig. 11.15 below CO reading for whole day on hour basis in the same location but during the weekend, same trend is noticed that there is a high level of Carbon monoxide (CO) gas during hour 5 of the day, never the less level of CO peak generally was lower throughout the day.

As we analyze reading in Jubail Industrial City itself we end up with the same conclusion as the peak of max CO emission occur at 8:30 morning which also rush time but slightly shifted because of starting time for plant workers which is 6:30 a. m. to 8:00 a.m.

We can conclude that emissions in Jubail industrial city are effected highly by vehicle emissions.

11.5 Volume of Pollution Saving

Total population in Jubail industrial city [2] is according to the Seventh Census Report for Jubail Industrial City, prepared in 2005, gives a resident population of 224,430 [2], not counting visitors who travel from nearby city every day either to attend colleges, schools and jobs in the city; an early we can calculate a rough figure of how much pollution we can save. Also considering that this figure is 8 years old it's a good approximate to use the same number 224,430 as number of vehicles in Jubail Industrial City.

Using www.terrapass.com as a carbon footprint calculator, two samples were calculated on 15,000 mile per year basis for two car samples:

(a) American car GMC model 2011, Yukun K1500, XL 4WD Carbon footprint was 16,183 lb CO_2 per year
(b) Japanese car Nissan model 2011, Pathfinder 4WD, Carbon footprint was 17,135 lb CO_2 per year

As a result we can give approximate number of carbon footprint print of CO_2 for the whole city per year:

(a) Based on American Car carbon footprint of $CO_2 = 224{,}430$ car $\times$ 16,183 lb $CO_2 = 3{,}631{,}950{,}690$ lb $= 1{,}647{,}425$ metric Ton $= 1.6$ Million Ton
(b) Based on Japanese Car carbon footprint of $CO_2 = 224{,}430$ car $\times$ 17,135 lb $CO_2 = 3{,}845{,}608{,}050$ lb $= 1{,}744{,}338$ metric Ton $= 1.7$ Million Ton

Taking the average Car carbon footprint of CO_2 in J.I.City $= 1.67$ Million Ton CO_2 per year.

11.6 Cost of Fuel Per Year

Assuming that global fuel costs \$3.333/gallon for regular unleaded gasoline, \$3.575/gallon for premium, KSA cost \$ 0.95/Gallon.

(a) Based on American Car (C1500 Yukon Xl 2wd) MPG $= 17$, regular fuel, 1 year Global Cost $=$ \$2,904.5, KSA cost $=$ \$827.9 [3]

(b) Based on Japanese combined MPG = 16, premium fuel, 1 year global cost = $3,313.26, KSA cost = $880.45 [4]

Taking the average global = $3,108.88
Taking the average KSA = $854.2

Taking the total average fuel cost in J.I.City (global) = 224,430 × $3,108.8 = $ 697.7 M
Taking the total average fuel cost in J.I.City (KSA) = 224,430 × $854.2 = $ 191.7 M

11.7 Results and Discussion

Car carbon footprint of CO_2 in J.I.City = 1.67 Million Ton CO_2 per year this amount of pollution coming only from vehicles in an industrial city noticing that this amount was calculated for model 2011 cars imagine the pollution for 5 years old car or more, this amount of pollution also reflected in the CO level at the beginning and end of business day see Figs. 11.14, 11.15 and 11.16.

We could save $697.7 M − $191.7 M = $506 M fuel cost, which is the difference between global fuel price and KSA fuel price, this amount could be used to develop the city.

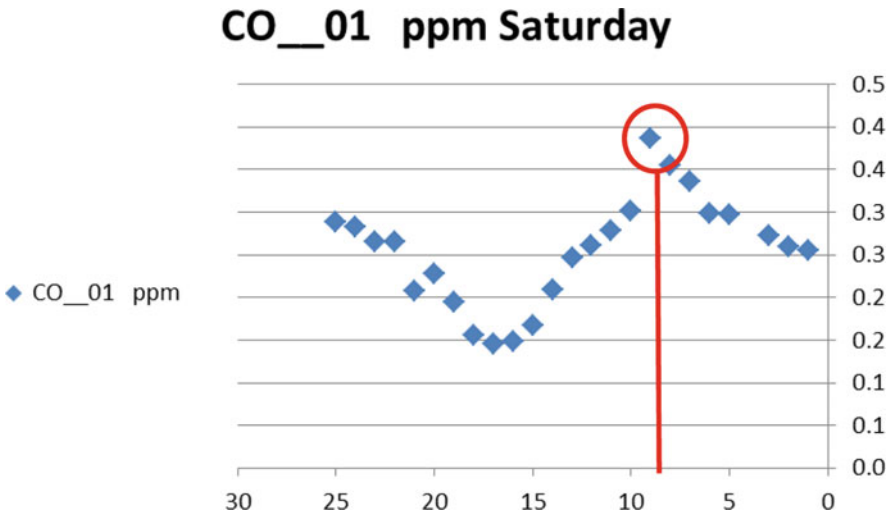

Fig. 11.16 CO level in measured in Jubail Industrial City location throughout the day

11.8 Conclusions

In conclusion transportations using fossil fuel should be stopped inside J.I.City in year 2015, electric public transportation should be developed inside the city, City Council should start using Electric Vehicle, and main industrial companies in the city should be convinced to do so also.

Car agencies should start selling EV in KSA.

I recommend Nissan Leave EV as suitable 70 mile range equivalent 112 km with a price $35,200 that sound reasonable, people already tried for 1 year and reported reasonable feedback [5].

Acknowledgement I here acknowledge all Departments in Royal Commission for Jubail (RC) for the support to finish this research, starting from Jubail Industrial College, Environment Department in RC and Roads Department.

Nomenclature

ppm Part per million

EV Electric vehicle

Superscripts

* Reference condition

Appendix

Questionnaire

This questionnaire is aimed to know the community's awareness of environmental pollution and provide solutions to reduce pollution. Your anticipated participation is greatly appreciated.

1 - Age:
a. 20 to 30 years
b. 31 to 50 years
c. 51 and above

2 - Gender:
a. Male
b. Female

3 - Position:
a. Student b. Admin. Staff c. Faculty Member
d. Technician e. Engineer

4 - Do you know that our environment is contaminated with sources of pollution other than industrial pollution?
a. Yes
b. No

5 - Do you know that your car or any vehicle using gasoline produces noise pollution?
a. Yes
b. No

6 - Do you know that your car or any vehicle pollutes the environment with toxic gases?
a. Yes
b. No

7 – Are you aware that an electric car doesn't pollute the environment, either with sound pollution or toxic gas?
a. Yes
b. No

8 – Have you ever known that the gas vehicles, which operate by natural gas, pollute the environment with a very low percentage of toxic gas?
a. Yes
b. No

9 – Do you support using electric or gas powered public transportation?
a. Yes
b. No

10 – Do you agree to stop every 200 kilometers to charge an electric car for at least 15 minutes to protect the environment?
a. Yes
b. No

11 - Are you ready to have an electric car or gas car instead of your current gasoline or diesel one?
a. Yes
b. No

12 - If you decide to buy an environmentally friendly vehicle, which one would you choose?
a. An electric car.
b. Gas-powered car.
c. Car powered by gasoline and electricity.
d. Car powered by natural gas and electricity.

13 - Any other comments or suggestions can be listed below.----------
---

---.

References

1. http://www.nutramed.com/environment/carsepa.htm. Accessed 3 July 2012
2. http://en.wikipedia.org/wiki/Jubail. Accessed 3 July 2012
3. http://www.terrapass.com/individuals-families/carbon-footprint-calculator/#air. Accessed 3 July 2012
4. http://www.mpgbuddy.com/vehicle-profile/30539/2011-nissan-pathfinder-4wd.html. Accessed 3 July 2012
5. http://news.discovery.com/autos/nissan-leaf-one-year-report-120327.html. Accessed 3 July 2012

Chapter 12
Design of a Nearly Zero Energy One-Family House in North-Centre Italy

Enzo Zanchini and Stefano Lazzari

Abstract The thermal design of a nearly zero energy one-family house, in North-Centre Italy, is described. The house has a timber frame, a wood-fiber thermal insulation for the roof and a wood-fiber plus YTONG blocks thermal insulation for the lateral walls. Forced ventilation with high efficiency heat recovery is employed. Heating and cooling is provided by an air-to-water heat pump connected to floor radiant panels. Domestic Hot Water is supplied by a thermal solar collector and a heat pump for DHW. The electric energy for the heat pumps and for the forced ventilation system is supplied by PV collectors, which provide also most of the electric energy for lighting and appliances. The thermal design is based on dynamic simulations performed through the code TRNSYS 16.

Keywords Nearly zero energy buildings • Air-to-water heat pumps • Thermal solar collectors • PV collectors • Hourly simulation

12.1 Introduction

Improving the energy efficiency of buildings, and possibly reach zero use of fossil fuels for space heating, cooling and dehumidifying, DHW production, and lighting is considered nowadays as an important technical target in most countries. In particular, in the USA, the Energy Independence and Security Act of 2007 (EISA 2007) authorizes the Net-Zero Energy Commercial Building Initiative to support the goal of net zero energy for all new commercial buildings by 2030. In Europe, the Directive 2010/31/UE on Energy Performance of Buildings, adopted in May 2010, establishes the "nearly zero energy target" from 2018 for all the new buildings owned or occupied by public authorities, and from 2020 for all new buildings. As a consequence, a broad research activity on the design and monitoring of nearly zero energy buildings (NZEB), as well as on the methods to assess their performance, has been developed.

E. Zanchini (✉) • S. Lazzari
Department of Industrial Engineering, School of Engineering and Architecture, University of Bologna, Viale Risorgimento 2, 40136 Bologna, Italy
e-mail: enzo.zanchini@unibo.it; stefano.lazzari@unibo.it

I. Dincer et al. (eds.), *Progress in Sustainable Energy Technologies Vol II: Creating Sustainable Development*, DOI 10.1007/978-3-319-07977-6_12

Thiers and Peuportier [1] used life cycle assessment (LCA) to evaluate the environmental impacts of two high-energy performance buildings, a renovated multi-family social housing building and two passive attached houses, both located in North of France. In 2011, Marszal et al. [2] analyzed the existing NZEB definitions and calculation methodologies in order to facilitate the development of a consistent NZEB definition and of a widely shared energy assessment method.

Terlizzese and Zanchini [3] analyzed the feasibility of two zero carbon emission plants for a residential building complex in North-Centre Italy, with respect to a conventional plant. The zero carbon plants are composed of either air-to-water heat pumps or ground coupled heat pumps, PV solar collectors, air dehumidifiers, thermal solar collectors and an auxiliary wood pellet boiler. The results show that the air-to-water heat pumps yield a shorter payback time, while the ground coupled heat pumps yield a higher exergy saving during the life cycle.

Gustavsson and Joelsson [4] investigated the primary energy use and the CO_2 emission for the production and operation of conventional and low-energy residential buildings. Different types of energy supply systems are considered. The results show that the primary energy used and the CO_2 emission resulting from production are lower for wood-framed constructions than for concrete-framed constructions.

Karlsson and Moshfegh [5] reported the results of a study of 20 low-energy houses situated on the west coast of Sweden. The ventilation performance, the energy demand, the households' perception of the building, the CO_2 emissions, the embodied and the operational energy, and the payback time with respect to ordinary Swedish buildings are investigated. Citherlet and Defaux [6] compared three variants of a family house in Switzerland, with standard, high and very high-energy performance, in order to evaluate the total environmental impacts during the whole building life cycle.

Relevant examples of NZEBs are described in the website "Net Zero Energy Buildings Database" of the International Energy Agency [7]. Among the buildings described there we can point out the Aldo Leopold Legacy Center, located at Baraboo, WI (1,100 m^2), the Audubon Center at Debs Park, located in Los Angeles, CA (467 m^2), the Challengers Tennis Club for Boys and Girls Los Angeles, CA (325 m^2), the Environmental Technology Center at Sonoma State University Rohnert Park, CA (204 m^2), the Hawaii Gateway Energy Center Kailua-Kona, HI (334 m^2), the Adam Joseph Lewis Center for Environmental Studies—Oberlin College, located at Oberlin, OH (1,260 m^2).

In this paper, the energy performance of a nearly zero energy one-family house under construction in North-Centre Italy, at Casalfiumanese (Bologna), is studied by dynamic simulations performed through the software TRNSYS 16. After construction, the house will be monitored and the evaluated performance will be compared with actual measurements.

The house has only one floor, and is composed of two bedrooms, two bathrooms, a living room and a kitchen. It has a timber frame and a thermal insulation composed mainly of wood-fiber and YTONG blocks. The hourly energy needs for heating, cooling, and summer dehumidifying are evaluated by means of TRNSYS 16; the monthly energy needs for domestic hot water supply are evaluated

according to UNI/TS 11300-2. The plant is composed of an air-to-water heat pump for heating and cooling, a solar collector and a heat pump for DHW production, a forced ventilation system with heat recovery, PV collectors designed to meet the whole electric energy use of the house, including lighting and domestic appliances. The hourly electric energy use for heating, cooling and dehumidifying is evaluated by considering the hourly energy need, the plant emission and regulation efficiency, the COP and EER data of the heat pump, given by the constructor, and the methods recommended by UNI/TS 11300-4 and UNI/TS 11300-3 to take into account the reduction of COP or EER due to intermittent operation.

12.2 Description of the Building

A layout of the house is reported in Fig. 12.1, where five thermal zones are evidenced: Night 1 (bedroom), Bath 1 (bathroom), Day (living room and kitchen), Night 2 (bedroom), Bath 2 (bathroom). The net heated floor area is 93.2 m^2. The roof has two pitches, with a slope of 14°, and two horizontal overhangs. The orientations of the main sides of the building, as well as of the roof pitches and overhangs, are 16° East of North and 16° West of South. The overhang with orientation 16° East of North has a width of 2.3 m, and has been required by the householders to have a more comfortable use of the outside space, which, on this side, faces a nice small lake. The overhang with orientation 16° West of South has a width of 2.0 m, and has been designed to provide a good shadowing of the windows facing South. A view of the North side of the house is reported in Fig. 12.2.

The vertical external wall has a thickness of 40 cm, and is composed of YTONG blocks, wood-fiber insulation, Celenit (fir fiber and mineral binders), OSB (cross-oriented layers of thin wooden strips, compressed and bonded together with wax and resin adhesives), air layers, two vapour barriers and a low emissivity layer. The main characteristics of the vertical external wall, in correspondence of the wood-fiber insulation (91.3 % of the whole length), are listed in Table 12.1. For the air layers, the effective thermal conductivity has been reported, evaluated by applying the standard UNI EN ISO 6946. If one takes into account the internal and external surface resistances recommended by UNI EN ISO 6946 (0.13 and 0.04 W/(m^2 K), respectively), the wall transmittance is 0.176 W/(m^2 K). In correspondence of the timber pillars (8.7 % of the whole length), the layers 4 and 5 of the Table are replaced by a timber layer with a thickness of 0.16 m (the pillar) and a thermal conductivity of 0.13 W/(m K). The transmittance of this part of the wall, according to UNI EN ISO 6946, is 0.295 W/(m^2 K). In TRNSYS, the convection and radiation heat exchanges are calculated separately and the standard surface resistances are not employed.

The roof has a thickness of 29 cm (excluding the timber beams, whose thermal resistance has not been considered), and is composed of a fir layer, a vapour barrier, Celenit, wood-fiber insulation, a ventilated air layer, OSB, a low emissivity layer and a steel sheet. The main properties of the layers of the roof, from inside to

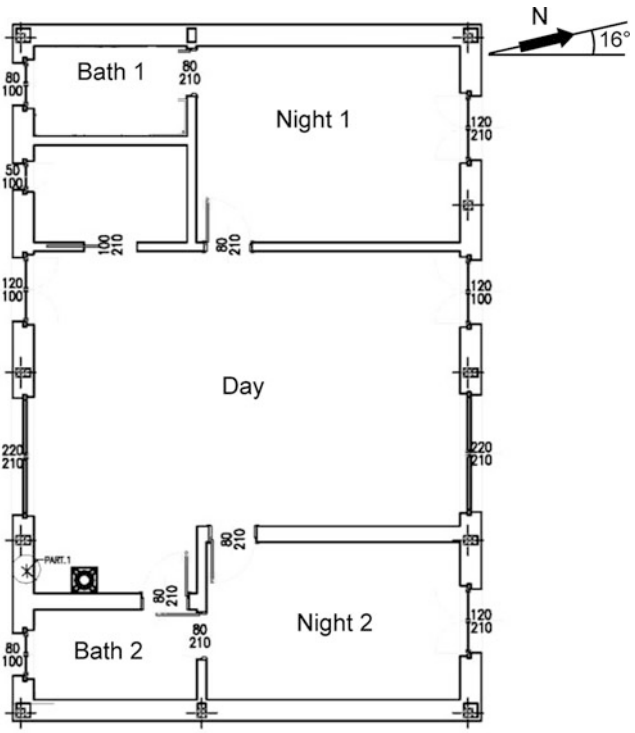

Fig. 12.1 Layout of the house

Fig. 12.2 View of the North side of the house (under construction)

Table 12.1 Layers of the vertical external wall, of the roof and of the floor

Layer	Thickness (m)	λ (W/(m K))	R (m^2 K/W)	ρ (kg/m^3)	Mass/area (kg/m^2)
Wall					
1. Cellulose-gypsum board	0.012	0.352	0.034	1,150	13.8
2. Vapour barrier	0.001	0.071	0.014	40	0.04
3. OSB	0.012	0.143	0.084	630	7.56
4. Wood-fiber	0.14	0.042	3.333	50	7
5. Air	0.02	0.109	0.183	1	0.02
6. OSB	0.012	0.143	0.084	630	7.56
7. Celenit	0.035	0.064	0.547	400	14
8. Low emissivity layer	0.001	0.071	0.014	40	0.04
9. Air	0.046	0.092	0.500	1	0.046
10. Vapour barrier	0.001	0.071	0.014	40	0.04
11. YTONG block	0.115	0.165	0.697	600	69
12. Plaster	0.005	0.9	0.006	1,800	9
Total	0.4	–	5.510	–	128.106
Roof					
1. Fir	0.025	0.18	0.139	450	11.25
2. Vapour barrier	0.001	0.071	0.014	40	0.04
3. Celenit	0.05	0.062	0.806	360	18
4. Wood-fiber	0.1	0.038	2.632	140	14
5. Wood-fiber	0.04	0.038	1.053	140	5.6
6. Air (ventilated)	0.06	–	0.000	1	0.06
7. OSB	0.012	–	0.000	630	7.56
8. Low emissivity layer	0.001	–	0.000	40	0.04
9. Steel	0.0005	–	0.000	7,870	3.94
Total	0.290	–	4.644	–	60.49
Floor					
1. Tiles	0.01	–	0.000	2,300	23
2. Concrete	0.05	–	0.000	2,000	100
3. Concrete with tubes	0.05	–	0.000	2,000	100
4. Isolex	0.12	0.035	3.429	360	43.2
5. Isocal 400	0.27	0.126	2.143	400	108
Total	0.5	–	5.571	–	374.2

outside, are reported in Table 12.1, below those of the wall. As prescribed by the standard UNI EN ISO 6946, the thermal resistances of the ventilated air layer and of the layers above it have been considered as vanishing. If one takes into account the internal and external surface resistances recommended by UNI EN ISO 6946 (0.10 and 0.04 W/(m^2 K), respectively), the roof transmittance is 0.209 W/(m^2 K).

The floor has a thickness of 50 cm, and is composed of tiles, a cement layer, a second cement layer which contains the tubes of the radiant panel system, two insulating layers whose principal component is expanded polystyrene. The main

Table 12.2 General properties of the windows

Property	Value	Unit
Glass transmittance	1.305	W/(m^2 K)
Frame transmittance	2.099	W/(m^2 K)
Frame thickness	0.06	m
Glass-frame thermal bridge UNI EN ISO 10077-1	0.08	W/(m K)
Additional thermal resistance, R_{add}	0.26	m^2 K/W
Use fraction of R_{add}	0.6	–

properties of the layers of the floor, from inside to outside, are reported in the end of Table 12.1. The thermal resistances of the layers above the tubes of the radiant panels have been considered as vanishing. The total thermal resistance of the insulating layers (below the tubes of the radiant panels) is 5.571 (m^2 K)/W, and corresponds to a transmittance of 0.179 W/(m^2 K).

To determine the heat exchanges between the house and the ground, the time evolution of the temperature of the ground, at the interface ground-floor, has been evaluated by means of a finite element simulation performed through the software COMSOL Multiphysics. The computational domain considered is a cross section of the floor and of the soil, with a depth of 16 m from the ground surface and a width of 16 m around the building.

The hourly values of the external air temperature of Bologna, in the typical meteorological year given by the software Meteonorm Version 5, available in TRNSYS 16, have been approximated by a sinusoidal function with mean value 14 °C and amplitude 12 °C. The temperature of the upper surface of the floor has been set equal to 20 °C during the heating period and equal to 26 °C during the cooling period. The obtained time evolution of the temperature at the surface between ground and floor has been approximated by the interpolating function

$$\theta_{gd} = 16.3 - 2.3 \sin\left(0.0007173\, t - 1\right) \tag{12.1}$$

where θ_{gd} is the temperature of the surface between ground and floor and t is time, in hours. Equation (12.1) has been employed in the dynamic simulation performed through TRNSYS.

The windows are double glazed, 4 mm glass—16 mm argon—4 mm glass, with a low emissivity layer and a wooden frame. The window sizes, in centimeters, are the following: 120 × 100 (2 windows), 120 × 210 (2 windows), 220 × 210 (2 windows), 80 × 100 (2 windows), 50 × 100 (1 window). The general properties of the windows are reported in Table 12.2. To insert the properties of the windows in TRNSYS the following procedure has been adopted. The window ID 13001, Saint Gobain CLIMAPLUS FUTUR AR 1.4 4/16/4, which has a glass transmittance of 1.43 W/(m^2 K) has been considered. To obtain a glass transmittance of 1.305 W/(m^2 K), an additional thermal resistance equal to 0.067 m^2 K/W has been applied to the glass surface. This resistance has been added to the whole window area, as a convective thermal resistance, and multiplied by the ratio between glass area and

total area. The 60 % use fraction of the additional thermal resistance R_{add} due to closed rolling shutter has been obtained by assuming that shutters are closed from 6 pm to 8 am.

The linear transmittances of the thermal bridges have been evaluated as prescribed by the standard UNI EN ISO 14683. The kinds and linear transmittances (with reference to the internal length) of the thermal bridges are: intersection of two vertical walls (C4), $\psi = 0.10$ W/(m K); connection wall-window (W16), $\psi = 0.15$ W/(m K); intersection wall-roof (R10), $\psi = 0.20$ W/(m K); intersection wall-floor (GF8), $\psi = 0.20$ W/(m K).

12.3 Climatic Data

The climatic data are available in the meteorological files of TRNSYS 16, which are taken from the software Meteonorm 5. The climatic data for Bologna refer to the exact values of latitude and longitude (44°30′ North, 11°21′ East), but to an altitude of 158 m, very close to that of Casalfiumanese (125 m). Therefore, they can be employed for Casalfiumanese without corrections. The values of the monthly averaged temperature of the external air during the Typical Meteorological Year (TMY) considered in Meteonorm 5, obtained by averaging the hourly data, are reported in Table 12.3. The simulation code TRNSYS evaluates the radiant energy incident on a plane with any slope and azimuth angle, during each hour. By employing the hourly data, we have determined the values of the radiant energy incident during each month on the PV panels, integrated in the roof pitch oriented towards South (slope 14°, azimuth 16°), and on the thermal solar collectors, oriented towards exact South with a slope of 60°. The results obtained are reported in Table 12.3. The radiant energy incident in a year on the above mentioned planes is 1,293 kWh/m^2 for the plane with slope 14° and azimuth 16°, and 1,219 kWh/m^2 for the plane with slope 60° and azimuth 0° (true South).

12.4 Forced Ventilation with Heat Recovery, Set Point Conditions and Internal Heat Gains

The volume flow rate of fresh air is evaluated according to the standard UNI EN 15251: 2008, by assuming that the building is a second-class one. During occupancy, the prescribed flow of fresh air is 0.42 l/(s m^2), and thus 39.14 l/s for the apartment. We assume $\dot{V}_{ve} = 40$ l/s (144 m^3/h). During the non-occupancy period, the prescribed flow rate is between 0.05 and 0.1 l/(s m^2). By considering 0.075 l/(s m^2) one obtains 6.99 l/s. We assume $\dot{V}_{ve} = 7$ l/s (25.2 m^3/h). Since the net internal volume of the building is 335 m^3, during occupancy one has an air change rate equal to 0.43 h^{-1}. We refer to a 50 % occupancy and consider, for

Table 12.3 Climatic data

Monthly averaged temperatures of the external air for Bologna, TMY of Meteonorm 5, °C												
	Jan.	Feb.	Mar.	Apr.	May	June	July	Aug.	Sept.	Oct.	Nov.	Dec.
	1.7	4.3	9.4	13.8	20.2	21.5	24.4	24.1	20.9	14.4	8.4	3.9
Monthly solar radiation per unit area on the planes of the PV and thermal collectors, W/m^2												
φ [°]	Jan.	Feb.	Mar.	Apr.	May	June	July	Aug.	Sept.	Oct.	Nov.	Dec.
14	47.72	55.19	98.04	126.15	156.00	172.91	183.85	165.03	122.87	83.68	44.64	37.29
60	66.87	63.47	102.92	114.00	123.49	132.16	143.37	144.25	123.69	98.23	55.99	50.75

the evaluation of ventilation heat losses, the average value $\dot{V}_{ve} = 23.5\,\text{l/s} = 0.0235\,\text{m}^3/\text{s} = 84.6\,\text{m}^3/\text{h}$. The forced ventilation system is provided with a heat recovery unit with efficiency $\eta_{hru} = 0.92$.

The lowest value of the internal air temperature has been set equal to 20 °C, for every hour and thermal zone. Similarly, the highest value of the internal air temperature has been set equal to 26 °C. The relative humidity control of the internal air, at 50 % relative humidity, is performed only during the cooling season (without winter humidification). In agreement with UNI TS 11300-1, the internal heat gains are evaluated through the equation

$$\dot{Q}_{int} = 5.924 \times A_f - 0.01557 \times A_f^2 \tag{12.2}$$

where $\dot{Q}_{int}$ is the power of internal gains in W, and A_f is the heated floor area in m^2. Since $A_f = 93.2\,\text{m}^2$, one has $\dot{Q}_{int} = 358.2$ W.

12.5 Thermal Energy Needs for Heating, Cooling and Dehumidifying

By employing the data reported in the preceding sections, TRNSYS evaluates directly the hourly needs of thermal energy for heating, cooling and dehumidifying. The hourly needs of thermal energy for heating and cooling are illustrated in Fig. 12.3; the monthly ones are illustrated in Fig. 12.4. The monthly energy needs for dehumidifying are illustrated in Fig. 12.5. The yearly need of thermal energy is 3,646.8 kWh (i.e. 39.13 kWh/m^2) for heating, 1,168.5 kWh for cooling, 368.9 kWh for dehumidifying.

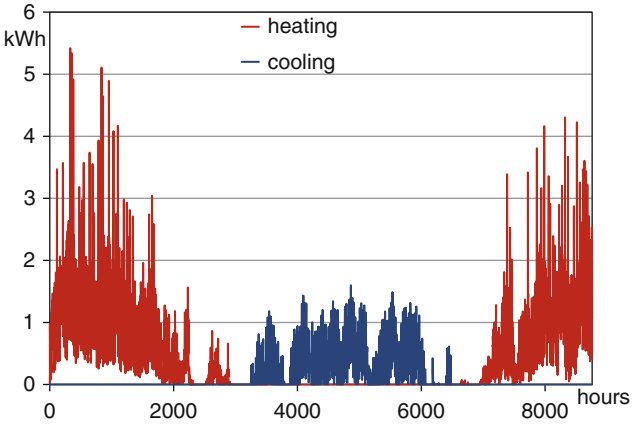

Fig. 12.3 Hourly energy needs for heating (*red*) and cooling (*blue*)

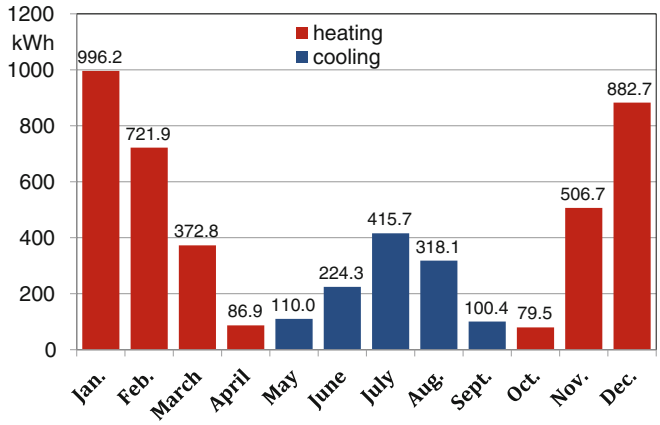

Fig. 12.4 Monthly energy needs for heating (*red*) and cooling (*blue*)

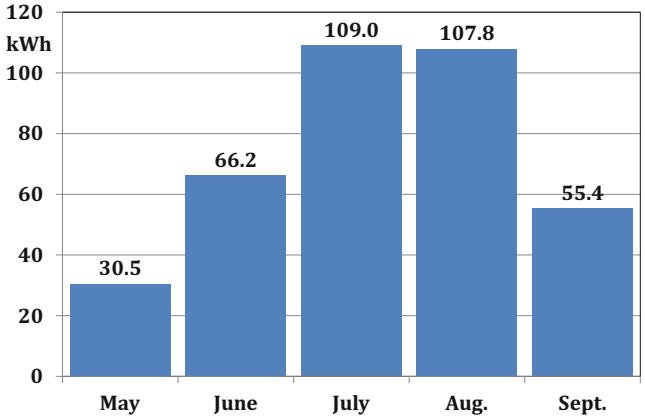

Fig. 12.5 Monthly energy needs for dehumidifying

12.6 Thermal Energy Needs for Domestic Hot Water (DHW)

The monthly energy need of thermal energy for DHW production has been evaluated as prescribed by the standard UNI/TS 11300-2. The thermal energy required in a month is given by

$$Q_{DHW} = \rho \times c \times V_W \times (\theta_{SW} - \theta_0) \times G \tag{12.3}$$

Table 12.4 Monthly needs of thermal energy for DHW production

Monthly needs of thermal energy for DHW production, kWh											
Jan.	Feb.	Mar.	Apr.	May	June	July	Aug.	Sept.	Oct.	Nov.	Dec.
129.6	117.1	129.6	125.4	129.6	125.4	129.6	129.6	125.4	129.6	125.4	129.6

where ρ is the water density, c is the specific heat capacity at constant pressure, V_W is the volume of water supplied in a day, θ_{SW} is the temperature of the supplied water, θ_0 is the temperature of water in waterworks, G is the number of days in the month.

One assumes, conventionally, $\theta_{SW} = 40$ °C and $\theta_0 = 15$ °C, so that $\theta_{SW} - \theta_0 = 25$ °C. For residences, the daily DHW use in liters is given by

$$V_W = a \times A_f \tag{12.4}$$

where A_f is the useful floor area (93.2 m^2) and a is a coefficient which, for values of A_f between 51 e 200 m^2, is given by the equation

$$a = 4.514 \times A_f^{-0.2356} \tag{12.5}$$

In the case under exam, one has $a = 1.551$ and $V_W = 144.54$ l/day. As a consequence, by employing for the density ρ the mean value between 15 and 40 °C (995.7 kg/m^3) and for c the conventional value recommended in UNI/TS 11300-2 (1.162 Wh/(kg K)), one obtains the daily need of thermal energy $Q_{DHW} = 4.181$ kWh/day. The monthly needs of thermal energy for DHW production are reported in Table 12.4. The annual need of thermal energy for DHW is 1,526 kWh, and corresponds to 41.8 % of that for space heating.

12.7 Description of the Heating, Cooling and Dehumidifying Plant

Space heating and cooling are accomplished by means of water circulation in floor radiant panels. The water inlet temperature in the radiant panels is 35 °C during winter and 18 °C during summer. The emission, control and distribution efficiencies are, respectively: $\eta_e = 0.99$ for heating and $\eta_e = 0.97$ for cooling; $\eta_c = 0.97$; $\eta_d = 0.998$; there is no storage. The total emission, control and distribution efficiency, for heating, is $\eta_{ecd} = 0.99 \times 0.97 \times 0.998 = 0.958$.

The water at the desired temperature is produced by an air-to-water heat pump with inverter, with nominal electric power 1.37 kW, nominal heating thermal power 5.80 kW and nominal cooling power 7.0 kW. The humidity control is performed by a dehumidifier with an absorption of 0.350 kW.

Table 12.5 COP of the heat pump for a water supply temperature of 35 °C

	% of nominal frequency								
θ_e (°C)	100 %	90 %	80 %	70 %	60 %	50 %	40 %	30 %	15 %
−10	2.69	2.72	2.75	2.79	2.83	2.86	2.87	2.88	2.88
−7	2.86	2.88	2.92	2.96	3.00	3.03	3.05	3.06	3.06
0	2.97	3.00	3.04	3.08	3.12	3.15	3.17	3.18	3.18
2	3.07	3.10	3.14	3.18	3.23	3.26	3.28	3.29	3.29
7	4.20	4.24	4.29	4.35	4.41	4.45	4.48	4.49	4.49
10	4.63	4.67	4.73	4.80	4.86	4.91	4.94	4.95	4.96
20	6.07	6.12	6.20	6.28	6.37	6.43	6.47	6.49	6.49
30	7.50	7.57	7.67	7.77	7.88	7.95	8.00	8.03	8.03

Table 12.6 Heating power of the heat pump for a water supply temperature of 35 °C, kW

	% of nominal frequency								
θ_e (°C)	100 %	90 %	80 %	70 %	60 %	50 %	40 %	30 %	15 %
−10	3.02	2.87	2.61	2.27	1.93	1.58	1.24	0.90	0.56
−7	3.26	3.09	2.81	2.45	2.08	1.71	1.34	0.97	0.61
0	3.99	3.78	3.44	2.99	2.54	2.09	1.64	1.19	0.74
2	4.20	3.80	3.62	3.15	2.67	2.20	1.72	1.25	0.78
7	5.82	5.52	5.02	4.37	3.71	3.05	2.39	1.73	1.08
10	6.32	5.99	5.45	4.74	4.02	3.31	2.59	1.88	1.18
20	7.98	7.57	6.88	5.99	5.08	4.18	3.28	2.38	1.49
30	9.64	9.15	8.32	7.24	6.14	5.05	3.96	2.87	1.79

Table 12.7 EER of the heat pump for a water supply temperature of 18 °C

	% of nominal frequency								
θ_e (°C)	100 %	90 %	80 %	70 %	60 %	50 %	40 %	30 %	15 %
5							12.87	15.41	19.03
15							10.48	12.55	15.50
25			5.72	6.02	6.27	6.55	7.16	8.57	10.58
35	3.61	3.79	4.04	4.19	4.37	4.69	5.13	6.14	7.58
45	2.64	2.84	2.99	3.10	3.15	3.43	3.74	4.48	5.54

The COP of the heat pump, for a water supply temperature of 35 °C, is reported in Table 12.5, as a function of the external temperature, θ_e, and of the percent of nominal frequency. The heating thermal power for a water supply temperature of 35 °C, is reported in Table 12.6, as a function of the external temperature and of the percent of nominal frequency.

The EER of the heat pump, for a water supply temperature of 18 °C, is reported in Table 12.7, as a function of the external temperature, θ_e, and of the percent of nominal frequency. The cooling thermal power for a water supply temperature of 18 °C is reported in Table 12.8, as a function of the external temperature and of the percent of nominal frequency. The EER of the air dehumidifier is assumed equal to 2.0.

Table 12.8 Cooling power of the heat pump for a water supply temperature of 18 °C, kW

	% of nominal frequency								
θ_e (°C)	100 %	90 %	80 %	70 %	60 %	50 %	40 %	30 %	15 %
5							4.01	2.90	1.75
15							3.66	2.63	1.57
25			6.58	5.82	5.02	4.19	3.30	2.35	1.38
35	7.00	6.57	5.94	5.24	4.52	3.75	2.95	2.08	1.20
45	6.24	5.85	5.25	4.63	3.98	3.29	2.57	1.79	1.00

12.8 Electric Energy Use for Heating

The electric energy used by the heat pump, for heating, is evaluated by considering, for each hour, the thermal power supplied by the heat pump (i.e., the thermal power required by the building divided by the total plant efficiency $\eta_{ecd} = 0.958$) and the external air temperature. This method allows one to determine, for each hour, the COP of the heat pump and, as a consequence, the use of electric energy for heating.

The data of the COP and of the heating power of the heat pump provided by the constructor, reported in Tables 12.5 and 12.6, are employed. Through proper interpolating equations of the COP as a function of the heating power $\dot{Q}_{HP}$, for each value of the external air temperature θ_e, one can associate with every pair of values (θ_e, $\dot{Q}_{HP}$) the corresponding COP of the heat pump. When the required heating power is lower than the minimum power which can be supplied by the heat pump without intermittence (at 15 % of the nominal frequency), the COP is evaluated through the expression

$$COP = f \times COP_{100} \tag{12.6}$$

where COP_{100} is the COP at 100 % of the nominal frequency at the external temperature under consideration and $f < 1$ is a correction coefficient introduced to take into account the intermittent operation. To determine f, the capacity ratio CR is introduced, given by

$$CR = \frac{\dot{Q}_{HP}}{\dot{Q}_{100}} \tag{12.7}$$

where $\dot{Q}_{100}$ is the heating power supplied at 100 % of the nominal frequency at the external temperature under consideration. Then, the following expression of f, recommended in [8], is employed

$$f = \frac{4 \times CR}{0.1 + 3.6 \times CR} \tag{12.8}$$

The values of the monthly use of electric energy for heating are reported in Table 12.10 (first row). The annual use of electric energy for heating is 1,115.0 kWh, while the annual use of thermal energy (annual energy need for heating divided by η_{ecd}) is 3,806.7 kWh. Thus, the seasonal *COP* is given by

$$SCOP = \frac{3806.7}{1115.0} = 3.414 \tag{12.9}$$

12.9 Electric Energy Use for Cooling and Dehumidifying

In analogy with the prescription of the standard UNI TS 11300-3 for monthly loads, the effective hourly load of thermal energy for cooling $\dot{Q}_{cr}$ is calculated by adding to the hourly energy need for cooling, $\dot{Q}_{C,nd}$, the emission and control losses,

$$\dot{Q}_{cr} = \dot{Q}_{C,nd} + \dot{Q}_e + \dot{Q}_c \tag{12.10}$$

The emission losses are given by

$$\dot{Q}_e = \dot{Q}_{C,nd} \frac{1 - \eta_e}{\eta_e} \tag{12.11}$$

where η_e is the emission efficiency, equal to 0.97 for floor radiant panels. The control losses are given by

$$\dot{Q}_c = \left(\dot{Q}_{C,nd} + \dot{Q}_e\right) \frac{1 - \eta_c}{\eta_c} \tag{12.12}$$

where η_c is the control efficiency, equal to 0.97 (modulating single room temperature control). The values of $\dot{Q}_{C,nd}$, for each hour, are calculated by TRNSYS.

To determine the *EER* of the heat pump for each hour, the following method is employed. For each hour, the partial load factor F is determined, defined as the ratio between the effective heat load for cooling $\dot{Q}_{cr}$ and the nominal cooling power of the heat pump, equal to 7 kW (100 % of nominal frequency, external air temperature 35 °C, water supplied to the radiant panels at 18 °C).

For $F > 0.15$, the data of the *EER* and of the cooling power of the heat pump reported in Tables 12.7 and 12.8 are employed. By proper interpolating equations of the *EER* as a function of the cooling power, one for each value of the external air temperature θ_e, a *EER* value is associated with every pair (θ_e, $\dot{Q}_{cr}$).

For $F < 0.15$, a coefficient $f < 1$ of the *EER* at 15 % of nominal frequency is introduced, to take into account the intermittent operation. The values of f recommended by UNI TS 11300-3 are employed, by replacing the tables with the interpolating function

$$f = 0.245 \ \ln F + 1.424 \tag{12.13}$$

By an interpolation of the data reported in Table 12.7, the following expression of the *EER* at 15 % of the nominal frequency, EER_{15}, as a function of the external air temperature is determined:

$$EER_{15} = 0.0035\theta_e^2 - 0.524\theta_e + 21.859 \tag{12.14}$$

Then, the *EER* is calculated by the expression

$$EER = f \ \ EER_{15} \tag{12.15}$$

By this method, the electric energy use for cooling for each hour is determined. The values of the monthly use of electric energy for cooling are reported in Table 12.10 (second row). The annual use of electric energy for cooling is equal to 150.7 kWh; the annual use of thermal energy for cooling (annual need of the building plus emission and regulation losses) is 1,241.9 kWh. Therefore the mean seasonal *EER* is

$$SEER = \frac{1241.9}{150.7} = 8.24 \tag{12.16}$$

The use of electric energy for dehumidifying, for each month, is obtained by dividing the thermal energy need for dehumidifying, reported in Fig. 12.5, by the *EER* of the dehumidifier, which is assumed equal to 2. The values of the monthly use of electric energy for dehumidifying are reported in Table 12.10 (third row). The annual use of electric energy for dehumidifying is equal to 184.4 kWh, a little higher than that for cooling.

12.10 Domestic Hot Water Production by a Thermal Solar Collector

DHW is produced by a thermal solar collector and by an air-to-water heat pump for DHW. A single-glazed solar collector with selective absorber, having the following features, is employed: aperture area $A = 2.29$ m^2; effective transmittance-absorptance product at normal incidence $\tau\ \alpha_0 = 0.770$; product of the heat removal factor F_R and the overall heat transfer coefficient U_L, $F_R\ U_L = 3.494$ W/(m^2 K). The overall efficiency for control, distribution and storage of the DHW production plant is assumed equal to $\eta_{DHW} = 0.95$. The values of the monthly use of thermal energy for DHW production (monthly need divided by η_{DHW}), in kWh, are reported in Table 12.9 (first row). The annual use of thermal energy is 1,606.3 kWh. The following additional data are assumed, for the solar DHW production plant: efficiency of the collector/storage heat exchanger 0.7; storage volume 131 kg/m^2

Table 12.9 Monthly values of the use of thermal energy for DHW production (kWh), of the fraction f supplied by the solar system, of the thermal energy supplied by the heat pump (kWh), and of the COP of the heat pump

	Jan.	Feb.	Mar.	Apr.	May	June	July	Aug.	Sept.	Oct.	Nov.	Dec.
$Q_{DHW,mth}$	136.4	123.2	136.4	132.0	136.4	132.0	136.4	136.4	132.0	136.4	132.0	136.4
f	0.466	0.505	0.763	0.872	0.933	1.000	1.000	1.000	0.959	0.756	0.418	0.333
$Q_{HP,mth}$	72.8	60.9	32.3	16.9	9.1	0.0	0.0	0.0	5.4	33.3	76.9	91.0
COP	1.80	2.01	2.48	2.92	3.61	3.75	4.07	4.04	3.69	2.99	2.38	1.98

(aperture area); collector orientation South with slope 60°. Only one collector is employed. The monthly values of the fraction f of the heat load supplied by the solar system are determined by the f-chart method, in agreement with the prescriptions of the standard UNI 8477-2: 1985, and are reported in Table 12.9 (second row). The mean value of f during the whole year is $f_m = 0.7518$.

12.11 Electric Energy Use for Domestic Hot Water Production

The monthly use of thermal energy for DHW production not supplied by the solar system is provided by an air-to-water heat pump for DHW, with highest electric absorption of 2.1 kW and a 300 l storage. By interpolating the data given by the constructor, the following expression of the COP of the heat pump as a function of the external air temperature, for a DHW supply temperature of 40 °C, is determined

$$COP = -0.0000267\ \theta_e^3 + 0.001759\ \theta_e^2 + 0.07131\ \theta_e + 1.6738 \qquad (12.17)$$

Equation (12.17) is employed with reference to the mean monthly values of the external air temperature. Monthly values of the thermal energy supplied by the heat pump ($Q_{HP,mth}$) and of the COP are reported in Table 12.9 (third and fourth rows). Monthly values of the use of electric energy for DHW production are reported in Table 12.10 (fourth row). The value of the thermal energy supplied by the heat pump during 1 year is $Q_{HP,yr} = 398.7$ kWh, the annual use of electric energy is 183.0 kWh, and the seasonal COP is $SCOP_{DHW} = 2.18$.

12.12 Electric Energy Use for Forced Ventilation

The fan of the forced ventilation system with heat recovery absorbs 80 W during the occupancy period, when $\dot{V}_{ve} = 144\ \mathrm{m^3/h}$, and 30 W during the non-occupancy period, when $\dot{V}_{ve} = 25.2\ \mathrm{m^3/h}$. Since the two periods have the same duration, one can consider the mean absorption, equal to 55 W. The values of the monthly use of electric energy for forced ventilation are reported in Table 12.10 (fifth row).

Table 12.10 Monthly use of electric energy for heating, cooling, dehumidifying, DHW, ventilating, and total monthly use, kWh

	Jan.	Feb.	Mar.	Apr.	May	June	July	Aug.	Sept.	Oct.	Nov.	Dec.
Heating	317.6	217.8	112.6	31.3	0.0	0.0	0.0	0.0	0.0	27.2	144.5	264.1
Cooling	0.0	0.0	0.0	0.0	14.9	28.7	51.2	42.0	13.8	0.0	0.0	0.0
Dehum.	0.0	0.0	0.0	0.0	15.2	33.1	54.5	53.9	27.7	0.0	0.0	0.0
DHW	40.5	30.3	13.0	5.8	2.5	0.0	0.0	0.0	1.5	11.2	32.3	46.0
Vent.	40.9	37.0	40.9	39.6	40.9	39.6	40.9	40.9	39.6	40.9	39.6	40.9
Total	399.0	285.0	166.5	76.7	73.6	101.5	146.7	136.8	82.6	79.2	216.4	351.1

12.13 Total Use of Electric Energy for Air Conditioning and Domestic Hot Water

The values of the monthly use of electric energy for heating, cooling, dehumidifying, DHW production and forced ventilation, as well as the sum of these values (total monthly use of electric energy for air conditioning and DHW production) are reported in Table 12.10. The total annual use of electric energy is 2,115.0 kWh; 52.7 % of total use is for heating, 22.8 % for ventilating, 8.7 % for dehumidifying, 8.7 % for DHW, 7.1 % for cooling.

12.14 Electric Energy Produced by the PV System

To obtain a quasi-zero energy building, completely self-sufficient for heating, cooling, dehumidifying, DHW production and forced ventilation, and nearly self-sufficient also for the electric energy use for lighting and appliances (including electric cooking), a PV system with a peak power of 6 kW is installed in the pitch of the roof oriented toward South. PV modules with polycrystalline cells having 15 % conversion efficiency are adopted; hence, the area necessary to obtain a peak power of 6 kW is 40 m^2. Since the modules are slightly ventilated, an overall system efficiency equal to 0.75 can be considered (UNI TS 11300-4).

For each hour, the electric energy produced by the PV system, per unit area, is calculated by multiplying the radiant energy incident on the plane of the PV panels, given by TRNSYS, by the cell conversion efficiency (0.15) and by the overall system efficiency (0.75). The monthly values of the electric energy produced by the PV system, with an area of 40 m^2, are reported in Fig. 12.6, where they are compared with the monthly values of the total energy use for air conditioning and DHW production. The electric energy produced in a year is 5,820 kWh, i.e., about 2.75 times the total energy use for air conditioning and DHW production. Therefore, the building has zero use of non-renewable energy sources for air conditioning and DHW production; moreover, the PV system supplies all, or nearly all, the electric energy for home appliances.

12.15 Energy Rating

The use of thermal energy for heating is $Q = 3{,}806.7$ kWh; the thermal energy coming from renewable sources (external air) is 2,691.7 kWh; the remaining part, 1,115 kWh, is PV electric energy. According to the Resolution 1366/2011 of the Region Emilia Romagna (Italy), the energy performance indicator for heating is

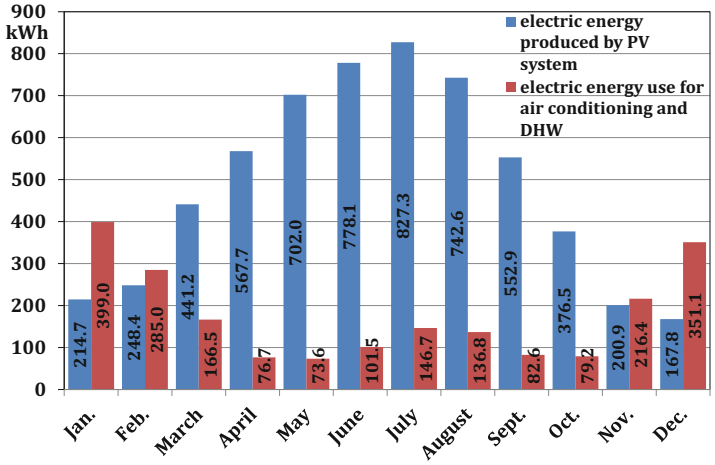

Fig. 12.6 Electric energy produced by PV system and use of electric energy for air conditioning and DHW

$$EP = \frac{1115}{93.2} = 11.96 \text{ kWh/m}^2 \tag{12.18}$$

The part of the thermal energy for DHW production not provided by renewable sources of thermal energy (thermal solar collectors, external air) is 183 kWh and, again, is PV electric energy. Thus, the energy performance indicator for DHW is

$$EP_{DHW} = \frac{183}{93.2} = 1.96 \text{ kWh/m}^2 \tag{12.19}$$

The total energy performance indicator is

$$EP_{TOT} = EP + EP_{DHW} = 13.9 \text{ kWh/m}^2 \tag{12.20}$$

so that the energy label of the building is A^+ ($EP_{TOT} < 25$ kWh/m^2).

12.16 Conclusions

A new nearly zero energy one-family house, in North-Centre Italy, has been designed and is under construction. The building (energy label A^+) has zero use of non-renewable energy sources for air conditioning and DHW production, and nearly zero use for lighting and appliances. About 71 % of the thermal energy used for heating is extracted from the external environment; about 29 % is PV electric energy. The electric energy used for cooling and dehumidifying (21 % of the thermal energy extracted from the house) is supplied by PV panels. About 75 %

of the annual energy use for DHW production is supplied by a thermal solar system; about 13.5 % is extracted from the external environment; about 11.5 % is PV electric energy.

Nomenclature

A	Area (m^2)
a	Dimensionless coefficient
c	Specific heat capacity (J/(kg K))
F	Partial load factor
f	Dimensionless coefficient
F_R	Heat removal factor
G	Number of days in a month
Q	Thermal energy (kWh)
$\dot{Q}$	Thermal power (W)
R	Thermal resistance per unit area (m^2 K/W)
t	Time (s)
U	Transmittance (W/(m^2 K))
V	Volume (m^3)
$\dot{V}$	Volume flow rate (m^3/s)

Greek Symbols

η	Efficiency
θ	Temperature (°C)
λ	Thermal conductivity (W/(m K))
ρ	Density (kg/m^3)
$\tau\ \alpha_0$	Effective transmittance-absorptance product at normal incidence
φ	Slope (°)
ψ	Linear transmittance (W/(m K))

Subscript and Superscripts

add	Additional
c	Control
C, nd	Cooling, need
cr	Cooling, real
d	Distribution
DHW	Domestic hot water
e	Emission, external
ecd	Emission, control, distribution
f	Heated floor
gd	Ground

HP Heat pump
hru Heat recovery unit
int Internal
L Overall
mth Month
SW Supplied water
TOT Total
u Useful
ve Ventilation
yr Year
0 *W*aterworks
100 100 % of nominal frequency
15 15 % of nominal frequency

Acronyms

COP Coefficient of performance
CR Capacity ratio
EER Energy efficiency ratio
EP Energy performance indicator
SCOP Seasonal COP
SEER Seasonal EER

References

1. Thiers S, Peuportier B (2012) Energy and environmental assessment of two high energy performance residential buildings. Build Environ 51:276–284
2. Marszal AJ, Heiselberg P, Bourrelle JS, Musall E, Voss K, Sartori I, Napolitano A (2011) Zero energy building—a review of definitions and calculation methodologies. Energy Buildings 43:971–979
3. Terlizzese T, Zanchini E (2011) Economic and exergy analysis of alternative plants for a zero carbon building complex. Energy Buildings 43:787–795
4. Gustavsson L, Joelsson A (2010) Life cycle primary energy analysis of residential buildings. Energy Buildings 42:210–220
5. Karlsson JF, Moshfegh B (2007) A comprehensive investigation of a low-energy building in Sweden. Renew Energy 32:1830–1841
6. Citherlet S, Defaux T (2007) Energy and environmental comparison of three variants of a family house during its whole life span. Build Environ 42:591–598
7. International Energy Agency (IEA) (2008) Net zero energy buildings database. http://iea40.buildinggreen.com/index.cfm
8. Scarpa M (2010) Procedure for the calculation of COP and capacities of heat pumps at any operating conditions. CTI Internal report, July 2010

Chapter 13
Integrative Approach for Desert Sustainable Ecohouse Design

Khaled A. Al-Sallal and Iman K. Al-Sallal

Abstract The study presents an integrative approach for desert sustainable architectural design that could be valuable to building professionals who might search for sound application models useful in harsh desert conditions. Following an integrated process of design and performance evaluation, a sustainable eco-friendly house was designed in light of Estidama guidelines, assessment method, and other design information documents (building codes, standards, and design guidance). The traditional courtyard form configuration was adapted and optimized to improve shading, natural ventilation through the courtyard assisted by wind towers to promote airflow, and special attention was also given to greenery and landscape elements to avoid heat and cool the house. All these systems were simulated and improved in order to achieve optimum energy performance. The design achieved considerable improvement over a typical Emirati house case; 59 % reduction in the greenhouse gas emissions and utility bill.

Keywords Sustainable design • Eco-house • Desert • Green roof • Landscape • Courtyard

13.1 Introduction

The climate of the UAE is considered to be one of the harshest within the globe; temperatures can reach up to 50 °C during the summer season. Indigenous people used to withstand such extremity through smart adaptation to the climate, local materials and architectural design strategies that can tolerate such temperatures. After oil was discovered in the UAE in the late 1950s, modern building technology was introduced to the region thus modern architecture was the result. Without keeping the influence to the environment in mind a lot of wrong practices were exercised such as the wrong building form and orientation for the climate, neglect

K.A. Al-Sallal (✉)
Architectural Engineering Department, UAE University, Al-Ain, UAE
e-mail: k.sallal@uaeu.ac.ae

I.K. Al-Sallal
SALA, University of British Columbia, Vancouver, BC, Canada V6T 1Z2
e-mail: iman.alsallal@gmail.com

I. Dincer et al. (eds.), *Progress in Sustainable Energy Technologies Vol II: Creating Sustainable Development*, DOI 10.1007/978-3-319-07977-6_13

of shading and passive systems, plantation with high irrigation needs, and excessive use of interlock pavement in the outdoors. These wrong practices generate unbearable levels of heat inside and outside of buildings; and eventually lead to high reliance on oversized systems for cooling, lighting, and other services.

Cooling and air conditioning of buildings in Abu Dhabi accounts for 75 % of electricity consumption in the summer months and is considered the major consumer of electricity [1]. This leads to very high levels of CO_2 and other greenhouse emissions. Landscape effect on heat gain mitigation on buildings has not been studied in the UAE. With the new policies in the UAE calling for green building such as Estidama guidelines and other codes, the consideration of landscape strategies to improve building environmental performance has become significant. Landscaping is considered as a challenging part due to its high water consumption and the scarcity of water resources especially in arid regions such as Abu Dhabi. In this study, the focus is on how landscape design contributes directly in enhancing the building energy performance; and thus lowering the overall energy consumption. Landscape elements such as green roofs, grass ground cover and greenery next to external walls were simulated to evaluate how it will integrate with other passive systems for an Eco-house design in order to achieve optimum energy performance. Where plants normally take a huge amount of water resources, the suitable plant types were carefully selected to consume the least amount of water.

13.2 Background

Designing buildings without taking into consideration proper design of building form, orientation, and envelope can lead to considerable increase in heat gains and energy use. A previous study on impact of urban patterns of residential buildings on energy use in Al-Ain city, UAE showed that 40 % of the total cooling energy is utilized to offset heat gains from walls and roof, and it could reach up to 75 % when combined with the glazing effect [2]. The area and orientation of glazing had a great impact on building energy use. Limiting the windows to only two elevations of the building resulted in a reduction of the total annual energy use by almost 55 %. To minimize energy use, the percentage of the glazing area per floor should be about 10–20 % of the surface area of the two elevations. Among the tested cases, buildings with perimeters ranging from 80 to 115 m with window to wall ratios of 1:6 performed better than others. The study also advised to minimize the area of glazing and shade windows when urban patterns force to use longer elevations on west and east elevations. Another study in the UAE investigated the thermal behavior of residential buildings with regard to orientation, shading devices on windows, walls and roofs, and night ventilation [3]. In terms of orientation, both north and south orientations performed better from the thermal behavior point of view. Windows' shading reduced room temperature by up to 3 °C, while wall and roof shading caused a reduction of 2 °C, and a combination of roof, wall and 80 % of window shading caused and extra 3 °C reduction. Summer night ventilation in a

room changing its air volume ten times per hour (10 ACH) resulted in a maximum room temperature of 37.4 °C.

Vegetation can reduce the heat reaching the building and penetrating its envelope by increasing the reflection of solar radiation and by providing shading. It can achieve evaporative cooling and take the heat away through the process of transpiration.

Vegetation surfaces and pavement materials heavily influence outdoor thermal environments. Field measurements performed in Singapore revealed there were clear effects of hard versus vegetation surfaces on globe temperature and mean radiant temperature (MRT) [4]. The characteristics of heat and water transfer processes in porous block pavement, asphalt, grass and ceramic porous pavement were analyzed using numerical modeling. The model revealed that the surface temperature of permeable pavement is appreciably lower than that of impermeable pavement [5]. A filed experiment conducted in Eastern Saudi Arabia found a good correlation between pavement temperature and air temperature [6]. Other experiments in Singapore showed that granite slab, terracotta bricks and concrete interlocking blocks provide lower surface temperatures and heat output than conventional asphalt concrete pavements [7]. An empirical study was performed on five pavements in three areas of Taiwan to study the seasonal influence of pavement on outdoor thermal environments [8]. The study found that asphalt concrete and concrete have higher temperature than interlocking blocks or interlocking blocks with grass infilling, and grass always has the lowest air temperature. The surface temperature of artificial pavements was 10 °C higher than that of vegetation surface at noon in the summer, but the difference among the various pavement types were not significant in winter.

Shade trees have great effect in reduction of cooling costs in hot climates. Akbari et al. [9] quantified the effect of shade trees on the cooling costs of two similar houses in Sacramento, California and the results showed that the trees reduced seasonal cooling costs by between 26 and 47 %. The same study modeled the effect of the trees on both houses using the DOE-2.1E3 simulation program and found that the model underestimated the energy savings of the trees by as much as twofold. Another study by Akbari and Taha [10], which used simulation to study the effect of trees on energy use in four Canadian cities, concluded that increasing the vegetative cover of a neighborhood by 30 % and increasing the albedo of houses by 20 % would decrease heating costs by 10–20 % and decrease cooling costs 30–100 %. A simulation study by Simpson and McPherson [11] found that trees shading the west side of houses in California had the biggest effect on cooling costs and that adding shade trees to a house on the west and east sides reduced annual cooling costs by 10–50 %. Another study by McPherson and Simpson [12], which used simulation modeling and aerial photography to estimate the energy savings of existing urban trees and new plantings in California indicated that existing trees could reduce peak energy load by 10 % resulting in annual savings of $779 million. They estimated that planting an additional 50 million trees on the east and west sides of houses would further reduce peak load by an average of 4.5 % over the next 15 years, which would result in total

savings for consumers of $3.6 billion or $71 per tree. In a recent study, Donovan and Butry [13] estimated the effect of shade trees on the summertime electricity use of 460 single-family homes in Sacramento, California. Results showed that trees on the west and south sides of a house reduced summertime electricity use by 185 kWh (5.2 %), whereas trees on the north side of a house increased summertime electricity use by 55 kWh (1.5 %). Results also showed that a London plane tree, planted on the west side of a house, can reduce carbon emissions from summertime electricity use by an average of 31 % over 100 years.

The effect of conventional landscape elements (i.e.; grass cover with shade trees) can further be improved if combined with a green roof. The term "*green roof*" generally represents vegetation and growing medium planted on the building rooftop. There are several environmental benefits associated with green roofs such as energy savings through building envelope thermal regulation, roof membrane protection and thus prolonged building's life cycle, sound insulation as green roofs act as an acoustic barrier and finally other benefits at the urban level such as mitigating urban heat island effect and storm water retention. With introducing circular no. 171, green roofs and vertical landscaping by Dubai Municipality (DM) that became effective since July 2009 [14], both building consultants and contractors have to integrate green roofs into their new buildings' design taking into consideration the selection of proper vegetation type, irrigation system, insulation materials and roof structural membrane system. Estidama also encourages applying the concept of green roofs and external landscaping in order to mitigate heat island effects [1, 15, 24]. NRC-IRC constructed a field roofing facility at its Ottawa campus to study the performance of garden roofs [16]. This energy demand was reduced from 6.5–7 to less than 1.0 kWh/day in the garden roof, a reduction of over 75 %. The garden roof was more effective in controlling heat gain than in reducing heat loss because of the various thermal mechanisms involved, shading, insulation, evapotranspiration and thermal mass. It reduced heat gain by 95 % and heat loss by 26 %. The study also predicted that in warmer regions where cooling rather than heating is the main concern, the results could be more significant. It also showed how garden roofs can lower the temperature and modify the temperature fluctuations experienced by the roofing membrane, which results in greater durability and an extended service life for the roof membrane. Another study [17] evaluated the life cycle environmental impacts of an eight story residential building, including the addition of a green roof (only 16 % of the building's exposed surface area), located in downtown Madrid, Spain using computer simulation. Due to a lower absorption of solar radiation and lower thermal conductance, the addition of a green roof was estimated to reduce annual energy consumption by 1.2 %. This was primarily due to summer cooling load reductions of over 6 %. For the upper floors, the peak hour cooling load was reduced by as much as 25 % relative to the common flat roof.

13.3 Design Approach

The developed design symbolizes an oasis stranded in the desert, withstanding harsh weather and sustaining itself from its difficult conditions. The oasis is represented by the luscious courtyard, landscape, water elements and the vast number of openings that are embraced by the house from inside, while the harsh climate is represented by the desert-like landscape and the image and texture of the building from the exterior. Amongst several effective strategies, two fundamental ones were given special attention: minimizing solar heat gain through shading and proper building envelope and maximizing passive cooling through natural ventilation. The traditional courtyard form configuration was adapted and optimized to improve shading and natural ventilation and wind towers were used to promote airflow. Special attention was also given to greenery as effective shading and passive cooling design elements, yet the plants were selected very carefully to satisfy the harsh conditions of the desert climate in terms of water scarcity and excessive heat.

13.3.1 Building Form/Footprint

Careful study is required by Estidama Guidelines (sec. 4.3.3) to arrive at a building footprint and orientation that work with the building envelope to maximize energy benefit [1]. It is best to choose a building footprint and shape that works with requirements for daylighting, cooling, and function. To achieve this, the eco-house is configured around a central courtyard. This form configuration is deeply rooted in the traditional architecture of the Arab Gulf house due to social, cultural, and ritual needs [18]. Using this kind of form in the desert regions is also recommended according to several studies [18–20] due to bioclimatic benefits such as solar shading and natural cooling (e.g., evaporative cooling and nocturnal night sky). The courtyard acts as a well into which the cooler air from the roof sinks, and so the downstairs rooms cool more rapidly during the night [20]. Regarding orientation, LEED for Homes [21] gives a design requirement in section Innovation and Design Process, ID-credit 1 Integrated Project Planning, 1.5 Building Orientation for Solar Design: glazing area on north and south facing walls of the building should be at least 50 % greater than the sum of the glazing area on the east and west facing walls. This was considered in the design of the eco-house. Figure 13.1 shows the site plan and a 3D view of the designed house.

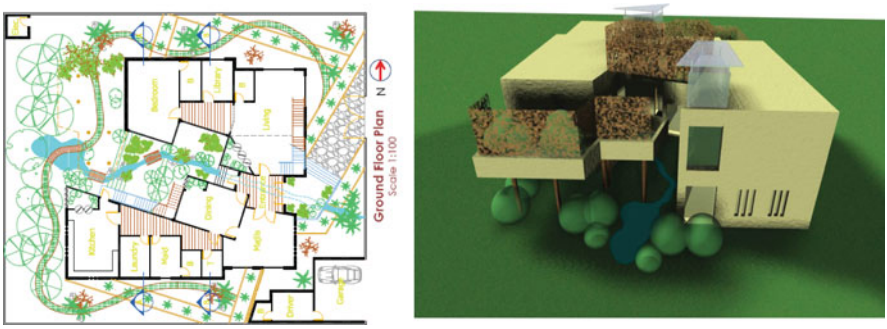

Fig. 13.1 Site showing landscape elements (*left*) and 3D view (*right*) of the Eco-House

13.3.2 Passive Systems

The design of the building form has integrated different passive architectural items derived from the Emirati vernacular architecture. These items are represented mainly in the design of the courtyard and wind towers, besides other innovative design features such as the green roof. These features qualify the design to earn Estidama Credit ADM5: Innovation in Design [15]. This can also qualify to earn ID-credit 3: Innovative or Regional Design in LEED for Homes [21]. Having a courtyard is preferred in warm and humid climates especially when the courtyard can induce ventilation due to the stack effect [22] where the wind direction should be taken into account. Thus, the central courtyard is located in the middle of the house mass, the shape consists of two squares joined together and inclined at an angle, the house surrounds it all but is opened at two sides to allow for movement of water through, and to welcome the north-west winds that would help a great deal in passive cooling. At the start and towards the end of the north-south axis are two wind towers incorporated into the house. These towers confine the winds and cool the house in return. Wind towers promote passive cooling using natural ventilation via stack effect. Stack effect works mainly when there is a difference in temperature where hot air rises at the top of the wind tower and exits the house taking excess interior heat. In cool days and nights, the wind tower captures cold wind and directs it into the house's interior.

Regarding the green roof, there are three roof gardens that integrate the house further with nature and aid in passive cooling. In hot climates, a green roof acts as a buffer that protects the building from extreme solar radiation, and hence reduces the net heat gain. Therefore, it helps in cooling the surrounding area, as well as regulating the internal building temperature and decreasing the amount of energy required to cool the building structure. Moreover, a green roof reduces the requirements for traditional insulation [14]. As for the green roof structure [16, 23], the whole roof area was 150 mm solid concrete slab, lined with a waterproof membrane insulated with Polyfoam Roofboard 200 mm thick (2×100 mm), covered with Polyfoam Slimline membrane. The Slimline membrane was overlaid with a root

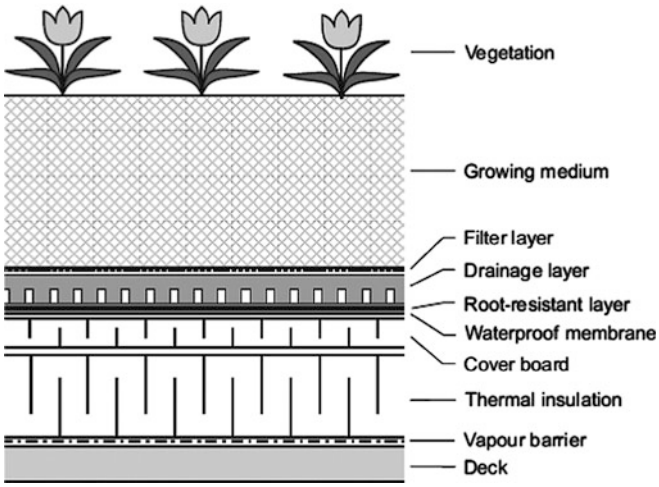

Fig. 13.2 Green roof structural elements, adapted from [16]

barrier/moisture reservoir as specified ensuring there were no overlapped gaps and edges. That was covered with a filtration layer, and growing matter as specified by Estidama [24] in order to match desert plants. That typical green roof section (see Fig. 13.2) has a U-value of 0.15 W/m^{2}K without considering the insulation value of the soil which varies with the water content.

13.3.3 Envelope

The use of construction materials in modern houses is another aspect that is greatly varied and hence it is difficult to assume one certain type. What was seen as more important than the type of construction was the U-value of the envelope components as specified by building codes. At the time of the study, Abu Dhabi Emirate did not have a code specifying the envelope U-values, hence the eco-house was designed to comply with the maximum permissible requirement of the U-value specified in Resolution 66 of Dubai Municipality (DM) for roofs, walls, and glazing components [25]. This required implementing the obligatory U-values of DM: 3.28 W/m^{2}K for glazing, 0.57 W/m^{2}K for walls, and 0.44 W/m^{2}K for floor slabs and roof slabs. By implementing the above U-values, an estimated energy reduction can reach up to 40 % according to DM resolution 66. To reach these required U-values, a thorough search in the local building material market was done before the final design of the walls, roof, and glazing assemblies. To evaluate the performance of the improved envelope, another reference case was created to represent the typical envelope material assemblies in the Emirati house. After this point, the improved envelope case was used as a baseline case to assess other improvements.

13.3.4 Landscape

Landscape design and location (whether horizontally or vertically) tend to maximize shading around the house especially near the windows, and minimize the load due to ground reflected solar radiation by using appropriate ground cover such as grass. The impact of the grass ground cover along with the shade trees on energy was evaluated in this eco-house. The exterior shade trees were set to provide only 50 % shading on walls and windows. Where plants normally take a huge amount of water resources, the suitable plants type was carefully selected. Palm trees, ornamental trees and aqueous plants such as Yucca Filamentosa and Yucca Aloifolia were recommended [14]. These desert plants are suitable for intensive greening, yet consume the least water. They are normally watered by drip irrigation and consume from 50 to 60 L/day for palm and ornamental trees, and as little as 15–20 L/m^2/day for the aqueous plants. According to Estidama credit (PW-2.1: Exterior Water Use Reduction: Landscaping) in areas with low rainfall or seasonal droughts, up to 60 % of total seasonal water usage can be attributed to irrigation [24]. As mentioned earlier, the main system used for plants irrigation is drip irrigation (mainly for roof gardens) besides a bioswale for the house's central courtyard. A bioswale is a densely vegetated open channel designed to attenuate and treat storm water runoff. It has gentle slopes to allow runoff to be filtered by vegetation planted on the bottom and sides of the swale (see Fig. 13.1).

13.3.5 Systems

Regarding water reuse in the house, a gray water system is being introduced. In this essence, it is known that domestic wastewater generated from washing, showering, cooking etc. is commonly referred to as grey water. A typical family of four produces about 360 L/day of Gray water = 135,000 L/year. Recycling this wastewater stream can reduce the demand for potable water supply. Grey water can be collected, treated and used for irrigation, cleaning, fire fighting top up, or for toilet flushing. That will allow the house to earn Estidama credits: ADW1: Water Consumption and ADW2: Monitoring of Water Usage [15]. As an appropriate cooling system for the type and size of the studied building, direct expansion split system with residential scale ductwork was considered. Since the design from the beginning adopted the courtyard (with greenery and water) as an optimized form for hot climate, considering the effect of natural ventilation was seen as an attractive option. This is considered in the simulation of the design case. Fluorescent lights with daylight-activated dimmers were also adopted in the design case as a green approach. These improvements were evaluated against the baseline case.

13.4 Methodology

To evaluate the performance of the proposed solutions, there was a need to create a case to represent the typical Emirati house. Because the form of the contemporary Emirati house is vastly varied and does not fit into a specific configuration type, this reference case was chosen as just a simple square. This was seen reasonable due to several factors. Firstly, the standard land plot that is given to the Emirati citizen is a square shape (e.g.; 30 m $\times$ 30 m in Abu Dhabi). Secondly, Most of the modern Emirati houses do not give much consideration to the issues of solar or wind orientation. Hence, a square could be seen as an average case with regard to the orientation issue. Other design variables such as the total built-up area, the total height, and the number of floors did not change between the typical and the design cases. All tested cases were simulated using Enerwin-EC software [26].

Due to lack of actual energy surveys for typical Emirati houses, there was a need to search for other useful reference values that help to estimate the magnitude of the problem. Based on the EIA-2005 [27] survey done in the U.S., the energy consumption per household for a single family detached house with five or more bedrooms, is 160 MBtu/year (46,950 kWh/year). This is equivalent to 33.22 metric tons of CO_2 emissions per household per year. The survey also showed the energy consumption as 55.1 kBtu/sq.ft (173.8 kWh/m^2 year) for a household size of 6^+ persons; which is equivalent to 0.123 metric tons of CO_2 emissions/m^2 year. When the typical Emirati house case was evaluated, the simulation results showed values that were double those of the EIA-2005; which gave a clear indication from the beginning of the magnitude of the problem and the critical need to make the typical designs more energy-efficient.

Typically at the UAE latitude (24° N), the heat gain through the roof component is usually the highest; then comes heat gain through the windows and walls; other building components have usually smaller effect compared to these main components. Thus, before improving the house performance to reduce heat gain, it was necessary to optimize its form design so that distribution of load becomes a bit more uniform with smaller magnitude at each component, and hence easier to solve. That was achieved by using a courtyard configuration. The window to wall ratio (WWR) as 0.20, 0.15, 0.20, and 0.10 for North, East, South, and West facades, respectively, was used in all cases.

One of the most important and challenging architectural targets in this design exercise was the proper landscaping. Landscape design went integrated with the other passive and active design components of the eco-house. Grass ground cover and greenery next to external walls (LS case) was simulated and considered as the landscape scenario. The effect of the green roof element was simulated in a separate scenario (GR case) and the results of both cases were compared against the reference house (REF case).

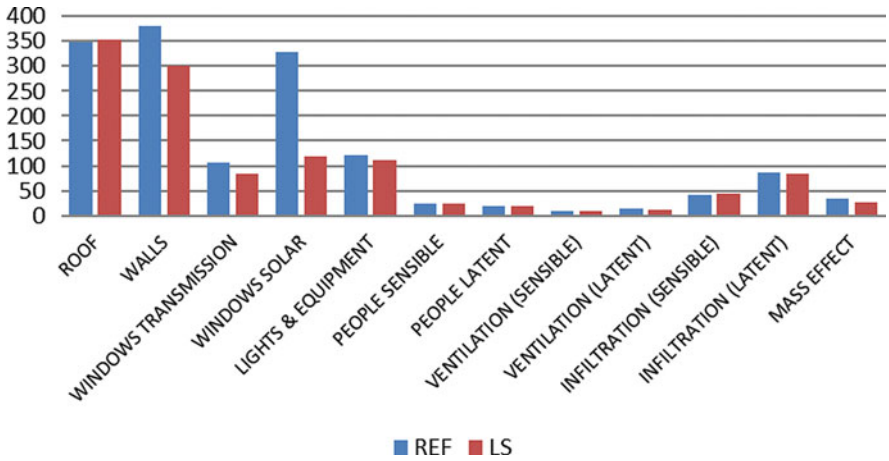

Fig. 13.3 Annual heat gain (GJ) by component for the Landscape (LS) case compared to the reference (REF) case

13.5 Results and Discussion

The simulation cases went through sequential design improvements to improve performance (see Fig. 13.3). The first step in reducing the energy consumption for cooling a building is to reduce the highest contributors of the load through design.

13.5.1 Stage 1

Stage 1 examined the potential of the courtyard form against another typically used square form equal in floor area. To make an accurate and fair comparison, all other variables related to the site (ground cover and plant shading), the envelope (construction materials and glazing), and systems were equalized. The typical house yielded load distribution as follows: 25 % for roof, 23.5 % windows solar, walls 20 %, and 30 % for other components. The courtyard configuration (referred to as the reference house or REF case in this study) helped to distribute the cooling loads as follows: 24.3 % for roof, 18.1 % for windows solar, 27.4 % for walls, and 30 % for other components; this helped to decrease the windows solar and roof loads' contributions. This new form configuration helped in reducing the total annual heat gain by 4.4 %. This resulted in reducing the cooling energy by 4 %, the fan energy by 2 %, and the lighting and equipment energy by 21 %. It also helped to reduce the greenhouse gas emissions, the electrical energy use, and the utility bill by 8 %. The proposed form configuration combined with other passive systems (i.e.; wind towers and green roofs) could help to earn Estidama credits ADM5: Innovation in

Design, ADIEQ3: Potential for Natural Ventilation and Ventilation Rates and ADIEQ4: Indoor Air Quality [15].

13.5.2 Stage 2

When the conservation level of the envelope was improved, the total heat gain dropped down greatly (77 % from the improved form case). This resulted in great savings in the cooling energy (67 % less) and fan energy (73 % less). It also helped to reduce the greenhouse gas emissions, the electrical energy use, and the utility bill by 49 %. This resulted in different load breakdown and accordingly other components had to be considered as priority improvements; which is arranged here in order: lights and equipment (21 %), infiltration-latent (15.8 %), walls (12.4 %), windows-solar (9.8 %), and thermal mass (9 %). Based on these results, some design decisions were made as described below. These improvements could help to earn Estidama credits ADE4: Information on Energy Use and Savings and ADE7 [15]: Cooling and Air Conditioning, whereby insulating the building will help to downsize the HVAC systems.

13.5.3 Stage 3

An early design decision was made to minimize direct and reflected solar heat gain by maximizing shading on walls and windows and improve ground cover. This would help to reduce the walls and windows-solar loads. Landscaping has great potential to provide these benefits and in the meantime attain other Estidama credits such as LV-R1: Urban Systems Assessment, LV-R2: Outdoor Thermal Comfort, RE-1: Improved Energy Performance [24]. This resulted in great reduction of the windows-solar (63.7 %), windows transmission (22.1 %), walls loads (20.7 %), and mass effect (16.9 %); and 21.5 % reduction in the total annual cooling load, compared to the base case (see Fig. 13.3). The energy use of the house (compared to the REF case) dropped down by 16 % for cooling and 18 % for fan operation (see Fig. 13.4). It also helped to reduce the greenhouse gas emissions and the electrical energy use by 9 % (see Fig. 13.5). Another decision made to reduce the high levels of heat gain through the roof was by adding a green roof. This resulted in great reduction of the heat gain through the roof (99.6 %), compared to the reference case (see Fig. 13.6). The energy use of the house (compared to the reference case) dropped down by 24 % for cooling and 27 % for fan operation (see Fig. 13.7). It also helped to reduce the greenhouse gas emissions and the electrical energy use by 19 % (see Fig. 13.8).

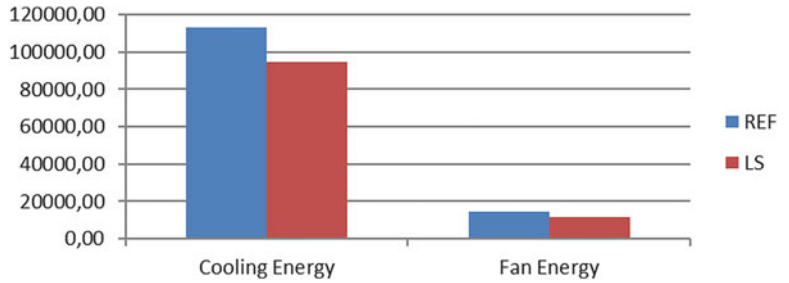

Fig. 13.4 Annual cooling and fan energy use (Kwh) for the Landscape (LS) case compared to the reference (REF) case

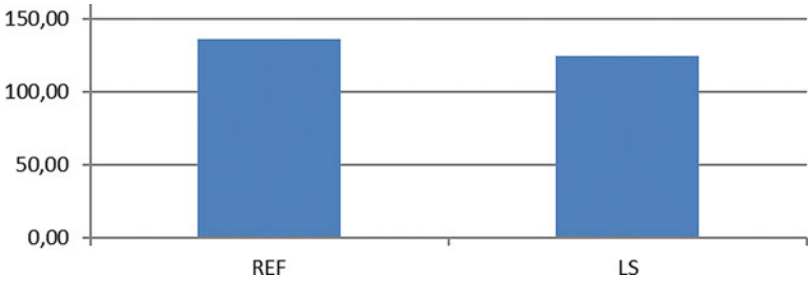

Fig. 13.5 Tons of CO_2/year for the Landscape (LS) case compared to the reference (REF) case

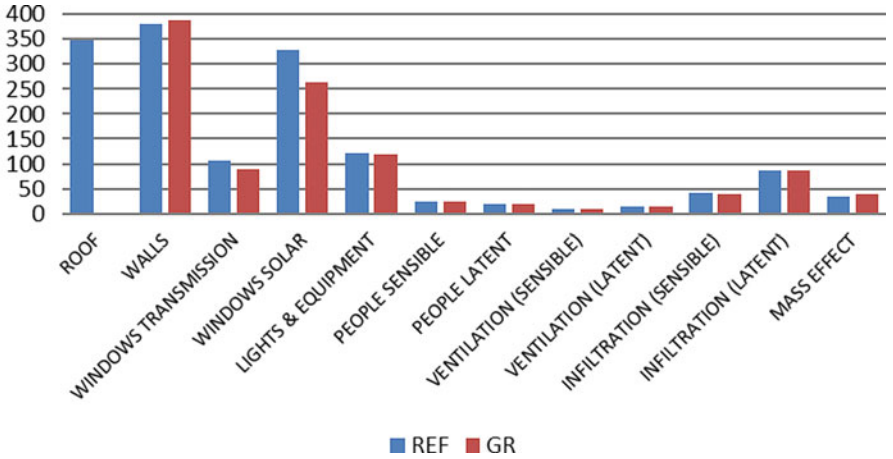

Fig. 13.6 Annual heat gain (GJ) by component for the Green Roof (GR) case compared to the reference (REF) case

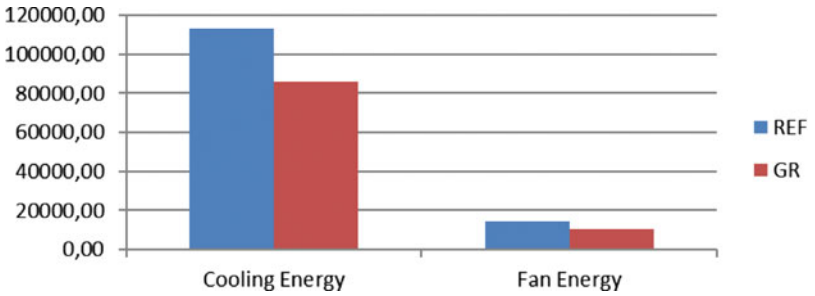

Fig. 13.7 Annual cooling and fan energy use (Kwh) for the Green Roof (GR) case compared to the reference (REF) case

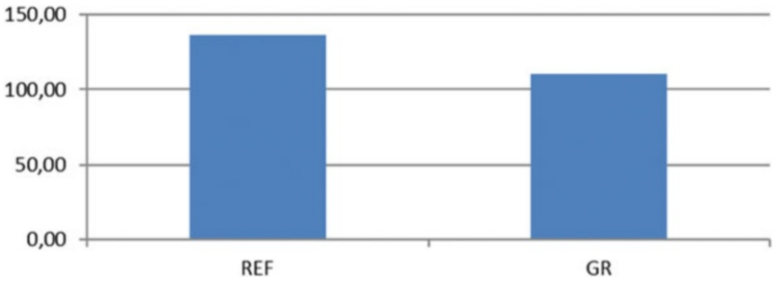

Fig. 13.8 Tons of CO_2/year for the Green Roof (GR) case compared to the reference (REF) case

13.5.4 Stage 4

In this stage, a decision was made to reduce the load of thermal mass by natural ventilation. Stage 4 examined the effect of natural ventilation. If there is a cooling load and the outdoor air temperature is less than the interior air, natural ventilation is permitted at the rate of 73.2 L/s/m^2. When this was examined, the results showed a great reduction in heat gain caused by thermal mass (approx. 50 %) and windows-solar (21.6 %). It also contributed in reducing a great deal of the internal heat gains generated by buildings occupants (36.9 %) and lights and equipment (21.2 %). The reduction in the total annual cooling load is 14 %, compared to the improved envelope case in stage 2. It also helped to reduce the greenhouse gas emissions, the electrical energy use, and the utility bill by 3 %. It showed a potential in reducing the cooling energy (compared to the improved envelope case) by 11 %. These improvements could help to earn Estidama credits ADE1: Reduction of CO_2 Emissions, ADE7: Cooling and Air Conditioning, ADIEQ3: Potential for Natural Ventilation and Ventilation Rates, and ADIEQ4: Indoor Air Quality, whereby natural ventilation supports well being and comfort of occupants [15].

13.5.5 Stage 5

The load of lights and equipment was reduced by relying more on daylighting; which was done by installing daylight-activated dimmers on the lighting system. This resulted in reducing the lights and equipment load by 19.3 % and the total annual cooling load by 4 %, compared to the improved envelope case in stage 2. It also helped to reduce the greenhouse gas emissions, the electrical energy use, and the utility bill by 7 %. It showed a potential in reducing the energy use of the house by 4 % for cooling, 5 % for fan operation, and 14 % for lighting and equipment. These improvements could help to earn Estidama credits ADE1: Reduction of CO_2 Emissions and ADIEQ1: Indoor Lighting, whereby daylighting improves health and comfort for building users [15].

13.5.6 Stage 6

The last stage examined the effect of using all previous retrofits together in one case, as a final optimized design case. The reduction in the total annual cooling load is 21.8 % compared to the improved envelope case and 74.8 % compared to the improved form case. The results showed a potential in reducing the energy use of the house (compared to the improved envelope or the baseline case) by 19 % for cooling and 13 % for lighting and equipment; and helped to reduce the greenhouse gas emissions and the utility bill by 12 %. This is considerable improvement over the square-form house (the typical house) and the basic courtyard house (envelope not yet improved) with 59 and 55 % reduction in the greenhouse gas emissions and the utility bill, respectively.

13.6 Conclusions

This study presented a holistic approach to design a sustainable house in the desert of Abu Dhabi. In a hot climate such as Abu Dhabi for an envelope-dominated building, most of the heat gain comes through the roof, the windows and the walls (approximately 70 %). This gave a clear indication about the critical need to minimize solar gain and improve the thermal conservation level of the building envelope. Utilizing the courtyard configuration helped in reducing the greenhouse gas emissions and the utility bill by 8 %. Improving the envelope helped to improve the performance by 49 %. Reducing the load of thermal mass by natural ventilation helped to improve the performance by 3 %. Relying more on daylighting helped to improve the performance by 7 %.

Using greenery to improve the building thermal performance can also result in other benefits such as improved air quality, visual comfort via daylight uniform

distribution, noise reduction, prolonged building structure (as green roof), outdoor and indoor thermal comfort, and aesthetics. The use of outdoor landscape (grass ground cover and shade trees) has made a 9 % improvement of performance over the base case regarding the electrical energy use and greenhouse gas emissions. The energy use of the house (compared to the reference case) dropped down by 16 % for cooling and 18 % for fan operation. With regards to the green roof scenario, a performance improvement of 19 % over the base case has been achieved. The energy use of the house dropped down by 24 % for cooling and 27 % for fan operation. Such strategies and improvement of performance would eventually help to earn several points in Estidama Pearl Rating System for Villas [24], such as: LV-R1: Urban systems assessment, LV-R2: Outdoor thermal comfort, LV-9: Indoor noise, IP-1: Innovative cultural & regional practices, IP-2: Innovating Practice, IDP-R1: Integrated Development Strategy, IDP-1: Life Cycle Costing, NS-R1: Natural systems assessment & protection, NS-1: Landscape design & management plan, NS-2: Landscape enhancement, PW-2.1: Exterior water use reduction: Landscaping, PW-3: Stormwater management, and RE-1: Improved Energy Performance.

The design achieved considerable improvement over the typical Emirati house case; 59 % reduction in the greenhouse gas emissions and the utility bill. Such a methodology could be valuable to professionals in the UAE who might search for a clear application model.

References

1. Estidama Sustainable buildings and communities and buildings program for the emirate of Abu Dhabi—design guidelines for new residential and commercial buildings (May 2008)
2. Aboul-Naga M, Al-Sallal KA, El Diasty R (2000) Impact of city urban patterns on building energy use: Al-Ain city as a case study for hot-arid climates. Architect Sci Rev 43:147–158
3. Abou-El-Fadl S (2006) Cooling energy saving in residential buildings in UAE by shading and night ventilation. Proceedings of the 5th UAE University Research conference, Al-Ain, UAE, pp 1–12
4. Wong N, Chen Y, Ong C, Sia A (2003) Investigation of thermal benefits of rooftop garden in the tropical environment. Build Environ 38(2):261–270
5. Asaeda T, Ca V (2000) Characteristics of permeable pavement during hot summer weather and impact on the thermal environment. Build Environ 35(4):363–375
6. Ramadhan R, Al-Abdul Wahhab H (1997) Temperature variation of flexible and rigid pavements in Eastern Saudi Arabia. Build Environ 32(4):367–373
7. Tan S, Fwa T (1992) Influence of pavement materials on the thermal environment of outdoor spaces. Build Environ 27(3):289–295
8. Tzu-Ping L, Yu-Feng H, Yu-Sung H (2007) Seasonal effect of pavement on outdoor thermal environments in subtropical Taiwan. Build Environ 42:4124–4131
9. Akbari H, Kurn D, Bretz S, Hanford J (1997) Peak power and cooling energy savings of shade trees. Energy Buildings 25:139–148
10. Akbari H, Taha H (1992) The impact of trees and white surfaces on residential heating and cooling energy use in four Canadian cities. Energy 17(2):141–149

11. Simpson J, McPherson E (1996) Potential of tree shade for reducing residential energy use in California. J Arboriculture 22(1):10–18
12. McPherson E, Simpson J (2003) Potential energy savings in buildings by an urban tree planting program in California. Urban Forestry Urban Greening 2:73–86
13. Donovan G, Butry D (2009) The value of shade: estimating the effect of urban trees on summertime electricity use. Energy Buildings 41:662–668
14. Dubai Municipality (2009) Green Roof Circular no. (171)
15. Estidama Sustainable buildings and communities and buildings program for the emirate of Abu Dhabi—assessment method for new residential and commercial buildings (May 2008)
16. Liu KY, Baskaran A (2005) Using garden roof systems to achieve sustainable building envelopes. Construction Technology Update No. 65, NRC-IRC—National Research Council of Canada, Institute for Research in Construction
17. Saiz S, Kennedy C, Bass B, Pressnail K (2006) Comparative life cycle assessment of standard and green roofs. Environ Sci Technol 40:4312–4316
18. Reynolds JS (2002) Courtyard: aesthetic, social, and thermal delight. Wiley, New York
19. Fathy H (1973) Architecture for the poor: an experiment in rural Egypt. University of Chicago Press, Chicago
20. Fathy H (1986) Natural energy and vernacular architecture (Shearer W, Sultan AA (eds)). Chicago, University of Chicago Press
21. LEED for Homes Rating System, U.S. Green Building Council (January 2008)
22. Bansal NK, Hauser G, Minke G (eds) (1994) Passive building design: a handbook of natural climatic control. Elsevier Science B.V, Amsterdam, Netherlands
23. Knauf Insulation Ltd, Merseyside, United Kingdom, June 2010. www.knaufinsulation.co.uk
24. Estidama—the Pearl Rating System for Estidama, emirate of Abu Dhabi, Abu Dhabi Urban Planning Council, Version 1.0, April 2010
25. Dubai Municipality (2003) Thermal Insulation Circular no. (66)
26. Enerwin-EC Software: energy simulation software for buildings with life-cycle costs, professional version 5.9. Texas A&M University & Degelman Engineering Group, Inc.
27. EIA-2005 Residential Energy Consumption Survey. Table US-3, total consumption by fuels used, 2005

Chapter 14
Ventilation and Architectural Design Strategies for Cooling Office Buildings in Different Climates of Chile

Waldo Bustamante Gómez, Felipe Encinas Pino, Sergio Vera Araya, and Francisco Sánchez de la Flor

Abstract In Office buildings in Chile, cooling energy demand is higher than heating demand. The climate of the country show important differences between cities by the ocean and those of interior regions. Main cities of Central Chile are Santiago and Valparaíso, both located at around 33°S. Santiago presents a Mediterranean climate, with a high temperature oscillation between day and night during cooling period. Valparaíso, by the coast, shows lower temperature fluctuation compared with Santiago during identical period. In order to define design strategies for energy efficiency of office buildings in mentioned cities, a sensitivity study has been made, considering variables like window to wall ratio, type of windows (clear and selective glazing, including low e, single and double glazing), use and type of external solar protection (ESP) and use of nocturnal or diurnal ventilation. In opaque facades, thermal insulation is considered. In case of walls, in order to increase thermal inertia external insulation is assumed. The sensitivity analysis is developed considering a square building containing office rooms on all four orientations. This 10 story building has been specially proposed and designed for this analysis. Methodology considers an evaluation of heating and cooling demand of the building in both cities. For this purpose, simulation software under dynamic conditions has been used (TAS). The lowest cooling energy demand is reached when using the lowest window to wall ratio (20 %), with ESP in east, west and

W. Bustamante Gómez (✉) • F. Encinas Pino
School of Architecture, Center for Sustainable Urban Development (CEDEUS), Pontificia Universidad Católica de Chile, Av. El Comendador 1916, Providencia, Santiago, Chile
e-mail: wbustamante@uc.cl; felipe.encinas@uc.cl

S. Vera Araya
Department of Construction Engineering and Management, School of Engineering, Center for Sustainable Urban Development (CEDEUS), Pontificia Universidad Católica de Chile, Av. Vicuña Mackenna 4860, Macul, Santiago, Chile
e-mail: svera@ing.puc.cl

F. Sánchez de la Flor
Escuela Superior de Ingeniería de Cádiz, Calle Chile 1, Cádiz, Spain
e-mail: francisco.flor@uca.es

I. Dincer et al. (eds.), *Progress in Sustainable Energy Technologies Vol II: Creating Sustainable Development*, DOI 10.1007/978-3-319-07977-6_14

north oriented glazed areas. In fact, fully glazed facades in both cities are not recommended. Nocturnal ventilation was highly effective for decreasing cooling demand in both cities. In the case of Valparaíso, due to relatively low temperature during cooling period (maximum lower than 26 °C), diurnal ventilation for cooling purposes is also effective.

Keywords Office buildings • Cooling energy demand • Nocturnal ventilation

14.1 Introduction

Chile shows a wide latitudinal variation (from around 17°30′S to 56°00′S), which generates high North–South climate differences. On the other hand, the presence of the Pacific Ocean and the Coastal and Andes mountains, generate important climate variation from East to West. Santiago (located in the foothills of the Andes) is the governmental capital and also the industrial and financial centre of the country. Valparaíso, the main port of Chile, is located at similar latitude of Santiago but by the coast.

Climate of Santiago is semiarid, showing high temperatures and solar radiation during spring and summer. For the warmest month of the year (January), mean value of maximum temperature is 29.7 °C and mean minimum is 13.0 °C. Mean temperatures of coldest month (July) are: 3.9 °C (mean minimum) and 14.9 °C (mean maximum). During summer and intermediate seasons, a high temperature fluctuation is observed. Climate of Valparaiso is influenced by the Pacific Ocean, showing lower temperature oscillation than Santiago. Mean value of maximum temperature is 20.8 °C and mean minimum is 13.5 °C for the warmest month of the year (Jan). For the coldest month (July), mean minimum is 9.2 °C and mean maximum is 14.3 °C [1].

In Chile, around 4.73 million of square meters of buildings of the Industry, Commerce and Financial Institutions sector were constructed during 2008 [2]. 53.2 % was built in Santiago and 6.6 % in Valparaíso. In the country there is no mandatory thermal behaviour requirements for office buildings and most of their design patterns are brought from developed countries, even if some architectural strategies, such as double skin, are not suitable—for example—in Central European countries due to the generation of overheating problems, especially when they are designed with fully glazed façades [3, 4].

Normally, in the country, office buildings show higher cooling than heating energy demand. Some studies have been done in order to study the impact of different architectural strategies on the energy demand [5, 6]. A study performed in 2004 in London for an office building, showed benefits in energy use if windows size, solar protection, and internal profit, are optimized. During two representative weeks, one with hot temperate climate and the other with extreme hot climate, 23 and 40 % of refrigeration energy reduction were respectively obtained, once previous modifications were applied. On the other hand, when nocturnal ventilation is applied to the optimized building, an additional reduction of 13 % is reached [7].

A study performed in 1998 in Sweden (predominantly cold climate), shows how important are the selection of type of glazing and window to façade ratio for reducing cooling and heating energy demand. Glass use with low U values and solar transmittance may mitigate overheating problems but it does not solve it [8].

In order to define architectural design strategies for reaching thermal and visual comfort with energy efficiency in office buildings of the mentioned cities—with different climates—a sensibility study has been made. Variables considered are the following: size of windows (window to wall ratio), type of windows (clear and selective glazing, including low e, single and double glazing), use and type of solar protection and use of nocturnal or diurnal ventilation. In opaque facades (walls and roofs), thermal insulation is considered. In case of walls, in order to increase thermal inertia and effectiveness of nocturnal ventilation, external insulation is assumed. This paper will mainly show results of this study related to the effect of diurnal and nocturnal ventilation on cooling energy demand.

14.2 Methodology

This study aims to analyse the thermal behaviour of an office building, for different design strategies, during a whole year. For this analysis, simulations are performed with TAS (www.edsl.net), software under dynamic conditions. The sensitivity analysis was developed with a 10 story building, specially designed for this study. Figure 14.1 shows the plan (16 × 16) building and 3D image. Each story contains 12 offices of typical dimensions (4 m × 4 m × 2.8 m height).

14.2.1 The Building

Main specifications of the building are the following:

- Walls: Reinforced concrete 150 mm with external EPS 30 mm. $U = 1.0$ W/m^2 °C.
- Roof: Reinforced concrete 150 mm with EPS 60 mm. $U = 0.59$ W/m^2 °C (in Valparaíso) and with 80 mm of EPS in Santiago. $U = 0.40$ W/m^2 °C.
- Windows: single glazing, clear. $U = 5.8$ W/m^2 °C, Lighting transmittance: 0.90 Solar transmittance: 0.87. In the case of windows, this corresponds to the initial situation. Type of glazing is changed during the sensitivity process. It is necessary to mention that it is still common to find new office buildings with single glazing in the country.

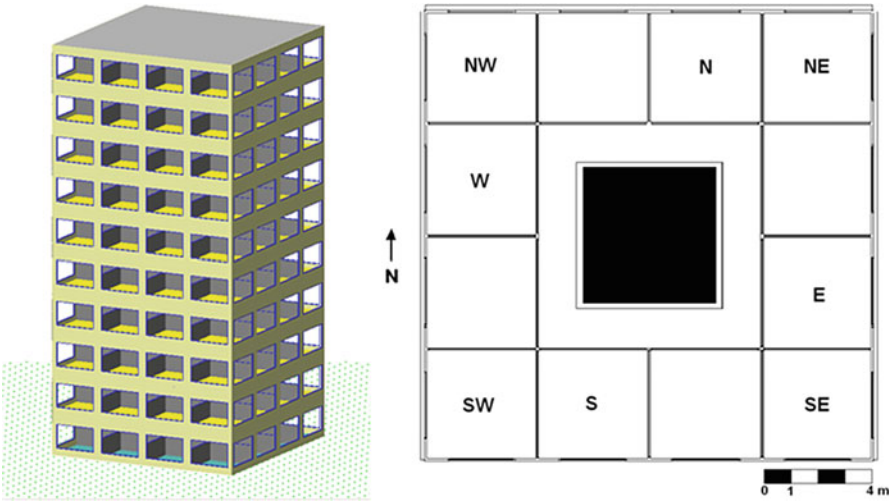

Fig. 14.1 Plan and 3D image of the building

14.2.2 Internal Gains and Internal Conditions

- Internal gains of the buildings considered are the following:
- People: 9.38 W/m^2 (sensible) 6.88 W/m^2 (latent).
- Lighting: 11 W/m^2.
- Equipment: 11.25 W/m^2.
- Temperature during week days: Maximum of 26 °C from 8:00 AM till 19:00 PM (for cooling demand estimation).
- Weekend days: No temperature restrictions.
- Infiltration rate: 0.3 ach.
- Ventilation rate: 1.0 ach during week days from 8:00 AM till 19:00 PM.

14.2.3 Sensitivity Analysis

For defining cases to be simulated, a factorial design was adopted. This involves a given number of samples per each input parameter and consequently running the model for all combination of samples [9]. This method is based on the sampling-based approach, where the model is repeatedly executed from the combination of input parameters sampled with some probability distribution. Since the design of this sensibility analysis consists in 4 input parameters with 3, 3, 4 and 8 parameters per each one, the total combination of samples gives a complete sample of 288 cases. Table 14.1 presents the different input parameters considered for this study and their associated variables.

Table 14.1 Input parameters for sensitivity analysis

Input parameters	Number of variables	Description of variables
Glazing ratio[a]	3	20 %
		50 %
		100 %
Types of solar protection devices	3	Without solar protection
		Overhang in N orientation and blinds for E and W orientations
		Blinds in N, E and W orientations
Types of glazing	4	Single glazing, clear
		Single glazing, selective
		Double glazing, clear
		Double glazing, selective
Orientations	8	All orientations (N, NE, E, SE, S, SW, W, NW)

[a]Ratio of the glazed area with respect to the total façade area

The 8 orientations correspond to different office rooms showed in Fig. 14.1 (N, NE, E, SE, S, SW, W and NW). For each one of these office rooms of 6th floor, the cooling and heating demand was estimated according to variation of type of glazing, types of solar protection and glazing ratio (see Table 14.1).

Simulations considered the following type of glazing: Clear single glazing clear (CS, 4 mm) selective single glazing (SS, 6 mm), clear double glazing (DGC) and selective double glazing (DGS). Properties of these types of glazing are shown in Table 14.2. LT: Light transmission, ST: Solar transmission.

After obtaining energy demand results and selecting cases with lower heating and cooling demand, simulations considering low e glazing were made. They showed a non-significant impact in lowering heating demand in both climates. As it will be observed, heating demand is significantly lower than cooling demand in office buildings in Chile. Also, for a selective number of cases, after obtaining the 288 mentioned results, ventilation strategies (diurnal and nocturnal) were studied, in order to observe their impact on reducing cooling demand in the building.

14.3 Results and Discussion

First of all, we have confirmed that heating energy demand for office buildings is significantly lower than cooling demand. In the case of Valparaíso, with only diurnal ventilation for maintaining quality of air in different offices, the lower energy demand was reached with selective double glazing, a WWR of 20 % and solar protection (Overhang in N orientation and blinds for E and W orientations). In this case annual cooling demand is 16.3 kWh/m^2 year and heating demand reaches 3.2 kWh/m^2 year. These values represent the energy demand of all 16 offices of the

Table 14.2 Properties of different types of glazing

	CS	SS	DGC	DGS
LT	0.90	0.60	0.82	0.54
ST	0.82	0.50	0.68	0.41
U ($W/m^{2\circ}C$)	5.80	5.70	2.78	2.76

6th floor of the building. In the case of Santiago, cooling demand for identical case is 31.8 kWh/m^2 year and 4.5 kWh/m^2 year as heating demand. When using selective and double glazing with low e, cooling demand increases in a 15 % in the case of Valparaíso and around 1 % in the case of Santiago (both with identical solar protection).

14.3.1 Sensitivity Analysis

Regarding the sensibility study and due to high output variability (cooling energy demand for each office)—as consequence of the input variability—the energy performance of office buildings is highly impacted by their façade glazing ratio. Differences on annual cooling demand according to window to wall ratio are significant. See Fig. 14.2 for the case of Valparaíso. Identical results were obtained for the case of Santiago. See Fig. 14.3.

On the contrary, Fig. 14.4 shows as the variability of the output results per orientation is reduced, which is even more critical regarding to the range of low cooling demand (cases with low window to wall ratio). Figure 14.4 shows variability on energy demand for all office rooms of 6th floor of the building. Very similar results were observed also in the case of Santiago. According to these results, it is clear that for any design strategy proposed for new office developments in Valparaiso and Santiago, the ratio of the glazed area with respect to the exposed façade should be prioritized with respect to orientation.

14.3.2 Ventilation Strategies

As mentioned, in order to decrease cooling energy demand on office buildings in cities of Santiago and Valparaíso, strategies of ventilation were studied. In the case of Santiago, where we may observe high diurnal temperatures during spring and summer (higher than 26 °C) but relatively low nocturnal temperatures (around 15 °C), night ventilation was studied. In the case of Valparaíso, where higher temperatures on spring and summer are commonly lower than 26 °C, diurnal ventilation for cooling was also studied.

Figure 14.5 shows the effect of nocturnal ventilation in cooling demand of office buildings in Santiago, when using 20 % of window to wall ratio with or without solar protection (SP). Types of glazing are: Single glazing (SG), double glazing

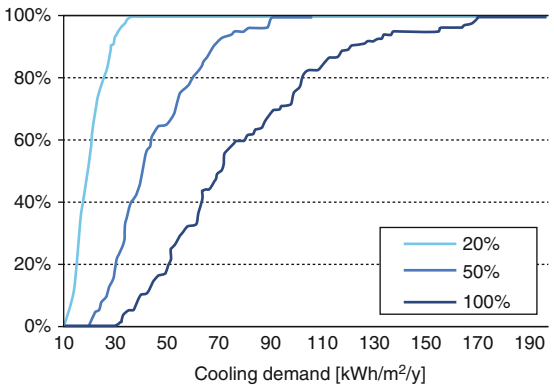

Fig. 14.2 Cumulative frequency (%) for cooling demand with respect to glazing ratio in the case of Valparaíso

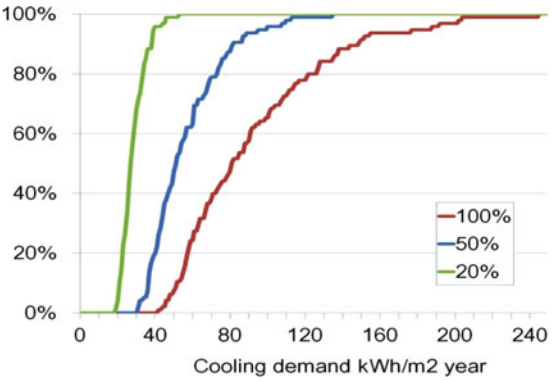

Fig. 14.3 Cumulative frequency (%) for cooling demand with respect to glazing ratio, in the case of Santiago

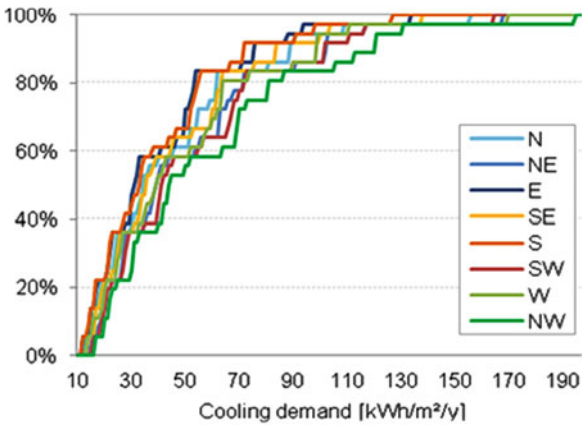

Fig. 14.4 Cumulative frequency (%) for cooling demand with respect to orientation in the case of Valparaiso

selective (DGS). It may be seen that nocturnal ventilation is very effective for getting energy efficiency in office buildings in Santiago. As we have already mentioned, envelope wall of the building is externally insulated, providing it higher

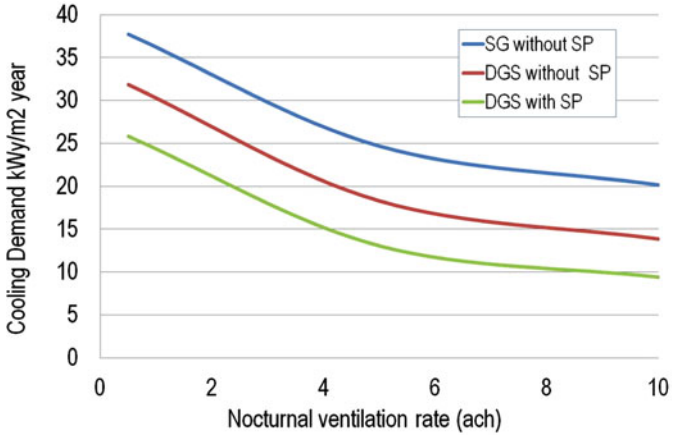

Fig. 14.5 Cooling demand of office buildings with respect to nocturnal ventilation rate

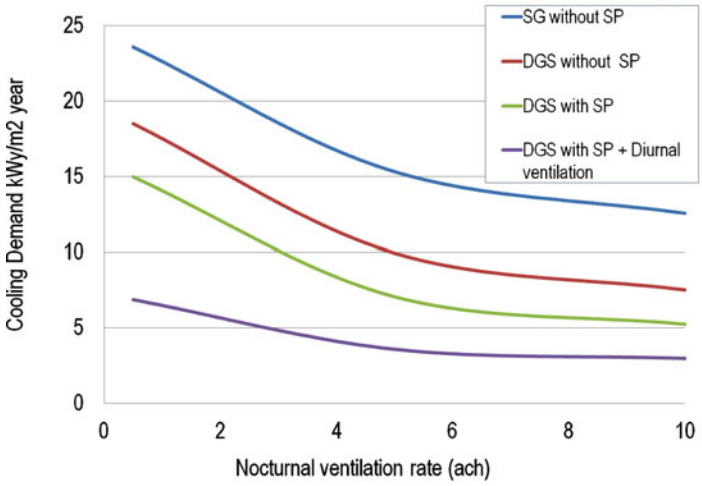

Fig. 14.6 Cooling demand of office buildings with respect to nocturnal ventilation rate

thermal inertia. Eight to ten air changes per hour for nocturnal ventilation may be recommended.

Figure 14.6 shows the case of Valparaíso, where identical cases than Santiago were studied. Nocturnal ventilation is also effective bur in this case diurnal ventilation may be recommended. Opening windows when external temperature is lower than 26 °C allow reaching a cooling demand 6.9 kWh/m^2 year, which decreases to 3.0 kWh/m^2 year when using diurnal and nocturnal ventilation. Both cases suppose windows with double glazing selective, solar protection and envelope walls with external insulation.

14.4 Conclusion

First of all, cooling energy demand in office buildings of Santiago and Valparaíso is significantly higher than heating energy demand. Attention on architectural design strategies for decreasing cooling demand is highly recommended. For lowering cooling demand, solar protection, size and type of windows and solar protection have been studied.

Double glazing selective may be recommended for reaching low cooling demand in both cities. Double glazing clear may also be recommended when using effective solar protection.

It has been showed that there is a high dependence between size of façade glazing area and the cooling energy demand on office buildings in both studied cities. The lower the window to wall ratio is, a better energy performance of the building is reached. On the contrary, orientation of offices is less relevant for reaching low cooling energy demand, which is more evident for lower window to wall ratio.

Finally, nocturnal ventilation is highly effective for reaching low cooling energy demand in the city of Santiago (with a Mediterranean climate). This strategy is less effective in the case of Valparaíso (with a climate influenced by the ocean). For energy efficiency in office buildings, in the case of Valparaíso, diurnal ventilation may also be applied. Nocturnal and diurnal ventilation may be combined with solar protection on windows and the lower window to floor ratio that may be possible to be used.

Acknowledgements This research has been carried out as part of the project FONDECYT N° 1090602 funded by CONICYT, Chile. The authors also gratefully acknowledge the research support provided by CEDEUS, CONICYT/FONDAP 15110020.

References

1. Instituto Nacional de Estadísticas (2008) Anuario de Edificación 2008. Instituto Nacional de Estadísticas, Santiago de Chile
2. Instituto Nacional de Normalización (2008) NCh 1079 of 2008. Arquitectura y construcción – Zonificación climático habitacional para Chile y recomendaciones para el diseño arquitectónico. Instituto Nacional de Normalización, Santiago de Chile
3. Manz H, Frank T (2005) Thermal simulation of buildings with double-skin façades. Energ Build 37:1114–1121
4. Gratia E, De Herde A (2007) Are energy consumption decreased with the addition of a double skin? Energ Build 39:605–619
5. Bustamante W, Encinas F, Otárola R, Pino A (2011) Strategies for improving thermal performance and visual comfort in office buildings of Central Chile. In: Bodart M, Evraud A (eds) Proceedings of passive and low energy architecture, PLEA 2011, Louvain la Neuve, Belgium
6. Pino A, Bustamante W, Escobar R, Encinas F (2012) Thermal and lighting behavior of office buildings in Santiago of Chile. Energ Build 47:441–449

7. Kolokotroni GI, Watkins R (2006) The effect of London heat island summer cooling demand and night ventilation strategies. Sol Energ 80:383–392
8. Bülow-Hube H (1998) The effect of glazing type and size on annual heating and cooling demand for Swedish offices. Proceedings of renewable energy technologies in cold climate 98. Montreal, Canada
9. Hamby DM (1994) A review of techniques for parameter sensitivity analysis of environmental models. Environ Monit Assess 32:135–154

Chapter 15
Investigations for the Thermal Influence of Glass Patterns on the Building Envelope

Shiang-Jiun Lin, Yong-Cheng Chen, and Po-Tao Sun

Abstract Indoor thermal distribution is strongly influenced by the transmission of solar energy. In summer, specifically, the solar energy intensity attains the maximum, which introduces a great heat load to enter indoors and drastically increases the temperature that often raises high enough to against the requisition of thermal comfort. Attempting to attenuate the transmitted radiant energy, this paper considers different types of patterns distributed throughout the surface of window glass and evaluates their thermal performances by comparing with that for the flat glass.

The modeling results provided by the commercial CFD package, ANSYS Fluent, indicates that the indoor thermal intensity can be reduced as the solar radiation passes through the glass patterns. Under identical ambient conditions and glass characteristics, the glass having the described trapezoidal–shaped patterns is able to dissipate the indoor heat flux from 146 to 134 W/m^2. The glass pattern in triangular shape gives better capacity on the thermal dissipation. Based on the triangular-shaped glass pattern, the thermal field approaching to the roof window obtains 1.3 °C lower than that for flat glass. Besides the pattern shape varies the transmitted solar load, the spacing between patterns can also be a parameter to change the solar effect on the thermal distribution of a building. According to the modeling results, more thermal reduction can be acquired as the pattern spacing is smaller.

It is very crucial today to develop skills to reduce the power consumptions in any occasions. For buildings, there many works have done the studies based on the

S.-J. Lin (✉)
National Kaohsiung University of Applied Sciences, 415 Chien-Kung Road, Kaohsiung 807, Taiwan
e-mail: kathysjlin@kuas.edu.tw

Y.-C. Chen
Sanyang Industry Company Ltd., 3 Chung Hua Rd. Hukou, Hsinchu 303, Taiwan
e-mail: jerry24568@hotmail.com

P.-T. Sun
3M Taiwan Limited, 66, 800 Lane, Chung Shang S. Road, Yangmei, Taoyuan 326, Taiwan
e-mail: jsun1@mmm.com

I. Dincer et al. (eds.), *Progress in Sustainable Energy Technologies Vol II: Creating Sustainable Development*, DOI 10.1007/978-3-319-07977-6_15

ventilation and glazing systems. In here, this paper provides investigations for the glass patterns on the reduction of thermal load in a building and demonstrates the transmitted solar load indeed can be attenuated if the glass incorporates with patterns over the surface.

Keywords Patterned glass • Building energy saving • Modeling simulation

15.1 Introduction

During the last decades, the natural fuels existing on the earth have been over-developed, which leads a significant decrease in natural energy available for many of power-demanded facilities. Therefore, as the natural energy rapidly diminishing and the renewal energy still costing, it is very crucial and urgent to develop new technologies that are able to give the reduction of energy consumption in any occasions. For buildings, the transmitted solar radiation passing through window panes or any types of fenestration system can be the primary source to vary the indoor thermal field and thermal comfort which is straightly associated with the energy demands. The energy consumption for a building can gain 10 % or above to attenuate the thermal effect resulting from the solar load. In summer season, especially, the air conditioning load can even drastically increase due to the excessive solar radiation. Therefore, many research works provided solutions to reduce the solar effect on the building envelope. Etzion and Erell [1] applied a rotatable frame supporting the two transparent and absorptive glazing components to establish a flexible glazing mechanism. Based on their novel design, the absorptive glazing with a low shading coefficient can be flexibly placed on the exterior or interior of the building as solar load changes. Such glazing system is promising to reduce the energy consumption and provide comfortable living environment. Chow et al. [2] evaluated the thermal performance for a photovoltaic (PV) ventilated window system applied on a small office room in Hong Kong. Their study reported that the transmittance of a solar cell obtained in the range of 0.45 and 0.55 could achieve the best energy saving. Low-emissivity glass with coatings can also alter the solar heat transferred into the building. Blue and green glasses tend to filter some infrared radiation, which can be used in warm climate as an outer pane of a double-glazed unit and achieve the cool daylight [3]. While these solutions perform good capacity on dissipating the interior heat load, they can be difficult or elaborative. Due to knowledge of the solar load related to the glass member [4] as well as recognizing the interest thermal solutions recently emphasizing on the glazing mechanism design, ventilation and glass coatings, the authors provide a new study that investigates the influence of glass patterns on the indoor thermal load, using commercial package ANSYS Fluent. Furthermore, the relation between glass thermal performance and pattern shapes is analyzed as well in this work.

15.2 Numerical Analysis and Results

The thermal field inside of a building can be strongly affected by the solar radiation. Through the heat transfer process, the solar load passing through a window pane will induce the heat flux entering interior of the building. As the solar radiation drastically increases in summer season, specifically, the transferred heat flux can be raised even high enough to against the thermal comfort acquisition and hence causes the increase in the air conditioning load that often results in great energy consumptions. Therefore, for buildings, reducing the transmitted radiant energy becomes a crucial issue to achieve energy savings.

Based on the energy conservation, the solar incident traveling in the ambience enters a glass pane can be expressed as Eq. (15.1).

$$Q_i = Q_r + Q_a + Q_t \tag{15.1}$$

Where Q_i is the solar incident energy, Q_r is the reflected radiation, Q_a is the energy absorbed by the glass and Q_t is the transmitted energy passing through the glass pane. According to Eq. (15.1), the glazing energy, the radiant energy entering a glass pane, can be represented in terms of the absorbed and transmitted energies as written in Eq. (15.2)

$$Q_{glazing} = Q_a + Q_t \tag{15.2}$$

Where $Q_{glazing}$ is the glazing energy. For a glass with flat surface as shown in Fig. 15.1a, the glazing energy can be determined as follows

$$\left(Q_{glazing}\right)_{flat} = \sum_{i=1}^{5} q_i \tag{15.3}$$

Where q_i is the component of glazing energy. Contrast with the conventional flat glass of Fig. 15.1a, b shows the glass containing discontinuous surfaces and whose corresponding glazing energy can be expressed as Eq. (15.4)

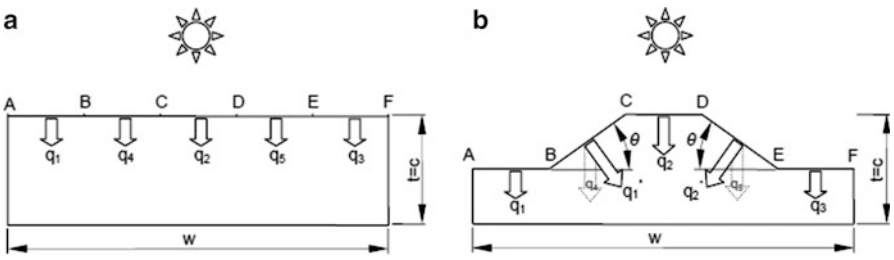

Fig. 15.1 Glazing energy for (**a**) flat and (**b**) discontinuous surface

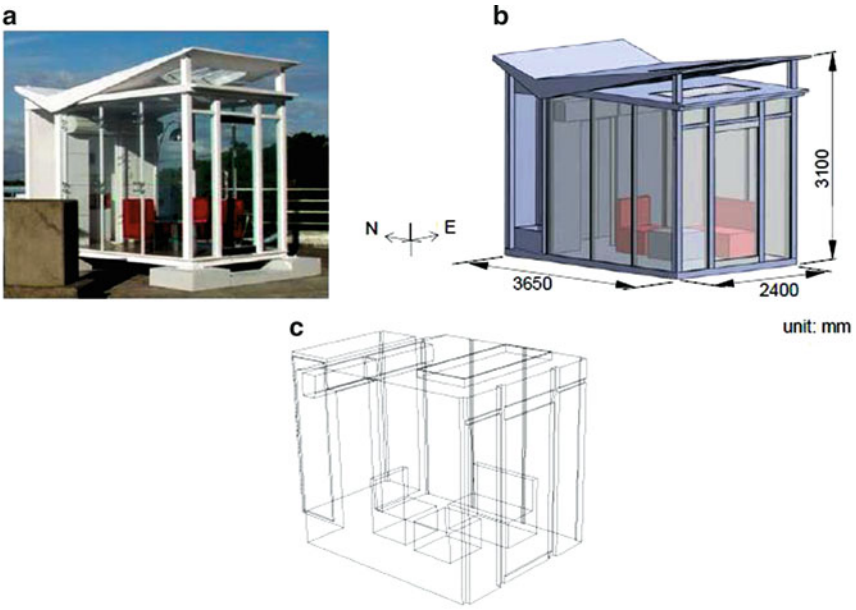

Fig. 15.2 The (**a**) image, (**b**) schematic graph and (**c**) analytical model of glass house

$$\left(Q_{glazing}\right)_{discontinuous} = \sum_{i=1}^{3} q_i + \sum_{j=1}^{2} q_j^{*};\ \ q_1^{*} \equiv f(q_4, \cos(\theta));\ \ q_2^{*} \equiv f(q_5, \cos(\theta)) \tag{15.4}$$

Where q_j* is the component of the glazing energy entering the discontinuous face of the glass pane. Assuming that the glass shown in Fig. 15.1a, b are identical in dimensions and the type, Eqs. (15.3) and (15.4) give that as θ of Fig. 15.1b is greater than zero, the glass pane with discontinuous surface results in less solar radiation entering the glass, comparing with that for the conventional flat glass ($\theta = 0°$). Consequently, a glass pane having flat surface throughout potentially allows the maximal radiant energy transmitting into the building. Therefore, this work designs glass patterns, forming the discontinuous surface, over the glass pane.

The analytical model used in this work refers from the furnished glass house located in 3 M Taiwan site, whose image and schematic feature are shown in Fig. 15.2a, b, respectively. The glass house having dimensions of 3,650 mm in length, 2,400 mm in width and 3,100 mm in height contains a roof window and twelve floor windows which appear highly glazing space facing on east, west and south, as can be seen in Fig. 15.2a, b. As the intensity of solar radiation attains maximum when it is approaching to noon, this research applies glass patterns on the roof pane. Furthermore, in order to fully investigate the influence of glass patterns

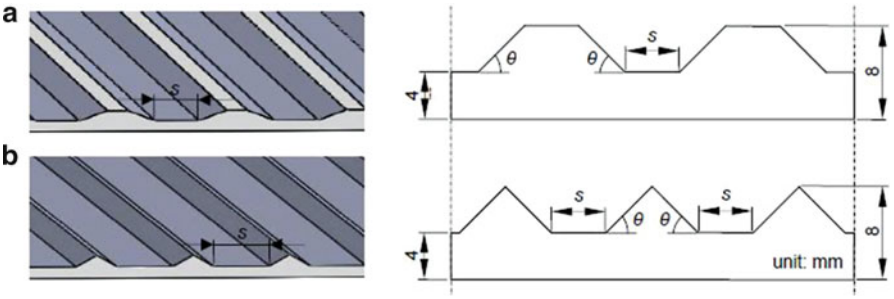

Fig. 15.3 Pattern feature in (**a**) trapezoidal (**b**) triangular shape

Table 15.1 Thermal and radiant properties of roof glass [5]

Thermal property		
Heat transfer coefficient (W/m^2 K)		4
Radiation property		
Absorption	Direct visible	0.49
	Direct IR	0.49
	Diffuse hemispherical	0.49
Transmission	Direct visible	0.30
	Direct IR	0.30
	Diffuse hemispherical	0.32

on the transmitted radiant energy, the analytical model obtained in Fig. 15.2c presently regards all of the floor windows as walls. Dimensions of the roof glass are 700 mm long, 1,600 mm wide and 8 mm thick.

To reduce the unpleasant solar radiation entering the interiors of the glass house, this work imposes glass patterns in trapezoidal and triangular shape over the exterior surface of the roof pane, respectively, as shown in Fig. 15.3. In addition, considering that the pattern parameters including the bottom angle θ and spacing s between the adjacent patterns as shown in Fig. 15.3 can alter the transmitted solar load, this work also analyzes the thermal performance for the patterned glass, varying the feature parameters, θ and s.

The present study applies commercial package, ANSYS Fluent, to investigate the thermal behaviors inside of the glass house based on the roof glass with flat and patterned surfaces, respectively. In the numerical analysis, the solar radiations including direct, diffuse and ground reflected radiations needed for this work were determined by the solar calculator based on fair weather conditions, which is programmed in ANSYS Fluent module. To simulate the summer season in Taiwan, this work takes the date of July 8th, 2011 and 120°16′ degrees in longitude and 22°16′ degrees in latitude. The thermal and radiation properties of the roof glass employed in this work were carried out from those for the coated glass provided by Ashrae [5]. Table 15.1 indicates thermal and radiant properties of roof glass.

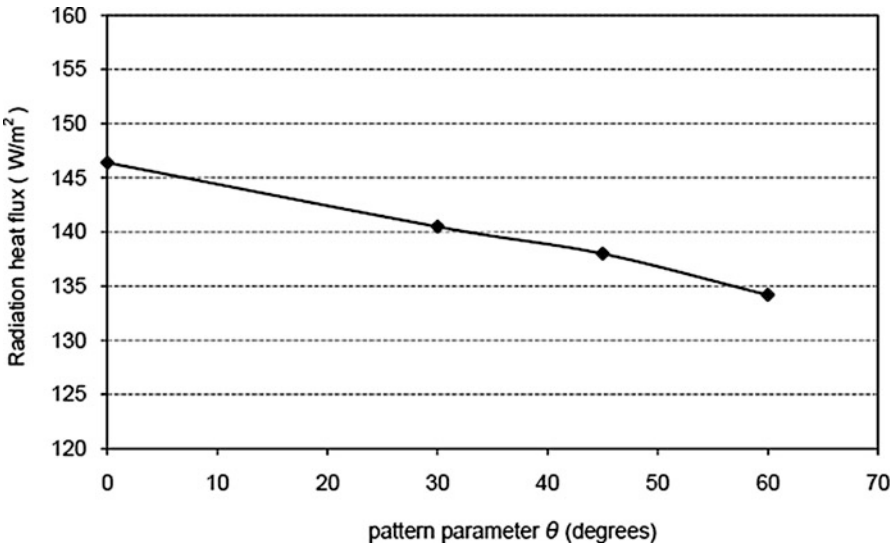

Fig. 15.4 Radiation heat flux on the inner face of the roof glass based on varying θ of trapezoidal-shaped patterns

Figures 15.4, 15.5, 15.6, and 15.7 obtain the analytical results based on applying the trapezoidal-shaped patterns throughout the external surface of the roof pane, as shown in Fig. 15.3. Fixed spacing s of 11 mm between the adjacent patterns, Fig. 15.4 plots the radiant heat flux on the inner face of the roof glass associated with the bottom angle θ, Fig. 15.3. The corresponding thermal fields located 100 mm away from the underneath of roof glass as indicated in Fig. 15.5a are shown in Fig. 15.5b, e. As obtained in Fig. 15.4, the transferred heat load slightly decreases as the bottom angle θ increases; hence there is only slight difference among the thermal fields shown in Fig. 15.5b, e. Remaining θ equal to 45° instead, Figs. 15.6 and 15.7 show the radiation heat flux and indoor thermal results based on varying the pattern space between 11 and 41 mm. In Fig. 15.6, the heat flux on the inner face of roof glass reduces from 146 to 138 W/m^2 as the pattern space decreases from 41 to 11 mm. It indicates that the interior heat load resulting from the transmitted solar radiations can be reduced as the pattern space decreases; however, due to the slight heat dissipation, the indoor temperature, where is even approaching to the roof pane shown in Fig. 15.7a, is not drastically decreased while one applies finer pattern space over the roof glass, as plotted in Fig. 15.7b.

The modeling results obtained in Figs. 15.4, 15.5, 15.6, and 15.7 give that the transmitted solar load can be attenuated if the glass incorporates trapezoidal-shaped patterned throughout the exterior surface as shown in Fig. 15.3. Moreover, applying greater θ with smaller pattern space, the trapezoidal shaped pattern performs better capacity on reducing the transmitted solar load passing through the window pane, although the radiant energy is slightly reduced based on such pattern feature.

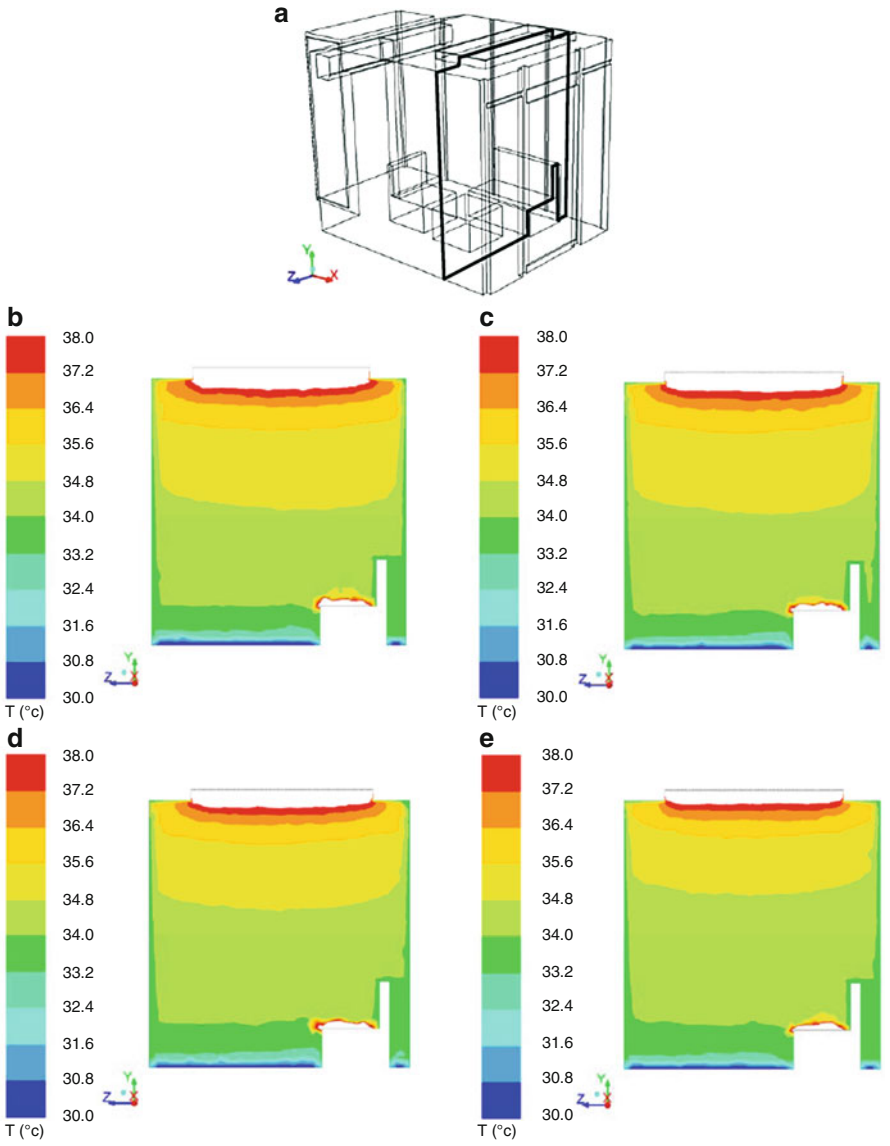

Fig. 15.5 Indoor temperature field throughout the interest face of (**a**) based on trapezoidal-shaped patterns with θ equal to (**b**) 0° (**c**) 30° (**d**) 45° (**e**) 60°

Besides analyzing the thermal performance for the trapezoidal-shaped patterns, this work interests the glass patterns in triangular shape as well. Based on the new finding in Fig. 15.6, it is advantageous to make the pattern space as small as possible; therefore, the roof glass analyzing here incorporates triangular-shaped patterns immediately adjacent to each other as shown in Fig. 15.8. Figure 15.9

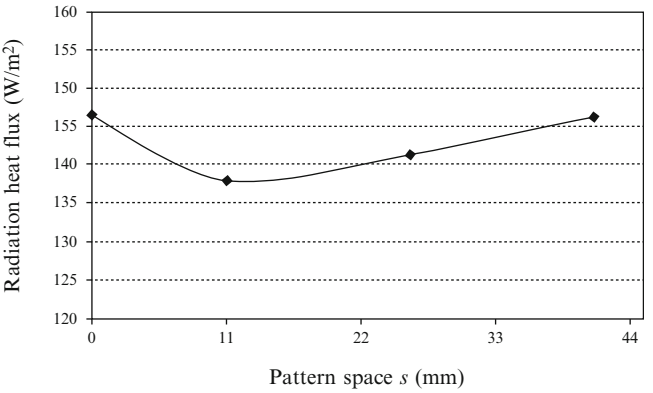

Fig. 15.6 The radiation heat flux on the inner face of the trapezoidal patterned glass versus pattern space *s*

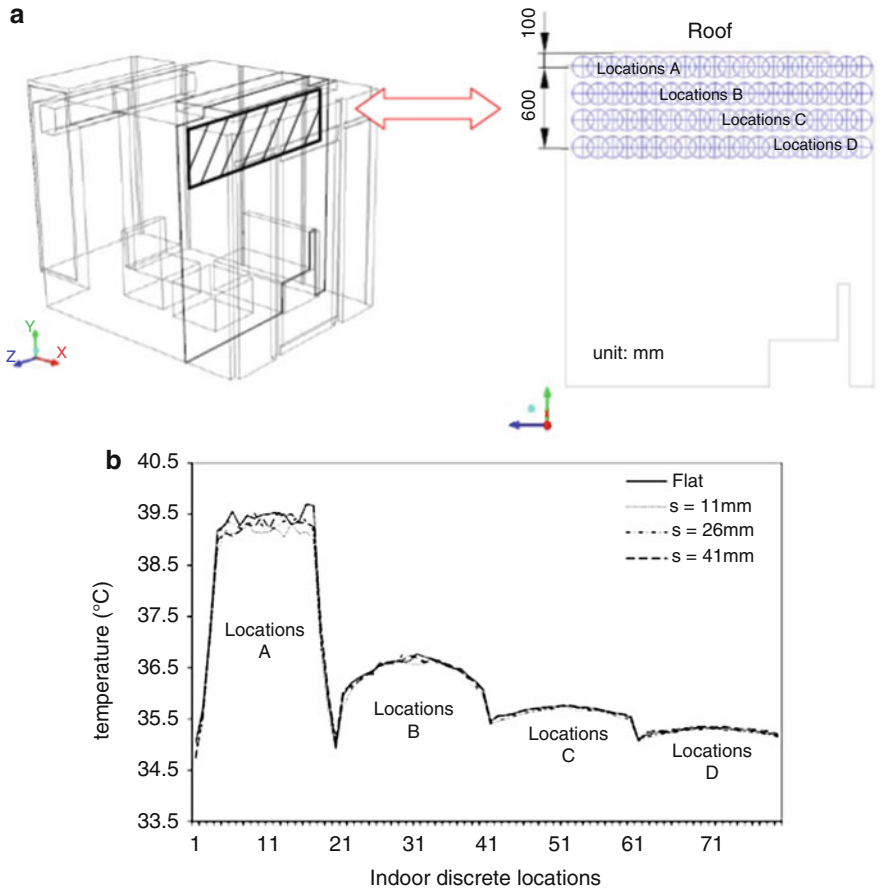

Fig. 15.7 Indoor temperature at discrete locations of (**a**) based on varying *s* of trapezoidal-shaped patterns

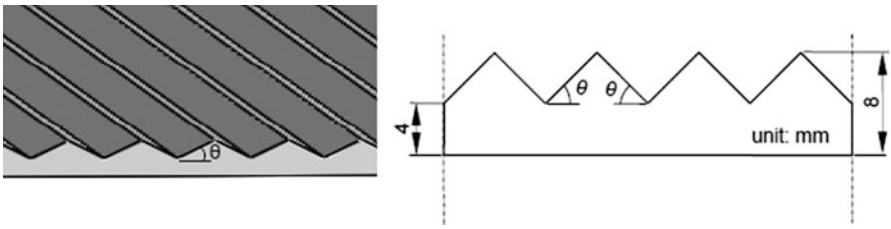

Fig. 15.8 Analytical roof glass patterned in triangular shape

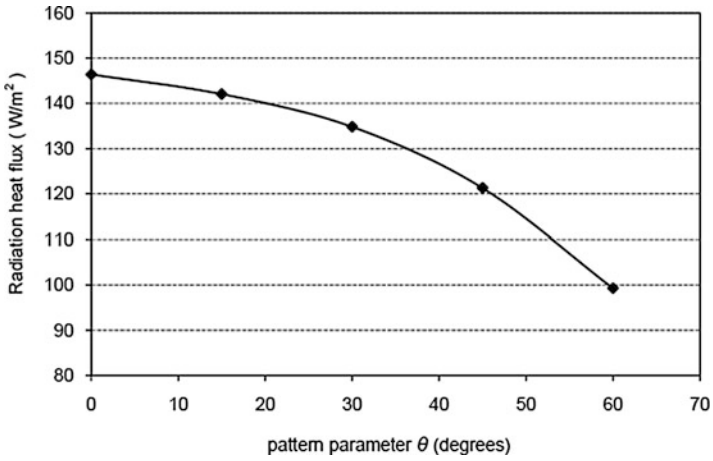

Fig. 15.9 Radiation heat flux on the inner face of the roof glass based on varying θ of triangular-shaped patterns

shows the transferred heat flux over the inner face of the roof pane related to the change in the bottom angle θ from 0 to 60°. Similar to the results obtained in Fig. 15.4 for the trapezoidal patterns, the transmitted solar radiation reduces as the triangular-shaped patterns applying greater θ. When θ equals 60°, the heat flux greatly decreases from 146 to 99 W/m^2 and which is about 32 % of that for flat glass, as obtained in Fig. 15.9. Moreover, the thermal distributions inside of the glass house obtained in Fig. 15.10 also indicate that the triangular-shaped pattern applying θ equal to 60° has a great capacity to dissipate heat load existing inside of the glass house, comparing with that for the flat roof glass, θ equal to 0°. Figure 15.11b displays the indoor temperature, located 100 mm vertically away from the roof pane as shown in Fig. 15.11a. According to Fig. 15.11b, it indicates that if one applies triangular-shaped patterns with θ equal to 60° throughout the surface of the roof glass, the maximum reduction of indoor temperature can attain about 1.3 °C.

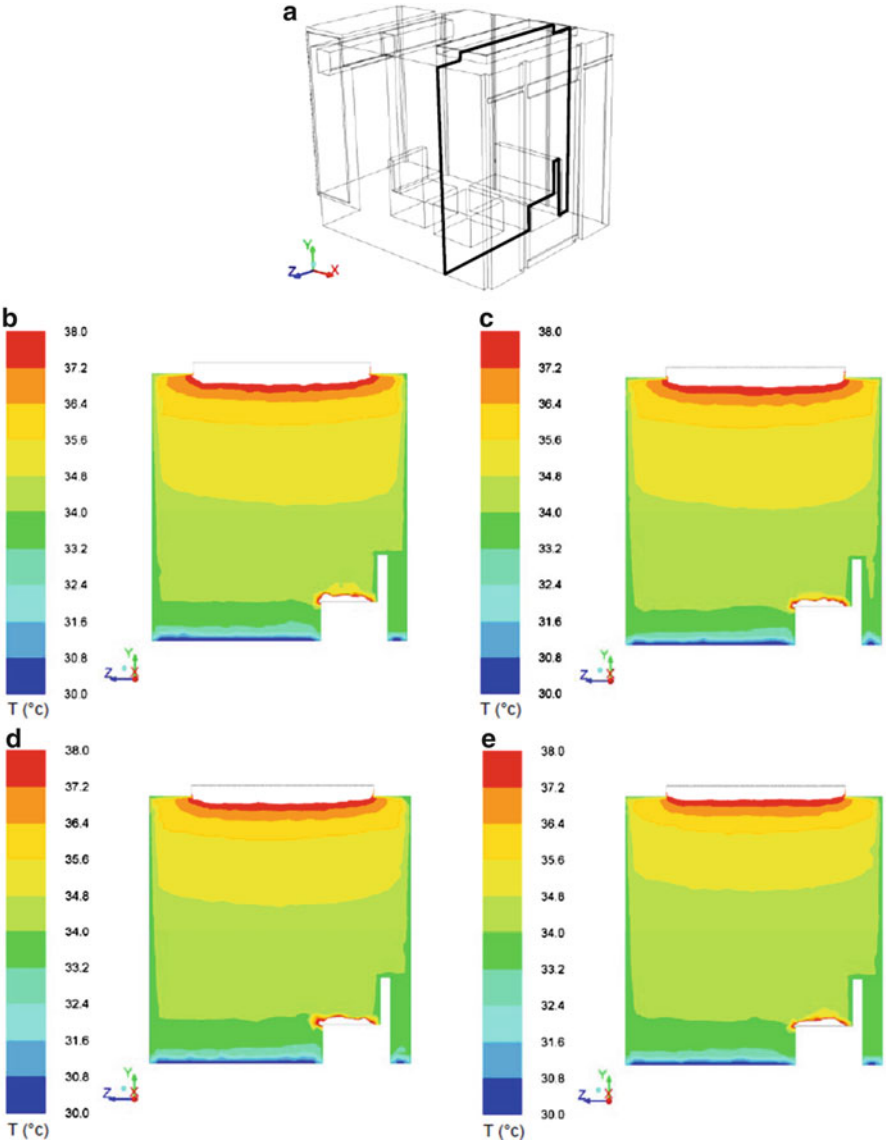

Fig. 15.10 Indoor temperature field throughout the interest face of (**a**) based on triangular-shaped patterns with θ equal to (**b**) 0° (**c**) 30° (**d**) 45° (**e**) 60°

15.3 Discussion

The objective of this work is to develop a skill that can perform the capacity to attenuate the solar load getting into the glass pane. Knowledge of the variation of transmitted solar radiation dependent on the glass component, this work imposes

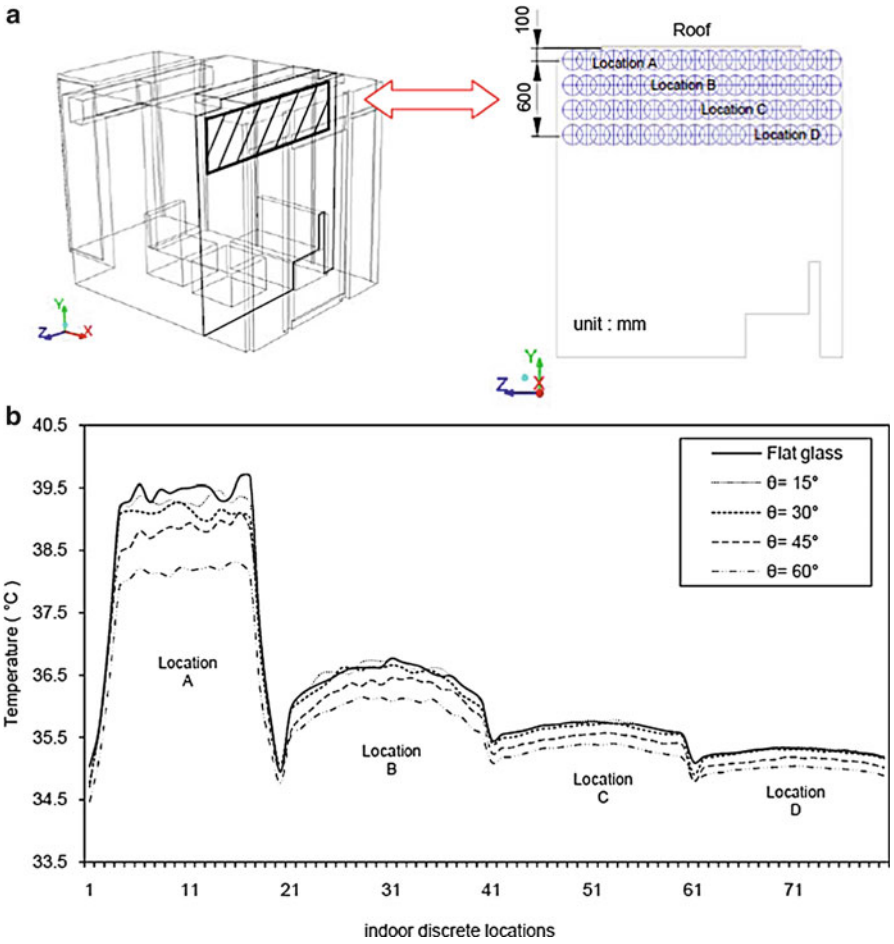

Fig. 15.11 Indoor temperature at discrete locations of (**a**) based on varying θ of triangular-shaped patterns

patterns in trapezoidal and triangular shape over the exterior face of the roof glass, rather than considering the conventional flat surface. Analytical results indicate that the transmitted solar load indeed can be reduced if one applies the described patterns on the roof glass, comparing with that for flat glass. The pattern feature parameters including θ and pattern space s shown in Fig. 15.3 can vary the thermal performance of the glass. The glass pattern applying greater θ results in the more reduction of heat load due to the glazing radiant energy associated with the function of $\cos(\theta)$ as expressed in Eq. (15.4). However, if θ is approaching or equal to 90°, the thermal behavior of the patterned glass will be approximately same as that for the conventional glass. It results from such patterns appearing nearly flat surface throughout as the flat glass does, although they distribute discontinuously over the

glass face. The spacing between adjacent patterns provides the flat area, as well, and where potentially allows the maximal radiant energy penetrating into the glass. Therefore, applying finer pattern space helps reduce the solar load entering indoors, as shown in Fig. 15.6.

The thermal performances based on trapezoidal and triangular-shaped patterns are shown in Figs. 15.4, 15.5, 15.6, 15.7, 15.9, 15.10, and 15.11, respectively. Under identical solar radiant conditions and glass characteristics, analytical results indicate that more heat dissipation is acquired by employing triangular-shaped patterns, comparing with that for the pattern in trapezoidal shape. As mentioned previously, the transmitted solar load can be attenuated by the patterned glass based on applying smaller s. The absence spacing between adjacent patterns and the geometric character like vertices for triangle give the triangular-shaped patterns as shown in Fig. 15.8 without flat areas appearing over the surface of the roof glass, which results in the significant reduction in the solar load getting into the glass. Therefore, such triangular-shaped patterned glass behaves superior capacity on the reduction of transferred heat flux, as can be seen in Fig. 15.9. If one applies triangular-shaped patterns having 60° for the bottom angle θ, for instance, throughout external face of the roof glass, the radiant heat flux on the inner face of roof pane can be reduced about 32 % of that for applying the flat glass.

The analytical results provided in this work substantiate the validity of the described skill for the reduction of glazing radiant energy. While this study emphasizes on the roof glass and presently neglects the floor windows in the glass house, in order to fully understand the thermal performance of the patterned glass, the authors are confident that applying the described patterns over the floor window will result in more heat dissipations inside of the glass house.

15.4 Conclusions

Transmitted solar radiation passing through a window can significantly affects the thermal field and thermal comfort for a building. This work demonstrates that if the glass incorporates with patterns throughout, the glazing radiant energy indeed can be attenuated, comparing with that for the conventional flat glass. Moreover, the heat load existing inside of the glass house can also be reduced, which is straightly advantageous for the decrease in the air conditioning load, specifically in warm seasons, and consequently attains the aim of energy savings.

Acknowledgement The authors appreciate the technical department of 3M Taiwan Ltd. for providing grants to support this work.

Nomenclature

Q Instantaneous radiant energy flux (W/m^2)
q The component of instantaneous radiant energy flux (W/m^2)

Greek Symbols

θ Incident angle

References

1. Etzion Y, Erell E (2000) Controlling the transmission of radiant energy through windows: a novel ventilated reversible glazing system. Build Environ 35:433–444
2. Chow TT, Fong KF, He WAL, Chan S (2007) Performance evaluation of a PV ventilated window applying to office building of Hong Kong. Energ Build 39:643–650
3. Schuman J (1992) Cool daylight. Prog Architect 73(4):136–141
4. Ismail KAR, Henriquez JR (2003) Modeling and simulation of a simple glass window. Sol Energ Mater Sol Cell 80:355–374
5. ASHRAE (2001) Fundamentals handbook – Table 13 of Chapter 30

Chapter 16
Choosing the Right Technology: Optimized Design of Renewable Supply Systems for Residential Houses

Christian Milan, Mads Pagh Nielsen, and Carsten Bojesen

Abstract The use of renewable energy sources (RES) has continuously increased throughout the last decade. In the residential building sector the trend goes towards energy supply systems based on multiple RES. This is mainly due to political requirements, governmental subsidies and fuel price development. These systems not only require an optimal design with respect to the installed capacities but also the right choice in combining the available technologies assuring a cost-effective solution.

The aim of this paper is to present an optimization methodology for residential on-site energy supply systems based on mixed integer linear programming. The methodology chooses the right combination of technologies and sizes the components based on on-site weather data and expected consumption profiles. Through this approach the fluctuations of RES as well as the user behavior are taken into account already during the planning process. The methodology allows for specifying a level of Net Zero Energy Building (Net ZEB) performance to investigate cost reductions when allowing shares of fossil fuel consumption. The outcome is an optimal supply technology combination and optimal installed capacities in terms of the overall costs including system installation and operating expenses. The approach is applied to a case study of a residential single family house under Danish conditions. It delivers rapidly site-specific solutions and can easily be used as an extension for common building energy simulation software.

In the case study several levels of Net ZEB performance have been investigated. The results show that supply systems based solely on renewable sources are still considerably more expensive than standard solutions and that substantial cost reductions can be reached by allowing a certain share of primary energy consumption.

Keywords Net zero energy buildings • Renewable energies • Linear programming • Investment optimization

C. Milan (✉) • M.P. Nielsen • C. Bojesen
Department of Energy Technology, Aalborg University, Pontoppidanstræde 101, Aalborg Øst 9220, Denmark
e-mail: cmi@et.aau.dk; mpn@et.aau.dk; cbo@et.aau.dk

I. Dincer et al. (eds.), *Progress in Sustainable Energy Technologies Vol II: Creating Sustainable Development*, DOI 10.1007/978-3-319-07977-6_16

16.1 Introduction

Mitigating climate change is one of the global challenges of the twenty-first century. To achieve this goal, the worldwide Greenhouse Gas (GHG) emissions have to be reduced drastically throughout the next decades [1]. The building sector is one of the major origins of these emissions with e.g. 40 % of the total GHG discharge in the European Union [2]. Therefore, efforts are being made to reduce the energy demand and the fossil fuel consumption in buildings.

16.1.1 From Single to Multi Source Supply Systems

Over the past two decades, the use of renewable energy sources (RES) in the building sector has increased continuously [3]. At first, only a single technology was installed besides the conventional fossil fuel systems, e.g. a solar thermal collector for hot water preparation. Lately, political guidelines and subsidies as well as technical improvements and cost reductions accompanied by the concept of low energy buildings led to the installation of several technologies in the same house [4]. The future trend and legislation goes towards residential supply systems, which are based totally on renewable sources [5]. Systems with several or solely renewable technologies are much more difficult to design due to the large diversity of technology options available and the interdependencies of the system components. Moreover, all the on-site conditions have to be included in the planning process. People in different countries have different consumption patterns. Likewise, weather conditions and consequently the availability of renewable energy resources differ considerably dependent on the geographical location.

16.1.2 Site-Specific Solutions but Consistent Methodology Needed

The above mentioned reasons necessitate a site-specific solution for each building and eliminate the possibility of applying standardized solutions. To develop these individual system designs, trial-and-error approaches are most common today in low energy building planning [6–8]. These approaches are very labor and cost-intensive and do not assure that a global optimum design is found. The solution obtained by these methods can be just a local optimum, since the whole solution area cannot be evaluated. In contrary, linear problems guarantee a global solution, since the optimum will always be located in the intersection of some of the constraints. Therefore, a consistent methodology is needed which allows for a fast optimum solution based on the specific on-site conditions. The existing energy analysis programs are mostly focused on regional or national levels and therefore

exclude the investigation of single supply systems or they have only specific technologies implemented but not a large variety [9]. Several studies have been conducted on the optimization of energy systems for low energy houses. However, these works include the design of the whole building and apply genetic algorithms or involve highly non-linear complex problems [6, 8, 10]. This leads to very calculation intensive solution procedures, which can require two months on standard processors for calculating a one year performance of the energy system [10]. Another important point is that low energy houses often involve by far higher investment costs compared to standard buildings due to special building materials and the installation of several renewable energy technologies [4]. Therefore, it would be desirable to have a tool for investigating the costs for several shares of renewable energies in the building supply system.

16.1.3 Developing a Ready-to-Use Program

The work presented in this paper attempts to close the gap of applicable models for residential renewable supply systems. A ready-to-use program is developed, which allows for identifying and analyzing the cost-optimal combination out of a wide range of technologies taking the fluctuations of RES and user behavior patterns into account. The approach is based on a mixed integer linear programming problem to minimize the computational expenses. It is a further developed and extended methodology of the work presented in [11]. The objective of the remaining chapters is to describe the methodology development and features. Firstly, the structure and mathematical theory will be presented followed by a description of the considered technologies and the implemented supply models of each technology. The approach is then used to investigate different cost optimal solutions for a typical Danish low energy house in a case study. The paper concludes with a discussion on the results and potential expansions of the model.

16.2 Optimizing Supply System Design

During the design phase of the supply system, several optimization objectives are possible. An important characteristic of energy conversion technologies applying RES at residential buildings are the considerably higher investment costs compared to standard fossil fuel solutions [12]. The objective function chosen in this paper is therefore to minimize the overall costs of the supply system rather than optimizing energy efficiency. In future, the methodology could also be extended into a multi-objective problem including environmental performance or system efficiency. Nevertheless, this study focusses on a purely financial analysis. In the following sections, the most important methodology features are described as well as the structure of the program and the mathematical theory behind is discussed.

Table 16.1 Used definition for net zero energy buildings

Type of supply system	Renewable energy supply options	Balancing period	Balancing unit	Balance border
Connected to public grid	On-site generation of on-site sources and off-site sources (biogas)	Annual	Consumed primary energy	Energy related to 1. Building operation and user appliances 2. Embodied energy of the energy supply technologies 3. Fossil-fuel consumption

16.2.1 Methodology Features

The methodology described in this paper is based on mixed integer linear programming and hence delivers fast site-specific solutions. The program uses hourly values for the consumption profiles and weather data and can easily be coupled with building engineering tools, such as EnergyPlus. The EnergyPlus software can calculate hourly energy demands based on the future architecture of the building and the chosen construction materials [13].

Furthermore, the purpose of the presented approach is to provide a tool for designers of low energy houses to investigate different cost optimal solutions towards so called Net Zero Energy Buildings (NetZEB). NetZEBs are houses which produce on an annual basis as much energy out of renewable sources as they consume. Currently the term "NetZEB" is still under development and many countries use different approaches when measuring net zero energy performance [14]. Therefore it is important to state the exact chosen definition, when dealing with NetZEBs. In this paper the definition of the Danish Strategic Research Centre on Zero Energy Buildings is applied with minor adaptations to the current case [15]. In Table 16.1 the main characteristics of this definition are listed.

A grid connected building is considered, which has to balance out the consumed primary energy on a yearly basis by feeding excess electricity to the grid. The renewable energy supply options include the generation at the building-site of on-site sources as well as using biogas as an off-site source. In the balance all the energy related to the building operation (space heating, domestic hot water, electricity for appliances and lighting), the annual share of the energy consumed during the manufacturing process of the different supply technologies, e.g. the Photovoltaic (PV) module, and the primary energy due to fossil fuel consumption are accounted for.

Based on this definition the program allows the building designer to define a certain degree of Net ZEB performance. The degree is defined as the share of allowable primary energy consumption by the building compared to the primary energy consumption, which a reference system based on a standard solution would

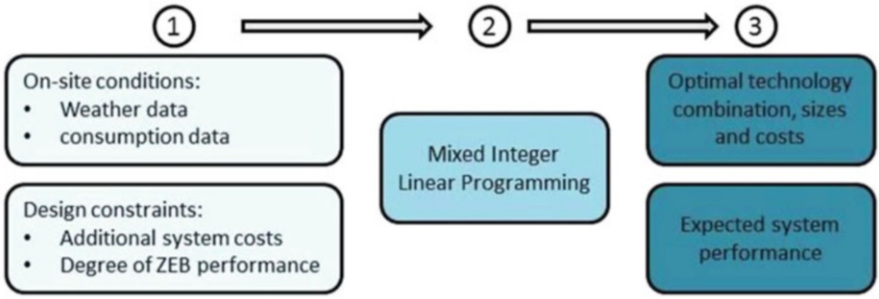

Fig. 16.1 The three basic steps of the optimization methodology

cause. In this case the reference system consists of a natural gas boiler for the heat supply and grid purchased electricity. This gives the possibility to the designer to investigate cost reductions by deviating from the Net ZEB performance.

16.2.2 Methodology Structure

The methodology consists of three basic units as depicted in Fig. 16.1. The first part consists mainly of the input data and constraints set by the building or system designer. The methodology uses hourly values for on-site weather data and consumption profiles. The second unit consists of the optimization problem itself which involves balance equations for heat, electricity and primary energy consumption connected to the objective function representing the overall costs of the system.

The last part consists of the simulation results after the problem has been solved. The cost optimal combination and installed capacities for each considered technology are determined together with the overall system costs including the investment, operational and decommissioning phase. During the calculation of the optimal configuration the energy balance equations have been solved for each hour of the year and therefore the program delivers in addition the expected system performance data.

16.2.3 Mathematical Formulation of the Optimization Problem

The methodology uses mixed integer linear programming to find the optimal system design and is a further development of the model described in [11]. For the sake of conciseness only the major equations are presented here. For the detailed

equations please refer to the earlier mentioned article. The general formulation of the optimization problem is:

$$\min p(x) = \left(y, P_{inst}^{T1}, P_{inst}^{T2}, \ldots, P_{inst}^{Tn}\right) \tag{16.1}$$

s.t.
$h_i(x) = 0$
$g_m(x) \leq 0$

The objective function $p(x)$ depends on the installed power P_{inst}^{Tn} of n considered technologies and the corresponding binary variables, which represent the selection (y = 1) or disregard (y = 0) of each technology. The function has to be minimized subject to $h_i(x)$ equality and $g_m(x)$ inequality constraints. These constraints are either due to physical restrictions or defined by the system designer. Minimizing the overall system costs is the main objective of the presented methodology. The objective function, shown in Eq. (16.2), represents these costs C_{NPC}^{System} discounted to the net present costs (NPC), since several expenses occur at later times than the initial investment.

$$p(x) = C_{NPC}^{System} = P_{inst}^{T1} * c_{NPC}^{T2} + P_{inst}^{T2} * c_{NPC}^{T2} + \cdots + P_{inst}^{Tn} * c_{NPC}^{Tn} + c_{NPC}^{grid} \tag{16.2}$$

s.t.

$$P_{inst}^{Tj} \geq 0$$

Each technology j has its specific cost c_{NPC}^{Tj}, which are multiplied by the installed power P_{inst}^{Tj} to obtain the total system costs. The installed power must not be negative. The expenses for buying electricity is included at total costs C_{NPC}^{grid}. The specific costs c_{NPC}^{Tj} are the sum of the investment costs c_{inv}^{Tj}, the expenses occurring during operation and maintenance (OM) of the system c_{OM}^{Tj}, and the decommissioning costs c_{dec}^{Tj} as referred to in Eq. (16.3). Both, the OM and decommissioning costs are discounted to NPC by the discount rate i. The OM costs can vary over time due to e.g. rising fuel prices and are for this reason discounted for each year of the operational lifetime N.

$$c_{NPC}^{Tj} = \left(c_{inv}^{Tj} + \sum_{t=1}^{N} \left(c_{ON,t}^{Tj} * (1+i)^{-t}\right) + c_{dec}^{Tj} * (1+i)^{-N}\right) \tag{16.3}$$

s.t.
$j \in \{1,\ldots,n\}$

The OM costs are calculated according to Eq. (16.4) including the yearly maintenance costs $c_{ma\,\mathrm{int}}^{Tj}$ plus the fuel price $c_{fuel,t}^{Tj}$ for the period t multiplied by the specific fuel consumption f_t^{Tj}:

$$c_{OM,t}^{Tj} = f_t^{Tj} * c_{fuel,t}^{Tj} + c_{maint}^{Tj} \tag{16.4}$$

As mentioned above, the methodology is also intended to enable the investigation and design of NetZEBs. To be able to measure, if a building is achieving net zero energy performance, a balancing unit is necessary. In the work presented, primary energy has been chosen for this purpose in accordance to [15]. The balance equation is shown in Eq. (16.5).

$$b \leq \frac{s_{T_1} * p_{inst}^{T_1} + s_{T_2} * p_{inst}^{T_2} + \cdots + s_{T_n} * p_{inst}^{Tn}}{N} + \sum_{t=0}^{t=N} \left(\gamma_{T1} * f_t^{T1} + \gamma_{T2} * f_t^{T2} + \cdots + \gamma_{Tn} * f_t^{Tn}\right) + \gamma_e * \sum_{t=0}^{t=N} \dot{e}_t^{grid} \tag{16.5}$$

The primary energy consumed during the fabrication process of each supply device is included in the balance and described by the first term. ε_{Tj} corresponds to the specific primary energy of the manufacturing process including installation of technology *Tj*. Since this energy only needs to be offset throughout the whole operational life span *N* of the system, a share for each year is calculated. The second term involves the fossil fuel consumption of the system for each technology during the balancing period, which is multiplied with the corresponding primary energy factor γ_{Tj} of each fuel. The last term respects the exchange with the public grid. By delivering energy to this network, the building can offset the consumed primary energy. In this case, the summation term is negative, since more energy is fed into the grid than it was purchased throughout the balancing period. For a NetZEB the presented primary energy balance has to be zero. In the current methodology it is possible to investigate different degrees of NetZEBs apart from the 100 % NetZEB case and therefore the variable *b* is introduced. This variable defines the allowed share of primary energy consumption compared to the primary energy consumption of the reference system, which represents a standard solution based on fossil fuels.

The aim of the next chapter is to give an overview of the technologies considered in this paper and the used reference system.

16.3 Supply System Components

Before sizing the supply system, the designer has to specify the technologies to consider in the optimization process. In Fig. 16.2a the flow scheme of the system with all implemented supply technologies is shown.

In order to cover the heat demand a solar thermal collector, a combined heat and power unit (CHP) fueled with biogas and a heat pump are investigated as potential supply technologies. The electricity demand can be covered by a photovoltaic (PV) module and the biogas CHP. Heat, which cannot be consumed immediately, is stored in a water tank. The reference system, as depicted in Fig. 16.2b consists of

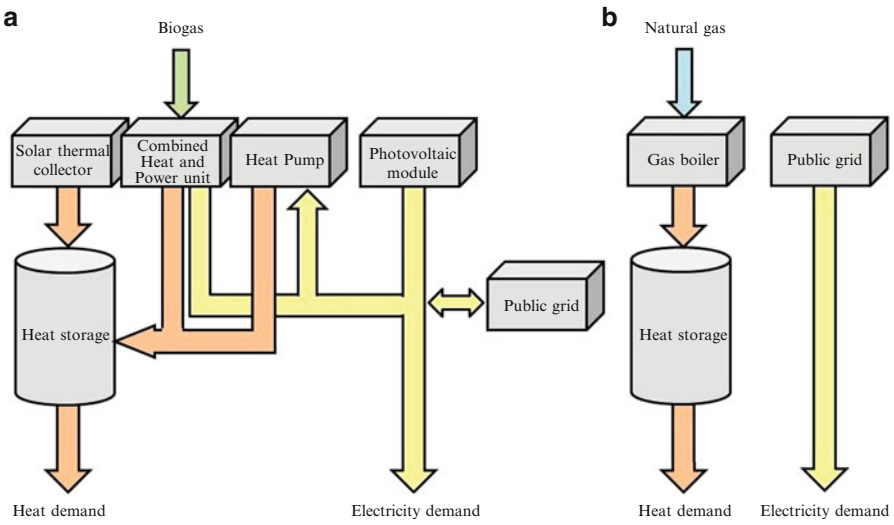

Fig. 16.2 (**a**) Flow scheme with all considered supply technologies (**b**) Flow scheme of the reference system

a natural gas boiler for the heat supply and a public grid connection for the purchase of electricity to cover all the energy demands.

16.3.1 Technology Comparison

The most important technical and economical specifications of all the considered technologies under Danish conditions are shown in Table 16.2. For each technology an allowed range of the installed capacity is defined to assure that the specifications are valid, since they refer to that specific range and often change for larger or smaller capacity scales. The heat storage size is fixed for both the reference system and the system to be optimized with a capacity of 200 l. The embodied primary energies are taken from scientific life-cycle analyses [16–18].

The investment costs are mainly based on commercial available products and have been expressed as a function of the installed capacity for the PV module, the solar-thermal collector and the heat pump, since the prices can vary quite substantially with the capacity [19–23]. The removal costs have been estimated as a share of 20 % for all technologies, except the heat pump, based on [19]. They have stated this factor only for a PV module and a solar-thermal collector, but since no precise data was available it was assumed to be in the same range for the Micro-CHP and the gas boiler. The heat pump removal costs have been assumed to be higher at around 30 % due to the piping in the soil.

Table 16.2 Comparison of considered technologies

	PV module	ST collector	Heat pump (HP)	Micro-CHP	Boiler	Heat storage
Technical parameter						
Type	Poly-crystalline	Glazed flat-plate	Water based ground source	Recipro-cating gas engine	Conden-sing boiler	Water tank
Efficiency [–]	0.12	0.79	4.9[a]	0.63[b] thermal 0.26[b] electric	0.85[b,c]	0,995/day (0.875[d])
Max. capacity [kW]	10	10	10	5	15	200 l
Embodied primary energy (kWh/kW)	6,000	1,172	1,612	883	1,029 kWh	7,637 kWh/m^3
Economical parameter						
Investment costs [€]	2,027+ P^{PV} * 3,661[e]	1,728+ P^{ST}*580[e]	12,406+ P^{HP}*696[e]	2,500 €/kW_{el}	4,933	1,126
Operation and Maintenance costs [€]	1 % of investment costs	1 % of investment costs	267	0,03 €/kWh	8.5 % of fuel costs	0
Removal costs [% of investment costs]	20	20	30	20	20	20

[a]Annual averaged COP
[b]Based on upper heating value
[c]Including typical standby losses
[d]Efficiency of the heat exchangers inside the tank
[e]As a function of the installed capacity

16.3.2 Development of Performance Models

For each technology a performance model has been developed and implemented in the mixed-integer linear problem. These performance models link the energy output of each device to the installed capacity. All models applied in this paper are based upon simplified approaches in order to keep the overall optimization problem linear. The equations for the PV module, the solar-thermal collector and the ground-source heat pump are not explicitly mentioned here for the sake of conciseness. For the detailed models please refer to [11]. The implemented equations for the CHP, the gas boiler and the heat storage are described in the following.

16.3.2.1 CHP

The CHP considered in this methodology represents a reciprocating engine within ranges of 0–5 kW. Eqs. (16.6) and (16.7) formulate the electricity and the heat output per hour dependent on the fuel consumption f_t^{CHP}. Besides the efficiency of the CHP, also a so-called load service rate η_{lsr}^{CHP} is introduced, which accounts for efficiency reductions due to starts, stops and half load operation of the CHP [24].

$$\dot{e}_t^{CHP} = \eta_{el}^{CHP} * \eta_{lsr}^{CHP} + UHV^{BG} * f_t^{CHP} \tag{16.6}$$

$$\dot{q}_t^{CHP} = \eta_{th}^{CHP} * \eta_{lsr}^{CHP} + UHV^{BG} * f_t^{CHP} \tag{16.7}$$

The installed electrical power of the CHP is linked to the electricity output by Eqs. (16.8) and (16.9). The electricity output per hour must not exceed the installed electrical power as demanded in Eq. (16.8):

$$P_{el}^{CHP} \geq \dot{e}_t^{CHP} \tag{16.8}$$

Equation (16.9) sets a limit to the annual produced electricity. In order to avoid too many interruptions in the CHP operation a minimum number of full load hours t_{fl} has been defined as a lower border for the annual electricity production.

$$P_{el}^{CHP} * t_{fl} \leq \sum\nolimits_t \dot{e}_t^{CHP} \leq P_{el}^{CHP} * t_{avail} \tag{16.9}$$

The upper limit is set by the maximal available hours t_{avail} of the CHP module. This is due to the fact that CHPs based on reciprocating engines are maintenance intensive and have to be serviced several times a year. During these times they are not available for power production [24].

16.3.2.2 Gas Boiler

For the reference case, a gas boiler fueled by natural gas has been implemented in the methodology. The equation for the hourly heat production is shown in Eq. (16.10) and is formulated analogously to the heat equation for the CHP. However, a low service rate is not included, since condensing boilers have very fast start-up times and in part load operation even higher efficiencies [25]. Therefore, also only one fixed boiler size is considered, because they can run in a large power range.

$$\dot{q}_t^{GB} = \eta^{GB} * UHV^{NG} * f_t^{GB} \tag{16.10}$$

The installed capacity is, analogue to Eq. (16.8) the limiting factor for the maximal heat production.

$$P^{GB} \geq \dot{q}_t^{GB} \tag{16.11}$$

Gas boilers need only very little maintenance and therefore no constraints have been set on the availability of the boiler.

16.3.2.3 Heat Storage

In the current model a water tank is used for heat storage. It is used for short time storage and has a fixed size of 200 l. Since temperature losses occur when heat is transferred to the tank or extracted from it, Eq. (16.12) accounts for these losses by involving the efficiency of the heat exchangers η^{HX} to and from the tank.

$$\dot{q}_t^{HS} = \frac{q_t^{HS,net}}{\eta^{HX}} \tag{16.12}$$

The calculated net heat $q_t^{HS,net}$ is used to determine the charge level l_t^{HS} of the storage tank as specified in Eq. (16.13). It is added to the heat already available in the tank from the previous hour. However, the tank has also losses to the surroundings, which are considered by the heat loss rate η^{HS}.

$$l_t^{HS} = l_{t-1}^{HS} * \left(1 - \eta^{HS}\right) + q_t^{HS,net} \tag{16.13}$$

To exclude an overcharging of the tank, the following constraint limits the maximum charge level to the installed capacity of the heat storage, defined in Eq. (16.14):

$$l_t^{HS} \leq P_{inst}^{HS} \tag{16.14}$$

16.3.2.4 Backup System

The methodology also accounts for a backup system in case of very large deviations of weather conditions or user consumption. The backup consists of a security margin of 10 % of installed electricity and heat production capacities, with which the system should be oversized. The backup installations are also allocated in a cost optimal way.

16.4 Case Study

The above presented methodology has been used to investigate a sample case of a fictitious low energy house under Danish conditions. In the following conducted simulations are described and the results are presented and discussed.

16.4.1 Description of the Simulations

The above described methodology has been implemented in the GAMS software platform, which is designed for solving optimization problems [26]. The main assumptions for the example case are listed in Table 16.3.

Future natural gas and electricity prices have been taken based on the actual estimations of the Danish Energy Agency [27, 28]. The actual biogas price was calculated for upgraded biogas, which can be delivered to the natural gas grid, and relates to the achievable price from an operating Danish biogas plant [29]. For the future biogas prices an annual increase of 3 % has been assumed. To all the prices current taxes and fees have been added to obtain the delivery price to a Danish household. A summary of the results is shown in Table 16.4.

16.4.2 Results and Discussion

The above specified residential building has been investigated by applying the methodology and solving the problem with the GAMS software. The calculations have been performed for different degrees of Net ZEB performance as seen in Fig. 16.3. The installed and the additional backup capacity are depicted for each technology. The lowest achievable share of Net ZEB performance with the given renewable energies is 23 %. To achieve even lower shares a technology using fossil fuels, such as a natural gas boiler, would be needed.

Table 16.3 Main assumptions for the case study

Parameter	Value
Building specifications	
Type of house	Low energy single family house
Number of occupants	2
South facing roof space	85 m^2
Economical parameters	
Operational life span of supply system	20 years
Discount rate	3 %
Security margin in installed capacity	10 %
National energy system	
Primary energy factor for grid electricity	2.5 $kWh_{prim}/kWh_{delivered}$
Primary energy factor for natural gas	1 $kWh_{prim}/kWh_{delivered}$

Table 16.4 Used future energy prices for households

Year	Electricity (€/kWh)	Natural gas (€/kWh)	Biogas (€/kWh)
2012	0.32	0.08	0.11
2015	0.34	0.10	0.12
2020	0.40	0.11	0.14
2025	0.38	0.12	0.16
2030	0.49	0.13	0.18

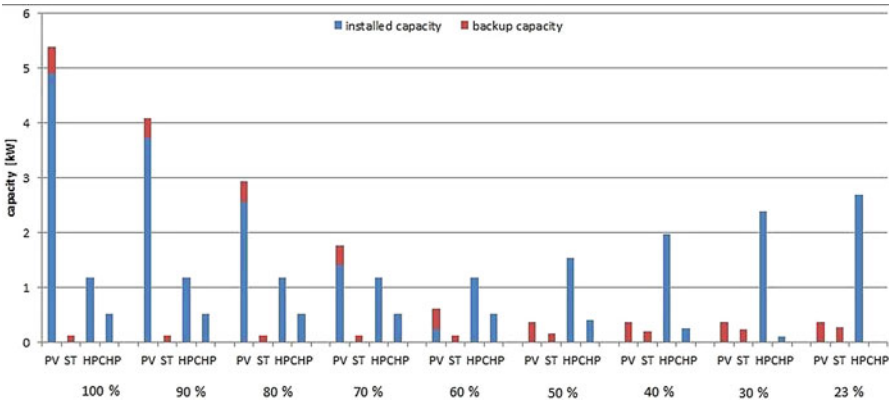

Fig. 16.3 Installed and backup capacities for each technology and degree of Net ZEB performance

It can be seen from the figure that very high degrees of ZEBs necessitate large PV modules to offset the electricity consumed from the grid. With lower shares of ZEB performance, the size of the PV module declines until it is eventually only considered as a backup source. The heat production is covered solely by the CHP plant and the heat pump for buildings close to Net ZEB conditions. A small solar

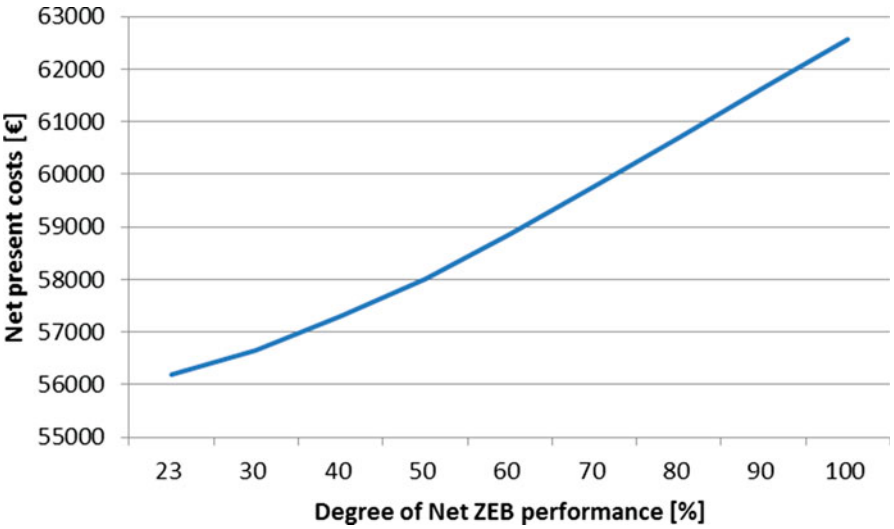

Fig. 16.4 Total supply system net present costs in relation to the degree of Net ZEB performance

thermal collector is intended to function as a backup source in case of large deviations of heat consumption. When increasing the allowed amount of consumable primary energy, the CHP capacity declines and the heat pump size is increased to cover the heat demand by using grid electricity.

The development of the total system costs as a function of the Net ZEB degree is depicted in Fig. 16.4. The net present costs decline considerably, if minor shares of primary energy consumption are allowed. The potential cost reductions become smaller the lower the Net ZEB degree is.

Investigating the composition of the total system costs, as listed in Table 16.5, it can be stated that the cost structure for supply systems achieving or being close to Net ZEB performance is very different to the standard reference solution. The investment costs prevail for these systems and the operational and maintenance costs are considerably lower. With increasing the share of primary energy consumption the trend goes towards lower investment costs and higher operational costs, since the PV module capacity is reduced and electricity is bought from the grid instead.

From the discussed results it can be concluded that the presented methodology determines a cost optimal solution based on the desired degree of Net ZEB performance. However, it should be stated that the considered technologies are solely using renewable energy sources. In regard to larger shares of allowed primary consumption higher cost reductions can be achieved by implementing fossil fuel technologies, such as a gas boiler. This is indicated by the very low costs of the reference system, which is still more than 20 % lower than the costs for the lowest Net ZEB performance of 23 %. Furthermore, it should be noted that the methodology applies continuous variables for the capacities. This might not reflect

Table 16.5 Comparison of total costs depending on the degree of NetZEB performance

	Reference system	100 %	90 %	80 %	70 %	60 %	50 %	40 %	30 %	23 %
Investment costs [€]	6,060	38,023	33,345	28,668	23,990	19,313	18,310	18,264	18,219	18,188
Total net present OM costs [€]	36,461	19,601	23,867	28,134	32,400	36,667	36,923	36,625	35,625	35,188
Net present costs for system removal [€]	671	4,943	4,425	3,907	3,389	2,871	2,773	2,785	2,797	2,805
Total system net present costs [€]	43,192	62,566	61,637	60,708	59,779	58,850	58,006	57,314	56,640	56,180

the market situation and a future improvement would be to implement available discrete sizes for the capacities. Finally, it has to be stated that the methodology neglects the control issues, which might arise in practical applications, when combining several supply technologies, such as a solar thermal collector and a heat pump. To implement these considerations in the methodology is a recommendation for future research.

16.5 Conclusions

In this paper a methodology was developed, which allows for determining the cost optimal combination and sizes of selected renewable energy technologies for a residential building. Furthermore, it compares the system performance to a reference system based on a standard configuration using a natural gas boiler. It was shown that by allowing minor shares of primary energy consumption, cost reductions can be achieved compared to a 100 % Net ZEB. The cost structure for Net ZEBs is characterized by very high investment costs but involves in return only little operation and maintenance costs. Finally, recommendations on future development of the methodology have been given.

Nomenclature

b	Allowed primary energy consumption kWh
e	Electricity generation per hour kWh/h
C	Total costs €
c	Specific costs €/kW and €/m^3
f	Specific fuel consumption m^3/kW
g(x)	Inequality constraint
h(x)	Equality constraint
l	Heat loss rate kWh/h
P	Capacity of each technology kW
p(x)	Objective function
q	Heat generation per hour kWh/h
s.t.	Subject to
t	Number of hours h
UHV	Upper heating value
y	Binary variable representing selection ($y = 1$) or neglection ($y = 0$) of a technology

Greek Letters

ε	Specific primary energy consumption kWh/kW
γ	Primary energy factor
η	Efficiency

Subscripts

avail	Availability
dec	Decommissioning
el	Electrical
fuel	Fuel type
inst	Installed capacity kW
inv	Investment costs €
l	Number of equality constraints
lsr	Load service rating factor
m	Number of inequality constraints
maint	Maintenance
NPC	Net present costs €
OM	Operational and maintenance
t	Time index
th	Thermal

Superscripts

BG	Biogas
CHP	Combined heat and power unit
GB	Gas boiler
grid	Public grid
HS	Heat exchanger
N	Number of total years of operation
n	Number of considered technologies
net	Net amount
NG	Natural gas
System	Total supply system
Tj	Relevant technology j

References

1. Pachauri RK et al (2007) Climate change 2007: synthesis report. Contribution of working groups I, II and III to the fourth assessment report of the intergovernmental panel on climate change, IPCC, Cambridge, UK and Cambridge University Press, New York, USA
2. Pérez-Lombard L, Ortiz J, Pout C (2008) A review on buildings energy consumption information. Energ Build 3:394–398

3. Edenhofer O et al (2011) The IPCC special report on renewable energy sources and climate change mitigation. Cambridge University Press, Cambridge, UK
4. Voss K, Musall E (2012) Net zero energy buildings: international comparison of carbon-neutral lifestyles. Birkhäuser Architektur, Basel
5. European Commission (2010) Directive 2010/31/EU of the European Parliament and of the Council of 19 May 2010 on the energy performance of buildings (recast). Official J Eur Union L153:13–35
6. Peippo K, Lund PD, Vartiainen E (1999) Multivariate optimization of design trade-offs for solar low energy buildings. Energ Build 2:189–205
7. Charron R, Athienitis A, Beausoleil-Morrison I (2005) Tools for the design of zero energy solar homes. 30th annual conference of the solar energy society of Canada, Vancouver
8. Wang W, Zmeureanu R, Rivard H (2005) Applying multi-objective genetic algorithms in green building design optimization. Build Environ 11:1512–1525
9. Connolly D et al (2010) A review of computer tools for analysing the integration of renewable energy into various energy systems. Appl Energ 4:1059–1082
10. Ooka R, Komamura K (2009) Optimal design method for building energy systems using genetic algorithms. Build Environ 7:1538–1544
11. Milan C, Bojesen C, Nielsen MP (2012) A cost optimization model for 100 % renewable residential energy supply systems. Energy 48(1):118–127
12. Kaltschmitt M, Streicher W, Wiese A (2007) Renewable energy: technology, economics, and environment. Springer, Berlin
13. U.S. Department of Energy (2012) http://apps1.eere.energy.gov/buildings/energyplus/. Accessed 4 July 2011
14. Marszal AJ et al (2011) Zero energy building – a review of definitions and calculation methodologies. Energ Build 4:971–979
15. Strategic Research Centre on Zero Emission Buildings (2012) http://www.en.zeb.aau.dk. Accessed 5 July 2012. (in Danish)
16. Bauer H, Bressler G, Günther-Pomhoff C (1996) Ganzheitliche Bilanzierung von elektrisch angetriebenen Wärmepumpen als Basis einer Ökobilanz. Final report. Forschungsstelle für Energiewirtschaft, Munich, (in German)
17. Ardente F et al (2005) Life cycle assessment of a solar thermal collector: sensitivity analysis, energy and environmental balances. Renew Energ 2:109–130
18. Haas R et al (2010) Mikro-KWK – Langfristige Szenarien der gesamtwirtschaftlich optimalen Integration von Mikro-KWK Anlagen in das österreichische Energiesystem. Final report. Institut für Elektrische Anlagen und Energiewirtschaft, TU Wien, (in German)
19. Antvorskov S, Knölke B (2001) Analyse af ydelses-og økonomiforhold for opsætning af solvarmeanlæg ved boligforeningen Herlevhuse. Technical Report SR-01-11. Danish Technical University, Copenhagen, (in Danish)
20. Gaia Solar, Data sheets (2011) http://www.altomsolceller.dk/. Accessed 15 May 2011 (in Danish)
21. VELUX (2011) http://www.velux.dk. Accessed 23 July 2011 (in Danish)
22. Byggecentrum (2011) http://www.byggecentrum.dk/produktadgang/vs-prisdata-startside/. Accessed 14 May 2011 (in Danish)
23. de Wit J (2006) Mini- og mikrokraftvarme: teknologi, potentiale og barrierer. Dansk Gasteknisk Center, Hørsholm
24. U.S. Environmental Protection Agency, Catalog of CHP Technologies (2008) http://www.epa.gov. Accessed 23 June 2012
25. Pistohl W (2009) Handbuch der Gebäudetechnik 2: Heizung/Lüftung/Beleuchtung/Energiesparen 7. neu bearbeitete und erweiterte. Werner, Neuwied, in German
26. GAMS Development Corporation (2010) http://www.gams.com. Accessed 5 May 2011

27. Danish Energy Agency, Forudsætninger for samfundsøkonomiske analyser på energiområdet (2011) http://www.ens.dk/. Accessed 5 July 2012 (in Danish)
28. Danish Energy Agency, Udviklingen i de fremtidige energipriser, herunder sikkerhed i tallene (2012) http://www.ens.dk/. Accessed 5 July 2012 (in Danish)
29. PlanEnergi (2009) Optimal udnyttelse af biogas i Lemvig. Mainreport. http://www.lemvigbiogas.com. Accessed 5 July 2012 (in Danish)

Chapter 17
State of the Art Review: Fuel Cell Technologies in the Domestic Built Environment

Theo Elmer and Saffa B. Riffat

Abstract The paper provides a state-of-the-art review of fuel cells operating in the domestic built environment. Fuel cells produce heat when generating electricity, thus they are of particular interest for combined heat and power (CHP) applications. As this paper's focus is the domestic built environment, only micro-CHP applications are considered.

The review commences with an examination of micro-CHP in the built environment and then appraises domestic fuel cell technology. It concludes with an assessment of the present development of, and future challenges for, domestic fuel cells; specifically the operational advantages they offer compared to conventional micro-CHP technologies. As fuel cells are an emergent technology the paper draws on a breadth of literature, data and experience, mostly from the UK, Japan, USA and Australia.

Keywords Fuel cells • Domestic buildings • Combined heat and power • Review

17.1 Introduction

It is now of global importance that greenhouse gas (GHG) emissions associated with energy production are substantially reduced in order to limit the effects of climate change. Agreements such as the 1997 Kyoto Protocol have been established in order to try and mitigate the effects of climate change by reducing the quantities of GHGs released into the atmosphere. More recently the UK set out in its 2007 Energy White Paper it would commit to an 80 % GHG emission reduction compared to 1990 levels by 2050 [1]. The UK's 2050 target is ambitious; however there is now a common trend amongst many countries towards aspirations of a low carbon future. In the 4th Inter-governmental Panel on Climate Change Assessment the built environment was identified as holding the largest economic potential for

T. Elmer (✉) • S.B. Riffat
Institute of Sustainable Energy Technology, School of Architecture and Built Environment, University of Nottingham, Nottingham NG7 2RD, UK
e-mail: laxte1@nottingham.ac.uk; saffa.riffat@nottingham.ac.uk

I. Dincer et al. (eds.), *Progress in Sustainable Energy Technologies Vol II: Creating Sustainable Development*, DOI 10.1007/978-3-319-07977-6_17

the reduction of CO_2 emissions [2]. Currently in the UK, over 30 % of CO_2 emissions are associated with the domestic housing sector. This illustrates the critical importance of decarbonising the domestic built environment if substantial CO_2 emission reductions are to be realised. Fuel cells have been identified as one of the promising technological options on the route to a zero carbon built environment [2].

Fuel cells are electrochemical devices which convert hydrogen and oxygen into water and in the process produce electricity. Invented in 1839, fuel cell technology is by no means new. However, in the past, fuel cells have struggled to flourish particularly in terms of commercialisation and market application. This stalled start has occurred for a variety of reasons; technological reliability, lack of interest, lack of infrastructure but mainly cost [3]. On the other hand, fuel cells have been used in bespoke projects. NASA used fuel cells in some of their early space shuttles to provide electrical power, heat and water. In more recent years fuel cells have started receiving much more attention with their use in the current major market application of automobiles, with cars such as the Honda FCX Clarity [4].

As a result of growing concerns of climate change, ever increasing cost and scarcity of fuel resources fuel cells have been identified as a key technological option for improving both building energy efficiency and reducing emissions [5]. Fuel cells are an attractive option for building applications because of their; high electrical efficiency (even at part load), low emissions, near silent operation, flexibility of fuel use and useful heat output. Owing to the variety of fuel cells on the market and their modularity, fuel cells have the ability to cover a range of building applications from single family homes to an entire hospital [5]. Ceramic Fuel Cells Ltd (CFCL) reported that the residential Solid oxide fuel cell (SOFC) market is around 17,000 kWe installed per annum, a large market potential. E.ON believes most UK homes are technically suitable for fuel cell micro-CHP, equal to a potential total installed capacity of 24 GWe [6]. In micro-CHP applications the heat output of the fuel cell can be used for the heating of water for domestic hot water (DHW) or space heating. Similarly combined cooling heat and power (CCHP) applications most commonly utilise the heat output in a heat driven cooling cycle such as vapour absorption, adsorption or desiccant [4]. Fuel cells are also of special interest in the built environment on account of their promise as a decentralised generator (DG). Fuel cells can provide both heat and power from a single fuel source at the end-point of use [4]. DG applications are of increasing interest because of; reduced electrical transmission losses, protection against attacks or damages to centralised plants, increased energy security and the option to utilise the commonly wasted heat from the power production process, therefore increasing overall efficiencies.

Fuel cells have been trialled at a variety of scales in CHP and CCHP configurations [2, 7–10]. However fuel cells in such applications are still not considered a mature technology with many technical, performance and operational uncertainties requiring further investigation [5]. However, EneFarm field trials of 1 kWe Proton exchange membrane fuel cells (PEMFC) in Japanese households has illustrated annual CO_2 emission reductions of 750–1,250 kg per annum, demonstrating the

potential fuel cells have in assisting decarbonisation of the domestic built environment [11]. It has been estimated that if 5.6 million homes were to install micro-CHP fuel cell technology the emission savings would be equivalent to the emissions of eight 750 MW combined cycle gas turbine (CCGT) power stations [12].

17.2 Micro-CHP in the Built Environment

CHP is defined as the generation of heat and power from a single fuel source, with the view to using both products. CHP system applications can range in size from large multi MW centralised power applications to a single kW domestic home. Domestic micro-CHP is defined by the Carbon Trust as any system size up to 3 kWe. Hawkes et al. [2] define micro-CHP as any system between $\leq$3 kWe and $\leq$20 kWth. It is suitable to define both the thermal and power output because if the thermal output of the CHP system is greater than the demands of the building it will severely limit the operating period of the CHP system, resulting in lower efficiencies, greater emissions and longer pay back periods. As Beaussoleil-Morrison [13] states, if the thermal output of the CHP device cannot be fully utilised, then the CHP system cannot expect to deliver a net benefit relative to grid electricity and a highly efficient condensing boiler. Therefore accurate energy load assessments and sizing of the CHP unit is essential.

17.2.1 Merits of Micro-CHP

The use of micro-CHP operating as a DG in the domestic built environment has many advantages associated with it compared to traditional centralised energy generation. These include:

- Improved system efficiency, otherwise wasted heat is utilised (heating or cooling), therefore system efficiency can be elevated from as low as 30–50 % in central power stations to around 70–85 % in micro-CHP. Figure 17.1 illustrates the energy savings possible when switching from centralised energy generation to decentralised micro-CHP.
- Decentralised micro-CHP eliminates transmission losses which account for 6–24 % in the European Union (EU) transmission network [14].
- Improved system efficiency and greater fuel utilisation leads to reduced operating costs and CO_2 emissions.
- Electricity is regarded as having an economic value of roughly three times that of gas. Therefore converting lower cost gas to electricity allows households to recover cost and reduce energy bills. This is an important factor in the fight against fuel poverty [15].

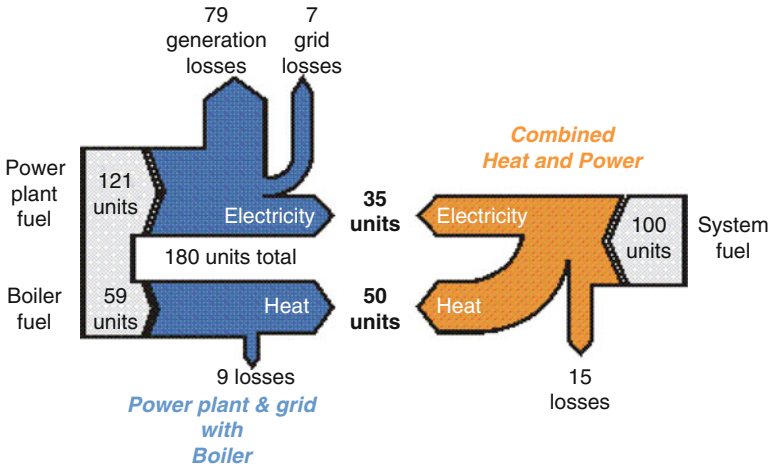

Fig. 17.1 Sankey diagram comparing CHP system efficiency and conventional energy generation [16]

- Centralised decarbonisation of electricity generation in many countries is problematic on account of opposition to both renewables and nuclear. Micro-CHP in consumers' homes offers an option to assist in both decarbonising electricity production and providing energy saving benefits directly to the home owner [15].

17.2.2 Micro-CHP Technologies

Currently there are three main technologies used as micro-CHP prime movers in the domestic built environment, all at varying levels of commercial and technological maturity; Internal combustion engine (ICE), Stirling engine (SE) and fuel cells. The performance and operational characteristics of these three technologies are summarised in Table 17.1. It is evident that fuel cells have some clear operational advantages, particularly when operating in the built environment. These include; higher electrical efficiencies, low heat to power ratios (H:P) and near silent operation. However, the relative infancy of fuel cells limits their extensive application and market involvement.

The H:P of a CHP unit is the quantity of heat energy produced per unit of electricity generated and is an important system characteristic. Conventional CHP systems are sized to thermal loads and are only operational when the demand for energy is both electrical and thermal i.e. it will only run when there is demand for the heat produced when generating electricity. Therefore a CHP system with a high H:P means the unit is severely limited in its operational period. When there is low or no heat demand, electricity is imported from the grid. Otherwise, producing

Table 17.1 Domestic micro-CHP technologies [2, 4, 15]

Parameter	Internal combustion engine	Stirling engine	Fuel cell
Electrical capacity	1 kW+	1 kW+	1 kW+
Electrical efficiency	20 %	10 %	35–60 %
Overall efficiency	85 %	90 %	85 %
Heat to power ratio	3:1	10:1	1:1
Able to vary output	No	No	Yes
Fuel used	Gas, biogas, liquid fuels	Gas, biogas, butane	Hydrocarbon fuel
Noise	Loud	Fair	Quiet
Maturity	High	Fair	Low
Companies producing	Baxi	Whispergen	Baxi, Bluegen (CFCL)

electricity when there is no thermal demand means heat has to be dumped, this severely reduces system efficiency and increases cost. In such a scenario centralised electricity is likely to be more viable both in terms of cost and CO_2 emission savings.

Table 17.1 shows that fuel cells have high electrical efficiencies, even at part loads which is a particular advantage for domestic applications because of time varying electrical demands [5]. High electrical efficiency also means fuel cells have a low H:P if appropriately designed. A low H:P means a fuel cell micro-CHP system can operate for a greater period of time per year. Even in the summer when the central heating is off, the fuel cell can produce electricity and the heat output is such that it can be stored in a hot water cylinder and used for DHW applications. No dumping of excess heat is required. As a result, a fuel cell system has a greater potential in reducing CO_2 emissions because they increase access and thus the benefits associated with generating electricity on site (normally met by the grid). Consequently the CO_2 emission and cost reductions achievable with a fuel cell system are such that it may make micro-CHP viable in a greater proportion of households compared to technologies with higher H:P such as SEs or ICEs. The Carbon Trust predicts annual CO_2 emission reductions are marginal through the use of conventional micro-CHP technologies (SE, ICE) and only attainable in the domestic sector in large homes with high heat demands. This is because these technologies have high H:P. However, newer more efficient builds, whose heat to power demands are beginning to align around 1:1 could now become suitable candidates for micro-CHP with the use of fuel cell technology with its low H:P output.

The micro-CHP technologies summarised in Table 17.1 show differing electrical efficiencies, but similar total system efficiencies. For the same total system efficiency, each kWh of electricity produced represents the opportunity cost of not producing 1 kWh of heat, but is worth the avoided cost of buying 1 kWh of electricity from the grid. On average 1 kWh of micro-CHP electricity costs 3.5p but is worth 12p. 1 kWh micro CHP electricity costs 0.22 kg CO_2 but is worth

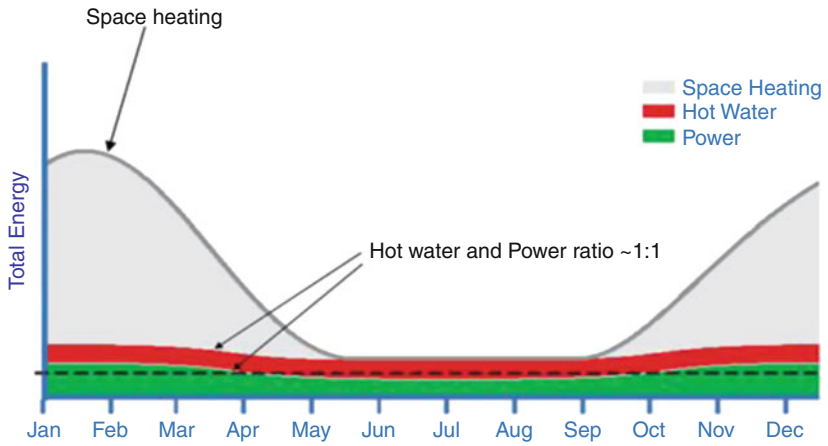

Fig. 17.2 Annual energy load profile [17]

0.568 kg CO_2 [6]. This illustrates the basic rationale for micro-CHP in the domestic built environment, additionally it demonstrates how best to operate the system i.e. micro-CHP generates economic value and it is always more cost effective to produce electricity at the opportunity cost of heat. The above also demonstrates the even greater benefit fuel cells can bring to micro-CHP economics. Because fuel cells are usually operated in electrical led mode they can create more value than conventional heat led technologies such as a SE. Additionally, fuel cells with their higher electrical efficiencies generate more value due to higher electrical production per unit input of fuel. Furthermore it is often stated that a disadvantage of SOFCs is their inability to effectively modulate electrical output, however when grid connected, it is of greatest benefit to the consumer to operate at maximum electrical output to produce greatest benefit.

Figure 17.2 shows a typical European home's annual energy load profile. It indicates a high space heating load in winter and a low load in summer. However, the DHW to electrical power demand aligns at around 1:1 throughout the year. A fuel cell with a H:P of around 1:1 is therefore well suited to such an application. The fuel cell can run continuously throughout the year and thermal constraints would not interfere in its operation therefore accessing the benefits associated with generating electricity on site. In this scenario, the fuel cell would be installed in addition to a boiler which would supply the space heating load. A SE micro-CHP unit with a H:P of up to 10:1 would, depending on the operating schedule, have to be shut off from April to October—reducing the systems potential benefit. Otherwise dumping of excess heat would be required which is not a viable option for both environmental and economic reasons.

Good quality CHP refers to CHP generation that is energy efficient in operation, meeting the standards set in the EU CHP Cogeneration directive. Three main parameters constitute good quality CHP; maximum utilisation of heat i.e. no

dumping, high overall system efficiency (greater than 85 %) and a low H:P (less than 1.5). Conventional micro-CHP technologies such as ICE and SE struggle to meet all of the parameters set. For example SEs have H:P far larger than 1.5 and as a result in the summer heat will most likely be dumped. Fuel cells however have high system efficiencies and low H:P, therefore even in the summer months heat does not need to be dumped. Additionally, as a result of a low thermal output, heat utilisation of a fuel cell system will be high. Further demonstrating the great potential and additional benefits fuel cells are able to deliver when operating in the domestic built environment as micro-CHP systems.

This section has served to provide an overview of current and future micro-CHP technologies operating in the domestic built environment. Limitations of current technologies have been highlighted and the operational advantages of fuel cell technology have been presented.

17.3 Fuel Cell Technology

Fuel cells are electrochemical devices operating on the principle of electrolytic charge exchange between two oppositely charged electrodes, similar to a battery. However, unlike a battery the fuel and oxidant are not integral parts. Fuel cells combine a fuel (hydrogen) and oxidant (oxygen) to produce water, electricity and heat. The fuel and oxidant are supplied as needed to provide the required power, whilst waste products are continuously removed.

Because fuel cells are electrochemical devices they are not governed by the thermodynamic laws of a heat engine, thus they can achieve much higher operational electrical efficiencies (i.e. greater than Carnot) compared to traditional centralised and decentralised electrical generation devices such as gas turbines or ICE [3]. Figure 17.3 shows a single fuel cell. A single cell is composed of a negatively charged anode where fuel is supplied and oxidation takes place, an electrolyte which conducts ions but not electrons, and a positively charged cathode where the oxidant is supplied and reduction takes place. An external circuit connects the anode to the cathode to allow electron flow (current). Cells are connected together in series to form stacks.

A single cell will generally produce around 0.75 V at 2 Amps, thus generating around 1.5 W of DC power [19]. Cells are connected in series to form stacks. Stacks are then connected in parallel to complete the fuel cell module. Cell/stack configuration is dependent on the voltage and current characteristics required of the fuel cell application. Hydrogen is the preferred fuel as it produces higher electrochemical performance and reduced cell degradation. Hydrogen fed in at the anode is stripped of its electrons, creating ions. The ions then pass through a conductive electrolyte to combine with oxygen at the cathode. Because a cell potential is generated, the free electrons create a current in the external circuit as they cannot

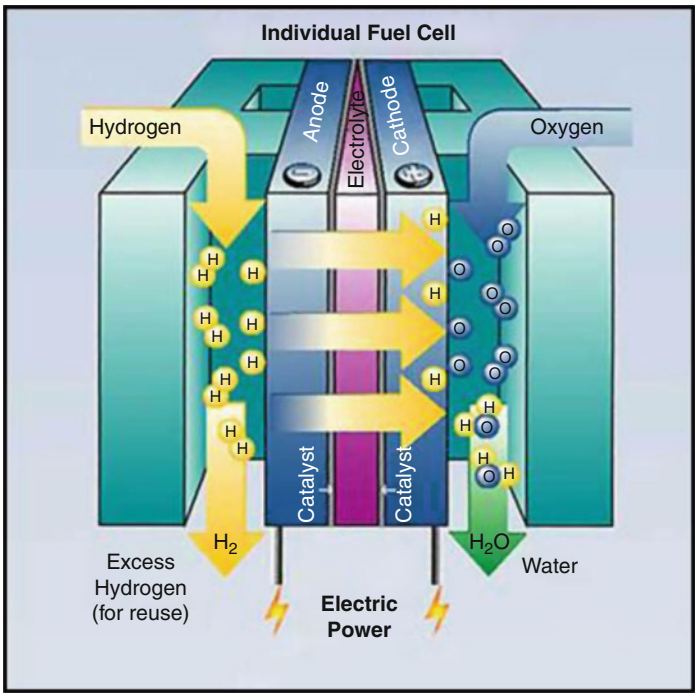

Fig. 17.3 Fuel cell basic concept [18]

pass through the electrolyte. Specific reactions are highly dependent upon the type of fuel cell, however the overall reaction is [20]:

$$H_2 + ½\ O_2 \rightarrow H_2O$$

Fuel cells are often categorised by the type of electrolyte. This is determined by the type and purity of the fuel, oxidant used and the operating temperature. There are currently six main types of well-developed fuel cell on the market [21]:

- Proton Exchange Membrane Fuel Cell (PEMFC).
- Alkaline Fuel Cell (AFC).
- Direct Methanol Fuel Cell (DMFC).
- Phosphoric Acid Fuel Cell (PAFC).
- Molten Carbonate Fuel Cell (MCFC).
- Solid Oxide Fuel Cell (SOFC).

The first three fuel cells are classified as low temperature fuel cells (80–250 °C), whilst the remaining three are medium to high temperature (250–1,000 °C). The operating temperature is often a significant factor when determining which type of fuel cell should be used in a particular application. This is due to a number of factors including; heat usability, start-up time and ability to vary output. Of the six fuel cell

Table 17.2 Summary of PEMFC and SOFC characteristics [2–4, 23]

Parameter	PEMFC	SOFC
Operating temperature	30–100 (°C)	500–1,000 (°C)
Electrical efficiency	35–45 %	45–60 %
Electrolyte	Solid polymeric membrane	Solid, stabilised zirconia ceramic matrix with free oxide ions
Charge carrier	H^+ ions	$O^=$ ions
Construction	Plastic, metal or carbon	Ceramic, high temperature metals
Fuels	Hydrocarbons or methanol	Natural gas or propane
Contaminants	CO, sulphur, NH_3	Sulphur
Cell configurations	Flat plate	Tubular, flat plate, planar
Applications	Automotive, stationery	Stationery
Companies	Baxi	CFCL, Ceres
Advantages	Quick start up time, can vary output quickly, compact, no corrosive fluid used	High temperature enables internal reforming, no liquid electrolyte used, useful high temperature heat output can be used in another cycle
Disadvantages	Expensive platinum catalysts required, high purity H_2 required	Long start up time, expensive heat resistant materials needed

variants listed above, the low temperature PEMFC and the high temperature SOFC demonstrate the greatest promise for early market application, generally attracting the most attention and investment in building application projects [3, 5, 22]. The discussions in this paper pertaining to building integrated fuel cells will focus on these two variants. Currently it is estimated SOFC developments are 5 years behind PEMFC. PEMFC and SOFC characteristics are summarised in Table 17.2.

Recent advances in low temperature SOFC technology using ceria-carbonate two or multi-phase nanocomposite has illustrated that high electrochemical performance (1.2 W/cm^2) can still be achieved at reduced temperatures (500 °C). This is a clear advantage for the domestic sector where high temperature operation results in technical complexity and consequently cost that inhibits commercialisation. Furthermore these developments mean SOFC stacks can be manufactured for prices below 400 €/kWe compared to 1,000 €/kWe for conventional SOFC systems [24].

17.3.1 Fuel Cell Systems

A fuel cell in principle is very simple, requiring few parts (even less moving) resulting in near silent operation and little maintenance required. In order to operate a fuel cell system i.e. a load supplied by a fuel cell, many auxiliary devices and

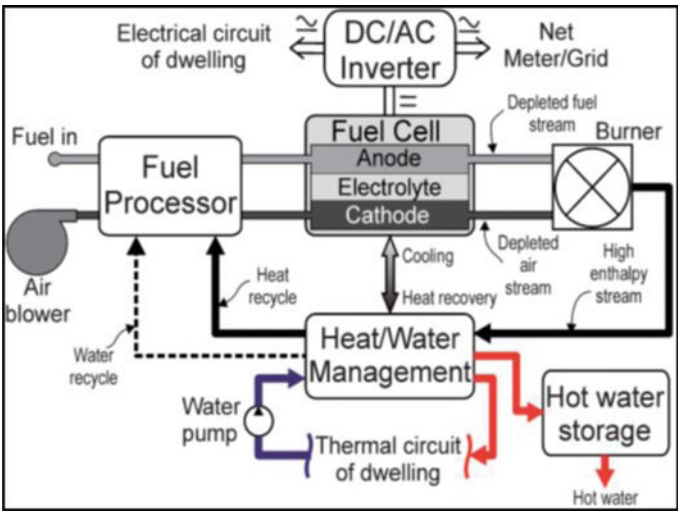

Fig. 17.4 Fuel cell micro-CHP system [2]

interconnects are needed for both the correct operation of the fuel cell and the delivery of heat and power to the load. Some of these auxiliary devices have a power demand, thus they are a parasitic load on the system. The electrical efficiency of the system can be between a fifth and third less than the quoted stack efficiency due to the parasitic loads. Auxiliary equipment also contributes to increased noise, vibrations and maintenance. However, without auxiliary equipment the fuel cell could not operate. A fuel cell micro-CHP system can expect to produce 0–55 dB, whereas an ICE is around 95 dB [2]. Figure 17.4 shows a schematic of a fuel cell micro-CHP system, with the main auxiliary equipment. When operating as a CCHP system the fuel cell auxiliary equipment will remain the same as the heat output is simply used in a heat driven cooling cycle.

The following list provides a brief explanation of the fuel cell system components in Fig. 17.4. Of course some of these components will differ from system to system and type of fuel cell used. It needs to be noted that the system description below is limited to the fuel cell requirements. For the fuel cell system to operate within a home as a micro-CHP system it is assumed an existing AC electrical ring main plus grid connection is present as well as a hot water system with boiler, storage and heat emitters.

17.3.2 Fuel Cell System Description

The components of a complete fuel cell system are described below.

1. *Fuel cell stack*. The stack is where electrical power is produced. Individual cells (anode, electrolyte and cathode) are electrically connected together using bipolar plates to form a stack. Bipolar plates not only provide the electrical connection but simultaneously supply fuel and oxidant to the cells and removes waste products [19].
2. *Fuel reformer*. Due to the lack of availability of pure hydrogen and supporting infrastructure, hydrocarbon fuels such as natural gas are most commonly used in the first generation of fuel cell micro-CHP systems. This is a result of natural gas' availability, well developed transport infrastructure (direct to homes) and current low cost. When using a hydrocarbon fuel stock, fuel reforming is one of the largest differences between the PEMFC and SOFC systems. Reforming is required to convert the fuel into hydrogen with a very low level of contaminants. PEMFCs require a very pure supply of hydrogen therefore a PEMFC's fuel reformer is a large and complicated system. Natural gas is most commonly converted to hydrogen in two stages: stage one; steam reforming owing to its ability to produce much higher concentrations of hydrogen. Stage two; a water-gas shift reaction converts any CO in the fuel stream in to hydrogen and CO_2. As a result of SOFC's much higher operating temperatures they are able to internally reform the hydrocarbon fuel, thus reducing the size and cost of the reformer; a clear advantage compared to PEMFCs. A SOFC's fuel processor consists of a de-sulphuriser and can include a pre-reformer. Both PEMFCs and SOFCs are highly sensitive to sulphur poisoning therefore this needs to be removed in the reforming stage.
3. *Inverter and power electronics*. This is used to convert the DC electrical output of the fuel cell stack into AC power. AC electrical power can then in turn serve the buildings energy loads or be fed back into the grid. For a 1 kWe domestic fuel cell, the inverter efficiency will be around 85–95 %.
4. *Water management*. This is required for two processes; one, high purity water is needed for the steam reforming process. Two, water is required for the hydration of the electrolyte in the PEMFC to ensure effective ion conduction.
5. *Heat Management*. Heat recovery from the fuel cell is essential in order to improve: (a) the system efficiency and (b) the environmental performance i.e. make it a CHP unit. Heat recovery differs slightly between PEMFC and SOFC systems. In a PEMFC system, heat recovery is achieved through the circulating cooling liquid that passes through the cooling plates of the PEMFC. The cooling liquid leaves the stack at around 80 °C, a suitable temperature for DHW or space heating. In a SOFC the heat recovery is more complex and is obtained using the cathode air flow. Excess air and unconsumed fuel leaving the stack are combusted in an afterburner, producing heat which serves the pre-reformer and pre-heats the input reactant streams. Excess heat from this is then available for DHW or space heating applications. In a PEMFC system an afterburner can also be employed to create a higher heat output.
6. *Reactant delivery system*. Domestic micro-CHP systems are not pressurised. Therefore, a blower is required to supply air, which is the main parasitic load on the system. The mains gas pressure is sufficient to operate the fuel cell.

7. *Afterburner*. Used to burn unreacted fuel. This is one way to alter the H:P ratio of the system depending on the load requirement, allowing the fuel cell system to operate for extended periods. In extreme scenarios the fuel cell stack could be by-passed, thus operating in boiler only mode.
8. *Control system*. Ensures the whole system functions in a safe, efficient manner for long term operation. The system can be designed to different levels of sophistication, either; fixed output or varying output responding to demands of the system.

This section has provided an introduction to the fundamentals of fuel cell technology, presenting and discussing the roles of the components required in a fuel cell micro-CHP system.

17.4 Fuel Cell Systems in the Domestic Built Environment

This section will provide an overview of fuel cell systems operating in the domestic built environment. Maintenance, durability, cost, CO_2 emission reductions and commercially available fuel cell products will be discussed. It is envisaged that the first generation of fuel cells for the domestic built environment will run on hydrocarbon fuels such as natural gas (methane) or propane. Following this, the second generation of fuel cells will run on pure hydrogen [3]. There are two reasons for the first and second generation stages of fuel use. One, the infrastructure to store, transport and deliver natural gas to individual homes is already present in both the UK and most developed countries. Two, currently the production of hydrogen is very expensive and, depending on the production method, can produce more emissions than that offset by the use of pure hydrogen. Braun, Klein et al. [25] ran a SOFC micro-CHP in a residential application under five different system configurations. When the system was fuelled with hydrogen it did not offer any efficiency advantages over methane. The transition from the first generation (hydrocarbon fuels) of fuel cells to the second generation (hydrogen) will offer benefits in terms of CO_2 emission reductions and the ability to use a variety of different types of fuel cell without onsite reformation.

17.4.1 Maintenance

As a result of the lack of moving parts in a fuel cell, regular maintenance work to the fuel cell module itself is hoped to be less in comparison to conventional micro-CHP technologies such as with an ICE or SE. However due to the size and complexity of the auxiliary equipment in a fuel cell system, this is the source of the majority of maintenance work. For systems using hydrocarbon fuels, the fuel processor will need to be changed periodically [2]. CFCL predict the SOFC stack in

their BlueGEN unit will need to be changed once every 5 years and the water/air filters annually [26].

17.4.2 Durability

Lifetime, reliability and durability of fuel cells are currently one of their largest limiting factors. Fuel cells need to meet both lifetime and stop-start operating targets in order for them to become viable as micro-CHP generators in the domestic built environment. These targets are critical if fuel cells are to compete with both current centralised generation and DG technologies. It is estimated that both PEMFC and SOFC stacks lose power at a rate of 0–5 % per 1,000 operating hours [2]. Currently the industry holds a target of 40,000 h for stationery applications. This gives around 10 years of operation if the unit is operated at regular intervals instead of continuously, which is a more likely scenario for the lower temperature PEMFC. CFCL with their SOFC BlueGEN unit envisage operation will be continuous due to long start up and shutdown times of SOFC systems, they have a target lifetime of 15 years, although this includes stack replacement every 5 years [26]. Laboratory tests of both PEMFC and SOFCs have shown the 40,000 h target is possible, nonetheless limited data is available regarding actual field data, and even more so for domestic micro-CHP systems.

In 2008 as part of the Ene-Farm Project, Panasonic's home use PEMFC demonstrated durability of 40,000 h with 4,000 start-stop cycles [27]. The latest Panasonic model, launched in April 2011 now has a quoted system lifetime of 50,000 h [28], showing great promise for the stationary market. SOFC systems have not been tested on such a large scale as PEMFCs. Limited data beyond 10,000 operational hours has been reported in the literature reviewed. The development of fuel cell technology has now matured to a point where stack technology is at a level commensurate with operational targets. It is the other relatively untried components of the fuel cell micro-CHP system that are causing reliability issues and require developmental work. However with the introduction of more fuel cell micro-CHP units to the market and increased volume of both field tests and commercial applications, it is hoped these teething problems will soon be dealt with.

17.4.3 Cost

Currently there is a lack of standard industry prices for micro-CHP fuel cell systems. However, they can be expected to be higher than those of conventional CHP systems because of fuel cells comparable immaturity. As time progresses and the volume of units produced increases, it is hoped the price of these systems will decrease. For demonstration projects, a quoted price in 2009 ranged from £10,000 to £100,000 for a 1 kWe demonstration unit [2]. Panasonic's EneFarm branded

micro-CHP 1 kWe PEMFC had a retail price of £26,500 in 2009, then in 2011 with the launch of the new model the price decreased to £21,000 [28]. It is predicted by 2015 the price of this unit will decrease further, by 2015 Panasonic believe they can offer the unit at a price of £3,500 to energy companies [29]. Again, data regarding SOFC system cost is limited in comparison to PEMFCs. This is due to the SOFC technologies less substantial commercial development. CFCL are currently charging £19,950 for their SOFC BlueGEN unit, however once in mass production the forecasted cost is around £5,000 [26]. Many commercial developers believe the future of cheaper fuel cell technology lies with SOFC systems. This is because they do not need to use expensive platinum catalysts like PEMFCs [29].

17.4.4 CO_2 Savings Achievable with Fuel Cell Micro-CHP

The likely contribution domestic fuel cell micro-CHP systems will provide regarding CO_2 emissions reduction will now be explored. Gas fed micro-CHP poses a potential challenge in terms of a transition to a low carbon economy [6]. However, it is an essential component in optimising the resource present today and ensuring the arrival at a zero carbon economy. As discussed in Section One, there is currently a limited bank of available data regarding the benefits of fuel cell technologies in the built environment; this is a result of the still premature level of implementation of such technology.

The *Annex 42* project [13] has carried out extensive performance assessment studies of both SOFC and PEMFC technologies operating as micro-CHP units in single (SFH) and multi-family homes (MFH), comparing them to a reference system. Beaussoleil-Morrison [13] states that results from the *Annex 42* assessment demonstrate that individual buildings employing co-generation fuel cell technology could reduce non-renewable primary energy (NRPE) demand compared to a conventional gas boiler system and grid electricity. However reductions are highly dependent upon the grid electricity generation mix i.e. the kg/CO_2/kWh. Key findings from the study showed that when the reference system utilised centralised electricity generation from a CCGT and an individual home heat pump, the electrical efficiency of the micro-CHP fuel cell unit had to be greater than 40 % (operational) in order for it to be competitive both on a cost and CO_2 emission level basis. In order to obtain maximum system efficiency and CO_2 emission reduction at least 80–90 % of the homes annual heat demand needs to be met by the fuel cell. Furthermore, the way in which the micro-CHP fuel cell unit was operated had a large impact on the benefits gained. When in heat led mode, the system showed the best energy efficiency. However, when in electrical led mode, it created the greatest cost savings. In general, base load sizing offered better energy savings than peak load sizing.

Field trials of PEMFC micro-CHP units in Japanese homes indicate a reduction of around 12GJ NRPE demand per annum are achievable when switching from grid electricity and gas heating to a fuel cell micro-CHP system. Simulations by

Hawkes et al. [2] based upon the UK illustrate fuel cell micro-CHP has the potential to reduce CO_2 emissions by 1.5 tonnes per annum for a high demand home, a figure which is consistent with previous simulations that predict around 1 tonne per annum are achievable for an average sized family home [30].

E.ON estimate that the BlueGEN system can achieve CO_2 emission reductions of 4.5 tonnes/house/year [6]. Ceres Power, a manufacturer of an intermediate temperature wall mountable 1 kWe SOFC, anticipate savings of up to 2.5 tonnes of CO_2 per year and £250 in energy bills are attainable for a UK residence when switching from grid electricity and gas boiler to their fuel cell unit [17]. Clearly the estimates made by these two firms are much larger than the other literature presented, and may be based upon a specific case. There is a danger of manufactures overselling the benefits of micro-CHP fuel cell systems. This needs to be curtailed until a sufficient bank of real operational data can be acquired in order to accurately verify the possible benefits.

From the literature presented in this section it is clear that there is no definitive set of figures concerning the CO_2 emission reductions achievable from fuel cell micro-CHP technology operating in the built environment. However, what is apparent is that fuel cell micro-CHP devices are currently providing CO_2 emission reductions. The extent of these reductions is highly dependent upon a large range of factors including; central electricity mix, homes annual demand and efficiency of the system. Furthermore, it is expected the CO_2 savings in the future will only improve, with the introduction of renewable biogas or hydrogen. In this case micro-CHP fuel cells could potentially reach 100 % CO_2 emission reductions.

17.4.5 Additional Benefits of Fuel Cell Micro-CHP Operating in the Domestic Built Environment

The introduction of fuel cell micro-CHP to the domestic built environment will not only deliver benefits such as reductions in CO_2 emissions and operating cost, but, many other valuable contributions. Two of which are discussed below. Firstly, if it can be justified investing in micro-CHP in its own right (i.e. the benefits are such that external support is not necessary), then any additional benefits gained from operating micro-CHP in the domestic built environment have no marginal cost. The additional benefits of micro-CHP include; avoided centralised generation and transmission network capacity deployment. This is a clear advantage to a countries energy system. E.ON state that the fuel cell micro-CHP generator BlueGEN will provide a value of around £300 a year to the network through peak shaving in high demand periods, reduced centralised generation capacity and transmission network capabilities. However, there will need to be some form of regulatory and infra-structure change to the energy system in order to permit the management of these additional advantages, allowing the benefits to be shared with the consumer [6].

Secondly, today in the UK the majority of heat is produced from the burning of fossil fuels. In the document *The Future of Heating: A strategic framework for low carbon heat in the UK* [31], the UK government sets out its aspirations to begin the decarbonisation of the heating sector. In this document electrical heat pumps are strongly favoured for individual building scale heat decarbonisation. If all 25 million UK homes switched to using heat pumps, electrical demand would increase enormously, and in response to this there would need to be an increase in centralised electrical generation and transmission capabilities. If UK electrical generation is not at a stage commensurate with low carbon electrical generation i.e. renewable, the carbon emissions associated with the heating sector could actually increase [6]. The UK should therefore resist increasing centralised electrical generation capacity to decarbonise its heating sector and look to alternatives such as DG. Fuel cell micro-CHP has the potential to mitigate the effects that heat pumps will have on the electrical generation network by producing low carbon onsite heat and power, reducing the required central network capacity.

17.4.6 Commercially Available Domestic Fuel Cell Micro-CHP Units

In terms of commercialisation, fuel cell micro-CHP in the domestic built environment is still in its infancy. Currently it is estimated that there are around 11,000 small scale stationary fuel cells in operation globally [12]. Around 7,000 of these are micro-CHP systems of less than 10 kWe, 80 % PEMFC and 20 % SOFC [2]. The USA is the largest manufacturer of fuel cell micro-CHP units. However, due to market uncertainty and lack of incentives, most of these are exported to Japan. As a result, Japan is currently the leader in terms of fuel cell micro-CHP technology in the domestic sector. As of 2008 over 3300 PEMFC units were under demonstration in residential buildings in Japan [32] and as of 2012 that figure is closer to 6,000 [12].

Most commercial suppliers of fuel cell micro-CHP units assume that they are to be installed alongside a highly efficient condensing boiler. The fuel cell would provide the electrical power and DHW. The boiler provides the space heating [6]. It is intended that a domestic fuel cell unit would operate continuously at a fixed output; this is to reduce degradation to the cells, and in the case of a SOFC prevent thermal cycling. Furthermore, constant operation will maximise the benefits gained from onsite electrical generation. Constant operation of the fuel cell micro-CHP unit means excess electrical generation may be sold back to the grid. In the UK as of February 2012 micro-CHP qualifies for the Feed in Tariff (FiT) for generators $\leq$2 kWe [33]. E.ON suggest that for the BlueGEN unit (2 kWe), producing 13,000 kWh of electricity per year, the net value per annum is £1,845 with the FiT and £650 without it [6]. This illustrates that fuel cell micro-CHP does provide almost immediate economic benefits to the operator, with or without external support. In this paper two manufacturers of fuel cell micro-CHP units designed

Table 17.3 Baxi Innotech GAMMA 1.0 specification [36]

Baxi Innotech GAMMA 1.0	
Fuel cell type	Low temperature PEMFC (60 °C)
Capacity	1 kWe, 1.7 kWth
Fuel	Natural gas
Electrical efficiency	32 %
CHP efficiency	85 %
Operating mode	>100 start-stop cycle p/a
Dimensions	600 mm × 600 mm × 1,600 mm
Operating hours	4,000–6,000 p/a

for the domestic housing sector will be discussed, one a PEMFC (Baxi) and the other a SOFC (BlueGEN).

17.4.6.1 Baxi Innotech: GAMMA 1.0 [34]

Since 2002 Baxi has been developing fuel cell micro-CHP units: Beta series (2002–2005), Beta 1.5 (2005), Beta 1.5 PLUS (2008) and GAMMA 1.0 (2010–2012). In each development stage Baxi has been trying to achieve the following; cost reduction, increased operational performance, gain service and maintenance experience, field trials of increasing numbers of units and regarding GAMMA 1.0 series prepare it for market application as of 2013. Extensive demonstrations and field trials of the GAMMA 1.0 have been carried out in Germany as part of the Callux project. The Callux project is the largest national field test of fuel cell heating appliances for homes [35]. The unit's specification is given in Table 17.3 and a picture in Fig. 17.5.

The GAMMA 1.0 series consists of three parts; fuel cell, heat storage unit and energy manager. These components can be adjusted accordingly to best suit load requirements and generate the optimum savings. Due to the heat storage unit and integrated auxiliary water heater, the heat energy can be utilised as and when required. The Baxi GAMMA 1.0 utilises a low temperature (60 °C) PEMFC; making the hot water output ideal for DHW applications. Baxi state that the fuel cell micro-CHP unit will provide 100 % of the heating demand of a SFH, produce 5,000–6,000 kWh of electricity per annum, covering 73 % of the annual electrical load. Looking forward, Baxi have produced a development road map of where they believe the GAMMA series technology will progress. By 2013/2014 it is planned the DELTA will be introduced with electrical efficiency of 35 %, CHP efficiency of >90 % and a durability of 60,000 h [34].

17.4.6.2 Ceramic Fuel Cells: BlueGEN [26]

The BlueGEN unit produced by CFCL is a fully functioning SOFC micro-CHP unit that can be connected to a home's natural gas supply to provide heat and power

Fig. 17.5 The Baxi Innotech GAMMA 1.0 [34]

directly to the user. Currently it has the highest electrical efficiency of any fuel cell system on the market. Consequently the unit has a low heat output. As a result the unit can operate for longer periods throughout the year, thus increasing the benefit of adopting micro-CHP [26]. It is estimated that the unit will run continuously, producing around 13,000 kWh of electricity per annum and 200 l of DHW; space heating will need to be addressed by an alternative device. CFCL are currently developing another fuel cell unit that will cover all power and thermal loads [37]. Table 17.4 details the system performance, whilst Fig. 17.6 shows a picture of the unit.

From extensive field trials in homes in Australia, CFCL estimate they can produce a kWh of electricity for around 7 pence (includes the value of heat and carbon credits). Although this is based upon an Australian study, it does highlight that these units are not only feasible environmentally, but also economically. CFCL currently quote a cost of £19,950 for their unit, however once in mass production it is forecasted to cost around £5,000, with a payback period of 7 years and a useable life of 15. However, the unit is still not at a level of commercialisation to allow it to be bought off the shelf by an individual, but is normally sold en mass to larger organisations such as E.ON. With regards to CO_2 emissions, CFCL state the BlueGEN unit can reduce a home's emissions by up to 75 %. CFCL and E.ON have now formed a partnership as part of the European Union Fuel Cell and Hydrogen Joint Undertaking's Joint Technology Initiative (JTI) fuel cell demonstration programme. The JTI project partners consist of E.ON, CFCL, Ideal Boilers Limited and HOMA Software BV of The Netherlands [37]. CFCL and E.ON have made this joint agreement with the aim to demonstrate domestic fuel cells in the UK. E.ON has placed an order for 45 BlueGEN units as part of a demonstration

Table 17.4 BlueGEN performance [26]

CFCL BlueGEN	
Fuel cell type	SOFC
Capacity	Up to 2 kWe, 1 kWth
Fuel	Natural gas
Electrical efficiency	60 % at 1.5 kWe
CHP efficiency	85 %
Power modulation	0–100 %
Operating hours	Constant
Start-up time	25 h
Noise level	<45 dBa

Fig. 17.6 BlueGEN by CFCL [26]

period. After the demonstration period E.ON would, subject to a minimum order of 100,000 units, become the sole UK supplier of CFCL products. The joint partnership with HOMA Software BV is part of the development of a 'virtual' grid. The proposal is to conglomerate many homes' fuel cell micro-CHP capacity and remotely manage generation in response to utility scale power demands. With enough combined units, the generation capacity could be equal to several centralised power plants. However, electrical and system efficiencies would be much higher [6]. The BlueGEN unit is currently the only fuel cell product on the market to be certified under the Micro-generation Certification Scheme in the UK, making it eligible for the micro-CHP FiT. Under this tariff, 10.5p/kWh of electricity produced is paid to the homeowner, with a further 3.1p/kWh paid for surplus electricity exported [38].

17.4.7 Fuel Cell Micro-CHP Demonstration Projects

Real world demonstrations of fuel cell systems are essential in the development of efficient, effective and usable systems. Two fuel cell micro-CHP projects are now discussed, one based upon PEMFC technology and the other SOFC.

EneFarm is a fuel cell research, development and demonstration project based in Japan, and is the largest of its kind anywhere in the world. The project started in the 1990s and involves many companies including Panasonic, Tokyo Gas Co., Ltd and Kyocera. The research and development stage began with the production of a 1 kWe PEMFC micro-CHP system that runs on natural gas. Demonstration has been carried out in three stages. Stage 1; small scale demonstration where 50 units were installed into homes between 2003 and 2005. Stage 2; large scale demonstration of 3000 PEMFC micro-CHP units ran until 2009. Stage 3; commercialisation phase ran from 2009 onwards and it is hoped as of 2012 there will be more than 20,000 units installed with the aid of Japanese government grants [11]. EneFarm users also benefit from a discounted gas price, further incentifying the use of the units [39].

The EneFarm project has facilitated the continual improvement of the fuel cell system and housing integration. As a result the efficiency, cost and size of the units produced have continued to improve. The fuel cell system developed can be operated both grid connected or disconnected. The PEMFC system is designed (due to its operational characteristics) not to run continuously. It is on during the day when demand is high and hot water can be stored. The system is then turned off at night when demand is low. However there is now a newly introduced SOFC system from Kyocera, which has a continuous operating programme, this is to avoid damage due to temperature variations. The introduction of a SOFC to the programme has been spearheaded due to its promise of lower capital cost [29]. EneFarm expected sales are predicted to continue, in 2012 alone it is hoped 20,000 units will be sold, with a sales target of 50,000 by 2015 and 2.5 million by 2030 [39]. With such large volumes of sales it can be anticipated that the cost of these systems will continue to decrease, hopefully permitting the widespread uptake of fuel cell technology in the domestic built environment, not only in Japan but across the world. This widespread use would allow fuel cells to deliver operational advantages of higher electrical efficiencies, lower emissions and silent operation.

Highlights for the EneFarm project include; the very first fuel cell micro-CHP system in the world supplied to the Japanese Prime Minister's residence in April 2005 and the world's first general launch of household fuel cell micro-CHP systems in May 2009. It can be concluded that the EneFarm project has facilitated the wider use of fuel cell technology in the built environment with many valuable lessons learnt. The project should form a suitable platform on which to base future fuel cell development programmes on.

Until now the EneFarm project has solely focussed on PEMFC demonstrations. SOFC demonstration projects are still around 5 years behind those of PEMFC

[2]. However, successful projects have been completed. In terms of SOFC development CFCL's BlueGEN unit is one of the market front runners. In Australia CFCL in conjunction with Ausgrid have been trialling their BlueGEN unit in a smart home in Sydney. At the 12 month benchmark, promising operational results show a run time of 8,700 h with an availability of 91 %. The system has been operating at an average electrical efficiency of 56 %, exporting 10,700 kWh of electricity and resulting in 7.8 tonnes of carbon savings [40]. BlueGEN has also been trialled in Germany in a low carbon office building which also incorporates PV, wind turbine and solar thermal technologies. The demonstration project aims to understand how BlueGEN interacts with other DG in a single development. Crucial lessons learnt at the 16 month mark include; constant operation yields better performance, at a 2 kWe output the system generated 17,500 kWh per annum. Additionally, optimisation of generators is required in multi-source installations for best performance [40]. Currently there are 84 BlueGEN demonstration systems installed in nine countries. Such installations are providing valuable results, not just for BlueGEN, but the use of SOFCs as micro-CHP systems in the domestic built environment.

17.5 Conclusions

This paper has served to provide a state-of-the-art review of fuel cell technologies operating in the domestic built environment. The paper has addressed three fundamental areas: micro-CHP in the built environment, fuel cell technology and fuel cell systems in the domestic built environment. Throughout, up to date specific examples have been used to highlight the central role fuel cell micro-CHP could have in the domestic built environment in reducing operational cost and assisting in the decarbonisation of the sector.

Fuel cells have high electrical efficiencies, resulting in a lower H:P compared to conventional micro-CHP technologies. A low H:P means the fuel cell can be operational for greater periods of time throughout the year, therefore increasing the benefit to the user due to greater onsite electrical generation. Currently there are many different estimates regarding the extent of carbon savings delivered by fuel cells operating in the built environment. Discrepancies between estimates can be attributed to the fact that all projects are different with varying requirements and user demands. What can be concluded from the literature reviewed is significant carbon savings are achievable but not constant. Furthermore, there is not currently a large enough wealth of operational data with regards to the carbon savings achievable with fuel cells. The EneFarm project has however provided in-valuable results with respect to fuel cells operating in the built environment, and with sales of 20,000 units expected in 2012 alone is the largest project of its kind. Additionally, with the development and imminent deployment of commercially available fuel cell units such as the GAMMA 1.0 and BlueGEN, it is hoped more operational data will be made available, thus solidifying the carbon benefits fuel cells can deliver.

This paper has also highlighted the operational advantages fuel cells offer compared to conventional micro-CHP technologies, such as; higher electrical efficiencies, reduced noise and vibrations during operation and flexibility of fuel use. With regards to the type of fuel cells being used, the low temperature PEMFC and the intermediate to high temperature SOFC currently show the greatest promise, with most building integrated projects focussing on these two technological variants. The PEMFC offers quick start up time, power modulation and useful direct hot water output, whilst the SOFC provides high electrical efficiency, ability to internally reform hydrocarbon fuels and a high temperature heat output which can be utilised in another cycle. Two of the major market players outside of Japan in fuel cell development for the domestic housing market have been introduced, Baxi and CFCL, with their respective PEMFC and SOFC products.

If the UK and other countries are serious about their aspirations of a low carbon future, the built environment and the domestic sector in particular will play a vital role. In order to create a real transformation, both operational and technological changes need to occur. Decentralised energy generation from fuel cells in the domestic built environment will lead to increased energy security, reduced operational cost for the user and lower total CO_2 emissions. All essential objectives for the future built environment. Nations can no longer rely on technologies of the past to help arrive at the destination of a low carbon sustainable society.

Fuel cells are a technology of the future, providing a change in the way heat and power are supplied to end users. Fuel cells could finally provide the means by which energy generation can transfer from centralised to decentralised locales.

17.5.1 Future Work and Development

This section will identify three specific opportunities for future research and development work in the use of fuel cells, and specifically how to maximise the benefits of fuel cells operating in the domestic built environment. Firstly, hydrogen energy systems (electrolyser, fuel cell and hydrogen store) could be used as an energy storage option in autonomous renewable energy settings, such as remote communities [41]. There are little or no standing losses in compressed hydrogen storage tanks, therefore it can be considered a form of long term inter-seasonal energy storage [42]. Secondly, continued technological improvements to fuel cells have facilitated an increased interest in CCHP systems [43]. CCHP fuel cell systems mean higher levels of overall efficiencies are achievable due to a greater utilisation of waste heat. Finally, the use of long term (inter-seasonal) thermal energy storage means that the fuel cell can operate for a greater period of time per year without having to dump heat. Minimising heat dumping means higher system efficiency, lower emissions and operating costs are achievable [44].

Nomenclature

Acronym

AC	Alternating current
AFC	Alkaline fuel cell
CCGT	Combined cycle gas turbine
CCHP	Combined cooling heat and power
CFCL	Ceramic Fuel Cells Ltd.
CHP	Combined heat and power
CO	Carbon monoxide
CO_2	Carbon dioxide
DC	Direct current
DG	Decentralised generator
DHW	Domestic hot water
DMFC	Direct methanol fuel cell
EU	European Union
GHG	Greenhouse gases
H:P	Heat to power
ICE	Internal combustion engine
MFH	Multi-family home
MCFC	Molten carbonate fuel cell
NRPE	Non-renewable primary energy
PEMFC	Proton exchange membrane fuel cell
PAFC	Phosphoric acid fuel cell
SE	Stirling engine
SFH	Single family home
SOFC	Sold oxide fuel cell
UK	United Kingdom
USA	United States of America

References

1. DECC (2008) Climate Change Act 2008. The Climate Change Act 2008 2013, Electronic article. http://www.decc.gov.uk/en/content/cms/legislation/en/content/cms/legislation/cc_act_08/cc_act_08.aspx. Accessed 15 Mar 2013
2. Hawkes A, Staffell I, Brett D, Brandon N (2009) Fuel cells for micro-combined heat and power generation. Energ Environ Sci 2:729–744
3. Gencoglu MT, Ural Z (2009) Design of a PEM fuel cell system for residential application. Int J Hydrogen Energ 34:5242–5248
4. Wu DW, Wang RZ (2006) Combined cooling, heating and power: a review. Prog Energ Combust Sci 32:459–495
5. Kazempoor P, Dorer V, Weber A (2011) Modelling and evaluation of building integrated SOFC systems. Int J Hydrogen Energ 36:13241–13249

6. Harrison J (2012) E.ON – smart homes with fuel cell micro CHP. In: Smart hydrogen & fuel cell power conference, Birmingham
7. Gigliucci G, Petruzzi L, Cerelli E, Garzisi A, La Mendola A (2004) Demonstration of a residential CHP system based on PEM fuel cells. J Power Sourc 131:62–68
8. Al-Sulaiman FA et al (2010) Energy analysis of a trigeneration plant based on solid oxide fuel cell and organic Rankine cycle. Int J Hydrogen Energ 35:5104–5113
9. Calise F (2011) Design of a hybrid polygeneration system with solar collectors and a solid oxide fuel cell: dynamic simulation and economic assessment. Int J Hydrogen Energ 36:6128–6150
10. Pilatowsky I, Romero RJ, Isaza CA, Gamboa SA, Rivera W, Sebastian PJ, Moreira J (2007) Simulation of an air conditioning absorption refrigeration system in a co-generation process combining a proton exchange membrane fuel cell. Int J Hydrogen Energ 32:3174–3182
11. Carter D (2012) Fuel cell residential micro-CHP developments in Japan, ENE.FARM. Accessed 12 Feb 2013
12. UKHFCA (2012) Fact sheet 1: stationary applications
13. Beaussoleil-Morrison I (2008) An experimental and simulation-based investigation of the performance of small scale fuel cell and combustion-based cogeneration devices serving residential buildings. Annex 42 of the International Energy Agency's Energy Conservation in Buildings and Community Systems Programme
14. Peht M, Cames M, Fischer C, Prateorius B, Schneider L, Schumacher K, Voss J (2006) Micro cogeneration towards dencentralized energy systems. Springer, Berlin
15. Staffell I (2009) Fuel cells for domestic heat and power: are they worth it? Chemical Engineering, Birmingham
16. Brett D (2007) Micro-generation. http://www.homepages.ucl.ac.uk/~ucecdbr/research.html. Accessed 9 May 2012
17. Flint B (2008) Fuel cell products for global energy markets. In: Gas industry micro CHP workshop, Paris
18. ElianEnergy (2011) Fuel cell cars. http://www.future-alternative-energy.net/fuel-cell-cars.html. Accessed 9 May 2012
19. Larmine J, Dicks A (2003) Fuel cell systems explained, 2nd edn. Wiley, Chichester
20. Pilatowsky I, Romero RJ, Isaza CA, Gamboa SA, Sebastian PJ, Rivera W (2011) Cogeneration fuel cell – sorption air conditioning systems. Springer, London
21. O'Hayre R, Cha SK, Colella W, Prinz FB (2006) Fuel cell fundamentals. Wiley, New York
22. Sammes NM, Boersma R (2000) Small-scale fuel cells for residential applications. J Power Sourc 86:98–110
23. Minh NQ (2004) Solid oxide fuel cell technology – features and applications. Solid State Ionics 174:271–277
24. Riffat S (2012) Durable solid oxide fuel cell tri-generation system for low carbon buildings
25. Braun RJ, Klein SA, Reindl DT (2006) Evaluation of system configurations for solid oxide fuel cell-based micro-combined heat and power generators in residential applications. J Power Sourc 158:1290–1305
26. CFCL (2009) BlueGEN modular generator – power and heat (electronic resource). http://www.bluegen.info/Assets/Files/BlueGen_Brochure_(ENG_GER)_April_2010.pdf. Accessed 8 Dec 2012
27. Panasonic (2008) Panasonic develops new fuel cell cogeneration system for home use (electronic resource). http://panasonic.co.jp/corp/news/official.data/data.dir/en080414-2/en080414-2.html. Accessed 27 Apr 2012
28. Panasonic (2011) Tokyo Gas and Panasonic to Launch New Improved "Ene-Farm" Home Fuel Cell with World-Highest*1 Power Generation Efficiency at More Affordable Price. http://panasonic.co.jp/corp/news/official.data/data.dir/en110209-2/en110209-2.html. Accessed 27 Apr 2012
29. Boyd J (2008) Home fuel cells to sell in Japan. http://spectrum.ieee.org/energy/renewables/home-fuel-cells-to-sell-in-japan. Accessed 27 Apr 2012

30. Peacock AD, Newborough M (2005) Impact of micro-CHP systems on domestic sector CO2 emissions. Appl Therm Eng 25:2653–2676
31. DECC (2012) The future of heating: a strategic framework for low carbon heat in the UK. Crown Copyright, London
32. Nishizaki K (2008) The Japanese experience in micro CHP for residential use. In: Gas industry micro CHP workshop, Paris
33. DECC (2012) Feed-in tariffs (FiTs) update (electronic article) http://www.decc.gov.uk/en/content/cms/meeting_energy/Renewable_ener/feedin_tariff/feedin_tariff.aspx. Accessed 15 Mar 2013
34. Klose P (2011) Baxi Innotech – Gamma 1.0 large scale demonstration of residential PEFC systems in Germany, status and outlook. In: 4th IPHE workshop – stationary fuel cells, Tokyo, Japan
35. Callux (2012) Practical tests for fuel cells in a domestic setting (web resource). http://www.callux.net/home.English.html. Accessed 10 Oct 2013
36. Baxi (2011) A new perspective the fuel cell heating unit. For home generation of heat and energy. http://www.baxi-innotech.de/. Accessed 9 May 2012
37. CFCL (2011) E.ON UK orders additional 105 ceramic fuel cells' products. http://www.cfcl.com.au/Assets/Files/20111128-JTI_and_E.ON_order.pdf
38. FCT (2011) Ceramic fuel cells receives substantial order from E.ON UK. Fuel Cell Today. http://www.fuelcelltoday.com/news-events/news-archive/2011/november/ceramic-fuel-cells-receives-substantial-order-from-eon-uk
39. TG (2009) ENE FARM residential fuel cells launched. http://www.tokyo-gas.co.jp/tgminutes/64.pdf. Accessed 15 May 2012
40. Rowe T, Foger K (2011) Market launch of BlueGen: essential experience from real-world field trials. In: Fuel cell seminar and exposition, Orlando, USA
41. Hamada Y et al (2011) Hybrid utilization of renewable energy and fuel cells for residential energy systems. Energ Build 43:3680–3684
42. Gammon R et al (2006) Beacon energy farm; hydrogen and renewables integration (HARI)
43. Yu Z, Han J, Cao X (2011) Investigation on performance of an integrated solid oxide fuel cell and absorption chiller tri-generation system. Int J Hydrogen Energ 36:12561–12573
44. Santangelo PE, Tartarini P (2007) Fuel cell systems and traditional technologies. Part I: experimental CHP approach. Appl Therm Eng 27:1278–1284

Chapter 18
Green Lab: A Strategic Design Framework to Develop Sustainable Research Laboratories

Rosalba Belibani, Elena Gigliarelli, and Jody Patterson

Abstract The aim of this paper is to present a system of design strategies, useful to technical institutes and universities, that endeavor to create more environmentally and socially sustainable laboratory spaces.

The Green Lab model is designed to promote sustainable education throughout the complete life cycle of smart buildings. This requires a critical departure from traditional practices, starting at the formative stage, as defined by Edward Mazria's 2010 Imperative and 2030 Challenge (http://architecture2030.org/): first the change required in education, making ecological literacy a central tenet; then the change enabled in design, required to reduce CO_2 emissions by building activity by 50 %. Green Lab assumes an alternative approach to design education, to deliver different results—rendering the education process itself innovative, interactive and sustainable, and demanding smart buildings with the same characteristics.

The Green Lab methodology has been developed through teaching and research experience, providing a forum to apply and test design principles and innovative construction technologies as well as an occasion to propose a shift in cultural paradigm, so that university and research institutions themselves become prototypes in the field of sustainable building and energy technologies. The building project must constitute an innovation epicenter for the study of sustainable technologies, representing in itself a testing ground for advanced "solutions in progress" which are continually integrated, evaluated and replaced.

The result of this sustainable education model is the design of an architectural organism conceived according to bioclimatic strategies for minimal environmental impact, using recycled materials and meeting the highest standards of energy

R. Belibani Ph.D. (✉)
"Sapienza" Università di Roma, Roma, Italy
e-mail: rosalba.belibani@uniroma1.it

E. Gigliarelli
ITABC, CNR National Research Institute, Bologna, Italy
e-mail: elena.gigliarelli@itabc.cnr.it

J. Patterson
University of Waterloo, Waterloo, ON, Canada N2L 3G1
e-mail: japatterson@uwaterloo.ca

I. Dincer et al. (eds.), *Progress in Sustainable Energy Technologies Vol II: Creating Sustainable Development*, DOI 10.1007/978-3-319-07977-6_18

efficiency—a Green Lab capable of sustaining itself, generating energy from renewable sources via its form, surfaces and volumes. The knowledge base of the design laboratory is in constant expansion, requiring active research contributions (via dedicated website DiarAmbiente) from all participants: students, professors, architects, engineers, and national researchers collaborate directly to maintain a highly dynamic multilateral learning environment, keeping the moving target of sustainable design in focus. Its outcomes are high-level design projects, demonstrating increased consciousness and commitment to sustainable building.

Keywords Sustainable education • Design studio • Research project • Green Lab • Adaptive reuse

18.1 Background

The initiative to start a research project within a design studio context—founded upon the themes, methodology, content and goals of sustainability education—came after a long process of enhancing ecological literacy in collaboration with Anna Gadola and Franca Bossalino, and expressed in the research published on the website DiarAmbiente [1].

In May 2005, American architect Edward Mazria challenged the international building community to take the lead in combating climate change. In June 2005, sixteen of the most important institutions worldwide in the field of architectural education signed the Declaration of Las Vegas, recognizing "the great responsibility that rests on the architectural profession to do everything possible to influence a significant reduction carbon emissions resulting from construction and the life cycle of the built environment."

In 2006, Mazria launched Imperative 2010 online—regarding the change required in education, whereby ecological literacy must become a central tenet of design education—along with the 2030 Challenge [2], to change building design in order to achieve a 50 % reduction in the level of CO_2 emissions produced by the building industry. The DiarAmbiente site was born thus, with the conviction that we can develop all of our theories into practical application within the Design Studios of the Architectural and Urban Design program, held for 2 years, within the 5-year degree course in Architecture of the EU at the Faculty of Architecture at Sapienza University of Rome.

18.2 Problem

It was decided to target the entire design studio experience—both teaching and learning—in order to integrate and develop the complex aspects of sustainability. The most difficult challenge to approach was to conceive a teaching methodology

that could be called sustainable within the context of the teaching tradition, coexisting with the difficulties inherent to the teaching discipline. The design exercises to be assigned to students were more easily identified and treated in an articulated manner:

- 'Ecological literacy' education as a central principle in ecological design project, aiming to reduce CO_2 emissions by 50 %.
- Deepening of technological and engineering aspects within an architectural language where form follows not function, but the evolution of the project.
- Analysis of the relationships between the project and its locality.
- Technical analysis of the composition process, highlighting the complexity of the design process wherein practical skills and theory must feed each other.
- Attention to all aspects of the environmental sustainability of the project which inform the architectural solution.

The final design project assigned was a scientific research laboratory facility, characterized as an artificial lung, with a contemporary and technologically advanced architectural structure, to be achieved on the site of the National Research Council of Rome (CNR) in the municipality of Montelibretti: a scientific campus of 70 ha, including 15 institutes and over 500 employees.

To ensure realistic adherence to the aims of the project, the teaching staff was enhanced with the participation of Arch. Luciano Cessari and Arch. Elena Gigliarelli, both of CNR-ITABC, and Jody A. Patterson, Visiting Professor at the Faculty of Architecture, as well as other staff with experience in teaching design, sustainability and sustainability assessment via LEED and ITACA protocols.

The assignment was to design an architectural organism, incorporating recyclable materials and the latest solutions for reducing energy use and implementing energy from renewable sources, characterized as a "green laboratory": a Green Lab with low environmental impact, which can sustain itself from an energy standpoint. The building must be a center for the study of innovative technologies in sustainability, applied to the understanding, conservation and renovation of our built heritage, representing in itself a prototype "in progress" for technologically advanced solutions, to be continuously integrated or replaced.

18.3 Context

Redeveloping an area of the National Research Council site was, therefore, the issue addressed in the Design Studio, for which students were encouraged to experiment with the design of new models of buildings for researchers and scientists, utilizing the latest solutions for energy saving and use of energy from renewable sources.

Teaching goals were established to elaborate a joint project, accomplished through a complex systems approach, to create new workspaces for scholars and researchers while at the same time leading to the improvement and enhancement—

on an environmental, landscape and architecture basis—of this important Italian Science and Technology Park. The aim of this design project is to improve the quality of research and sustainability of the entire complex, via a systematic and coherent set of interventions on existing buildings, open and green spaces, but also to develop a model for science parks (CNR research area of Rome) that encourages cooperation between public research universities, public and private industry. Research laboratories so designed can encourage interaction between scientists from various disciplines, promote the recruitment of top researchers and facilitate the association and development of scientific activities. The challenge in designing a laboratory for scientific research contained in a contemporary and technologically advanced architectural organism, involved the creation of a self-sustaining low-impact "Green Lab."

18.4 Approach

The design studio, which aims to provide students with the theoretical knowledge and practical skills necessary for project development, is traditionally organized into lectures, exercises and design activities in the classroom. Usually, the student is a passive subject during lessons and intervenes only during reviews, showing the progress of their project. To transform, therefore, the design studio into an educational experiment—as sustainable as possible—we attempted to shift the student into an active role, taking a share in the teaching work from which the student is traditionally excluded. Sustainable design issues approached during the course were developed through the following activities:

- Three interim hand-ins of maquettes at different scales.
- Various tutorials on complex topics agreed with or chosen by the student.
- Presentation of systems for assessing the sustainability of a project, both specific to Italy (ITACA) and international (LEED), applied as an analysis exercise to projects chosen by the student.
- Ongoing reviews to check the progress of individual projects and permit a more personal relationship between teacher and student.

Students were also required to keep a studio album in which to collect notes, drawings, thoughts, ideas, sketches, impressions, images, references to other projects or specific theoretical references.

Two introductory lectures were delivered by Professor Franca Bossalino, long engaged in a campaign to improve the ecological literacy of architecture students. Within the Architectural and Urban Design IV studio, which served as a testing ground for this new approach to sustainability as applied to didactic activity and content, there are two Training Modules (approximately 30 h each) of "Systems" and "Technologies," which, in applying a structured model for sustainable education, offered substantial contributions to the development of an integrated design project.

The architectural project was developed during three intense months, taking a holistic approach and applying bioclimatic design processes governed by effective elements and best-practice solutions for sustainable design (buffer zones, curtain walls, green roofs, green walls, use of geothermal energy, appropriate use of integrated solar panels, etc.) The course website also provided a means to share the extensive and detailed bibliography and an notable collection of web-links with important information for project development.

18.5 Methodology

Studio teaching was approached as an experiment to define a design methodology around innovative and sustainable laboratories, to be implemented at a Science Park operated by Italy's most significant research agency. Choosing the CNR Rome site for the Studio intervention gives strict boundaries to the development of the theme, based in thorough analysis of the context and the scale of the intervention area. An environment of 70 acres at high landscape value, veined with a network of laboratories and scientific institutions developed in various phases over 40 years, posed the problem of supporting critical functionality of these headquarters while enhancing the area as a green and attractive place for research excellence: seeking an architectural intervention that can begin a process of regeneration of the entire campus.

The theme of the redevelopment of the site thereby intersected with a teaching methodology aiming to develop sustainable solutions and models for a new type of research laboratory, a "social incubator" that encourages interaction and team-based research, while providing the flexibility to allow ongoing evolution and change (Fig. 18.1).

Departing from the classical approach of functional laboratory, the research site was no longer seen as a machine for the development of techno-scientific processes but as a place of intellectual work and open and flexible experiments, connected to social and scientific networks and populated by "nomadic workers," operating within a crowd sourcing framework that foresees the collaboration of many researchers who via these networks will accomplish a particular job—all of this with obvious reflections on building design and architectural solutions.

It was therefore requested that the proposed project express levels of in-depth research and design on the following topics:

1. A Green Lab, called "LARIS Laboratory for Interactive Research on Sustainability."
2. A Science Center.
3. The archaeological museum display area of Colle del Forno.

Fig. 18.1 Master plans

18.5.1 LARIS Green Lab

The LARIS Green Lab was thought of as a 'living laboratory' in which researchers and partners in conservation can carry out research and evaluation on current and future systems and technologies at a high degree of performance and sustainability. In this sense LARIS will be used as a platform to test and demonstrate the technical performance and usability features of their technologies and systems. Product evaluation (via technical analysis and compatibility testing) performed by an independent public research entity can reduce the public burden of product development and create early market demand. Advanced visualization systems and simulation technologies will be used to involve all those involved in conservation efforts for built heritage (architects, restorers, superintendents, manufacturers of environmentally sustainable materials, etc.) (Fig. 18.1).

18.5.2 Science Center

The architectural organism assigned also had to include a Science Center, able to promote the dissemination of scientific research findings and discoveries in the very facility and in the field of sustainability, as well as those developed in other institutions in the area. This "Thematic Center" was to open to the public the contents of discoveries and innovations in this field, proposing itself as a platform for communication and exchange between the institute and the scientific community. To satisfy these needs, a room for multimedia exhibit was also requested for the display and dissemination of scientific culture: a place to perform interactive simulations of the performance and use of the building and explore alternative scenarios with sustainable strategies. This should include: a multimedia theater featuring advanced visualization (high-quality, high-scale screens to exhibit graphics and audio) and technologies of interaction with the public; reconfigurable

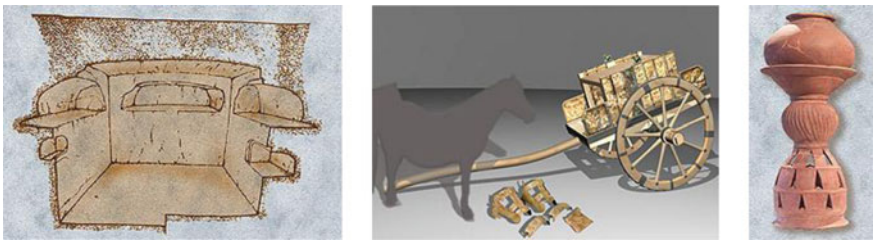

Fig. 18.2 Archaeological context

screens to maximize flexibility and allow experimentation with this same equipment; fixed seats with LCD touch screen panels wired for interactive participation and interconnected to a large screen display.

18.5.3 Colle del Forno Archaeological Area

The architectural design was also to include a hypothesis for the linking and integration of the new complex with the archaeological area called Colle del Forno, located on the crest of a hill that dominates the area, represented by a pre-Roman necropolis and currently inaccessible to the public. To relate the building organism with the necropolis, an open-air museum display area was called into play to provide a system of trails and facilities for visiting and reading in experimental ways (Fig. 18.2).

Laboratories constitute a unique challenge for sustainable design because of their intense energy use, stringent health and safety requirements, and complex environmental systems. Because of this, growing public awareness of sustainable design and construction has not gone unnoticed by the scientific community. The U.S. Green Building Council (USGBC), the Leadership in Energy and Environmental Design (LEED) program and the EPA/DOE's Labs21 were considered as guides and organizational tools supporting the sustainable design process for this specific area. From a spatial point of view the building must achieve an appropriate balance between open and closed type laboratories, developed on one or more levels, integrating with other agencies and with the surrounding topography, structured and populated with existing and new vegetation. The results of this Design Studio have shown a panorama of architectural solutions in which these scientific buildings were linked to issues of environmental sustainability and energy savings.

18.5.4 Program Requirements

Student projects must include the following components:

- Structured spaces for technology labs.

- Flexible wireless space for researchers.
- Multimedia center for technology simulations, design and science exhibits.
- Space for meetings and conferences.
- Offices for management of activities.
- Common areas.
- Toilets, a kitchen etc.

18.5.5 Project Requirements

Students were required to design a building defined by function rather than style, that can either be characterized as a strong architectural landmark—distinctive of the CNR campus—or as a compositionally light structure, morphologically and most of all ecologically. Technologically, the building must be designed as a living organism, able to generate energy via its own form, mass and volumes, utilizing primarily passive design strategies and systems. High level sustainability can include advanced water recycling systems and natural ventilation, favoring daylit interiors (Fig. 18.3).

18.6 Results

The results achieved by the final projects submitted were all of good quality, with a notable percentage of high quality, convincing the faculty to proceed with this teaching method. With regard to the project requirements in terms of sustainability and energy conservation, it is necessary to state that students have shown themselves highly receptive and capable to acquire a new design language, inspired by the themes proposed by the innovative use of bioclimatic strategies and skilful application of materials and vegetation. Even the interiors, which required some degree of design has been developed to the satisfaction of the choices made by the student.

18.7 Conclusions

This research shows its originality not only in the approach to teaching sustainability issues, but, of course, in the strategic content of the Green Lab projects themselves and especially in the teaching methodology used, unequivocally confirmed by the value of its results. All areas of the research support the potential for future development and areas of application.

Fig. 18.3 Sample of student work

References

1. http://www.diarambiente.it
2. http://architecture2030.org/

Bibliography

Abdu-Khader MM, Speight JG (2004) The concepts of energy, environment, and cost for process design. Int J Green Energ 1:137–151

(2008) Area n.99, Save energy. In: Rivista di architettura e arti del progetto
Open House International (2008) The quest for zero carbon housing solutions – La domanda di abitazioni a zero emissioni. 33(3)
Bell B (2004) Good deeds, good design. Community service through architecture. Princeton Architectural Press, New York
Benyus JM (2002) Biomimicry. Innovation inspired by nature. Harper Perennial
Brown LR (2008) PIANO B 3.0 Mobilitarsi per salvare la civiltà. Ambiente
Brown LR (2010) PIANO B 4.0 Mobilitarsi per salvare la civiltà, Ambiente
Butera FM (2007) Dalla caverna alla casa ecologica, storia del comfort e dell'energia. Ambiente
Coyle D (2012) Economia dell'abbastanza Gestire l'economia come se del futuro ci importasse qualcosa. Edizione Ambiente
Dall'Ò G, Gamberale M, Silvestrini G (2008) Manuale della certificazione energetica degli edifici. Norme, procedure e strategie d'intervento. Ambiente, Milano
Falcione M (2008) Diritto dell'Energia – Fonti rinnovabili e risparmio energetico. In: Collana "Quaderni dell'AIEE" (Associazione Italiana Economisti dell'energia)
Fassi A, Maina L (2006) L'isolamento ecoefficiente. Ambiente, Milano
Friedman TL (2008) Hot, flat, and crowded. Why we need a green revolution – and how it can renew America. Straus & Giroux, Farrar
Goleman D (2009) Ecological intelligence: how knowing the hidden impacts of what we buy can change everything. Broadway Books, New York
Henderson H, Ikeda D (2005) Cittadini del Mondo, L'impegno di ognuno per costruire un futuro sostenibile. Sperling & Kupfer
Hopkins R (2009) Manuale Pratico della Transizione, Arianna
Johnson, Bart R, Hill K (2001) Ecology and design, frameworks for learning. Island Press, Washington, DC
Karr JR (2002) What from ecology is relevant to design and planning? In: Johnson BR, Hill K (eds) Ecology and design: frameworks for learning
Kreith F, Kreider J (1978) Principles of solar engineering. Hemisphere-McGraw-Hill, New York
Krugman P (2010) Un'altra economia. In: Internazionale, vol 843. pp 23/29
Lovelock J (2006) La rivolta di Gaia. Rizzoli editore
Mercalli L (2011) Prepariamoci. Un piano per salvarci, Chiare Lettere
Moggridge B (2007) Designing interactions. MIT Press, Cambridge, MA
Orr DW (2009) Down to the wire. Oxford University Press
Pallante M (2009) La decrescita felice, Per la decrescita felice
Pallante M (2009) La Felicità Sostenibile, Rizzoli
Palleroni S, Merkelbach E, Eichbaum C (2004) Studio at large, architecture in service of global communities. University of Washington Press, Seattle
Sassi P (2008) Strategie per l'architettura sostenibile. I fondamenti di un nuovo approccio al progetto, Ambiente
Shiva V (2002) Terra Madre – Sopravvivere allo sviluppo, UTET Libreria
Sinclair C, Stohr K (2006) Design like you give a Damn. Architectural responses to humanitarian crises. Architecture for humanity
Steffen A (2006) Worldchanging. A user's guide for the 21st century. Henry N. Abrams Inc., New York
Stern N (2009) Un piano per salvare il pianeta. Feltrinelli
Todd, Nancy Jack & John (2007) Progettare secondo natura. Eleuthera, Milano
Villeneuve, Claude-Richard, François (2008) Vivere i Cambiamenti Climatici. Muzzio
Ward B (1976) La casa dell'uomo, come inventare la città futura. Arnoldo Mondadori
Weisman A (2008) Il mondo senza di noi. Che cosa succederebbe sul nostro pianeta con la scomparsa dell'uomo? Einaudi Stile libero extra
Williams DE (2007) Sustainable design, ecology, architecture, and planning
Worldwatch Institute (a cura di Gianfranco Bologna) (2011) State of the world 2011: Nutrire il pianeta. Ambiente

http://architecture2030.org/
http://www.diarambiente.it
http://www.kyotoclub.org/prossimi-eventi/2012-giu-5/smart_cities/docId=2827
http://www.genitronsviluppo.com/
MOBILE-SCHOOL: La Scuola Costruisce la Scuola

Chapter 19
Integrated System Concept for Energy Efficient Smart Buildings and Cities

Hasan Ufuk Gökçe and Kamil Umut Gökçe

Abstract The quality of life in Europe's cities states that although quality of life has improved in many areas, in other areas such as environmental issues and energy efficiency have deteriorated. In such places, people, companies and public authorities experience specific needs and demands regarding domains such as energy efficiency, environment and transportation services. These domains are increasingly enabled and facilitated by web-based applications, service oriented architectures, ubiquitous sensing infrastructure, advanced information management applications such as data warehousing and data mining technologies which generate actionable information for intelligent and predictive control for further optimised smart buildings and cities.

The engineering and deployment of off-the-grid energy production systems for buildings addressing the renewable energy technologies (e.g. wind, solar, geothermal) and integration of these systems to the city level grid applications with the ICT-based sub-systems becomes a necessity.

This paper addresses an integrated building concept that operates on energy-efficient basis while capturing retrofit opportunities that scale from a single building to multiple buildings at cities level. The proposed concept is developed based on two research areas; (1) Building energy supply-side (microgrid) management and (2) Building energy demand-side management complementing with the integrated energy production from renewable energy sources, building energy diagnostics and predictive control, ubiquitous wireless sensing technologies, and microgrid power electronics and power control to exploit the potential for reduction of building energy consumption, thus addressing the deficit of insufficient tool support.

The research findings will be demonstrated in an appropriately selected building in Hannover, Germany with EOS Sustainable Energy Solutions GmbH. This will be achieved by integrating different energy generation systems addressing the renewable energy technologies coupled with energy storage systems and building energy management systems comprising scalable and robust sensing network platforms, energy performance monitoring and data warehouse technologies.

H.U. Gökçe (✉) • K.U. Gökçe
Department of Civil and Environmental Engineering, Faculty of Engineering, University of Alberta, Edmonton, AB, Canada T6G 2R3
e-mail: ufuk.gokce@eos-energy-solutions.de; umut.gokce@eos-energy-solutions.de

I. Dincer et al. (eds.), *Progress in Sustainable Energy Technologies Vol II: Creating Sustainable Development*, DOI 10.1007/978-3-319-07977-6_19

Keywords Renewable energy • Energy efficiency • Smart buildings • Artificial intelligence

19.1 Introduction

Cities all over the world exhibit complex dynamics. As cities grow, planners devise "complex systems to deal with food supplies on an international scale, water supplies over long distances and local waste disposal, urban traffic management systems and so on; (. . .) and the quality of all such urban inputs defines the quality of life of urban dwellers" [1].

Notwithstanding the enormous formidable challenges and disadvantages associated with urban agglomerations, the world population has been steadily concentrating in cities.

In addition, there is a substantial increase in the average size of urban areas. This has been made possible by a simultaneous upward shift in the urban technological frontier, so that a city could accommodate more inhabitants. Problems associated with urban agglomerations have usually been solved by means of creativity, human capital, cooperation among relevant stakeholders, and bright scientific ideas: in a nutshell, 'smart' solutions. The label 'smart city' should therefore point to clever solutions allowing modern cities to thrive, through quantitative and qualitative improvement in productivity and efficiency.

The concept of smart cities has different meanings. A useful definition is to call a city "smart" when "investments in human and social capital and traditional (transportation) and modern (ICT-based) infrastructure fuel sustainable economic growth and a high quality of life, with a wise management of natural resources, through participatory government" [2]. Other definitions identify significant characteristics such as energy efficiency, environmental issues, productive economy, and define rankings based on measurable underlying indicators. Smart cities can be also understood as places generating a particular form of spatial intelligence and innovation, based on sensors, embedded devices, large data sets, and real-time information processing and response.

A recent and interesting project conducted by the Centre of Regional Science at the Vienna University of Technology identifies six main 'axes' (dimensions) along which a ranking of 70 European middle size cities can be made [3]. These axes are: a smart economy; smart mobility; a smart environment; smart people; smart living; and, finally, smart governance. These six axes connect with traditional regional and neoclassical theories of urban growth and development. In particular, the axes are based—respectively—on theories of regional competitiveness, transport and ICT economics, natural resources, human and social capital, quality of life, and participation of societies in cities.

A report of the European Environmental Agency [4] concerning quality of life in Europe's cities states that although quality of life has improved in many areas, in other areas such as health, environmental issues and energy efficiency have

deteriorated. In such places, people, companies and public authorities experience specific needs and demands regarding domains such as healthcare, energy efficiency and the environment, as well as safety and public services. These domains are increasingly enabled and facilitated by web-based applications, service oriented architectures, ubiquitous sensing infrastructure, advanced information management applications such as data warehousing and data mining technologies which generate actionable information for intelligent and predictive control for further optimised smart cities.

On the basis of on-going research in the area of energy efficiency and legislative drivers launched by the national and international organizations, the role of integration concepts, performance monitoring and analysis methodologies and sophisticated control strategies through the seamless integration of people, ICT devices and computational resources gain significant importance for reducing the energy consumption and the operational costs for buildings as well as cities. According to European standard "EN 15232 Energy Performance of Buildings-Impact of Building Automation" building operation systems can, depending on building type and equipment standard, produce the following potential savings of energy: restaurants 31 %, hotels 25 %, offices 39 %, shopping centers 49 %, hospitals 18 %, schools/universities 34 % and residential 27 % [5, 6]. This is a major contribution to the "Kyoto-Protocol-Process" in which the EU outlined the objective to reduce energy consumption by 20 % by 2020. Also, it is often faster and less costly to integrate building energy systems than it is to insulate building shells. At the moment sophisticated building energy management systems are available for facilities management. Most of the larger non-residential buildings younger than 30 years are already equipped with wired building automation systems in Europe. However, their focus on energy performance rating of buildings is at best sporadic often consisting of an ad hoc combination of off-the-shelf building management systems (BMS). This ad hoc combination presents many difficulties for building owners in relation to the management and upgrade of these systems, as the BMS can consist of a number of components utilizing various information exchange protocols that have to be integrated within the monitoring and targeting (M&T) software packages. The optimization of these systems for energy management adds another layer of complexity to the design and management procedures [7]. It requires analyzing the system, developing new interfaces, replacing devices, and optimizing parameters. Furthermore the engineering and deployment of efficient energy production systems for buildings addressing the renewable energy technologies, phase change materials, energy harvesting facades and integration of these systems with the ICT-based sub-systems becomes a necessity. Integrated IT tool support for these activities does not exist; available tools are stand-alone products, often tied to specific standards, and focus on development from scratch. There is not a procedure defined which describe information exchange between different domains for different energy generation and management systems. This lack of appropriate descriptions and tools currently outweighs the benefit of software interoperability. As this technology gap spans for all application domains, it will likely hamper further adoption of IT solutions. In this regard, the prospective consequence of the

building behaviour and the needs of the building occupant/operator which would manage energy production/consumption efficiently would not be predictable with a single combined information, communication, hardware and tool platform. A promising approach, to overcome these shortcomings, is the implementation of a holistic, modular infrastructure for building energy supply and demand sides.

19.2 Approach

The agenda in this research is build on the need of integration structures, holistic monitoring and analysis methodologies, life-cycle oriented management and decision support of both facilities and service teams with considering two key research areas; (1) Building energy supply-side (microgrid) management which addresses the energy management systems capable of optimal integration and control of energy production addressing renewable energy technologies such as photovoltaic/hot water solar panels, geothermal heat pumps, small scale wind turbines, biomass and the communication and intelligence required to work cooperatively with local authorities/grid operators and (2) Building energy demand-side management which comprises a scalable, robust wireless sensing/actuation network platform that computation and actuation to collect build-use data through advance data monitoring and data mining technologies which lead to develop optimal control algorithms that adjust Lighting, Heating, Ventilation, Cooling set points as well as controlling of appliances to adapt to occupancy, weather loads and their predictions, minimizing total energy consumption and balancing peak demand while maintaining the indoor environment within user preferred comfort parameters.

The proposed concept depicted in Fig. 19.1 above consists of three parts: (1) Building Energy Supply (BES) side. This consists of conventional energy supply from the grid and Off-the-Grid energy generation systems such as photovoltaic/hot water solar panels, geothermal heat pumps, small scale wind turbines, biomass and storage technologies maintains optimal integration and control of off-the-grid energy generation systems for building energy supply side, (2) Building Energy Demand (BED) side which consists of HVAC systems, lighting systems and appliances, (3) Multi Dimensional Energy Monitoring, Analysis and Optimisation System consisting of wireless sensors/meters/actuators, multi dimensional information management platform, intelligent control module and monitoring tools.

19.3 Concept

At present, off the grid energy generation technologies are usually provided by the companies which solely focus on specific areas such as wind, solar, geothermal, biomass and storage as there is a very limited number of companies that provide a "*total service concept*." Therefore, holistic design between various energy

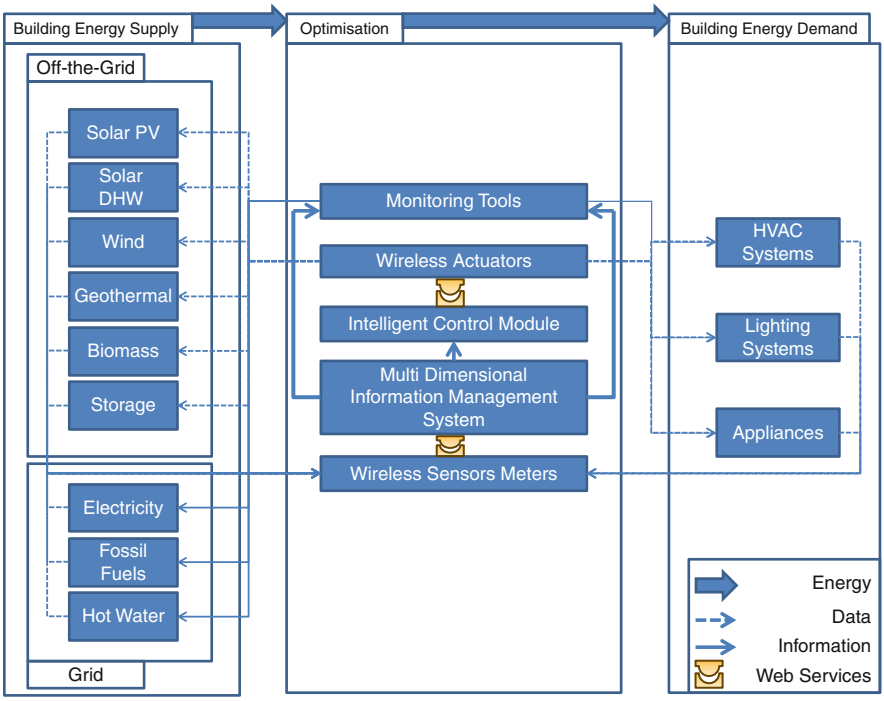

Fig. 19.1 A smart building concept integrated with off-the-grid energy generation systems

generation systems hasn't been provided in an expected granularity due to the lack of integration concepts.

Moreover, the control of energy performance of buildings is often provided by an ad hoc combination of off-the-shelf building management components, distributed data metering equipment, glued together by M&T software tools. The absence of building management systems standardization coupled with competition for market share results in independent and non-compatible system development. In this regard BACnetTM was developed to provide an open, non-proprietary protocol specification that allows building automation controllers of different manufacturers to communicate with each other [8]. However Building Management Systems/ Energy Management Systems still operate on non-standardized proprietary interfaces. Consequently they are becoming more complex over time and are difficult for the average operator to understand given the educational and experience [9]. Additional training overhead is required for each new system or system updates. Moreover [10] states that in the absence of compatible hardware and communication protocols maintenance can become extremely problematic as seamlessly integrating these systems is an inefficient overhead.

However, in conjunction with traditional procurement policy it is conceivable that numerous systems which would provide an integrated system chain enabling the efficient use of renewable energy resources and energy management systems in

a holistic building-supply and building-demand side energy management concept complementing with a modular approach should appear, as can be seen in this research.

In this regard two research concepts are provided by defining: (1) Integration and optimisation of off-the-grid energy generation systems. (2) Multi Dimensional Energy Monitoring, Analysis and Optimisation System.

19.3.1 Integration and Optimisation of Off-the-Grid Energy Generation Systems

Integration and optimisation of off-the-grid energy generation systems involves two complementing phases (1) the design of small scale house type renewable energy technologies e.g. wind, solar, geothermal and storage systems for off-the-grid energy generation and storage in buildings through an integrated structure based on the requirements analysis including energy demand and grid supply patterns and (2) the development of an optimisation middleware for energy-supply, in order to control the various systems in an integrated and optimized way.

19.3.1.1 Off-the-Grid Energy Generation and Storage Systems

Off-the-grid renewable energy technologies for energy generation for buildings usually addresses individual systems integration, e.g. a wind turbine is combined with adequate storage devices or energy harvesting facades are combined with actuators or blind control systems. Several tools supporting the integration of these components exist with manufacturers having usually their own preferences.

Therefore the definition of optimal processes and interfaces allowing the integration of different systems e.g. integration of small scale battery charging wind turbines and photo-voltaic solar cells which feed a common storage system (battery bank) and control of energy production on the basis of environmental conditions e.g. wind speed, day light period, etc. can be accepted as one of the prerequisites of a holistic, modular approach.

In this research, in order to integrate different type of systems in an optimized way, the requirement and the state-of-the art analysis which would allow optimized integrations have been obtained with researching the systems given below. This preliminary state-of-the art analysis will be used to develop the middleware for building energy supply.

Small Scale Battery Charging Wind Turbines

After examining, different type of home use small scale wind turbines in the market, 600W 24VDC battery charging wind turbine with 6 Blade type has been chosen to optimise small scale renewable energy output which is compatible with our application scenarios. Its cut-in speed is low in order to facilitate continuous generation and auxiliary energy source. The wind speeds in excess of 150 km/h has been approved. This type of home use wind turbines generally comprises of a single axial flux permanent magnet brushless alternator. The six blade design supports a self-regulating aerodynamic rotor that achieves speed control through blade turbulence, which controls the speed of the rotor with no moving parts and no obtrusive noise. The diameter is 1.5 m.

Solar Panels Made of Photo-Voltaic Solar Cells

In this research, four major types of Solar Technology Panels have been examined (1) polycrystalline cells which are the most common and cheapest panels with conversion efficiency 13–15 % (sunlight to electricity), however, under elevated temperatures of 50 °C panel temperature, the efficiency drops by around 20 %, (2) panels made from monocrystalline cells which are used in high reliability applications such as telecommunications and remote power with conversion efficiency is typically 14–17.5 % (higher than the polycrystalline cells), however, at elevated temperatures, the efficiency only drops by 10–15 % so they are more consistent in output (3) Panels made from amorphous cells which have been used in portable items for many years with conversion efficiency of sunlight to electricity is 5–7 %, about half that of the other panels but unlike the other types, their output does not decrease in elevated temperatures. Panels made of thin film cell CIGS technology (Copper, Indium, Gallium, diSelenide) are flexible, durable, and provide slightly higher efficiency than other flexible solar cells, typical sizes less than 60 W and can be mounted to curved surfaces. The critical item that delivers the current to charge the batteries is the solar controller. There are 3 major types of controller: (1) Standard single phase controller, (2) Multistage controller, and (3) Maximum Power Point Tracking Controller (MPPT). The first 2 controllers provide roughly 70 % of the panels power to the batteries as they reduce the voltage of the solar panels but do not increase the current. MPPT Controllers are true "State of the Art" technology with 96 % + output. The final critical factor is the location of the controller, the mounting the controller at the battery end of the solar panel cable allows batteries fully charged. In summary, the way to compare the relative output capacity of panels is by the current output charging batteries at around 13.5 V.

In our case with considering the current systems, the high quality polycrystalline solar panels for home solar power systems and MPPT controllers are used in this research.

Solar Vacuum-Tube Collectors for Hot Water

In order to heat water using solar energy, a collector, often fastened to a roof or a wall facing the sun, heats working fluid that is either pumped (active system) or driven by natural convection (passive system) through it. Residential solar thermal installations fall into two groups: passive and active systems. Both typically include an auxiliary energy source (electric heating element or connection to a gas or fuel oil central heating system) that is activated when the water in the tank falls below a minimum temperature setting such as 55 °C. Hence, hot water is always available. The combination of solar water heating and using the back-up heat from a wood stove chimney to heat water can enable a hot water system to work all year round in cooler climates, without the supplemental heat requirement of a solar water heating system being met with fossil fuels or electricity. For this research Viessmann Vitosol 300T type SP 3A Vacuum-tube solar collectors with dry connection heat tubes have been chosen. The system has gross area of 2.88 m^2 and the absorber area of 2.00 m^2.

Geothermal Heat Pumps

A geothermal heat pump, ground source heat pump (GSHP), or ground heat pump is a central heating and/or cooling system that pumps heat to or from the ground. It uses the earth as a heat source (in the winter) or a heat sink (in the summer). In a fridge, heat is transferred from the inside to the outside. With a heat pump, this happens exactly the other way round. Heat from the air or the ground is transferred into the living space via the heating system. Vapour from a refrigerant is compressed to increase the temperature, to make it high enough for central heating and DHW (Domestic Hot Water) heating. For this research, the selected Viessmann Vitocal 350-G reaches up to 72 °C. These heat pumps can therefore also be used for modernisation as they can provide a sufficiently high flow temperature for central heating with radiators. The compression process is vital for the efficiency of a heat pump. To generate heat, for example, heat is extracted from the ambient air and used to evaporate a refrigerant that boils at low temperature. Getting hotter towards the centre—from an initial temperature of between 5 and 18 °C, a flow temperature of up to 72 °C is achieved. The gas created is compressed by the scroll compressor, which causes it to heat up. The gas heated in this way transfers its heat via the condenser to the heating water or DHW heating system, and thereby condenses again. Finally, the refrigerant, which is still under pressure, is expanded in an expansion valve, and the circuit begins again. A heat pump can make use of the following energy sources: (a) Air—practically unlimited availability; lowest investment costs (b) Ground—via geothermal collector or geothermal probe. (c) Water—efficiency depends on the water temperature. (d) Waste heat—subject to availability, volume and temperature level of the waste heat. In this regard, the best heat source for each individual case depends on local conditions and the actual heat demand.

Energy Storage Systems

For energy storage systems two types of batteries have been examined, (1) Lead Acid Deep Cycle Batteries which are designed to have stored current discharged between charging sessions, with very heavy non-porous battery plates to withstand repeated major discharging and charging cycles (deep cycles) and (2) Nickel Alloy Batteries Nickel Cadmium (NiCad) and Nickel Iron batteries, rather than consisting of lead plates submerged in a sulfuric acid solution, feature nickel alloy plates in an alkaline solution.

In this research, we have chosen nickel alloy battery types for our experiments with considering the facts such as they are well suited for home power use, although much less common and much more expensive than lead acid types. The nickel alloy battery can have up to 50 years of useful life, compared to 20 years with a well-maintained lead acid battery. They can also sit for extended periods of time partially or fully discharged without suffering damage, unlike lead acid types and they need lower maintenance. On the other hand a lead acid battery should never be completely discharged, meaning they need to be more closely monitored. Nickel alloy batteries operate better at lower temperatures, and can discharge more of their total amp-hour capacity as useful current.

A battery bank is the main part of the energy storage systems and enables a constant level of power to the house. Without the battery bank, the entire electrical system of a house would be limited by the immediate output of renewable energy resources. A wind turbine would be subject to constant power fluctuations as the wind speed increased, dropped or disappeared entirely. At night, a solar-run house would have no electrical power available. Therefore in order to provide a constant level of power without causing problems for households, a grid connection to the battery banks would be necessary during non-peak hours, thereby the house-use power can be available regardless of weather conditions with convenient electricity prices.

In our case, we designed our system based on three separate battery sections composed of nickel alloy batteries. The first section is connected with the small scale battery charging wind turbine, the second section is connected with the high quality polycrystalline solar panel while the third section connected to the central electricity grid. Therefore the wind generator and solar panel can deliver power to the battery bank regardless of current power usage, so excess power can be stored during low use times (generally the middle of the day and middle of the night) and be available during high use times (usually morning and evening). In our case an inventer DC–AC which is used to convert the DC power from the battery bank to AC power for the house power systems, a rectifier AC–DC which converts AC grid power to DC power for the use of battery charging, a control relay which provides a direct connection between the house and the grid in the event that all stored energy is depleted or a problem occurs in the battery bank.

19.3.1.2 Optimisation Middleware for Building Energy Supply Systems

This is considered for the integration of off-the-grid power generation systems and central electricity/gas/water grid and optimal control of these systems on the basis of occupant needs and environmental factors. In order to provide this, a novel model-based system development approach is investigated that automates code development. In the model-based system development approach, we propose to adopt the software product line paradigm. It starts with requirement engineering for the envisaged systems specifying the functionality to be implemented. From these requirements the source codes are individually generated from software modules to fulfil the requirements and optimally use the system resources. Information about the implemented functions, requirements, and software function blocks are stored in the form of Electronic System Descriptions. This repository contains descriptions of individual systems for integration purposes. Consequently on the basis of specified descriptions which allow controlling of optimal management of wind turbines, solar panels, geothermal systems etc. The middleware is designed with considering the functionalities given below.

The middleware is in control of charging the batteries when out of power from either the grid or renewable energy systems occurred. It will supply the hot water by taking into consideration of the occupant requirements and environmental factors. The middleware also be in control of providing stored power to the house whenever possible. It is designed for running the system in the most cost effective manner by considering carbon emissions. It would decide when to charge the batteries and from which source. The middleware is designed to provide stored power to the house whenever present and only switch to grid power if all stored power is depleted. Moreover it provides charging the batteries from the grid power during non-peak hours and only if the systems could not provide enough power for the house use.

19.3.2 Multi Dimensional Energy Monitoring, Analysis and Optimisation System

Multi Dimensional Energy Monitoring, Analysis and Optimisation System is implemented on the basis of four complementing components as (1) Building Information Model, (2) wireless sensor/meter/actuator network platform, (3) multi dimensional information management platform, (4) Intelligent Control Module and (5) Monitoring tools.

19.3.2.1 Building Information Model (BIM)

In order to simplify the requirement engineering, information about the building (location, building systems, etc.) can be imported from the systems which support architectural and building systems design. Architectural designs are typically developed with the Computer Aided Design (CAD) tools such as Autodesk Revit, Microstation, ArchiCAD and DDS-CAD. They support standardised, extensible Building Information Models (BIM) based on product modelling standards such as IFC (Industrial Foundation Classes).

The concept of a BIM describes an integrated data model that stores all information relevant to a building throughout the building life cycle. In our case, it is envisioned to extend the BIM with the system design, e.g. the number and kind of wireless sensors and communication devices in order represent deployment in different rooms and their interaction within each other and with the building itself.

In order to predict and model building energy performance, energy simulation models should be considered. These models enable the building operator to perform comparisons between design intent and actual energy performance data. For example, in order to perform an energy simulation on the Revit MEP model, the IES plug-in is used in our simulations to complete BIM Model comprising energy performance aspect.

19.3.2.2 Wireless Sensor/Meter/Actuator Network Platform

Wireless Sensor Network (WSN) is a wireless network consisting of spatially distributed autonomous devices using sensors that allow the physical environment to be monitored at high resolution. These sensors also called motes are installed in particular locations or can be deployed in a particular zone to gather information such as temperature, humidity, CO_2, lux level, etc. The real functionality of sensors comes with wireless sensor networks when these sensors start communicating with each other through wireless protocols. WSN can shuffle the information collected through the sensors and transfer it to the public internet and or a local area network. Finally, the information is collected in the data warehouse where it is analysed.

In this project the wireless sensor network architecture is implemented based on the recently released IETF 6LoWPAN (RFC 4944) open standard for IP communication over low-power radio links—IEEE 802.15.4 represents one such link. WSN LoWPAN networks are connected to other IP networks through one or more border routers forwarding packets between different media including Ethernet, Wi-Fi or GPRS. The IP architecture offers widespread commercial adoption and broad interoperability due to its attributes such as openness, flexibility, scalability and manageability. Many industrial standards, including BACNet, LonTalk, CIP and SCADA, introduced an IP using either TCP/IP or UDP/IP over Ethernet.

In this research the wireless sensors have been chosen to detect and measure various parameters such as temperature, humidity and water/gas/electricity meter

readings. In our case the motes, mainly consists of 3 components; the sensor interface which actually measures the physical attributes like humidity level, the radio interface which communicates with other motes and the CPU which performs computations and transfers information between the two components. The used board is equipped with an Atmega1281 MCU and EM2420 radio chip. The platform includes sensors for monitoring air-temperature, air-humidity and light. Moreover incorporates electricity meters as well as the interface for controlling (on/off) an AC load are utilised. The platform runs the recently released b6LoWPAN stack. Soekris embedded PC boards [11] with Atheros CM9 Wi-Fi cards and a single IEEE802.15.4 node form a backbone network will be used in all the rooms of the sample building.

19.3.2.3 Multi Dimensional Information Management System

The objective of the data warehouse development is to provide a multi dimensional information management platform to store integrate and analyse complex data sets from multiple information sources such as model editors, energy simulation tools and performance framework specification tools as well as data streams collected from wired and wireless sensors and meters in order to analyse building performance data and to support decision making process of the stakeholders. The data extracted from the Building Information Model and from the wireless sensor/meter/actuator network platform is aggregated in the data warehouse core in order to provide actionable information to the intelligent control module. Simultaneously aggregated data is presented through specific Graphical User Interfaces (GUIs) concerning different stakeholder requirements. The developed system is explained in detail by [12–14].

19.3.2.4 Intelligent Control Module

The actionable information generated by the Multi Dimensional Information Management System is processed within the intelligent control module for low energy building operation in order to control and optimise both building energy supply side and building energy demand side in run time.

The intelligent control module contains algorithms for the defined building operation scenarios (e.g. heating, cooling, and lighting) and interacts with the data warehouse core to compute control parameters, which are then passed to the wireless network for actuation. The detailed description of the intelligent control module has been provided by [12–14].

19.3.2.5 Monitoring Tools

The common goal of the graphical user interfaces is to represent the building performance information to the end users at the Building Energy Demand (BED) side and to the grid operators (stakeholders) at the Building Energy Supply (BES) side concerning their roles and functions. The aim of the proposed system's monitoring tools is designing and implementing user friendly, customized and context sensitive Graphical User Interfaces (GUIs) for defined end users and stakeholders. In order to achieve this, Java and Service Oriented Architecture (SOA) based interfaces are developed which enables end users automated querying without dealing with complex SQL statements [12–14].

19.4 Conclusions

In this paper an integrated building energy management system composed of (1) Building energy supply-side and (2) Building energy demand-side management is described. The proposed concept integrates energy production systems from renewable energy sources, building energy diagnostics and predictive control, ubiquitous wireless sensing technologies, and microgrid power electronics and power control. The research focuses on an innovative model-driven development approach that integrates systems in building energy supply-side and building energy demand-side to provide optimized energy production/consumption. The research findings will be demonstrated in an appropriately selected building in Hannover, Germany with EOS Sustainable Energy Solutions GmbH [15] integrating different energy efficient production/consumption systems addressing the renewable energy technologies, energy storage systems and building energy management systems comprising scalable and robust sensing network platforms, energy performance monitoring and data mining technologies. The initial research findings will be used to extend this research to the smart cities level.

References

1. The Science Museum (2004) Urban development. http://www.makingthemodernworld.org.uk/learning_modules/geography/04.TU.01/?section = 2. Accessed 3 Apr 2009
2. Caragliu A, Del Bo C, Nijkamp P (2009) Smart Cities in Europe. Series Research Memoranda 0048. Free University Amsterdam, Faculty of Economics, Business Administration and Econometrics
3. Komninos N, Schaffers H, Pallot M (2011) Developing a policy roadmap for Smart Cities and the Future Internet. In: Proceedings of the eChallenges 2011 conference, Florence, 24–26 Oct 2011
4. EEA (European Environmental Agency) (2009) Ensuring quality of life in Europe's cities and towns. EEA Report 5/2009

5. DIN (Deutsches Institut für Normung e.V.) (Herausgeber) (2007) DIN EN 15232: Energieeffizienz von Gebäuden Einfluss von Gebäudeautomation und Gebäudemanagement, Deutsche Fassung EN 15232:2007. Berlin, Germany
6. VDMA (German Engineering Federation) (2008) Energy-efficiency of buildings. Beuth Verlag GmbH 2007, Germany, p 79
7. Nikolaus K (2008) Pictures of the future spring 2008. http://w1.siemens.com/innovation/en/publikationen/publications_pdf/. (Last download 2008)
8. ASHRAE (2003) HVAC systems and equipment. ASHRAE, Atlanta, GA
9. Lowry G (2002) Modelling user acceptance of building management systems. Automat Constr 11(6):695–705
10. Hatley D, Meador R, Katipamula S, Brambley M, Lt.Cokl CW (2005) Energy management and control system: desired capabilities and functionality prepared for HQ air mobility command (AMC/CEO) PNNL-15074, Richland, WA
11. Soekris Board (2012) http://www.soekris.com/. (Last download 2012
12. Gökçe HU (2010) Multi-dimensional analysis of building performance data for energy efficient building operation. Ph.D. thesis, National University of Ireland, Cork, Ireland
13. Gökçe KU, Gökçe HU (2011) Multi dimensional information management platform for wireless embedded monitoring of building performance data. In: Hans-Joachim Bargstädt, Karin Ailland (eds) Proceedings of the 11th international conference on construction applications of virtual reality, Weimar, Germany, 3–4 Nov, Heft 21, ISBN: 978-3-86068-458-0
14. Gökçe HU, Gökçe KU (2013) Integrated system platform for energy efficient building operations. J Comput Civil Eng 10.1061/(ASCE)CP.1943-5487.0000288 (5 Jan 2013). SCIA, Ranking
15. EOS (2012) http://www.eos-energy-solutions.de. Germany

Chapter 20
Interoperable ICT Platform for Energy Efficient Smart Buildings

Hasan Ufuk Gökçe and Kamil Umut Gökçe

Abstract Europe's objective under the 20-20-20 target is to reduce energy consumption by 20 % and increase the renewable energy sources by 20 % in the overall energy mix. The European Union currently imports two third of its oil and gas which makes it the world's leading importer of these fuels. Due to increasing energy prices and relatively high percentage of building related energy consumption much effort is invested for energy efficient buildings. Apart from meaningful building insulation measures, the only means of achieving marked improvements in the energy efficiency of buildings is to make use of efficient building automation technologies which comprises performance monitoring, analysis and intelligent control. This research addresses the need for integration concepts, holistic monitoring and analysis methodologies, life-cycle oriented decision support and scenario based control strategies through the seamless integration of ubiquitous sensing infrastructures, simulation tools, Building Information Modelling (BIM) tools, service oriented architectures and data warehouse technologies. This paper introduces an interoperable Information and Communication Technologies (ICT) platform integrating IT systems at design, construction and operation stages of buildings so that monitoring, analysis and optimization of building energy performance can be achieved. The developed prototype has been demonstrated with EOS Sustainable Energy Solutions GmbH which is Hannover, Germany based R&D company, on a sample building of Technology Center Hannover within the scope of Dynamic System Architecture for Energy Efficient Building Operations (DASSEB) Project.

Keywords Energy efficiency • Renewable energy • Artificial intelligence • Wireless embedded devices

H.U. Gökçe (✉) • K.U. Gökçe
Department of Civil and Environmental Engineering, Faculty of Engineering, University of Alberta, Edmonton, AB, Canada T6G 2R3
e-mail: ufuk.gokce@eos-energy-solutions.de; umut.gokce@eos-energy-solutions.de

I. Dincer et al. (eds.), *Progress in Sustainable Energy Technologies Vol II: Creating Sustainable Development*, DOI 10.1007/978-3-319-07977-6_20

20.1 Introduction

As contribution to the legislative drivers such as Kyoto-Protocol, Copenhagen Summit (COP15) and Durban Summit (COP 17), the European Union (EU) outlined the objective to reduce energy consumption by 20 % until 2020. The EU currently imports 82 % of its oil and 57 % of its gas [1]. The EU can have little influence on external energy markets and energy supply but can influence domestic energy demand. One possible solution to both the above problems is to reduce energy consumption by increasing energy efficiency.

In terms of energy efficiency buildings provide significant potential for energy and energy related CO_2 emissions savings since buildings account for 40 % of the total energy usage and 30 % of total energy related CO_2 emissions in Europe [2, 3].

Apart from meaningful building insulation measures, the only means of achieving marked improvements in the energy efficiency of buildings is to make use of efficient building automation technologies (VDMA 2008). According to European standard "*EN 15232 Energy Performance of Buildings-Impact of Building Automation*" building automation systems can, depending on building type and equipment standard, produce the following potential savings of energy: restaurants 31 %, hotels 25 %, offices 39 %, shopping centres 49 %, hospitals 18 %, schools/universities 34 % and residential 27 % [4, 5]. Also, it is often faster and less costly to automate building systems than it is to insulate building shells [6]. Thus, flexible and easy to handle monitoring and control technologies are essential. Presently, many sophisticated building services systems are available for facilities management. However, their focus on energy performance rating of buildings is at best sporadic, often comprising an ad hoc combination of off-the-shelf building management systems (BMS) with some extensions. Such systems provide many problems to building owners with regard to interoperability. The optimization of these systems for energy management adds another layer of complexity to the design and management procedures. It requires analyzing the system, developing new interfaces, replacing devices, newly adjusting and optimizing parameters.

In this regard, the prospective consequence of the building behaviour and the needs of the building occupant/operator which would manage energy consumption efficiently would not be predictable with a single combined information and communication platform. A promising approach, to overcome these shortcomings, is the implementation of an integrated, modular infrastructure.

In order to address this aim, a project named "DASSEB—Dynamic System Architecture for Energy Efficient Building Operations" which is supported by the Scientific and Technological Research Council was granted in 2010 and the developed concept has been demonstrated with EOS Sustainable Energy Solutions GmbH [7] which is Hannover, Germany based R&D company, on a sample building of Technology Centre Hannover in Germany.

20.2 System Architecture

The developed system architecture covers the implementation of a modular platform as depicted in Fig. 20.1, that integrates multiple dimensions of building information such as performance data (e.g. energy consumption, temperature, lighting level), system data (e.g. status, switch settings) and process data (e.g. inspection, maintenance, repair) which supports integration concepts, holistic monitoring and analysis methodologies, life cycle oriented decision support and information and communication technologies. This is implemented as an extension to international standards (e.g. IFC 2x3 ISO/PAS 16739).

The proposed system architecture (see Fig. 20.1 above) consists of three application layers such as (1) Data Layer, (2) Information Layer, and (3) Tool Layer. These layers will be explained with their components in the following sections.

20.2.1 Data Layer

Data layer provides data collection from multiple sources such as wireless sensors and actuators which collects relevant measurements and system status [8]. Since this data is raw it requires definition data in order to classify and categorise

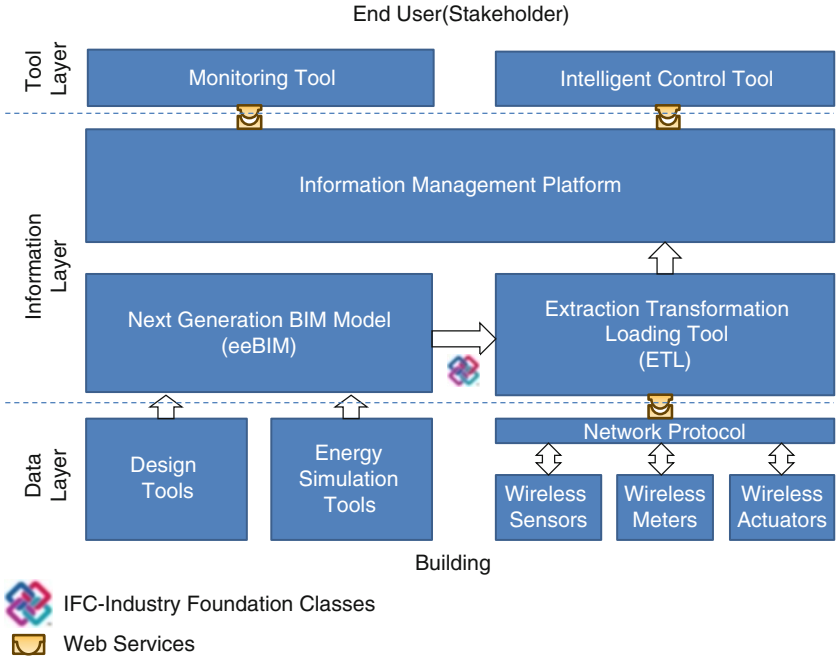

Fig. 20.1 Integrated system architecture for energy efficient smart buildings

measurements for analysis purposes. Various Model Editors are required to define and categorise the sensed data.

Data Layer consists of: (1) Wireless network embedded systems such as wireless sensors, meters and actuators, (2) Design Tools, and (3) Energy Simulation Tools.

20.2.1.1 Wireless Network Embedded Systems

This consists of wireless sensors and actuators. For this research the applicability of flexible wireless sensing and actuation infrastructure with novel miniaturised sensor nodes and actuators that allow long-term embedding into the building fabric is searched. Also, self-configurable, self-optimised and self-healed wireless sensor and actuation infrastructures are specified to identify architectural approaches.

Furthermore, the specification of a web-service based Network Protocol is provided to enable the wireless network embedded devices to interact with the information management platform via web-service protocols.

20.2.1.2 Design and Energy Simulation Tools

These are required to categorise and classify the raw data collected from the Network Embedded Systems. Existing off-the-shelf design and energy simulation tools are examined in order to support 4D design and Energy Simulation Models.

20.2.2 Information Layer

This is the information management layer of the proposed architecture. The data collected within the data layer is processed, analysed and aggregated within this layer to provide actionable information for the Tool Layer. Information layer consists of three components.

These are: (1) Next Generation Building Information Model; Energy Efficient BIM (eeBIM), (2) Extraction Transformation and Loading (ETL) Tool, and (3) Information Management Platform (Data Warehouse Services).

20.2.2.1 Next Generation Building Information Model (eeBIM Model)

This is based on Industry Foundation Classes (IFC) for energy efficient building operations. The BIM specification utilising formal standard definitions (data & functions) of engineering building components (e.g. pumps, valves), systems (e.g. air handling units, heat pumps, solar panels) and sensors (temperature, relative humidity, CO_2, VOC's) as specified by professional engineering institutions CIBSE and ASHRAE is developed based on the Model View Definitions (MVD) Format of

the IFC. The IFC data exchange scenario is developed to provide exchange of BIM between Design, and Energy Simulation tools and Information Management Platform, for more information see [9].

20.2.2.2 ETL Tool

Data needs to be loaded to the data warehouse regularly. To do this, data from one or more operational systems needs to be extracted and loaded into the warehouse. The process of extracting data from source systems and bringing it into the data warehouse is commonly called ETL, which stands for Extraction, Transformation, and Loading [10]. For the proposed system the ETL tool is used to populate the fact data table which stores long term dynamic data such as measurement stream. Also, ETL Tool can be used to populate Dimensional Tables which stores relatively static data such as architectural data and building HVAC systems data [1].

The ETL process developed for this research populates fact data table by performing the following steps:

- Extracts data from the current building management system (BMS) comma separated values (CSV) file archive.
- Eliminates inconsistencies such as duplicate rows.
- Transforms the CSV file structure to the data warehouse fact data table structure.
- Loads the CSV files to the data warehouse fact data table.

Also, the ETL tool is used to populate the dimensional tables. HVAC equipment dimension, location dimension and sensing device dimension tables can be populated by extracting the data from the CAD tool. A detailed description of the ETL tool is provided by [1, 11].

20.2.2.3 Information Management Platform

The information collected from various sources needs to be processed and aggregated for the requirements of the developed tools (e.g. monitoring and intelligent control tools) and the stakeholders. This requires a multi dimensional information management platform [1].

Data warehouse systems allow a number of alternative ways to integrate and query information stored in it. Thus, a data warehouse coupled with On-Line Analysis Processing (OLAP) enables end-users to creatively approach, analyze and understand the building performance under different circumstances [1].

The data warehouse stores summarized information instead of operational data. This summarized information is time-variant and provides effective answers to queries such as “Energy consumption of a particular room in a particular building when the outside temperature is 21 °C” [1].

The aim of the data warehouse component of the proposed system is to:

1. Collect dynamic data from different sources such as wired/wireless sensors and meters.
2. Map the dynamic data with data extracted from CAD tools, energy simulation tools and performance specification tools.
3. Perform multi-dimensional data aggregation to support decision making process.

Data Warehouse component consists of three sub-components [1]. These are:

- Operational Data Store: ODS is a database designed to integrate current valued subject oriented, volatile and real time data from multiple sources such as building management system, wireless sensor network and energy unit prices.
- Fact Data and Dimensional Data: This is the main repository for long term storage of dynamic data. Data collected and temporally stored in the ODS populates the fact data table.
- Aggregated Data: This is the decision support level of the multi-dimensional data warehouse. Fact data become meaningful when it is associated with the dimensional data and provides the end user the means to "slice and dice" data.

A detailed description of the Information management platform tool is provided by Gökçe [1, 11].

20.2.3 Tool Layer

The actionable information provided by the Information Layer is utilised by the Tool Layer in order to perform various operations such as monitoring and intelligent control. Depending on the stakeholder requirements and application scenarios different types of tools (i.e. maintenance scheduling) can be developed as a modular structure. For the proposed system Monitoring and Intelligent Control tools are developed.

20.2.3.1 Monitoring Tool

The actionable information generated by the information layer is visualized through context sensitive and user friendly Monitoring Tools; Graphical User Interfaces (GUIs).

The common goal of the GUIs is to represent the building performance information to the end users (stakeholders) concerning their roles and functions. In order to achieve this, Java and SOA based interfaces are developed which enables end users automated querying without dealing with complex SQL statements [1].

Stakeholders include any person or organization that may be affected by the success or failure of the software [12].

Four principle stakeholders identified for the developed system. Their data requirements and roles are described below [1]:

- Building Owner: (a) Reviews the overall energy consumption and CO_2 emissions of facilities, (b) Reviews the energy consumption and CO_2 emissions of a particular organization, occupant or zone, (c) Generates consumption bills and audits the costs of facilities.
- Facilities Manager: (a) Monitors and analyses the building performance data with regards to particular zone, organization/occupant, building system and/or time interval, (b) Maintains optimum occupant comfort level.
- Occupant/Tenant: (a) Monitors relevant energy consumption and CO_2 emissions, (b) Views real time energy consumption costs, (c) Requests user comfort.
- Building Technician: (a) Compares actual and intended performance of building systems (HVAC Systems) in order to perform preventive maintenance activities.

20.2.3.2 Intelligent Control Tool

An Intelligent Control module which contains scenario based algorithms interacts with the defined building operation scenarios (e.g. heating, cooling, and lighting) and with the DW core to compute control parameters, which are then passed to the wireless network for actuation [1].

In order to test and validate the proposed system three initial control scenarios are determined, for more information see [1, 9, 11]. These are:

1. Energy consumption monitoring: Real time energy consumption visualization of the each energy consuming object in the building.
2. Heating system controlling: Controlling the temperatures of individual zones (rooms) via controlling wireless controllers/actuators for panel radiators in each zone (room). For example, "Maintain 24 °C of room temperature unless occupant leaves the room for longer than X amount of minutes."
3. Lighting system controlling: Controlling the lighting levels (Lux Levels) of individual zones (rooms) via controlling wireless adjustable lighting switches. For Example "Maintain 500 Lux in the room unless the room is not occupied."

20.3 Validation

In order to validate and test the proposed system in the scope of DASSEB research project, the first scenario, Data Aggregation and Representation is applied in one of the buildings of Technology Centre Hannover located in Hannover Germany. The sample building is a social housing tower block. The building has 12 floors including a single basement.

The following steps are undertaken to apply the Data Aggregation and Representation scenario:

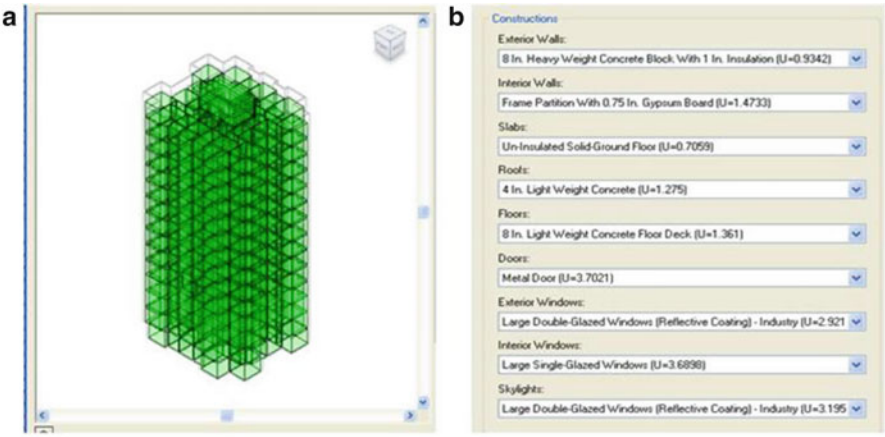

Fig. 20.2 (**a**) Setting heating and cooling loads and (**b**) Setting building element construction

(1) Building and building systems are modelled using Autodesk Revit [13], (2) Building energy performance is simulated using the energy simulation tool EIS, (3) Wireless devices and wireless sensor and actuation network (WSAN) are deployed, and (4) Information Management Platform is implemented in the building (Fig. 20.2).

20.3.1 Possible Energy Saving Improvements

Based on the deployment of a WSAN and the information provided by the BIM, results of the case study have demonstrated possible energy saving improvements that can be applied:

- Centralized Heating Plant: On large mixed use developments, as in our case the diversity which can be applied to heating is as low as 12–15 %. For example if one home required a maximum load of 10 kW heating, then 100 homes would only require 120–150 kW of the central plant, not 1 MW.
- Centralized Ventilation: This could be implemented but requires too much vertical ventilation space. Also, ownership and maintenance issues would cause complexities.
- Heat Recovery: Air to air heat recovery devices can retain up to 75 % of heat. These devices are not as efficient in summer because of the lower temperature difference between internal and external air.
- Night Purge: This works by allowing cooler night air to naturally enter a space and remove heat from the building. The very heavy thermal mass of the building can be utilised for free cooling of buildings in summer. The construction of the building is already suited to this.

- Solar Thermal Heating: The panels on the roof and the shades on south facing facades could provide a sizable amount of hot water requirements for domestic washing and cleaning. These panels are economically viable and should also prove useful in Turkey.
- Photovoltaic: This could be utilised for electricity generation in Turkey with relatively longer sunshine hours and opportunity to sell the surplus energy back to grid (€28 cent per kWh).

20.4 Conclusions

The Interoperable ICT platform for energy efficient smart buildings described in this research enables a continuous assessment process throughout the BLC by combining the data from different sources and phases in a single data repository. A single data warehouse processing geometrical, material, simulated and real time data provides enhanced decision making capabilities to the stakeholders. Model editors and simulation tools with industry standardised interoperability capabilities provide a dynamic information flow for efficient building operations. The case study demonstrates the potential of the proposed system. Based on initial results, it enabled continuous building energy analysis from design through building operation. Also, the results lead to possible energy saving improvements.

As an extension to our current research we are integrating off-the-grid building energy generating systems (e.g. solar panels) with electricity grids to optimize the consumption by considering energy usage patterns of the occupants [14]. As a secondary function It also can feed information to the diagnosis activities regarding control problems (i.e., the control system is not behaving as expected), as well as the Maintenance Management System, to request repairs of known faults. The developed system will be further expanded to predictive control. Through the implementation of knowledge discovery (KDD) and data mining methodologies, the data aggregated within the DW core can be used to discover predictive patterns such as the user preferences and the weather predictions.

References

1. Gökçe HU (2010) Multi-dimensional analysis of building performance data for energy efficient building operation. PhD thesis. National University of Ireland, Cork, Ireland
2. EC-European Commission (2007) New EU energy plan-more security, less pollution. http://ec.europa.eu/news/energy/070110_1_en.htm. Accessed 21 Sept 2011
3. Itard L, Meijer F, Vrins E, Hoiting H (2008) Building renovation and modernisation in Europe: state of the art review. ERABUILD. TU Delft, The Netherlands
4. EC-European Commission (2009) Environment – climate change – emission trading system. http://ec.europa.eu/environment/climat/emission/index_en.htm. Accessed 21 Sept 2011

5. DIN (Deutsches Institut für Normung e.V.) (Herausgeber) (2007) DIN EN 15232: Energieeffizienz von Gebäuden Einfluss von Gebäudeautomation und Gebäudemanagement, Deutsche Fassung EN 15232:2007. Berlin, Germany
6. IEA-International Energy Agency (2008) CO_2 Emissions from fuel combustion. 2008 Edition
7. EOS (2012) http://www.eos-energy-solutions.de. Germany
8. Gökçe KU, Gökçe HU, Katranuschkov P (2012) IFC based product catalogue formalization for software interoperability. J Comput Civil Eng 10.1061/(ASCE)CP.1943-5487.0000194. Ranking: SCI A
9. Gökçe KU, Gökçe HU, Scherer RJ (2012) eeBIM for energy efficient building operations. Proceedings of the 14th international conference on computing in civil and building engineering, Moscow State University of Civil Engineering, Moscow, Russia, 27–29 June 2012, ISBN 978-5-93093-881-4
10. Loney K (2004) Oracle database 10 g the complete reference. Oracle Press McGraw-Hill/Osborne, California, ISBN-13: 978-0072253511
11. Gökçe HU, Gökçe KU (2014) Multi dimensional energy monitoring, analysis and optimization system for energy efficient building operations. J Sustainable Cities Soc 10:161–173, Elsevier Press
12. Marinilli M (2006) Professional java user interfaces. Wiley, New York, ISBN: 978-0-471-48696-1
13. Autodesk (2012) Revit architecture. http://www.revit.com/. Accessed 5 Mar 2012
14. Gökçe HU, Gökçe KU (2012) Integrated system architecture for optimized building operations. In: Gudnason G, Scherer R (eds) Proceedings of the 9th European conference of product and process modeling, eWork and eBusiness in Architecture, Engineering and Construction, Reykjavik, Iceland, © 2012 Taylor & Francis Group, London, 25–27 July ISBN 978-0-415-62128-1

Chapter 21
Software Interoperability for Energy Efficient Building Operations Based on the IFC Data Model Standard

Hasan Ufuk Gökçe and Kamil Umut Gökçe

Abstract The Industry Foundation Classes (IFC) object model as a standard data model which has a quite large scope is proposed as a standard approach (ISO-PAS 16730 IFC2x platform specification) to identify the specifications and enables interoperability between the AEC (Architecture Engineering and Construction) applications. Currently the majority of AEC software and system developers use IFC APIs (Application Protocols) that are capable of importing and exporting IFC/STEP files, however the IFC based applications in the energy efficiency domain has not yet well articulated. Current BEMS (Building Energy Management Systems) focus on energy performance rating of buildings is at best sporadic often consisting of an ad hoc combination of off-the-shelf building energy management systems. This ad hoc combination presents many difficulties as the BEMS is consist of a number of components utilizing various information exchange protocols that have to be integrated within the M&T software packages. However, even though various solutions have been proposed in the last years, a general approach based on an acknowledged standard is still missing. In this paper, a new integration methodology is presented, which comply with the data schema of the IFC standard. It allows for coherent integration of different information, helping to achieve the interoperability of the involved tools and services in collaborative working environments. The essence of the developed interoperability approach is in the consistent definition of partial IFC models for energy efficient building operations which have been tested in a demonstration test bed in Hannover—Germany.

Keywords Energy efficiency • Building information model (BIM) • Data Warehouse Technologies • Artificial intelligence

H.U. Gökçe (✉) • K.U. Gökçe
Department of Civil and Environmental Engineering, Faculty of Engineering, University of Alberta, Edmonton, AB, Canada T6G 2R3
e-mail: ufuk.gokce@eos-energy-solutions.de; umut.gokce@eos-energy-solutions.de

I. Dincer et al. (eds.), *Progress in Sustainable Energy Technologies Vol II: Creating Sustainable Development*, DOI 10.1007/978-3-319-07977-6_21

21.1 Introduction

Interoperability of the heterogeneous applications in the domain of energy efficiency can be best achieved by using generalized and standardized representations of the needed product and process data from various services, thereby enabling optimized and energy efficient building operations [2]. Therefore, in the last years several IT systems integrating various application domains have been developed to obtain networked-based environments. Such systems typically combine energy management systems and services thereby allowing reducing operation costs, and increasing work efficiency. However, the developed solutions largely lack generality in terms of data and process interoperability. Integration of product and process information is based on the specific internal data models of the used component systems, and not on generally applicable and hence standardized data models [2]. All this significantly decreases flexibility, multi-dimensional data analysis, and last but not least holistic system design. In spite of its promising potential, a standardized Building Information Model (BIM) based on the IFC product model of the BuildingSMART initiative is still practically unused for energy efficiency purposes, even though "the majority of AEC software developers already provide IFC APIs that are capable of importing and exporting IFC/STEP files" [3].

Furthermore the engineering and deployment aspects of current systems require extensive manual work with much trial-and-error in programming devices, composing applications from devices, deploying devices in buildings with complex radio propagation characteristics, developing data structures for data acquisition, and analyzing tasks [4] Integrated IT tool support for these activities does not exist; available tools are stand-alone products, often tied to specific standards. These existing tools neither support the exchange of information between different application stages, nor do they consider the extension of an existing wired or wireless monitoring and control systems during operation [5]. This lack of appropriate tools currently outweighs the benefit of software interoperability.

In this regard, a single combined information and communication platform would not adequately predict the consequences of the building performance behavior and the needs of the building occupant/operator to manage energy consumption efficiently [6]. In order to avoid these shortcomings, a promising approach is the implementation of a dynamic modular infrastructure based on the acknowledged standard models.

21.2 Objectives

In this paper, we address the existing gap between the data provided in the application domains and services used for energy efficient building operations on the one side and their association to the BIM data contained in the IFC model on the

other side. In this regard, we propose a new methodology that provides coherent integration of product and process information based on the IFC data model standard. This methodology supports the interoperability of the involved tools and services. The essence of this newly developed approach is in the consistent definition and use of newly developed IFC Partial Models for energy efficiency that pulls together the needed product data to provide seamless information flow through standardized product and process information.

By developing the IFC Partial Models, the management of large-scale complex networks, services and mobile applications complying with the new network and management protocols which supports seamless end-to-end network composition and service operation through sensor hardware can be facilitated [2]. Thereby a model-driven approach integrating application domains and intelligent services based on the IFC model which provides monitoring, analysis and control of performance, with regard to energy usage, at all stages of the buildings' lifecycle can be developed. In order to address this aim, a project namely "DASSEB—Dynamic System Architecture for Energy Efficient Building Operations" which is supported by the Scientific and Technological Research Council has been granted in 2010 and the developed concept has been tested on a sample building in Hannover Germany.

21.3 Background

In the last decades, various research and development initiatives have examined heterogeneous integration of software and hardware systems to create user-sensitive, networked-based environments for inter organizational collaborations which complement context-based managerial views coupled with the IFC model data standard. This research initiatives include Process Matrix approach, based on an extended application of Generic Process Protocol coupled with the dedicated use of the Unified Modeling Language [7], IFC-compliant integrated AEC systems using smart objects [8], process oriented information modeling methodology for IFC model development [9] and the development of product model based processes and data exchange procedures in the ProIT project, compiling design guidelines necessary for product modeling and establishing model structures for the re-use of product libraries [10]. However, the goal of lossless, incremental data flow through different application systems which would allow seamless system integration is still not fully articulated. This can be changed by switching to a more structured way of defining partial models, as suggested in the BLIS project [11]. BLIS developed concepts allowing to start with the high level IFC classes, such as IfcWall, IfcBeam etc., which are then detailed step by step to reach the low level classes related to geometry, material, and various systemic properties. Accordingly, in this approach a partial model can be defined in two ways: (1) generally, by using an engineering ontology representing the content of the targeted product data model, and (2) specifically, by mapping the general view to an existing release of the product data

model e.g. IFC2x3 [12]. A set of diagrams and form sheets are used to improve comprehensibility and maintenance. However, the definitions developed in such a way are not directly applicable as data queries.

21.4 Integration Methodology

In order to realize software interoperability for energy efficient building operations in this research, a principal methodology for creating IFC Partial Models and their binding to requirements through functional parts have been developed as part of the Information Delivery Manual (IDM) [13]. Furthermore a comprehensive study of the current IFC model has been conducted to reveal entities, attributes and relations covered by IFC with regard to identified information resources. This study identifies gaps and suggests the associated modifications and re-structuring needs. The relevancies of the information resources in relation to IFC objects are examined according to IFC model requirements. This examination provides a mapping between the information resources and the IFC classes. An information resource defines one to several partial IFC classes. Usually product model classes cannot be used as single entities, but they are embedded in a network of classes defined as IFC Concepts [2].

Overall, the grouping of IFC Concepts enables the implementation of adaptable IFC Partial Models (Views) that are required for standardized system integration. The aim in forming a concept is to obtain a clear definition and reuse ideas and software code [14]. In our approach, IFC Partial Models and IFC Concepts are defined by using the General Model Subset Definition schema, GMSD [15, 16]. GMSD is a schema which allows a neutral definition format for different types of data exchange as well as client/server implementations. It has the ability to define generic views as well as specifically needed model subsets formally.

21.5 Developing an IFC Partial Model for Energy Efficient Building Operations

In order to identify the basic content of the IFC Partial Models (IFC Views) for energy efficient building operations based on IFC 2x3 version (IFC 2x3 ISO/PAS 16739), all required attribute values and objects' possible relationships have to be modeled to support the identified requirements. High level requirements' mapping to IFC views are illustrated in Fig. 21.1.

In this regard, each requirement related with the application domains and services has been considered. These requirements (as primary keys) lead to a respective structuring of related IFC classes (as foreign keys). The primary key of the given relational table uniquely identifies each requirement. It is an attribute that

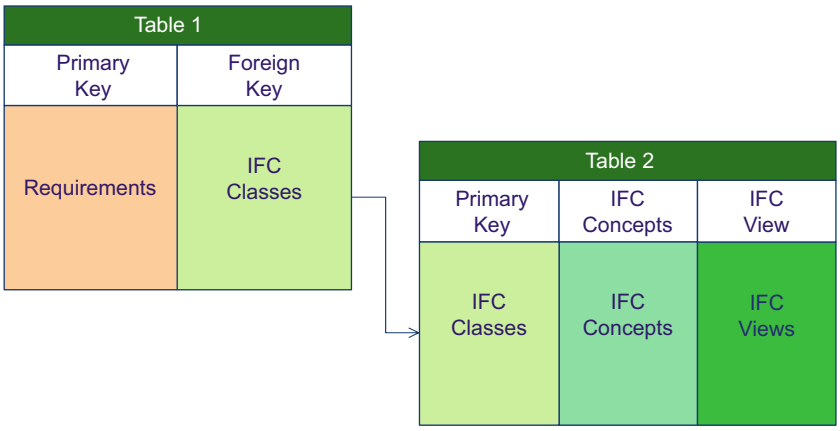

Fig. 21.1 Table formalization from requirements to IFC view formalizations

is guaranteed to be unique or it can be generated as a globally unique identifier. Primary keys consist of a single attribute or multiple attributes in combination. The foreign key identifies a column or a set of columns in one (referencing) table that refers to a set of columns in another (referenced) table. The columns in the referencing table must be the primary key in the referenced table. The values in one row of the referencing columns must occur in a single row in the referenced table. In our case, the formulated IFC classes (as primary keys) are brought together under IFC Concepts. These concepts are gathered to provide the related IFC Partial Model definitions for energy efficient building operations. Different parts of the IFC product data model are provided as IFC Concepts. An IFC Concept is a grouping of an IFC model subset so that one IFC Concept describes an object, such as a building element's objects, certain specific characteristics or bundled properties [10].

In this context, IFC Concepts are developed based on the proposed IFC Model View Definition Format [17] of the BuildingSMART initiative. Based on the collected IFC classes referenced by the requirements the concepts which are needed for the realization of the IFC Partial Models for energy efficient building operations can be provided. Each IFC Concept uses one (1:1) or many (1:n) IFC classes in its composition. On the other hand, IFC classes can be represented in one (1:1) or many (1:m) concepts to support different demands. For example in IfcClassification, arrangement of objects into classes and assignment of classification notation to objects have to be represented separately.

21.6 Requirement Analysis

The requirements needed for the IFC Partial Models for energy efficient building operation are examined based on four scenarios: (1) Data Representation and Aggregation, (2) Building Performance Analysis and Diagnostics, (3) Management of Maintenance Activities and (4) Intelligent and Predictive Building Control. These scenarios are proposed based an integrated platform suggested by [2]. The developed system architecture covers the implementation of a modular platform as depicted in Fig. 21.1, that integrates multiple dimensions of building information such as performance data (e.g. energy consumption, temperature, light), system data (e.g. status, switch settings) and process data (e.g. inspection, maintenance, repair) which supports integration concepts, holistic monitoring and analysis methodologies, life cycle oriented decision support and information and communication technologies. This is implemented as an extension to international standards (e.g. IFC 2x3 ISO/PAS 16739) (Fig. 21.2).

In this paper, the requirements associated with the first scenario Data Representation and Aggregation, and their mapping to IFC classes will be partially presented. In this context, the dynamic data collected from the network embedded systems (sensor & actuation network) and the persistent data extracted from the BIM tools (design and energy simulation tools) are stored, aggregated and represented to the stakeholders for performing multi-dimensional analysis of the building performance. The system extracts sensor data from wireless sensor/meter network via a developed middleware for WSAN. The proposed Information Management Platform is composed of: (1) Operational data store, (2) Extraction Transformation and Loading (ETL) tool, and (3) Data Warehouse core. Collected sensor/meter data is stored in the operational data store for data cleansing and redundancy

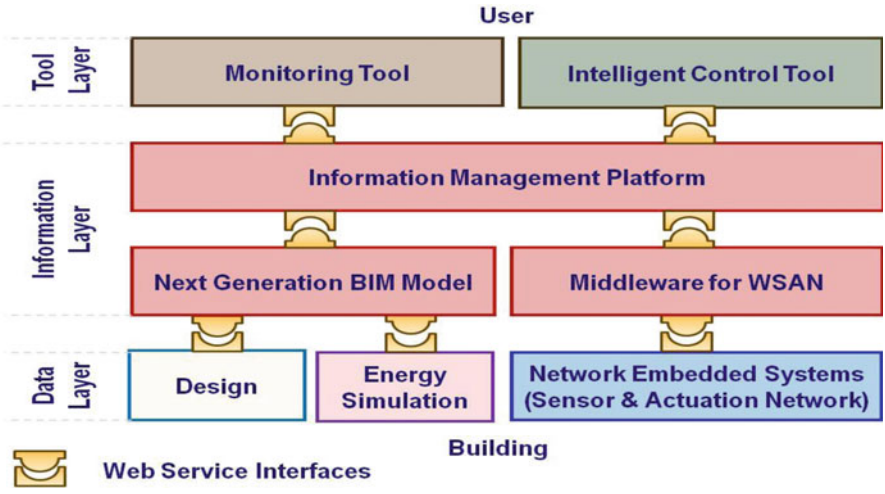

Fig. 21.2 Application layers for holistic system architecture

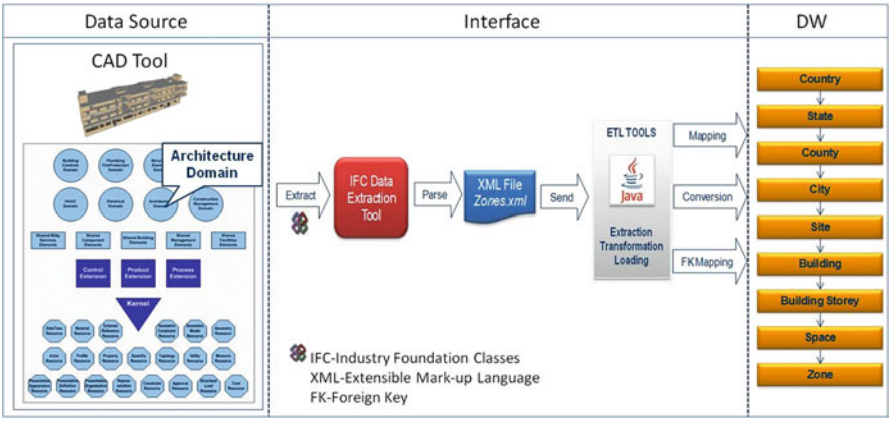

Fig. 21.3 The ETL process for populating the location dimension table

Table 21.1 Requirements mapping—location dimension to IFC classes (partial representation)

Requirements for location dimension	IFC classes referenced by the requirements for location dimension
IDs	**IfcRoot*
Building	**IfcBuilding*, *IfcBuildingStorey*
Building zones	**IfcZone*
Building spaces	**IfcSpace*, *IfcSpaceType*

check processes. This pre-processed data is loaded to the fact data section of the data warehouse system via an Extraction, Transformation, and Loading (ETL) tool. The ETL tool is also used to populate the dimensional tables by extracting data from the BIM tools as depicted in Fig. 21.3. Loaded fact data and dimensional data is aggregated with regards to different stakeholder requirements in the data warehouse core and presented through specific Graphical User Interfaces.

In this case, the IFC Partial Models can be developed based on the requirements of the dimensions such as location dimension, organization dimension, HVAC dimension and time dimension developed for complex data queries. In order to formalize the transition from exchange requirements to an IFC Partial Model definition, the information defined in these dimensions is examined with regard to the IFC data model. An established requirement can define one or several IFC Classes as given in Table 21.1.

An IFC Partial Model contains one to several IFC Classes. These classes are represented in a network of mutual inter-dependencies that collectively define IFC Concepts, specified as standard one page description of the new IFC Model View Definition Format [2]. An IFC Partial Model View comprises several IFC Concepts which define the complete set of needed IFC Classes as depicted in Table 21.2.

Table 21.2 Mapping of IFC classes to IFC concepts for IFC partial model development (partial representation)

IFC classes referenced by the requirements for location dimension	IFC concept for location dimension	IFC partial model for energy efficient building operation
**IfcRoot*	*Location concept	The integration of concepts provides the IFC partial model for energy efficient building operations
**IfcBuilding*, *IfcBuildingStorey*		
**IfcZone*		
**IfcSpace*, *IfcSpaceType*		

GMSD is used to formalize the proposed views and to explicate the respective IFC Subset Content.

21.7 Case Study

This new methodology has been applied in Hanover—Germany. The sample building is an office building. The building has 6 storeys including a basement. The following steps were undertaken to apply this scenario: (1) Building and Building systems have been modeled using building information modeling editor (Autodesk Revit), (2) Building energy performance has been simulated using the energy simulation tool (IES), (3) Wireless systems have been deployed, and (4) Data Warehouse services have been implemented based on the developed IFC Partial Models.

In this context, newly developed IFC Data Extraction Tool as depicted in Fig. 21.4 extracts the data from a source application (e.g. CAD and Simulation Tools) and loads the extracted data to the Target Application (in XML file) based on the developed partial models.

The processes of the tool involve: (1) Information instances (based on developed dimensions) in the source application (e.g. CAD and Energy Simulation Tools) are extracted by the translator, (2) Extracted data is assigned to appropriate IFC classes, (3) the entity instance data are then mapped from IFC classes into a text file format defined by the ISO-STEP Part 21 (based on developed IFC Concepts), (4) this file is then received by the other application and interpreted by the receiving application's translator in terms of the IFC object instances it represents, (5) the translator in the target application (e.g. XML File) writes the relevant IFC objects into its native data structure based on the proposed IFC partial models.

The IFC data exchange scenario depicted in Fig. 21.4 is used to provide exchange of IFC based standard data between Design, Energy Simulation tools and Data Warehouse Core.

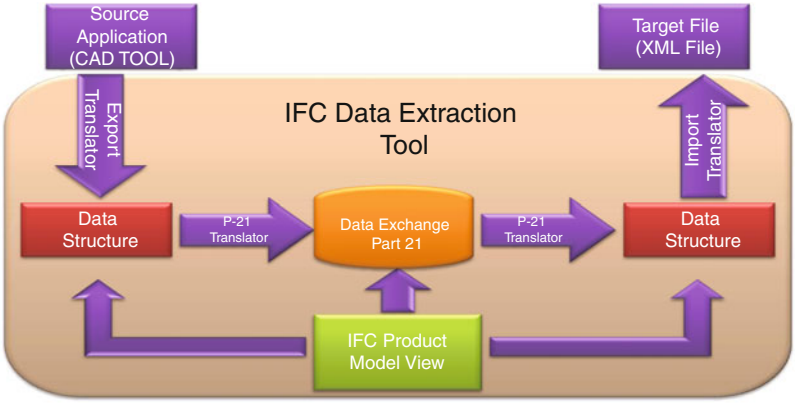

Fig. 21.4 IFC data extraction tool

21.8 Conclusions

In order to provide exchange of energy related data, based on the IFC data model standard in this work, a new methodology is proposed to develop IFC Partial Models for energy efficient building operations, which include minimal set of new IFC classes, data types and object relations. These IFC Partial Models support the exchange of energy related information based on defined requirements associated with dimensions structured in the data warehouse core.

The mapping between dimensions' requirements and IFC classes is provided. These classes are brought together in a network of classes using so called IFC Concepts. The grouping of IFC Concepts enables the implementation of IFC Partial Models. This approach leads to the development of an integration methodology for existing domain applications and intelligent services.

In order to formalize IFC Partial Models, IFC Concepts are developed based on the IFC View Definition Format of the BuildingSMART initiative. However, due to the specific requirements of our model, such as the representation of classes in EXPRESS-G, appropriate modifications are made in the formalizations.

Realization of the IFC Partial Models based on the IFC Concepts is accomplished using the General Model Subset Definition Schema (GMSD) method. Validation of the developed concepts is provided with the help of the GMSD support tools.

For applications on the field, a sample building in Hanover is used. In this context, a new IFC Data Extraction Tool is developed to extract the data from source applications (e.g. CAD and Simulation Tools) and loads the extracted data to the Target Application.

References

1. Standard: ISO 16730, – IFC2x platform specification
2. Gökçe KU, Gökçe HU, Scherer RJ (2012) eeBIM for energy efficient building operations. Proceedings of the 14th international conference on computing in civil and building engineering, 27–29 June 2012, Moscow State University of Civil Engineering, Moscow, Russia, ISBN 978-5-93093-881-4
3. Nour M (2007) Manipulating IFC sub-models in collaborative teamwork environments. In: Rebolj D (ed) W78 24th conference on information technology in construction, 'Bringing ITC Knowledge to Work,' Maribor, Slovenia
4. Gökçe HU, Gökçe KU (2014) Multi dimensional energy monitoring, analysis and optimization system for energy efficient building operations. J Sustainable Cities Soc 10:161–73, Elsevier Press
5. Gökçe HU (2010) Multi-dimensional analysis of building performance data for energy efficient building operation. Ph.D. thesis, National University of Ireland, Cork, Ireland
6. Gökçe HU, Gökçe KU, Scherer RJ (2011) Holistic system architecture for low energy building operations. Proceedings of the 10th international conference in sustainable energy technologies, Istanbul, Turkey, 4–7 Sept, ISBN: 978-605-88549-1-8
7. Katranuschkov P, Gehre A, Scherer RJ, Wix J, Liebich T (2004) User requirements capture in distributed project environments: a process-centred approach. In: Beucke K et al (eds) Proceedings of the Xth international conference on computing in civil and building engineering (ICCCBE-X)
8. Halfawy M, Froese T (2005) Building integrated architecture/engineering/construction systems using smart objects: 'Methodology and Implementation'. J Comput Civil Eng 19(2):172–181
9. Chen P-H, Wana C, Tionga RLK, Tinga SK, Yang Q (2004) Augmented IDEF1-based process-oriented information modeling. Autom Construct 13(6):735–750
10. ProIT (2004) Product model data in the construction process. © IAI International Solutions
11. Hietanen J (ed) (2002) Building lifecycle interoperable software (BLIS). http://www.blis-project.org/index2.html. Accessed July 2004
12. Gökçe KU (2008) IT supported construction project management methodology based on process and product model and quality management, Ph.D. thesis, TU Dresden, Germany
13. Wix J (ed) (2005) Information delivery and framework. Presentation at the IAI International Council in Oslo, Norway. http://www.nibs.org/FMOC/71305/2_InformationDeliveryAnd Framework.pdf
14. Gökçe HU, Gökçe KU (2013) Holistic system architecture for energy efficient building operations. J Sustainable Cities Soc 6:77–84, Elsevier Press
15. Weise M, Katranuschkov P, Scherer RJ (2003) Generalised model subset definition schema. In: Amor R (ed) Construction IT: bridging the distance, proceedings of the CIB-W78 Workshop, Waiheke Island, Auckland, New Zealand
16. Weise M, Katranuschkov P (2005) Supporting state-based transactions in collaborative product modelling environments. In: Scherer RJ, Katranuschkov P, Schapke S-E (eds) Proceedings CIB-W78 22nd conference on information technology in construction, Dresden, Institute for Construction Informatics, TU Dresden, Germany
17. Hietanen J (2006) IFC view definition format, Version 1., © 2006 IAI International Alliance for Interoperability. ISO 16793, – IFC2x Platform Specification

Chapter 22
Virtual Energy Platform for Low Energy Building Operations

Hasan Ufuk Gökçe and Kamil Umut Gökçe

Abstract In this research, a new Virtual Energy Platform is proposed to represent a new and affordable ICT platform for energy-intensive systems for low energy building operations targeting: (1) design and simulation of energy use profiles addressing energy-intensive systems, building equipments, and services, (2) intelligent and interactive management of energy consumptions via intelligent metering, monitoring and control, and (3) innovative tools for energy efficiency service provision providing continuous and accurate information to end-users and decision makers. The proposed system architecture is composed of three integrated layers: (1) data, (2) information, and (3) tool layers. For physical applications: (1) integrated design tools, (2) energy simulation tools, (3) wireless sensors and actuators, (4) wireless sensor networks, (5) middleware technologies, (6) data warehouse technologies, (7) artificial intelligence based control systems and (8) monitoring tools are addressed. The system architecture is implemented as an extension to international standards (e.g. IFC 2×3 ISO/PAS 16730). The proposed system is tested in a demonstration test-bed in Hannover, Germany.

Keywords Energy efficiency • Artificial intelligence • Wireless embedded devices • BIM

22.1 Introduction

At the moment sophisticated Building Energy Management (BEM) systems are available worldwide. Building Energy Management (BEM) aims at the effective and efficient usage of energy to maintain high building performance operation [1]. However, their focus on energy performance rating of buildings is at best sporadic often consisting of an ad-hoc combination of off-the-shelf building energy management systems [2]. The absence of compatible hardware and communication

H.U. Gökçe (✉) • K.U. Gökçe
Faculty of Engineering, Department of Civil & Environmental Engineering,
University of Alberta, Edmonton, AB, Canada T6G 2R3
e-mail: ufuk.gokce@eos-energy-solutions.de; ufuk@ualberta.ca;
umut.gokce@eos-energy-solutions.de; umut@ualberta.ca

I. Dincer et al. (eds.), *Progress in Sustainable Energy Technologies Vol II: Creating Sustainable Development*, DOI 10.1007/978-3-319-07977-6_22

protocols can become extremely problematic as seamlessly integrating these systems is an inefficient overhead.

Furthermore the engineering and deployment aspects of current systems require extensive manual work with much trial-and-error in programming devices, composing applications from devices, deploying devices in buildings with complex radio propagation characteristics, and developing data structures for data acquisition and analyzing tasks [3]. Integrated IT tool support for these activities does not exist; available tools are stand-alone products, often tied to specific standards. These existing tools neither support the exchange of information between different application stages nor do they consider the extension of an existing wired or wireless monitoring and control systems during operation. This lack of appropriate tools currently outweighs the benefit of software interoperability [4].

A promising approach to achieve a consistent structure considers the implementation of a modular platform that integrates multiple dimensions of building information such as performance data (e.g. energy consumption, temperature, light), system data (e.g., status, switch settings) and process data (e.g. inspection, maintenance, repair) which supports integration concepts, holistic monitoring and analysis methodologies, life cycle oriented decision support and information and communication technologies.

22.2 Research Objectives

This research aims to provide a holistic extensible and an integrated model driven virtual system platform to enhance the management of large-scale complex networks, services and tools. In this context new network and management protocols have been considered to develop frameworks and algorithms in order to support mixed initiative configurations for energy efficient building operations. This provides seamless end-to-end network composition and service operation through sensor and actuator hardware with dynamic features.

In order to address this aim, a project named “DASSEB - Dynamic System Architecture for Energy Efficient Building Operations” which is supported by the Scientific and Technological Research Council of Turkey was granted in 2010 and the developed concept has been tested in a demonstration test-bed in Hanover-Germany.

22.3 System Architecture

The virtual energy platform proposed for energy-intensive systems is depicted in Fig. 22.1. The developed system architecture addresses the implementation of a modular platform composed of ICT building blocks that integrates multiple dimensions of building information such as: performance data, system data and process data which supports integration concepts, holistic monitoring, analyses and control

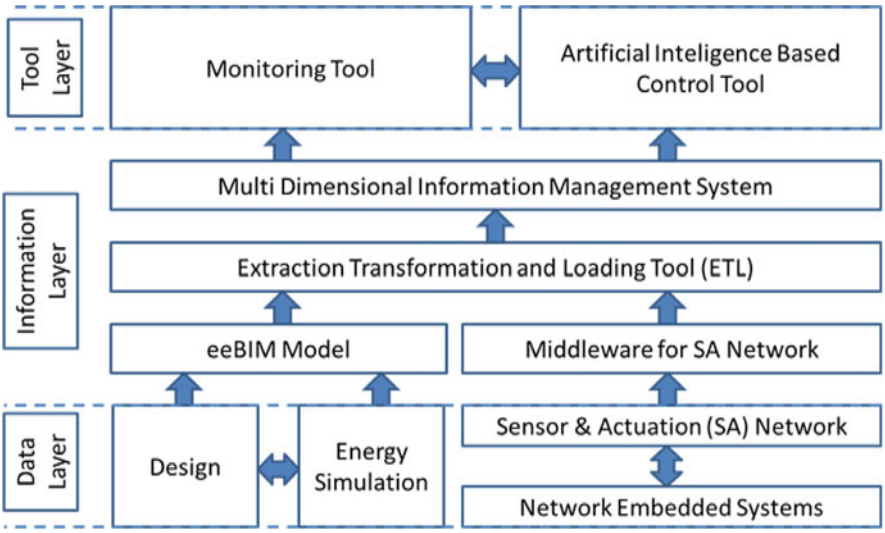

Fig. 22.1 Application layers for Virtual Energy Platform

methodologies. In the provided platform, the system architecture is implemented as an extension to international standards (e.g. IFC 2×3 ISO/PAS 16730), that complement and empower existing tools for design and operation management (FM). This allows evaluating, simulating and optimizing the energy efficiency of built facilities and facility components in variations of real life scenarios.

The Virtual Energy Platform is provided in three integrated layers.

22.3.1 Data Layer

22.3.1.1 Network Embedded Systems: Wireless Sensor and Actuation (SA) Network

(1) Sensors, (2) Actuators.

Network Embedded Systems & SA Network research addresses the development of wireless sensing infrastructure with novel miniaturized sensor nodes. The main aim is to specify self-configurable, self-optimized, and self-healed wireless sensor infrastructures.

22.3.1.2 Model Editors

(1) Design, (2) Energy Simulation.

The existing off the shelf design and energy simulation tools, are used to provide 4D design, energy simulation models and associated interfaces.

22.3.2 Information Layer

22.3.2.1 eeBIM (Building Information Model for Energy Efficiency)

(1) Building Product Model (IFC), (2) Building Performance Model (IFCExt).

- A new product and process partial model specification "eeBIM" is proposed utilizing formal standard definitions (data & functions) of engineering building components (e.g. pumps, valves), systems (e.g. Air handling units, heat pumps, solar panels) and sensors (temperature, relative humidity, CO_2, VOC's) as specified by professional institutions CIBSE and ASHRAE.
- The proposed eeBIM partial model is developed based on an ISO standard data model (Industry Foundation Classes (IFC) ISO16730) that facilitates seamless interoperability of the BIM with upstream activities that include information management platform and downstream activities that include communication with the design and energy simulation models.

22.3.2.2 Middleware for Sensor and Actuation Network (SA)

- A prototype of an embedded web-service based middleware is addressed to enable the wireless sensor/actuator network to interact with the information management platform via web-service protocols.

22.3.2.3 Extraction Transformation, Loading Tool

- Extraction, Transformation, Loading Tool (ETL) is developed to support integrated system applications. In this research, the proposed ETL Tool can extract, transform and load required data from heterogeneous models and applications i.e. sensed data from SA network, 4D building and energy simulation models from CAD and energy simulation tools to be used in information management platform.

22.3.2.4 Information Management Platform

- Data warehouse core is addressed that stores summarized information instead of operational data. This summarized information is time-variant and provides effective answers to queries such as "Energy consumption of a particular room in a particular building when the outside temperature is 21 °C." [5]. The aim of the data warehouse component of the proposed system is to: (1) Collect dynamic data from different sources such as wired/wireless sensors and meters; (2) Map the dynamic data with data extracted from CAD tools and energy simulation tools; (3) Perform multi-dimensional data aggregation to support decision making process.

22.3.3 Tool Layer

22.3.3.1 Monitoring Tool

- A monitoring tool is developed to perform building performance monitoring enabling more efficient performance analysis. This is achieved based on a Java based interface which enables end users easy querying without dealing with complex SQL statements.

22.3.3.2 AI Based Control Tool

- An artificial intelligence (AI) based control tool is addressed which optimizes user comfort and energy efficiency, based on preference-based control system. The learning algorithms which will be used to estimate the expected occupant comfort degree based on a database of previous responses is researched.

22.4 System Components

The complexity of the proposed platform requires scenarios. In this context four scenarios are developed: (1) Data Aggregation and Representation, (2) Building Performance Analysis and Diagnostics, (3) Management of Maintenance Activities, and (4) Intelligent Building Control.

In this paper, the details associated with the first scenario, Data Aggregation and Representation is presented. In this case, the dynamic data collected from the wired/wireless sensor/meter network and the persistent data extracted from the BIM tools should be stored, aggregated and represented to the end-users for performing multi-dimensional analysis of the building performance. The system extracts sensor data from building management systems and from the wireless sensor/meter network. Collected sensor/meter data is stored in the operational data store for data cleansing and redundancy check processes. This pre-processed data is loaded to the fact data section of the data warehouse system via an Extraction, Transformation, and Loading (ETL) tool. Simultaneously, data gathered from the building information model is loaded to the dimensional data section of the data warehouse. Loaded fact data and dimensional data is aggregated with regards to different stakeholder requirements in the data warehouse system and presented through specific Graphical User Interfaces [5]

The first scenario addresses: (1) Model Editors (development of eeBIM partial model), (2) Network Embedded Systems, (3) Wireless Sensor & Actuation Network, (4) Information Management Platform, (Middleware for SA networks, ETL tool and Data Warehouse Services), and (5) Monitoring Tool.

22.4.1 Model Editors

In this context, two model editors have been considered as: (1) Design Tool to develop BIM Model, and (2) Energy Simulation Tool to develop Energy Simulation Model.

22.4.2 Design Tool: Building Information Model

The design tool provides the 3D Building Information Model (BIM) for the energy simulations and the information management platform. The required information is formed based on the IFC View for eeBIM (partial IFC model for energy efficient building operations), (for details see [6]). In our case, four different Computer Aided Design (CAD) systems have been considered and their capabilities have been analyzed: (1) Autodesk Revit, (2) Microstation, (3) ArchiCAD, and (4) DDS-CAD. The interoperability of these tools with other software tools has been examined. In particular the Industry Foundation Classes (IFC) compatibility is researched. In terms of IFC, all CAD systems are compatible with the latest version of IFC2×3. From an interoperability perspective, all CAD systems claim to offer some form of import/export functions between systems. In this regard, Autodesk Revit has been chosen which is composed of Revit Architecture and Revit MEP (Mechanical Electrical and Plumbing). Autodesk Revit Architecture [7] is a 3D drawing tool which encompasses all the information aspects necessary to cover the lifecycle of a building. This allows for intelligent, 3D and parametric object-based design [7]. In this way, Revit provides full bi-directional associative integration. A change anywhere is a change everywhere, instantly, with no user interaction to manually update any view. Revit MEP is specialized specifically for design and documentation of building services [7]. It combines all of the tools and capabilities of Revit Architecture with realistic and detailed building services equipment. An important feature of Revit MEP is the availability of product libraries which contain families of accurate parts and equipment used for construction [7].

22.4.3 Energy Simulation Tool: Energy Simulation Model

Current Energy Simulation tools can be used to model and predict building energy performance. With the proposed Virtual Energy Platform in this research, it is possible to compare the design intent and actual energy performance data which supports calibration of BIM models. For this purpose, the Integrated Environmental Solutions (IES) plug-in which provides energy simulations on the Revit MEP Model has been chosen. IES is an energy simulation software package [8]. IES's

Revit plug-in Toolbar allows Revit Architecture and MEP to import a 3D BIM model into IES's software and undertake energy and thermal analysis [8]. Information is required regarding building type, construction materials, and heating and cooling system types which are determined in the IFC View for eeBIM model specified in the information management platform. Once the model is established, all IES performance analyses are accessible for the model. While Revit has excellent drafting and 3D modeling properties, and often plays a central role in projects, it currently does not perform its own energy simulation. Rather, it relies entirely on IES. Therefore, from an energy simulation point of view, the use of Revit MEP cannot be justified. In this sense, it's only function is to create the building geometry and properties before exporting to IES [4].

22.4.4 eeBIM: Partial IFC Model for Energy Efficient Building Operations

The output of 3D BIM and Energy Simulation models combined in "eeBIM" partial IFC model. The required data is specified based on the (1) developed energy management sub-schemas, and (2) dimensions developed in the information management platform addressing different requirements (for details see [6]). The partial IFC model omits object classes that are not relevant for the targeted energy requirements. These requirements defined based on data queries for different systems and stakeholders complying with the formal standard definitions.

22.4.5 Wireless Sensor and Actuation Network

A Wireless Sensor & Actuation Network (WSAN) consists of spatially distributed autonomous devices using: (1) sensors and (2) actuators, in order to monitor and control the physical environment at high resolution. The sensors, also called motes are installed in particular locations or can be sprayed in a particular zone to gather information such as temperature, humidity, CO_2, and Lux level. The real functionality of these sensors and actuators is demonstrated when they start communicating with each other within wireless sensor & actuation networks. WSAN can shuffle the information collected through the sensors and transfer it to the public internet and or a local area network. Finally, the information is collected in the data warehouse where it is analyzed, are used to manage and control zones with installed actuators on specific systems, tools, components e.g. on windows, doors, home appliances.

22.4.6 Wireless Sensor Network Design for Prototype Development

Wireless systems are composed of wireless sensors, meters, and actuators, on top of which rests a wireless network platform. In this research the wireless sensor network architecture is developed based on recently released IETF 6LoWPAN (RFC 4944) open standard for IP communication over low-power radio links – IEEE 802.15.4. LoWPAN networks are connected to other IP networks through one or more border routers forwarding information packets between different media including Ethernet, Wi-Fi or GPRS. The IP architecture offers widespread commercial adoption and broad interoperability due to its openness, flexibility, scalability and manageability. A number of industrial standards, including BACNet, LonTalk and CIP, introduced an IP using either TCP/IP or UDP/IP over Ethernet.

22.4.7 IEEE 802.15.4 Sensor Nodes Forming 6LoWPAN Network

Wireless sensors can be developed to detect and measure various parameters such as temperature, humidity and water/gas/electricity meter readings. A sensor node in a network, called a mote, mainly consists of three components: the sensor interface, which measures the physical attributes such as the humidity level; the radio interface, which communicates with other motes; and the CPU, which performs computations and transfers information between the two components. The used board in our case is equipped with an Atmega1281 MCU and EM2420 radio chip. The platform includes sensors for monitoring air–temperature, air–humidity and light. Moreover the platform incorporates electricity meters as well as the interface for controlling (on/off) an AC load are utilized. The platform runs the recently released b6LoWPAN stack.

22.4.8 IEEE 802.11 Gateways as 6lowPAN/IPv6 Routers

Soekris embedded PC boards [9] with Atheros CM9 Wi-Fi cards and a single IEEE802.15.4 node form a backbone network spanning all the rooms of the test building. Soekris net4521 is a compact, low-power, low-cost computer based on a 133 MHz 486 class processor which supports power over ethernet (PoE). These features make Soekris an attractive solution when selecting a wireless communication backbone for the sensor networks. It has also been optimized for use as wireless router and has been designed for FreeBSD, NetBSD, OpenBSD and Linux.

22.4.9 Middleware for Sensor and Actuation Network (SA)

Middleware is a software layer that lies between the operating system and applications on each side of a distributed computing system in a network [10]. Middleware is especially integral to modern information technology based on XML, SOAP, Web services, and service-oriented architecture. Service-Oriented Architecture (SOA) is an approach to organize IT resources and data collectively in order to enable integration between different technologies and allow for standardized data interaction [11]. SOA focuses on interoperable, robust, reusable, and compassable services that abstract the application functionality and data of each technology. Two important aspects of implementing a successful SOA are Web Services and Ontologies. While Web Services are partially integrated in Building Management Systems a consistent SOA is still missing [12–15]. Modern information management technologies allow reducing the parameterization effort, thus capable to respond to complex query profiles required for sophisticated decision support. However, the specific content is to be imported from other data sources such as BIM, WSAN and even existing Building Energy Management Systems for data analyses to represent the building energy performance data. In our case, a prototype of an embedded web-service based middleware is addressed to enable the wireless sensor/actuator network to interact with the information management platform via web-service protocols. The proposed middleware platform aggregates the required data via web-service protocols. The integrated model to ensure consistency across the system's interfaces and middleware services provided.

22.4.10 Extraction Transformation and Loading Tool

Data needs to be loaded to the data warehouse regularly [3]. In order to do this, data from one or more operational systems needs to be extracted and loaded into the warehouse. The process of extracting data from source systems and bringing it into the data warehouse is commonly called ETL, which stands for Extraction, Transformation, and Loading [16]. For the proposed system, the ETL tool is used to populate the fact data table which stores long term dynamic data such as the measurement stream. Also, the ETL Tool can be used to populate Dimensional Tables which stores relatively static data such as architectural data and building HVAC systems data [5]. The ETL process developed for this research populates the fact data table [5];

- Extracts data from the current building management system (BMS) comma separated values (CSV) file archive,
- Eliminates inconsistencies such as duplicate rows,
- Transforms the CSV file structure to the data warehouse fact data table structure,
- Loads the CSV files to the data warehouse fact data table.

Also, the ETL tool is used to populate the dimensional tables which can be populated by extracting data from the CAD tool.

22.4.11 Information Management Platform (Data Warehouse Services)

The proposed system enables continuous monitoring to tune building systems for optimal comfort and peak efficiency based on current operational requirements. As a result, the holistic N-dimensional information management system, which is supported by data warehouse technology to provide required tools and methods for building performance monitoring, enables more efficient performance analysis and dramatic energy savings [5]. In this case, the Information Management Platform is structured based on the Data Warehouse Core.

22.4.12 Data Warehouse Core

Data warehousing systems provide a number of alternative ways to integrate and query stored information. Thus, a data warehouse coupled with On-Line Analysis Processing (OLAP) enables end-users to creatively approach, analyze and understand the building performance under different circumstances [5]. The data warehouse stores summarized information instead of operational data. This summarized information is time-variant and provides effective answers to queries such as "Energy consumption of a particular room in a particular building when the outside temperature is 21 °C." [5].

The aim of the data warehouse component of the proposed system is to:

- Collect dynamic data from different sources such as wired/wireless sensors and meters.
- Map the dynamic data with data extracted from CAD tools, energy simulation tools and performance specification tools.
- Perform N-dimensional data aggregation to support the decision making process.

The Data Warehouse component consists of three sub-components [5]:

- Operational Data Store: ODS is a database designed to integrate current valued subject oriented, volatile and real time data from multiple sources such as the building management system, wireless sensor network and energy unit prices.
- Fact Data and Dimensional Data: This is the main repository for long term storage of dynamic data. Data collected and temporally stored in the ODS populates the fact data table.

- Aggregated Data: This is the decision support level of the multi-dimensional data warehouse. Fact data become meaningful when it is associated with the dimensional data and provides the end user the means to "slice and dice" data.

22.4.13 Monitoring Tool

The common goal of the Monitoring Tool is to represent the building performance information to the end users in regards to their roles and functions [2]. The aim is to design and implement a user friendly Graphical User Interface (GUI). In order to achieve this, a Java based interface is developed which enables end users to query without dealing with complex SQL statements. Also, this GUI can represent query results both in graphical format and/or tabular format according to the end user's preference. There are two main utilization scenarios considered for the system, performance monitoring and on-site diagnostics, resulting in the application of two different types of user interfaces: (1) Desktop Application for performance evaluation (2) Mobile Application for facility management and building diagnostics.

22.5 Case Study

The first scenario, Data Representation and Aggregation has been currently in validation in Hanover – Germany. The sample building is an office building. The building has 5 storeys including a basement. The following steps were undertaken to apply this scenario: (1) Building and Building systems have been modeled using building information modeling editor (Autodesk Revit); (2) Building energy performance has been simulated using the energy simulation tool (EIS); (3) Wireless sensors and actuator have been deployed in two rooms for comparison purposes; and (4) Data warehouse services have been implemented.

22.6 Possible Energy Saving Improvements

Based on the deployment of a WSAN and the information provided by the BIM, results of the case study have demonstrated possible energy saving improvements that can be applied:

- Centralised Heating Plant: On large mixed use developments, as in our case the diversity which can be applied to heating is as low as 12–15 %.
- Centralised Ventilation: This could be implemented but requires too much vertical ventilation space. Also, ownership and maintenance issues would cause complexities.

- Heat Recovery: Air to air heat recovery devices can retain up to 75 % of heat. These devices are not as efficient in summer because of the lower temperature difference between internal and external air.
- Night Purge: This works by allowing cooler night air to naturally enter a space and remove heat from the building. The very heavy thermal mass of the building can be utilised for free cooling of buildings in summer. The construction of the building is already suited to this.
- Solar Thermal Heating: The panels on the roof and the shades on south facing facades could provide a sizable amount of hot water requirements for domestic washing and cleaning. These panels are economically viable and should also prove useful in Germany.
- Photovoltaic: This could be utilised for electricity generation in Germany with longer sunshine hours and opportunity to sell the surplus energy back to grid.

22.7 Conclusions

The European directive EPBD (Energy Performance Building Directive 2002/91/EC-2006/32/EC) requires a dramatic change in the way buildings are analysed [4]. Current building performance analysis focuses on assessment at earlier stages of the building life cycle (BLC) with less analysis at the later stages of operation and maintenance. The Virtual Energy Platform for Energy Efficient Buildings described in this research enables a continuous assessment process throughout the Building Life-cycle by combining the data from different sources and phases in a single data repository. A single data warehouse processing geometrical, material, simulated and real time data provides enhanced decision making capabilities to the stakeholders. Model editors and simulation tools with industry standardized inter-operability capabilities provide a dynamic information flow for efficient building operations. The test bed demonstrates the potential of the proposed system. Based on initial results, it enabled continuous building energy analysis from design through building operation. Also, the results lead to possible energy saving improvements. Finally, the system maintains the basis for: improving building performance, developing intelligent control routines, and implementing fault diagnosis measures.

References

1. Capehar BL, Turner WC, Kennedy WJ (2008) Guide to energy management. Fairmont Press, Lilburn, GA
2. Gökçe HU, Gökçe KU (2013) Integrated system platform for energy efficient building operations. J Comput Civil Eng, 10.1061/(ASCE)CP.1943-5487.0000288 (5 Jan 2013). Ranking: SCI A

3. Gökçe HU, Gökçe KU (2013) Holistic system architecture for energy efficient building operations. J Sustainable Cities Soc 6:77–84. Elsevier Press
4. Gökçe HU, Gökçe KU (2014) Multi dimensional energy monitoring, analysis and optimization system for energy efficient building operations. J Sustainable Cities Soc, 10:161–173. Elsevier Press
5. Gökçe HU (2010) Multi-dimensional analysis of building performance data for energy efficient building operation. PhD Thesis, National University of Ireland, Cork, Ireland
6. Gökçe KU, Gökçe HU, Katranuschkov P (2012) IFC based product catalogue formalization for software interoperability. J Comput Civil Eng, 10.1061/(ASCE) CP.1943-5487.0000194. Ranking: SCI A
7. AUTODESK (2012) Revit architecture. www.revit.com, Accessed 21 April 2012
8. IES (2011) IES. www.iesve.com, Accessed 18 Dec 2011
9. SOEKRIS (2011) Soekris board. www.soekris.com, Accessed 28 Aug 2011
10. Krakowiak S (2005) What's middleware?. ObjectWeb.org. http://middleware.objectweb.org/. Accessed 14 Jun 2011
11. Mensah K (2005) Oracle Database Programming Using Java and Web Services. Digital Press. ISBN-13: 978-1555583293
12. Wang S, Xie J (2002) Integrating building management system and facilities management on the internet. Autom Constr 11(6):707–715, Elsevier
13. Wang S, Xu Z, Cao J, Zhang J (2007) A middleware for web service-enabled integration and interoperation of intelligent building systems. Autom Constr 16(1):112–121
14. Jang W, Healy WM, Skibniewski MJ (2008) Wireless sensor networks as part of a web-based building environmental monitoring system. Autom Constr 17(6):729–736
15. Malatras A, Asgari A, Baugé T, Irons M (2008) A service-oriented architecture for building services integration. J Facilities Manag 6(2):132–151, Emerald Group Publishing Limited
16. Loney K (2004) Oracle Database 10g The Complete Reference, California: Oracle Press McGraw-Hil/Osborne. ISBN-13: 978-0072253511 2004

Chapter 23
The Studies of Environmental Ionizing Radiation Curriculum Indicators for Taiwan's Elementary and Junior High School

Chien-kuo Ku and Cheng Da Wu

Abstract This studies aims at constructing environmental ionizing radiation curriculum indicators for Taiwan's elementary and junior high school, and providing guidelines for schools and education administration to promote ionizing radiation curriculum. This studies utilizes Fuzzy Delphi and Analytical Hierarchy Process to undertake two stages of questionnaires, compile opinions and views from 25 experts, in order to construct environmental ionizing radiation curriculum indicators. Research results shows: (1) Utilizes Fuzzy Delphi and selected 36 evaluation indicators under five levels of "knowing radiation", "the application of radiation in daily life", "the monitor of ionizing radiation", and "emergency measures for nuclear accidents". (2) Utilizes Analytical Hierarchy Process to decide the priority of the environmental ionizing radiation curriculum indicators.

The structure of ionizing radiation curriculum indicators and opinions made by experts in questionnaires are referred, and summed up some key elements to implement. For Taiwan elementary and junior high schools, they can refer to environmental ionizing radiation curriculum indicators, in order to develop and evaluate the implementation and effectiveness. The priority can be referred when select the topics.

Keywords Ionizing radiation • Curriculum indicators • Fuzzy Delphi

C.-k. Ku (✉)
Department of Applied of Physics and Chemistry, University of Taipei, Taiwan, No.1, Ai Kuo West Road, Chung Zheng District, 10048 Taipei, Taiwan
e-mail: 2007ckku@gmail.com

C. Da Wu
Department of Applied of Physics and Chemistry, Ming Zhi Elementary School, Tai Shan Area, New Taipei, Taiwan
e-mail: wuta@mail.mjes.ntpc.edu.tw

I. Dincer et al. (eds.), *Progress in Sustainable Energy Technologies Vol II: Creating Sustainable Development*, DOI 10.1007/978-3-319-07977-6_23

23.1 Foreword

Since the discovery of X ray, radiation is closely connected with human daily life. In fact, radiation is always surrounded, but people are just unaware about that, and we even enjoy some service brought by the radiation.

In March 11, 2011, Japan occurred huge earthquake at local time 1426, which induced tsunami, and Fukushima's nuclear incidents. As Taiwan is only a few hundred miles from Japan, it certainly caused panic among Taiwan people toward ionizing radiation. Therefore, how to plan for the environmental ionizing radiation education, understanding natural radiation and man-made radiation, increase the knowledge of prevention and protection of nuclear incidents, integrate into schools' curriculum and provide people with knowledge of ionizing radiation, become an urgent education task.

Atomic Energy Council, Executive Yuan has indicated radiation prevention and protection, nuclear safety, radioactive material, nuclear incident emergent measures, knowing atomic energy law and environmental radiation monitor are the major education campaign. Taipower Company has also listed items like natural background radiation, radiation regulations, radioactive emission control, radiation monitor items and range, radiation monitor results and radiation monitor quality as important announcement content.

As New Taipei City has located first nuclear plant, second nuclear plant, and fourth nuclear plant which is going to be operated soon, therefore new Taipei city government is especially concerned about related prevention and safety mechanism and educational campaign. Thus, in the official disaster webpage, it introduced Japan earthquake, tsunami, nuclear disaster related issue Q&A, what to do during nuclear accidents, and temporary shelter in the education campaign site. It also established nuclear energy zone, provided the introduction of emergency measures during nuclear accidents, and nuclear energy Q&A, and even used online link to provide nuclear education transparent data system, to let the public understand radiation and nuclear energy related information.

Therefore, the research purpose is to construct the range and learning indicators of environmental ionizing radiation curriculum, based on the six main factors promoted by the Energy Atomic Council, Executive Yuan, collect related literature to construct elementary and high school environmental ionizing radiation curriculum indicators, and provide references for the educational administration in terms of implementation and goals of implementation.

The main purpose of the research:

- Understanding content and implementation factors of local and international environmental ionizing radiation curriculum indicators.
- Constructing the promotion and implementation items of environmental ionizing radiation curriculum in elementary and high schools.
- Exploring the priority relationship between the promotion and implementation of environmental ionizing radiation curriculum.

23.2 Introduction

Since our environment is full of radiation, and affect our life, such as agricultural products, watches, clocks, smoke detectors and other daily articles, and even industry application, and environmental protection application [1–3]. This society is inevitable with the radiation. Therefore the radiation is existed in the society. The public should have the right and obligation to know more about radiation. The topics that contain in local and international environmental ionizing radiation curriculum are compiled in Table 23.1.

In order to let people understand, the content has to be adjusted. Therefore, this paper outlined the related indicators from simple to difficult, to construct environmental ionizing radiation curriculum indicators in a systematic way. And below is the implementation of local and international environmental ionizing radiation curriculum (Table 23.2).

23.3 Research Method

The research utilizes Fuzzy Delphi and AHP [13–16], which consult experts regarding some topics to make some prediction. At the same time, related literature is analyzed, school environmental education indicators are referred, and a compilation of the curriculum indicators structure is completed. And the research utilized Fuzzy Delphi questionnaires to obtain opinions from 25 scholars and experts, and integrated the first stage of results, and utilizes Analytical Hierarchy Process to decide the priority and comparative priority of each evaluation indicators. The research procedure is as follows (Fig. 23.1):

23.4 Research Results and Discussion

- Fuzzy Delphi and calibration analysis
  The first stage of expert questionnaire is based on Fuzzy Delphi, and also the concept of triangle fuzzy to select the curriculum indicators of environmental ionizing radiation indicators, which is a total of 35 indicator items. In the first stage of questionnaire, there is one to ten selection items according to priority, and also adding "not agree" as evaluation item, so that expert's opinions should be more complete. In the first stage of questionnaire, the average score of disagree opinion is 1, which is 4 % of all experts. The setting of the research original evaluation indicators are the minimum score for fuzzy value 6.3894, geometric average score of 8.1787, and maximum score 9.2660, and created a triangle fuzzy value Wwk = (6.3894, 8.1787, 9.2660), and used center of gravity to turn into single value Sk = 7.9447, as the threshold for self evaluation

Table 23.1 Compilation of environmental ionizing education related literature review

Scholars/experts	Environmental ionizing radiation curriculum
Bao-Shan, Ong [4]	Provide reference and teaching material for "Radiation Application" senior course. Radiation education should include: 1. The measurement and quantity of radiation 2. Biology effectiveness and prevention standard 3. The source of natural radiation 4. The kinds of natural radioactive and radiation 5. The application of natural radiation. 6. The source of medical used radiation. 7. The study of radiation source. 8. Nuclear plants and radiation safety. 9. The industry application of radioisotope. 10. Other application of radioisotope. 11. X-ray camera technique. 12. The concept of neutron camera technique and industry application.
Tian-ge Wang [5]	Topics of books about atomy, nuclear and radiation which are targeting youngsters are as follows: 1. What forms the world. 2. The mystery of radiation. 3. Mysterious world. 4. Nuclear era. 5. What do you know about radiation.
Shu-Ren, Cheng [6]	The application of radioactive elements: 1. The discovery of radioactive elements. 2. The characteristics of radioactive elements 3. The decay of radioactive elements. 4. Man-made radioactive elements. 5. The basic principle of radio isotope application. 6. The application of radioisotope in research studies. 7. The application of radioisotope in transportation and military. 8. The application of radioisotope in hydrology and earth science. 9. The application of radioisotope in drugs and food industry. 10. The application of radioisotope in agriculture and fish industry. 11. The application of radioisotope in medical industry. 12. The application of radioisotope in industry. 13. The application of radioisotope in nuclear power. 14. The prevention and monitor of radioactive elements. 15. The disposal of nuclear waster.
Zheng-Yi, Lin, Zao-chong, Liao, Shao-Pei, Su, Jun-Quan, Yao, Jin-Yuan, Yu, Hai-Nan, Xiao [7]	Provide with nuclear power related topics: 1. Knowing nuclear power 2. The heart of nuclear plant-nuclear reactor 3. Radiation and radiation prevention. 4. The operation and risk of nuclear plant 5. Nuclear safety and emergency plans.

(continued)

Table 23.1 (continued)

Scholars/experts	Environmental ionizing radiation curriculum
	6. Radiation waste. 7. Environmental protection of nuclear plants. 8. Earthquake prevention of nuclear plants. 9. Nuclear plants are not atomic bombs. 10. The development of international nuclear development.
Atomic Energy Council, Executive Yuan [8]	O Knowledge about nuclear power are as follows: 1. The introduction of nuclear water plants. 2. The safety concept of nuclear power. 3. The control of nuclear safety. 4. The prevention of radiation. 5. The management of radiation waste. 6. Environment protection. 7. The nuclear energy campaign and communication. 8. International cooperation. 9. The peaceful use of atomic energy.
Fuel Cycle and Materials Administration, Atomic Energy Council, Executive Yuan [9]	Knowing Radiation Waste 1. Knowing radiation. 2. The source of radiation waste. 3. The characteristic of radiation waste. 4. The classification of radiation. 5. The life of radiation waste.

indicators. The selection principle is that the number of people of assessment factor is more than 90 %, and the fuzzy priority is more than Sk ≧ 7.9447. When both are met, then they will be listed in the assessment factors (Table 23.3).

- The survey of hierarchy analysis and test analysis
  The second stage of questionnaire is hierarchy analysis questionnaire. The first stage of Fuzzy Delphi has sifted five groups of curriculum indicators and 35 curriculum indicators, and has gone through comparative in pairs, to obtain priority among indicators. This second stage of questionnaire analysis is calculated based on Expert Choice (11.5version), included major priority, secondary priority, and unity indicator C.I. After the analysis of statistics, qualitative research is used to describe environmental ionizing radiation curriculum indicators, as the foundation of environmental ionizing radiation indicators. After the analysis of experts' questionnaire, the local priority of the environmental ionizing curriculum indicators are described in Table 23.4, in order to understand indicators of the local priority in the same level.

Overall, on the third level of 35 indicators, the first nine priorities are "4-1-1 Taiwan's environmental monitor" 0.132, "5-1-1How people carry out radiation prevention and protection"0.114, "1-4-1Health effect"0.096, "4-1-2 Environmental radiation monitoring management" 0.082, "5-1-2 Radiation safety consultancy 0.062", "3-1-1 characteristic of nuclear power generation"0.054, "3-3-3 prevention of nuclear power generation"0.042, "1-3-1general ionizing radiation volume"0.034, "1-5-2prevention of ionizing radiation"0.033. For the first nine

Table 23.2 Constructing indicators of environmental ionizing radiation curriculum

Literature source	Cases of promotion and content
Environmental protection Group, Ministry of Education "Radiation and Nuclear Energy" [10]	In order to build up accurate concept about nuclear energy and radiation prevention and protection for students, the environmental protection group has outlined "nuclear energy and adiation education" teaching mode for the use of schools. The contents are as below: 1. What is radiation? 2. The radiation's application and influence towards human. 3. The prevention and protection of radiation. 4. The monitor of environmental radiation. 5. The nuclear plants and radiation monitoring.
Japan's Ministry of Education, Culture, Sports, Science and Technology Radiation supplementary teaching material Elementary School [11]	1. What is radiation? 2. Radiation, what is it for? 3. What will radiate? 4. What will happen after radiation is exposed? 5. How to measure radiation? 6. How to protect oneself from radiation?
Tsing-Hua University TEENS [12]	The content of Science Education Center are as follows: 1. Online exhibition of nuclear knowledge. (a) Knowing nuclear energy (b) The history of nuclear energy (c) The safety of nuclear energy (d) Knowing nuclear power generation. (e) What is nuclear waste 2. Knowing nuclear power generation-introduce (a) Chain reaction (b) Continuous nuclear fission (c) Types of reactors. 3. Our neighbor-Fubao, introduction of e-comics. (a) Radiation and radioactive material (b) The principle of nuclear power generation and nuclear plants safety (c) Emergency plan for nuclear plants. 4. Introductions of atomic scientists

indicators, levels of "knowing radiation", "monitoring environmental radiation", and "the emergency measure of nuclear accidents" sweep up seven indicators. This shows that experts emphasized on those three levels of indicators.

The priority of each indicator can be references to the development of environmental ionizing radiation education or the implementation of certain indicators, in order to meet the demands of each school. The following is the priority of the third level of indicators, and it is graded in percentage, please see Table 23.5.

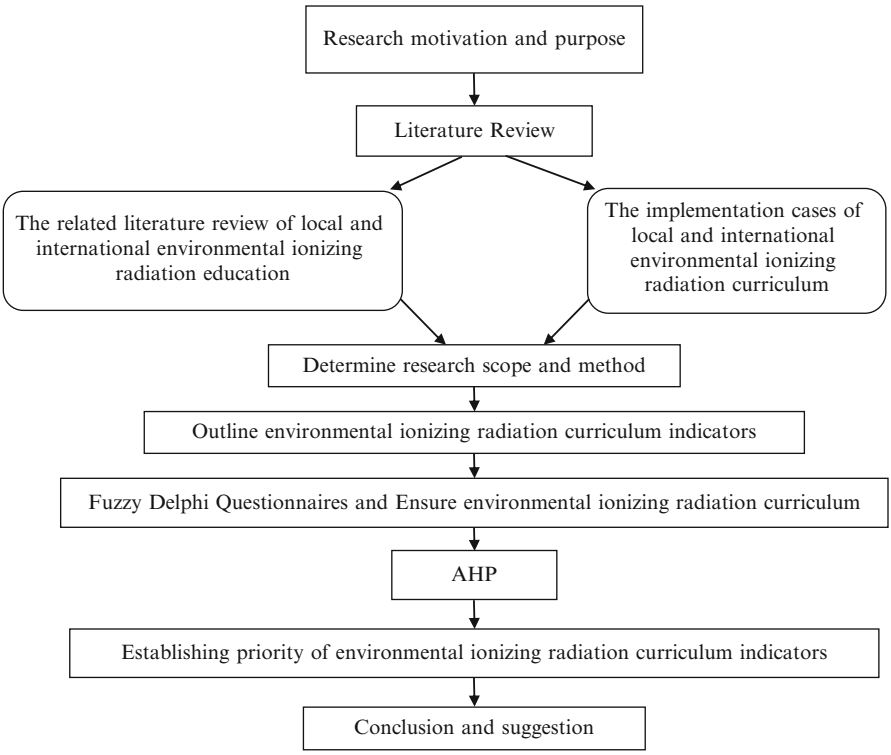

Fig. 23.1 Research procedure

Table 23.3 The revised table of environmental ionizing radiation curriculum

First level of indicator	Second level of indicators	Third level of indicators
1. Knowing radiation	1-1types of radiation	1-1-1Ionizing radiation.
		1-1-2Non-ionizing radiation.
	1-2source of ionizing radiation	1-2-1Natural radiation.
		1-2-2Man-made radiation.
	1-3Measurement of radiation	1-3-1volume of normal ionizing radiation.
	1-4The influence of radiation toward human	1-4-1Health effect.
	1-5The characteristic, prevention, protection and warming of radiation.	1-5-1The characteristic of radiation materials.
		1-5-2The prevention of ionizing radiation.
		1-5-3Labels of warning.

(continued)

Table 23.3 (continued)

First level of indicator	Second level of indicators	Third level of indicators
2. The application of radiation in daily life.	2-1Medical application.	2-1-1Medical checkup
		2-1-2Cancer treatment.
		2-1-3Volume of medical ionizing radiation.
	2-2Agricultural application.	2-2-1Plant disease prevention.
		2-2-2Improvement of agricultural products
	2-3Industrial application.	2-3-1Examination of X ray
		2-3-2Measurement of thickness and height.
		2-3-3Followup leaking.
		2-3-4 Sterilization and harden
	2-4Research	2-4-1 Measure and decide the year and fault.
		2-4-2Detect the leaking of reservoir
	2-5The application of security	2-5-1The security of police and military
		2-5-2Security of airports and custom
		2-5-3 Fire and Smoke detector.
3. Radiation and nuclear plants.	3-1Nuclear power generation.	3-1-1The characteristic of nuclear power generation.
	3-2Radioactive waste	3-2-1 Source of radioactive waste
		3-2-2The disposal of radioactive waste
		3-2-3 The storage of radioactive waste
		3-2-4The settling of radioactive waste
	3-3Taiwan's nuclear plants	3-3-1 The distribution of nuclear plants
		3-3-2 The power generation principle of nuclear plants
		3-3-3 Security of nuclear power
4. The monitor of environmental ionizing radiation.	4-1the monitor of environmental radiation.	4-1-1Taiwan environmental radiation monitoring.
		4-1-2 The management of environmental radiation
5. Emergency measures of nuclear incidents.	5-1The prevention measures of nuclear accidents	5-1-1 Public's prevention measures during nuclear accidents
		5-1-2 Radiation safety consultancy

Table 23.4 Main, secondary and third levels of indicators

Main indicators	Priority	Order	Second level of indicators	Priority	Order	Third level of indicators	Priority	Order
Knowing priority	0.296	1	Types of radiation	0.131	4	Ionizing radiation	0.090	6
						Non-ionizing radiation.	0.036	9
			Radiation source	0.170	3	Natural radiation	0.093	5
						Man-made radiation.	0.090	6
			The measurement of radiation	0.116	5	Average volume of radiation.	0.086	8
			The influence of radiation toward human	0.323	1	Health effect	0.209	1
			ChCharacteristic, prevention and warning labels.	0.259	2	Characteristic of radioactive material	0.126	3
						Prevention of radiation	0.143	2
						Warning label	0.126	3
The application of radiation in daily life	0.158	4	Medical application	0.407	1	Medical checkup	0.159	1
						Cancer treatment	0.153	2
						The volume of radiation.	0.136	3
			Agricultural application	0.103	5	Prevention of plant disease	0.039	10
						Improvement of agricultural products.	0.039	10
			Industrial application.	0.184	3	Examination of X ray	0.057	7
						Measurement of thickness and height.	0.051	8
						Traces of leaking	0.034	12
						Sterilization and harden	0.043	9
			Application of research	0.119	4	Measure and decide the year and fault.	0.027	14
						Detect leaking of reservoir	0.034	12
			Application of safe check	0.187	2	Security of airports and custom	0.061	6
						Security check of airports and custom	0.080	5
						Smoke detector.	0.086	4

(continued)

Table 23.4 (continued)

Main indicators	Priority	Order	Second level of indicators	Priority	Order	Third level of indicators	Priority	Order
Radiation and nuclear plants	0.157	5	Nuclear power generation	0.157	3	the characteristic of nuclear power generation.	0.131	3
			Radioactive waste	0.208	2	Source of radioactive waste	0.102	4
						The disposal of radioactive waste	0.070	7
						The storage of radioactive waste	0.079	6
						The settling of radioactive waste	0.054	8
			Taiwan nuclear power plants	0.450	1	The distribution of nuclear plants	0.080	5
						The power generation principle of nuclear plants	0.158	2
						Security of nuclear power.	0.326	1
Monitor of environmental ionizing radiation.	0.214	2	environmental radiation monitoring	0.616	1	Taiwan environmental radiation monitoring	0.569	1
			The monitoring management of environmental radiation	0.384	2	The monitoring management of environmental radiation	0.431	2
Emergency of nuclear accidents.	0.176	3	Public's prevention measures during nuclear accidents變方法	0.649	1	Public's prevention measures during nuclear accidents	0.710	1
			Radiation safety consultancy	0.351	2	Radiation safety consultancy	0.290	2

Table 23.5 Scores of indicators on the third level

Third level of indicators	Priority value (A)	Scores of indicators (A*100 %)
1-1-1Ionizing radiation	0.022	2.20 %
1-1-2Non-ionizing radiation	0.009	0.9 %
1-2-1Natural radiation	0.023	2.3 %
1-2-2Man-man radiation	0.022	2.2 %
1-3-1Volume of general ionizing radiation	0.021	2.1 %
1-4-1Health effect	0.052	5.2 %
1-5-1Characteristic of radioactive material	0.031	3.1 %
1-5-2The prevention of ionizing radiation	0.035	3.5 %
1-5-3Warning label	0.031	3.1 %
2-1-1Medical checkup	0.042	4.2 %
2-1-2Cancer treatment	0.040	4.0 %
2-1-3Volume of medical ionizing radiation	0.036	3.6 %
2-2-1The prevention of plant disease.	0.010	1.0 %
2-2-2Improvement of agricultural products.	0.010	1.0 %
2-3-1Checkup of Xray	0.015	1.5 %
2-3-2Measurement of thickness and height.	0.013	1.3 %
2-3-3Detect leaking.	0.009	0.9 %
2-3-4Sterilization and harden	0.011	1.1 %
2-4-1Trace the year and fault.	0.007	0.7 %
2-4-2Detect the leaking of reservoir	0.009	0.9 %
2-5-1The security of police and military	0.016	1.6 %
2-5-2Security of airports and custom	0.021	2.1 %
2-5-3Fire control and smoke detector	0.023	2.3 %
3-1-1The characteristic of nuclear power generation	0.018	1.8 %
3-2-1Source of radioactive waste	0.014	1.4 %
3-2-2The disposal of radioactive waste	0.010	1.0 %
3-2-3The storage of radioactive waste	0.011	1.1 %
3-2-4The settling of radioactive waste	0.008	0.8 %
3-3-1The distribution of nuclear plants	0.011	1.1 %
3-3-2The principle of nuclear power generation	0.022	2.2 %
3-3-3Security of nuclear power	0.045	4.5 %
4-1-1Taiwan environmental radiation monitoring.	0.077	7.7 %
4-1-2The monitoring management of environmental radiation	0.059	5.9 %
5-1-1Public's prevention and safety measures during nuclear accidents	0.153	15.3 %
5-1-2Radiation safety consultancy	0.062	6.2 %
	0.998	99.8 %

23.5 Conclusion

This research aims at constructing environmental ionizing radiation curriculum indicators, based on the environmental ionizing radiation related education and campaign implemented by Atomic Energy Council, Executive Yuan. The construction of the indicators is to provide references for each school in promoting environmental ionizing radiation curriculum, so that Taiwan elementary and high school can establish implementation program of the environmental ionizing radiation curriculum, in the mode of environmental education.

This research undertakes questionnaires through Fuzzy Delphi and Analytical Hierarchy Process, in order to establish the structure of Taiwan's elementary and high school environmental ionizing radiation curriculum. It is hoped that Taiwan's elementary and high school, educational administration institute can refer to the indicators while promoting environmental ionizing radiation curriculum. According to the literature, the initial structure is outlined, and sifted through Fuzzy Delphi questionnaires, to construct environmental ionizing curriculum indicators. There are a total of five main indicators in the first level, "knowing radiation", "radiation in daily life application", "radiation and nuclear plants", "the monitoring of environmental ionizing radiation", and "the emergency measures of nuclear accidents", and 35 indicators underneath.

- Main indicators-the priority of first level of self evaluation : According to the priority value of the original survey, the priority of self-evaluation indicators analysis is "the level of knowing radiation" 0.296, "the monitoring of environmental ionizing radiation" 0.214, "the level of emergency measures of nuclear accidents" 0.176, "the application of radiation in daily life" 0.158, "the level of radiation and nuclear plants" 0.157.
- The overall priority of second level to the third level indicators: In 35 self evaluation indicators, the priorities are 4-1-1 Taiwan environmental radiation monitoring, 5-1-1 Public's prevention and safety measures during nuclear accidents 0.077, 1-4-1 health effect0.065, "4-1-2 environmental radiation monitoring management unit" 0.056, 1-5-2 the prevention of ionizing radiation0.052, 3-3-3the safety and prevention of nuclear power 0.048, "2-1-1medical checkup" 0.043, "5-1-2 radiation safety consultancy"0.042, and "1-5-3warning labels"0.039.

After reviewing some environmental education, radiation and energy related literature, and also going through the first stage of fuzzy Delphi questionnaires for experts, some indicators can be referred to.

- Knowing radiation: The first step of implementing environmental ionizing curriculum is to "understand what is radiation", the contents are divided into "the classification of radiation", and "where is radiation". Therefore, in the expert's questionnaires, the indicator of "the influence of radiation toward human health" has gained the highest recognition. While indicators of ionizing radiation characteristic, prevention and warning labels, after the detail

introduction and understanding in the courses, and in coordination with the complete environmental ionizing radiation curriculum, students should deeply understand that ionizing radiation in daily life is very common, and not a dreadful monster, should be cautious when facing radiation, but should avoid being panic due to ignorance.

- The application level of radiation: The most important part for construction of environmental ionizing radiation is the implementation of "curriculum and teaching". It is needed to combine with curriculum, the important element is to outline school based curriculum, or integrate radiation curriculum indicators into other courses, or organize "environmental ionizing radiation classroom theme event. Experts hold the same view that the implementation of radiation course should be based on school-based curriculum for each grade, and integrate into curriculum, and the principle is not to burden the tasks of teachers and not necessarily design curriculum for each semester year. The related references are energy education integrated into each learning fields, medical radiation integrated into health and sport fields, and natural disaster prevention activities in each semester year.
- Radiation and Nuclear Power Plants: The third step of environmental ionizing radiation curriculum indicators is "radiation and nuclear power plants", the implementation factors are "knowing nuclear power plants", and "diverse energy", which aims at allowing students to understand nuclear power plants are not nuclear weapons, and a way of power generation of reducing CO_2, and the cost is lower than other power generation, and moreover, it has tight safety prevention. The opinions of expert toward knowing radiation and nuclear power plants should be emphasized on the basic safety prevention facilities and mechanism, and should explain the power generation principle of nuclear power plants and material in used, so as to differentiate nuclear power plants and nuclear weapons.
- The monitoring of environmental ionizing radiation: The fourth indicator of environmental ionizing curriculum is the "monitoring of environmental ionizing radiation", which includes "monitoring ionizing radiation", "real time inquiry", and "monitoring unit". The updated of the monitoring of environmental ionizing radiation will help to improve people's confidence toward nuclear plants and other related radiation facilities, and reduce worries of people on the safety of nuclear plants and radiation. As not every school has the ability of carry out radiation monitoring actions, therefore Atomic Energy Council, Executive Yuan and Taipower Company set up 36 monitoring stations and post real time monitoring data on the website, allowing people to know the scale of radiation around the island or the adjoining area of nuclear plants, so that the monitoring data is transparent to the public. Experts think that in implementing environmental ionizing radiation monitoring actions, the meaning of monitoring and understanding of executive units should be added, and so, in the item of curriculum indicators, it is added the meaning of executive units and explanation of executive units.
- The emergency measures of nuclear accidents: The fifth indicator is the "emergency measure of nuclear accidents, which included "the public' prevention

measures of nuclear accidents", and "the safety radiation consultancy". The professional improvement of teachers will help students understand the prevention of radiation, and guide students to react during nuclear accidents. Thus it is important to encourage teachers to establish environmental ionizing radiation teaching groups, or participate in the related education training courses, seminars or workshop, to enhance teachers' professional knowledge. Also, it is advised to introduce expert resources, to help schools in promoting the depth and scope of environmental ionizing radiation curriculum, and also through the cooperation and interaction with other schools, it is hoped to provide some guidelines during implementation. Organizing related teachers' empowerment activities, or in cooperation with Atomic Energy Council to share resources, are the important resources. Experts think that in promoting nuclear emergency measure, it should add up detailed explanation steps, and thus in the items of curriculum indicators, it is listed that how people undergo radiation prevention and protection during the execution and radiation safety consultancy strategies.

Acknowledgment This research thank for NSC-101-NU-E-133-001-NU support.

References

1. Turner J (1995) Atoms, radiation and radiation protection, 2nd edn. Wiley, New York, NY
2. Ran M-Y, Xue J-W (2009) Prediction model of the radiation from ground surface to the occupant in outdoor space. J Civil Eng Architect 3:70–79
3. Qin-Sen S (ed) (1995) The application of radiation. Taiwan Dung-Hua, Taipei
4. Bao-Shan O (1999) Taiwan radiation source and application. Wunan, Taipei
5. Tian-Ge W (1997) Atom, nuclear, radiation. Taiwan Bookstore, Taipei
6. Shu-Ren C (1997) The application of radioactive material. Taiwan Bookstore, Taipei
7. Zheng-Yi L (1992) The compilation of nuclear knowledge. Taipower Company, Taiwan
8. Atomic Energy Council (1995) X-ray adventurous trip. Atomic Energy Council, Taipei
9. Fuel Cycle and Materials Administration, Atomic Energy Council, Executive Yuan. http://gamma1.aec.gov.tw/fcma/know_activity_junk_a.asp
10. Radiation and Nuclear Energy, Environmental Protection Group Worldwide Web, the Ministry of Education, Executive Yuan http://www.edu.tw/environmental/download.aspx?download_sn=3867&pages=0&site_content_sn=8133
11. Radiation Supplementary Teaching Material, Japan Ministry of Education, Culture, Sports, Science and Technology http://www.mext.go.jp/b_menu/shuppan/sonota/attach/1313004.htm
12. Science Education Center, TEENS, National Tsing-Hua University http://vm.nthu.edu.tw/science/
13. You-Hua Y, Zhang Y-C (1999) Sustainable development indicators. Environ Education J 37:53–74
14. Chen C-J, Cai Z-J, Zhang L-Z (2004) The studies of Taiwan's elementary and high school greening effectiveness indicators. Environ Education J 3:75–85
15. Zhang Z-C (2007) The studies of constructing environmental education indicators in government agencies. Studies Environ Education 4(2):1–21
16. Wang S-M (2009) The studies of green school indicators and the history of evaluation tools. Studies Environ Education 6(1):119–160

Chapter 24
An Energy Strategy in a Liberalized Environment in Slovakia

Milena Sviteková, Henrieta Pavolová, and Barbara Hlavňová

Abstract The article deals with the state energy policy and strategy in Slovakia and also compares the basic principles of energy policy in the European Union. The goal is to outline the objectives of energy policy of the Slovak Republic, the strategy for reducing energy consumption and increasing energy efficiency. It also describes the system of financing energy policy measures and highlights the current state of research and development positions in the energy sector in Slovakia. It briefly defines the process of liberalization of energy market, restructuring and privatization in Slovakia. The author also presents a view of an enlarged regional cooperation that is essential (the Visegrad Group—V4). V4 was established as a tool for cooperation in several sectors, the group is led by the Presidency, which varies annually. One of the effects of the gas crisis was the elaboration of V4 + Budapest Declaration, 24 February 2010, which created a specific framework for the flagship project of common gas connections of V4 and further development of this cooperation—Bratislava Declaration of January 25, the 2011th. Regional cooperation promoted by the European Commission—the establishment of the High Level Group for north–south connections (countries V4, Croatia, Bulgaria, Romania) and its integration into strategic documents of European Union. Briefly stated the key role of nuclear energy in the energy mix in Slovakia. A major source of energy are renewable sources of energy that are an important part of Slovak politics of climate change. Also contributing to the economic "green" growth (job creation) and security of supply. The goal is 14 % share of renewable energy in gross final consumption in 2020 and 10 % share of renewable energy in the transport sector in 2020. It defines the usable potential of renewable resources (hydropower, biomass, biofuels, biogas, wind energy, geothermal energy) and also shows the expected evolution of total electricity consumption and maximum

M. Sviteková (✉)
Department of Communications, Faculty of Operation and Economics of Transport and Communications, University of Žilina, Univerzitná 1, 010 26, Žilina, Slovakia, UK
e-mail: milena.svitekova@gmail.com

H. Pavolová • B. Hlavňová
Faculty of Mining, Ecology, Process Control and Geotechnologies, Technical University of Košice, Slovak Republic, Letná 9, 042 00 Košice, Slovakia, UK
e-mail: henrieta.pavolova@tuke.sk; barbara.hlavnova@tuke.sk

I. Dincer et al. (eds.), *Progress in Sustainable Energy Technologies Vol II: Creating Sustainable Development*, DOI 10.1007/978-3-319-07977-6_24

possible development of electricity generation by 2030. The paper contains a discussion of in-depth energy audit and energy policy, i.e. In-Depth Review (IDR), conducted by the International Energy Agency (IEA) in a comparison of results obtained in selected EU countries. At the end of the article the author provides a real situation during the liberalization from his point of view in a selected energy company in Slovakia.

Keywords Energy policy • Economic policy • Renewable resources

24.1 Introduction

Free market economy is the best way to increase wealth and prosperity for all citizens. It must be maintained in operation by responsible fiscal policy without indebtedness, monetary policy ensuring a stable price level, or functioning security and defense guaranteeing effective access to justice and equality before the law. The government may not grant privileges to narrow interest groups, because that would be harming other sectors and consumers. Successful economic policy focuses on measures aimed at strengthening accountability in the public service in all areas and remove existing distortions. The common denominator of all measures is the need for careful analysis of their effects. Economic policy must motivate to work, to effort and to enterprise. It must not be short-sighted and must take into account the long-term effects.

For the competitiveness of enterprises is important that the legislative environment is as stable as possible, and to the future devotement of the conceptual and predictable.

Direct government intervention should be exceptional and adequately justified, aimed at meeting the objectives, provision of which is outside the consideration of market mechanism (for example, removal of regional disparities in the poorest regions). Their benefits and costs must always be precisely analyzed. Incentives and tax breaks can deficiencies in the business environment (e.g. lack of motorways) can be replaced for a short and temporary, and therefore should be continued in the radical trend of their cushioning. Market-based solutions often yield the best results even in areas where the state is has a strong position—whether as to healthcare, the provision of social services or outsourcing some services for state and public administration through transparent competition. An important measure to improve the quality of the business environment was the launching of the project Singapore by Ministry of Economy of the Slovak Republic. It contains more than one hundred concrete measures to reduce the administrative burden on business and saving companies 100 million euros a year. Today is ready more than 200 measures to eliminate bureaucracy and unnecessary costs on business, so that bureaucracy costs fell by more than a quarter—that is more important than requested by the European Union. The three strategic objectives of economic policy for Slovakia are

Table 24.1 Expected development of lignite mining in 2030 (m.j.) kt) [1]

Year	2005	2010	2015	2020	2030
Mining of lignite	2,400	2,400	2,100	1,800	900

Table 24.2 Estimated growth of gas consumption upto 2030 (billion m^3) [1]

Year	2005	2010	2020	2030
Total consumption of natural gas	6.5	6.9	7.0	7.1

Table 24.3 The available potential of renewable resources (PJ—Peta Joules) [1]

Source	Exploitable potential	
	PJ	GWh
Hydropower	23.8	6,600
Large-scale hydropower	20.2	5,600
Small hydropower plants	3.6	1,000
Biomass	75.6	21,000
Dendromass	47.0	13,055
Agricultural biomass	28.6	7,945
Biofuels	5.0	1,389
Biogas	6.9	1,917
Wind energy	2.2	600
Geothermal energy	22.7	6,300
Solar energy	18.7	5,200
Total	154.9	43,006

Table 24.4 Estimated evolution of the total electricity consumption and maximum possible power generation (in TWh) [1]

Year	Consumption	Production	Difference
2006	29.4	31.0	1.6
2007	29.7	28.4	−1.3
2008	30.1	28.7	−1.4
2009	30.5	26.1	−4.4
2010	31.0	26.5	−4.5
2015	32.9	38.1	5.2
2020	34.8	38.1	3.3
2030	38.0	35.5	−2.5

(1) reducing bureaucracy in business and improving the business environment; (2) continuation of bannering of all relations in the energy sector and improving the regulatory framework and (3) brand building Slovakia for investors and promoting tourism [1].

24.2 Energy Policy in the Slovak Republic

Energy policy is part of a national economic strategy of the Slovak Republic as to maximize its economic growth in terms of sustainable development is conditional on the reliability of supply at optimum cost and adequate protection of the environment.

Energy policy is the basis for the future direction of development, particularly electricity, thermal energy, gas, mining, processing and transport of oil, coal and renewable energies. The aim of the energy policy is to create conditions to ensure sufficient energy, its efficient use, safe and continuous delivery and maximize savings on the demand side. By the implementation of energy policy we can achieve provision of the energy needs of the Slovak Republic, the path to sustained reduction of energy consumption, creating a competitive environment in the energy market to reduce costs at all levels and eliminate one-sided dependence on energy suppliers. At the same time it paves the way for implementation of energy efficiency [1].

The main objective of energy policy of EU member states are: provide enough energy to maximize energy savings on the consumption side and ensure safe and continuous supply of energy in a balanced structure of its components, so that in case of failure of one energy source that could be replaced by another source. In recent years in all EU member states is becoming a key issue for diversifying energy sources and not just by different types of energy sources, but also according to their geographic area of origin. EU member states at present nearly half of its energy consumption is covered by imports from the territory of third countries. Considering expected growth in energy consumption in the future and opportunities to exploit domestic energy sources to meet growth in consumption can expect growth in import dependence. The most frequently used source of domestic energy in the EU countries is coal. Clean coal technologies enable the use of relatively large reserves of coal with minimal environmental impact. Brown coal provides mainly domestic mining, the need for coal imports is also provided outside the territory of EU Member States. The risk for the EU countries is high dependence on imported oil and its derivatives from third countries because they lack the EU market, and because of the instability of prices. Although gradually moving away from electricity and heat production of petroleum products, the overall demand for these products remains high, mainly due to rising consumption in transport. The biggest development in the current record consumption of natural gas through its acceptance of its impact on the environment. The problem is its limited availability in the common market and its dependence on the price of crude oil prices. Recently, increasing supply needs of the common market in natural gas supplies from Algeria, Norway and Russia. About a third of consumed electricity in the EU is produced in nuclear power plants. Due to the increasing consumption of electricity and the need to reduce greenhouse gas emissions have recently begun to change the negative attitude of some EU member states towards nuclear energy. For further development of its use is to be completed particular the issue of security of their

operations, as well as the issue of spent nuclear waste. To enhance energy independence, EU member states put more emphasis on renewable energy sources. To promote the use of renewable energy has created a number of institutional and financial instruments and schemes. The biggest boom reaches the use of wind energy and biomass. Renewable energy sources are an important component of the structure of energy sources, but their ability to substitute other energy sources in coming years is limited [1].

The implementation of energy policy for the last 3 years, in accordance with the direction of energy policy EU, meant the gradual liberalization of energy markets. In the energy sector after 2000, the big restructuring was conducted, which resulted in increasing economic efficiency of the sector. The restructuring was accompanied by the transformation and privatization. Today we can state that the process of privatization in the energy sector is completed, the result was a change in ownership, which was carried by input out foreign investors into transformed energy companies. Major foreign investors have entered into a distribution company and before the end is also the entry of a foreign investor into production of electricity. Is not considered the privatization of the carrier and distributor of gas and oil carrier or the privatization of the electricity transmission system. The goal of liberalization was to create a competitive environment and the existence of natural monopolies and allow the one hand, consumers of electricity and gas supplier choice and on the other hand to offer the existence of equal competition between suppliers, gradually creating a natural pressure to improve economic efficiency. At the energy market was created free competition on a level of production and supply, supply and trade in electricity and gas, based on transparent rules without discriminatory or contrary to favor any of the suppliers. By introduction of new market rules was made a room for the benefits that may arise in the internal market in electricity and gas in terms of greater efficiency of operating systems and networks, better levels of service provision, pressure on cutting prices and greater competitiveness. There remains room for the implementation of measures aimed at ensuring equal conditions for all market participants to reduce the risk of a dominant position of market participants and exploitative behavior, as well as to ensure the application of non-discriminatory tariff for transmission for distribution of electricity and gas transmission and distribution and this is on the basis of published tariffs prior to their entry into force, as well as to safeguard the rights of customers [1].

The liberalization of energy markets requires systemic changes throughout the business environment not only for businessmen in the energy sector. As the nature of the operation of energy networks can't introduce full competition, a key role in this area has a regulation that provides non-discriminatory and transparent performance in network industries, application of regulatory measures aimed at reducing the risk of infringing competition rules, abuse of dominant position in the energy market and services, protection of consumers, the application of measures to ensure the reliable, economic and quality of energy supply and provision of related services. For the purpose of establishing a functioning electricity market and creating a competitive environment in the energy, conditions are created to allow rebalancing of prices, respectively tariffs to their differentiation depending on the

type of customer (up sampling) in the context of a general EU practice and principles specifying that prices and tariffs reflect costs. For the period after 2007 it would appear advisable to implement based on clear and transparent rules for rebalancing prices, respectively in electricity tariff. European Parliament and Council adopted Directive. 2003/54/EC concerning common rules for the internal market in electricity and Directive. 2003/55/EC concerning common rules for the internal gas market will become the basis for unification of rules necessary for the functioning of the internal market in electricity and gas and to create a functioning internal market in all EU countries, not excluding the Slovak Republic. Except restructuring, implementation of key guidelines governing the ES internal market in electricity and gas was required by the service providers the introduction of such rules to allow non-discriminatory and transparent functioning of the competitive environment in the energy sector. It is necessary to monitor the impact of legislation on energy market liberalization, to analyze the barriers of real market opening in electricity and gas take appropriate legislative measures to eliminate these barriers [1].

24.2.1 The Objectives and Priorities of Energy Policy of the Slovak Republic Upto 2020 and Outlook to 2030

The SR energy policy in the long term is to ensure that the volume of electricity, which covers the demand for cost-effective principle, while ensuring maximum efficiency with safe and reliable supply of all forms of energy in the required quantity and quality. An important part of energy policy aims of SR is to reduce the ratio of gross domestic energy consumption to gross domestic product—reducing energy demands. To achieve the objectives of energy policy, the SR provides the following basic priorities: replace electricity production facilities in order to ensure the production of electricity, which primarily covers the domestic demand for cost-effective principle; take measures aimed at saving energy and increasing energy efficiency on the demand side; reduce dependence on energy supplies from risk areas—Diversification of acquisition of sourcing energy and transport routes; use of indigenous primary energy sources for electricity and heat on economically effective principle; to increased use of combined heat and power; use of nuclear energy as a diversified, economically efficient and environmentally acceptable option of electricity production; ensure nuclear safety operation of nuclear power plants; increase the share of renewable energy for electricity and heat to create the appropriate additional funds needed to cover domestic demand; complete system and network to be able to ensure safe and reliable transmission, transportation and distribution of electricity and gas; build a new connecting lines in order to improve links to the EU internal market as well as third-country markets; encourage use of alternative fuels in transport [1].

24.2.2 Starting Points to Achieve the Objectives of Energy Policy: Balance Resources and Needs

The Slovak Republic provides nearly 90 % of primary energy by purchases outside the territory of the EU internal market. The only significant domestic energy source is lignite, because the extraction, natural gas and crude oil is insignificant. For this reason still increase an importance of renewable energy sources (biomass, water, geothermal, solar, wind). Based on the analyzes we can be expect in the long term (until 2030) that a major role in satisfying consumption will play a greater use of nuclear fuel, natural gas and renewable energy. This development assumes that a tightening of emission limits will decrease consumption of coal. The same scenario can be expected even if the emission limits sufficiently discourage the use of coal. Due to the replacement of petroleum constituents biofuels it is expected only a slight increase in oil consumption especially in transport. Based on long-term forecasts of gross domestic consumption can be expected following the pattern of consumption of primary energy sources [1].

24.2.3 Starting Points to Achieve the Objectives of Energy Policy: Balance Resources and Needs

The Slovak Republic provides nearly 90 % of primary energy by purchases outside the territory of the EU internal market. The only significant domestic energy source is lignite, because the extraction, natural gas and crude oil is insignificant. For this reason still increase an importance of renewable energy sources (biomass, water, geothermal, solar, wind). Based on the analyzes we can be expect in the long term (until 2030) that a major role in satisfying consumption will play a greater use of nuclear fuel, natural gas and renewable energy. This development assumes that a tightening of emission limits will decrease consumption of coal. The same scenario can be expected even if the emission limits sufficiently discourage the use of coal. Due to the replacement of petroleum constituents biofuels it is expected only a slight increase in oil consumption especially in transport. Based on long-term forecasts of gross domestic consumption can be expected following the pattern of consumption of primary energy sources [1].

Coal—Domestic brown coal currently accounts for approximately 79 % of the consumption of brown coal needed to produce electricity and heat. It plays an important role in ensuring security of electricity supply. Other necessary amount of brown coal and all coal by imports (Fig. 24.1).

Natural gas—Annual natural gas consumption is about 7 billion m^3. This consumption is domestic mining contributes about 3 %. Other natural gas imported from Russia [1].

In the next period is expected slight increase in consumption of natural gas mainly due to consumption growth in industry and in production of electricity and

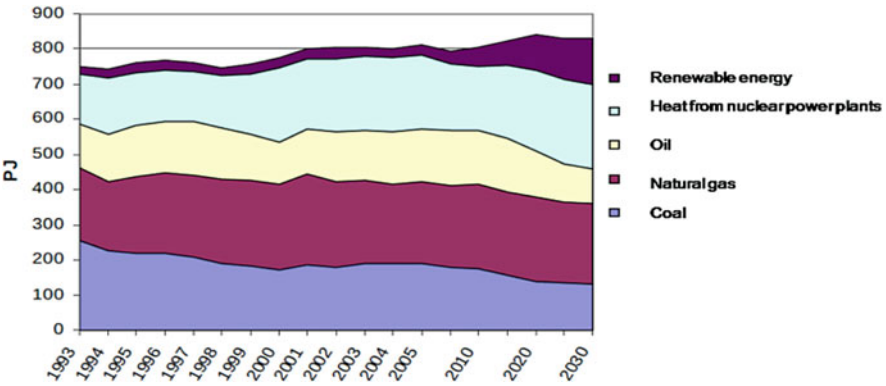

Fig. 24.1 Development of consumption of primary energy sources [1]

heat. The use of gas is also suitable because of minimal environmental impact. This assumption is based on the conservation programs of natural gas prices compared to other primary sources. In the event of a significant change in the price of natural gas programs we can also expect changes in total consumption [1].

Oil—Slovakia imports annually about 5.5 million tons of oil. This volume is guaranteed by long-term international agreement with the Russian Federation. From the amount of imported oil to meet domestic consumption is used 3.2 million tons. Domestic extraction is involved in oil consumption of about 2 %. Oil security, security of oil supplies and related activities at the time of shortage, are addressed in the legislation of the Slovak Republic. Currently SR does not meets the 90-day supply of oil and oil products [1].

Nuclear fuel—Today, more than 55 % of the electricity produced in nuclear power plants. Nuclear fuel supply is ensured by long-term contracts from the Russian Federation. It is useful to support the transition to improved fuel with better use of nuclear material in nuclear fuel, which results in a reduction of its consumption per unit of electricity. In connection with Nuclear Power ablactation V1 in Jaslovské Bohunice (JU V1) decreased supply of nuclear fuel. In connection with the use of nuclear fuel to generate electricity is a key issue in solving storage of spent nuclear fuel as well as the question of disposal of decommissioned nuclear power plants (JEZ). Slovak Republic in resolving these issues will proceed in accordance with EU policies taking into consideration the maximum safety and reliability of nuclear energy at all stages of the life cycle of JEZ [1].

Renewable—Currently from renewable energy, including the use of large hydropower potential of hydro power produces about 19 % of domestic electricity consumption. The total exploitable potential of individual types of renewable energy provides opportunities to increase their share in total production of electricity to 24 % in 2020 and 27 % in 2030. Most promising renewable sources for heat is biomass, where the total annual potential suitable for energy use is about 75.6 PJ. Biomass is a promising source for production of electricity. Nevertheless, the most used source remains the use of hydropower potential. As for other renewable

sources (wind energy, geothermal energy, solar energy) their use will be only additional resources for the safety and reliability of electricity and heat, while an important factor remains the question of prices of electricity and heat from renewable sources [1].

The population living in Slovakia as well as to achieve a comparable level with the developed EU countries has an impact, inter alia, sufficient electricity at a price that will not only ensure the competitiveness of the economy, but also its accessibility to citizens. Economic growth in recent years has been also provided by declining energy intensity as evidenced by the indicator of total electricity consumption, which increased in 2004 compared to 1995 by 6.5 % over the same period increased HDP at constant prices 1995 by 35.7 %. Further development of electricity consumption is an important factor for strategic planning at all levels. Electricity consumption is affected by several factors, of which a key is price. Expected development of electricity consumption over a longer period of time is therefore based himself in a high degree of uncertainty. Assuming the development of overall electricity consumption was based on the annual growth of 1.2 %, this growth has been taken into account energy saving measures on the demand side. It refers to the current development of production and for a basis was determined 2001 data, i.e. so maximum production of 32 TWh, which was gradually reduced each year due to closure of the production of electricity resources. By the end of 2008 this fall amounted to 7.2 TWh. Assuming the development of electricity generation have been considered and the effects of measures to increase performance of production resources as well as measures aimed at construction of new generating resources [1].

From the estimated power generation potential is obvious that gradually since 2007 and until 2010 production of electricity did not cover the projected electricity consumption. After weaning, JE V1, despite measures to increase enforcement of existing capacity will not be possible without the implementation of construction of new generating capacity to cover the estimated consumption of electricity, even though it will implement all measures to reduce overall electricity consumption. To meet the objective of energy policy is necessary to ensure the volume of electricity, which covers the demand for cost-effective principle and also be necessary to replace the decommissioned JE V1 reliable source that will be able to provide electricity production at an economically efficient basis. Due to the termination of electricity generation in JE V1 will need to address a temporary shortfall between electricity consumption and electricity production. These can be addressed such as the purchase of electricity in the internal EC market, buying electricity on third markets, and/or taking measures to reduce electricity consumption and taking steps to improve performance of existing production facilities. The key question for deciding which option will be implemented in particular electricity price and estimate its future development, the capacity of the transmission system i.e. ability to make cross-border transmission of electricity efficiency measures to reduce electricity consumption. It will also be needed to ensure greater use of renewable energy. It is anticipated that in 2015, after commissioning JE Mochovce (EMO) 3 and 4 and after the implementation of new plants using renewable energy

sources will be a temporary surplus of electricity in Slovakia. After 2020, due to the closure of JE V2 after a life of its surplus electricity over. To achieve one of the main energy policy objectives of ensuring that the volume of electricity, which covers the demand for cost-effective principle, only be so that there is sufficient productive resources to produce it. To realize the main objective of energy policy is possible by increasing the performance of existing production facilities and building new production facilities. The decision about measures oriented to build new production facilities will be based on the assumption what kind of role will play in the future different energy sources in satisfying consumption. Perspective have the following types of production facilities: hydropower—construction of a hydropower plant on the river Ipeľ or on a watercourse; power plants using renewable sources—e.g. biomass, solar sources, wind; power plants with combined production of heat and power; thermal power plant and questionable prospects has the nuclear power plant—the implementation of the completion of EMO 3 and 4. The EUR 2.775 bn construction of Mochovce units 3 and 4 is developed by Slovak power plant 66 % owned by the power company Enel SpA and 34 % by the Slovak National Property Fund. It is the biggest investment ever undertaken by a private investor in the history of Slovakia. Once up and running, Mochovce units 3 and 4 along with already operational units 1 and 2 will restore Slovakia's energy independence by meeting around 45 % of the domestic power demand. Video http://www.youtube.com/watch?v=_QBKcVLQ5VE&feature=player_embedded. The final determination of the specific measures which will achieve the objectives of energy policy will take into account the economic efficiency of the proposed solutions and return on funds spent on implementation [1].

Last year's earthquake in Japan which led to the biggest nuclear disaster of Chernobyl, changing the form of World Energy. After the tragedy in Fukushima power production from nuclear power started to diverge more advanced Western countries. Global player's redrawn maps and set new strategic economic objectives. A decision to fall today in the neighboring countries, will help define the future face Slovakian nuclear power. The development, which directly affects Slovakia is currently happening in the Czech Republic, where in the first week of July 2012 restarted construction power plant Temelín. Semi-public company CEZ got on the table now offers companies that are competing for a huge energy contract. Consortia are preparing for the competition, unofficially expect that victory in the Czech Republic will open their doors to Slovakia. Whether they ever will continue to consider new nuclear units at Jaslovské Bohunice, it should be clear later this year. State Nuclear and Decommissioning Company (JAVYS) and CEZ formed a joint venture nuclear power company Slovakia (JESS) for building new nuclear power plant. Although it is not yet one hundred percent clear whether the new units at Bohunice will be built or not. Finally, this year should tell more feasibility study. Of course, it will have to find a strong company that will be able to power plant construction as politician's promise a new source should be built without the participation of the state budget. Of course, it will have to find a strong company that will be able to invest in power plant construction, as politicians promise that a new source should be built without the participation of the state budget. This is

quite tight even without such mega projects. CEZ itself to such an investor does not happen and the construction of power plants in Slovakia will not be able to let go. Must cope with their own non-critical issues of foreign expansion and seek funding system Temelin. This process will be closely monitored by the Slovak energy sector, because it will be like here, where they do not officially think of funding system. Ambition of applicants to associate business in both countries for Czech nuclear power plant is not yet confirmed. As in Temelin, also for the construction at Jaslovské Bohunice, is planned most advanced PWR generation III/III +. However, it is because as Czech and Slovak nuclear power historically uses pressurized water technology. Completion of two at least 1,000 MW blocks should cost around 200 billion crowns (7.8 billion euros). The Czechs want to enter the construction of power plant to a selected firm by standard procedures. A probably similar know-how CEZ wants to use in future in Slovakia. In Temelin contract are interested American Westinghouse from a group of Japanese Toshiba, the French Areva and russian consortium MIR 1200, which connects Gazprombank, controlled Czech Skoda JS and firms Gidropress and Atomstroyexport from Rosatom state portfolio. Who gets the business, it should be clear at the end of next year and the actual construction should start in 2016. For all of the companies are contracts in the middle of Europe extremely important, after the German government and the Italians decided to withdraw from the Nuclear Energy Future and German energy company RWE and Eon announced withdrawal from the project Horizont on construction of nuclear power plants in the UK. Britain itself still wants nuclear plants, so he is looking for a company that would assume elaborated German project on the islands. Despite the Fukushima tragedy there are still signed new contracts to build nuclear power plants. All key business benefit of the Chinese market. All key firms benefit of the Chinese market. The Russians are building in Vietnam, Iran, India and Turkey, where the power plants not only build and finance, but are also the end user. New references from Central or Western Europe would come in handy for all companies that want to convince that Fukushima was just an episode. And there is no reason for the business not to grow further. Although not yet know how to deal with spent nuclear fuel from many reactors worldwide. While developments around the Temelin power engineers monitor as determining the potential also for future Jaslovske Bohunice, out of focus is not project the completion of Mochovce. Slovak Power (SE) have trouble with the completion of two new blocks. Company itself is loath to admit it and about the construction does not inform, except optimistic statements. In January they sent a message to agencies that both units will be built in time: the third block construction work will be completed later this year and the next will follow in 2013. But last year penetrated the information from Mochovce that is not an ideal. Control of the whole building in the beginning took the Italian company Enel Ingegneria & Innovazione (EII) and that has no experience with the construction of Russia's nuclear units. Italians thought that the building would be cheaper than if they ordered it with a completely different company. Lack of experience had to prove particularly at a time. At the end of May 2012 SE had already admitted that the construction has been delayed about a year and the first block will be in

readiness for launch in late 2013 and another 8-month delay. Officially the building has been delayed for implementation of new safety standards. Builders themselves have an extremely complicated situation in Mochovce. Nuclear power projects are from 80 years of the last century. Since then, has not only technology been changed, but the conditions has tightened for the operation of nuclear power plants. Fukushima crash shook confidence in the safety nuclear plants, and that operators and supervisors still want to implement a new security "fuse." All this, however, can be incorporated in Slovakia-Russian projects and in long time ago built foundations gradually. The actual third and fourth units began to build in 1985, but just before the separation of Czechoslovakia, in 1992, the construction stopped. It was restarted in 2008 under the original russian concept of pressurized water reactors VVER. New Mochovce would deliver after completion supply to the network twice to 470 MW. Mochovce follows the standard financial tradition of the most new European nuclear plants. Final accounts properly calculated exceed the numbers. The planned investment of 2.8 billion. € should raise about 200 million more. After construction, the country of Slovakia will become capable of greater electricity export [2].

Reducing energy consumption is one of the basic pillars of sustainable development. Sustainable development must ensure the current needs of the population without limitation of the ability of future generations to meet their own needs. To achieve sustainable development is necessary to change the production technology for the production and consumption and to alter the procedures and habits on the production side and on the demand side. To ensure the development of the Slovak Republic is required that sustainable energy solutions and technologies available using its own energy resources become part of sustainable development. Influencing the amount of energy consumption with an aim to reduce the gross domestic energy consumption can be achieved mainly by favoring those investments that will ensure greater energy efficiency from measures that are based incurring additional investments to increase production capacity or measures aimed at disrupting the supply of energy in cases where preferred investments are more efficient and economically more favorable solution with regard to their positive impact on the environment. Reducing energy consumption in the long run will reduce the negative impacts on the environment, particularly by reducing emissions of greenhouse gases and this will fulfill the commitments under the Kyoto Protocol. One way of reducing energy consumption is increasing energy efficiency. Energy efficiency is a cross-sectional area, which extends to all areas of the economy, covering measures to ensure energy savings on the production side and on the demand side. Increasing energy efficiency is the result of many decisions mainly on the state party and government, third sector, the very consumers and producers appliances, but also on the production side, particularly the use of new technology available, energy-saving measures in the transmission, transportation and distribution of energy. Increasing energy efficiency is ultimately revealed as a total energy savings. By increased energy efficiency will result in reduction of consumption of primary energy sources, which results in reducing their dependence on imports, reducing the burden on the environment and reducing the impact of energy prices on consumers.

Measures aimed for increasing energy efficiency will be as follows: information campaign to disseminate information on energy consumption; make room for a comfortable and efficient energy services; the benchmarking of energy efficiency appliances and support the development and equipment production and innovative technologies with high energy efficiency [1].

Research and development in the energy sector in any economy is the subject of priority interest. Currently, the main problem of research and development in the energy sector is in particular low levels of funding and the fact that in the management of research and development in energy is not an independent scientific workplace available. In the past, research focused mainly on the area of nuclear energy for coal, gas and hydro resources. Research and development in renewable energy is insufficient. To ensure appropriate development in the area Due to several forms of these sources is extremely difficult. Comprehensive and successful solution is hard to imagine without support in this area. Research and development activity has been poorly funded by the state budget through "state research and development" and "state orders for research and development." For the energy sector has been created a national cross-sectional research and development program "Application of progressive principles of production and transformation of energy." The priority focus of research and development will be field of energy that will bring benefit the whole society and will result in the introduction of such technologies that enhance the competitiveness of the Slovak economy. To support specific projects for international cooperation to use funds from the Structural Funds [1].

Providing some of the measures to achieve energy policy objectives in the long run would be complete without the direct support of funds from public sources. This requirement is particularly topical in the case of the implementation of measures to use renewable sources for heat and power production, increasing energy efficiency, reducing energy intensity and research and development in energy. Possible sources of funding projects in different areas are: resources of project; resources coming from EU structural funds; state budget; funds obtained through the implementation of methods for Public—Private—Partnerships and obtained by alternative financing—financing by third parties. Apart from the question of funding plays a key role in the use of renewable sources for electricity and heat, also regulator of pricing policy. Therefore, in the next period the basic aim in this area will create space for the stability of the regulatory framework, its identification of longer term (over 5 years) so as to ensure a reasonable return on investment. Contractor of individual measures will have clear rules for the calculation of return on investments [1].

The Visegrad Group—V4 was established as a tool for cooperation in several sectors, the group is led by the Presidency, which is changed every year. One of the effects of the gas crisis was the elaboration V4 + Budapest Declaration, 24 February 2010, which created a framework for: flagship project of common gas connections of V4 countries and further development of this cooperation-Bratislava Declaration from January 25, the 2011th. It has since the cooperation was expanded, set up the working group V4 + for sectors of oil, energy security and strategic issues of EU. Regional cooperation promoted by the European Commission—the

Fig. 24.2 The cooperation of the Visegrad V4 [3]

establishment of the High Level Group for north–south connections (V4, Croatia, Bulgaria, Romania) and its integration into strategic documents: covers all sectors (electricity, gas, oil); study prepared by a private company and action plan with a list of projects. Strengthened regional cooperation by ENTSO-G and ENTSO-E, also supported by Regulation 994/2010 of security of gas supply (common preventive and emergency action plans). As an example, short-term electricity market with the Czech Republic [3] (Fig. 24.2).

Economic policy of the Slovak Republic from the perspective of low-carbon economy presents basic pillars of medium-term objectives as follows: reduction of greenhouse gas emissions by 20 % in 2020 compared with 1990; Slovakia does not yet have a comprehensive strategy for low-carbon economy—but available are from a number of sectoral strategies, policies and measures, climate change policy; government prepared a revision of institutional coordination—climate change policy and other policies; Slovakia continually meets and exceeds short term goals of greenhouse gas emission saving; between 1993 and 2010, CO_2 emissions per unit of HDP fell by more than 60 % and reduction of that parameter confirms massive technological restructuring and the transition from coal to burning oil and gas [3].

National Action Plan for renewable energy set targets for individual sectors and technologies, planned production and consumption. The total estimate of the share

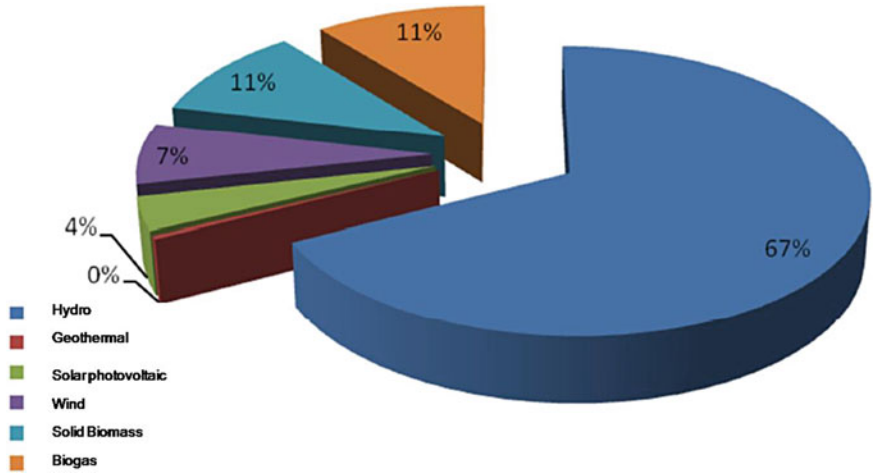

Fig. 24.3 Target for the production of electricity from renewable energy in 2002 by technologies GWh [4]

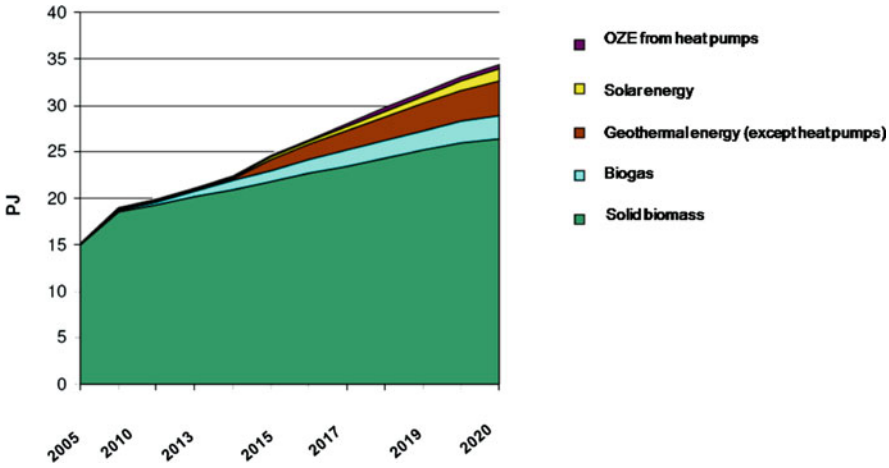

Fig. 24.4 Target for heat production from renewable sources in 2020 by technology (PJ) [4]

of renewables in gross final consumption is 15.3 %. Then it describes existing and planned systems of support and legislative framework for Slovakia. On Fig. 24.3 is introduced target of electricity production from renewable energy sources for 2020 by technology [4].

Subsequently Fig. 24.4 presents the historical development of heat production from renewable energy sources in Slovakia and the forecast for 2020 by technology.

Within the application and use of renewable energy legislative framework has been modified in practice (Law on the promotion of renewable energy and high-efficiency cogeneration). Changes in the law on renewable energy sources—development of the sector of photovoltaic (PV) has proved to be unsustainable particularly for high impact on consumer prices and concerns about land use. Adjustments in the law were mainly related to support equipment of PV with a maximum capacity of 100 kW, exclusive installation on the roofs of buildings and flexible purchase prices reflecting the cost of investors [1].

24.3 System Analysis

2nd In-Depth Review: Report of the Slovak Republic (2011).

Evaluation criteria were based on common goals IEA (Shared Goals en.)—defined 4 June 1993 at a meeting in Paris. The evaluation team conducted working visits in selected institutions in Slovakia during the 21st–26 November 2010. Composition of the team was as follows: Roman Portužák (Head)—The Ministry of Industry and Trade CR, representatives of 5 other IEA member countries, 1 European Commission representative, 1 representative of the Agency OECD for nuclear energy, 4 representatives of the IEA, comments and editorial assistance: other experts IEA Slovakia has a reserve in energy policy, according to the International Energy Agency (IEA). Slovakia should add the question of strengthening of energy security and competitiveness of industry. According to a survey of energy policy of Slovakia, Slovakia should also continue in diversify energy resources and deepen regional integration. Strengthening of regional cooperation, particularly in the gas development and electricity interconnection, represents a major step to increase energy security and market competition. IEA Report, which charts the years 2005–2010, recommends to Slovakia's energy efficiency to focus on implementation, to ensure full utilization of the potential energy savings, including the modernization of district heating. Slovakia should also aim at reducing greenhouse gas emissions according to the report. Slovakia should continue to implement policies that facilitate the transition to a low carbon economy. Nuclear energy and renewable energy should make this issue a critical role [5].

24.3.1 SWOT Analysis of the Evaluation Survey

In view of formal aspect is a unique strength of clear and logical structure of the text under three main headings: Policy Analysis SECTOR ANALYSIS + ENERGY TECHNOLOGY. Also consider for the strength the sub-themes under headings: 3 + 7 + 1 topics within three main areas and a transparent structure processing individual topics (usually similar for all subjects). Appropriate use of

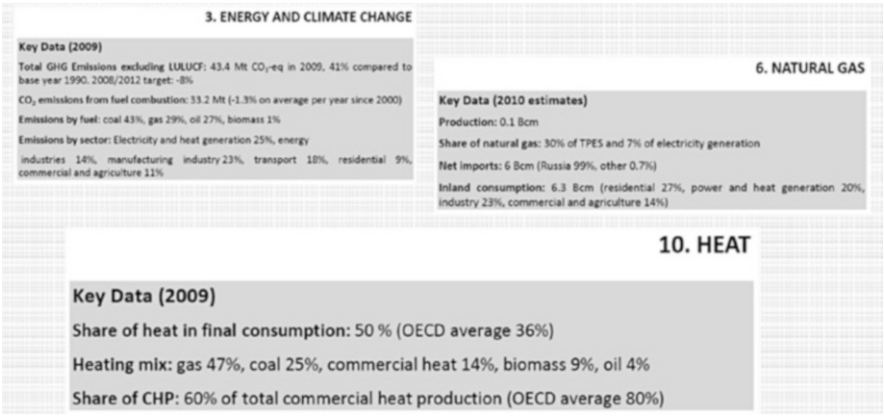

Fig. 24.5 Some examples of basic summary at the beginning of chapters [4]

graphs, whose aim is to bring Slovakia comparison with other IEA member countries by selected indicators, we characterize as the last of the strengths of the formal point of view. Strength is evaluated in terms of content rich statistical data (including historical data and future expectations of government). In terms of methodology is evaluated as a weakness selection of respondents, i.e. only 21 institutions (5 ministries, 2 regulators, 3 other government agencies, 4 academic institutions, 5 (semi) public companies, 2 business associations). In our view, should be addressed another big company (SE, MOL, heating companies, etc.)., DSOs (particularly electricity), more alternative energy suppliers (households, small commercials, wholesale), the research-oriented companies and institutions (Geothermal Anywhere, SOVVA—a center of excellence stub), Energy analysts also (ESI, energia.sk). Weakness in terms of data update in mind and accuracy are unclear Timing of data updates (interviews 2010, references in the text—and the 2011 edition of the study: 09/01/2011, Publication: 11/21/2011). Study also does not reflect many significant changes in 2011 (market opening, sunny "boom," etc.). We evaluate as weakness sometimes confused logic when interpretation of data, i.e. "Lobby" for wind and sun (?) causality between OZE and energy efficiency (?), market coupling vs. flow-based method in the context of the single energy market, a number of factual inaccuracies: vague definition of regulatory authorities in the institutional framework (URSO + RADA), CZ-SK intra-day market coupling 2005, NJF problems—lack of income from electricity customers + NJF defined only descriptively, factual inaccuracies in the report is unfortunately quite a lot [5–9] (Fig. 24.5).

24.4 Results and Discussion: Partial Introduction of Methodology Depth Survey

24.4.1 Conclusions and Recommendations for the Subsequent Realization of Research

Based on the implemented SWOT analysis we are putting forward proposals for the implementation of subsequent surveys in the EU economy countries, including Slovakia. Recommendations: assessment of the development from the last in-depth review; evaluation of major achievements and not achieved objectives of the Government of SR from the last in-depth review; use of selected case studies (case studies) to illustrate the achievement of objectives compared with the previous in-depth review; deeper analysis of the positions and views of major players in the energy sector (government, regulator, business, analytical centers); extension of the respondents and precise definition of data updates [5].

24.4.1.1 Partial View of the Author to the Energy Market in Slovakia

At the energy market, there are anomalies and these are their system of trading with emission allowances, production support of renewable sources as well as capacity payments to producers for maintaining power system stability. The original intention of emissions trading is gone. The trading of emission allowances false market, because it impossible to predict future developments. When the investor cannot predict what will be a few years, it is unrealistic to want to invest. From emissions trading has become a huge business. Emission allowances were allocated free of charge, but ultimately is still reflected in the price of electricity. By selling emission allowances, many companies have created huge profits. Market so consequently did not generate investment incentives, and only a tiny portion of these earnings was invested in the original intent. Emission allowances should had been used initially as an investment incentive to build cleaner sources that did need emissions. The point was completely lost. A market was created that works on political decisions and not on fundamentals. Emissions trading is clearly influenced by political decisions. This is related to corruption and cronyism. The current situation is that the system is the stockpiling by allowances at least till 2015. Another anomaly of the energy market is guaranteed by the state support of electricity from renewable sources. In the case of subsidy mechanisms comes to artificial investments that are not supported by the natural evolution of the market. The guaranteed prices for 15 years ahead of production has become a green clean energy business without any risk and original noble purpose of manufacturing “clean” energy has been denied. During 2010, the return on investment was given for 5 years. For 10 years it is the net earnings for the investor. Another anomaly is the capacity market payments to producers for maintaining power system stability. The energy source would have been able to collect fund an annual basis regardless of whether it actually

manufactures or produces electricity. To stabilize the market by removing the anomaly becomes necessary. The solution can be integrated intraday (intra-day) market and change of strategies to promote renewable energy. Doing business without risk is unthinkable. Alternative energy must therefore become an active participant in the market [5–9].

24.4.1.2 Sub-personal View of the Author to the Privatization of Power Distribution Network Companies

The privatization of energy distribution companies in Slovakia took place from the first view in a standard way. At the end of 2005 The Slovak Government finally approved the sale of shares of West Energetics, Inc. (ZSE) Currently owns 40 % stake of distribution companies ZSE German company E.ON The remaining 10 % stake FNM sold through the capital market. The European bank for reconstruction and development (EBOR) owns 9 % shares in ZSE. Ministri of Economy wanted to do likewise in a case of privatization of Central Slovak Energetics (SSE), Inc. Zilina and Eastern Slovak Energetics (VSE), Inc. Kosice, where 10 % of shares were supposed to sell through the capital market. The plan of privatization of other two energy companies, however, did not take place as originally planned. The minority 49 % stake of shares in the company of the SSE's from October 2002 is owned by the French company Electricité de France. German energy company RWE Energy is the owner of 49 % of the shares of VSE Company from 2003. The remaining 51 % stake in both companies is owned by FNM. A contract concluded between the Fund of National Property of the Slovak Republic, Slovak Republic represented by the Ministry of Economy and each shareholder of EDF, or EON or RWE were from at least one reason unsuitable for SR. From the first point of view the minority stake of EDF company for example becomes redundant with the agreed terms of the majority occupy managerial positions in the energy distribution company. Any decision-making powers are clearly in the hands of the French shareholders. So basically the majority owner holds the decision-making is a quasi-foreign minority owner. Sapidity is a description of the decisive influence, which means that in relation to any person or shares, the opportunity directly or indirectly manage or direct the management of a person or shares through stock ownership, voting rights, corporate, shareholder or other agreement governing ownership interests, or otherwise. Logically follows that the majority owner of shares i.e. 51 % of Slovak shareholder has a decisive influence. But compared with the real distribution board in the energy distribution company in five members, which the board representing the Slovak shareholder has only two members of and French shareholder has three members, has become a very lucrative business for French shareholders. Is inconceivable that the Slovak shareholder made this situation when with the full knowledge agreed and sold quasi all the energy sector with a positive lock for the foreign investor, that can attack the general public in front of media about the major responsibility of the SR for decisions made in the above energy

distribution companies, which manager representing the Slovak shareholder has no decisive influence and reach [5–9].

24.5 Conclusions

The main recommendations for Slovakia from the viewpoint of the authors are mainly to create a coordinated policy to optimize the environment in key sectors for market with the priority aim of improving the climate in Slovakia and the EU, including the specific cap-and-trade. Implement a comprehensive national energy efficiency of strategy aimed at reducing energy consumption, with an explicit focus on transport policy and construction industry and exploiting strategic position between the EU and Ukraine and Russia in terms of the position of the distributor—to create the optimal infrastructure necessary to facilitate the supply and access to markets. One of the major recommendation in carbon capture and storage (CCS) is to reduce CO_2 emissions from electricity generation from fossil fuels, mainly coal and gas, but CCS can be applied in the CO_2-intensive sectors, refineries, cement production, iron and steel, petrochemicals, oil and gas processing and elsewhere. The application of carbon technology in the industrial environment becomes a whole new line of business, thereby creating a new business sector, which will be beneficial to human health, the environment, rationalize the use of energy resources, entrepreneurs in this sector will benefit from the expertise of energy and other industry and economy depend on combustion plant. Recommendations of the international energy agency under research are as follows: The government of the Slovak Republic should enhance energy security by supporting infrastructure projects which diversify energy supply sources and routes and continue to pursue its national energy policy objectives within a regional context, strengthening regional co-operation, integrating regional energy markets and supporting increased interconnections. At the next part the government of the Slovak Republic should step up CO_2 emissions reduction efforts, notably in the transport and buildings sectors, including through the creation of a detailed plan with specific actions and interim targets and an assessment of the cost-effectiveness of different mitigation measures, to ensure the national target for non-ETS emissions is achieved and ensure timely implementation of energy efficiency policies and measures and raise public awareness of energy efficiency improvement options, given the critical importance of energy efficiency for energy security, climate change mitigation and economic competitiveness. At the last part the government of the Slovak Republic should ensure a stable and predictable legislative framework, with an independent and adequately resourced regulator, to encourage investments in energy projects in accordance with the long-term national energy strategy [5–9].

Nomenclature

E Energy (kJ) The joule (J) is a derived unit of energy, work, or amount of heat in the International System of Units. The petajoule (PJ) is equal to one quadrillion (10^{15}) joules
$\dot{E}$ Energy flow rate (kW)
E Energy: the terrawatt hour (TWh). The gigawatt hour (GWh)

Acronyms

CCS	Carbon capture and storage
CEZ	Czech power plants (České energetické závody)
CO_2	Carbon dioxide
CZ	Czech Republic
EBOR	The European bank for reconstruction and development
EII	Enel Ingegneria & Innovazione
EMO	Nuclear power plant (Jadrová elektráreň Mochovce)
FNM	National property fund
HDP	Gross domestic product
IDR	In-depth review
IEC	International energy agency
JEZ	Nuclear power plants
JU V1	Jaslovské Bohunice
MHSR	Ministry of Economy of the Slovak Republic
SE	Slovak power
SK	Slovak Republic
SSE	Stredoslovenská energetika a.s.
SWOT	Analysis (strengths weaknesses, opportunities, and threats)
URSO	Regulatory Office for Network Industries (Úrad pre reguláciu sieťových odvetví)
VSE	Východoslovenská energetika a.s.
V4	The Visegrad Group
ZSE	Západoslovenská energetika a.s.

References

1. Internal Document MHSR (2012) The internal material of the ministry of economy of the Slovak Republic

2. Beer G (2012) Slovak nucleus after Fukushima. J Trend 1336–2674. ISSN 1336-2674
3. Žáková A (2011) Energy policy of the Slovak Republic, of the ministry of economy. Conference: common EU energy policy and energy security of Slovakia
4. Portužák R (2011) Common EU energy policy and energy security of Slovakia. Conference: common EU energy policy and energy security of Slovakia
5. Portužák R (2012) The conference: 9th annual energy conference ENKO. Bratislava, Slovensko
6. Website SEAS: http://www.seas.sk/sk/elektrarne/typy-elektrarni/fotovoltika/fotovolticky-system-mochovce. Accessed 29 June 2011
7. Website SSE: http://www.sse.sk. Accessed 29 June 2012
8. Website ZSE: http://www.zse.sk. Accessed 29 June 2012
9. Website VSE: http://www.vse.sk. Accessed 29 June 2012

Chapter 25
Towards an Integrated Value Optimizing Ecosystem in Natural Gas Liquids Operations and Related Facilities

Farayi Musharavati

Abstract Although natural gas is one of the cleanest fuels on earth, natural gas operations and related facilities are still associated with visible ecological and waste management problems. While managing regulated waste is a direct cost to operations, managing unregulated waste is an indirect cost. However, waste becomes 'waste' when a production operation is totally isolated from the rest of the world. For example, Natural Gas Liquids (NGL) plants process natural gas into raw natural gas liquids, lean gas or refinery products. In doing so, a number of 'losses' may take place along the process system through either leaks and/or process upsets. Such loses can be considered as wastes due to inefficiencies and ineffectiveness of the process system. On the other hand, excess gas may be flared or be reinjected to enrich reservoirs. In such a case, the flared gas is a missed opportunity which also has negative consequences such CO_2 and greenhouse gas emissions. Although excess gas reinjection is a more responsible alternative, it cannot be guaranteed that 100 % of the excess gas ear marked for reinjection will be actually reinjected to enrich the resource. This scenario leads to the issue of depleting finite resources. Whatever the case may be, any form of 'waste' does not give value to the business, employees or consumers of the end product. As such, it is important for operations to look beyond their boundaries for possibilities of creating value out of inevitable 'waste.' One way of meeting this challenge is to develop an integrated value optimizing ecosystem that seeks to eliminate waste or at least convert 'waste' into value. In this paper, it is postulated that value can be created through utilizing 'waste' by integrating NGL operations and related facilities. In order to allow the ecosystem to evolve as and when required, a framework for continuously creating, maintaining and sustaining value in NGL operations and related facilities is proposed. The operational aspects of such a framework are discussed with the aid of an NGL plant case study. It is shown that in an integrated value optimizing industrial ecosystem 'waste' can be eliminated or at least be reduced to a minimum while value to the customer and business operations is increased. This allows operations

F. Musharavati (✉)
Department of Mechanical and Industrial Engineering, Qatar University,
Box 2713, Doha, Qatar
e-mail: farayi@qu.edu.qa

I. Dincer et al. (eds.), *Progress in Sustainable Energy Technologies Vol II: Creating Sustainable Development*, DOI 10.1007/978-3-319-07977-6_25

to progressively move towards a closed loop operating system where 'wastes' become inputs for current, new and future processes.

Keywords Integrated value optimization • Industrial ecology • Ecosystem • Symbiosis • Closed loop operating system • Natural gas liquids (NGL) • Natural gas

25.1 Introduction

To date the concepts of green engineering and sustainable operations have been accepted in most oil and gas processing operations and related facilities. A number of methods, mechanisms and techniques on emerging technologies and their potential applications and impact on the oil and gas industry have been discussed for quite some time [1]. These methods, mechanisms and techniques have: (a) enabled realizations of improved operating efficiencies; (b) boosted confidence, potential and possibilities of reducing and/or eliminating waste (solids, liquids and gases); (c) helped companies to understand and gain mileage on critical issues such as, extending the life of non-renewable and recoverable resource reserves; (d) helped companies to be more conscious about the impact of CO_2 emissions and greenhouse gas (GHG) emissions; and (e) helped companies to realize that beyond greening lies a great challenge and responsibility of sustainable operations, development and growth. Despite all these efforts, oil and gas processing operations and facilities are yet to realize leading value indicators of sustainable operations and manufacturing excellence. There is, therefore, an inherent need to develop new operational systems that can scale the heights of operational excellence in a sustainable and cost effective manner.

Managing regulated waste is still an inevitable practice in the oil and gas industry even though it is clearly known that regulated waste is a direct cost to operations. On the other hand, managing unregulated waste is an indirect cost associated with CO_2 emissions, GHG emissions, ecological problems and environmental degradation. Managing both regulated and unregulated waste in a complex system composed of different types of processes, different operations in different facilities is not an easy task. A possible solution suggested in this paper is to develop and implement an integrated value optimizing ecosystem that can address the challenges of optimizing the exploitation of non-renewable resources, maximizing recovery of recoverable materials and energy, and meeting unexpected supply and demand targets.

Waste does not give value to the business, employees or consumers of the end product. As such, it is important for operations to look beyond their boundaries (plants, companies) for possibilities of creating value out of the inevitable 'waste.' One way of meeting this challenge is to develop an integrated value optimizing ecosystem that seeks to increase value and eliminate waste or at least convert 'waste' into value. For NGL production, value can be created through utilizing 'waste' by integrating all NGL operations and related facilities. Such an integrated

approach allows the creation of an industrial ecosystem that evolves as and when required. This requires transparency, information and data availability, reliable communication systems, dependable and real-time collaboration and a framework for continuously creating, maintaining and sustaining value in NGL operations and related facilities. Such a framework allows operations to progressively move towards a closed loop operating system where 'wastes' become inputs for current, new and future processes.

The aim of this paper is to explore, investigate and identify key components for creating an integrated value optimizing ecosystem in natural gas liquids operations and related facilities. In natural gas processing operations there are interactions between people (workers), materials, energy and a number of processes that are used to covert inputs to desired outputs. For the discussions in this paper the term related facilities is used to describe all operations, other than the NGL extraction and production plant, that need products and/or by-products of the NGL production for direct or indirect use or for further processing into other products. The approach used in this paper takes a systems view of natural gas processing operations and related facilities. In this way, the dynamics of the interactions among people, materials, energy, processing plants and related facilities can be analyzed in order to identify system parameters and constraints that impact on an optimum match of system inputs and outputs within the limits of local and global carrying capacity.

25.2 Background

Ideas of industrial ecosystems originated from environmental studies that considered an ecosystem as a limited space within which living beings interact with nonliving matter at a high level of interdependence to form an environmental unit [2]. These ideas were latter conceptualized for applications in industrial settings by Frosch and Gallopoulos [3]. Since then, many researchers have discussed and developed concepts for implementing industrial ecosystems. These include: Allenby and Richards [4]; Hard and Grundel [5]; Gondkar et al. [6]; and Tsvetkova and Gustafsson [7].

Most researchers, for example [4, 6] discuss and develop industrial ecosystems based on analogical references to natural ecology. In this view, the various components of production operations such as; workers, raw materials, energy, water, consumers of the products, factory wastes (liquids, solids and gasses); by-products, recoverables, and consumables are analogous to biological organisms in natural ecology. As such, most industrial ecosystems research has focused on exchange of resources, mentioned above, among production-consumption units or a cluster of companies. Examples of such approaches can be found in [7–9].

Despite the various efforts and progress in studies of industrial ecosystems a number of loose ends are yet to be tied. For example, a unified theory that describes characteristics and behavior of industrial ecosystems is yet to be desired [10]. Therefore, the actual dynamics of an industrial ecosystem are not known and, therefore,

not well understood. In addition, the economics and the business side of industrial ecosystems offer little incentives. Obvious economic advantages of industrial ecosystems include efficient and effective use of resources. While this advantage has significant impact on sustainability, its impact on the business side (i.e. reduce costs and increase benefits) is relatively less. Moreover, the dynamics of how the costs and benefits will be apportioned among the network of companies in a given industrial ecosystem are not known beforehand.

Since the concept of industrial ecosystems originated from ecology and biological organisms, the issue of evolution in industrial ecosystems cannot be ignored. Therefore, an important fact that cannot be ignored is how to maintain and/or sustain (a) a functional industrial ecosystem, (b) environmental benefits, the business aspect and the economic advantages of inter-company network in given and evolving industrial ecosystems. The issues raised above can be partially addressed by putting in place mechanisms for; effective information flows across the network of companies, effective cooperative management, and continuous real-time collaboration and by developing an inter-company culture that support the continuous and smooth evolution of the industrial ecosystem.

Discussions in the previous paragraphs have revealed a number of drawbacks in the establishment of industrial ecosystems. Such drawbacks include: (1) lack of economic incentives, (2) lack of willingness to invest in technologies that support industrial ecosystems, (3) lack of efficient information flows to and from the companies that constitute an industrial ecosystem, (4) lack of cooperative management, (5) the need for continuous collaboration and (6) the establishment of a culture that supports a functional industrial ecosystem. Albeit, the underlying concept in industrial ecosystems is that one company's products, by-products or wastes (solids, liquids and gases) can become inputs in other companies within the industrial ecosystem. This concept requires an understanding of the functional dynamics of inter-company resource flows and resources exchanges. This concept also goes beyond exchange of resources to inter-company exchange of by-products and wastes. Thus, value can be added to by-products and wastes in an industrial ecosystem. Hence, progressive assessment methods and sustained production optimization are vital tools in any given industrial ecosystem.

The concepts described above are relevant to the oil and gas industry, in particular natural gas processing and related facilities. A prominent example that will be used as a case study in this paper is a Natural Gas Processing Complex (NGPC) consisting of four Natural Gas Liquid (NGL) plants and Storage and Loading Facilities (SLF). The NGL plants and related facilities in the NGPC were commissioned at different times and they underwent a number of changes, upgrades and retrofits over the years. This NGPC processes natural gas into: (a) products, some of which are sent to SLF for export-these are mainly heavy hydrocarbons, while some of the products such as lean gas are sent directly to consumers such as power plants and the industry in general; (b) useful (value added) intermediate materials such as raw natural gas liquids, which are inputs to other NGL plants; (c) by-products such as; NGL condensate—which is sent to SLF, stabilized condensate—which is either sent to refineries or exported, and liquid

sulphur which is sent to two different companies in which the liquid sulphur is a raw material input; and (d) surplus natural gas which is re-injected into natural gas reservoirs or flared. This description shows that in the NGPC, materials and energy can be allowed to flow among a network of different companies and related facilities while by-products and value added intermediaries are exchanged and thus effectively recycled in a symbiotic manner that, if effectively managed and coordinated through effective collaboration among the various plants and related facilities, will result in operations that resemble natural ecosystems. In order for such a complex industrial ecosystem to function in a manner that is sustainable, an integrated value optimizing framework is required. Such a framework would overcome some of the drawbacks mentioned earlier on since the business aspect (value adding and value optimization) is dynamically incorporated into the various activities, operations, energy and materials exchange, and cooperative management through right-time collaborative links among all players (i.e. suppliers of raw materials inputs, producers of products, intermediaries and by-products as well as consumers of products, intermediaries and by-products) in the purported industrial ecosystem.

25.3 Method

25.3.1 Integrated Production Operations

As discussed in [11], process integration and process optimization are crucial ingredients for sustainability initiatives. While little progress has been achieved in terms of process integration and process optimization, some of the oil and gas companies are still falling short of improving plant performance against leading value indicators of process manufacturing enhancement and operational excellence. These observations represent some of the inherent challenges associated with sustainability initiatives through the concept of industrial ecosystems.

An industrial ecosystem can be considered as a network of companies that interact through exchanging and making use of available resources, materials and/or energy in order to increase energy efficiency and increase the amount and types of process outputs that have market value [6]. A number of issues can be identified from this statement. Creating a network of companies essentially means connecting the various companies into 'one system,' i.e. an industrial ecosystem, and ensuring that the companies function together as a 'system.' In order to realize a functional network of inter-company relationships, the various players must be willing and must be committed to the development and realization of such an inter-play. This can be made even easier if all players in the network of inter-companies will gain either economically, environmentally or both. For smooth interaction to take place, interfaces and relationships among the companies must be identified and developed. This calls for transparency, cooperative management and strong

right-time collaboration. A critical issue in the development of an industrial ecosystem is improving value of inputs and outputs in the network of companies. The inputs and outputs in an integrated production operation include: products, by-products, intermediaries and wastes generated in the industrial ecosystem.

Albeit, the interrelationships among players in an industrial ecosystem require a method for assessing the performance of the ecosystem and a mechanism for integrated value optimization. The method of assessment allows the players in the ecosystem to initiate implement and evaluate sustainability performances of the various operations in terms of environmental benefits and societal behavior of the industrial ecosystem. On the other hand, value optimization mechanisms are required to continuously add value and capabilities of interactions among companies in the ecosystem. In addition, value optimization mechanisms can be used to evaluate and hence improve the economic performance of an industrial ecosystem. Moreover, continuous value optimization may become a significant factor in maintaining interrelationships among players, thereby sustaining the integrated production operations.

From discussions in the previous paragraphs, three challenges in developing industrial ecosystems can be identified as follows: (1) how to integrate a number of production operations/units/facilities in an industrial ecosystem, (2) how to optimize value of products/by-products/intermediaries in an industrial ecosystem, and (3) how to sustain the integrated production operations. These challenges require unique production operations models and/or frameworks that address the issues mentioned above in a sustainable and cost-effective manner.

25.3.2 NGL Case Study

The case study discussed in this paper is a Natural Gas Processing Complex (NGPC) consisting of natural gas processing operations and related facilities. Related facilities use the products, by-products and/or intermediary value added materials. As such natural gas processing offers great potential for the design and development of industrial ecosystems.

In analyzing natural gas processing (NGP) for industrial ecosystem development, it is crucial to ensure that there is a strong link between NGP operations and natural gas extraction (NGE) operations. This is because the type and quality of the extracted natural gas will affect the outputs and inputs (i.e. products, by-products and intermediaries) as well as process performances within the ecosystem. In addition, disruptions in natural gas supply will affect the whole ecosystem in terms of economic and environmental benefits. Therefore, natural gas supply operations must be integrated with natural gas processing operations. On the other hand, disruptions in downstream processing operations and related facilities will equally affect the industrial ecosystem. For example, if the demand for NGP products; by-products and/or intermediaries changes (increase or decrease) for any reason (e.g. maintenance, shutdown, breakdown malfunctions or malpractices) the

already extracted natural gas has to go somewhere. This excess gas can be stored (if provision for storage is available) otherwise this gas may have to be re-injected into predetermine reservoirs (if they exist) or it may have to be flared. While flaring is an opportunity cost, flaring also contributes to CO_2 and GHG emissions. Therefore, downstream natural gas processing operations and related facilities must be integrated to NGP and NGE operations. Therefore all extraction, production, processing and consuming operations/units/facilities must be integrated in order to function as a system i.e. an industrial ecosystem.

The various players, operations and facilities in the natural gas processing complex can be summarized as follows: a compendium of natural gas extraction (CNGE) platforms, i.e. NGE1, NGE2 and NGE3 supply natural gas (associated and non-associated) to a compendium of natural gas processing (CNGP) plants. In the CNGP plants, two natural gas processing (NGP) plants i.e. NGP1 and NGP2 receive natural gas directly from the compendium of natural gas extraction platforms. NGE1, NGE2 and NGE3 are offshore operations separated from each other. Plants NGP1, NGP2, NGP3, and NGP4 are physically separated from each other, although they are located in the same industrial area.

NGP1 plant process natural gas into; products, intermediaries and by-products. Hydrocarbon products from NGP1 include methane, ethane, propane and butane. Most of the hydrocarbons are sent to the storage and loading facilities (SLFs) for export, while ethane is sent to two different companies, company A and company B. Company A processes ethane to polyethylene and 1-hexene while company B further processes ethane into products such as ethylene and polyethylene. The other product from NGP1 is pipeline quality gas which is sent directly to natural gas consumers (NGCs) of two types i.e. power plants (NGC_A) and the industry in general (NGC_B). Intermediaries from NGP1 include richer raw natural gas which is supplied to NGP3 and NGP4 for further processing. By-products include natural gas liquid condensate and liquid sulphur. Liquid sulphur is sent to company B where it is used as feedstock to produce sulphur. Natural gas liquid condensate is either sent to SLF for export or used as an input in a refinery for crude spiking. Surplus natural gas from NGP1 is re-injected into a reservoir. This usually happens when consumer limitations and/or plant process upsets prevail. On the other hand, the NGP2 plant processes natural gas into hydrocarbon products such as methane, ethane, propane and butane. Like NGP1, most of the hydrocarbons are sent to the storage and loading facilities (SLFs) for export, while ethane is sent to companies A and B for further processing.

NGP3 and NGP4 plants receive relatively richer raw natural gas from NGP1. NGP3 processes the natural gas into hydrocarbon products, such as propane, butane and pentane. These are sent to the SLFs for export. Ethane rich gas from NGP3 is also sent to company A. Another product from NGP3 is natural gas condensate, which is also sent to the SLFs. On the other hand, NGP4 produces hydrocarbons such as propane, butane and pentane as well as gasoline. The hydrocarbons are also sent to the SLFs. Ethane rich gas from NGP4 is sent to companies A and B. It is obvious, from the summary of operations and facilities described above, that that there are inherent relationships among the various players. These relationships need

to be recognized, developed, established, maintained and sustained in order to initiate, develop, and consolidate the existence of an industrial ecosystem. An important observation is that there is need for integrating all production operations and related facilities. Such integration will help in synchronizing the various activities in the different operations and related facilities.

Achieving inter-company integration requires an understanding of all production operations, the various production processes and activities in each of the players that are intended to function as an industrial ecosystem. While this requirement may be difficult, time consuming and possibly prohibitive, it offers a number of benefits to all players. Besides economic and environmental benefits, other benefits include the realization that value should be achieved and maintained along the upstream in extraction plants and operations through production processing operations to downstream operations, production operations and any other related activities.

A number of technologies currently available in most modern oil and gas processing operations and related facilities can be leveraged to enhance, design and develop integrated production operations along the supply-production-distribution and consumption value chain. Example of such technologies include: intelligent predictive applications, which reduces reactive decisions and solutions; real-time collaborative links that allows collaborated decisions and solutions, process visualizations and visual interactive process simulations that allow a greater level of total process awareness and understanding; real-time process management and control, which will allow real-time intervisions to correct, adjust, improve and/or optimize production operations and processes in cases of disturbances, process upsets, and supplier-customer limitations across the integrated production chain; cooperative management, which prevents loss and eliminate or at least reduce performance problems as and when they surface and thus preventing such problems from compromising the effectiveness and efficiency of the integrated production operations. These technologies can also allow improved decision making as well as reduce risks associated with any operational activities, malpractices and malfunctions.

While most of the technologies described in the previous paragraph are available, they need to be assembled into a framework that defines how such technologies can be implemented in an industrial ecosystem. While multiple process integration (i.e. system integration of all players in the ecosystem) and process optimization are key ingredients to the success of an industrial ecosystem, other issues such as; performance degradation in any one of the players, plant availability, and variations in supply and demand may result in sub-optimal operations that often lead to production losses and hence unequitability in terms of economic and environmental gains and benefits among players in an industrial ecosystem. Therefore, production optimization must be continuous in order to sustain the relationships, connecting links and interfaces in the industrial ecosystem. A method for strategizing integrated production operations as a sustainable value optimizing ecosystem will be discussed in the following sections.

25.3.3 Value Optimizing Ecosystem

Technologies that are required to functionalize an integrated value optimizing ecosystem include; intelligent monitoring and control, model-based simulation, automated diagnostics and collaborative technologies. However, what is currently missing is an operational framework that allows an ecosystem to function as well as continuously assess and improve value. To realize the benefits of a value optimization ecosystem, integrated production operations (IPOs) must be functional and the functionality must be sustained throughout the life span of the ecosystem. Since the IPOs are composed of different processes that are interrelated and hence interconnected, total process knowledge and information must be available at the right time in order to facilitate concurrent process optimization, concurrent process management and concurrent as well as collaborative decision making across the IPOs. Since the ecosystem will evolve, optimization parameters for the IPOs are essentially moving targets that may prove difficult to identify, track and implement in order to sustain optimization.

The relationships among the players in an industrial ecosystem can be viewed as consisting of suppliers of inputs (i.e. products, intermediaries and by-products) and customers of outputs. The suppliers need to understand the type of services they are offering in the industrial ecosystem. They need to know that they are supplying the right product, the correct amounts, and the right quality of supplies. This requires regular discussions with the respective players about the services and solutions that their unit provides. Such discussions will ensure value and also strengthens the relationships among the suppliers and customers in the ecosystem. In addition, regular and continuous dialogue also assures a timely and quality delivery of supplier-customer services. In order to sustain the ecosystem, it is also necessary to cooperatively manage and collaboratively improve the value exchange interfaces of the various services offered.

Besides the challenges of designing and developing an industrial ecosystem (as discussed in the previous sub-section), operating an industrial ecosystem is another challenge. As pointed out previously, maintaining and sustaining value in an ecosystem is vital to the continued existence of the ecosystem. All players in the ecosystem must continue to realize value. An ecosystem offers a number of benefits to the players. These benefits include; economic, environmental and societal. Players in an ecosystem will continue to be engaged and committed as long as the perceived benefits continue to accrue. This continuity will also help to sustain IPOs. For the ecosystem to function and continuously generate environmental and economic benefits, a value optimizing framework is required. A proposed NGL industrial ecosystem and the value optimizing framework within the industrial ecosystem will be discussed in the following section.

25.4 Results and Discussions

An overview of relationships among players in the proposed NGL industrial ecosystem is shown in Fig. 25.1. Figure 25.1 shows a total of fourteen separate entities of different sizes and located in different geographic areas within a country. These entities include: 3 natural gas extraction operations (NGE1, NGE2 and NGE3); 4 natural gas processing operations (NGP1, NGP2, NGP3, and NGP4); 2 different pipeline quality natural gas consumers (i.e. power plants and industries); 2 different companies (A and B) that use products and by-products from the natural gas processing complex, 1 storage and loading facility (SLF) which receives hydrocarbon products from the natural gas processing complex for export; 1 refinery which uses a by-product from the natural gas processing complex and 1 facility that distributes gasoline for local consumption.

In Fig. 25.1 it can be observed that one entity's product, value-added intermediary, by-product or waste (liquids, solids or gases) is either used as feedstock in another entity's or is consumed directly. An example of a product from one entity that becomes feedstock of another entity is the ethane rich gas that is produced from the entity NGP4. After production the ethane rich gas it is sent two different entities

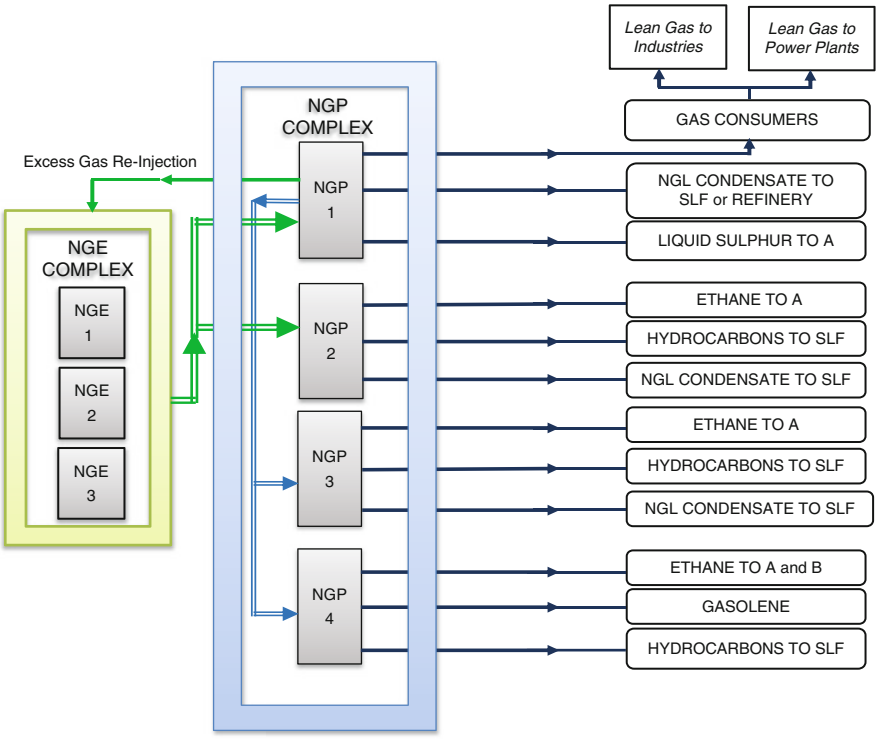

Fig. 25.1 Overview of the natural gas processing complex and related facilities (NGPCRFs) ecosystem

(companies A and B), where it is used as feedstock for producing different types of products. Examples of value-added intermediaries produced from entity NGP1 are raw natural gas liquids (NGLs). The produced raw NGLs are then sent to either NGP3 or NGP4 as feedstock for producing hydrocarbons that are stored for export in a SLF. An example of a liquid waste that is produced from the entity NGP1 is liquid sulphur, which is sent to entity company A where it is used as feedstock to produce different types of products. The relationships described above illustrate symbiotic relationships (ecological input and output) that naturally lend itself as a potential industrial ecosystem.

Table 25.1 shows the input–output relationships of the various entities in the proposed industrial ecosystem. The materials in Table 25.1 exclude the usual wastes (solids, liquids and gases) and emissions that are associated with natural gas processing and related facilities. These wastes also represent other opportunities for intercompany resource exchange in the proposed industrial ecosystem.

25.4.1 Integrated NGL Ecosystem

For the integrated NGL ecosystem to work effectively, a common collaborative environment that contains all the necessary and critical data and information about the various processes and operations in all players must be created on a common platform that is easily accessible by all players. Such an environment must be able to provide accurate real time data and information which can then be used for cooperative management and collaborative decision making. The data and information should capture both the necessary and critical data in order to enable better management of the ecosystem in a sustainable and cost effective manner. The real time collaborative environment will leverage the available technology by providing decision analysis and decision support; total process monitoring and control across all players; prediction and optimization capabilities in the integrated NGL ecosystem; total process safety monitoring; error detection and recovery capabilities as well as maintenance and repair diagnostics. At present these technology are scattered all over public literature and have been used to manage and control complex adaptive systems [10]. Such technologies can be easily adapted for use and implementation to enhance production operations and improve operations towards manufacturing excellence and leading indicators of industrial ecosystems.

Since the optimization performance of the ecosystem will evolve with time, software integration of total process models can also be leveraged in real time in order to track moving optimization targets as the ecosystem evolves. This feature will resolve any conflicting objectives during the evolution process and can be used to execute a moving horizon optimization strategy for the integrated NGL ecosystem. Such a strategy will help in sustaining optimization across multiple processes over the life of the ecosystem. The main production-critical equipment in an ecosystem requires accurate interpretation and prediction of performance data. This data can be used for cooperative management and collaborative decision

Table 25.1 Input–output symbiotic relationships (intercompany resource exchange) among the various entities in the proposed industrial ecosystem

Entity type	Typical operations	Inputs (supplier)	Outputs (receiver)	End-use	Typical emissions
NGE 1	Natural gas extraction from field	Natural gas extraction resources and accessories	Natural gas (NGP complex)	NG consumption (NGC_A & NGC_B)	Flue gases
NGE 2				Hydrocarbons (to SLF for export)	Insignificant
NGE 3					
NGP 1	Natural gas processing & recoveries (NGPCRF)	Raw natural gas from field operations (NGEC)	Raw natural gas (to NGP3 & NGP 4)	Ethane to A & B Hydrocarbons, NGL condensate & gasoline to SLF	Flue gases and regulated flared emissions
NGP 2			Hydrocarbons NGL condensate Gasoline (to SLF)		Insignificant
NGP 3		Raw natural gas from NGP 1			
NGP 4					
SLF	Storage, loading for local and international export	Storage and loading resources and facilities	Hydrocarbons Gasoline NGL condensate (consumers)	Consumption Exports	Insignificant
Refinery	Refining operations	Stabilized condensate (NGP complex)	NGL condensate (to SLF for export)	Export	Insignificant
Gasoline	Storage, loading for local and international export	Storage and loading resources and facilities	Consumption	Consumption	Flue gases
NGC_A	Power plant operations	Power plant resources and facilities	Consumption	Consumption	Flue gases and regulated flared emissions
NGC_B	Various industry sectors	Industry resources and facilities	Consumption	Consumption	Flue gases and regulated flared emissions
A	Ethane recovery processing	Ethane rich gas (NGP complex)	Polyethylene & 1-hexene	Consumption	Flue gases
B	Ethane recovery Processing Sulphur processing Operations	Ethane rich gas (NGP complex) Liquid sulphur (NGP complex)	Ethylene & polyethylene Sulphur	Consumption	Flue gases

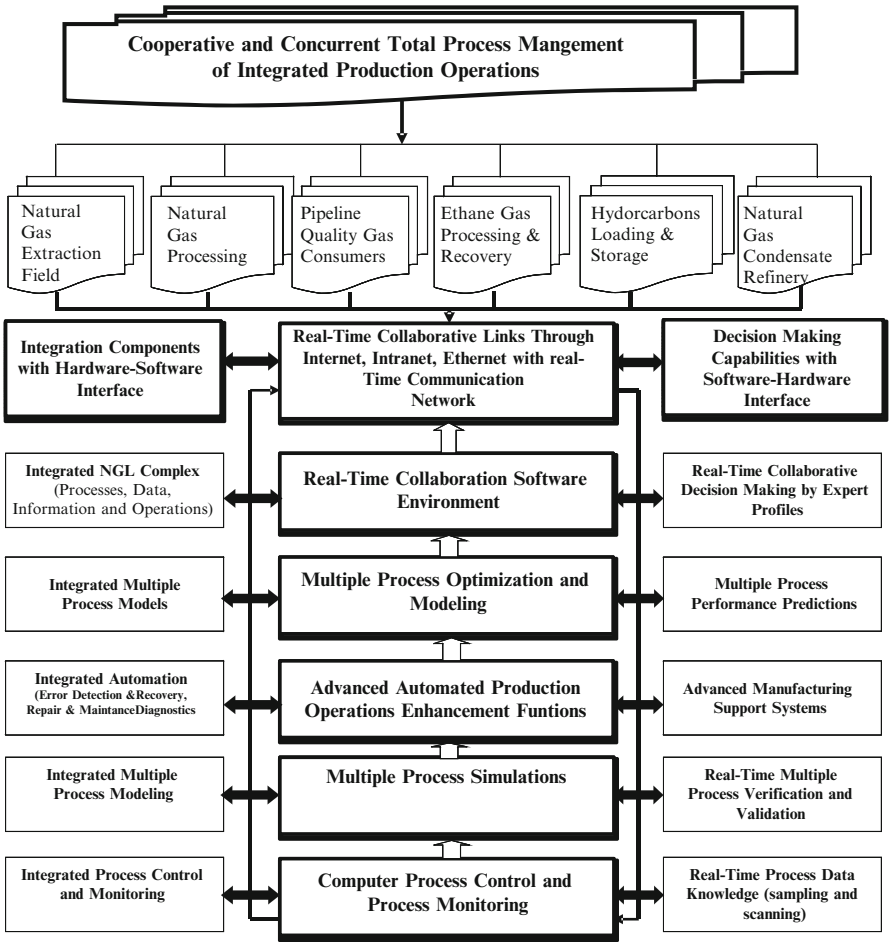

Fig. 25.2 Operational framework for an integrated natural gas processing and related facilities complex

making in bid to avoid reactive management. The software and hardware features that enables the operations of an integrated NGL ecosystem can be designed to operate as a closed-loop control system enhanced with advanced automation functions that provide real time multiple process adaptive control feedback. Figure 25.2 shows an operational mechanism for deploying functionality in an integrated NGL ecosystem.

Figure 25.2 shows that there are some feedback loops that are used in a continual decision making fashion. Closed loop management and control (through collaborated and cooperative process performance feedbacks) allows the integrated NGL production operations to track the moving optimal point targets. The accumulated data will act as an expert support resource (in addition to human expert profiles) that can be used

to verify and validate multiple process models and simulations in order to provide updated data and information. This updated data can be used to optimize the supply-production-distribution-consumption chain in a collaborative environment. The central goals of the collaborative environment include; continuous integrated production enhancement, achieving operational excellence, realizing sustained production optimization, reducing operating costs and maximizing return on investments.

25.4.2 Value Optimizing Framework in an NGL Ecosystem

Like sustainability, the move towards an industrial ecosystem usually suffers the drawback of lack and reluctance to invest in environmental innovations [7]. In order to realize the move towards industrial ecosystems, innovative value creating mechanisms, methods and frameworks that mitigate this drawback need to be developed. Figure 25.3 shows components of a value optimizing framework for supporting, maintaining and sustaining value an integrated NGL ecosystem.

The integrated NGL ecosystem has been visualized as consisting of a chain of suppliers, producers, distributors and consumers of products, value added intermediaries, by-products, and wastes. While the underlying concepts of an industrial ecosystem revolve around economic, environmental and societal benefits, the most important benefit i.e. economic are not directly realized by all players in the ecosystem. However, environmental and societal benefits can be directly realized. Therefore, value creation is critical to the design, development and continuity of an ecosystem. This requires innovative mechanisms and methods that can assess, evaluate and derive value from the various interactions within the network of players in the ecosystem. Continuous creation of value can be done by critically examining the input output relationships among the network of players. All wastes (solids, liquids and gases) can be considered as opportunities for continuous value creation. continuous value creation (tangible, non-tangible) tends to position operations towards leading value indicators through production enhancements and operational excellence. It has already been shown that the input output relationships in an integrated NGL production operations has many products (e.g. hydrocarbons) intermediaries (e.g. raw natural gas) and by-products (e.g. liquid sulphur) all of which may act as feedstock in different processes to create a diverse range of products that are required by distributors, producers, consumers and customers.

Creating value in an integrated NGL production operation would, for example, involve the production of the right quality and right-first-time hydrocarbons. Since these hydrocarbons are sold to other players within the network (local, regional or international) producing high value hydrocarbons would eliminate or at least reduce the need for multistage recoveries and purification processes on the part of the producer. This effectively reduces production costs (tangible economic benefit) on one hand while the producer receives reputation to deliver (intangible benefit) the right quality, the right offering, at the right price for the right company (i.e. since the company receiving the hydrocarbons will be part of the ecological ecosystem).

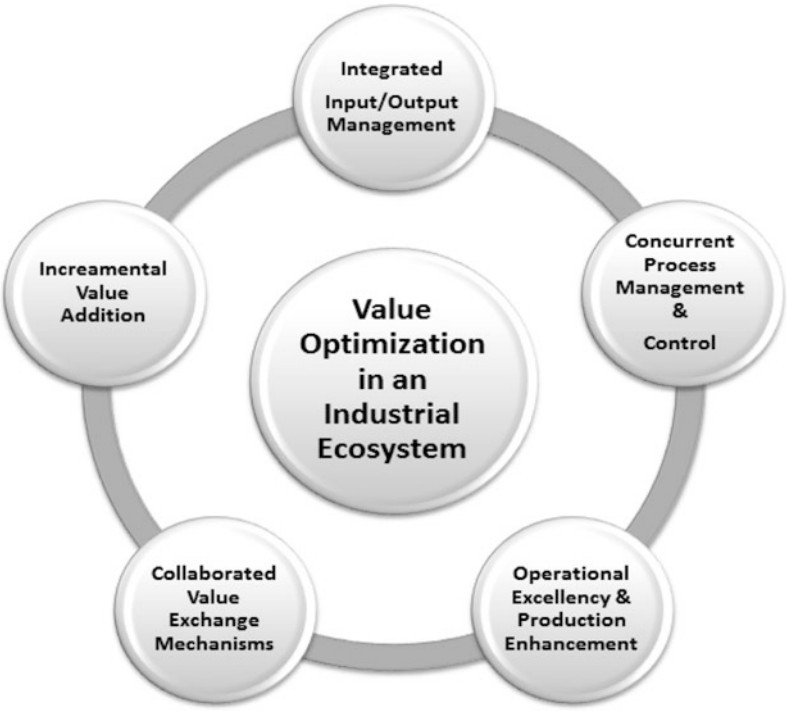

Fig. 25.3 Value optimizing framework for a functional NGL ecosystem

The receiver of the high value and high quality hydrocarbons benefits from using a good product. If the receiver will further process the high value high quality hydrocarbons, this will eliminate any pre-processing operations and the emissions and effluents will be relatively less. On the other hand, innovative ideas to create value out of, for example, gaseous emissions (i.e. indirect value linked to meeting stringent environmental regulations and directives) will result in societal benefits. This can be further improved towards achieving leading environmental indicators and best practice.

Figure 25.3 shows that in order to optimize value in an ecosystem, a basic step is to create an integrated input–output management process that examines and account for all forms of inputs and outputs (solids, liquids, gasses, and resources). This integrated approach helps to organize and execute input–output relationships in an optimal and cost effective manner. Since it will be a collaborated effort throughout the integrated NGL production operations, efficiency and effectiveness are guaranteed. The integrated input–output management process also ensures that all players know exactly what services their suppliers and customers require i.e. at what time in what quantities and for how long. In a typical NGL production operation, excess gas usually builds up for many reasons one of which is customer limitations. This often leads to regulated flares with the consequences of GHG

emissions and related costs. While the related costs may be shouldered to the limiting customer, frequent customer limitations may be undesirable. In a functional ecosystem, customer limitations can be known in advance through predictive simulation tools. Details of this limitation can be made available to all players through a collaborative environment thus reducing the frequency of unexpected flaring. Integrated input–output management also ensures that customers' expectations, perceptions and expected responsiveness are cooperatively understood and agreed upon beforehand. This will avoid dissatisfaction on the part of suppliers and producers, thus building trust and cementing the important links within the ecosystem.

In Fig. 25.3, concurrent process management and control is a function that assesses, evaluates and matches production-consumption capacities within the ecosystem. Operational excellence and production enhancements ensures that process performance is consistent, will be maintained and hence value in the ecosystem will be sustained. The logic is that total process awareness and knowledge, cooperative management and collaborative real-time decision making can embed and continuously create value into the integrated process. Collaborated value exchange finders and analysis will aim to moderate customers' perceptions and process constraints in a transparent and cost-effective manner. For this to be achieved in a transparent manner it is necessary to define and agree upon value indicators and expected service levels. Incremental value addition is an important step that ensures the continued existence of mechanisms for continuously identifying, establishing, achieving and improving value within the ecosystem. This will help to target and measure progress towards an integrated value optimizing industrial ecosystem.

25.5 Concluding Remarks

This paper has identified a number of technologies (mature, new, and emerging) that can leverage production operations into integrated production operations strategies, management and control. While integrated production operations management has been accepted as an effective and efficient way of benefiting from collaborative links and cooperative management, crucial ingredients for realizing the full benefits of integrated production operations management and control are still disconnected in most operations. In this paper, the underlying theme has been that if these technologies, methods and mechanisms are assembled together in an effective and optimal way, companies can benefit from cooperative management and cooperative decision making based on real-time data, information, historical patterns and experience. In order to illustrate this concept the necessary ingredients for moving towards an integrated value optimizing ecosystem have been discussed with reference to natural gas processing operations and related facilities.

It has been acknowledged that an ecological input–output exchange of materials, resources and energy can be cast in a way that reveals economic, environmental, and societal benefits of an ecosystem. While economic benefits may not be directly

realized, the need for optimizing value in an ecosystem has been emphasized. In this respect, a proposed integrated natural gas processing and related facilities ecosystem has been discussed. An operational framework that describes the input–output symbiotic relationships among the various players in an ecosystem was outlined. In addition, a value optimizing mechanism that aims to continuously search for incremental value addition along the supplier-producer-distributor-consumer-customer chain has been suggested as an alternative way for achieving integrated value optimization within an NGL production operations ecosystem. In the proposed ecosystem, symbiotic value adding relationships were identified and communicated through cooperative management and control of resource flows through the NGL production network.

Acknowledgements This research was made possible by a UREP award [UREP 09-078-2-021] from the Qatar National Research Fund (a member of The Qatar Foundation). The statements made herein are solely the responsibility of the author(s).

References

1. Global Oil and Gas Industry Association for Environmental and Social Issues (IPIECA), the American Petroleum Institute (API) and the International Association of Oil & Gas Producers (OGP) (2010) Oil and gas industry guidance on voluntary sustainability reporting. http://www.ipieca.org/sites/default/files/publications/sustainablity_reporting_guidance.pdf. Accessed July 2010
2. Dansereau P Ecosystem, In Canadian Encyclopaedia Historica-Dominion Retrieved 2012 from http://thecanadianencyclopedia.com/en/article/ecosystem/
3. Frosch R, Gallopoulos N (1989) Strategies for manufacturing. Sci Am 261(3):94–102
4. Allenby BR, Richards DJ (1994) The greening of industrial ecosystems. National Academy Press, Washington, DC
5. Hardy C, Graedel TE (2002) Industrial ecosystems as food webs. J Ind Ecol 6(1):29–38
6. Gondkar S, Sreeramagiri S, Zondervan E (2012) Methodology for assessment and optimization of industrial eco-systems. Challenges 2012(3):49–69
7. Tsvetkova A, Gustafsson M (2012) Business models for industrial ecosystems: a modular approach. J Clean Prod 29–30:246–254
8. Korhonen J, von Malmborg F, Strachan PA, Ehrenfeld JE (2004) Management and policy aspects of industrial ecology: an emerging research agenda. Bus Strat Environ 13(5):289–305
9. Liao W, Heijungs W, Huppes G (2012) Thermodynamic analysis of human-environment systems: a review focused on industrial ecology. Ecol Model 228:76–88
10. Chertow MR, Ehrenfeld JR (2012) Organizing self-organizing systems: toward a theory of industrial symbiosis. J Ind Ecol 16(1):13–27
11. Klemes J, Friedler F, Bulatov I, Varbanov P (2011) Sustainability in the process industry, integration and optimization. McGraw Hill, New York

Chapter 26
Mass Transfer and Bubble Flow Dynamics in Aqueous Solutions for Hydrogen Production Cycles

O.A. Jianu, M.A. Rosen, G.F. Naterer, and Z. Wang

Abstract The hydrogen economy is one potential avenue to a clean energy system, and a promising option for hydrogen production is thermochemical water decomposition. This process involves multiple steps, some consisting of multiphase reaction systems. Here, the thermodynamics and kinetics of vapour diffusion and entrainment for ascending bubbles in a vertical column are examined through experimental studies for various gas production rates. The vapour entrainment is interpreted in terms of the phase transition rate, and its dependence on such operating parameters as gas bubble size, liquid depth, temperature, pressure and concentration is examined. These effects are investigated experimentally, and a phase transition correlation is developed to analyze these parameters. Also, a predictive model is developed to simulate the physical processes of bubble transport in a vertical liquid column, as it occurs in water splitting processes such as oxygen generation in the copper-chlorine thermochemical cycle, as well as hydrogen generation in electrolytic and photocatalytic processes.

26.1 Introduction

Due to increasing impacts on ecosystems, the economic costs associated with climate change and other environmental impacts, engineers, scientists and others are increasingly pursuing clean energy technologies. A hydrogen economy in which the two main energy carriers are hydrogen and electricity is one promising

O.A. Jianu (✉) • M.A. Rosen • Z. Wang
Faculty of Engineering and Applied Science, University of Ontario Institute of Technology, 2000 Simcoe Street North, Oshawa, ON, Canada
e-mail: Ofelia.Jianu@uoit.ca; Marc.Rosen@uoit.ca; Forest.Wang@uoit.ca

G.F. Naterer
Faculty of Engineering and Applied Science, Memorial University of Newfoundland, St. John's, NL, Canada A1B 3X5
e-mail: GNaterer@mun.ca

I. Dincer et al. (eds.), *Progress in Sustainable Energy Technologies Vol II: Creating Sustainable Development*, DOI 10.1007/978-3-319-07977-6_26

approach. Hydrogen energy systems can have a significant role in providing environmental sustainability [1]. Hydrogen production is an important aspect of a hydrogen economy. Current methods of hydrogen production are often unsustainable as they are based primarily on fossil fuels such as natural gas or coal, which release CO_2 into the atmosphere. Promising alternatives for sustainable hydrogen production are thermochemical water decomposition cycles for large-scale production and electrolytic and photoelectrolytic cycles for smaller scale production. Thermochemical cycles may prove particularly beneficial for large-scale hydrogen production. One such cycle that has the advantage of operating at lower temperatures (below 600 °C) is the copper-chlorine thermochemical cycle, which uses mainly thermal energy to split water into hydrogen and oxygen [2]. This is achieved by continuously recycling the intermediate compounds (i.e. copper and chlorine) without releasing pollutants into the environment. A thermochemical hydrogen production cycle usually involves multiple steps, some consisting of multiphase reaction systems [3, 4]. To improve efficiency and cost-effectiveness, it is important to optimize the multiphase system design and the process integration.

Another method of water splitting is conventional water electrolysis, which has been used for hydrogen production since the early nineteenth century. It yields hydrogen at about 99.99 % purity compared with 98 % purity obtained from fossil fuel based methods [5]. Electrolysis produces hydrogen already separated from oxygen. However, electrolysis is relatively costly compared to other methods such as steam methane reforming (SMR). In water electrolysis, the water is split into hydrogen and oxygen using an electric current. The overall efficiency of hydrogen production through water electrolysis depends on two factors: electricity-to-hydrogen efficiency and energy source-to electricity conversion efficiency [6]. Therefore, the electricity-to-hydrogen performance of electrolytic processes is intrinsically related to mass transfer effects, which are influenced by hydrodynamics. The electrical and thermal properties of the electrolyte, diffusive transport of electroactive species and current density are modified by the dispersed phase (i.e. gas bubbles) and affect the macroscopic cell performance [7]. Fluid flow in the cell depends on the release of gas bubbles which depends on the cell design, so understanding gas–liquid flows in electrolytic systems is important for addressing mass transport, system optimization and efficiency improvement.

The gases released at the electrode surface rise upward due to buoyancy. The presence of the gas phase at the electrodes can be detrimental to the overall performance of the process as it blocks the active surface area of the electrodes and increases the resistance of the electrolyte [8]. The presence of gas bubbles and their motion has a significant impact on the performance of the electrolytic cell [9]. Boissonneau and Byrne investigated the velocity field in an electrolytic cell with vertical electrodes through Laser Doppler Anemometry and Particle Image Velocimetry (PIV) [8]. Their experiment related the gas evolution to the hydrodynamics of electrolyte flow through a narrow vertical channel. Although the flow was laminar, the bubbles induce local turbulence which causes velocity fluctuations due to the interactions with the continuous phase.

Ali and Pushpavanam [10] studied the effects of gas evolution on hydrodynamics of water electrolysis in a partitioned electrolytic system using PIV. Their research was conducted for various electrode designs and different operating conditions such as voltage and concentration. As a result, they determined that the optimum condition for mixing was based on liquid circulation. Circulation was computed as a measure of irrotationality or irreversibility in the system. The results were verified further quantitatively by analyzing time averaged velocity profiles along a line. The temporal variation of liquid velocity at a point was also analyzed. It was found that velocity components exhibit turbulent fluctuations about a mean value [10].

Photoelectrolysis uses solar irradiance to decompose water into hydrogen and oxygen. The process may use two doped semiconductor materials. A p-type and n-type are brought together forming a p–n junction [6, 10]. A permanent electric field is formed at the junction when the charges in the n-type material rearrange. When a photon with energy greater than the semiconductor material's bandgap is absorbed at the junction, an electron is released and a hole is formed [11]. The hole and electron are forced to move in opposite directions due to the electric field. As a result, an electric current is created when an external load is connected [12].

Similarly, in photoelectrolysis, water is decomposed into hydrogen and oxygen when a photocathode, p-type material with excess holes, or a photoanode, n-type of material with excess electrons, is immersed in an aqueous electrolyte [6, 12, 13]. Holladay et al. [11] summarized the process in four steps. First, a photon with greater energy than the bandgap strikes the anode, creating an electron-hole pair. Second, the holes decompose water at the anode's front surface to form hydrogen ions and gaseous oxygen, while the electrons flow through the back of the anode, which is electrically connected to the cathode. Third, the hydrogen ions pass through the electrolyte and react with the electrons at the cathode to form hydrogen gas. In the last step, the oxygen and hydrogen gases are separated by the use of a semi-permeable membrane. The separated gases are then processed and stored [11].

The efficiency is directly related to the semiconductor band gap, which limits the usage of different wavelengths. This is the energy difference between the bottom of the conduction band and the top of the valence band. Efficiency is also related to the band edge alignments, since the material or device must have sufficient energy to split water [11]. In order to increase the efficiency of the system, electron transfer catalysts may be used. However, these can minimize the surface over-potentials in relation to the water and facilitate the reaction kinetics, decreasing the electricity losses in the system [11]. As a result, appropriate surface catalysts for the systems are being sought. Such catalysts must remain active for as many as 10^8 redox reaction cycles, which is the equivalent of 20 years of operation [6]. Researchers also suggested the use of suspended metal complexes in solution as the photochemical catalysts [14]. Typically, nano-particles of ZnO, Nb_2O_5 and TiO_2 have been used [11, 15].

Gas bubbles exist in gas-liquid, gas-solid, and gas-liquid-solid systems such as the prior systems. The formation of bubbles through nozzles or orifices submerged

in viscous liquids represents an important process in gas–liquid flow contacting equipment such as bubble columns, sieve plate columns, and sparged vessels. In general, particulate systems are classified on the basis of the state of the particle present as gas bubbles, liquid drops, or solid particles/agglomerates [16]. The prediction of gas-liquid contact through bubbles is complex. To understand the process of gas bubbling in a liquid pool, it is necessary to understand the process of bubble formation. The process of bubble formation is governed by many operating parameters (i.e., gas flow rate through the orifice, mode of operation, flow condition of the liquid), system properties (dependent on orifice dimensions, orifice chamber volume), and also the physicochemical properties, such as liquid viscosity, liquid density, and nature of the liquid (i.e., polar or nonpolar), which affect the mode of bubble formation and subsequently bubble size. The main forces acting on a moving bubble are gravity, buoyancy, drag, viscous forces, added mass force, and the lift force. In many cases, the gas-liquid properties, orifice dimensions and the type of fluid govern these forces. The flow rate of gas through an orifice and orifice dimensions mainly affect the bubble frequency and thus the detachment time. Similarly, the orifice chamber volume affects the back pressure on the bubble and hence bubble sizes in general [16].

Studies by Clift at al. [17] and Duineveld [18] reported that bubbles with diameters less than 1 mm rise through water and retain their spherical shape due to surface tension. Also, the trajectory follows a nearly straight line. However, this is not the case for larger bubbles. Researchers reported deformations due to the increase in hydrostatic and dynamic pressures over a bubble's surface [19, 20]. Therefore, large bubbles first deform into oblate spheroids, then become ellipsoidal, and with further increase in size, switch into a spherical or ellipsoidal cap shape [21]. The gas-phase density can be increased by increasing the pressure or using a higher molecular weight gas. As a result of increased gas density, the difference between the densities of two phases decreases, resulting in smaller sized bubbles and also a reduction in the buoyancy force [16]. According to this model, the bubble volume at the end of detachment remains the same for all bubbles generated from all holes on a porous plate [22]. Since the sizes of bubbles after its formation and its wake affect the rise velocity and direction of rise, i.e., trajectory in the liquid, they influence the above-mentioned dynamic processes, overall turbulence in the system and performance of the equipment to some extent [16, 23, 24].

With rising bubbles, past studies have shown a rectilinear path becomes a zigzag or spiral pattern, then quasi-rectilinear as the bubble size increases until it becomes a spherical cap. This has been observed in liquids of small Morton number [21]. However, the bubble size does not affect the trajectory in large Morton numbers as a rectilinear path is observed regardless of diameter [25]. Researchers also observed rocking motions for different Reynolds numbers [26]. Ohta et al. [23] discussed the trajectory of a larger bubble consisting of primary and secondary structures. The primary structure is defined as the structure where the bubble begins to oscillate and rise in a zigzag motion as soon as the bubble is released and reaches

the terminal velocity. The secondary structure follows soon after when the bubble attains a special shape at terminal velocity.

In this paper, both experimental and modeling studies are performed to examine the dynamics of bubble flows and kinetics of water vapour transfer, particularly related to processes of hydrogen production at a liquid-solid interface. The solid could be a electrode, catalyst, or reactant. Experimental data are obtained and correlated with non-dimensional parameters involving the bubble diameter, velocity and trajectories such that the water vapour transfer rate can be quantified under different operating conditions for various hydrogen production methods.

26.2 Experimental Setup

In an electrolytic step of a conventional hydrogen production cycle, water is split to produce hydrogen by means of an electric current. Hydrogen gas is produced on the cathode of the electrolyzer, whereas oxygen gas is produced on the anode. The gas bubbles rise to the surface, carrying a certain amount of moisture from the water.

Furthermore, in the decomposition step of the Cu-Cl cycle, oxygen gas rises through the molten salt (i.e. molten CuCl). Due to the motion of oxygen, CuCl mass is transferred across the interfacial boundary. The temperature out of the reactor quickly decreases, causing the molten salt to solidify which ultimately may clog the outlet of the reactor. Additionally, unreacted solid particles of Cu_2OCl_2 are descending as the oxygen bubbles are rising. These solid particles affect the motion of the oxygen bubbles, which in turn may affect the reaction rate. Modeling of the multiphase flow is needed to better understand the processes and develop methods that prevent pipe clogging. An experimental loop was designed and built at the University of Ontario Institute of Technology (UOIT) in the Clean Energy Research Laboratory (CERL) to facilitate better understanding of the physics of gas-liquid systems and to quantify the mass transferred across the boundaries of the bubbles in multiphase flows.

The apparatus consists of a 270.8 mm high, 203 mm diameter, clear PVC vertical column filled with liquid. Nitrogen gas is supplied and bubbles are generated through a porous surface. The size and number of bubbles varies with the nitrogen flow rate such that less bubbles with bigger diameters are formed for lower flow rates, while more bubbles with smaller diameters are formed for higher flow rates. The flow rate of nitrogen is set manually using rotameters. Bubbles flowing through the porous surface rise up through the water. Due to the motion of a bubble through water, some of the water molecules from the liquid diffuse across the boundary of the bubble and they are carried out of the water column. In order to determine the amount of water carried to the surface, a humidity analyzer was installed at the gas exit. Type T thermocouples have also been installed at five different locations in order to record the temperature of the water as well as the temperature of the gas. LabVIEW software was used to view and record the data

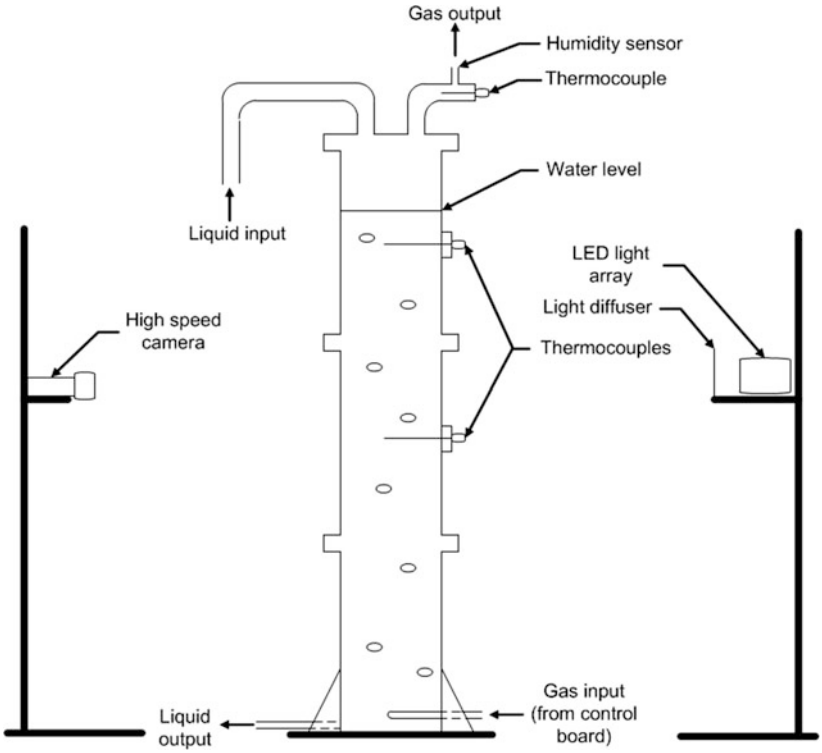

Fig. 26.1 Schematic of experimental setup

captured by the humidity sensor and thermocouples. A schematic of the experimental setup is presented in Fig. 26.1.

In order to better understand the flows with bubble generation and dynamics, it is important to map the bubble size, bubble number, and bubble velocity as bubbles rise through the liquid. Hence, DynamicStudio Shadow Sizer was employed to measure the bubble dynamics. The particles rising through the medium are backlit with an LED light source with a trigger frequency of 400 Hz, pulse of 100 μs and delay of 10 μs. A glass diffuser is used in order to obtain an even light sheet so that the camera can acquire a shadow image of the moving particles. A FlowSense 2ME camera with an effective sensor size of 1,600 by 300 pixels was used to capture images. Images were captured in single frame mode with a trigger frequency of 91 Hz, delay to open of 3.5 μs, delay to close of 10,920 μs and exposure time of 95 μs. The particle in motion was frozen with the aid of a short light flash and a sychronization device. The timer box for imaging applications started automatically so that the camera and LED light array were synchronized at the start of the acquisition process. The camera and light system were set up as shown in Fig. 26.1. The stands were custom built so that images can be taken at precise specified heights from the gas exit.

26.3 Bubble Flow Model

26.3.1 Assumptions

Various assumptions similar to past studies [16] were adopted. It was assumed that the wall does not significantly influence the ascending gas bubbles. Since the volume of the liquid within the column was much larger than the volume of the bubbles formed, it was assumed that the liquid is a semi-infinite medium in comparison to bubble volume. Also, viscous effects were neglected on the change of bubble size. It was assumed that the gas followed ideal gas and incompressible flow. Since the gas injection rate was constant, it was assumed that the bubble velocity was proportional to the flow rate with no allowance for a change in bubble cross-section during ascension. Additionally, the motion of the bubble was not affected by the presence of another bubble immediately above it. During motion, the gas-liquid interface was acted on by a pressure difference between the gas and liquid and by surface tension forces, which are constant and uniform. The gas bubbles were assumed to be spherical.

26.3.2 Dimensionless Parameters

This subsection presents a new predictive model involving the mass transfer across the boundary of the gas bubble with respect to its size, shape, velocity and height traveled. The trajectories of bubbles are strongly influenced by bubble deformations and the surrounding liquid flow [19]. Past studies have shown that the Reynolds (Re), Eotvos (Eo) and Morton (Mo) numbers are useful for describing a rising bubble motion because the shape and terminal velocity of the bubble are influenced by these three dimensionless parameters [23]. In order to better understand how the three numbers describe the bubble's motion, it is necessary to determine their values. The Reynolds number is the ratio of inertia forces to viscous forces in the fluid:

$$Re = \frac{VL_c}{\upsilon} = \frac{\rho V L_c}{\mu} \tag{26.1}$$

where V is the bubble's velocity in m/s, L_c is the diameter of the bubble in units of m, μ is the dynamic viscosity of the fluid in units of Pa s, ρ is the density of the fluid in units of kg/m^3 and $\upsilon = \frac{\mu}{\rho}$ is the kinematic viscosity of the fluid in units of m^2/s. The Eotvos number characterizes the shape of the bubble and it is proportional to the buoyancy force divided by the surface tension force:

$$Eo = \frac{\Delta\rho g L_c^2}{\sigma} \tag{26.2}$$

where $\Delta\rho$ is the density change of the two phases and σ is the surface tension in units of N/m. The Morton number is used together with the Eo number in order to characterize the bubble's shape:

$$Mo = \frac{g\mu^4\Delta\rho}{\rho_c^2\sigma^3} \tag{26.3}$$

When a drop deforms, its surface area increases with respect to a spherical drop of the same volume. Mass transfer between a droplet and a liquid is proportional to the surface area of the droplet [27].

26.3.3 Mass Transfer in Bubbles

Mass transfer between a droplet and a fluid has been extensively studied in the past. Theoretical models for mass transfer rate predictions from rising bubbles have been developed. Some of these models have been used for non-Newtonian fluids [28–31], whereas others for different Reynolds numbers [27–29, 32–36]. Analogous to heat transfer, mass transfer occurs due to diffusion and convection. The rate of mass diffusion of a chemical species A in a stationary medium in the direction of x is proportional to the concentration gradient dC/dx in that direction and it is expressed by Fick's law of diffusion [27]:

$$\dot{m}_{diff} = -D_{AB}\frac{dC_A}{dx} \tag{26.4}$$

where D_{AB} is the molecular diffusion coefficient in units of m^2/s and C_A is the concentration of species in the mixture at that location in units of kg/m^3.

Different types of diffusion have been reported in the past [37]. Diffusion takes place when the primary driving mechanism is a concentration gradient. Thermal diffusion takes place as a result of temperature gradients. Forced diffusion occurs when an external force field such as electric or magnetic field is applied to the mixture in order to separate molecules from the mixture. Knudsen diffusion refers to diffusion between a porous solid with pores smaller than the mean free path of a gas molecule. Also, surface diffusion results when the size of gas molecules is comparable to the pore size and molecules are absorbed along the pore walls. All of these diffusion processes occur when the two mediums are stationary. A different type of mass transfer occurs when the media are in motion. Convection mass transfer refers to the transfer of mass between a surface and a moving medium as a result of both mass diffusion and bulk fluid motion [37]. Similar to heat transfer, mass transfer is influenced by surface geometry, flow velocity, flow regime, fluid

properties and composition. Due to the processes that arise as a result of fluid motion and its properties, mass transfer is determined based on experimental data. Therefore, the relative magnitude of molecular momentum and mass diffusion in the velocity and concentration boundary layers are expressed by the dimensionless Schmidt number defined as follows [37]:

$$Sc = \frac{\upsilon}{D_{AB}} \tag{26.5}$$

In heat transfer analysis, it is convenient to express the heat transfer coefficient in terms of the dimensionless Nusselt number. Likewise, in mass transfer, the mass transfer coefficient is expressed in terms of the dimensionless Sherwood number [37]:

$$Sh = \frac{h_{mass} L_c}{D_{AB}} \tag{26.6}$$

where h_{mass} is the mass transfer coefficient in units of m/s primarily indicating the convective contribution, and D_{AB} is the molecular diffusivity in units of m^2/s indicating the diffusive contribution.

Considering external flow with a free stream condition, $w_{A,\infty}$, the mass transfer condition at the surface can be expressed as [37]:

$$j_{A,i} = -D_{AB} \frac{\partial w_A}{\partial y}\bigg|_{y=0} = h_{mass}(w_{A,i} - w_{A,\infty}) \tag{26.7}$$

where $j_{A,i}$ is the mass transfer flux in kg/s m^2, $w_{A,s}$ is the mass or mole fraction of medium A at the surface, depends on the units of mass transfer flux. This paper will adopt mass fraction.

For an internal flow and using bulk motion properties, the above relation can be rewritten as:

$$\frac{d[(w_A - w_{A,i})/(w_{A,\infty} - w_{A,i})]}{d(y/L_c)}\bigg|_{y=0} = \frac{h_{mass} L_c}{D_{AB}} = Sh \tag{26.8}$$

Another method to determine the Sherwood number is given in terms of the Reynolds and Schmidt numbers. The expression is given as follows [38]:

$$Sh = cRe^{1/2} Sc^{1/3} \tag{26.9}$$

where c is a constant. This expression is used when the bubble can be assumed to be rigid and non-deforming.

Table 26.1 Various parameters influencing the mass transfer

Variable	Description	SI units	Dimension
h_{mass}	Mass transfer coefficient	m/s	LT^{-1}
L_c	Diameter of gas bubble	m	L
ρ_l	Density of liquid	kg/m^3	ML^{-3}
ρ_g	Density of gas within bubble	kg/m^3	ML^{-3}
μ_l	Dynamic viscosity of liquid	Pa s	$ML^{-1}\ T^{-1}$
μ_g	Dynamic viscosity of gas	Pa s	$ML^{-1}\ T^{-1}$
D_{lg}	Diffusivity of liquid into gas	m^2/s	L^2T^{-1}
D_{gl}	Diffusivity of gas into liquid	m^2/s	L^2T^{-1}
σ	Surface tension	kg/s^2	MT^{-2}
V	Velocity	m/s	LT^{-1}

26.3.4 Non-dimensional Correlations

The non-dimensional correlation will have the following form [39, 40]:

$$y = C_0 t_1^{C_1} t_2^{C_2} \ldots t_n^{C_n} \tag{26.10}$$

where values of t are the various independent parameters influencing the mass transfer and C are the coefficients. A dimensional analysis is necessary in order to determine relations among physical quantities governing the mass transfer coefficient and obtain a general empirical equation. Mass transfer across the boundary of a gas bubble is dependent on different variables such as the velocity of the rising bubble, size and shape of the bubble, distance it travels and the temperature of the surrounding fluid. Table 26.1 lists the key parameters needed for the analysis of mass transfer across the interface, their units and dimensions in terms of mass (M), length (L), time (T) and temperature (K).

The Buckingham Π theorem was used for the purpose of non-dimensional groups. An equation expressing the mass transfer coefficient as a function of the mass transfer parameters can be written as follows:

$$h_{mass} = f\left(L_c, \rho_l, \rho_g, \mu_l, \mu_g, D_{AB}, D_{BA}, V\right) \tag{26.11}$$

After investigating the dimensions, three dimensionless Π terms were determined. The terms are expressed in Table 26.2.

The following equation was obtained based on the above dimensional analysis:

$$\Pi_1 = f(\Pi_2, \Pi_3) \tag{26.12}$$

Equation 26.13 can be represented in terms of the dimensionless groups as:

$$Sh = cRe^{n_1} Eo^{n_2} \tag{26.13}$$

Table 26.2 Correlations of Π terms

Π terms	Dimensionless group	Name
Π_1	$\frac{h_{mass}L_c}{D_{AB}}$	Sherwood number
Π_2	$\frac{\rho V L_c}{\mu}$	Reynolds number
Π_3	$\frac{\Delta\rho g L_c^2}{\sigma}$	Eotvos number

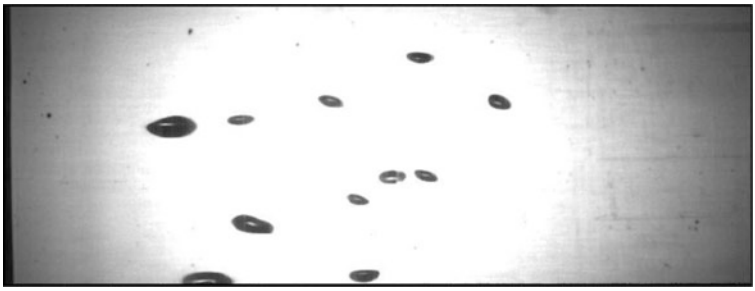

Fig. 26.2 Aquired image for 2 L/min

where n_1 and n_2 are coefficients to be determined. In order to determine the coefficients in Eq. (26.13), experimental data were utilized. Diameters of gas bubbles were obtained using DynamicStudio using the steps described in the previous section.

26.4 Results and Discussion

DynamicStudio software, an advanced edge detection algorithm to extract the bubble shape information, was used to acquire and process the images. The "shadow sizer processing" method was used to extract information such as size, position, shape and velocity of bubbles. Prior to image processing, a set of calibration images was acquired. This step was necessary because it enables the measurement of a scale factor. The scale factor was used to determine the conversion of pixel units into metric units. Figure 26.2 depicts the acquired image at a flow rate of 2 L/min)

It can be seen that the gas bubbles are irregular in shape and their diameters are different. Each bubble carries a different amount of moisture. Due to their iregular shape, more mass is transferred across the boundary compared to spherical bubbles. The size of the bubbles also affects the amount of mass transferred across the boundary; more moisture is carried by the larger diameter bubbles. It is important to note that bubbles rise up in a spiral motion which enhances the mass transfer across the interface. After aquiring the images, they were processed using the Shadow Image module of DynamicStudio. In order to ensure that all gas bubbles were analyzed by the software, a grey level profile of the bubbles was determined.

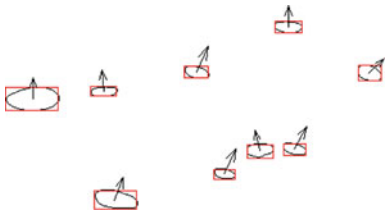

Fig. 26.3 Processed image for 2 L/min

The images were then processed in order to obtain useful information such as diameter, area, shape, position and velocity of the bubbles. The velocity information was extracted by combining a correlation algorithm and measuring displacement between two successive images via a dedicated particle-tracking algorithm. Figure 26.3 depicts the processed image with velocity vectors.

All bubbles from the acquired image were analyzed by the software due to the choice in the grey level profile. The results obtained after analyzing the image are listed in Table 26.3.

These results have been used to calculate the Sherwood, Reynolds and Eotvos numbers in order to develop correlations that determine the amount of mass transfer across the interface of the gas bubble as it rises through the liquid. Diffusive mass transfer occurs across the interfacial boundaries of the gas bubbles. In order to determine the amount of mass transferred and carried out of the column, a humidity sensor was used to measure the change in relative humidity. The change in relative humidity is shown in Fig. 26.4.

Since a change in relative humidity was observed, it was necessary to develop a correlation relating the change in relative humidity (i.e. mass transfer) to the parameters causing this change. A set of 165 data points was compiled and used for analysis. Once the diameters of different size gas bubbles were obtained using DynamicStudio, it was possible to calculate the three dimensionless groups represented in Table 26.2. The dimensionless groups were calculated using MATLAB. Equations (26.1), (26.2) and (26.9) were used to calculate the Reynolds number, Eotvos number and Sherwood number, respectively. The constant c in Eq. (26.9) was chosen to be the change in relative humidity. Scatter plots were then generated using MS Excel. The plotted data were then analyzed using a log-log scale as seen in Fig. 26.5.

The slope of the log-log regression obtained from the equation of the line provides the coefficient for the associated scatter plot. From the equation of the line, a slope of 0.435 was obtained, therefore, the coefficient n_1 in Eq. (26.13) becomes $n_1 = 0.435$. The statistical R^2 value of 0.908 is an indication that data correlate at this point. The next step was to determine the coefficient of the Eotvos number. The effect of Re is included in the second plot. Figure 26.6 depicts the scatter plot of Eo versus the other Π terms.

From the equation of the line, a slope of 0.279 was obtained. This becomes the coefficient of the Eo number such that $n_2 = 0.279$. The R^2 value of 0.993 is also a

Table 26.3 Results with DynamicStudio for 2 L/min

Centroid X[a] (mm)	Centroid Y[a] (mm)	Area (mm^2)	Perimeter (mm)	Equivalent diameter (mm)	Major axis[b] (mm)	Minor axis[c] (mm)	X-direction velocity (m/s)	Y-direction velocity (m/s)
27.18	19.87	166.70	18.30	5.69	4.28	1.90	0.00	0.30
38.49	18.68	38.59	9.30	2.74	2.30	0.82	-0.03	0.31
40.19	35.89	110.11	15.10	4.62	3.66	1.49	0.12	0.32
53.20	15.62	40.87	8.69	2.82	2.10	0.96	0.16	0.37
57.60	31.77	31.26	7.63	2.46	1.80	0.86	0.16	0.36
63.25	27.98	50.33	9.76	3.13	2.22	1.11	-0.06	0.28
67.83	8.42	46.21	9.61	3.00	2.35	0.97	0.01	0.30
68.77	27.81	36.76	8.24	2.67	1.97	0.92	0.18	0.32
80.72	15.78	53.23	9.15	3.21	2.06	1.28	0.21	0.21

[a]Measured with reference to the frame of the image
[b]X-direction axis
[c]Y-direction axis

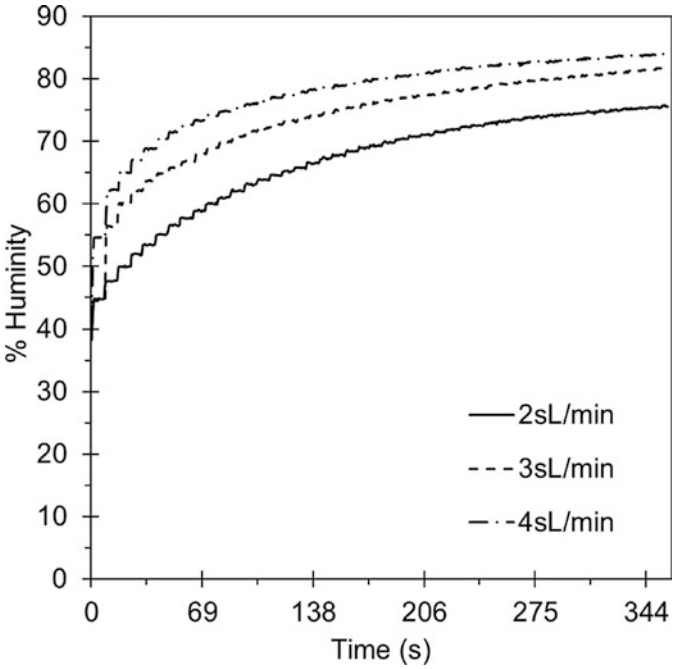

Fig. 26.4 Change in humidity for different flow rates

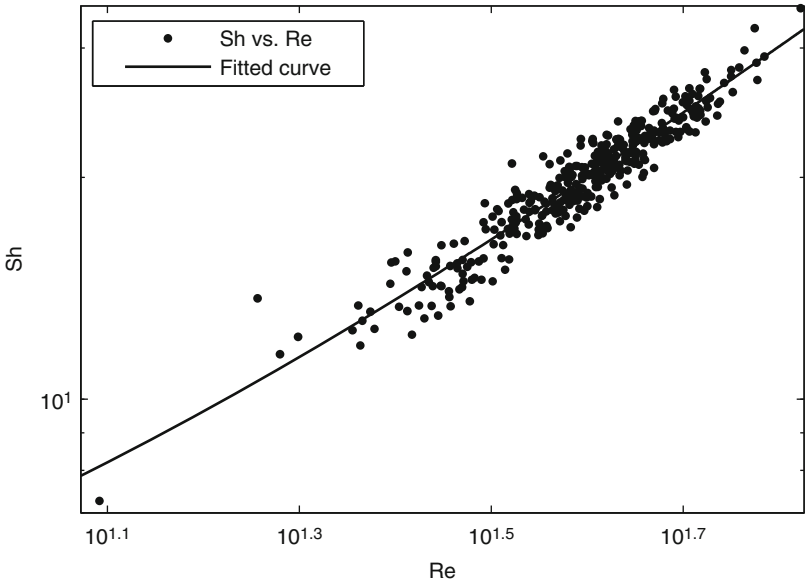

Fig. 26.5 Scatter plot and linear regression for Re versus Sh

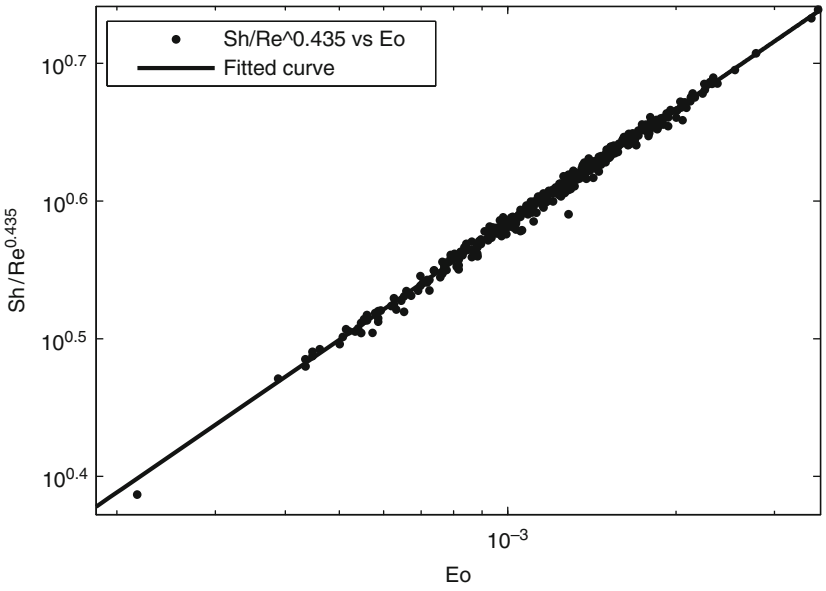

Fig. 26.6 Scatter plot of Sh/Re$^{0.435}$ versus Eo

good indication that the data correlates. Thus, a correlation has been attained as follows:

$$Sh = Re^{0.435} Eo^{0.279} \tag{26.14}$$

This experimental data and correlation provide useful information for better understanding of diffusive mass transfer through bubbles, particularly for applications related to hydrogen production.

26.5 Conclusions

Relations between the flow dynamics and mass transfer kinetics of multiphase flows involving gas bubbles and the amount of water vapour entrained by the vapour phase have been examined. Experimental data were obtained for the change of bubble moisture and velocity to simulate the hydrogen and oxygen bubbles rising in a quiescent liquid. A new correlation was developed to relate the bubble dynamics and water vapour generation rate with Reynolds and Sherwood numbers particularly involving the amount of mass transferred across the interfacial boundary. The experimental data and model presented in this paper can provide a better understanding of the gas bubble dynamics and water vapour generation kinetics related to hydrogen production.

Acknowledgements Financial support from the Ontario Research Excellence Fund and Atomic Energy of Canada Limited (AECL) is gratefully acknowledged.

Nomenclature

C	Concentration kg/m^3
D	Diffusivity m^2/s
Eo	Eotvos number
h_{mass}	Mass transfer coefficient m/s
$j_{A,i}$	Diffusive mass flux kg/s m^2
L_c	Diameter of the bubble m
Mo	Morton number
Re	Reynolds number
Sc	Schmidt number
Sh	Sherwood number
V	Bubble velocity m/s
w	Mass mole fraction

Greek Letters

μ	Dynamic viscosity of the fluid Pa s
ρ	Density kg/m^3
σ	Surface tension kg/s^2

Subscripts

A	Species A
B	Species B
g	Gas
l	Surrounding liquid
i	Interface

References

1. Dincer I (2012) Green methods for hydrogen production. Int J Hydrogen Energ 37:1954–1971
2. Rosen MA (2010) Advances in hydrogen production by thermochemical water decomposition: a review. Energy 35:1068–1076
3. Naterer GF, Suppiah S, Stolberg L, Lewis M, Ferrandon M, Wang Z et al (2011) Clean hydrogen production with the Cu-Cl cycle – progress of international consortium, I: experimental unit operations. Int J Hydrogen Energ 35:15472–15485

4. Naterer G, Suppiah S, Lewis M, Gabriel K, Dincer I, Rosen MA et al (2009) Recent Canadian advances in nuclear-based hydrogen production and the thermochemical Cu-Cl cycle. Int J Hydrogen Energ 34:2901–2917
5. Bockris JO'M, Bandapani B, Cocke D, Ghoroghchian J (1985) On the splitting of water. Int J Hydrogen Energ 10:179–201
6. Wang Z, Roberts RR, Naterer GF, Gabriel KS (2012) Comparison of thermochemical, electrolytic, photoelectrolytic and photochemical solar-to-hydrogen production technologies. Int J Hydrogen Energ 37:16287–16301
7. Mat MD, Aldasb K (2005) Application of a two-phase flow model for natural convection in an electrochemical cell. Int J Hydrogen Energ 30:411–420
8. Boissonneau P, Byrne P (2000) An experimental investigation of bubble-induced free convection in a small electrochemical cell. J Appl Electrochem 30:767–775
9. Dahlkild AA (2001) Modeling the two-phase flow and current distribution along a vertical gas-evolving electrode. J Fluid Mech 428:249–272
10. Ali BA, Pushpavanam S (2011) Analysis of liquid circulation and mixing in a partitioned electrolytic tank. Int J Multiphas Flow 37:1191–1200
11. Holladay JD, Hu J, King DL, Wang Y (2009) An overview of hydrogen production technologies. Catal Today 139:244–260
12. Turner J, Sverdrup G, Mann MK, Maness PC, Kroposki B, Ghirardi M, Evans RJ, Blake D (2008) Renewable hydrogen production. Int J Hydrogen Energ 32:379–407
13. Aroutiounian VM, Arakelyan VM, Shahnazaryan GE (2005) Metal oxide photoelectrodes for hydrogen generation using solar radiation-driven water splitting. Sol Energ 78:581–592
14. Gratzel M (2000) Perspectives for dye-sensitized nanocrystalline solar cells. Prog Photovolt Res Appl 8:171–185
15. Norbeck JM, Heffel JW, Durbin TD, Tabbara B, Bowden JM, Montani MC (1996) Hydrogen fuel for surface transportation. Society of Automotive Engineers Inc., Warrendale
16. Kulkarni AA, Joshi JB (2005) Bubble formation and bubble rise velocity in gas-liquid systems: a review. Ind Eng Chem Res 44:5873–5931
17. Clift R, Grace JR, Weber ME (1978) Bubbles, drops and particles. Academic, New York
18. Duineveld PC (1995) The rise velocity and shape of bubbles in pure water at high Reynolds number. J Fluid Mech 292:325–332
19. Ellingsen K, Risso F (2001) On the rise of an ellipsoidal bubble in water: oscillatory paths and liquid induced velocity. J Fluid Mech 440:235–268
20. Magnaudet J, Eames I (2000) The motion of high-Reynolds-number bubbles in inhomogeneous flows. Annu Rev Fluid Mech 32:659–708
21. Hassan NMS, Khan MMK, Rasul MG (2010) A modelling and experimental study of the bubble trajectory in a non-Newtonian crystal suspension. Fluid Dynam Res 42:065502
22. Miyahara T, Takahashi T (1986) Coalescence phenomena at the moment of bubble formation at adjacent holes. Chem Eng Res Des 64:320
23. Ohta M, Kikuchi D, Yoshida Y, Sussman M (2011) Robust numerical analysis of the dynamic bubble formation process in a viscous liquid. Int J Multiphas Flow 37:1059–1071
24. Buwa VV, Deo DS, Ranade VV (2006) Eulerian-Lagrangian simulations of unsteady gas-liquid flows in a bubble column. Int J Multiphas Flow 32:864–885
25. Yang B (2006) Numerical studies of single gas and vapor bubble flows. Ph.D. thesis. Department of Mechanical Engineering, The Johns Hopkins University, Baltimore, MD
26. Aybers NM, Tapucu A (1969) The motion of gas bubbles rising through stagnant liquid. Heat Mass Tran 2:118–128
27. Favelukis M, Raphael S (1996) Mass transfer between a slender bubble and a viscous liquid in axisymmetric extensional flow. Chem Eng Sci 51:1169–1172
28. Kawase YY, Ulbrecht JJ (1981) Drag and mass transfer in non-Newtonian flows through multi-particle systems at low Reynolds numbers. Chem Eng Sci 36:1193–1202
29. Kawase YY, Moo-Young M (1986) Approximate solutions for power law fluid flow past a particle at low Reynolds numbers. J Non-Newtonian Fluid Mech 21:167–177

30. Jarzebski AB, Malinowski JJ (1986) Transient mass and heat transfer from drops or bubbles in slow non Newtonian flows. Chem Eng Sci 41:2575–2578
31. Feng ZG, Michaelides EE (2000) Mass and heat transfer from fluid spheres at low Reynolds numbers. Powder Technol 112:63–69
32. Ruckenstein E (1982) Prediction of rates of heat or mass transfer in complex situations by interpolating between simpler limiting cases. Chem Eng Sci 37:1505–1511
33. Nakano Y, Tien C (1967) Approximate solutions of viscous incompressible flow around fluid spheres at intermediate Reynolds numbers. Can J Chem Eng 45:135–140
34. Kishore N, Chhabra RP, Eswaran V (2008) Bubble swarms in power-law liquids at moderate Reynolds numbers: drag and mass transfer. Chem Eng Res Des 86:39–53
35. Martin M, Montes FJ, Galan MA (2010) Approximate theoretical solution for the Sherwood number of oscillating bubbles at different Reynolds numbers. Chem Eng Process 49:245–254
36. Baird MHL, Hamielec AE (1962) Forced convection transfer around sphere at intermediate Reynolds numbers. Can J Chem Eng 40:119–121
37. Cengel YA (2007) Heat and mass transfer: a practical approach. McGraw Hill, Boston
38. Vasconcelos JMT, Orvalho SP, Alves SS (2002) Gas–liquid mass transfer to single bubbles: effect of surface contamination. Am Inst Chem Eng J 48:1145–1154
39. Mokry S (2009) Development of heat-transfer correlation for superficial water in SCWR applications. Masters thesis. Faculty of Engineering and Applied Science, University of Ontario Institute of Technology, Oshawa, ON, Canada
40. Wang X, Naterer GF, Bibeau E (2007) Convective droplet impact and heat transfer from a NACA airfoil. J Thermophys Heat Tran 21:536–542

Chapter 27
Numerical Analysis of the Thermo-mechanical Behavior of Energy Piles

Heng Zhao, Ping Cui, Lin Lu, and Zhaohong Fang

Abstract A finite element model is developed to investigate the thermo-mechanical behavior of the energy pile in detail. In the model, soil is regarded as a kind of thermo-elastic-perfectly plastic material, and the interaction between the pile and soil is modeled by contact elements. In order to save the computing time, the U-tubes in the energy pile are simulated by line elements, which are proved to be suitable for calculating the temperature of the pile. To deal with the thermo-mechanical multi-field problem, the sequential coupling method is utilized. The simulation results show that the thermally induced stress and deformation in the pile can be significantly influenced by the properties of the soil, the applied mechanical load and the restraint condition at the pile head. Long-time simulations of the energy pile with cyclic heat injections and extractions indicate that the thermal cycles would induce an unrecoverable settlement of the pile, and the ultimate bearing capacity of the energy pile may need to be redefined in view of its long-time performance.

Keywords Energy pile • Thermo-mechanical behavior • Numerical analysis • U-tube • Load

H. Zhao
Postdoctoral Workstation, Shandong Fangya GSHP Technology Co., Ltd., Jinan, China
e-mail: zhaohtsing@gmail.com

P. Cui
Shandong Key Laboratory of Building Energy Saving Technologies, Shandong Jianzhu University, Jinan, China
e-mail: nature_cui@126.com

L. Lu
Department of Building Service Engineering, Hong Kong Polytechnic University, Hong Kong, China
e-mail: vivien.lu@polyu.edu.hk

Z. Fang (✉)
Postdoctoral Workstation, Shandong Fangya GSHP Technology Co., Ltd., Jinan, China

Shandong Key Laboratory of Building Energy Saving Technologies, Shandong Jianzhu University, Jinan, China
e-mail: fangzh_45@163.com

I. Dincer et al. (eds.), *Progress in Sustainable Energy Technologies Vol II: Creating Sustainable Development*, DOI 10.1007/978-3-319-07977-6_27

27.1 Introduction

The Ground-Coupled Heat Pump (GCHP) technology now has been widely utilized for space heating and cooling due to its high energy efficiency and environmental friendliness [1]. In this technology, the ground heat exchangers (GHEs) for absorbing and transporting thermal energy from ground are traditionally consisted of vertically or horizontally buried high-density polyethylene tubes with circulated anti-freezing fluid inside. As the traditional GHEs especially for the ones consisted of vertically buried tubes often require a higher initial cost and a large plot of land, a new kind of GHEs named energy piles, in which the tubes are buried in the piles, has become a better choice recently [2–4].

Different from the traditional pile mainly used to support the upper structure, the energy pile has to work as a GHE with temperature changing in the entire pile foundation. As a result, thermal strain and stress would be generated in the pile and surrounding soil, and influence the pile's mechanical behavior. This thermo-mechanical behavior of the energy pile has been noted by many researchers, and some preliminary studies have been carried out. The results from two in-situ tests indicated that the increase of compressive stress or the total tensile stress could get up to 2 MPa with a temperature change of 20 °C in the pile [5, 6], implying that it is possible for the pile to fail. Moreover, a centrifuge model test indicated that the temperate change even has a significant effect on the pile's ultimate bearing capacity due to the change of contact pressure on the pile–soil interface [7, 8]. A few models have been present to analyze the energy pile's thermo-mechanical behavior, such as the finite element model [9], the revised load transfer method [10]. In these studies there are more or less some factors presumed not to be considered but without knowledge on that to what extent they can be neglected, such as the soil's thermal deformation, the cyclic thermal load, and etc. More importantly, there is almost no study on the long-time behavior of energy piles.

In this paper, a finite element model is developed to investigate the thermo-mechanical behavior of energy pile in detail, including the thermally induced stress and displacement in the pile and the pile's bearing capacity. With parametric analysis, the influence of soil's properties and the applied mechanical load is analyzed. Based on the long-time thermo-mechanical coupling simulations, the influence of cyclic thermal loadings is studied.

In this paper, the positive value of stress, if not noted, represents compression, and the pile's displacement is defined as positive when it is in the up direction.

27.2 Model Development and Verifications

The commercial software ANSYS is employed to operate the numerical analysis, with the sequential coupling method utilized to deal with the thermo-mechanical multi-field problem. To reasonably simulate the energy pile, there are some key

points including the constitutive laws of the soil and pile, the simulation of the pile–soil interface, the modeling of U-tubs and the initial and boundary conditions.

27.2.1 Materials' Constitutive Laws

The thermo-mechanical behavior of soil is very complex, for which several advanced but complicated constitutive models have been developed. Here we employ a simple thermo-elastic-perfectly plastic constitutive model based on Drucker-Prager failure criteria. In this model, the behavior of soil is divided into two stages: the thermo-elastic stage and the perfectly plastic stage. In the thermo-elastic stage, the relation between the soil's strain and stress can be expressed as

$$\varepsilon_{ij}^{\mathrm{e}} = D_{ijkl}\sigma_{kl} + \alpha\Delta T\delta_{ij} \tag{27.1}$$

where $\varepsilon^{\mathrm{e}}{}_{ij}$ is the thermo-elastic strain tensor, σ_{kl} the stress tensor, D_{ijkl} the compliance tensor, δ_{ij} the Kronecher delta, α the coefficient of thermal expansion, and ΔT is the temperature change. In the perfectly plastic stage, the stress satisfies

$$f = \frac{2\sin\phi}{\sqrt{3}(3-\sin\phi)}I_{\sigma,1} + I_{\sigma,2} - \frac{6c\cos\phi}{\sqrt{3}(3-\sin\phi)} = 0 \tag{27.2}$$

where $I_{\sigma,1}$ and $I_{\sigma,2}$ are the first and second invariants of the stress tensor respectively, ϕ and c are the soil's internal friction angle and cohesion respectively. In this stage, the plastic strain $\varepsilon^{\mathrm{p}}{}_{ij}$ would occur. With an associate flow rule it satisfies

$$\mathrm{d}\varepsilon_{ij}^{\mathrm{p}} = \mathrm{d}\lambda\partial f/\partial\sigma_{ij} \tag{27.3}$$

where $\mathrm{d}\varepsilon^{\mathrm{p}}{}_{ij}$ is the increment tensor of plastic strain, and $\mathrm{d}\lambda$ is a non-negative scalar. The total strain of the soil ε_{ij} is the sum of the thermo-elastic strain and the plastic strain, i.e.,

$$\varepsilon_{ij} = \varepsilon_{ij}^{\mathrm{e}} + \varepsilon_{ij}^{\mathrm{p}} \tag{27.4}$$

The material of the energy pile is regarded to be isotropic and thermo-elastic. Its modulus E_{p} can be estimated by the proportions of its cross section as

$$E_{\mathrm{p}} = (A_{\mathrm{c}}E_{\mathrm{c}} + A_{\mathrm{s}}E_{\mathrm{s}})/A_{\mathrm{p}} \tag{27.5}$$

where E_{c} and E_{s} are the elastic modulus of concrete and steel respectively, A_{c} and A_{s} are the corresponding area, and A_{p} is the total area of the cross section. Actually, E_{p} in Eq. (27.5) is the pile's vertical elastic modulus, but very near to the modulus in other directions.

27.2.2 Pile–Soil Interface

The pile–soil interface is used to transfer the interacting force between the pile and soil. To correctly simulating the pile's behavior, the model of the pile–soil interface is very important. Here we employ the contact elements which describe the interface as rigid-perfectly plastic. To account for the strength loss on the interface, the friction coefficient and cohesion are set to be 2/3 times the soil's corresponding value. Contact elements are also applied under the pile toe, which implies that there will be no tensile stress at the pile toe. For the energy pile which is often long, during the construction it is usual difficult to clean the base of the drilling hole completely. So it is reasonable to think that the residual gravel and soil would make the pile toe unbearable to any tensile force.

In order to verify the contact elements, a simulation of a published in-situ pile test [11] is made. In the test, a traditional pile was constructed near the University of California, Berkeley campus. The diameter of the pile was 0.76 m and the length was 5.8 m. Unconfined compression tests showed that the un-drained shear strength of the soil is 84kPa. Compared with the results from the in-situ test, the simulated load-displacement curve is illustrated in Fig. 27.1. It can be seen that the contact elements can model the pile–soil interface well.

27.2.3 U-Tubes

In the finite element model, as the temperature gradient near the U-tube is very steep, a fine mesh is often required. It obviously will increase the calculation time and memory consumption. However, for the thermo-mechanical behavior analysis of the energy pile which mainly focuses on the total temperature change in the whole pile, the domain near U-tubes can be meshed coarsely with the U-tubes modeled by line elements, as illustrated in Fig. 27.2a. Even so, it should be noted that as the line elements neglect the diameter of the tubes, the calculated U-tube temperature will be totally different from the actual value, regardless of the mesh size in the nearby domain.

To make sure that the line elements are suitable, a more accurate finite element model is also built in which the U-tubes are model as real tubes by solid elements, as shown in Fig. 27.2b. Using these two different models, the heat transfer process of an energy pile with 4 U-tubes is simulated, in which the pile keeps injecting heat into the ground at a constant power $W = 1$ kW. Their calculated average temperature changes in the pile are illustrated in Fig. 27.3, which shows that the two models give almost the same results.

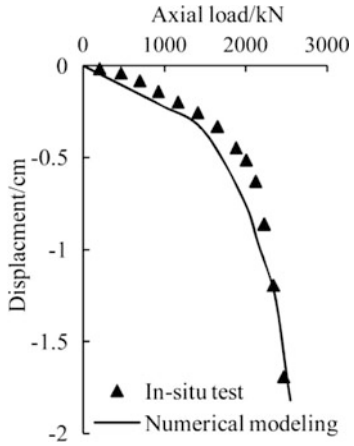

Fig. 27.1 Calculated load-displacement curve by the contact elements

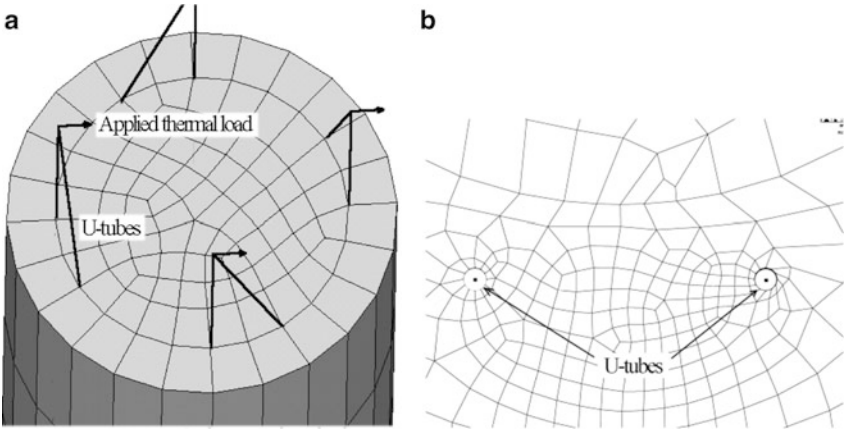

Fig. 27.2 Mesh of the energy pile with U-tubes modeled by (**a**) line elements; (**b**) solid elements

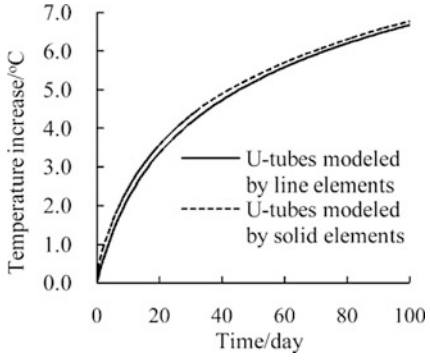

Fig. 27.3 Comparison of the pile's calculated average temperature using two different models in which U-tubes modeled by different kinds of elements

27.2.4 Initial/Boundary Conditions

The initial temperature of the pile and soil is assumed to be uniform. The initial stress in the soil due to the gravity is calculated first by the numerical model, and then applied in the model without strain. The outer boundary of the numerical model should be determined with consideration of the influence domain of the energy piles from both the heat transfer and mechanical aspects. In this model, as simulations of many years' heat transfer process will be carried out, the horizontal outer boundary mainly depends on the thermal influence domain. Considering the mechanical influence depth of the pile, the vertical outer boundary is set to be 0.5 times the pile length.

The reaction of upper structure on the energy pile is represented by the mechanical load applied on the pile head. To apply the thermal load, the inlet and outlet of the U-tubes are connected above the pile head, and the thermal load is applied at the connecting point, as shown in Fig. 27.2a. In the U-tubes, the forced convection heat transfer of the water flow with the heat conduction is considered.

27.3 Simulating Results and Discussion

A typical two-layer soil model is built to investigate the energy pile's thermo-mechanical behavior, as illustrated in Fig. 27.4. The two soil layers, labeled as 1# and 2#, are interfaced at the pile toe. The length of the pile is 30 m, and the diameter is 0.6 m. In the pile there are 8 U-tubes distributed uniformly at a distance of 0.25 m from the pile center. A mechanical load P is applied on the pile head. The horizontal outer boundary of the model is 50 m far from the pile center. In order to analyze the influence of soil properties on the pile's thermo-mechanical behavior, different elastic modulus and thermal expansion coefficients are assigned to each layer of soil. The values of the pile and soil's parameters are listed in Table 27.1.

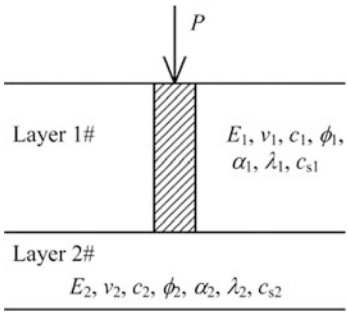

Fig. 27.4 Two layers of soil and energy pile

Table 27.1 Parameters of the pile and soil

Mechanical parameters	Soil		Pile
	1#	2#	
Elastic modulus E (MPa)	13, 26, 52	26, 260, 26,000	2.1×10^4
Poisson's ratio v	0.35	0.35	0.2
Coefficient of thermal expansion α ($°C^{-1}$)	0, 1×10^{-5}, 5×10^{-5}	1×10^{-5}	1×10^{-5}
Internal friction angle ϕ (°)	30.5	30.5	–
Cohesion c (kPa)	20	20	–
Thermal conductivity λ (W m^{-1} $°C^{-1}$)	1.2	1.2	2.0
Specific heat capacity c_s (J kg^{-1} $°C^{-1}$)	1×10^3	1×10^3	0.97×10^3

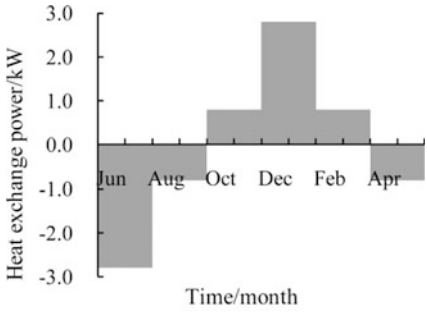

Fig. 27.5 Simplified annual thermal load

27.3.1 Temperature Change in the Pile

The thermal load applied to the energy pile is assumed to be the same annually. To save the computing time, the annual thermal load is divided into six constant power periods as illustrated in Fig. 27.5. With the thermal load, a 2-year heat transfer process is simulated, and the corresponding temperature change on the middle cross section of the energy pile is shown in Fig. 27.6. It can be seen that the difference between the temperature changes at the pile center and edge is minor. Moreover, as the size of the length of the pile is much larger than its diameter, the temperature distribution along the length is almost uniform. So for the thermo-mechanical analysis, the temperature distribution in the pile can be regarded as uniform, and the effect caused by its variation in space can be neglected.

27.3.2 Thermal Stress and Deformation

In Fig. 27.6, two time points A and B, when the temperature in the pile reaches its highest or lowest value respectively, are chosen to represent the worst conditions for the pile's mechanical behavior. Assuming a reference condition that the layers

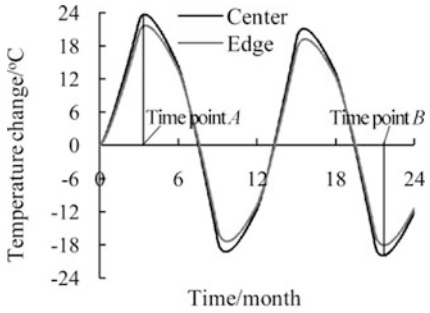

Fig. 27.6 Temperature changes at the center and edge on the middle cross section of the pile

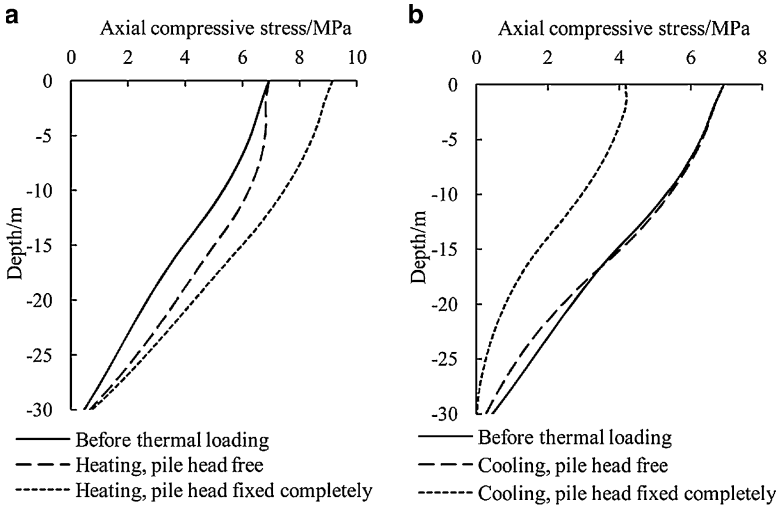

Fig. 27.7 Distribution of the axial compressive stress in the pile before the thermal loading and at (**a**) time point *A*, (**b**) time point *B*

of soil 1# and 2# have the same properties, for which $E_1 = E_2 = 26$ MPa, $\alpha_1 = \alpha_2 = 1 \times 10^{-5}$ °C^{-1}, $P = 1{,}960$ kN, the distribution of the axial compressive stress in the pile before thermal loading and at time points *A* and *B* are calculated. For comparison, two kinds of restraint at the pile head are considered, i.e., being free or fixed by the upper structure completely. The results shown in Fig. 27.7 indicate that the restraint condition at the pile head has large influence on the thermally induced stress. If the pile head is fixed completely, the change of stress at the pile head can reach 2–3 MPa, which obviously can make the pile fail when the initial stress caused by the mechanical load is close to the concrete strength.

However, here we assume the pile head to be free, and mainly focus on the influence of soil properties and the applied mechanical load to the thermally induced stress and deformation in the pile. It may be argued that the pile head is linked to the upper structure and cannot be regarded as free. But in fact, for a common condition that the upper structure is totally supported by a group of similar energy piles, all the pile heads would have nearly equal displacements along with

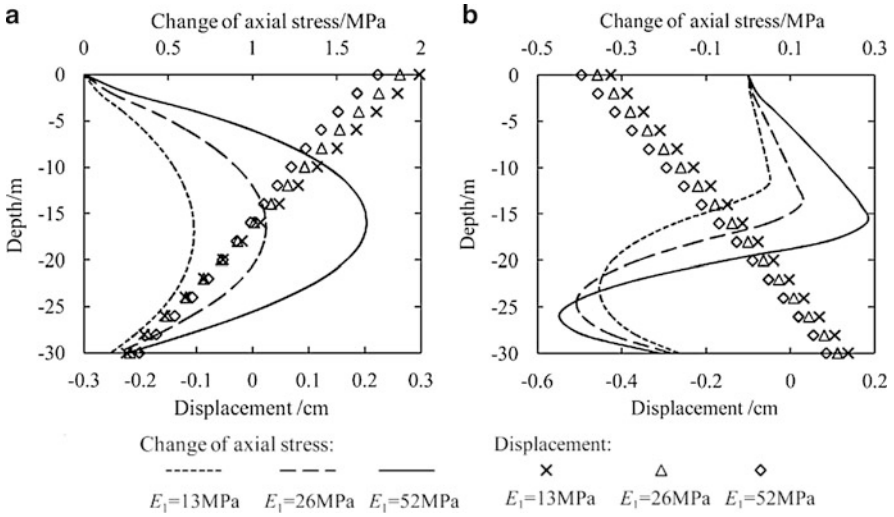

Fig. 27.8 For different modulus of the surrounding soil E_1, the pile's displacement and the change of axial stress at (**a**) time point *A*, (**b**) time point *B*

the bottom of the upper structure and actually can move freely. Moreover, if the pile head is really restrained in some conditions, such as in the case when the upper structure is partly supported by traditional piles, then, it is difficult to determine the degree of the restraint for a single pile, i.e., the relation between the restraint force and the displacement of pile head. For these conditions, a feasible way is to build the structure–pile–soil interaction model, for which the detailed investigation of pile–soil interaction without upper structure restraint is the foundation.

27.3.2.1 Influence of the Properties of the Soil Surrounding the Shaft

As energy piles are often long, the soil surrounding the shaft (layer 1# in Fig. 27.4) plays an important part to support the upper structure, and also can influence the thermally induced stress and deformation significantly. For different modulus of the surrounding soil E_1, with other parametric values identical to those of the reference condition, the thermally induced stress and pile displacement are illustrated in Fig. 27.8. For different coefficient of thermal expansion α_1, the results are shown in Fig. 27.9.

The calculated results show that with the parameter values in reasonable ranges the modulus can affect the pile's thermo-mechanical behavior more than the coefficient of thermal expansion. In fact, during the cooling period, the coefficient of thermal expansion almost has no influence. That is because the temperature variation in the soil diminishes quickly as the distance from the pile center increases. For an energy pile group, if the spacing of the piles is not very small, as a conservative result the surrounding soil's coefficient of thermal expansion can be set to zero.

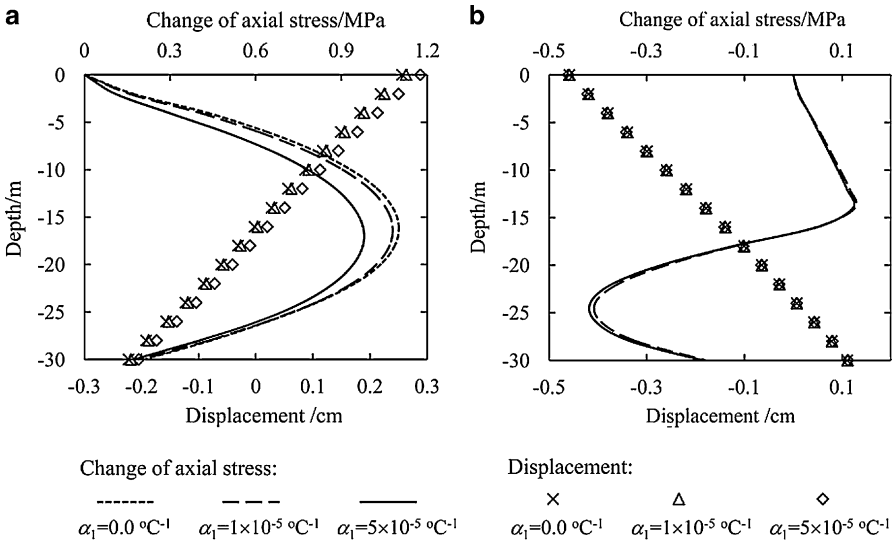

Fig. 27.9 For different coefficient of thermal expansion α_1, the pile's displacement and the change of axial stress at (**a**) time point *A*, (**b**) time point *B*

From Figs. 27.8 and 27.9, it can be seen that the change of axial stress during the heating pile period is larger than that during the cooling pile period, and the pile's displacement is just the opposite. During the heating pile period, the stress increases in the entire pile, and the fixed-point, where the pile's displacement is zero and the change of stress reaches its largest value, is located near the midpoint. During the cooling pile period, the stress increases in the upper part of the pile and decreases in the lower part, with fixed-point located near the pile toe. The reason for the increase of stress in the upper part is that the shaft shear stress near the pile head often reaches its ultimate value, and the ultimate value will decrease during the cooling pile period as the normal compressive stress on pile–soil interface becomes smaller due to the contraction of the pile.

In general, when the modulus of surrounding soil increases or its coefficient of thermal expansion decreases, the thermally induced stress in the pile will become larger, and the pile's displacement will become smaller.

27.3.2.2 Influence of the Properties of the Soil Under the Pile Toe

The soil under the pile toe provides the tip resistance, and also can be regarded as a restraint at the pile toe. The degree of the restraint mainly depends on the modulus of the soil. For different soil modulus E_2, with other parametric values identical to those in the reference condition, the thermally induced stress and pile's displacement are calculated as shown in Fig. 27.10. In general, as the modulus increases, the change of stress will become larger with the displacement smaller, and the fixed-

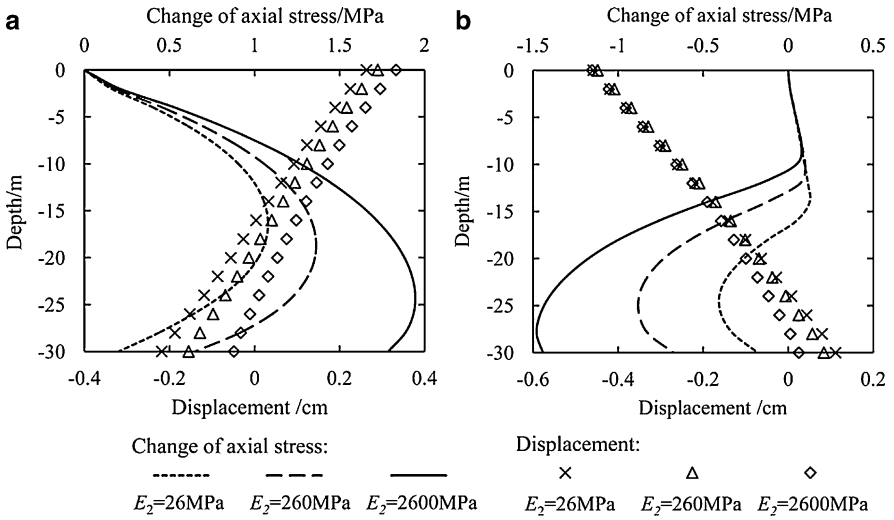

Fig. 27.10 For different modulus of the soil under the pile toe E_2, the pile's displacement and the change of axial stress at (**a**) time point *A*, (**b**) time point *B*

point will move downward. If the pile toe is located on the rock stratum, such as $E_2 = 2{,}600$ MPa, during the heating pile period the stress near the pile toe will increase significantly. During the cooling pile period, the stress changes in the upper part of the pile are almost the same, for which the reason is similar to the reason for the stress increase in the upper part described above.

27.3.2.3 Influence of the Applied Mechanical Load

With different mechanical loads *P*, the thermally induced displacement of the pile and the change of stress are calculated as illustrated in Fig. 27.11. The results show that when the mechanical load increases, the displacement will become larger, the change of stress will become smaller, and the fixed-point will move upward in the heating pile period and move download in the cooling pile period.

The influence of the mechanical load on the pile's thermo-mechanical behavior is due to the nonlinear behavior of the pile–soil interface. As the temperature changes, the increased shaft shear stress will make part of the pile–soil interface be in plastic stage, which weakens the restraint of surrounding soil. The larger the mechanical load, the more the part of interface is in the plastic stage. During the heating pile period, the plastic part of the interface is mainly on the lower part of the shaft, where the ultimate shear stress is larger than a certain value, so only the mechanical load large enough can have influence. During the cooling pile period, the plastic part of the interface is near the pile head, where the ultimate shear stress is small, thus, the mechanical load of any value can have influence.

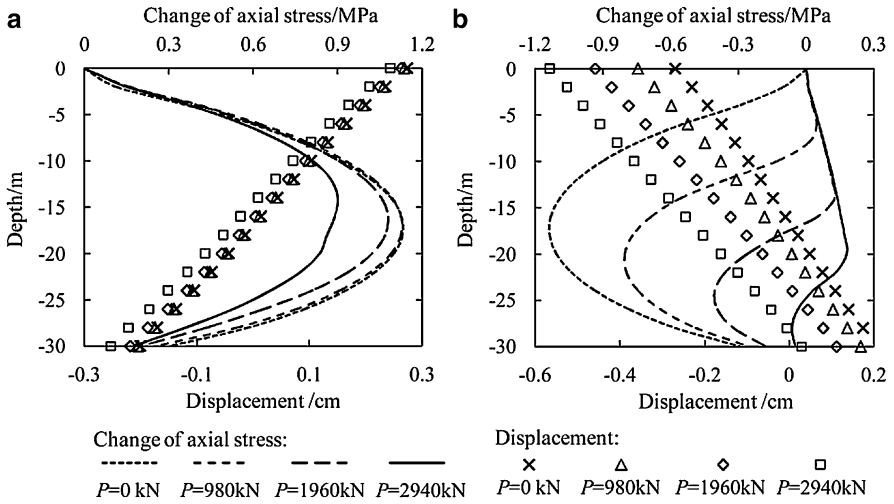

Fig. 27.11 For different modulus of the soil under the pile toe E_2, the pile's displacement and the change of axial stress at (**a**) time point *A*, (**b**) time point *B*

27.3.3 Bearing Capacity

Since the soil is a type of cohesive-frictional material, the ultimate shaft resistance on the pile–soil interface is related to the normal compressive stress on it. When the pile contracts or expands during the heating or cooling pile period, the normal compressive stress will increase or decrease, as shown in Fig. 27.12. Then the pile's bearing capacity, which is comprised of the ultimate shaft resistance and the ultimate tip resistance, will also change. Assuming the applied mechanical load $P = 1{,}960$ kN, with other parametric value same to those in the reference condition mentioned above, the load-displacement curves for the pile at time points *A* and *B* are calculated and compared to the original load-displacement curve before thermal loading, as illustrated in Fig. 27.13. With these curves, the ultimate bearing capacity can be determined by the point at which the curve slope decreases suddenly. The result shows that for this simulated condition the pile's bearing capacity can have a variation of nearly 10 %, which seems to be not significant. But in fact the variation will increase if the pile's diameter become larger or the surrounding soil becomes stronger.

27.3.4 Long-Time Behavior

In the long-time operation, the energy pile will bear the cyclic thermal load. As a result, the pile will cyclically move up and down. During the cyclical relative

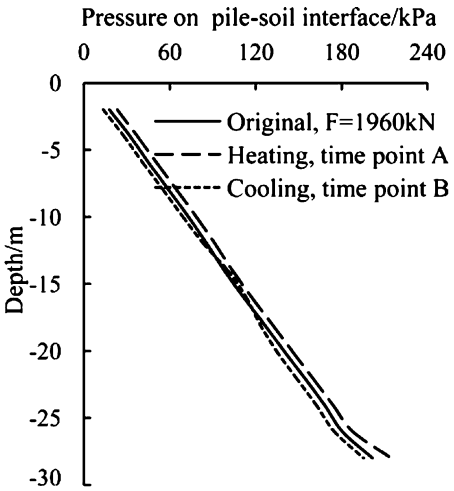

Fig. 27.12 Distribution of normal stress on the pile–soil interface before and during thermal loading

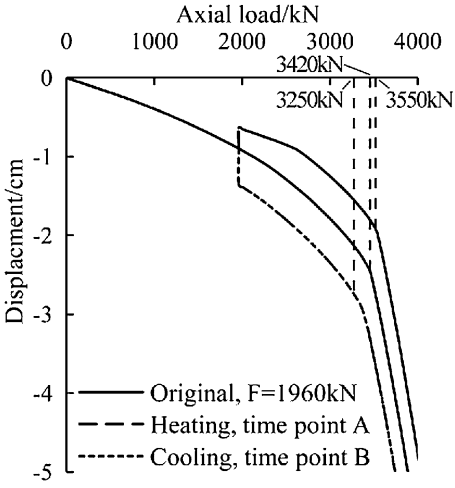

Fig. 27.13 Load-displacement curves of the pile with the corresponding ultimate bearing capacity before and during thermal loading

movement between the pile and soil, if part of the pile–soil interface is in the plastic stage, the pile's permanent displacement may be generated. To investigate the pile's displacement induced by the cyclic thermal load, the tong-time simulations of the pile with different mechanical loads are carried out. Using the average value of the maximum and minimum displacements in a thermal cycle to represent the average displacement of this cycle, the pile head's average displacement is illustrated in Fig. 27.14. It can be seen that the cyclic thermal load causes the pile to subside permanently, and the settlement will increase with the number of cycles until it converges to a stable value. The final settlement and the number of cycles for it to be stable will increase as the mechanical load becomes larger.

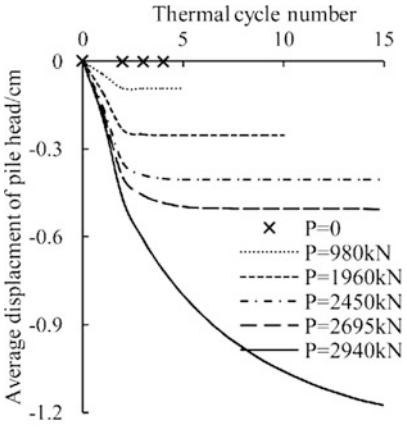

Fig. 27.14 Average displacement of the pile head induced by the cyclic thermal load

But if the mechanical load is large enough, it seems that the settlement will not turn stable, such as in the case of $P = 2{,}940$ kN in Fig. 27.14. It is supposed that there may be a threshold value for the mechanical load, above which the settlement will not cease increasing as the thermal cycle continues, and then, the pile will fail certainly. Obviously, the threshold value is less than the ultimate bearing capacity, as the pile's bearing capacity is 3,420 kN shown in Fig. 27.13, which implies that for energy piles the ultimate bearing capacity should be redefined in view of its long-time performance.

In fact, the results shown in Fig. 27.14 underestimate, more or less, the effect of thermal cycles with the elastic-perfectly plastic model employed for soil. In this model, plastic deformation can be generated only when the shear stress on the shaft reaches its ultimate value. Actually, plastic deformation can be generated as long as the soil is to be deformed.

27.4 Conclusions

The use of energy piles and other thermo-active ground structures as GHEs has become promising in the GCHP industry recently. However, the influence of temperature change on the structures' mechanical behavior has not been well understood. In this paper, based on numerical simulations, the energy pile's thermo-mechanical behavior has been investigated in detail. In the numerical model, the soil is modeled as a kind of thermo-elastic-perfectly plastic material, and the pile–soil interface is simulated by contact elements. The reliability of contact elements has been verified by an in-situ test. To save the computing time, the U-tubes in the pile are modeled by line elements, which are proved to be suitable for calculating the temperature in the pile.

The influence of soil properties and the applied mechanical load on the energy pile's thermo-mechanical behavior has been investigated through parametric analysis. The results show that the restraint condition at the pile head, the modulus of the soil and the mechanical load can significantly affect the thermally induced stress and the displacement in the pile. In a general condition, the thermal deformation of the surrounding soil can be neglected. Because of the decease of contact stress on the pile–soil interface during the cooling pile period, the change of stress is generally smaller than that during the heating pile period, but the corresponding displacement is larger. In general, when the soil is strong or the applied mechanical load is small, the thermally induced stress will be large, and the displacement will be small.

For the reference condition defined in this paper, the bearing capacity of the energy pile can vary 10 % due to the temperature change. As the variation can be enhanced by a larger diameter pile or stronger soil, the bearing capacity need to be further studied.

The long-time simulation of the energy pile's thermo-mechanical behavior indicates that the cyclic thermal load can induce a permanent settlement of the pile, and the final settlement is related to the applied mechanical load. More importantly, the results imply that there may be a threshold value for the mechanical load, above which the settlement will not cease increasing when the thermal cycle continues. Obviously, for energy piles, this threshold value is more suitable to be regarded as the pile's ultimate bearing capacity.

Acknowledgments The research is supported jointly by a grant from National Natural Science Foundation (Project No. 51208286) and a grant from 12th Five-Year National Science and Technology Support Program (2012BAJ06B03-01).

Nomenclature

a Area m^2
c Cohesion Pa
c_s Specific heat J/kg °C
d Compliance Pa^{-1}
e Elastic modulus Pa
t Temperature °C

Greek Letters

α Coefficient of thermal expansion $°C^{-1}$
ε Strain unit
λ Thermal conductivity W/m °C
v Poisson's ratio unit
σ Stress Pa

ϕ Internal friction angle °
ρ Density kg/m^3

Subscripts

p Pile
s Steel

Superscripts

e Elastic
p Plastic

References

1. Spitler JD (2005) Ground-source heat pump system research past, present and future. HVAC&R Res 11(2):165–167
2. Brandl H (2006) Energy foundations and other thermo-active ground structures. Geotechnique 56(2):81–122
3. Wood CJ, Liu H, Riffat SB (2009) Use of energy piles in a residential building, and effects on ground temperature and heat pump efficiency. Geotechnique 59(3):287–290
4. Moel M, Bach P, Bouazza A (2010) Technological advances and applications of geothermal energy pile foundations and their feasibility in Australia. Renew Sustain Energ Rev 14:2683–2696
5. Laloui L, Moreni M, Vulliet L (2003) Comportement d'un pieu bi-fonction, fondation et échangeur de chaleur. Can Geotech J 40(2):388–402
6. Bourne-Webb PJ, Amatya B, Soga K (2009) Energy pile test at Lambeth College, London: geotechnical and thermodynamics aspects of pile response to heat cycles. Geotechnique 59 (3):237–248
7. Rosenberg JE (2010) Centrifuge modeling of soil structure interaction in thermo-active foundations. University of Colorado at Boulder, M.S. thesis
8. McCartney JS, Rosenberg JE (2011) Impact of heat exchanger on slide shear in thermo-active foundations. Geo-Frontiers 2011, ASCE
9. Laloui L, Nuth M, Vulliet L (2006) Experimental and numerical investigations of the behaviour of a heat exchanger pile. Int J Numer Anal Meth Geomech 30:763–781
10. Knellwolf C, Peron H, Laloui L (2011) Geotechnical analysis of heat exchanger piles. J Geotech Geoenviron Eng 137(10):890–902
11. Wang G, Sitar N (2004) Numerical analysis of piles in elasto-plastic soils under axial loading. 17th ASCE engineering mechanics conference, Newark, DE

Chapter 28
An Equivalent-Capacitance Approach for Determining the Performance of a Refrigerant Coil

Chun Kwong Lee and Hong Nam Lam

Abstract An equivalent-capacitance approach (ECA) was proposed to determine the performance of a heat exchanger with a change in the physical state of one of the working fluids. The new methodology was an alternative form of the popular log-mean-temperature-difference approach (LMTDA) which could avoid the often troublesome iterative computations involving natural logarithms. Sample simulations were made using both methods for a refrigerant condenser and an evaporator. It was found that whenever convergence was achieved, both methods gave very similar results. However, the iteration stability of the ECA was much better, especially when the heat transfer value (UA) of the heat exchanger was large. Consequently, the ECA was considered to be a better alternative to the LMTDA in determining the performance of a refrigerant coil.

Keywords Heat exchanger • Temperature effectiveness • Log-mean-temperature difference • Overall heat transfer value • Capacitance rate

28.1 Introduction

Heat exchangers are commonly used in HVAC systems, particularly those in which there is a change in the physical state of one of the working fluids. They can appear as standalone devices or components of an item of air-conditioning equipment such as the condenser and the evaporator of a conventional vapour-compression chiller as well as the generator and absorber of an absorption refrigeration system. Hence, the determination of the performance of such kinds of heat exchangers is important in the modelling of a HVAC system. For a refrigerant coil used to exchange heat with a fluid, the simplest approach [1–4] assumes that the change in the physical state of the refrigerant proceeds at a constant temperature. Consequently, a

C.K. Lee (✉) • H.N. Lam
Department of Mechanical Engineering, University of Hong Kong, Pokfulam Road, Hong Kong, China
e-mail: a8304506@graduate.hku.hk; hn.lam.hku@hku.hk

I. Dincer et al. (eds.), *Progress in Sustainable Energy Technologies Vol II: Creating Sustainable Development*, DOI 10.1007/978-3-319-07977-6_28

temperature effectiveness (ε) can be defined and the capacity of the heat exchanger (Q) can be found as follows:

$$\varepsilon = 1 - e^{-\frac{UA}{C_f}} \quad \text{and} \quad Q = C_f\left(T_{f,i} - T_{rs}\right)\varepsilon \tag{28.1}$$

Here, the temperature effectiveness depends on the average overall heat transfer value of the coil (UA) and the capacitance rate of the fluid (C_f). The difference between the fluid inlet temperature ($T_{f,i}$) and the refrigerant saturation temperature (T_{rs}) is considered to be the maximum temperature change allowed for the fluid. The outlet conditions of the coil are then calculated directly from:

$$T_{f,o} = T_{f,i} - \frac{Q}{C_f} \tag{28.2}$$

$$h_{r,o} = h_{r,i} + \frac{Q}{m_r} \tag{28.3}$$

The main advantage of the temperature-effectiveness approach (TEA) is that the performance of the refrigerant coil is determined explicitly through Eqs. (28.1)–(28.3). However, it has one drawback. While the calculated fluid leaving temperature ($T_{f,o}$) is safeguarded by the temperature effectiveness so that it will not go beyond the feasible limit, there is no such guarantee on the refrigerant side. In actual practice, the refrigerant enters a condenser as a superheated gas and may leave the condenser as a sub-cooled liquid, while the refrigerant is usually a saturated mixture at the evaporator inlet and becomes a superheated gas when it leaves the evaporator. Figure 28.1 depicts the temperature variation inside a counter-flow (CF) condenser and an evaporator where 1 and 2 denote the two ends of the heat exchangers. As the mass flow rate of the refrigerant is usually much smaller than that of the other fluid, the temperature change of the refrigerant outside the saturated region can be very large. The situation is especially significant for the superheated refrigerant gas. Hence, if the enthalpy change of the refrigerant across the coil is high, the refrigerant may leave the coil at a temperature ($T_{r,o}$) which falls beyond the feasible limit. This can happen when UA is large or the difference between the fluid inlet temperature and the refrigerant saturation temperature is large. Another possible situation in which the said condition can occur is when the refrigerant mass flow rate is low. This occurs for a variable-speed vapour-compression system when the compressor is running at a low speed during the part-load operation.

To solve the problem, the log-mean-temperature-difference approach (LMTDA), was employed [5–7] as shown below:

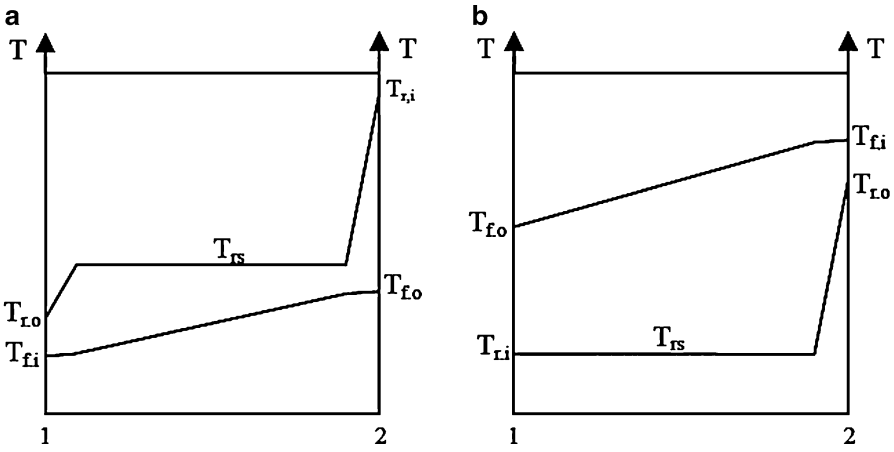

Fig. 28.1 Variation of temperature inside a counter-flow (**a**) condenser and (**b**) evaporator

$$\Delta T_m = \frac{\left(T_{f,2} - T_{r,2}\right) - \left(T_{f,1} - T_{r,1}\right)}{\ln\left(\frac{T_{f,2} - T_{r,2}}{T_{f,1} - T_{r,1}}\right)} \tag{28.4}$$

$$Q = UA\Delta T_m \tag{28.5}$$

Here, a log-mean-temperature difference (ΔT_m) is defined to calculate the capacity of the coil based on the temperatures of both fluids at the two ends of the coil. This methodology was also adopted in modelling the performance of the absorber and the regenerator in an absorption refrigeration system [8–10]. For a counter-flow design, Eq. (28.5) becomes

$$\Delta T_m = \frac{\left(T_{f,o} - T_{r,i}\right) - \left(T_{f,i} - T_{r,o}\right)}{\ln\left(\frac{T_{f,o} - T_{r,i}}{T_{f,i} - T_{r,o}}\right)} \tag{28.6}$$

The corresponding formulation for a parallel-flow (PF) design is

$$\Delta T_m = \frac{\left(T_{f,o} - T_{r,o}\right) - \left(T_{f,i} - T_{r,i}\right)}{\ln\left(\frac{T_{f,o} - T_{r,o}}{T_{f,i} - T_{r,i}}\right)} \tag{28.7}$$

Again, Eqs. (28.2) and (28.3) are used to determine the outlet conditions of the coil. However, unlike the TEA, the solution for the LMTDA has to be solved iteratively. This can be troublesome when calculating ΔT_m, as there is a natural logarithm in the denominator which limits the feasible combinations for the temperatures during the iteration. To overcome this problem, various limiting conditions have to be set. In case the refrigerant lies outside the saturated region at the coil outlet, $T_{r,o}$ may approach $T_{f,i}$. In these circumstances, the imposed limiting

conditions will affect the convergence of the iteration and results in a long computation time. The final solution may also be incorrect. To solve the problem, an equivalent-capacitance approach (ECA) is proposed in this study which avoids the calculation of the natural logarithm, and thus no limiting conditions are required. The results and the iteration cycles based on the ECA and LMTDA are compared to assess the validity and strength of the ECA.

28.2 Mathematical Formulations

By defining an equivalent capacitance rate (C_r, C_f) for the refrigerant and the other fluid, Eq. (28.6) can be re-written as

$$\frac{Q}{UA} = \frac{T_{f,o} - T_{f,i} + T_{r,o} - T_{r,i}}{\ln\left(\frac{T_{f,o}-T_{r,i}}{T_{f,i}-T_{r,o}}\right)} = \frac{-\frac{Q}{C_f} + \frac{Q}{C_r}}{\ln\left(\frac{T_{f,o}-T_{r,i}}{T_{f,i}-T_{r,o}}\right)}$$

$$UA\left(\frac{1}{C_r} - \frac{1}{C_f}\right) = \ln\left(\frac{T_{f,o} - T_{r,i}}{T_{f,i} - T_{r,o}}\right) \tag{28.8}$$

By denoting the left-hand side of Eq. (28.8) as α,

$$\alpha = \ln\left(\frac{T_{f,o} - T_{f,i} + T_{f,i} - T_{r,i}}{T_{f,i} - T_{r,i} + T_{r,i} - T_{r,o}}\right) = \ln\left(\frac{-\frac{Q}{C_h} + \Delta T_i}{\Delta T_i - \frac{Q}{C_c}}\right)$$

where $\Delta T_i = T_{f,i} - T_{r,i}$

$$e^{\alpha}\left(\Delta T_i - \frac{Q}{C_r}\right) = -\frac{Q}{C_f} + \Delta T_i$$

$$Q = \frac{\Delta T_i(1 - e^{\alpha})}{\frac{1}{C_f} - \frac{e^{\alpha}}{C_r}} \tag{28.9}$$

The refrigerant leaving temperature is determined from

$$T_{r,o} = T_{r,i} + \frac{Q}{C_r} \tag{28.10}$$

The performance of the heat exchanger can then be calculated by using Eqs. (28.2) and (28.10) if C_r and C_f are known. Hence, the key issue is how the equivalent-capacitances are defined. For the refrigerant,

$$C_r = m_r \frac{h_{r,o} - h_{r,i}}{T_{r,o} - T_{r,i}} \tag{28.11}$$

In case the refrigerant lies within the saturated region at a constant temperature, $1/C_r$ can be taken as zero. In this circumstance, Q can still be calculated. Equation (28.11) is also applicable to any other fluid with a change in the physical state in the exchanger such as the liquid desiccant in the generator of an absorption chiller. For the other fluid without a change in the physical state,

$$C_f = m_f c_f \tag{28.12}$$

Again, the performance of the heat exchanger is determined by solving Eqs. (28.2), (28.9)–(28.12) using an iterative approach. As no natural logarithm needs to be calculated, no limiting conditions are required. Equation (28.9) fails when $C_f = C_r$ although it rarely happens. To solve the problem, as $C_f \to C_r$, $\alpha \to 0$ and $e^{\alpha} \approx 1 + \alpha$. Hence, Eq. (28.9) can be re-written as

$$Q \approx \frac{-\Delta T_i \alpha}{\frac{1}{C_f} - \frac{1+\alpha}{C_r}} \approx \frac{-\Delta T_i \alpha}{-\frac{\alpha}{UA} - \frac{\alpha}{C_r}} \approx \frac{\Delta T_i UAC_r}{UA + C_r} \tag{28.13}$$

Equation (28.13) is the same as the one derived based on the TEA when the capacitance ratio is unity. For a PF heat exchanger, the same manipulation applied to Eq. (28.7) yields

$$Q = \frac{\Delta T_i \left(1 - e^{\beta}\right)}{\frac{1}{C_f} + \frac{1}{C_r}} = \frac{\Delta T_i UA \left(e^{\beta} - 1\right)}{\beta} \tag{28.14}$$

where

$$\beta = -UA\left(\frac{1}{C_f} + \frac{1}{C_r}\right) \tag{28.15}$$

Unlike Eq. (28.9) for a CF design, Eq. (28.14) is valid for all capacitance ratios.

28.3 Results and Discussion

With the formulation for the ECA established, comparisons of the calculated heat exchanger performances were made with those based on the LMTDA when applied to a refrigerant condenser and an evaporator using the commercial software EES [11] at different values for UA. EES offered many built-in functions for calculating the properties of numerous refrigerants. R134a was chosen in this study and water was employed to exchange heat with the refrigerant. Both the PF and CF

Table 28.1 Entering conditions of water and refrigerant

	Condenser	Evaporator
Water mass flow rate (kg/s)	1.0	1.0
Water temperature (°C)	30.0	10.0
Refrigerant mass flow rate (kg/s)	0.2	0.2
Refrigerant pressure (kPa)	1,100	250
Degree of superheat of refrigerant at inlet (°C)	30.0	Not applicable
Quality of refrigerant at inlet	Not applicable	0.2

Table 28.2 Simulated performance of a condenser based on different modelling approaches

LMTDA/ECA/TEA				
Type	*UA* (kW/K)	$T_{f,o}$ (°C)	$T_{r,o}$ (°C)	*nit*
CF	2.0	39.39/39.39/34.91	40.28/40.27/42.95	299/34/NA[a]
	4.0	40.00/40.00/37.96	31.66/31.66/42.95	88/28/NA[a]
	6.0	40.09/40.09/39.86	30.32/30.32/33.67	41/27/NA[a]
	8.0	40.09/40.11/41.03	30.30/30.07/16.37	500/26/NA[a]
	10.0	40.11/40.11/41.76	30.01/30.01/5.213	500/26/NA[a]
PF	2.0	38.25/38.25/34.91	42.95/42.95/42.95	500/157/NA[a]
	4.0	39.41/39.41/37.96	39.99/39.99/42.95	79/28/NA[a]
	6.0	39.44/39.44/39.86	39.65/39.51/33.67	500/27/NA[a]
	8.0	39.80/39.45/41.03	39.81/39.45/16.37	500/27/NA[a]
	10.0	40.11/39.45/41.76	40.12/39.45/5.213	500/27/NA[a]

[a]*NA* not applicable

configurations were investigated. Table 28.1 summarised the design entering conditions for the water and the refrigerant when used in the condenser and the evaporator. The specific heat capacity of water was taken as 4.19 kJ/kg K.

Various limiting conditions were set for the refrigerant leaving temperature when applying the LMTDA which depended on the flow configuration and the function of the coil as shown below:

1. For a PF condenser, $T_{r,o} - T_{f,o} \geq 0.01$ °C.
2. For a PF evaporator, $T_{r,o} - T_{f,o} \leq 0.01$ °C.
3. For a CF condenser, $T_{r,o} - T_{f,i} \geq 0.01$ °C.
4. For a CF evaporator, $T_{r,o} - T_{f,i} \leq 0.01$ °C.

Table 28.2 compared the simulated performances of the PF and CF condenser at different values of *UA* based on various modeling approaches including the TEA. Here, *nit* was the number of iterations required with a maximum of 500 set in the simulation models. It could be observed that in all cases, the iterations converged readily when the ECA was used. On the other hand, convergence might fail when using the LMTDA, especially when *UA* was large and *nit* reached 500. In fact, the simulated performance of the PF condenser oscillated when *UA* was large. In all the cases when convergence was met, the simulated results obtained by using the ECA

Table 28.3 Simulated performance of an evaporator based on different modelling approaches

LMTDA/ECA/TEA				
Type	UA (kW/K)	$T_{f,o}$ (°C)	$T_{r,o}$ (°C)	*nit*
CF	2.0	4.579/4.571/4.571	−4.302/−4.302/−4.302	500/78/NA[a]
	4.0	2.128/2.127/1.203	−0.377/−0.378/21.79	189/25/NA[a]
	6.0	1.909/1.909/−0.886	4.875/4.875/70.13	101/16/NA[a]
	8.0	1.815/1.815/−2.183	7.135/7.135/98.54	67/12/NA[a]
	10.0	1.768/1.768/−2.987	8.280/8.281/115.6	49/10/NA[a]
PF	2.0	4.579/4.571/4.571	−4.302/−4.302/−4.302	500/78/NA[a]
	4.0	2.192/2.193/1.203	−1.925/−1.923/21.79	160/20/NA[a]
	6.0	2.083/2.082/−0.886	0.701/0.700/70.13	76/14/NA[a]
	8.0	2.049/2.048/−2.183	1.526/1.525/98.54	45/14/NA[a]
	10.0	2.060/2.035/−2.987	1.249/1.825/115.6	500/14/NA[a]

[a]*NA* not applicable

were basically the same as those based on the LTMDA. In this respect, the ECA was considered to be a better alternative to the LMTDA in determining the performance of a heat exchanger. With a CF design, the fluid leaving temperature can be even higher than the refrigerant leaving temperature, and a higher heat transfer rate could be achieved as compared to a PF design. This explained why a CF heat exchanger was more common than a PF one. From Table 28.2, the calculated $T_{r,o}$ based on the TEA fell below $T_{f,i}$ or 30 °C when UA was more than 6.0 kW/K. Moreover, $T_{r,o}$ was higher than $T_{f,o}$ for a PF design when UA was over 4.0 kW/K. Both situations were infeasible. This highlighted the weakness of the TEA as already mentioned in the introduction. On the other hand, both the LMTDA and the ECA guaranteed that the calculated coil performance was feasible. As the TEA assumed a constant refrigerant temperature inside the heat exchanger, the simulated coil performance was the same regardless of a CF or a PF design.

Table 28.3 showed the corresponding results for an evaporator. When UA was 2.0 kW/K, the refrigerant still lay in the saturated region when it left the evaporator. Hence, the three approaches basically yielded the same results. Moreover, the coil performance was the same between a CF and a PF design. When UA was increased to 4.0 kW/K and higher, the refrigerant became a superheated gas at the evaporator outlet, and the differences in the simulated results between those based on the LMTDA/ECA and those using the TEA became significant. The calculated $T_{r,o}$ was much higher than $T_{f,i}$ or 10 °C when the TEA was employed. Again, this was impossible. For the CF design, contrary to the situations for the condenser, the simulated $T_{r,o}$ at the evaporator outlet had not yet reached the limiting condition with the use of the LMTDA/ECA even if UA was up to 10.0 kW/K. This could be explained by the much higher difference between the entering fluid and refrigerant temperatures for the condenser. If a smaller degree of superheat for the refrigerant was employed at the condenser inlet, a similar trend could be obtained. Nevertheless, non-convergence or oscillation in the simulated results could still be observed for the PF evaporator with UA taken as 10.0 kW/K when using the LMTDA. Meanwhile, a monotonic trend could be obtained when employing the ECA.

28.4 Conclusions

A better modelling methodology, namely the equivalent-capacitance approach (ECA), was developed to determine the performance of a heat exchanger in which at least one of the working fluids experienced a change in the physical state. An equivalent capacitance rate was defined based on the enthalpy and temperature changes across the heat exchanger. The new method was an alternative form of the log-mean-temperature-difference approach (LMTDA). Both methods required iterative calculations but guaranteed that feasible results could always be obtained as opposed to the simple explicit temperature-effectiveness approach (TEA). By avoiding the calculation of a natural logarithm as required in the LMTDA, no limiting conditions needed to be set in the ECA. This could improve the convergence of the iterations and reduce the computation time.

Sample comparisons were made on the simulated results obtained using the three approaches for a refrigerant condenser and an evaporator under different flow configurations and overall heat transfer values (UA). It was found that whenever convergence was achieved, both the LMTDA and the ECA generated very similar results. However, the ECA offered a much better iteration stability, especially when UA was large. In fact, oscillation in the iteration could be observed for a parallel-flow design when using the LMTDA based on a large UA. Meanwhile, infeasible results could arise when using the TEA. In view of all the above-mentioned advantages in comparison with the disadvantages of LMTDA, the ECA should be a better choice for determining the performance of a refrigerant coil.

Acknowledgement The authors would like to gratefully acknowledge the funding support provided to this research work by the Research Grants Council of Hong Kong under the General Research Fund for Project Number 713710.

Nomenclature

C	Capacitance rate (kW/K)
c	Specific heat capacity (kJ/kg K)
h	Specific enthalpy (kJ/kg)
m	Mass flow rate (kg/s)
nit	Number of iterations
Q	Heat exchanger capacity (kW)
T	Temperature (K)
UA	Overall heat transfer value (kW/K)

Greek Symbols

$\alpha \quad = UA\left(\frac{1}{C_c} - \frac{1}{C_h}\right)$

$\beta \quad = -UA\left(\frac{1}{C_c} + \frac{1}{C_h}\right)$

ΔT_i Temperature difference between the entering fluid and refrigerant (°C)
ΔT_m Log-mean-temperature difference (°C)

Subscript and Superscripts

f Fluid
i Inlet
o Outlet
r Refrigerant
rs Refrigerant at saturated state
1,2 Two ends of a heat exchanger

Acronyms

CF	Counter-flow
ECA	Equivalent-capacitance approach
LMTDA	Log-mean-temperature-difference approach
TEA	Temperature-effectiveness approach
PF	Parallel-flow

References

1. Pieve M, Salvadori G (2011) Performance of an air-cooled steam condenser for a waste-to-energy plant over its whole operating range. Energ Convers Manag 52(4):1908–1913
2. Karlsson F, Fahlen P (2007) Capacity-controlled ground source heat pumps in hydronic heating systems. Int J Refrig 30(2):221–229
3. Jin H, Spitler JD (2002) A parameter estimation based model of water-to-water heat pumps for use in energy calculation programs. ASHRAE Trans 108(1):3–17
4. Herbas TB, Berlinck EC, Uriu CAT, Marques RP, Parise JAR (1993) Steady-state simulation of vapor-compression heat pumps. Int J Energ Res 17(9):801–816
5. ASHRAE (2009) ASHRAE handbook: fundamentals. ASHRAE, Atlanta
6. Yu FW, Chan KT (2007) Part load performance of air-cooled centrifugal chillers with variable speed condenser fan control. Build Environ 42(11):3816–3829
7. Cecchini C, Marchal D (1991) A simulation model of refrigerant and air-conditioning equipment based on experimental data. AHSRAE Trans 97(2):388–393
8. Fong KF, Lee CK, Chow TT (2012) Comparative study of solar cooling systems with building-integrated solar collectors for use in sub-tropical regions like Hong Kong. Appl Energ 90 (1):189–195
9. Mehrabian MA, Shahbeik AE (2005) Thermodynamic modelling of a single-effect LiBr_H2O absorption refrigeration cycle. Proc Inst Mech Eng E J Process Mech Eng 219(3):261–273
10. Florides GA, Kalogirou SA, Tassou SA, Wrobel LC (2003) Design and construction of a LiBr-water absorption machine. Energ Convers Manag 44(15):2483–2508
11. EES (2001) Engineering equation solver. F-Chart Software

Chapter 29
Perspectives on Sustainability in Natural-Gas-Liquids Operations Through a Cleaner Production Framework

Reem Fahd and Farayi Musharavati

Abstract Sustainability in design and operation of industrial processes has become a global issue in process engineering. Of late, there has been keen interest in operationalizing sustainability particularly in the oil and gas processing industries. One way of operationalizing sustainability is to combine 'process integration' and 'process optimization' in a framework that allows engineers to significantly improve operating efficiencies. In this study, methods, mechanisms and perspectives for integrating waste minimization and process parameter optimization in order to improve operating efficiencies in natural-gas-liquids (NGL) process systems are discussed. The aim of the analysis is to provide a basis for; reducing wastes, increasing the efficiency of materials processing, as well as optimize the consumption of natural gas in NGL operations and processing facilities. The solution trajectory for operationalizing sustainability was developed by creating an innovative cleaner-production-based framework that addresses sustainability concepts through process system optimization and implementation of optimal production operation strategies. To this end, opportunities for cleaner production assessments in NGL operations and processing systems were investigated. Cleaner production alternatives were examined and evaluated with respect to in-place environmental management systems. An adapted cleaner production model that dynamically incorporates; (a) process integration, (b) process optimization, (c) optimal production operation strategies, and (d) operational excellence in a bid to deploy sustainability concepts in NGL plants was developed. The applicability of the proposed model was illustrated through a case study of an existing NGL plant in Qatar. It was concluded that innovative cleaner production models that take cognizance of existing environmental management systems can quickly reveal sustainability initiatives in NGL process systems.

Keywords Sustainability • Cleaner production • Process integration • Process optimization • Natural gas liquids (NGL) • Natural gas

R. Fahd • F. Musharavati (✉)
Department of Mechanical and Industrial Engineering, Qatar University,
Box 2713, Doha, Qatar
e-mail: reem.khir@qu.edu.qa; farayi@qu.edu.qa

I. Dincer et al. (eds.), *Progress in Sustainable Energy Technologies Vol II: Creating Sustainable Development*, DOI 10.1007/978-3-319-07977-6_29

29.1 Introduction

Oil and gas production industries deal with the global processes of; exploration, extraction, refining, storage, transporting, and marketing of oil and gas products. The largest volume products of this industry are fuel oil and gasoline. Part of the oil and gas products are used as raw materials for many chemical products including; pharmaceuticals, solvents, fertilizers, pesticides, and plastics. Therefore, the importance of the oil and gas production industry can never be over emphasized.

In the State of Qatar, a number of companies play a vital role in global oil and gas processing. This includes; exploration, storage, distribution and exportation of oil and gas products. Over the years, companies in Qatar have gained the experience and expertise in the upstream, midstream and downstream aspects of the oil and gas industry. Some of these companies produce crude oil that is partially fed to refineries for crude oil products. Other companies produce natural gas that is further processed to produce; pipeline quality gas, liquid petroleum gas, and natural gas liquids (NGL) for local use as well as for export.

Natural gas is a mixture of hydrocarbons and is often found in the ground together with petroleum. Natural gas is burnt directly to produce energy. In comparison to fossil fuels, natural gas burns with a cleaner blue flame and therefore causes relatively less pollution problems. Uses of natural gas include producing electricity for cooking and heating in buildings. Natural gas is also used as fuel for cars as well as to make fertilizers and plastic products. Many vehicles such as trucks, boats, cars, excavators, big rigs, and airplanes use natural gas as a fuel. Therefore, the supply and demand channels for natural gas in midstream and downstream operations are limitless. Such channels can be used to diversify, and hence optimize, the use of extracted natural gas with the added advantage of improved environmental performance.

Today, natural gas is highly demanded world-wide to cope with human activities and meet the needs of life in many forms. Although natural gas is considered to be one of the cleanest fuels, natural gas from different gas fields often contains harmful substances such as: mercury (Hg), Carbon Dioxide (CO_2), Hydrogen Sulfide (H_2S), Mercaptan Compounds (RSH) and Carbonyl Sulfide (COS). As a result, natural gas processing operations and facilities are often associated with; purification processes, filtrations, recovery units and waste management as well as waste disposal units. Such associations are end-of-pipe approaches that act as prominent indicators for the need for improving the sustainability of operations. These indicators are often measured in terms of effluent emissions. Therefore, the sustainability of an industrial process depends on minimizing these effluents. A better status and hence improvement in sustainability of operations would be to implement cleaner production options that aim at reducing and/or preventing waste generation at the source rather than end-of-pipe approaches.

Besides the visible environmental degradation and potential ecological problems associated with oil and gas processing plants, another major indicator for the need for sustainable operations is the rapid consumption of the natural gas resources. In

this context, end-of-pipe approaches mentioned above do very little in terms of matching or limiting the extraction or consumptions of natural gas to the correct and/or required levels. This often leads to extracting and consuming more than is required thus resulting in over consumptions of the natural gas reserves. Over consumption of natural gas reserves is often measured in terms of matching the resource intake to operations requirements. The correct balance is usually obtained by improving operating efficiencies, particularly fine tuning process parameters towards optimal design values.

The discussions in this study take inspiration from the two forms of sustainability indicators described above, namely; (a) minimization of waste generation (i.e. solid, liquid and gaseous wastes), and (b) optimization of resource intake. These two indicators form the basis for sustainability concepts discussed in this study. The logic lies in that minimization of waste generation and optimization of resource intake have a direct impact on the sustainability of industrial processes. In the public literature, two key concepts that support sustainable process design and synthesis have been identified, namely; (1) process integration, and (2) process optimization [1]. Process optimization involves adjusting process parameters so as to maximize operating efficiencies. When operating efficiencies are maximized, it is easier to match resource intake to operations-resource optimization. On the other hand, process integration implies a systems view of process operations in which unit operations aim to achieve targeted values with optimized energy consumption (i.e. reducing energy wastes) and increased efficiency of materials processing. Both process optimization and process integration have a direct impact on improving the sustainability of industrial processes. For example, process integration provides a basis for integrating the generation of waste along the process system while process parameter optimization sets the platform for improving operating efficiencies in natural gas processing systems. In the analysis the two, i.e. process integration and process optimization, provide a basis for reducing waste in the process system and thus optimizing the consumption of natural gas. A key methodology that shares similar concepts is cleaner production.

Cleaner production is a preventive methodology for minimizing waste and emissions in industrial processes through source reduction strategies. The general aim in implementing cleaner production concepts is to produce 'clean' products that perform the same function but produce them without waste. Since cleaner production models share similar concepts in terms of reducing process wastes and optimizing resource usage and resource consumption, the approach proposed in this work is to deploy the concepts of process integration and process optimization through a cleaner production framework. Therefore, the goal of this study is to explore, examine and investigate the roles of process integration and process optimization as the agents of change for sustainability in natural gas processing operations and facilities. The underlying logic is that a cleaner production model that is configured to deploy specific aspects of process integration and process optimization can go a long way in operationalizing sustainability in natural gas processing operations and facilities. The issues and methodology related to the application of cleaner production at the level of industrial production systems and

their corresponding unit operation and materials will be examined. The investigation will be illustrated through a case study of a natural gas processing operation. The case study will focus on macro-level and meso-level for natural gas liquids (NGL) processing plants.

29.2 Literature Review

Natural gas processing and production systems consist of processes that change raw materials into useful products by removing impurities. In order to reach the desired product, a number of operations such as heating, cooling, moving, separation, mixing, and chemical reactions are carried out. These operations need to be investigated thoroughly in a bid to identify opportunities for improving sustainability.

In order to extract natural gas from the ground, industries use sophisticated technology. With further and continued development of natural gas process system technologies, the natural gas processing industry has been facilitated with more efficient, safe and environmental conscious technologies and techniques. To date, the process of technology improvements focused on availing environmentally friendly technologies is continuously proceeding. Therefore, analytical process system investigations that identify opportunities for improving sustainability are, in most cases, complimentary and/or supplementary to the quest for more environmentally friendly process system technologies.

Most modern oil and gas processing operations are equipped with the best available technologies (BATs) and techniques. The amount and efforts for continuous process system changes for improved environmental performance demonstrate that the concept of greening has been widely accepted in natural gas processing operations. Traditionally, such changes have been implemented through recommendations from existing environmental management systems (EMSs). However, BATs constitutes moving targets on practices, since developing societal values and advancing techniques may change what is currently regarded as ‘best available’ [2]. This is evident from the fact that the oil and gas processing industry is still associated with upgrades in terms of; purification processes, recovery processes, pollution control measure and waste minimization measures, in a bid to meet ‘recent’ stringent industrial emissions directives. In addition, this industry is also associated with process system changes and upgrades that are entirely driven by environmental parameters. Hence, process integration, process optimization and cleaner production initiatives are important to the sustainable growth of the oil and gas processing industry.

29.2.1 Process Integration

Early perspectives on process integration were geared towards heat integration [3]. Since then, process integration concepts were discussed and utilized in heat exchanger networks, and pinch analysis [4]. A more general definition of process integration has been stated as: systematic and general methods for designing integrated production systems ranging from individual processes to total sites and with special emphasis on the efficient use of energy and reducing environmental effects [5]. Since inception, process integration has been regarded as a family of methodologies for combining several processes in order to reduce consumption of resources or reduce waste [1].

Process integration methods have been applied in various industries including: fluid catalytic cracking process in petrochemicals; energy integration of a hospital complex; sunflower oil production; and whisky distillery [1]. In most of the cited works, process integration is used as a methodology for solving various kinds of problems along the process system. In this study, process integration will be used as a concept that is integrated into a cleaner production methodology.

29.2.2 Process Optimization

In some applications, process optimization is used as a methodology for sustainable process design and synthesis. Process optimization is used as a means of formulating sustainability tasks as optimization problems. In this view, a number of optimization models have been utilized successfully as detailed in [1]. In this study, process optimization is used as a concept within a cleaner production methodology. Process optimization is used to capture the interactions and connections among the various inputs and outputs along the process system. This feature is key in minimizing resource demands and deciding which design parameters and operating policies are suitable for reducing environmental impacts.

29.2.3 Cleaner Production

Generally, the cleaner production method can be implemented through different alternatives [6]. These alternatives can be implemented individually or simultaneously depending on the situation. Successful implementation usually depends on the practicality of the solutions and the economic and technical feasibility of the available alternatives. In the public literature, Berkel [7] defined cleaner production as a proactive and preventive approach to industrial environmental management which aims for process and product integrated solutions that are both environmentally and economically efficient. As such, cleaner production is a strategy that

provides continuous preventive improvement of environmental performance of organizations. The goal of cleaner production is to prevent the pollution at the source rather than treat it after being created [8]. The link between cleaner production and process integration is quite evident from the definition given above. In a cleaner production framework, the concept of integration goes beyond the process system to include the product in the analysis.

Cleaner production aims at progressive reductions of environmental impacts of processes, products and services through preventative approaches rather than control and management of pollutants and waste after they have been produced. For processes, cleaner production aims to thoroughly conserve raw materials and energy, eliminate toxic raw materials, and decrease the quantity and toxicity of all releases and waste before processing. In the case of products, cleaner production aims at reducing the environmental impact along the life cycle of a product, i.e. from raw materials extraction to its final disposal. For services, cleaner production entails the incorporation of environmental concerns into designing and delivering services. Ultimately, cleaner production requires a change in attitudes, responsible environmental management and evaluation of technology options. This leads to the goal of zero waste [8].

From the discussions above, it can be observed that the cleaner production concept is dynamic. The older cleaner production approaches focused on waste minimization, pollution prevention and reduction in the use of toxins. On the other hand, modern preventive approaches in cleaner production aims at reducing the environmental impact through life cycle assessment of a process, product or service.

In [7], the engineering or assessment of cleaner production was classified into three levels, namely; macro scale; meso-scale and micro scale. The macro-scale level investigates the flow of materials from natural resources drawing out to consumer product discarding. The opportunities of improvement in the macro-level are implemented in areas like dematerialization, design for reuse, design for recycling, substitution of toxic and scarce materials , reuse of waste streams from one process to use it as input to another process.

The second scale level is the meso scale level which is concerned with the chemicals of the process. The area of improvements here can be done through process optimization, substitution of process technology, substitution of equipment, implementation of better operational and maintenance practices. The last level is the micro-scale level that deals with molecular interactions which is achieved by means of alternative catalyst systems, alternative process chemistry and use of alternative feedstock for processes. The discussions in this study focus on the macro and meso-scale levels.

When fuels are burned up, gases such as carbon dioxide and acids are produced. These gases cause global warming, which has terrible consequences on the environment worldwide. For NGL plants, emissions will come from gas sweetening units when acid waste gas is burned or incinerated. Most frequently, the acid waste gas is used as a feedstock in sulphur recovery units or in sulphuric acid plants. While flaring is often expected in NGL plants, the major poison and pollutant of

concern is SO_2. Most plants employ elevated smokeless flares or gas incinerators for combustion of all waste gas constituent, including tail gas incinerator in which H_2S is oxidized to SO_2. Such practices are not sustainable. Cleaner production can be implemented to reduce and/or eliminate gas flaring or incinerations from NGL plants.

29.3 Methodology

A number of methods and models were used for analyzing data collected from the case study. Input/output models were used to summarize the materials flow. The input/output models were appropriately used to provide quick answers based on a pre-determined set of input parameters. The input/output models were also used as a tool to determine feed materials, outputs and different streams such as by-products, flares or any other stream released by the process.

In using the materials balance model, the flows and compositions of each material were identified and, the balances over each individual process in the NGL plant were conducted. The mass conservation law implies that the mass of an input to several processes should be equivalent to the mass of the output of that process [9]. The material balance procedure used in the case study was based on the discussions in [10].

29.3.1 Cleaner Production Method

The case study is a modern NGL plant. The NGL case study was both ISO 9000 and ISO 14000 certified and a number of programs were in place to check measure and monitor the requirements for these certifications. Therefore, an active environmental management system (EMS) was in place. Within the EMS framework, the case study plant was implementing environmental reporting and pollution control methods. In comparison to the cleaner production concepts, the technical issues of ISO 14000 share commonalities with cleaner production. The environmental management system determines the environmental position and performance of the organization and their continuous improvements. The environmental management tools and systems are covered by ISO 14000 series which provide specifications and guidance for an environmental management system. The EMS does not help in defining the significance of environmental impact, so the organization itself has to set rules, procedures and policies to measure the significance. In addition, the case study plant used best available technologies (BATs) as and when required. The BATs were usually sought after and implemented in response to the need for continuously improving the organization's environmental performance. Aspects of cleaner production considered were: (1) process technology, (2) operational practices, and (3) waste and emissions.

29.3.1.1 Process Technology

The cleaner production framework advocates examining current process technology change for equipment improvements and improved process control. For such changes to be both effective and efficient in operations a systems view of the production process is required. The production process systems view should include both the process and product issues. This can be ensured by observing both process and product integration concepts in the assessment and analysis for process technology change. While this is sufficient, an optimization perspective must be used in order to avoid implementing process changes that results in sub-optimal operations. Thus, the process technology changes should not affect the economic performance of the production system in addition to improving the environmental performance of the production system. Hence, process integration and process optimization concepts are fundamental to a successful process technology change in a cleaner production framework. Process technology changes may include: implementing new technology (which may be BATs at that particular period); equipment modifications i.e. modify the existing production equipment and utilities in order to run the processes at higher efficiency and at lower waste and emission generation rates; improved processing conditions in order to run the processes more efficiently and at lower waste and emission generation rates. Other aspects of process technology change include: retrofitting, automation, and improved process control.

29.3.1.2 Operational Practice

The cleaner production framework advocates improved operations management and practices. For the NGL process, this includes effectively managing process upsets, preventing leaks and spills and enforcing good operational instructions. The basic idea is to achieve or benchmark best practice, improve operating efficiencies and practice efficient production planning. Other aspects of good operating practices include: effective energy management such as avoiding high-peak energy consumption and preventing unnecessary power consumption. Other additional aspects include; effective maintenance engineering and management, and implementing proper working instructions and procedures. In the case study plant, the later aspects of good operational practice were adequately covered through an active environmental management system.

29.3.1.3 Waste and Emissions

The cleaner production framework advocates elimination or at least minimization of waste and emissions. In the case study plant, waste accumulates along the process system and is sometimes taken out of the system through flaring or

collected either for disposal or for reprocessing in other companies. As such, an integrated treatment of waste and emissions was necessary. Based on the various cleaner production methods discussed above, an appropriate cleaner production assessment model was developed for implementation in the case study plant.

29.3.1.4 Cleaner Production Assessment

Due to the strong presence of a well-defined EMS backed by an active ISO 14000 certification, the general cleaner production model had to be modified to acknowledge case study efforts on environmental issues based on the implemented environmental management system [11]. In the case study, for example, issues to do with housekeeping were thoroughly covered under an updated environmental management system. In addition, process/technology changes had also been made in a bid to meet changes in acceptable emission levels as stipulated by the local environmental authorities. A modified cleaner production model suitable for the case study is shown in Fig. 29.1.

The model shown in Fig. 29.1 indicates that the first step when thinking about implementing cleaner production within an environmental management system framework that uses best available technologies in order to improve the organization's environmental performance is to evaluate the current environmental performance "as-is.' This evaluation is facilitated by procedures and systems within the ISO 14000 standard and any other environment initiatives based on the existing EMS. These initiatives may include environmental reporting and pollution control measures. This initial step is important because there are some commonalities in cleaner production, EMS and ISO 14000 implementations. Assessing the current performance will help to define the level at which cleaner production initiatives can begin.

By identifying weak areas that need improvements along the process system, cleaner production opportunities may be availed. Solutions can then be generated to address the weaknesses. This has a dual benefit of improving operational efficiencies and reducing wastes in the process systems. From the identified alternatives, cleaner production initiatives with the highest impact may be implemented first. Other solutions may be addressed during cleaner production continuous improvements. After implementation, the performance should be measured and compared to the previous performance in terms of amount of wastes, flaring and different types of emissions. This will then lead to cleaner production benchmarking. Benchmarking with organization which has implemented the Best Available Technologies (BATs) comes into the picture as part of the implementation cycle. By benchmarking with those organizations that are implementing cleaner production it is possible to close the cleaner production gaps gradually.

Continuous improvement is also required since cleaner production concepts are implemented in incremental iterations towards zero waste and emission. However, assessment of waste and emissions are usually related to the technology being implemented. Therefore, a best available technology consideration is important for

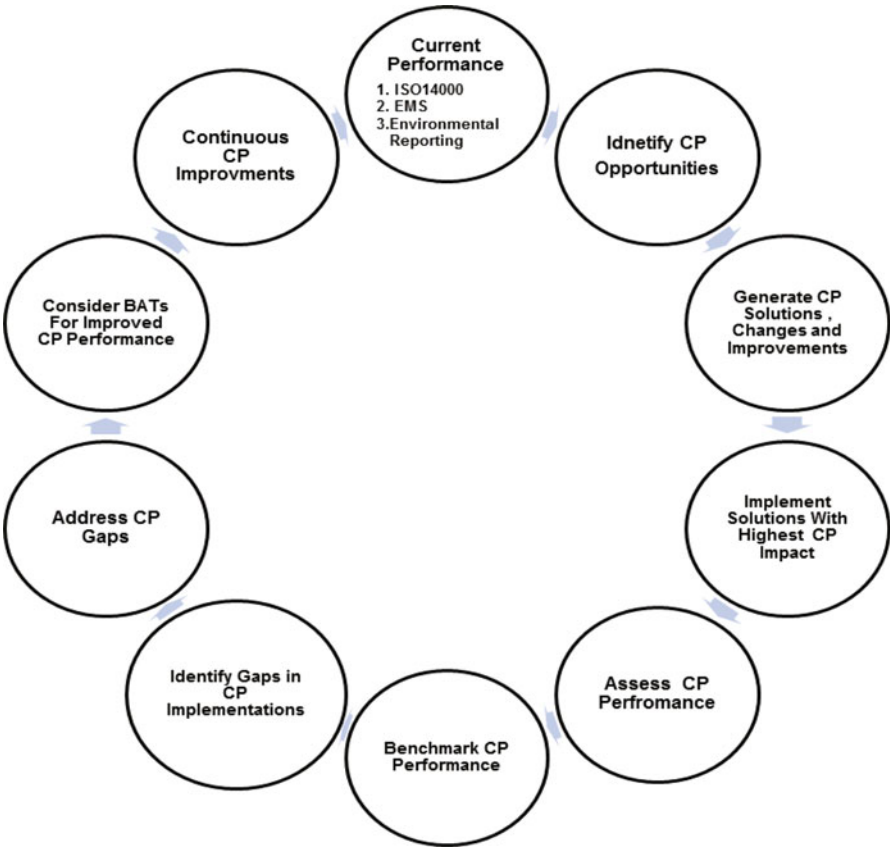

Fig. 29.1 Modified cleaner production model for NGL case study plant

cleaner production initiatives. In addition, best practices and implementation of optimum parameters have a significant contribution to cleaner production implementation. The cleaner production continuous improvement part of the proposed model is important since operating parameters need to be monitored and a cleaner production culture needs to be developed.

29.3.2 Case Study Process System

After analyzing the NGL process system in the case study, the research efforts were focused on: sulphur, carbon dioxide and water removal processes. Process analysis showed that the natural gas feed contains significant quantities of hydrogen sulfide (H_2S) and carbon dioxide (CO_2). Hydrogen sulfide (H_2S) is a dangerous and acidic element in oil and natural gas which must be separated from the hydrocarbons

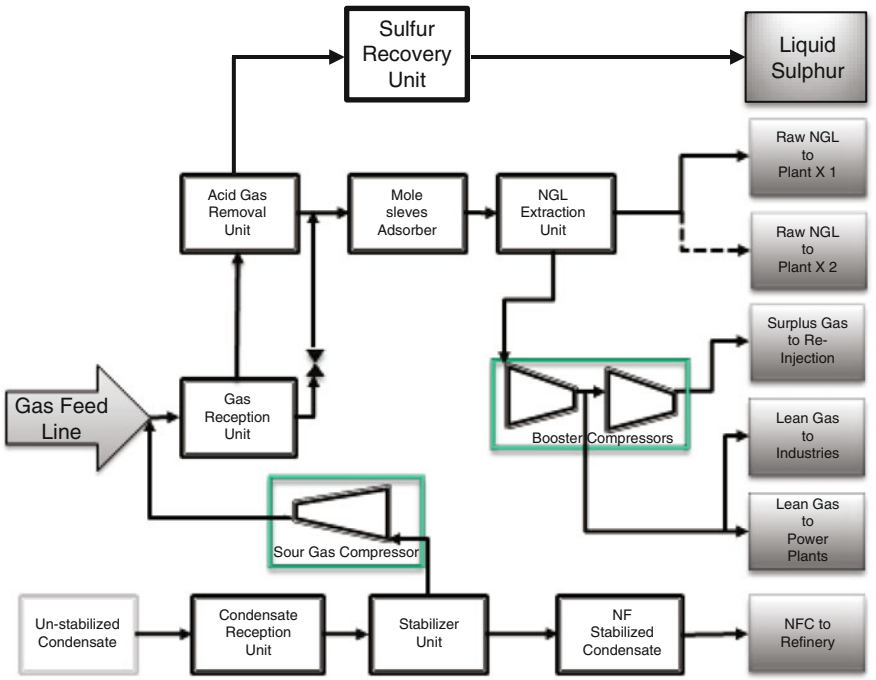

Fig. 29.2 Simplified sketch of the case study plant showing gas feed, processing units and plant outputs

before the natural gas is supplied to the customer. Hydrogen sulfides are usually removed in a mid-stream gas processing facility by iron sponges. Depending on the downstream processing steps and the concentration of the sour gas components, it may be necessary to eliminate H_2S and CO_2 from the natural gas. Amine solutions are usually used to eliminate the hydrogen sulfide—sweetening process. Furthermore, a glycol dehydration unit that uses a liquid desiccant is used to eliminate water from the natural gas and natural gas liquids (NGLs). The main reasons for dehydrating natural gas are: the natural gas can join with liquid or free water to form undesirable solid hydrates; water can pack-in in the pipeline causing slug flow and probable erosion and corrosion; water vapor raises the amount and reduces the heating rate of the gas; dehydrating permits operation of cryogenic and refrigerated absorption plants without freeze-ups and , if not isolated from the produced water, the natural gas is corrosive mainly due to the presents of CO_2 and/or H_2S. Figure 29.2 shows a simplified sketch of the case study plant.

The feed stream is sweetened in the Acid Gas Removal Unit. The sweetened gas is dehydrated in the Mole Sieves Adsorbers. After dehydration, the dried gas is sent to NGL Extraction Unit. In NGL Extraction Unit, lean gas is extracted and distributed to various gas consumers. Surplus gas is injected into a reservoir. Figure 29.2 shows that the NGL case study process system consists of various

operations. In the Acid Gas Removal Unit, sulphur will be absorbed by a solvent. Once the sulphur has been absorbed, the sulphur is taken to the Sulphur Recovery Unit while the raw liquid gas is sent to the moisture removal (glycol) unit in which it is passed through a glycol contactor.

The case study NGL plant shown in Fig. 29.2 consists of a number of unit operations, namely: Acid Gas Removal Unit (AGRU), Sulphur Recovery Unit (SRU), and the Glycol Dehydration Unit (GDU). An input/output model for AGRU revealed that there are two undesirable streams i.e. sour water and acid gas flares. These streams constitute cleaner production issues that need to be addressed in this unit operation. For the GDU, an identified cleaner production issue was to do with acid gas flare. In the SRU, a cleaner production issue was to do with sulphur recovery. In addition, a cleaner production issue related to the GDU is the use of water makeup to compensate for lost water, if any.

To summarize, a common cleaner production issue with the units identified above is flaring and acid gas incineration. In the AGRU, sulphur is absorbed by a solvent and then passed onto the SRU. The amount of sulphur that cannot be recovered is incinerated into the outside surroundings. The incinerated acid gas contains CO_2 and H_2S. This effluent acid gas incineration leads to greenhouse gas emissions, acid rain, and hence contributes to global warming. A materials balance estimate indicated small amounts of loses along the process system. These include: carbon dioxide—0.001 kg/h, Nitrogen—0.001 kg/h, and propane 0.001 kg/h. Besides materials balance and process assessments other cleaner production initiatives come from analysis of raw materials, process changes/designs and redesigns, recycling, reusing, improvements in housekeeping as well parameter optimization that aims at using energy and material resources effectively and efficiently.

In the analysis, data was collected from the case study for a preliminary assessment and analysis of cleaner production opportunities and initiatives. Data collection methods included; interviews with a number of multi-discipline personnel working at the case study location and industrial visits and observations of the operations at the case study.

29.4 Results and Analysis

29.4.1 Raw Materials

The cleaner production concept of raw materials substitution implies effective and efficient use of raw materials (to minimize losses along the process system) as well as using different raw materials that will not generate waste during processing. This concept also further implies re-using materials or using recycled materials. In an NGL process system, this means: (1) changing the source of raw gas feed and substituting the feed with a feed that will produce less waste in the process

system; (2) changing chemicals for other chemical reactions in the process by substituting them with different chemicals that will not generate waste and that are more environmentally friendly and safe to process or use. This ultimately translates to reformulating and redesigning products that will be environment friendly. After the analysis, it was observed that, the concept of raw materials substitution is insignificant in natural gas process operations since it is difficult to find a different source of raw gas within the same geographical location. A possible solution could be using a different field of high purity natural gas. Although it is well known that the degree of purities differs depending on where the natural gas is extracted from, the raw materials substitution concept was found to be of academic relevance.

29.4.2 Process or Technology Change

This concept involves modifications/replacement/retrofitting existing technology/process in a bid to improve environmental performance and attain operational excellence. For the NGL case study, this concept has been applied several times to the various unit operations over a number of years. In particular, the SRU at the case study was changed several times in the life time of the plant in a bid to meet the dynamic changes in acceptable emission levels. However, it was noted that this change was not driven through cleaner production but was a reactive approach that aimed at meeting the specified acceptable level of emissions as stipulated by local environment authorities.

29.4.3 Improvements in Housekeeping

Improvement in housekeeping can be considered as a cleaner production initiative. The logic is that operating, utilization, efficiency, and maintenance decisions are daily practices which must be set correctly. For the case study, operating systems, procedures and standard documents have been developed. The behavior of the process, normal performance and limits for the performance has been specified and are monitored automatically. Maintenance strategies and routine maintenance procedures were in place. However, what was lacking in the NGL plant case study was a cleaner production culture and personnel awareness of cleaner production concepts. Otherwise, most of the issues on housekeeping were observed through ISO 14000 and an active EMS.

One of the major cleaner production issues in the case study was gas flaring. Although flaring was done in accordance with standards set by the local environment authorities, flaring has no part in any cleaner production framework. To control air pollution for flue gas from heaters and flares in the NGL case study, measurements of the amount of various SO_X and NO_X were conducted. Since the

case study was implementing an EMS, the measured results would, from time to time, be compared with the requirements of the ministry of environment. Besides flaring, other less harmful liquid and solid wastes from the case study were discharged into the sea water in different quantities.

29.4.4 Opportunities for Cleaner Production

If an organization is already implementing an EMS, environmental reporting can reveal areas along the natural gas process system where cleaner production assessments can be carried out. For example, the sustainability concept component in an existing environmental management system can be considered as an opportunity for introducing cleaner production assessments since the sustainability concept is concerned with the use of resources and reservation of those resources for future generation. In addition, consumption of resources, i.e. natural gas in the case study, must not exceed the earth carrying capacity (both local and global). For clarification, in a typical process which has inputs and outputs, during the processing there may be some leaks and loses of materials and energy. These leaks and losses are in conflict with sustainability issues. However, cleaner production methods can be implemented to eliminate such losses thereby reducing the consumption of non-renewable resources. This is an example demonstration of the complimentary or supplementary effect of cleaner production in an EMS framework.

Alternatively, looking at the resources which are being used to process the raw materials and the end product will give an insight about other types of losses that cannot be eliminated unless certain changes e.g. process system redesign, are done. The mere presence of by-products e.g. waste water, acid gas flares, fugitive emissions and excess natural gas, means more resources are being consumed than what is needed. This implies that consumption is exceeding the need. The energy losses, the heat loses; the flares which are discharged are all signs of inefficiency in distributing and balancing the natural resources. In the case study, a number of projects have been executed that were purely environment driven through the existing EMS. In addition, a considerable number of in-house studies and process retrofits were made in bid to meet changing and stringent environmental regulations implemented through the existing EMS. Such project constitutes potential cleaner production opportunities.

A prominent environmental action in the case study was the introduction of the SRU that deals with acid gas (rich with H_2S) removal by producing sulphur. Although this was a good move, the implemented sulphur recovery unit was the best available technology in "those days." With the continued changes in stringent and stiffer environmental regulations, the existing sulphur recovery unit had undergone several upgrades and updates. After sometime, the unit could no longer meet new acceptable emission levels. Thus, it was necessary throughout the life of the NGL plant, to scout for more efficient sulphur recovery units in response to new emission levels and directives as published from time to time by the local authorities.

The major limitation in sulphur recovery was due to the fact that the recovered stream consisted of 65 % of CO_2, and 35 % of H_2S. If richer with H_2S, then recovery should theoretically increase. The specific recommendation made for this issue were as follows: (1) to inject the acid gas after liquefaction in deep geological formation into natural gas reservoir, (2) to separate the CO_2 from the feed so that it is rich in H_2S while CO_2 is being injected to the gas reservoir, (3) to separate the CO_2 from the feed before entering the recovery unit in order to enhance the recovery. A viable solution to the CO_2 issue in the case study would be to utilize it as a feed stock for methanol production in another facility.

The process system re-designs for improved environmental performance illustrate one of the major weaknesses of EMSs that lack input from cleaner production concepts. Firstly, process system re-designs or changes for improved environmental performance are only made in response to changes in acceptable emission levels, mostly at national/local level. Therefore, if a company's philosophy is to address environmental issues based on published acceptable emission levels, then the number of process system re-design changes will be proportional to the number of changes in acceptable emission levels and the availability of more advanced technology or BATs. Such process system redesigns and changes are also costly and may be uneconomic when compared to a one-time-change based on cleaner production assessments. The logic is that since cleaner production advocates zero emissions, process redesign for zero emission will meet even the most stringent environmental regulation for the life time of plant operations. Although the initial investment may be high, it may in the long run, offset the budget and hustles associated with a series of plant redesigns, plant updates and plant upgrades in order to meet continuously changing acceptable emission levels.

A second weakness of process changes in response to published acceptable emission levels is that vendors of process system technologies that aim at improving the environmental performance of process plant technologies may tailor their so called BATs in line with expected acceptable emission levels. This will damage technology innovativeness and creativity as well as tie operations to the then BATs. Hence, what is "best" currently may not be "the best" tomorrow. Consequently, greenhouse gas emissions and wastes will continue to damage the natural environment despite any measures taken.

The cited changes in the previous paragraphs are just a few examples of process system re-designs for improved environmental performance. Such and similar projects constitute many opportunities for cleaner production assessments in modern oil and gas processing operations. More potential cleaner production actions can be identified along the natural gas processing line at those points where unit operations such as purification, recycling and waste treatment have been installed based on recommendations from an existing EMS. Another opportunity for cleaner production initiatives in the case study was the process parameter optimization that aims to determine the optimum environmental performance of natural gas processing plants. Of course, this must be synchronized with operational excellence.

Table 29.1 Environmental performance levels of selected components in the case study versus permissible local limits

Effluent components	Emission limits (mg/L)	Case study emissions (EMS) (mg/L)	CP ideals
Chlorine residual (CI_2)	0.05	0.05	Near zero
Mercury (Hg)	0.001	0.001	Near zero
Oil and grease	15	10	Near zero
Total suspended solids (TSS)	10	10	Near zero
Biochemical oxygen demand	10	10	Near zero
Chemical oxygen demand	150	150	Near zero
Free residual chlorine Cl_2	0.1	0.1	Near zero

29.4.5 Environmental Performance of the Case Study Plant

After studying and analyzing data from the case study plant, it was observed that among many, sustainability issues can be operationalized under two aspects, namely; flaring and recovery. In the case study plant a lot of recovery techniques were in place, including: gas recovery systems for Ethane, Propane and Butane; Liquid recovery systems in vessels for storing feed gas and liquid off specification products that are consequences of process upset, and sulphur recovery systems. A number of gas incineration and acid gas flaring were part of the practice.

For assessing potential sustainability improvements in the case study, environmental performance was limited to feed gas utilizations, sulphur recovery and flaring. In the operations, the feed gas was found to be heavier than anticipated thus causing problems associated with feed gas utilization i.e. less gas was being utilized than was extracted. In addition, flaring was necessary due to the buildup of excess gas from process upsets, storage of feed streams and customer limitations. The excess gas was being flared through a controlled flaring procedure. Improvements in the flaring technologies and techniques also resulted in emission reductions. Acid gas flaring was also practiced whenever there was process upset or process malfunctions. Table 29.1 shows that the EMS in the case study plant was active. However, the last column shows the ultimate goal in implementing a cleaner production (CP) framework since CP ambitiously advocates zero emissions.

The relative differences between emissions in the case study (EMS) and those advocated by CP implementation (CP ideals) indicate the potentials for sustainability improvements in the case study. Figure 29.3 shows a relative comparison of flared emissions reductions in an EMS framework and a cleaner production (CP) framework. It can be observed from Fig. 29.3 that the relative reductions under a cleaner production framework are slightly better than those under an EMS framework. The relative differences between emissions reductions under an EMS framework and the reductions under a cleaner production framework indicate the potentials for sustainability improvements in the case study plant.

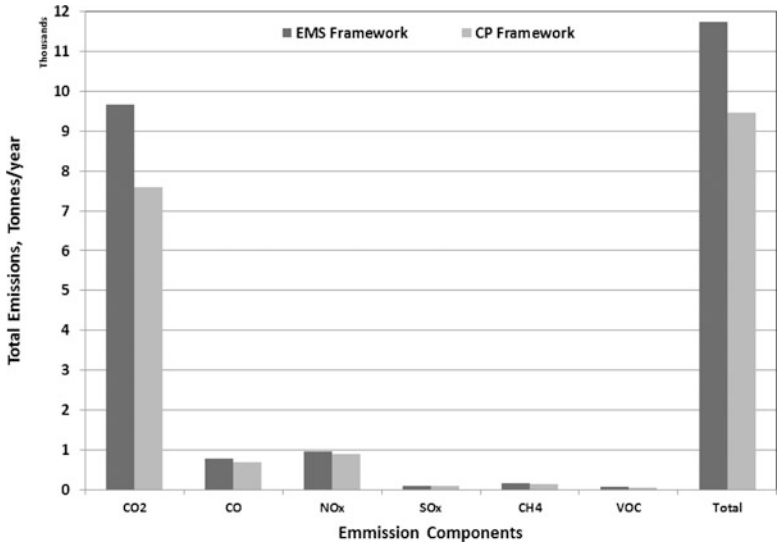

Fig. 29.3 Relative comparison of total emissions reductions under an environmental management system (EMS) and cleaner production (CP) framework

A comparison of sustainability initiatives in an EMS framework and cleaner production framework is shown in Table 29.2. Values for the CP framework were derived from the fact that CP advocates the following: (a) extraction of the correct levels of resources required, (b) full utilization of extracted resources, (c) operations at plant design specifications, (d) implementations of the BATs for best material recoveries and (e) optimum production operations and optimized plant parameter values. Although the values for the CP framework are theoretical, they serve to indicate potential movements of plant design and operations towards sustainability. The iterations in Table 29.2 represent historical changes discussed in this paper which are raised through the in place environmental management system. As can be observed from Table 29.2, for some time the case study plant under performed due to extraction unit problems which were later rectified to allow optimum resource extraction. The case study plant also chose to operate for some time with low carbon recovery equipment. In a cleaner production framework, this low recovery equipment could have been replaced earlier on to avoid losses and consequences. The same can be said for the design production.

As for sulphur recovery, the case study chose to implement a sulphur recovery technology that was capable of meeting the stipulated emission levels at "that time." This was in response to EMS indicators based on local allowable limits. Although the technology for better recovery could have been available, the 85 % recovery equipment sufficed at that time. However, as is always the case with EMS framework, when the emission targets change, the technology has to be upgraded again. On the other hand, the best available technology could have been implemented the first time (if available) in a cleaner production framework since

Table 29.2 Relative comparison of feed gas utilization, hydrocarbon recovery and sulphur recovery under an EMS framework and a CP framework

	EMS framework				Cleaner production (CP) framework			
Plant iterations	NGL extraction throughput	C2 recovery (%)	Production	Sulphur recovery (%)	NGL extraction throughput	C2 recovery (%)	Production	Sulphur recovery (%)
1	780	38	2,800	85	1,023	85	4,500	93
2	1,023	38	3,700	85	1,023	85	4,500	93
3	1,023	85	4,500	85	1,023	85	4,500	93
4	1,023	85	4,500	85	1,023	85	4,500	93
5	1,023	85	4,200	85	1,023	85	4,500	94
6	1,023	85	4,200	85	1,023	85	4,500	94
7	1,023	85	4,300	85	1,023	85	4,500	94
8	1,023	85	4,300	85	1,023	85	4,500	99
9	1,023	85	4,500	85	1,023	85	4,500	99
10	1,023	85	4,500	85	1,023	85	4,500	99
11	1,023	85	4,500	99.5	1,023	85	4,500	99

the cleaner production target (though ideal) is not the acceptable sulphur recover level but 100 % recovery.

29.5 Concluding Remarks

In this study, perspectives on how to operationalize sustainability through a cleaner production methodology have been discussed. Sustainability initiatives were exposed through cleaner production assessments in an existing NGL plant. The concepts of process integration and process parameter optimization were used to cast sustainability issues by focusing on natural gas resource intake, utilization and consumption as well as the flaring practices and recovery processes along the process system. The combination of 'process integration' and 'process optimization' in a cleaner production framework was found to be useful in casting sustainability transmission in a manner that does not result in sub-optimal process operations. Methods, mechanisms, techniques and perspectives for integrating waste minimization and process parameter optimization in order to improve operating efficiencies in natural-gas-liquids (NGL) process systems have been discussed.

A platform for reducing wastes, increasing the efficiency of materials processing as well as optimize the utilization and consumption of natural gas in NGL operations and processing facilities was also outlined. It was observed that the proposed cleaner production method is applicable in NGL plants. However, the extent of applicability depends on the types of the production process, process system technology as well as the raw materials and nature of the product being produced in a given plant. Opportunities for implementing cleaner production were revealed through (a) analyzing materials flows in the process system, (b) conducting materials balance calculations, and (c) focusing on issues raised in an existing EMS. This study acknowledges the valuable input of existing EMSs and BATs into cleaner production assessments, opportunities, initiatives and implementations. It was observed that implementing cleaner production concepts and techniques is complimentary and/or supplementary to an existing EMS depending on how effective the existing EMS is and how committed the organization is to the existing EMS. This relationship bears the marks of commonalities between continuously updated EMSs and cleaner production initiatives both of which are significant inputs into sustainability of process operations.

A modified cleaner production model for typical NGL plants was implemented. Cleaner production alternatives were examined and evaluated qualitatively based on: (a) NGL case study plant feed streams analysis for potential substitutions with 'cleaner' raw materials, and (b) alternative NGL plant process systems design and/or systems re-design for improved plant environmental performance. Due to the nature and limitations in alternative sources of raw natural gas, the cleaner production concept of raw materials substitutions, in particular alternative feed streams for NGL process plants, was found to be less applicable. However,

materials substitution issues based on the green chemistry concept may be feasible and applicable in some unit operations where chemical inputs are required in auxiliary sub-processes. The most technically applicable cleaner production concept was found to be the issue of process systems design and/or redesign for improved environmental performance. To this end, the environmental effects of the natural gas extraction units, acid gas removal unit and the sulphur recovery unit were discussed. Based on this case study, it was concluded that integrating an in-place EMS with cleaner production concepts has a complimentary benefit that significantly contributes towards meeting stringent legal international environmental compliance.

Acknowledgement This research was made possible by a UREP award [UREP 09-078-2-021] from the Qatar National Research Fund (a member of The Qatar Foundation). The statements made herein are solely the responsibility of the author.

Nomenclature

Hg	Mercury
CO_2	Carbon dioxide
H_2S	Hydrogen sulphide
RSH	Mercaptan compounds
COS	Carbonyl sulphide
CO	Carbon monoxide
CH_4	Methane
VOC	Volatile organic compounds
SO_2	Sulphur dioxide
Cl_2	Residual chlorine
SO_x	Sulphur oxides
NO_x	Nitrogen oxides

Acronyms

NGL	Natural gas liquids
BATs	Best available technologies
EMS	Environmental management systems
CP	Cleaner production
AGRU	Acid gas removal unit
SRU	Sulphur recovery unit
GDU	Glycol dehydration unit

References

1. Klemes J, Friedler F, Bulatov I, Varbanov P (2011) Sustainability in the process industry, integration and optimization. McGraw Hill, New York
2. Dennis P, Shobirin M (2009) Reducing environmental risks to as low as reasonably practicable in South East Asia, Doi: 10.2118/122724-MS
3. Linnhoff B, Vredeveld DR (1984) Pinch technology has come of age. Chem Eng Progr 80 (7):33–40
4. Tan R, Foo DCY (2007) Pinch analysis approach to carbon-constrained energy sector planning. Energy 32(8):1422–1429
5. Gundersen T (2000) A process integration primer-implementing agreement on process integration Trondheim. International Energy Agency, SINTEF Energy Research, Norway
6. Rivera A, Gonzalez J, Carrillo R, Martinez J (2009) Operational change as a profitable cleaner production tool for a brewery. J Cleaner Prod 17:137–142
7. Berkel RV (2000) Overview of the cleaner production concept and relation with other environmental management strategies, cleaner production for process industries, pp 1–14, www.p2pays.org/ref/13/12031.pdf
8. Kjaerheim G (2005) Cleaner production and sustainability. J Cleaner Prod 13:329–339
9. Himmelblau M (1967) Basic principles and calculations in chemical engineering, 2nd edn. Prentice-Hall, Englewood Cliffs, NJ
10. Morris, A. E., Geiger, G. and Fine, H. A. (2011) Fundamentals of Material Balances with Applications to Non-Reacting Systems, in Handbook on Material and Energy Balance Calculations in Material Processing, Third Edition, John Wiley & Sons, Inc., Hoboken, NJ, USA
11. Musharavati F (2012) Cleaner Production Opportunities for Natural-Gas-Liquids Operations That Implement BATs Within an Environmental Management Framework, In Abdelwahab Aroussi and Farid Benyahia (eds) Proceedings of the 3rd Gas Processing Symposium, Volume 3 in Advances in Gas Processing Pages 50–57

Chapter 30
Energy Savings Through Applications of Lean Manufacturing Principles

Roba Salim, Buthaina Ali, and Farayi Musharavati

Abstract This study explores and investigates the applicability of lean manufacturing principles and concepts in Dual Purpose Water and Electricity (DPWE) production plants. An existing DPWE production plant in the State of Qatar was used as a case study. The aim of the investigation was to identify opportunities for energy savings by analyzing plant energy use through Lean Value Stream Mapping. To this end, lean principles were employed to investigate energy wastes in the power and water production chains. 'Lean deadly wastes' were used to identify potential 'wastes' along the DPWE production system. Tools and techniques for analyzing, evaluating, and assessing energy use in the DPWE production plant were developed. Areas of energy wastes along the process system were identified and lean concepts were applied to reveal quick, non-capital energy saving opportunities. Energy assessments were carried out through the value stream mapping method that helped in the identification and detection of energy and operating efficiency improvement opportunities. The multi-stage flash distillation process was identified as the section that consumed relatively the largest energy. Other energy efficiency opportunities were revealed by virtually reconfiguring the DPWE production plant in the framework of lean principles and concepts. Results of the case study shows that a number of energy saving opportunities and energy efficiency initiatives exist in the various sections of the DPWE production plant. Therefore, lean principles are powerful concepts that can help in identifying energy saving opportunities and energy efficiency initiatives in DPWE production plants. Such opportunities and initiatives can be implemented to improve operating efficiencies and reduce production costs with the added advantage of improved environmental performance.

Keywords Lean principles • Energy use • Energy saving • Energy efficiency • Value stream mapping • Dual purpose water and electricity (DPWE) production plants

R. Salim • B. Ali • F. Musharavati (✉)
Department of Mechanical and Industrial Engineering, Qatar University, Box 2713, Doha, Qatar
e-mail: roba.salem@qu.edu.qa; buthali@hotmail.com; farayi@qu.edu.qa

I. Dincer et al. (eds.), *Progress in Sustainable Energy Technologies Vol II: Creating Sustainable Development*, DOI 10.1007/978-3-319-07977-6_30

30.1 Introduction

Lean manufacturing is a competitive strategy that has been adopted by many successful organizations worldwide [1–3]. Companies involved in lean manufacturing do so to improve overall company performance in terms of; productivity, profitability, efficiency and reducing operations and maintenance costs. In this study, lean principles, concepts and techniques are used to reveal energy saving opportunities in a dual purpose water and electricity (DPWE) production plant. A case study of an existing DPWE production plant, herein after referred to as the generating company, was used to illustrate the merits and demerits of using lean principles for identifying energy wastes (and hence energy savings) along the DPWE production system. The DPWE production system consists of two chains; (a) the power production chain and (b) the water production chain. This study focused on operational performance improvements related to elimination of wastes (energy and materials) along these two process chains through application of lean principles and concepts. The logic behind the undertaking was that operational performance improvements may lead to significant reductions in operating and production costs thereby reducing the unit cost of freshwater and electricity.

Lean thinking involves defining value for the customer, focusing on adding value, driving out wastes, reducing cycle times and ensuring smooth flow of work at the pull of the customer [4]. While this comprehensive perspective is usually desired in all implementations of lean, the nature of the plant under study may not accommodate implementations of the whole spectrum of lean. In such a case, a study usually focuses on those parts of the lean framework that are applicable in a given situation. This is usually true for new and unfamiliar applications of lean in environments that exhibit operational and design variations in comparison to the parent domain from which lean principles were derived; i.e. discrete parts manufacturing.

A review of research on the applications of lean principles shows that although lean principles were initially introduced in manufacturing operations, lean principles have been successfully implemented in other industrial sectors such as banking, insurance, finance, sales, marketing, customer service, product development, and healthcare systems [5, 6]. However, very little research is available in the public literature on lean implementations in power generating and/or water desalination plants. This study focuses on the perspectives of implementing lean in DPWE production plants.

As has been the case in other earlier ventures on lean implementations in new and unfamiliar areas, the actual system dynamics of lean implementations in DPWE production plants are not known. Neither are these dynamics well understood before hand. This gap presents a challenge that will be addressed in this investigation on the application and implementation of lean principles in DPWE production plants. Unlike the commonly used thermodynamic efficiency approach, this study focuses on improving the efficiency of installed capacity. The underlying argument in this investigation is that wasteful processes and resources increase

production costs while maximization of resource usage improves the operating efficiencies of an organization. Consequently, the analysis in this paper focuses more on dealing with minimization of wastes (i.e. materials and energy) in processes and systems and maximization of resource capabilities through improvements in the operations of a DPWE production plant.

Key energy savings, operating efficiency improvements and optimization initiatives of installed capacity in the generating company were identified through applications of lean principles and techniques. Since improving the energy efficiency of installations eliminates energy wastes, the analysis for energy efficiency of installed capacity naturally fits into the lean manufacturing philosophy [7]. Therefore, lean principles were employed to improve the overall operating efficiency of installed capacity by eliminating unnecessary actions and activities in the power and water production chains. Moreover, by reconfiguring the power and water plant processes in the framework of lean concepts and principles, opportunities arise for making additional changes to improve energy use efficiency at lower marginal costs.

Energy conservation measures provide opportunities for saving energy. Energy conservation measures discussed in this paper include; maintenance, operation and process improvement measures. Most of the process improvement measures are analyzed through the lean framework. The main applications for conservation opportunities that will be discussed in this study include: boilers, waste heat recovery and cogeneration. Cogeneration in this case implies the power production chain and water production chain.

The goal of the study is to identify possible operational and design modifications for energy savings opportunities and optimization initiatives in the generating company. In order to achieve the mentioned goal, the following specific objectives will be addressed:

- To identify the link between energy efficiency and lean principles in a bid to leverage costs and energy efficiency benefits.
- To critically examine and assess operational activities in the generating company through a lean framework.
- To carryout energy use assessments in order to reveal areas of ‘energy wastes’ (or energy savings) along the process system through application of the value stream mapping method.

The remainder of the study is organized as follows: initially, a background on lean concepts is provided followed by a description of the various methods used in this paper. The results of the study are then presented and discussed and finally concluding remarks are given.

30.2 Background

30.2.1 Lean Principles

The details and description of the classical lean manufacturing philosophy and tools are well documented by some of the early researchers of the lean system [8, 9]. A recent review on lean manufacturing can be found in [10]. Analytical approaches to study lean manufacturing systems include the work in [11] in which a group of qualitative and quantitative rules to implement lean manufacturing were presented. The approach in [11] focused more on how to change the mass production operation of industries to a lean operation. An approach based on queuing theory was proposed in [12]. In [12] the researchers investigated the necessary and sufficient conditions for the optimality of a single control point as well as multiple control points in a multi-stage system. Axiomatic design principles based on lean concepts were applied in [13] to design lean manufacturing systems with a focus on line segmentation. In [13] the authors showed that integrating axiomatic design rules with lean management improved the design and performance of manufacturing systems. In spite of large volumes of lean and lean implementations, some of which are cited above, fewer works have been presented to provide guidelines for implementing lean in DPWE production plants. This study contributes to reducing this gap by proposing methods for lean implementation in DPWE production plants.

A number of lean methodologies have been discussed in the public literature. In the present study, a lean system is perceived to be a system that focuses on creating value and removing waste [14]. The fundamental logic is that all work that people perform is the sum of value-adding activities and waste activities. A common trait in the lean philosophy is to eliminate non-value adding actions or at least reduce them to a minimum.

Historically, the term “lean” has been used to describe an approach that was observed as the Toyota Motor Company endeavored to eliminate process waste and to improve operational efficiency. To this end, five basic lean principles have been identified in the public literature [15]: namely;

1. *Specify value*—value can only be defined by the ultimate customer. It is specified in terms of satisfying customers’ needs by providing products and/or services with desired capabilities at a competitive price and lead time.
2. *Identify the value stream*—this is a set of all actions required to bring a product through problem-solving, information management, and physical transformation tasks. Here, value refers to the nature of activity being carried out. The value stream is the set of actions that transform a product or service.
3. *Make the value flow*—by reducing cycle times and batch sizes to the absolute minimum, ensuring each operation is visible, defined, and has a visible status to eliminate possible stoppages in the production process.

4. *Let the customer pull*—processes or products are to be produced and delivered on-demand from the customers.
5. *Pursue perfection*—even if the other four lean principles are followed, if the mindset for pursuing perfection has not been developed across the enterprise, any improvement will only deliver a one-off benefit.

The case study in which lean was implemented is described in the following sub-section.

30.2.2 Case Study

The case study plant is a dual purpose water and electricity production plant. Electricity is generated by using natural gas as the primary fuel. Therefore, the power production chain starts with natural gas feed which is burnt to release chemical energy which in turn is converted into mechanical energy that turns a turbine which is connected to an electricity generator. The generated electricity is then send to a distribution company (separate from the generating company) that is responsible for distributing electricity to consumers in the State of Qatar. Simultaneously, water is produced through multi-stage flash desalination of sea water. Exhaust gases from the gas turbines are used in the heat recovery boilers to produce steam which is passed through a heat recovery section and then enters the heat rejection section were heat is absorbed by sea water, through the cross flow principle. The distillate is then send to the water treatment plant before it is pumped to the distribution company. Figure 30.1 shows a simplified process flow description of the generating plant.

The case study plant (the generating company) owns and operates electricity generation and water desalination stations. The relationship between the generating company and the distribution company is shown in the Fig. 30.2.

In line with the five lean principles mentioned earlier on, the transmission and distribution company is the customer of the generating company while consumers of both water and electricity are customers of the transmission and distribution company. As such, value with respect to the transmission and distribution company simply means providing water and electricity capacities that are commensurate with the general needs of water and electricity consumers in the State of Qatar. Although the generating company is not in direct contact with the ultimate customer, the generating company has an obligation to keep pace with Qatar's ever increasing requirements for electricity and water. Therefore, achieving operational excellence through improving operating and energy use efficiencies in power and water production chains can effectively increase the capabilities of the generating company to provide adequate water and electricity at relatively favorable rates.

The generating company uses natural gas as primary energy for driving the DPWE production plant. Therefore, the value stream for the generating company consists of the nature of all activities carried out in the water and electricity

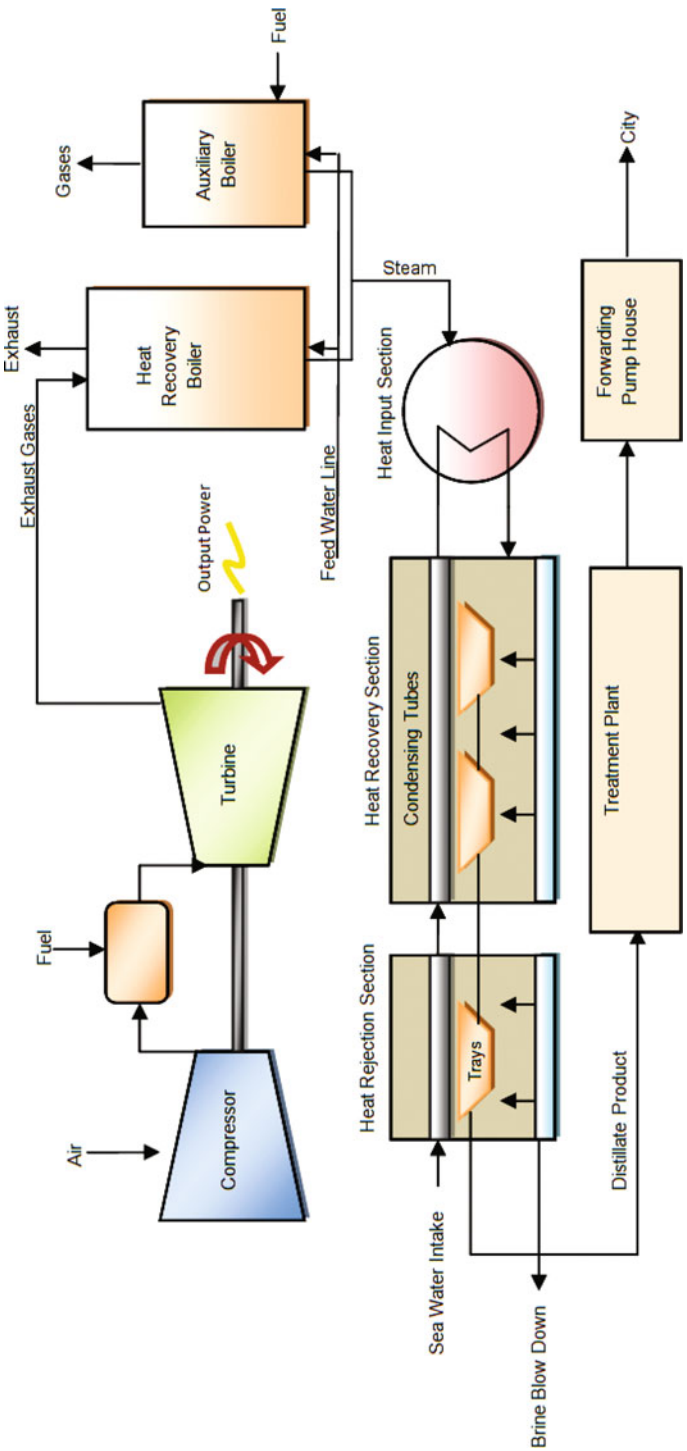

Fig. 30.1 Simplified schematic of the dual purpose water and electricity production plant

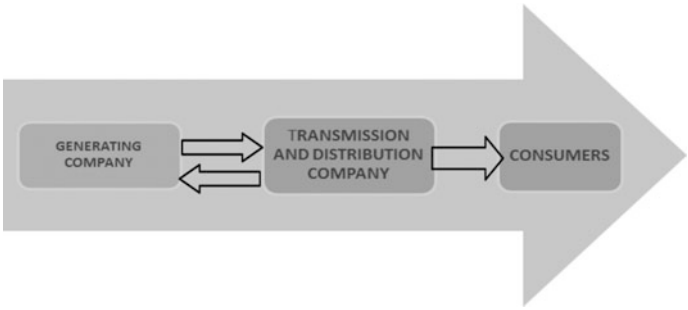

Fig. 30.2 Relationships between the generating company, the transmission and distribution company and the consumers of water and electricity

production chains. This set of actions start from natural gas feed, the primary fuel, up to the production of the water and electricity capacities as required by the transmission and distribution company. The natural gas, used as the primary fuel, is a non-renewable resource. Therefore, improving operating efficiencies is important since it translate to reductions in natural gas consumption, which in turn is a fundamental achievement in the journey towards sustainability.

Other lean principles highlighted in the five basic lean principles mentioned earlier on are; value flow, customer pull and the pursuance of perfection. Smooth flow of value in the generating company has been assured by effective maintenance strategies based on accumulated experience with plant operations. In order to eliminate the possibility of stoppages, duplicate lines and standby capacity were included in the design of the generating company facilities. On the other hand, customer pull (i.e. on demand delivery) is catered for by observing and maintaining a specific level of sea water reservoir at the generating company. The basic idea is that all things being equal, observing and maintaining a specific sea water reservoir level of a dedicated reservoir of sea water, the capacities for both electricity and water are satisfied simultaneously. While the issue of pursuing perfection is an important principle of lean, it can however, be satisfied by developing a lean culture in the generating company, which ensures the perpetual undertaking of continuous improvement actions in the operations of the DPWE production plant.

30.3 Plant Energy Assessment Methods

Based on the discussions in the previous sections, the analysis in this study focuses more on the first two lean principles; i.e. specifying value and identifying the value stream. To this end, the value stream mapping tool was used in the preliminary energy assessments while energy audits and other energy use efficiency techniques were used to provide more focused and more detailed energy assessments in areas of concern as revealed by the value stream mapping. The general energy assessment

methodology applied to the case study was as follows: (a) case study plant energy assessments were carried out by collecting and analyzing available energy utilities related process data in order to establish energy requirements of the DPWE production plant, and (b) component-based energy efficiency optimization opportunities were identified from an operating cost point of view. The various energy assessment methods used and techniques implemented are outlined in the following sub-sections.

30.3.1 Energy Audit

Energy audit refers to energy use studies of a plant through either a quick walk-through of a facility to identify major problem areas or a comprehensive analysis of energy use evaluation and assessments [16]. Two phases of energy audit methods were used in the case study. These included; (1) a preliminary audit phase, and (2) a general audit phase. The preliminary audit was implemented through lean's value stream mapping tool. This involved minimal interviews with site operating personnel, a brief review of facility utility bills and other operating data, and a structured virtual "walk-through" of the case study facility. The virtual walk-through of the plant was facilitated by studying process simulations of the case study. The data collected through these activities were then used as inputs to the values stream mapping. The general audit phase involved collecting more detailed information about facility operation and performing a more detailed evaluation of energy conservation measures. The following steps were used in the general energy audit phase:

- Interviews with key facility personnel.
- More detailed virtual "tours" of the facility by studying the process system simulations.
- Case study document reviews.
- Facility inspection with a focus on the major energy consuming processes and energy equipment.
- Staff interviews (as a follow up to preliminary audit phase investigations).
- Utility analysis, which involved a detailed review of energy use and energy sources.
- Identification and evaluation of feasible energy saving areas and energy conservation measures.

Although the energy audit method is usually given first preference in energy use analysis and assessments, auditing energy may not be effective enough since energy audit is the study of energy end uses and performance of a facility as a whole that one may not really know which process or process step uses the most energy [7]. Therefore, conventional energy audit methods were supplemented by appropriate lean techniques. In the actual implementation, activities on lean methodology and the energy audit method were done simultaneously whenever possible.

A unique approach used in this work was to use the lean values stream mapping method as the preliminary 'energy audit' phase while conventional energy audits were used in the general energy audit sessions. In this way, the results of lean value stream mapping were used to identify those areas in the process system were more detailed energy assessments were required. Such areas became the focal point of the general energy audit phase.

The preliminary energy audit phase indicated that relatively more loses were taking place on the following equipment; heat recovery boilers, auxiliary boilers, turbine sections, compressor sections, and the distillation sections of the process system. Typical loses on boiler sections included: dry gas loses, non-burned combustibles, losses due to moisture formed by hydrogen combustion, loses due to moisture in the fuel and loses due to moisture in the air. Typical loses on the turbine section included: heat rejected with cycle, heat rejected due to turbine cylinder problems and terminal parameters, losses due to pressure and temperature differences in feed, losses due to pressure and temperature changes in condensing system. Typical losses in the compressor sections included: exhaust gas losses, engine cooling losses, mechanical friction losses, heat leaks and loses due to pressure drops.

30.3.2 Lean Methods

Lean methodology is the concept of streamlining processes and eliminating waste in order to keep costs low, while maintaining high quality products and or services [17]. The lean methodology was used to identify optimization initiatives for increasing operating efficiency and reducing production costs. The underlying theme in applying the lean methodology was to develop and analyze lean aspects related to the case study and provide recommendations that if put in place would save time and money. Thus, by reducing waste (materials and energy), the case study plant will be able to reduce their overhead expenses and by saving time the case study plant would produce more in the same (or less) amount of time. Such changes would lead to general improvements in operating efficiencies and, therefore, will contribute to achieving operational excellence. Lean thinking uses a wide variety of powerful tools for standardization and simplification [18]. In order to critically examine and assess operational activities through a lean framework, the following lean tools were used: (a) lean's deadly wastes, and (b) the value stream mapping tool.

30.3.2.1 Energy Wastes in Relation to Lean's Deadly Wastes

The core philosophy in lean applications is to continuously improve a process by removing non-value added steps or 'waste.' In the lean framework, waste has been defined as all elements of production that only increase cost without adding value

that customers are willing to purchase [14]. In most implementation, all lean initiatives begin by identifying, along the process chain, what creates value for the customer. In general, any operation or process consist of value adding and non-value adding activities. In the lean framework, all non-value adding activities are considered as waste. Since not all non-value adding activities can be eliminated in a given process lean operates with two types of waste, namely; Type 1 and Type 2. Type 1 wastes are activities that do not add value for the customer but that currently are necessary to maintain operations, for example by assisting management to control and run the business. As such, Type 1 waste is easy to add in a process but difficult to remove since it is fundamental to the realization of transformation activities along the process system. As a guideline, it has been suggested that the amount of necessary but non-value adding activities should be kept at a minimum and is normally reduced by simplifying the process. Type 2 waste creates no value for any stakeholder and should be eliminated completely. Lean has identified seven deadly wastes in an organization. These can be summarized as waste of; overproduction, waiting, motion, inventory, transportation, defects and extra processing. Environmental and energy wastes are not explicitly included in the seven deadly wastes of lean discussed above. This is because energy and environmental wastes are embedded in, or related to, the seven deadly wastes. For the case study plant, some of the seven deadly wastes are not directly relevant. Therefore, in the analysis only relevant wastes were included.

30.3.2.2 Value Stream Mapping

Value stream mapping is a lean process-mapping method for understanding the sequence of activities used to produce a product in order to identify sources of non-value added time or materials; identify opportunities to increase efficiency; and develop a plan for implementing improvements [19]. Value stream maps serve as a critical tool during the review process and can reveal substantial opportunities to reduce costs, improve production flow, save time, reduce inventory, and has the added advantage of improving the environmental performance of an organization [20]. A current state value stream map was developed for the case study plant. More detailed energy uses assessments were then based on the results of the value stream map.

30.3.2.3 Examining Energy Use Through Value Stream Mapping

In general, conventional value stream maps can overlook environmental wastes such as energy, water, or raw materials used in excess of what is needed to meet the needs. To avoid this, an effective way that was used to understand energy use in the case study was to integrate energy analysis into the lean value stream mapping process. This approach was found suitable for identifying areas where the largest sources of waste exist in the value stream and hence prioritize process-improvement efforts.

The approach taken was to integrate a materials line in the value stream mapping in addition to the time line. In this way, the integrated materials line would focus on mapping the resources consumed and waste generated in the production of power and water. Incorporating energy use data directly into the current state value stream mapping made it easier to spot key energy saving opportunities in the context of other improvement opportunities. Since value stream mapping takes a systems approach i.e. views the plant processes as a system, conventional energy use assessments and energy audits were used to evaluate and assess energy wastes in those actual areas that were identified through value stream mapping as key energy saving opportunities. In addition, the energy audit was used as a crucial step in assessing and improving energy use efficiency on the process flow by identifying ways of providing more output with less energy input. In order to analyze energy use in the case study plant through value stream mapping, the following activities were carried out:

1. Understanding of the combined process of generating water and electricity at the plant. Figure 30.1 shows a simplified illustration of the process plant with inputs and outputs.
2. Data about energy use for individual process steps along the process system were collected.
3. Data was collected for the materials line (a variation of a time line used in conventional value stream mapping).
4. Collected data was then mapped using a lean value stream mapping tool.
5. The largest sources of waste were identified.

The results of the analyses based on the methods described in this section are presented in the following section.

30.4 Results and Discussions

Lean manufacturing principles were applied in the case study plant to assess energy use. Strategies and techniques for understanding how energy in the plant should be used will be discussed in this section. Opportunities for reducing energy wastes and costs were identified and are discussed in the following sub-sections.

30.4.1 Lean Deadly Wastes in the Case Study

Lean deadly wastes identified in the case study included:

1. Overproduction: i.e. producing more than needed. For the case study plant, this was interpreted to mean producing more electricity and water than is required by the distribution company. This also lead to the waste of inventory.

2. Waiting: i.e. idle operator or machine time. For the case study, this may mean just-in-case standby capacities, duplicate water and power production lines and energy equipment.
3. Motion: i.e. movement of people or machine that does not add value. This includes start and stop characteristics of production equipment during maintenance, shut downs or switching over to standby capacity of duplicate production line.
4. Inventory: i.e. any supply in excess of required quantities (demand for water or electricity). For the water production chain, it was noticed that the generating company has an inventory reservoir which in lean thinking can be considered as a waste.
5. Transportation: i.e. any material movement that does not directly support value added operations. In a DPWE production plant, a number of movements that do not add value to the power and water chains can be observed. For the water production chain these include: flow of sea water from sea up to the sea water intake at the plant, flow of brine discharge, flow of distillate product from distillers to the treatment plant, flow of steam from the boilers to the heat input section as well as pumping of desalinated water to the distribution. Although these can be considered as wastes of motion in the lean framework, more specifically they are Type 1 wastes i.e. activities that are necessary to maintain and complete the transformation process. For the power production chain, Type 1 wastes of motion include: flow of compressed air into the combustion chamber, transportation of natural gas from its source to the combustion chamber, movement of exhaust gases from turbines to heat recovery boilers, and transmission of generated power to the distribution company.
6. Defects: i.e. making defective parts/product. Since there are mechanisms along the DPWE production plant to ensure the right quality of water and electricity, this type of waste is relatively less applicable in the DPWE production plant. However, efforts made in say enforcing water treatment prior to sending to the distribution company can also be classified under this type of waste. In the case study plant no such efforts were encountered.
7. Extra processing: i.e. any process that does not add value to the product. This type of waste is also less applicable in the power and water production chains of DPWE production plants.

The listing presented above reveal a number of aspects related to the applicability of lean principles to DPWE production plants. For example the analysis shows that water is produced in excess. According to lean deadly wastes, this is a waste of overproduction. In addition, the reserve capacity in the case study was found to be too large than may be required (unless of course if the size of the reservoir was meant to provide cushions in the whole life stages of the plant). This reserve capacity is actually viewed as waste of inventory in the lean framework. However, these comments are made within the scope of the case study which in this case supplies only a fraction of the water required in the State of Qatar. In addition, the demand was based on estimates of how much of the population is actually

supplied by water produced from the case study plant. The reserve capacity may also have been designed to support other water supply stations when there is maintenance or a breakdown. Therefore, an analysis that considers all plants that supply water and electricity would provide more information for decision making and developing an optimal production policy.

It was also noted that the case study plant operates with a duplicate power and water production plant. In addition there is a lot of redundancy in the form of standby equipment. In a lean framework, the duplicate line and the redundancy are classified as wastes. However, reliability concepts tell us that critical plants such as those that provide water and electricity should always have some built-in redundancy. However, this redundancy must be optimized at the design stage.

30.4.2 Value Stream Map

Figure 30.3 shows the result of the energy map obtained through the lean value stream mapping method. Figure 30.3 shows that there are differences in the values of energy used and energy needed along the process system of the case study plant. Figure 30.4 summarizes the differences between the total energy actually used and the total energy needed for the various sections along the process system. Figure 30.4 shows that there is a potential of 10 % energy savings by providing and using the exact amount of energy required by the various energy equipment considered in the value stream mapping.

Figure 30.5 shows the relative energy consumption of the various energy equipment. Figure 30.6 shows the potential savings (differences in the used and needed values) from each sections of the case study plant. In the lean framework, this situation is classified as a waste i.e. supplying more energy than is needed. Therefore, the relative differences in the various amounts of energy used and energy supplied can be used as a starting point for a detailed thermodynamic or thermo-economic analysis that targets at find optimal solutions in each of these energy components.

Simple operational suggestions for solving the identified non-capital energy problems include:

- Provide the correct amount of energy needed by each energy equipment or unit process.
- Review maintenance schedules to upkeep equipment so as to reduce inefficiencies that often result in over estimations of energy required.
- Review energy equipment and benchmark with the best available technology. If necessary replace or retrofit and integrate best available technologies.

It can also be observed that a large amount of energy is wasted in the distillation process, particularly in the distillers. This gives an indication that this process step is the most inefficient step and hence it requires a more comprehensive thermodynamic analysis.

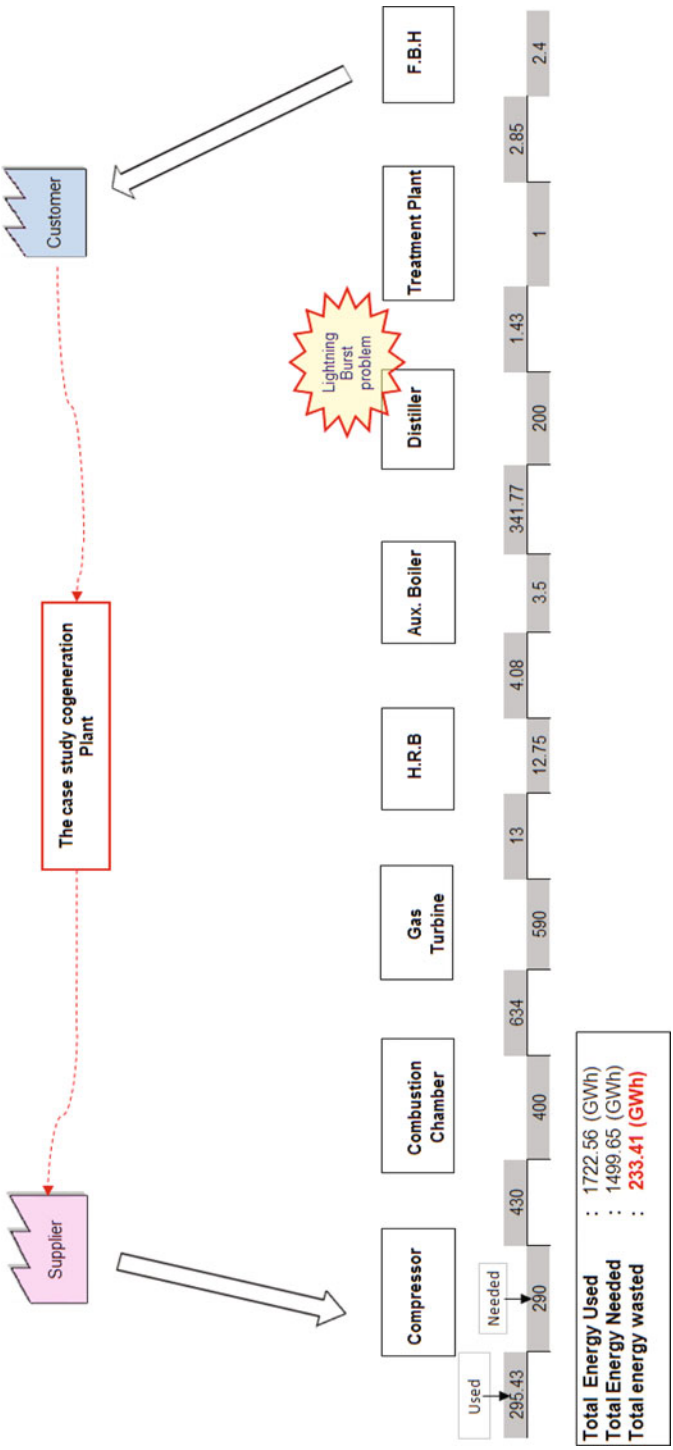

Fig. 30.3 Value stream map for the case study process system

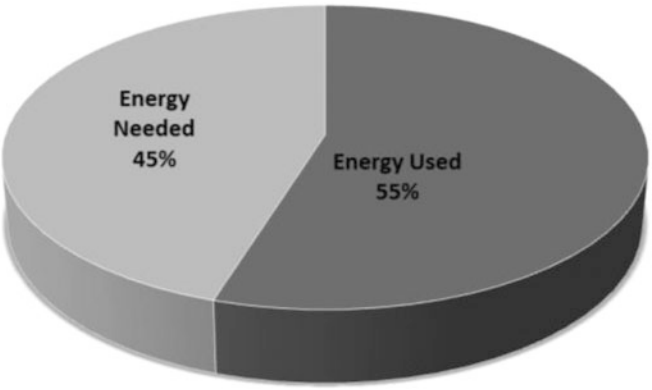

Fig. 30.4 Summary of total energy actually used and total energy needed

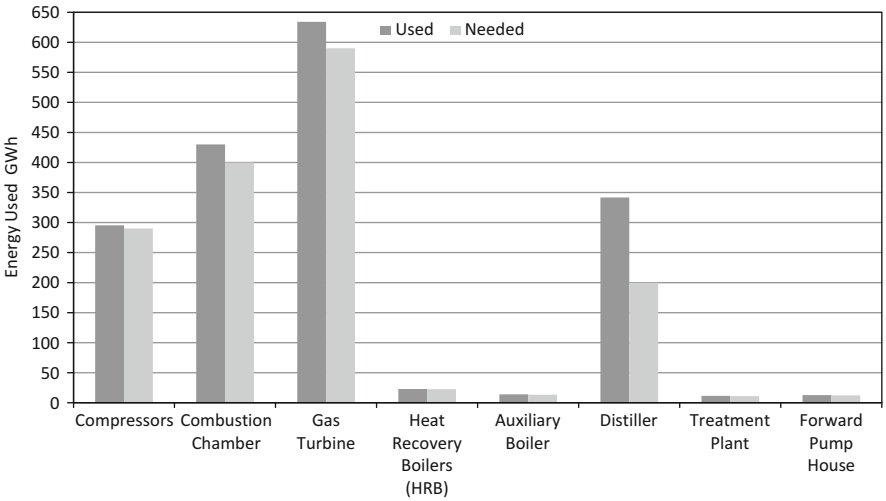

Fig. 30.5 Comparison of energy used and energy needed for the various equipment in the case study plant

The significant result from lean tool analysis is that the highest "energy waste" is in the distillers followed by the gas turbine, combustion chamber, and the compressors. Besides the distillers, the greater percentage of wasted energy in the gas turbine, compressors and combustion chamber (i.e. power chain) are most probably due to limitations in the installed technology. The relatively large percentage energy saving in the distillation process was somewhat expected since literature review had indicated that the desalination process is energy intensive. This means that a number of opportunities for energy savings and improvements in operational efficiencies exist in the distillation process. Because the desalination process is

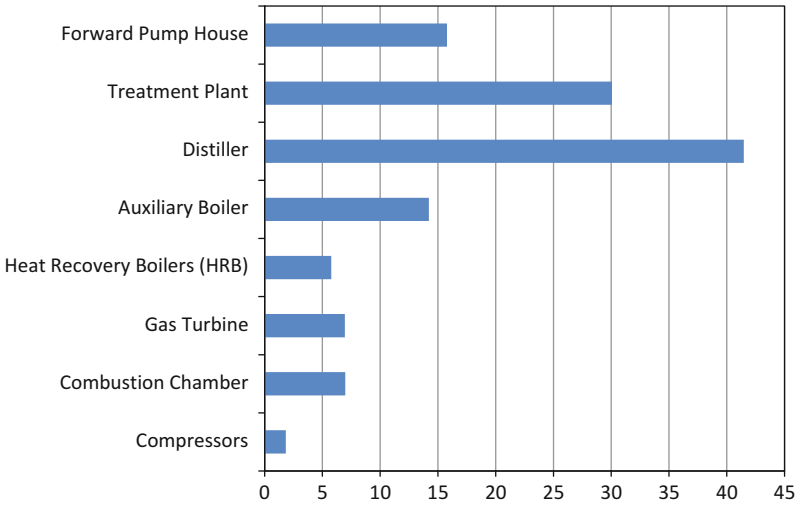

Fig. 30.6 Potential percentage energy savings for the various sections of the plant

energy intensive, care must be taken to reduce energy consumption which will in turn reduce production costs thereby lowering the unit cost of fresh water.

30.4.3 Multi-stage Flash Distillation Energy Consumption

A relative comparison of the thermal and electrical energy of the MSF desalination process in the case study with that of its nearest rival (MSF with a back pressure steam turbine to drive the brine recirculation pump) is shown in Fig. 30.7. Figure 30.7 shows that a significant amount of energy can be saved by replacing the MSF in the case study with an MSF that implements a back pressure turbine. An alternative way of reducing the energy consumption of the MSF is to review the design and operating parameters of distillers. The MSF process requires both thermal and mechanical energy. The former is required for heating recycled brine in the heat input section while the latter is required for driving pumps. Energy consumption of the MSF distillers can be reduced by increasing the performance ratio. The performance ratio is usually defined based on the top brine temperature (TBT). Thus, an Increase in TBT increases the flash range which will simultaneously increase distillate production and thermal performance.

The MSF plant in the case study operates with a TBT range of 90–112 °C [22]. This range can be increased by acid dosing which removes bicarbonate from seawater feed and allows evaporators to operate at an increased top temperature of 120 °C. Notable approaches for pre-treatment of seawater include using nano-filtration membrane which opens the possibility of increasing the TBT above 120 °C. This achievement may significantly reduce energy consumption.

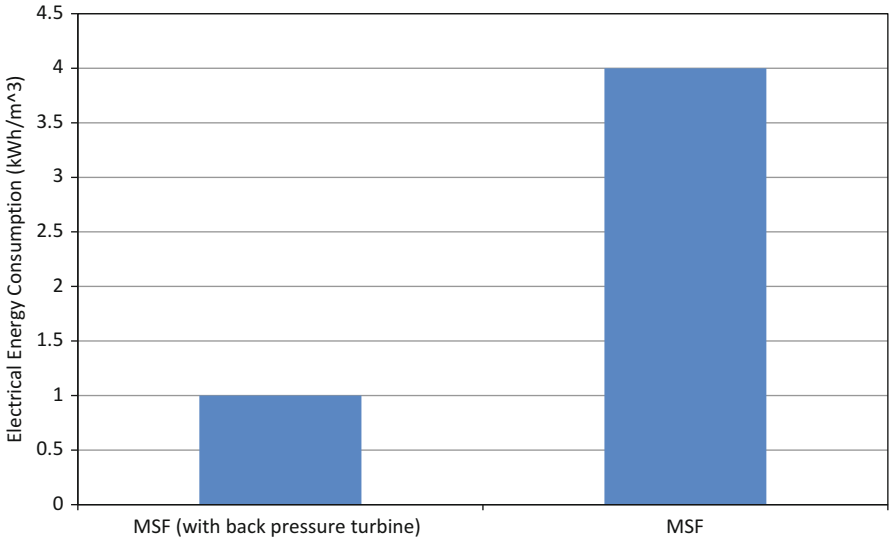

Fig. 30.7 Comparison of relative consumption of electrical energy by case study MSF and MSF in which the drive of the brine recirculation pump is a back-pressure steam turbine [21]

Retrofit options include increasing the number of stages thereby increasing the performance ratio. Other operational issues include frequently acid cleaning to ensure clean heat transfer surfaces and to restore the design performance ratio. Thermo-economic analysis of the hybrid cycles have revealed that the production cost of water could be reduced by as much as 30 % [23].

30.5 Conclusion

Dual purpose water and electricity (DPWE) production plants are a cost effective way of producing power and water in arid and semi-arid regions of the world. Over the years, these plants have become the conventional way of providing electricity and water in the gulf region. In this study, a case study of an existing DPWE production plant was used to illustrate how optimization initiatives for reducing energy consumptions and for conserving energy can be identified through applications of lean manufacturing principles and concepts. The discussions presented in this study have shown how a combination of lean principles and energy efficiency techniques can be used to leverage operating efficiencies and improve energy use efficiencies in DPWE production plants. Investigations based on lean manufacturing principles (value stream mapping) revealed that the highest energy waste in the case study plant was found in the distillation process. Therefore, improvements in the operating characteristics and operating modes of the desalination unit can result in significant energy savings. This may translate to reductions in the production

costs of water and electricity. The results also show that a number of optimization initiatives existed in the case study plant. For example differences in the energy actually used and energy needed can be reduced through non-capital intensive projects thus resulting in a series of energy savings on the various sections considered. Suggestions on how to improve the energy efficiency and to reduce the energy consumption of the distillation process were outlined.

The investigation also showed how lean tools such as value stream mapping can be an effective tool when extending it to analyze energy or material use and wastes. The lean value stream mapping tool was used to provide a broad overview of the energy profile for a DPWE production plant. The main purpose of this tool (as used in this study) was to point the user to further resources and tools for energy savings, energy conservation and improvements in operating performances. In this regard, lean tools can be used as a road map that helps the user understand the facility's current energy situation and provides directions for exploring more targeted ways of saving and conserving energy.

Acknowledgement This paper was made possible by a UREP award [UREP09-076-2-020] from the Qatar National Research Fund (a member of The Qatar Foundation). The statements made herein are solely the responsibility of the author[s].

Nomenclature

Acronyms

DPWE	Dual purpose water and electricity
HRB	Heat recovery boilers
MSF	Multistage flash
TBT	Top brine temperature
FBH	Forwarding board house

References

1. Shah R, Ward PT (2003) Lean manufacturing: context, practice bundles, and performance. J Oper Manag 21(2):129–149
2. Hopp WJ, Spearman ML (2004) To pull or not to pull: what is the question? Manuf Serv Oper Manag 6(2):133–148
3. Liker JK (2004) The Toyota way. 14 management principles from the world's greatest manufacturer. McGraw-Hill, New York
4. Monden Y (1981) Adaptable Kanban system helps Toyota maintain just-in-time production. Ind Eng 13(5):29–46
5. Gras JM, Philippe M (2007) Application of the Six Sigma concept in clinical laboratories: a review. Clin Chem Lab Med 45(6):789–796
6. Doolen TL, Hacker ME (2005) A review of lean assessment in organizations: an exploratory study of lean practices by electronics manufacturers. J Manuf Syst 24(1):55–67

7. Wachter B (2009) Lean manufacturing and energy efficiency. http://www.leonardo-energy.org/lean-manufacturing-and-energy-efficiency. Accessed May 2011
8. Hall RW (1983) Zero inventories. Dow Jones-Irwin, Home Wood, IL
9. Shingo S (1989) A study of the Toyota production system from an industrial engineering viewpoint. Productivity Press, Portland, OR
10. Shah R, Ward P (2007) Defining and developing of lean production. J Oper Manag 25:785–805
11. Black JT (2007) Design rules for implementing the Toyota production systems. Int J Prod Res 45(16):3639–3664
12. Askin R, Krishnan S (2009) Defining inventory control points in multi-product stochastic pull systems. Int J Prod Econ 120(2):418–429
13. Cochran D, Eversheim W, Kubic G, Sesterhenn ML (2000) The application of axiomatic design and lean management principles in the scope of production system segmentation. Int J Prod Res 38(6):1377–1396
14. Pettersen J (2009) Defining lean production: some conceptual and practical issues. TQM J 21:127–142
15. Womack JP, Jones DT (1996) Lean thinking: banish waste and create wealth in your corporation. Simon & Schuster, New York
16. EPA (2011) http://www.epa.gov/lean/environment/toolkits/environment/. Accessed Nov 2012
17. Abdul AH, Shaari MH, Zakuan NM, Hassan B (2010) Lean manufacturing assessment in Malaysia small medium enterprise: a case study. World engineering congress, Kuching, Sarawak, Malaysia, 2–5 Aug
18. Feld WM (2000) Lean manufacturing: tools, techniques, and how to use them. The St Lucie Press, London
19. Chen L, Meng B (2010) The application of value stream mapping based lean production system. Int J Bus Manag 5:203–209
20. Abdulmalek FA, Rajgopal J (2007) Analyzing the benefits of lean manufacturing and value stream mapping via simulation: a process sector case study. Int J Prod Econ 107:223–236
21. Wangnick K (2000) Present status of thermal seawater desalination techniques. http://www.idswater.com/Common/Paper/Paper_51/Present%20Status%20of%20Thermal%20Seawater%20Desalination.htm. Accessed June 2012
22. Hamed OA, Al-Sofi MA, Imam M, Mustafa GM, Ba-Mardouf K, Al-Washmi H (2000) Thermodynamic analysis Of Al-Jubail power/water co-generation cycles. Thermodynamic%20analysis%20of%20%20al-jubail%20power%20water%20co-generati.pdf. Accessed June 2012
23. Hamed OA, Mustafa GM, Ba-Mardouf K, Al-Washmi H (2001) Prospects of improving energy consumption of the multi-stage flash distillation process. Proceedings of the fourth annual workshop on water conservation in the Kingdom, Dhahran, 23–25 Apr

Chapter 31
Empirical Formulation of Shear Modulus Functions for Tubular Pinewood Specimens Under Torsion

Ezgi Günay, Cevdet Aygün, and Emre Uludoğan

Abstract In this study, tubular pinewood (Pinus Sylvestris L.) specimens are tested and shear strain measurements are performed by applying torsion in z-direction. Strain gauge measurements are performed for the maximum shear stresses which develop on the tubular specimen, along the radial r (r_{in}, r_{out}), circumferential ϕ (ϕ_{in}, ϕ_{out}) and z directions, in a point-wise (pw) manner. The data is gathered and examined for the determination of the local variations of empirical shear modulus functions on transversely isotropic surfaces of the specimens. The coordinate dependent shear modulus functions of $G_{z\phi}(r)$, $G_{z\phi}(\phi)$, $G_{z\phi}(z)$ are derived for $G_{z\phi}(r, \phi, z)$ as the function of r, ϕ and z, respectively, by analyzing the gathered data. It is proposed to represent the shear modulus functions, $G_{z\phi}(\phi)$ and $G_{z\phi}(z)$ with the parabolic polynomials, and, to represent the shear modulus function $G_{z\phi}(r)$ with a linear equation.

Keywords Wood • Torsion loading • Strain measurements • Stress variation • Shear modulus • Composite material

31.1 Introduction

It is a current trend today that completely wooden houses, apart from the houses with wood components, are gaining ground all over the residential districts of the world's metropolitan areas. In today's world, structural elements which require extra strength and robustness and are directly taken from nature such as trees and bamboos are being rediscovered for the usage in the construction of the buildings and the residential facilities as well as in the manufacture of the new echelon furniture and other household goods. Many parts of the world are just beginning to tap the wind which is clean, renewable and widely distributed. In this sense, a much greener alternative for the structures of the wind turbine towers are being

E. Günay (✉) • C. Aygün • E. Uludoğan
Faculty of Engineering, Mechanical Engineering Department, Gazi University, 06570 Maltepe, Ankara, Turkey
e-mail: egunay@gazi.edu.tr; caygun@gazi.edu.tr; emreuludogan@gmail.com

I. Dincer et al. (eds.), *Progress in Sustainable Energy Technologies Vol II: Creating Sustainable Development*, DOI 10.1007/978-3-319-07977-6_31

offered. Engineered wood is an ideal material for these towers since they are carbon-neutral, renewable, as well as strong and durable and cost-competitive compared to steel and concrete. Wood components are still being used in boat, yacht and small tonnage ship building industries, in many of world's developed and developing countries. As raw material abundantly available in the nature, wood is still being used to manufacture carriages and other transport means by peoples of developing world. In addition, wood is used widely to make most of the sports equipment. As the areas of usage for wood requiring strength and endurance is quite wide, assurance of safety carries weight with usage of all kinds of goods made up of wood. On the other hand, it is known that wood material is made up of either general orthotropic or transversely isotropic material which closely resembles composite material. Physical conclusions deducted from this study will equally be applicable to materials with similar physical properties, such as wood plastic composites (WPC) and other sorts of composites.

Wood is modeled as a fiber composite material of transversely isotropic type. The elastic material constants of fiber composites changes on the surface of each cross-section along the radial and circumferential directions but it remains same along the fiber directions. It is known that; the wood material behaves like a nonlinearly elastic composite structure under torsion loading. However, in addition to this phenomenon, it also exhibits visco-elastic properties. Transversely isotropic structure of wood is related to the natural growth of a tree. Annual rings of the wood form fairly regular concentric circles in nature, giving the wood cylindrically symmetric structure.

Coordinate dependent material elastic constants which were represented with mathematical equations, were studied analytically by scientists [1–5]. A new relationship to calculate the shear modulus G_{12} in terms of off-axis modulus of elasticity E_0 of orthotropic specimens such as wood-based panels was proposed [4]. An extensive body of experimental data according to the variation of in-plane shear modulus $G(\phi)$, and the variation of Young's modulus $E(\phi)$ of plywood panels were gathered and analyzed, in this sense. The mathematical relations between elastic properties of fiber and matrix structure and the wood polymer elastic constants in micromechanical level were studied [5]. The verification of shear modulus transformation rules to obtain basic engineering constants that agrees with reliable test data and the anisotropic elasticity theory was performed [6]. The shear stress versus shear strain expressions of transversely isotropic cylindrical bar under torsion, having a finite length, was described in terms of partial differential equations [7, 8]. Shear properties of clear softwood from Norway spruce were investigated by means of the Arcan shear test [9]. Bilinear and Voce adaptation of experimental shear stress–strain curve on principal coordinate system LR.

In the current study, two coordinate systems were used to define the coordinate dependent strain variations of pinewood specimens under torque, applied in z-direction. The results which were obtained by performing pw incremental measurements were illustrated as curves of shear stress $(\tau_{z\phi})_{pw}$ versus shear strain $(\gamma_{z\phi})_{pw}$, along the principal directions at the gauge locations. The torque loading

was applied to the specimen in the $(r-\phi)$ plane at one end, while the other end was fixed. The related data which was gathered from all these points was shown as separate curves for each test case. The purpose was to show the variations of the $G_{z\phi}(r, \phi, z)$ as functions of r, ϕ, z [10–12]. Consequently, these curves were formulated as empirical mathematical equations. In each test case, the coordinate dependent variations of the shear modulus functions $G_{z\phi}(r)$, $G_{z\phi}(\phi)$ and $G_{z\phi}(z)$ along the r, ϕ, z directions, resp., were generated on the all surfaces of the tubular specimen.

31.2 Experiment and Method

Test instruments and specimens are explained in this section. Tubular pinewood specimens were used in this study. In order to specify the test conditions different equipment was used. The average moisture content of the material was measured by using a Delmhorst Instrument BD-10 moisture meter [13]. Value of the moisture was measured as 6–7 %. All experiments were performed in room temperature by making use of uniaxial and triaxial rosette gauges KFG-5-120-C1-1, KFG-10-120-C1-1, KFG-10-120-D17 [14]. These gauges were bonded onto the specimens. The geometry of the specimens was formed by taking fillet depths equal to the radius of the outer portion of the wood shaft. Thus, it became possible to minimize stress concentrations (Fig. 31.1a). In order to minimize the deviations in the test results; these specimens were manufactured from a single tree trunk. The forming procedure was performed on the wood specimens in such a way that their fibers lay longitudinally parallel to the trunk. However, there were intrinsic structural differences stemming from the number and radii of annual rings in the part of the trunk from which the specimen was taken out.

The experimental set-up was displayed as a schematic diagram in Fig. 31.2. The torsion loading was applied by using a TQSM-21 [15] torsion testing machine. Data was collected by employing specialized units [16, 17]. As a first step, the normal strain values were obtained by reading the voltage differences ΔV_o from the display of the unit, and as a second step, these normal strains were converted into shear strains by using Mohr's circle [18].

The set-up included torsion test machine and two different data acquisition systems. The generated coordinate dependent pw shear strain data $\gamma_{z\phi}$ generated by the applied torque ($\vec{T} = T_z \vec{k}$) was simultaneously stored in terms of output voltage (V_o). The torsion load was applied on the transverse plane ($r-\phi$ plane, Fig. 31.1b) which had a unit normal vector $\vec{k}$ along the z-direction.

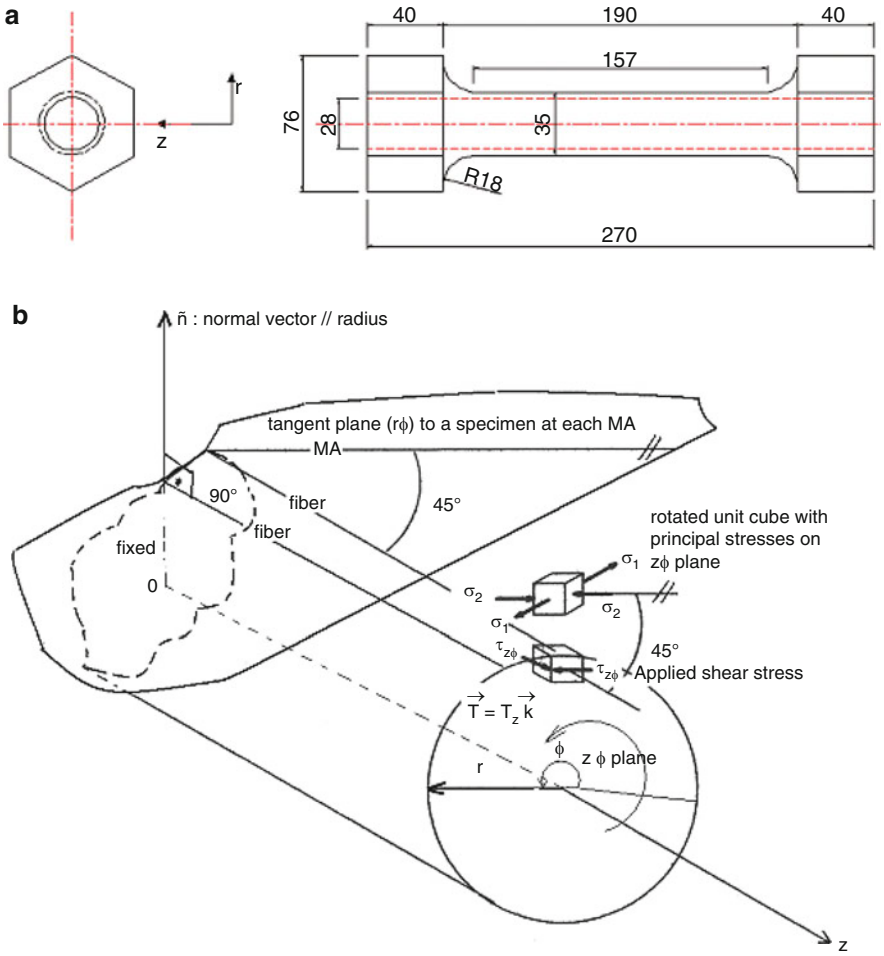

Fig. 31.1 (**a**) Geometrical dimensions of tubular wood specimen (mm). (**b**) In this figure, MA stands for measurement axis which is taken at 45° from fiber direction on the tangent plane. The first coordinate system was the cylindrical coordinate system with r, ϕ, z coordinates (global system). The second coordinate system was fiber oriented principal axes system, 1 – 2 – 3 or (LRT). (**c**) The specimen was modeled by employing two different coordinate systems

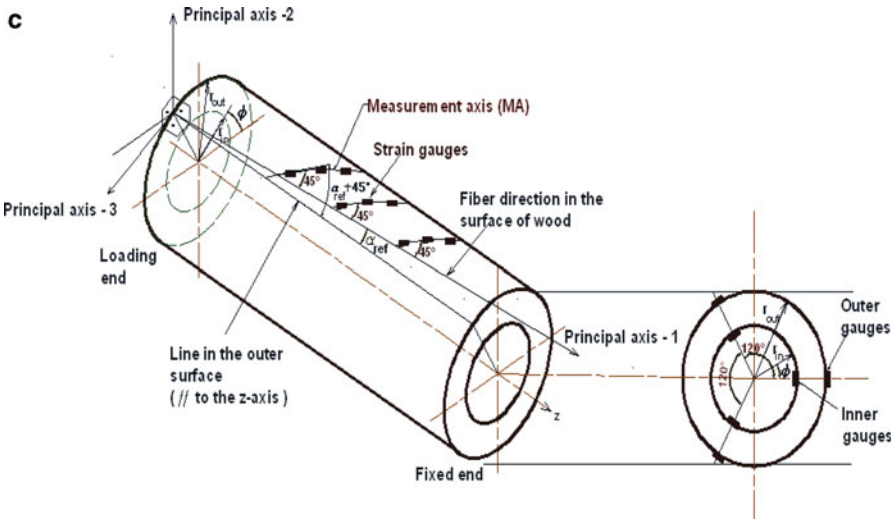

Fig. 31.1 (continued)

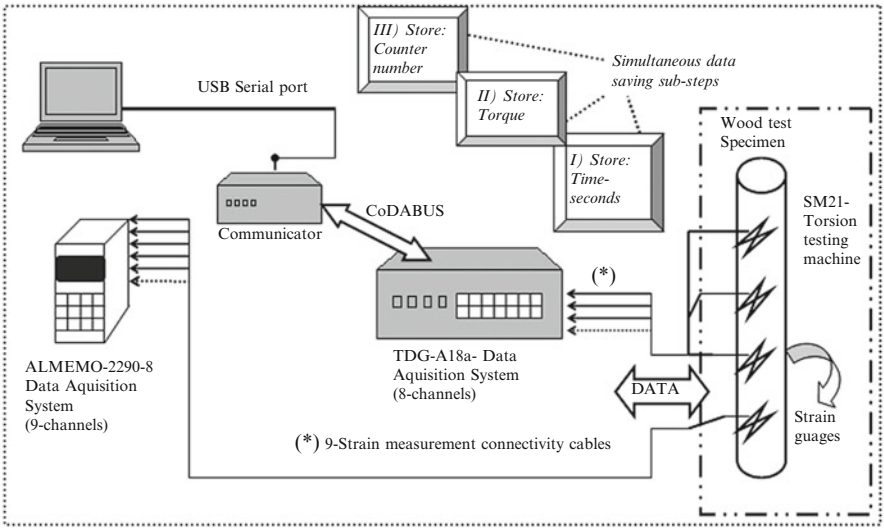

Fig. 31.2 Schematic diagram of the experimental test set-up with data acquisition systems, cables, tubular specimen with strain gauges on it. Additionally, sequences of the experimental operations were also shown

31.3 Measurements

In the consideration of the resultant curves $(\tau_{z\phi} - \gamma_{z\phi})_{pw}$, different failure stresses were established at the forward and backward rotation directions. Directions of forward and backward torque loadings, $+\alpha_{ref}$ or $-\alpha_{ref}$, indicated the fiber angles [11]. Only the forward loading case was considered in the empirical formulation of this study. Results of the experimental studies were analyzed mainly in two steps. Firstly, specific locations were defined along the r, ϕ, z directions on the specimens and shear stress versus strain $(\tau_{z\phi} - \gamma_{z\phi})_{pw}$ curves were obtained for each location. Secondly, the variations of pw shear modulus values of each specimen were shown as shear modulii $G_{z\phi}(r)$, $G_{z\phi}(\phi)$, $G_{z\phi}(z)$ versus r, ϕ, z directions [10]. Subscripts of shear modulus $z - \phi$ represent the cross-sectional surface; on which the torque was applied. On the other hand, circumferential surface is represented by using subscripts $(r - \phi)$. Strain gauges, on which measurements were taken, were installed along the *z* axis (Fig. 31.1c). At the following step of the experiment; exponential and quadratic equations of the variations were tabulated.

Measurements were performed by considering two reference coordinate systems in order to explain the wood specimen behaviour: global cylindrical coordinate system (r, ϕ, z) and local coordinate system (wood fiber arrangement based on principal material directions; 1, 2, 3) (Fig. 31.1c). The local and global coordinate systems were used together for the definition of MA (measurement axis). MA served as a variable of wood fiber direction $(0^o \leq \alpha_{ref} \leq 15^o)$. The angular positions of the strain gauges on the circumferential surface relative to *z*-axis, were aligned with respect to maximum shear stress. The maximum shear stress was the stress formed around MA. These angular positions were denoted as MAA (Measurement Axis Angle) and they were taken as $MAA = \alpha_{ref} + 45^o$. Each MA lies on the 1–3 principal planes which correspond to $r - \phi$ plane (Fig. 31.1c). Measurement axis angle $(MAA = \alpha_{ref} + 45^o)$ is relatively different from the geometrical central axis angle ϕ. MAA was defined on the 1–3 principal material planes which were attached on the surface of the cylinder. The first strain gauge was attached with $+45^o$ angle in the principal material axis-1. All other gauges were also located along this direction (Figs. 31.1b–c). Application of gauges in r_{in}, r_{out}, ϕ_{in}, ϕ_{out} locations were repeated in similar way. In the rest of the study, *z* axis was rotated to be z′ such that it coincided with MA.

Invariants I_1, I_2, I_3 remain constant with respect to coordinate transformations. Stress and strain components were coupled along the principal directions for $2\theta_{p_1} = 0^o$ and $2\theta_{p_1} = 90^o$. Only along the principal directions, stress and strain values of the isotropic materials coincided with the values of fiber composite materials [19]. Thus, it became easier to understand the behaviour of the wood material under torsion and to compare it with that of the isotropic material. Accordingly, the shear modulus functions were derived along the MA directions for the corresponding principal stresses and strains.

The torque value T was measured incrementally. Variation of $(\tau_{z\phi} - \gamma_{z\phi})_{pw}$ were plotted by using the inner or outer shear stresses $\tau_{z\phi}$ and their corresponding principal shear strains. Consequently, shear modulus functions for the principal

shear strains and corresponding shear stresses were expressed in terms of r, ϕ, z in Eq. (31.1) and Table 31.2.

$$\begin{matrix} G_{z\phi}\left(r\left(MA = \alpha_{ref} \pm 45^{o}\right)\right), \\ G_{z\phi}\left(\phi\left(MA = \alpha_{ref} \pm 45^{o}\right)\right), \\ G_{z\phi}\left(z\left(MA = \alpha_{ref} \pm 45^{o}\right)\right) \end{matrix} \tag{31.1}$$

Experimental results were discussed in the following section.

31.4 Results and Discussion

Empirical shear modulus functions and related plots are presented in this section. Average and equivalent mechanical properties of shear modulus values G_{avg} corresponding to the average shear stresses $\tau_{z\phi}$ for different types of wood (pine, oak, chestnut, hornbeam) were measured and results were listed in Table 31.1. These measurements were performed without using strain gauges and the related data was obtained from the second form of the nonlinear exact trilinear curve $(\tau_{z\phi} - \gamma_{z\phi})$. In the application direction of torsion loading; since the resultant curves $(\tau_{z\phi} - \gamma_{z\phi})$ were affected, different failure values were formed. Applied loading directions $+\alpha_{ref}$ or $-\alpha_{ref}$, represent the backward and forward loadings of torque, respectively. Forward loading applications yield higher failure values than the backward ones (Table 31.1).

Table 31.1 Average shear modulus values of typical wood types obtained without using strain gauges ($0^{o} \leq \alpha_{ref} \leq 15^{o}$)

Types of specimens	Shear modulus (GPa) G_{avg} (test#1/test#2/test#3/test#4)	Forward (+) and backward (−) torque directions (test#1/test#2/test#3/test#4)	Average shear modulus values (GPa) G_{avg}	Standard deviation (S_y)
Pine (tube)	0.29/0.46/0.27/0.32	−/−/+/+	0.34	0.085
Pine (solid)	0.35/0.46/0.27/0.32	−/−/+/+	0.35	0.080
Hornbeam (tube)	0.46/0.46/0.40	+/+/+	0.44	0.035
Hornbeam (solid)	0.38/0.43/0.39	+/+/+	0.40	0.026
Oak (tube)	0.32/0.36/0.40/0.43	+/+/+/+	0.38	0.048
Oak (solid)	0.47/0.43/0.3	+/+/+	0.40	0.089
Chestnut (tube)	0.45/0.47/0.41	+/+/+	0.44	0.031
Chestnut (solid)	0.31/0.31/0.36	+/+/+	0.33	0.029

Table 31.2 Empirical shear modulus functions of pinewood specimens

Fiber angle	Quadratic expressions (Pa)			Exponential expressions (Pa)		
MAA	$G_{z\,\phi}(r)$	$G_{z\,\phi}(\phi)$	$G_{z\,\phi}(z)$	$G_{z\,\phi}(r)$	$G_{z\,\phi}(\phi)$	$G_{z\,\phi}(z)$
45° (inner/outer)	$G = -4 \times 10^8 r + 8 \times 10^9$			$G = 3 \times 10^{11} e^{-0.345 r}$		
45° (outer)			$G = -4.3 \times 10^3 z^2 + 4 \times 10^6 z + 4 \times 10^7$			$G = 2 \times 10^8 e^{0.0062z}$
45° (outer)		$G = 9.9 \times 10^4 \phi^2 - 2 \times 10^7 \phi + 8 \times 10^9$			$G = 7 \times 10^9 e^{0.0009\phi}$	
45° (inner/outer)	$G = -2 \times 10^{10} r + 3 \times 10^{11}$			$G = 8 \times 10^{14} e^{-0.6607 r}$		

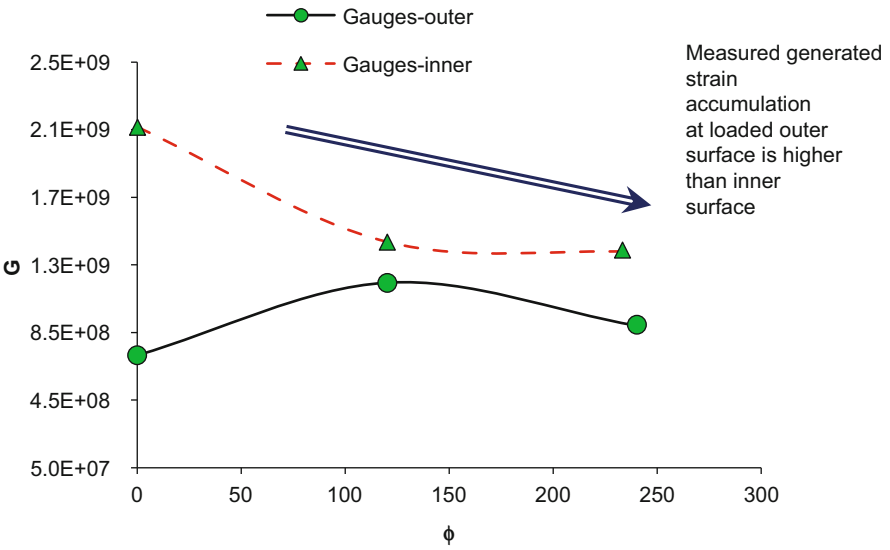

Fig. 31.3 Plots of $G_{z\,\phi}(\phi)$ versus ϕ at $z = 200$ mm (Gauges are located at $\phi = 0^o, 120^o, 240^o$)

The empirical equations of $G_{r\phi}(\phi)$, $G_{z\phi}(z)$ and $G_{z\phi}(r)$ were expressed in terms of various functions and were listed in Table 31.2. The descriptions of the results were explained according to the relative differences of slopes in shear stress–strain $(\tau_{z\phi} - \gamma_{z\phi})_{pw}$ and their corresponding $G_{z\phi}(r)$, $G_{z\phi}(\phi)$, $G_{z\phi}(z)$ versus r, ϕ, z curves for forward loading applications.

Figure 31.3 presents $G_{z\phi}(\phi)$ versus ϕ distribution of data obtained from six gauges at $\phi = 0^o, 120^o, 240^o$ for the tubular specimen. This distribution is obtained through the specified coordinates of MAA at the outer and/or inner surfaces of specimens (see Fig. 31.1c). In the figure, the outer and inner surface $G_{z\phi}(\phi)$ reactions due to the shear stress–strain distributions were formed in reverse orders at the measurement point ($z = 200$ mm). Through the circumferential direction, $G_{z\phi}(\phi)$ forms an convex curve at the inner surface and $G_{z\phi}(\phi)$ forms a concave curve at the outer surface.

Figure 31.4 presents $G_{z\phi}(z)$ versus z distribution from 4 gauges at $z = 65$, 157, 177, and 200 mm. for the tubular specimen. Variation of $G_{z\phi}(z)$, shows parabolic distribution. It is concluded that $G_{z\phi}(z)$ at the loaded end is bigger than $G_{z\phi}(z)$ at the fixed end.

Figure 31.5 presents $G_{z\phi}(r)$ versus r distribution at $\phi = 0^o/120^o/240^o$ for the data obtained from six gauges at $z = 200$ mm. Figure 31.5 demonstrate dependency of $G_{z\phi}(r)$ versus r on the MA angles ϕ. In these tests, gauges were located on both inner and outer surfaces with $\phi = 0^o, 120^o, 240^o$. At these locations of ϕ, the variations of $G_{z\phi}(r)$ from inner to outer surface decrease. Hence, it is concluded that;

1. $G_{z\phi}(r)$ versus r varies linearly on the cross-sectional surface. This is a consequence of $G_{z\phi}(r)$ values on the inner surface are being bigger than $G_{z\phi}(r)$ values on the outer surface.

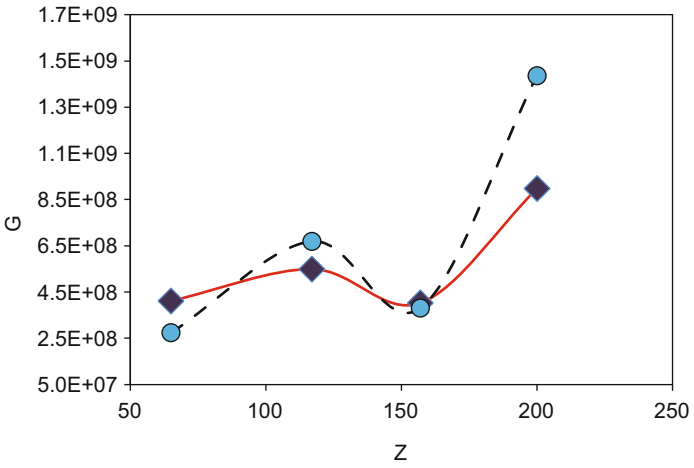

Fig. 31.4 Plots of $G_{z\,\phi}(z)$ versus z (Gauges are located at z = 65, 177, 157, and 200 mm)

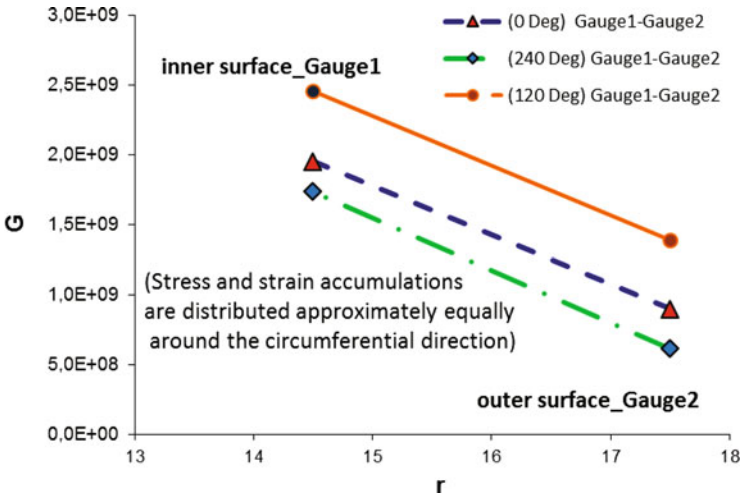

Fig. 31.5 Plots of $G_{z\,\phi}(r)$ versus r at z = 200 mm

2. Shear stresses formed on the outer surface are smaller than the shear stresses formed on the inner surface because shear stresses on the inner surface accumulate densely and shear stresses on the outer surface do not accumulate that densely.

Empirical expressions of $G_{z\phi}(\phi)$, $G_{z\phi}(z)$ and $G_{z\phi}(r)$ were obtained for tubular specimens (Fig. 31.6) by statistically evaluating the coefficients A_{avg}, B_{avg}, C_{avg} from the related experimental data and these coefficients were tabulated in Table 31.3 in five groups (GPa) with their statistical parameters.

(a) Coefficients of the linear $G_{z\phi}(r)$ expression were found to be $A_{avg} = -0.24$, $B_{avg} = 5.1$, and the coefficients of the exponential $G_{z\phi}(r)$ expression were found to be $A_{avg} = 83.1$, $B_{avg} = -0.1876$.

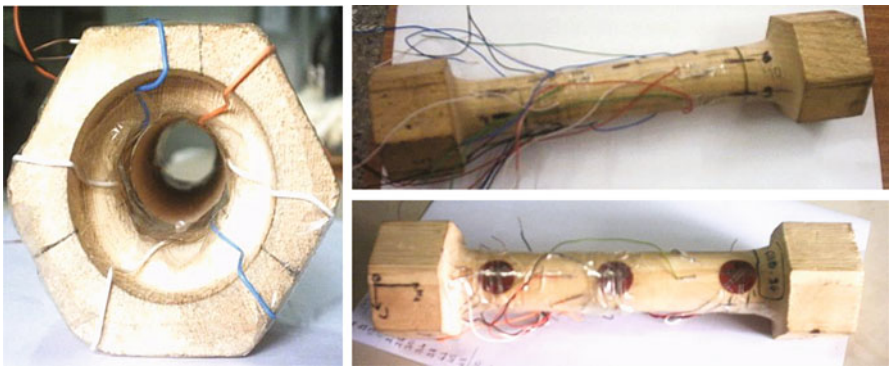

Fig. 31.6 Tubular pinewood specimens with strain gauges on them

(b) Coefficients of the parabolic $G_{z\phi}(\phi)$ expression were found to be $A_{avg} = -2.35 \times 10^4$, $B_{avg} = 1.76 \times 10^6$ and $C_{avg} = 6.2 \times 10^8$, and the coefficients of the exponential expression $G_{z\phi}(\phi)$ were found to be $A_{avg} = 1.19$, $B_{avg} = 0.0004$.

(c) Coefficients of the parabolic $G_{z\phi}(\phi)$ expression on the inner surface were found to be $A_{avg} = -3.78 \times 10^4$, $B_{avg} = 2.65 \times 10^6$, $C_{avg} = 6.875 \times 10^8$ and the coefficients of the exponential expression $G_{z\phi}(\phi)$ on the inner surface were found to be $A_{avg} = 10.13$, $B_{avg} = 0.000175$.

(d) Coefficients of the parabolic $G_{z\phi}(\phi)$ expression on the outer surface were found to be $A_{avg} = -0.72 \times 10^4$, $B_{avg} = 0.74 \times 10^6$, $C_{avg} = 5.43 \times 10^8$ and the coefficients of the exponential expression $G_{z\phi}(\phi)$ on the outer surface were found to be $A_{avg} = 13.75$, $B_{avg} = 0.000613$.

(e) Coefficients of the parabolic expression $G_{z\phi}(z)$ on the outer surface were found to be $A_{avg} = -0.5 \times 10^4$, $B_{avg} = -3.65 \times 10^6$ and $C_{avg} = 14.3 \times 10^8$, and the coefficients of the exponential expression $G_{z\phi}(z)$ on the outer surface were found to be $A_{avg} = 0.21$, $B_{avg} = 0.0075$.

31.5 Conclusions

In this study, variations of the shear modulus of transversely isotropic pinewood specimens under torsion were examined. The set of equations of shear modulus in $z - \phi$ and $r - \phi$ planes along the principal directions were formulated. All measurements were performed in terms of local coordinate system.

As an extension of the current study, it is suggested to calculate the additional shear modulus functions and the related coefficients by performing the experiments of the other types of loadings on other types of woods in a future experimental study. It is known that the elastic constants' matrix C_{ij} appearing in the Hooke's general law, is used to define the elastic constants of the materials. In this matrix,

Table 31.3 Empirical shear modulus functions for tubular specimens including the statistical values of coefficients (GPa)

Groups of average shear modulus functions	Linear function $G_{z\phi}(r) = A_{avg}r + B_{avg}$				Exponential function $G_{z\phi}(r) = A_{avg}\ e^{B_{avg}\ r}$			
(Group I) $G_{z\phi}(r)_{outer}$	Σ(exp) : 18	A_{avg}	B_{avg}	C_{avg}	Σ(exp) : 11	A_{avg}	B_{avg}	C_{avg}
	c.v. (%)	−136.3	80.9	–	c.v. (%)	137.1	−85.6	–
	S_Y	3.31	4.65	–	S_Y	30.69	0.11	–
	Mean (Pa)	-0.24×10^9	5.74×10^9		Mean (Pa)	22.4×10^9	0.13×10^9	–
	Parabolic function $G_{z\phi}(\phi) = A_{avg}\phi^2 + B_{avg}\phi + C_{avg}$				Exponential function $G_{z\phi}(\phi) = A_{avg}\ e^{B_{avg}\phi}$			
(Group II) $G_{z\phi}(\phi)_{outer}$	Σ(exp) : 15	A_{avg}	B_{avg}	C_{avg}	Σ(exp) : 16	A_{avg}	B_{avg}	C_{avg}
	c.v. (%)	−187.39	−751.4	70.1	c.v. (%)	137.1	363.03	–
	S_Y	4.41	13.21	4.35	S_Y	1.64	0.0014	–
	Mean (Pa)	-2.35×10^4	1.76×10^6	6.2×10^8	Mean (Pa)	1.19×10^9	0.000394	
	Parabolic function $G_{z\phi}(\phi)_{inner} = A_{avg}\phi^2 + B_{avg}\phi + C_{avg}$				Exponential function $G_{z\phi}(\phi)_{inner} = A_{avg}\ e^{B_{avg}\phi}$			
(Group III) $G_{z\phi}(\phi)_{inner}$	Σ(exp) : 8	A_{avg}	B_{avg}	C_{avg}	Σ(exp) : 8	A_{avg}	B_{avg}	C_{avg}
	c.v. (%)	−145.46	681.87	82.07	c.v. (%)	64.97	795.17	–
	S_Y	5.51	18.08	5.64	S_Y	6.58	0.00139	–
	Mean (Pa)	-3.78×10^4	2.65×10^6	6.88×10^8	Mean (Pa)	10.1×10^4	0.000175	–
	Parabolic function $G_{z\phi}(\phi)_{outer} = A_{avg}\phi^2 + B_{avg}\phi + C_{avg}$				Exponential function $G_{z\phi}(\phi)_{outer} = A_{avg}\ e^{B_{avg}\phi}$			

(Group IV) $G_{z\phi}(\phi)_{outer}$	Σ(exp) : 7	A_{avg}	B_{avg}	C_{avg}	Σ(exp) : 7	A_{avg}	B_{avg}	C_{avg}
	c.v. (%)	−285.64	654.06	43.66	c.v. (%)	166.33	249.36	–
	S_Y	2.06	4.81	2.37	S_Y	22.87	0.00152	–
	Mean (Pa)	0.72×10^4	0.74×10^6	5.43×10^8	Mean (Pa)	13.75×10^4	0.000613	–
	Parabolic function $G_{rz}(z) = A_{avg}z^2 + B_{avg}z + C_{avg}$				Exponential function $G_{z\phi}(z) = A_{avg}\, e^{B_{avg}z}$			
(Group V) $G_{z\phi}(z)_{outer}$	Σ(exp) : 8	A_{avg}	B_{avg}	C_{avg}	Σ(exp) : 7	A_{avg}	B_{avg}	C_{avg}
	c.v. (%)	−1,005	−279.21	157.2	c.v. (%)	49.89	36.31	–
	S_Y	5.03	10.19	22.48	S_Y	1.07	0.0027	–
	Mean (Pa)	-0.5×10^4	-3.65×10^6	14.3×10^8	Mean (Pa)	0.21×10^9	0.0075	–

it will be possible to define these constants in the form of the mathematical functions by replacing $G_{z\phi}(r)$, $G_{z\phi}(\phi)$ and $G_{z\phi}(z)$ with G_{13}, G_{23}, and G_{21}, for the wood material.

The results were summarized as follows;

1. It was shown that $\tau_{z\phi}$ and $\tau_{r\phi}$ can be written in terms of $\tau_{z\phi}(r, \phi, z)$ and $\tau_{r\phi}(r, \phi, z)$ and they can be calculated by writing Hooke's general law as $\tau_{\phi z} = C_{14}\varepsilon_r + C_{24}\varepsilon_\phi + C_{34}\varepsilon_z + C_{44}\gamma_{\phi z} + C_{45}\gamma_{rz} + C_{46}\gamma_{r\phi}$ and $\tau_{r\phi} = C_{16}\varepsilon_r + C_{26}\varepsilon_\phi + C_{36}\varepsilon_z + C_{46}\gamma_{\phi z} + C_{56}\gamma_{rz} + C_{66}\gamma_{r\phi}$ and substituting the values of the normal strain components $\varepsilon_r, \varepsilon_\phi, \varepsilon_z$ and the shear strain terms $\gamma_{r\phi}, \gamma_{z\phi}, \gamma_{rz}$ in these equations.
2. It was concluded that, $G_{z\phi}(z)$ values at $z = 200$ mm are greater than the $G_{z\phi}(z)$ values at $z = 70$ mm

   Similarly, $G_{z\phi}(\phi)_{outer}$ values are smaller than the $G_{z\phi}(\phi)_{inner}$ values, and, $G_{z\phi}(r)$ values at $z = 200$ mm are larger than $G_{z\phi}(r)$ values at $z = 70$ mm. Here, $z = 70$ and 200 mm represents two different locations at which measurements were taken.
3. It was shown that, the obtained shear modulus values along the (0°) fibers are larger than the other two (45° and 90°) directed measurements with triaxial rosette gauges. Results of the measurements along the 0° MA directions yield very small positive or negative shear strain values. Forward or backward loadings cause extension or contraction along the fibers and in turn, this generates positive or negative shear strains.

   The negative shear strains which develop at the measurement points as a consequence of applying the forward loading can be explained as the contraction of the material along the fibers. In other words, shear strains are defined with respect to coordinate system. Thus, behaviour of the shear strains are dependent upon arrangement of fibers and the direction of applied loading (Table 31.3).
4. It was concluded from the measurements along the MA directions $0^o, 45^o, 90^o$ with triaxial rosette gauges that the relative shear strain changes between $0^o - 45^o$ and $45^o - 90^o$ angles are not equal to each other. The difference of shear strains between the $0^o - 45^o$ directions is smaller than the one between $45^o - 90^o$ directions.

   In order to further understand the complex wood behaviour under torsion loading, it is planned to perform additional experiments. The phenomenon of the stress accumulations which develop at the critical points along the wood fibers will be supported by a new experimental study.

Acknowledgement The authors acknowledge gratefully the support of the work by the Gazi University Scientific Research Projects Department_Research Foundation (BAP) under contract 6/2003-21.

Nomenclature

$A_{avg}, B_{avg}, C_{avg}$	Average coefficients of parabolic equation
c.v.	Spread of data (coefficient of variation)
C_{ij}	Matrix of elastic constants
Deg	Degree
$G_{z\phi}(r), G_{z\phi}(\phi)$	Shear modulus functions generated in the $r-\phi$ planes along the r, ϕ and z-directions as
$G_{z\phi}(z)$	Modes of function
G_{avg}	Average shear modulus (GPa)
pw	Point-wise
MA	Measurement axis
MAA	Measurement axis angle
Mean	Average
r_{in}, r_{out}	Inner and outer radiuses of tubular wood (m)
S_Y	Standard deviation
$T_z, \vec{T}$	Applied z-directional torsion moment (N. m) and its vector notation
V_o	Output voltage (Volt)

Greek Symbols

α_{ref}	Grain angle of wood specimen on the surface of the cylindrical wood bar which is measured from the main axis-z (degree)
ϕ	Rotation angle on ($r\phi$) plane of the specimen (rad)
ϕ_{in}, ϕ_{out}	Inner and outer circumferential angles of tubular wood specimen (degree)
$\sum(exp)$	Total number of experiments
$(\tau_{z\phi} - \gamma_{z\phi})_{pw}$	Applied shear stress and developing shear strain distribution along point-wise direction
$\tau_{rz}, \tau_{z\phi}, \tau_{r\phi}$	Shear stress components (MPa)
$\varepsilon_r, \varepsilon_\phi, \varepsilon_z$	Normal strain components
$\gamma_{rz}, \gamma_{z\phi}, \gamma_{r\phi}$	Shear strain components (radian)
$\gamma, \gamma_{out}, \gamma_{in}$	Average shear strain, shear strains at outer and inner surfaces of the specimen (radian)

References

1. Bozorth RM (1951) Ferromagnetism. Van Nostrand, New York, NY
2. Wooster WA (1949) A textbook on crystal physics. Cambridge University Press, London
3. Turley J, Sines G (1971) The anisotropy of Young's modulus shear modulus and Poisson's ratio in cubic materials. J Phys D Appl Phys 4:264–271

4. Saliklis EP, Falk RH (2000) Correlating off-axis tension tests to shear modulus of wood-based panels. J Struct Eng 126(5):621–625
5. Salmén L (2004) Micromechanical understanding of the cell-wall structure. CR Biologies 327:873–880
6. Liu JY, Ross RJ (2005) Relationship between radial compressive modulus of elasticity and shear modulus of wood. Wood Fiber Sci 37(2):201–206
7. Günay E, Konaklı S (2004) The new formed shear modulus formulations for the transversely isotropic fiber composite bars under torsion loading. J Fac Eng Arch Gazi Univ 19(1):1–12
8. Günay E, Konaklı S (2006) Formation of shear stress equations for transversely isotropic finite length bar under torsion. Sci Eng Compos Mater 13:255–269
9. Dalh KB, Malo KA (2009) Nonlinear shear properties of spruce softwood: experimental results. Wood Sci Technol 43:539–558
10. Uludoğan E (2005) Coordinate dependent experimental determination of shear modulus for transversely isotropic composites by using wood torsion specimens. M.Sc. Thesis, Gazi University, Institute of Science and Technology, Ankara
11. Günay E, Orçan Y (2007) Experimental investigation of the mechanical behavior of solid and tubular wood species under torsional loading. Turkish J Eng Env Sci 31:89–118
12. Günay E, Uludoğan E (2007) Experimental determination of shear modulii variation of typical transversely isotropic wood specimens. J Mach Des Manuf 9:67–87
13. http://www.delmhorst.com/, Delmhorst Instr. Co., 51 Indian Lane East, Towaco, NJ 07082-1025, USA
14. http://www.kyowa-ei.co.jp/eng, Kyowa Electronic Instruments Co. Ltd., Tokyo
15. http://www.tecquipment.com/, TQSM21, Torsion testing machine manual, TecQuipment Ltd., Bonsall Street Long Eaton, Nottingham NG10 2AN, UK
16. http://www.teknikdestek.com.tr/, TDG-AI8a_Data Acquisition System, Ankara, Turkey
17. http://www.ahlborn.com/. ALMEMO_Datalogger Unit. Manual V5 AHLBORN Mess-und Regelungstechnik GmbH, Berlin: Medewitzer Straße14 02633 Gaussig
18. Inan M (1970) Strength of materials. Ofset Printing Ltd., Istanbul
19. Gibson RF (1994) Principles of composite material mechanics. McGraw-Hill Inc., Singapore

Chapter 32
Robust Control Techniques of ASVC-Based Var Flow Compensation

Mansour Benyamina and Benyounes Mazari

Abstract Advanced Static Var Compensators (ASVCs) are high power electronics based devices used to provide fast variable reactive power compensation to power networks. They should be properly controlled to ensure fast and continuous reactive power to meet a certain fluctuating load demand and enhance the transient stability of the power system. The effectiveness of these compensators depends on the choice of the control strategy.

In this paper, we deal with the application of the Internal Model Control technique (IMC) and the State Feedback Control (SFC) concept to adjust the ASVC Var flow with the ac transmission network. These controllers are evaluated under a variety of operating conditions where performances and robustness have been analyzed and compared to a conventional PI controller.

Simulation results in the case of a non linear model show that SFC and IMC controllers, suitable for real time implementation, lead to improved transient response and hence provide fast reactive power compensation to ac transmission networks.

Keywords FACTS • ASVC • IMC control • State feedback control

32.1 Introduction

The configurations of static compensators of reactive power based on switched inverters are today the most used in electric current transmission systems. The apparition of high-powered electronic devises in the design of power electronic converters has resulted in a solid-state Var source with a more simple structure namely the Advanced Static Var Compensator (ASVC) [4, 6]. The ASVC uses a

M. Benyamina
Electrical Engineering Department, University of Mostaganem, BP. 227 route Belhacel, 27000 Mostaganem, Algeria
e-mail: mansour_benyamina@yahoo.fr

B. Mazari (✉)
Laboratory of Electrical Drives LDEE, Faculty of Electrical Engineering, University of Sciences and Technology of Oran—USTO, B.P 1505, EL-Mnaouer, 31000 Oran, Algeria
e-mail: mazari_dz@yahoo.fr

I. Dincer et al. (eds.), *Progress in Sustainable Energy Technologies Vol II: Creating Sustainable Development*, DOI 10.1007/978-3-319-07977-6_32

PWM controlled dc/ac Voltage-Source Inverter (VSI) with a capacitor as a dc power storage device.

The ASVC is connected in derivation that can operate in networks of transport as well as of distribution to generate or absorb reactive power, without using bank of condensers or inductors, in order to provide fast variable and continuous reactive power compensation following large, fluctuating load demands.

Power transmission performances with higher long line transmission capacity and transient stability are achieved by controlling the reactive current injected or absorbed from the transmission line. The effectiveness of these compensators depends mainly on the choice of the control strategy which allows greater control of the power flow in real time taking into account network condition changes and responding almost instantaneously to stability problems. Various control approaches have been proposed in the literature [1, 2, 5, 8] where conventional voltage regulation loops used are based principally on a proportional-integral (PI) controller. These produce satisfactory performance only for limited operating range conditions. In this paper, we consider the application of the Internal Model Control technique (IMC) and the State Feedback Control (SFC) concept to adjust the ASVC Var flow with the ac system. The performances of the closed loop control systems are analysed and the effectiveness of the ASVC proposed controllers under a variety of operating conditions are demonstrated and compared to a conventional PI controller.

32.2 Overview and Modeling of the ASVC

The basic ASVC scheme is illustrated in Fig. 32.1. The ASVC circuit consists of six-pulse VSI with a dc capacitor and a PWM modulator. Connection of the ASVC to the transmission line is via a coupling transformer where Rs and Ls are the coupling transformer active losses and leakage respectively as shown in the three-phase equivalent circuit of the ASVC connected to a transmission line of Fig. 32.2.

Basically, the ASVC supplies reactive power to the ac transmission system if the magnitude of the inverter voltage is greater than the ac terminal voltage. It draws reactive power from the ac transmission system if the magnitude of the ac terminal voltage is greater to the inverter voltage. Var exchange is zero when the two voltages are equal [7].

It is assumed that the source is a balanced sinusoidal three-phase voltage supply with frequency ω.

Applying d-q transform to the ac circuit and combining the dc circuit equation, the ASVC model is obtained as:

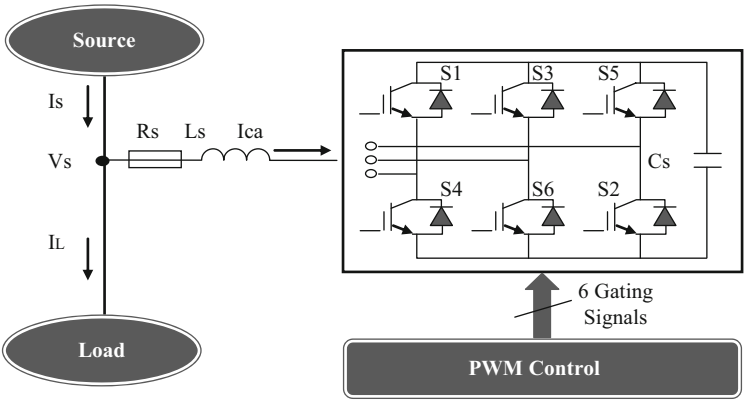

Fig. 32.1 Circuit diagram of the ASVC

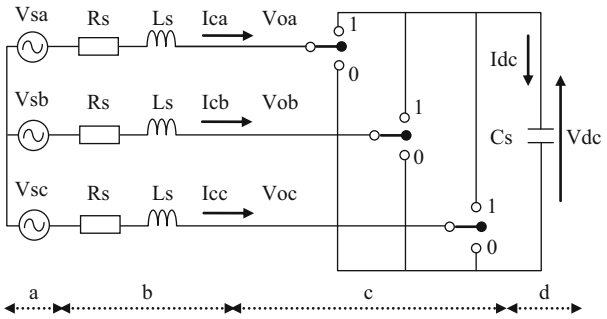

Fig. 32.2 Three-phase equivalent circuit of the ASVC. *a*—Three-phase source voltage, *b*–coupling transformer, *c*—PWM voltage source inverter, *d*—DC-side capacitor

$$\frac{d}{dt}\begin{bmatrix} i_q \\ i_d \\ V_{dc} \end{bmatrix} = \begin{bmatrix} -\frac{R_s}{L_s} & -\omega & 0 \\ \omega & -\frac{R_s}{L_s} & -\frac{m}{L_s} \\ 0 & -\frac{m}{C_s} & 0 \end{bmatrix} \begin{bmatrix} i_q \\ i_d \\ V_{dc} \end{bmatrix} + \frac{V_s}{L_s}\begin{bmatrix} \sin\alpha \\ \cos\alpha \\ 0 \end{bmatrix} \tag{32.1}$$

The modulation index (MI) relates the maximum phase voltage to the dc link voltage.

$$MI = \sqrt{\frac{2}{3}}m = \frac{(V_0)_{peak}}{V_{dc}} \tag{32.2}$$

The state equation is non-linear with respect to the control variable α which is related to the phase difference between the source voltage and inverter output

voltage. In the range of small values of α (|α| < 5°), the small signal equivalent state equations are expressed as:

$$\frac{d}{dt}\begin{bmatrix}\Delta i_q\\ \Delta i_d\\ \Delta V_{dc}\end{bmatrix}=\begin{bmatrix}-\frac{R_s}{L_s} & -\omega & 0\\ \omega & -\frac{R_s}{L_s} & -\frac{m}{L_s}\\ 0 & -\frac{m}{C_s} & 0\end{bmatrix}\begin{bmatrix}\Delta i_q\\ \Delta i_d\\ \Delta V_{dc}\end{bmatrix}+\frac{V_s}{L_s}\begin{bmatrix}-1\\ 0\\ 0\end{bmatrix}\quad \Delta\alpha \tag{32.3}$$

The system input is the control variable deviation Δα and the output is the generated reactive power given by:

$$\Delta Q_c=\begin{bmatrix}-V_s & 0 & 0\end{bmatrix} \tag{32.4}$$

Hence the system transfer function is given by:

$$\frac{\Delta Q_c(s)}{\Delta\alpha(s)}=\frac{V_s^2\left[\frac{s^2}{L_s}+\frac{R_s}{L_s}s+\frac{m^2}{L_s^2C_s}\right]}{s^3+2s^2\frac{R_s}{L_s}+\left(\omega^2+\frac{R_s^2}{L_s^2}+\frac{m^2}{L_sC_s}\right)s+m^2\frac{R_s}{L_s^2C_s}} \tag{32.5}$$

32.3 Control Scheme of the ASVC

32.3.1 Internal Model Controller

The overall closed loop control system is pictured in Fig. 32.3 and the basic architecture of a classical IMC is illustrated by Fig. 32.4 [3]. A system model is placed in parallel with the actual system. The difference is used to adjust the command signal. An attractive feature of IMC is that it produces an offset-free response even when the system is subjected to a constant disturbance.

With reference to Fig. 32.4, the control and output signal are expressed as:

$$\alpha(z)=\{1+C_0(z)[G(z)-G_m(z)]\}^{-1}C(z)[Q^*(z)-D(z)]$$
$$Q_c(z)=G(z)\{1+C_0(z)[G(z)-G_m(z)]\}^{-1}C(z)[Q^*(z)-D(z)]+D(z)$$

If a perfect model is assumed (G(z) = Gm(z)) then the closed loop system is stable if the controller C(z) and the system are stable. However under mismatch conditions (G(z) ≠ Gm(z)), a low pass filter is introduced in the feedback loop to improve the controller robustness with respect to modeling errors.

The design filter has the following transfer function

$$F(z)=\frac{(1-\beta)\quad z}{(z-\beta)}\qquad 0<\beta<1 \tag{32.6}$$

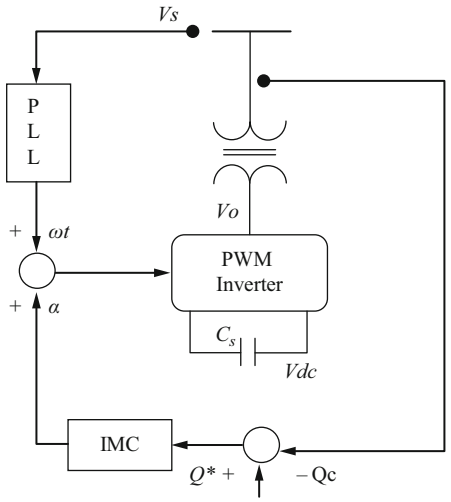

Fig. 32.3 ASVC closed loop control system

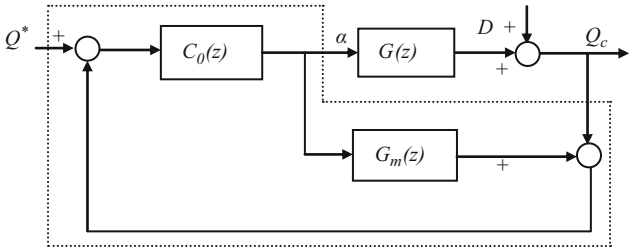

Fig. 32.4 Basic IMC structure

In what follows β has been fixed to 0.002.

Since the controller is the inverse of the system model (i.e. C0(z) = Gm(z)−1) then Qc(z) = Q*(z) and consequently the inverse system model should be stable. Furthermore if C0(1) = Gm(1)−1 the controller produces an offset-free response.

With Ts = 0.005 s, the discrete-time transfer function of the system is obtained as:

$$G(z) = \frac{220^2(0.3441z^2 + 0.3819z + 0.2207)}{z^3 + 0.269z^2 - 0.187z - 0.1353} \tag{32.7}$$

By taking Gm(z) = G(z) then the poles and zeroes of Gm(z) are p1,2 = −0.407 ± j0.2943, p3 = 0.5404, and z1,2 = −0.5549 ± j0.5775.

Then, the controller transfer function is given by:

$$C_0(z) = \frac{1}{220^2}\left[\frac{z^3 + 0.269z^2 - 0.187z - 0.1353}{0.9467z^3}\right] \tag{32.8}$$

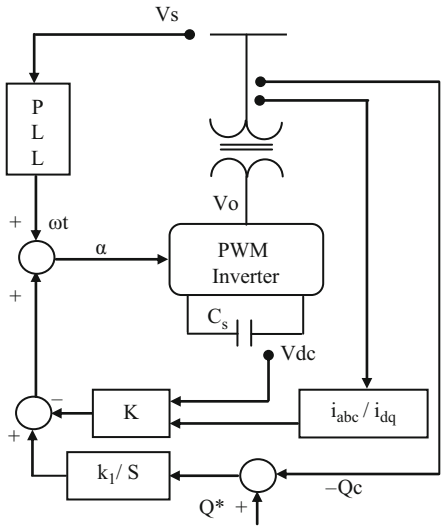

Fig. 32.5 ASVC closed loop control system

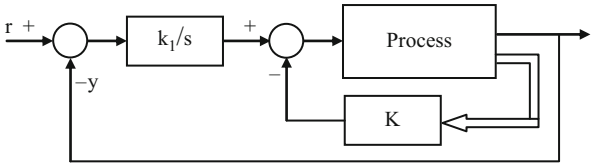

Fig. 32.6 Basic state feedback control structure

32.3.2 State Feedback Controller

The overall closed loop control system with SFC control technique is shown in Fig. 32.5 and the cascade control system of the state-feedback configuration is given in Fig. 32.6 [3]. The controlled variable y is compared with the set-point value r and the control error is fed back to an integrator. The former feedforward gain k1 is now the gain of the integrator. This configuration shows that the gain K in the internal closed-loop is a feedback parameter.

The basic principle of the designed system is to insert an integrator in the feed forward path between the error comparator and the process as shown in Fig. 32.7.

From this diagram we obtain:

$$\dot{x} = A\,x + B\,u \tag{32.9}$$

$$y = C\,x \tag{32.10}$$

$$u = -K\,x + k1\,\xi \tag{32.11}$$

$$\dot{\xi} = r - y = r - Cx \tag{32.12}$$

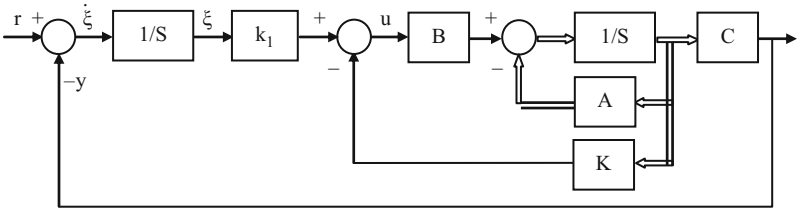

Fig. 32.7 Type 1 servo system where the plant has an integrator

We assume that the plant given by Eq. 32.9 is completely state controllable. The transfer function of the plant can be given by:

$$GP(s) = C\,[sI - A] - 1B \tag{32.13}$$

The system dynamics can be described by an equation that is combination of Eqs. 32.9 and 32.12.

$$\begin{bmatrix} \dot{x}(t) \\ \dot{\xi}(t) \end{bmatrix} = \begin{bmatrix} A & 0 \\ -C & 0 \end{bmatrix} \begin{bmatrix} x(t) \\ \xi(t) \end{bmatrix} + \begin{bmatrix} B \\ 0 \end{bmatrix} u(t) + \begin{bmatrix} 0 \\ 1 \end{bmatrix} r(t) \tag{32.14}$$

$$y = [\,C \quad 0\,] \begin{bmatrix} x(t) \\ \xi(t) \end{bmatrix} \tag{32.15}$$

Where

$$u = [\,-K \quad k_1\,] \begin{bmatrix} x(t) \\ \xi(t) \end{bmatrix} \tag{32.16}$$

We shall design an asymptotically stable system such that $x(\infty)$, $\xi(\infty)$, and $u(\infty)$ approach constant values, respectively. Then, at steady state $\dot{\xi}(\infty) = 0$, and we get $y(\infty) = r$.

Where

$$\hat{A} = \begin{bmatrix} A & 0 \\ -C & 0 \end{bmatrix} \qquad \hat{B} = \begin{bmatrix} B \\ 0 \end{bmatrix} \tag{32.17}$$

32.4 State Space Method Control Applied to the ASVC System

The state space representation of the system becomes:

$$\dot{x} = A\,x + B\,u \tag{32.18}$$

$$Qc = C\,x \tag{32.19}$$

Where

$$A = \begin{bmatrix} -\frac{R_s}{L_s} & -\omega & 0 \\ \omega & -\frac{R_s}{L_s} & -\frac{m}{L_s} \\ 0 & -\frac{m}{C_s} & 0 \end{bmatrix} \qquad B = \frac{V_s}{L_s}\begin{bmatrix} -1 \\ 0 \\ 0 \end{bmatrix} \qquad C = [-Vs \quad 0 \quad 0]$$

Hence

$$A = \begin{bmatrix} -200 & -314 & 0 \\ 314 & -200 & -129.3 \\ 0 & -1293.3 & 0 \end{bmatrix} \qquad B = \begin{bmatrix} -44000 \\ 0 \\ 0 \end{bmatrix} \qquad C = [-220 \;\; 0 \;\; 0]$$

The poles selected for a good dynamic response of the closed loop system are determined by the Ackermann algorithm where:

$$p1 = -500;\ p2 = -600;\ p3 = -700;\ p4 = -750.$$

Hence

$$\hat{A} = \begin{bmatrix} -200 & -314 & 0 & 0 \\ 314 & 200 & -129.3 & 0 \\ 0 & -1293.3 & 0 & 0 \\ 220 & 0 & 0 & 0 \end{bmatrix} \quad ; \quad \hat{B} = \begin{bmatrix} -44000 \\ 0 \\ 0 \\ 0 \end{bmatrix}$$

We shall determine the necessary state feedback gain matrix K using the pole placement technique, where:

$$\hat{K} = [K \vdots \quad -k_1] = [-0.0489 \quad -0.0537 \quad -0.0241 \quad -0.0973]$$

32.5 Results and Discussion

Simulations were performed under Matlab/Simulink environment with the following ASVC parameters:

$$Rs = 1\ \Omega \quad Ls = 5.10 - 3\ H \quad Cs = 500.10^{-6}\ F \quad Vs = 220\ V$$
$$m = 0.646 \quad \omega = 100\pi\ rad/s$$

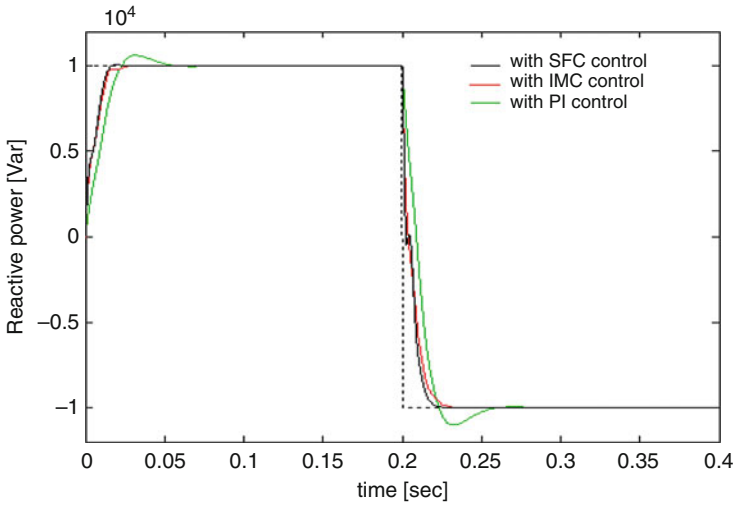

Fig. 32.8 Reactive power response under step change from inductive to capacitive with the non-linear model

The PI parameters are obtained using root locus design for a damping factor of 0.7 where the following controller gains are obtained: $Kp = 7.5 \times 10^{-6}$ $Ki = 2.5 \times 10^{-3}$.

The IMC and SFC controllers were evaluated under more realistic simulation condition when the ASVC devices were controlled by PWM control circuit.

Figure 32.8 shows the transient response in the case of IMC and SFC controllers based on the non-linear model of the ASVC. The Var command was varied from 10 Kvar (inductive) to −10 Kvar (capacitive) to swing the system from leading to lagging mode at time 0.2 s.

The results obtained show that by the IMC and the SFC controller lead to a faster transient response with a shorter settling time and with no overshoot. It can be observed also that the SFC control produces a better performance than IMC and PI control which demonstrates its robustness under model mismatch situations.

Figures 32.9 and 32.10 show the reactive power responses under IMC and SFC controllers compared to a PI controller and Figs. 32.11 and 32.12 show the current waveforms behavior. It is observed from Fig. 32.11 how the current injected into the transmission line swings instantaneously in response to a capacitive Var demand.

Figures 32.13 and 32.14 show the transient response of the dc-side voltage V_{dc}, and I_d, I_q ac current components respectively with IMC and SFC controllers. We notice that the response is faster and smooth in tw case of SFC control.

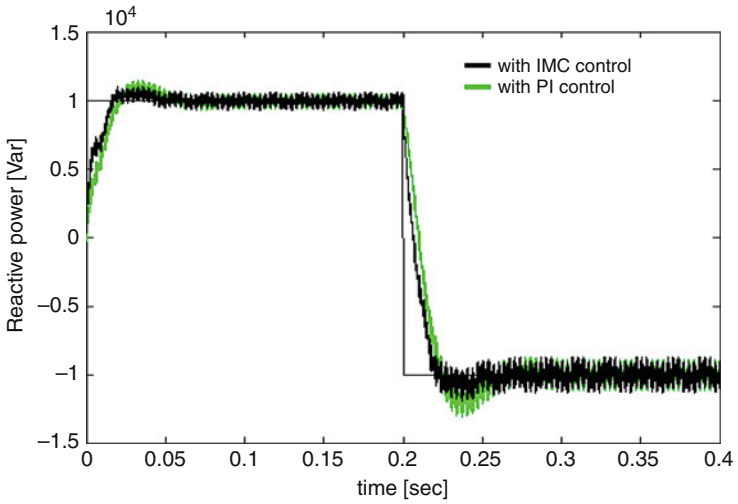

Fig. 32.9 Reactive power transient response under a step change from 10 Kvar leading to 10 Kvar lagging

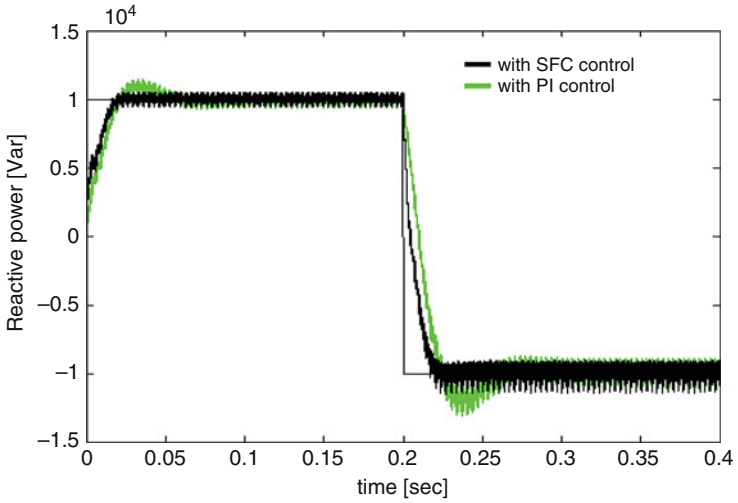

Fig. 32.10 Reactive power transient response under a step change from 10 Kvar leading to 10 Kvar lagging

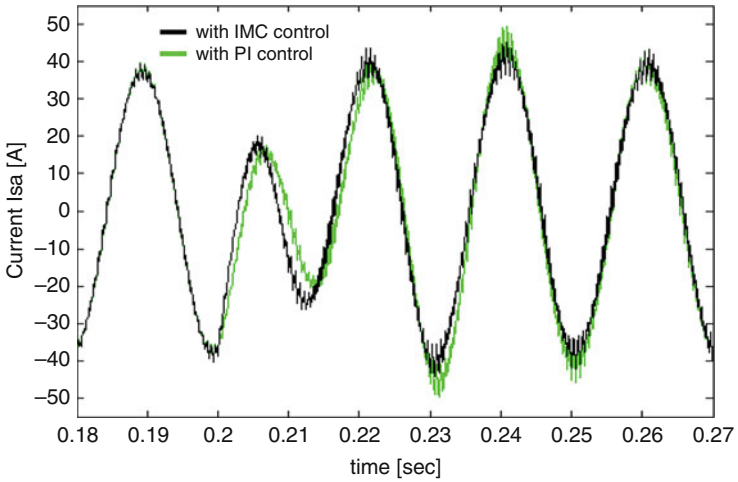

Fig. 32.11 Phase current response with IMC control

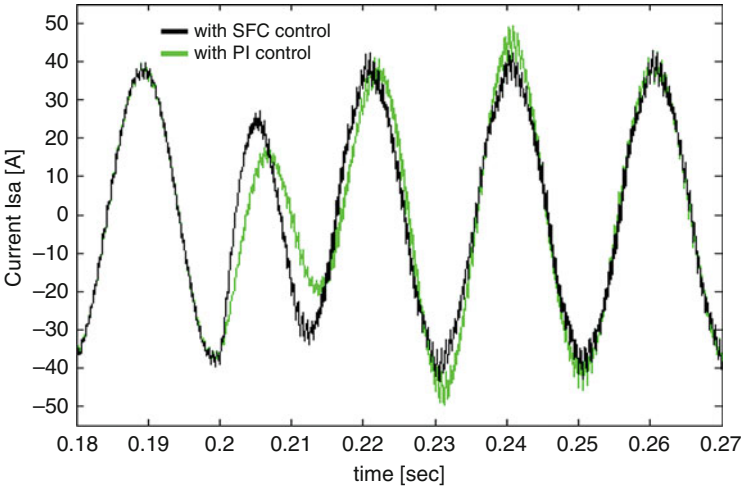

Fig. 32.12 Phase current response with SFC control

32.6 Conclusion

Internal Model Control and State Feedback Control techniques applied to an advanced static var compensator were presented in this work. Performance and robustness of IMC and SFC have been evaluated and compared to a conventional PI controller.

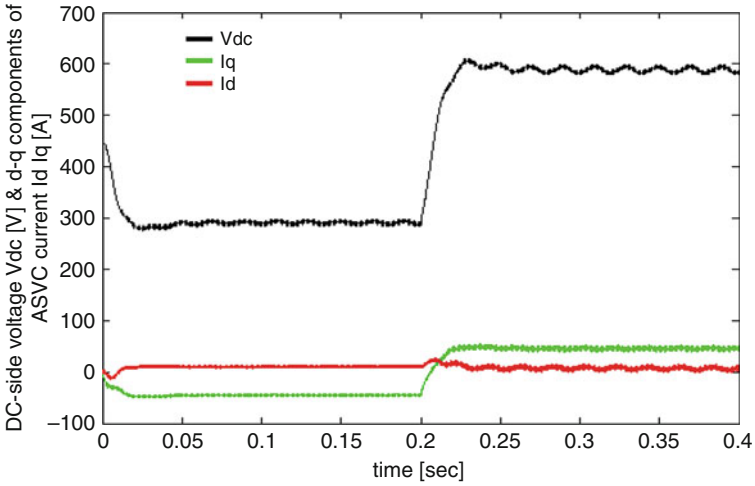

Fig. 32.13 DC-side voltage V_{dc}, and I_d I_q ac current components with IMC control

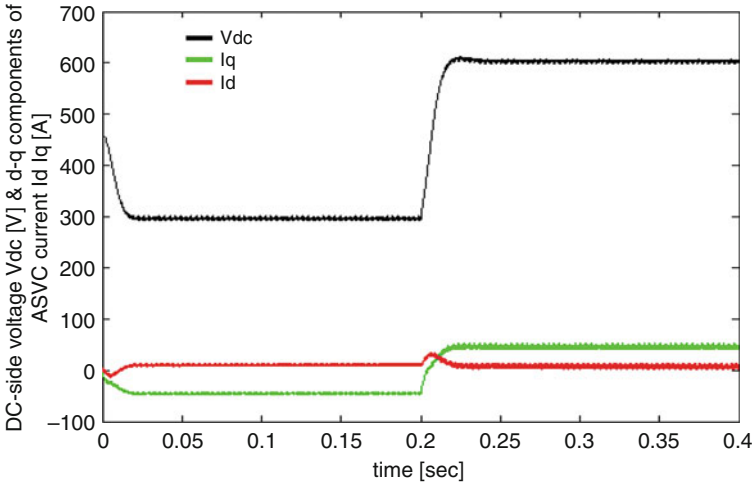

Fig. 32.14 DC-side voltage V_{dc}, and I_d I_q ac current components with SFC control

Simulation results demonstrate that the proposed strategy is feasible, it can be concluded that SFC and IMC control lead to improved transient response and hence provide fast reactive power compensation to the ac transmission network. Also the SFC controller is better than the IMC controller and can be easily tuned and very suitable for real time experimental implementation.

Nomenclature

Acronyms

ASVC	Advanced static Var compensator
IMC	Internal model controller
MI	Modulation index
SFC	State feedback controller

Subscript and Superscripts

ω	Supply frequency
A	$n \times n$ constant matrix
B	$n \times l$ constant matrix
C	$l \times n$ constant matrix
Co(z)	Controller transfer function
Cs	Source capacitor
F(z)	Filter transfer function
G(z)	Discrete-time transfer function
I_{ca} I_{cb}, I_{cc}	ASVC currents
I_s I_L	Source and load currents
K	Gain matrix K
Kp Ki	PI parameters
Ls	Source inductance
r	Reference input signal (step function scalar)
Rs	Source resistor
s	Laplace operator
u	Control signal (scalar)
V_{dc} I_{dc}	dc-side voltage and current
V_{sa} V_{sb}, V_{sc}	Source voltages
x	State vector of the plant (n-vector)
y	Output signal (scalar)

Greek Symbols

α	Control variable
$\Delta\alpha$	Control variable deviation
ξ	State variable

References

1. Abbasian M (2009) Robust control of STATCOM based on sliding mode technique. International Conference on renewable energies and power
2. Benyamina M, Mazari B, Tahri A (2007) A comparative study of robust control for an ASVC-based Var flow compensation. Int Rev Electric Eng 2(5):681–686
3. Bouhamida M (2005) Power system stabilizer design based on robust control techniques. ACSE Journal of Automatic Control and System Engineering. 5(3)
4. Grunbaum R (1999) FACTS: les systèmes performants pour le transport flexible de l'énergie électrique. Revue ABB review 4:4–17
5. Morari M, Zafiriou E (1989) Robust process control. Prentice Hall, Englewood Cliffs, NJ
6. Qader MR (2006) Optimal location of advanced static VAR compensator (ASVC) applied to non-linear load model. Energy 31:1761–1768
7. Trabelsi M (2008) Modélisation et commande directe d'un convertisseur multi-niveau monophasé. Congrés jeunes chercheurs en génie électrique, France 08
8. Sato Y, Kataoka T (1993) State feedback control of current-type PWM AC-to-DC converters. IEEE Trans. on Industry Application 29(6):1090–1097

Chapter 33
Thermogravimetric Studies on Co-combustion Characteristics of Mengxi Coal and Poplar

Kaiqi Shi, Tao Wu, Jiefeng Yan, Haitao Zhao, Philip Hall, and Edward Lester

Abstract In this paper, co-combustion characteristics of Mengxi coal (MC) and poplar (PP) blends and the effects of biomass ash on co-combustion process were investigated. A 'model poplar' (mPP) was prepared with pure cellulose, hemicellulose and lignin basing on the lignocellulosic contents of PP. Thermogravimetric analyses were performed on MC, PP, mPP, MC/PP blends with 10, 30, 50 % (wt%) of poplar, MC/mPP blends with 10, 30, 50 % (wt%) mPP samples. The devolatilization temperature, ignition temperature, peak temperature and burnout temperature were used to evaluate the co-combustion behaviour of different samples. Activation energy and pre-exponential facts for different processes were determined. It is evident that the combination between components in PP and ash of PP has marked impacts on devolatilization process of coal/biomass blends. It is also clear that poplar ash has a catalytic effect on the co-combustion process which makes the ignition of blends with higher biomass blending level takes place easily at lower temperatures. The ash matter in poplar lowers the decomposing rate of cellulose in biomass and the highest decomposing rate is observed at a lower temperature. Furthermore, poplar ash also affects weight loss rates of blends during combustion process. Impacts on burnout temperature of the blends are not significantly affected by blending poplar at low level. From data of active energy and pre-exponential factor, the ash in biomass reduces the reactivity of the blends at lower temperatures between 200 and 400 °C, but makes major co-combustion process at temperature 400–600 °C easily take place at lower biomass ratio.

K. Shi • T. Wu (✉) • J. Yan • H. Zhao • P. Hall
Division of Engineering, The University of Nottingham Ningbo China, No.199 Taikang East Road, Ningbo 315100, China
e-mail: kaiqi.shi@nottingham.edu.cn; tao.wu@nottingham.edu.cn; jiefeng.yan@nottingham.edu.cn; haitao.zhao@nottingham.edu.cn; philip.hall@nottingham.edu.cn

E. Lester
School of Chemical and Environmental Engineering, The University of Nottingham, Nottingham NG7 2RD, UK
e-mail: edward.lester@nottingham.ac.uk

I. Dincer et al. (eds.), *Progress in Sustainable Energy Technologies Vol II: Creating Sustainable Development*, DOI 10.1007/978-3-319-07977-6_33

Keywords Thermogravimetric analysis • Co-combustion • Coal • Biomass • Kinetics

33.1 Introduction

Biomass is one of the renewable energy sources, which has a great potential in meeting the world's increasing energy demand. Fossil fuels, such as coal and crude oil, are non-renewable and their reserves are limited. It is therefore vital to find some alternative energy sources to replace a proportion of coal and subsequently reduce the fossil fuel usage in energy sector [1]. The co-firing of biomass with coal in conventional coal-fired utility boilers is an attractive option for biomass utilization in the power generation [2], which has been proved to be one of the most economic technologies for the significant reduction of greenhouse gases emissions [3]. Currently, more than 150 coal-fired power plants had experience with co-firing of coal with biomass or waste [2]. There has been a considerably rapid progress over the past decade in the development of technologies for the co-utilization of biomass and coal.

Although coal was formed from biomass hundreds of millions years ago, the combustion characteristics of coal are significantly different from those of biomass. The understanding of how biomass addition affects the overall combustion characteristics of the blends is of particular importance for utility boiler operators due to its potential impacts on the safe operation of the boilers. Significant synergistic effects were observed between biomass and lignite blends [1, 4]. Effects were also made to understand the reactivity of the blends by the determination of pre-exponential factor and activation energy of the reaction assuming that the combustion process is a single step process [5–7]. In addition, it is found that the ash in the blends does not have any significant impacts on deposition and corrosion problems in boilers compared with coal combustion only [8].

Although a number of studies on co-combustion with TGA have been reported [1, 3, 5, 7, 9–12], very few attempts were made to understand the impact of ash on co-combustion process [8, 13]. Little information is available on the effects of biomass ash on the co-combustion of coal/biomass blends and its kinetics. In this study, model biomass samples were prepared basing on the lignocellulosic contents of real biomass with pure cellulose, hemicellulose and lignin [14], which are ash-free. TGA was employed to compare the co-combustion characteristics of poplar/coal blends and model poplar/coal blends. Combustion kinetics of blends were studied to understand how the co-combustion processes are affected by biomass blending. The synergistic effect during the course of co-combustion was also studied via the comparison of major combustion characteristics among coal, biomass and their blends together with the model biomass/coal blends.

33.2 Experimental

A Chinese coal, Mengxi coal (MC), and biomass, poplar (PP), were used for this study. MC and PP samples were prepared following the standard [15]. Approximate 1 kg of each sample was ground to a particle size <212 μm for future use.

The moisture, volatile, fixed carbon and ash contents were determined using TGA (EXSTAR TG/DTA 6300, Japan) following the procedures adopted elsewhere [16]. Approximately 5 mg of air-dried sample was used in each test which was manually ground prior to testing to eliminating possible diffusion effects. The heating program started at 30–105 °C at 10 °C/min under 200 mL/min N_2 purging. After holding for 20 min at 105 °C, the temperature was then further increased to 900 °C at 20 °C/min with 200 mL/min N_2, holding for 120 min. Further, the temperature was cooled to 850 °C and the gas was switched to air at 200 mL/min, holding for 60 min. The proximate contents were calculated with weigh loss percentage.

The carbon (C), hydrogen (H), nitrogen (N) and sulphur (S) contents in coal and biomass samples were determined using the CHNS/O Element Analyzer (PE2400II, USA). Approximately 2.0 mg of dried fine powder sample was used for each test. The oxygen (O) content was calculated by difference on ash and moisture free base.

The cellulose, hemicellulose and lignin contents of biomass were determined via acid detergent fiber (ADF), neutral detergent fiber (NDF) and acid detergent lignin (ADL) methods analyses respectively [17]. Around 1.00 g dried biomass sample was transferred into a round bottomed flask with condensing device and then added with 100 mL preheated neutral detergent solution (30 g sodium lauryl sulphate, 18.61 g EDTA disodium salt, 6.81 g sodium borate decahydrate, 4.56 g disodium hydrogen phosphate, and 10 mL 2-ethoxy ethanol dissolved in 1-L distilled water). The mixture was heated at its boiling temperature for 1 h. The solution was cooled and then filtered. The residue was washed three times with hot distilled water, and then three times with acetone and vacuum dried afterwards. Further drying was carried out at 105 °C over for 3 h. The initial and final weight difference was recorded as NDF. The ADF analysis is similar to that of NDF except for the different detergent solution called acid detergent solution (20 g cetyl trimethylammonium bromide was dissolved in 700 mL distilled water. 27.56 mL of 96.7 % acid sulphuric was then added to the solution and the topped up to 1 L with distilled water). The ADL analysis was started by covering the residues from ADF analysis with 72 % H_2SO_4 (15 °C) solution and stirred three times at an hourly intervals. The mixture was then filtered, washed with hot water and then dried in 105 °C oven for 3 h and then cooled. The residue was ignited in 500 °C furnace for 2 h. The still hot crucibles were transferred into oven a 100 °C for an hour before cooled in desiccators and then weighed. The initial and final weight difference of this analysis was recorded as ADL. The percentages of cellulose, hemicelluloses and lignin of the biomass were then calculated using the relationships shown as the Eqs. (33.1, 33.2, and 33.3):

$$\text{Cellulose}\ (\%) = \text{ADF} - \text{ADL} \tag{33.1}$$

$$\text{Hemi-cellulose}\ (\%) = \text{NDF} - \text{ADF} \tag{33.2}$$

$$\text{Lignin}\ (\%) = \text{ADL} \tag{33.3}$$

Basing on lignocellulosic contents, model poplar (mPP) was prepared by mixing pure cellulose (microgranular, Sigma, CAS9004-34-6), xylan (Poly(β-D-xylopyranose(1-4)), Sigma, CAS9014-63-5) and lignin (alkali lignin, Sigma, CAS 8068-05-1) together to represent the biomass sample without ash. Poplar and model poplar were then mixed with Mengxi coal at 10, 30, 50 wt% of biomass respectively to produce blends for testing.

Combustion characteristics of MC, PP, mPP, cellulose, xylan, lignin, MC/PP and MC/mPP blends were measured using EXSTAR TG/DTA 6300. The obtained thermogravimetric (TG) and derivative thermogravimetric (DTG) data were used to determine combustion characteristics.

Approximately 5.0 mg of sample was used for the testing. The sample is firstly heated from 35 to 900 °C at a heating rate of 20 °C/min and is held at 900 °C for 30 min. Then the sample is cooled down from 900 to 850 °C with a cooling rate of 20 °C/min and held for 30 min. The whole process is carried out in air with an air flowrate of 200 mL/min.

The TG and DTG profiles were then analyzed to show the characteristics of combustion, such as devolatilization temperature [12], ignition temperature [11], peak temperature and, burnout temperature [18].

Activation energy (E) and pre-exponential factors (A) are studied to evaluate the difficulty and intensity of thermal chemistry reactions for the different fuels, under the same combustion conditions. The devolatilization and combustion kinetics and weight loss rate can be expressed as Eqs. (33.4) and (33.5):

$$k = Ae^{-E/RT} \tag{33.4}$$

$$-\frac{dm}{dT} = -ka \tag{33.5}$$

where k is the decomposition rate, A is the pre-exponential factor, E is the activation energy, R is the universal gas constant, T is absolute temperature, and a is the remaining quota of residuals.

33.3 Results and Discussion

The proximate and ultimate analyses of MC and PP are shown in Table 33.1 together with lignocellulosic analysis data. The fixed carbon content of MC (45.5 %) is considerably higher than that of PP. The volatile content is 77.4 % for PP, much higher than that of MC, which is around 34.2 %. Both MC and PP have similar moisture content and ash content. In ultimate analysis, carbon content of

Table 33.1 Properties of Mengxi coal and poplar

Properties	MC	PP
Moisture content (wt%)	4.2	4.3
Proximate analysis (wt%)[a]		
Volatile matter	34.2	77.4
Fixed carbon	45.5	1.4
Ash	20.3	21.2
Ultimate analysis (wt%)[a, b]		
C	87.5	45.3
H	6.5	5.3
O[c]	3.5	46.4
N	1.0	1.4
S	1.5	1.6
Lignocellulosic content (wt%)[a]		
Cellulose	–	33.1
Hemicellulose	–	12.3
Lignin	–	10.8

[a]Dry basis
[b]Ash free basis
[c]By difference

MC is 87.5 %, which is nearly twice as that of PP. PP has higher O content than MC. The total lignocellulosic content of PP was only 56.2 % because PP has higher ash content (21.2 %) and other organic constituents such as tannin, ester and so on [19, 20].

Figure 33.1 shows the TG and DTG curves of PP and pure lignocellulosic constituents, i.e. cellulose, xylan and lignin. The weight loss rates of cellulose, xylan and lignin reach the highest value of 72.0, 10.7 and 28.5 %/min at 350, 278 and 504 °C respectively. Compared with the decomposition of pure lignocellulosic constituents, the three major peaks of DTG curve of PP are at 320, 349, and 488 °C. These are attributed to the decomposition of hemicellulose, cellulose and lignin respectively as shown in Table 33.2.

Ignition temperature, peak temperature and burnout temperature of PP, cellulose, xylan and lignin are shown in Table 33.2. Comparing the ignition temperatures of PP and pure lignocelluloses constituents, it is obvious that the xylan start to burn at a lower temperature of 247 °C. The ignition temperatures of cellulose and lignin are 341 and 458 °C respectively which are higher than that of xylan. The ignition temperature of PP is higher than that of pure xylan mainly because breaking the linkage between hemicellulose and cellulose needs more energy input. The burnout temperature of PP is 515 °C, which is higher than that of pure cellulose and xylan, but lower than that of pure lignin. During the combustion process, hemicelluloses and cellulose in PP burn first, and heat therefore generated would accelerate the burning of lignin in PP, which leads to a lower burnout temperature of PP compared with that of pure lignin. Therefore, the characteristic combustion parameters of PP are different to the pure lignocelluloses to a certain

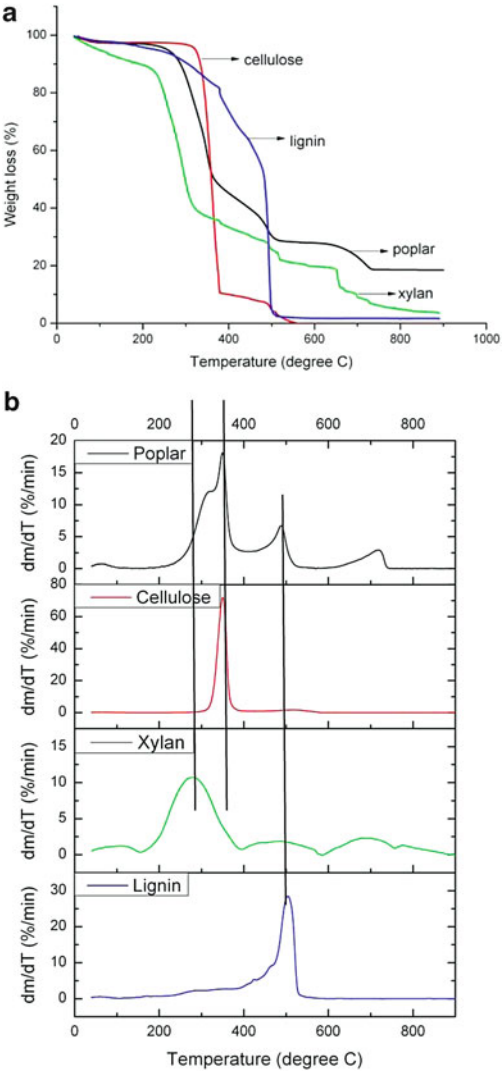

Fig. 33.1 Decomposition TG curve (**a**) and DTG curve (**b**) of PP and lignocelluloses

Table 33.2 Characteristics of TG and DTG profiles

	Ignition temperature (°C)	Peak temperature (°C)			Burnout temperature (°C)
		Hemicellulose	Cellulose	Lignin	
PP	297	320	349	488	515
Xylan	247	278	–	–	384
Cellulose	341	–	350	–	402
Lignin	458	–	–	504	533

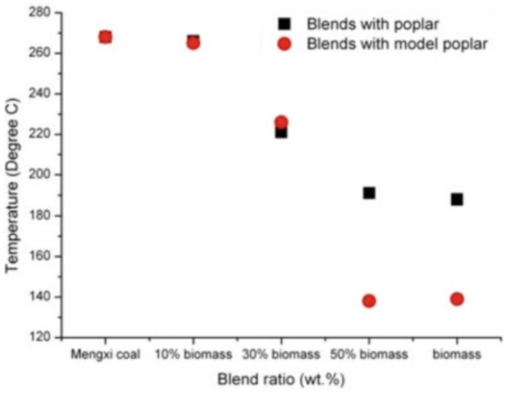

Fig. 33.2 Effect of blending on volatile release temperature

extent. The speculated reason for such deviation is that minerals in PP might have some catalytic effects.

Devolatilization usually takes place before ignition. As shown in Fig. 33.2, devolatilization of PP and mPP starts at 188 and 139 °C respectively. Both of them have much lower devolatilization temperature than MC because of higher volatile content of biomass and more easily decomposed constituents like cellulose and hemicelluloses in biomass [3]. With biomass blending ratio increasing, the devolatilization temperature decreases and levels off when the biomass content is greater than 50 %. Blends of PP and mPP almost have the same devolatilization temperature when biomass contents are smaller than 30 %. Once the biomass content in blends is greater than 30 %, the blends with model biomass have much lower devolatilization temperature compared with the blends with actual PP. The main difference between actual PP and model PP is their mineral contents. It is very likely that some minerals in actual PP have some catalytic effects on the devolatilization process. This catalytic effect becomes more obvious when more than 50 % of actual PP is added in the blends, which raises the mineral content to a critical level.

Table 33.3 shows the TG and DTG curves of MC/PP and MC/mPP blends. From Table 33.3, it is clear that there are four stages of weight loss observed from TG and DTG profiles. The first stage corresponds to the moisture removal. The decomposing and combustion of cellulose and hemicellulose in blends is observed in the second stage. In the third stage, char and lignin combustion occurs, whilst at a temperature around 700 °C, the non-lignocellulose compound starts to burn, which is the fourth stage of the whole combustion process. However, there are three stages during co-combustion of MC, mPP and MC/mPP blends, which are as the same as the first three stages of the co-combustion of MC, PP and MC/PP blends. Comparing DTG curves of MC/PP blends with that of MC/mPP blends, it is evident that decomposing rate of MC/PP blends during co-firing process is lower than that of MC/mPP blend. This is likely due to the ash in actual biomass.

The findings reveal that devolatilization of actual PP takes place at a temperature (188 °C) higher than that of mPP, but lower than that of MC. However, both the

Table 33.3 TG and DTG curves of the co-combustion of MC/PP blends and MC/mPP blends

TG/DTG			TG/DTG		
MC		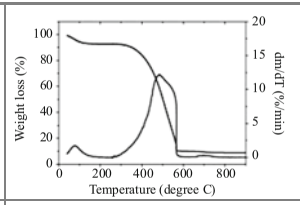	MC		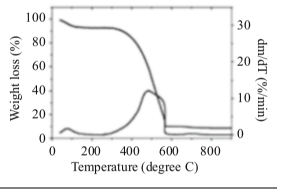
MC/PP blends	PP 10 %	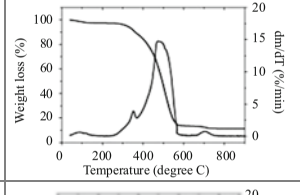	MC/mPP blends	mPP 10 %	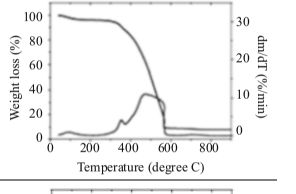
	PP 30 %	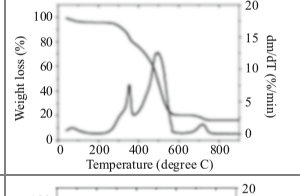		mPP 30 %	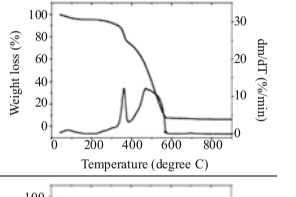
	PP 50 %	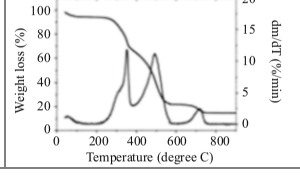		mPP 50 %	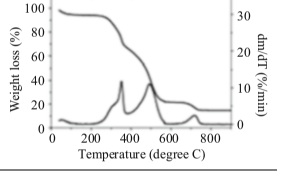

dm/dT (%/min)
30
20
10
0
Weight loss (%)
100
80
60
40
20
0
0
200
400
600
800
Temperature (degree C)

mPP

dm/dT (%/min)
20
15
10
5
0
Weight loss (%)
100
80
60
40
20
0
0
200
400
600
800
Temperature (degree C)

PP

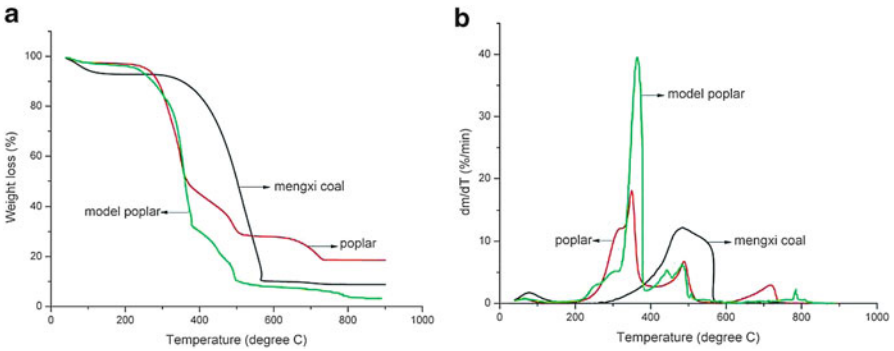

Fig. 33.3 TG curve (**a**) and DTG curve (**b**) of MC, PP, and mPP

Table 33.4 Characteristics of TG and DTG profiles

	Volatile release temperature (°C)	Ignition temperature (°C)	Peak temperature (°C)			Burnout temperature (°C)
			Peak 1	Peak 2	Peak 3	
MC	268	403	–	487	–	566
PP	188	297	349	488	718	515
mPP	139	333	364	484	–	508

ignition temperature and peak temperature of PP are lower than those of mPP and MC (as shown in Fig. 33.3a and Table 33.4). The MC starts burning at a temperature around 403 °C, which is higher than that of the actual biomass, which indicates that the combustion of coal and biomass does not take place simultaneously. From Fig. 33.3b, it is clear that the weight loss rate of MC reaches a peak of 12.2 wt%/min at a higher temperature of 487 °C. The highest weight loss rate of PP (18.8 %/min) occurs at 350 °C. At 488 °C, lignin of PP reaches its highest decomposition rate, which is very similar as that of the MC.

Compared the combustion of model biomass with actual biomass, it can be seen that ash in actual biomass has some catalytic effects on its combustion. It is shown in Fig. 33.3b and Table 33.4 that the peak temperature of mPP is 364 °C due to the decomposition of cellulose, which is higher than that of PP with a peak temperature around 350 °C. The other peak temperature for both mPP and PP is around 480 °C. The exact peak of hemicellulose in mPP or PP is not distinguishable because the decomposition of hemicellulose and cellulose occurs simultaneously. The highest weight loss rate of mPP (39.4 %/min) is higher than the rate of actual PP (18.8 %/min). Therefore, it is speculated that the ash matter in PP lowers the decomposition rate of cellulose. Furthermore, ash matter in actual PP also decreases the ignition temperature, peak temperature and burnout temperature of actual PP.

The ignition temperatures of MC/PP blends and MC/mPP show different trends with the increase in the biomass contents as shown in Fig. 33.4. When blending ratio is smaller than 30 %, the ignition temperatures of MC and actual PP blends change slightly around 400 °C, whilst the ignition temperatures of MC and model PP decrease from 400 to 330 °C. When the blending ratio is greater than 30 %, there

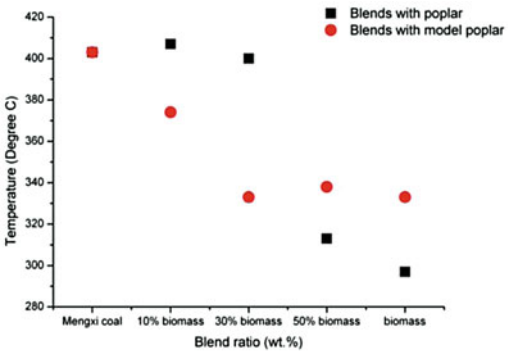

Fig. 33.4 Effect of blending on ignition temperature

Table 33.5 Peak temperatures of the combustion of MC/PP blends and MC/mPP blends

	MC blends					
	PP			mPP		
	10 %	30 %	50 %	10 %	30 %	50 %
Peak temperature (°C) (cellulose + hemicellulose)	354	354	353	356	362	365
Weight loss rate (%/min) (cellulose + hemicellulose)	3.9	7.7	11.8	4.1	12.2	19.1
Peak temperature (°C) (lignin + MC)	481	492	492	475	470	489
Weight loss rate (%/min) (lignin + MC)	14.7	12.5	11.2	11.0	12.3	11.5
Peak temperature (°C) (non-lignocellulosic compound)	706	718	716	–	–	–
Weight loss rate (%/min) (non-lignocellulosic compound)	0.7	1.5	2.5	–	–	–

is a significant decrease in ignition temperature of blends with actual PP. However, the ignition temperatures of blends of MC with model PP level off at around 330 °C. It is obvious that more actual PP blended with coal helps to initiate the ignition of the blends. Furthermore, with higher blend ratio than 30 %, blends with PP have lower ignition temperatures than blends with model biomass. Since ash in actual PP may have a catalytic effect on the combustion process which makes the ignition of blends with higher biomass blending level take place easily at lower temperatures.

The peak temperatures of different blends are listed in Table 33.5. The peaks of DTG curves are found around 360, 480, and 710 °C, which correspond to the decomposition of cellulose & hemicellulose, lignin & MC and non-lignocellulosic compound respectively. With the increasing actual PP or model PP contents of the blends, the weight loss rate of cellulose and hemicellulose increases from 3.9 % to 11.8 %/min for MC/PP blends and from 4.1 % to 19.1 %/min for MC/mPP blends separately. The weight loss rate of cellulose and hemicellulose in MC/mPP blends is higher than the rate of MC/PP blends in similar biomass blending level. However,

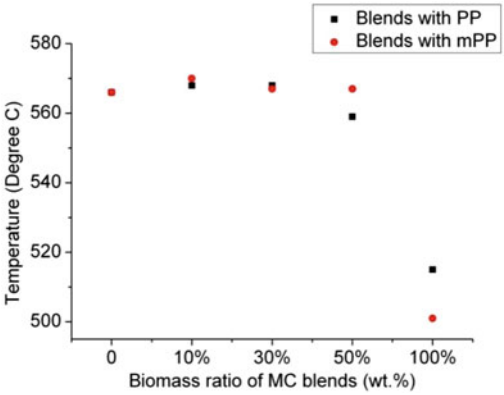

Fig. 33.5 Effect of blending on burnout temperature

Table 33.6 Kinetic parameters of TGA analysis

MC blends		Region 1		Region 2		Region 3	
PP or mPP ratio	MC ratio	E (kJ/mol)	A (min^{-1})	E (kJ/mol)	A (min^{-1})	E (kJ/mol)	A (min^{-1})
0	100 %	–	–	74.04	2.6836E6	–	–
PP 10 %	90 %	126.26	4.6744E12	72.27	2.5201E6	320.60	1.1439E18
PP 30 %	70 %	110.70	1.9067E11	80.53	9.2048E6	277.84	5.9234E15
PP 50 %	50 %	96.77	1.2409E10	80.686	9.3221E6	294.09	5.9138E16
PP 100 %	0	81.44	4.5992E8	74.61	3.8248E6	279.87	2.2589E16
mPP 10 %	90 %	93.22	4.5409E9	77.25	4.9093E6	–	–
mPP 30 %	70 %	92.94	3.9621E9	81.53	8.9519E6	–	–
mPP 50 %	50 %	87.54	1.1774E9	89.89	3.2486E7	–	–
mPP 100 %	0	77.50	2.0532E8	153.60	2.4600E12	–	–

the weight loss rate of lignin & MC in MC/PP blends decreases when the content of actual PP in MC/PP blends varies from 10 to 50 %. The weight loss rate of lignin & MC in MC and model PP blends firstly increases from 11.2 to 12.3 % and then decreases to 11.5 % as the content of mPP in MC/mPP blends increases from 10 to 50 %. There is no obvious difference in terms of peak temperatures regardless of the type and percentage of the biomass in the blends.

As shown in Fig. 33.5, the burnout temperature of the blends at low blending level is almost the same as that of the coal. However, the burnout temperature of MC/PP blends decreases from 570 to 515 °C when PP ratio increases from 50 to 100 %. When mPP ratio in the blends is greater than 50 %, the burnout temperature of the blend decreases rapidly from 570 to 500 °C. Therefore, it seems that at low blending level, the burnout temperature is not affected by the type of biomass being blended in the mixture, which is different from the work of Biagini et al. [21].

The values of E and A of the combustion of coal and biomass blends are calculated following the methods described elsewhere [5, 6]. The results are listed in Table 33.6.

The combustion of MC takes place between 230 and 630 °C so that there is only one region for MC. For PP, mPP and MC/mPP blends, there are two main regions due to the decomposition of cellulose and the simultaneous burning of lignin and coal, which are between 410–560 °C and 560–750 °C for PP, 190–390 °C and 390–500 °C for mPP, 205–390 °C and 370–600 °C for MC/mPP blends, respectively. MC/PP blends has three stages during co-combustion, which are approximate190–380 °C (Region 1), 370–625 °C (Region 2) and 600–775 °C (Region 3) dependent on the ratio of biomass in blends.

At lower temperatures, the values of E and A in region 1 decrease with the increasing percentage of PP or mPP in the blends. It is generally the case that blends with higher biomass ratio are more easily to realise volatiles and start to burn. In region 1, E and A of the blends with actual PP are higher than those of the blends with mPP at same blending level, which indicates that the ash in PP reduces the reactivity of the blends at lower temperature range due to ash inhibition effect [22]. However in main combustion region 2, blends with PP have lower E than blends with mPP at same blending level. Co-combustion of blends with actual PP takes place more easily than blends with mPP. Therefore, ash in PP lowers the E of combustion of MC/PP blends. The blends with PP has region 3 at higher temperature due to the stable non-lignocellulose compound in PP. These improvements in this section highlight the influence of PP ash on co-combustion with MC, which gives a favourable guide to practical application.

33.4 Conclusions

- During the combustion of PP process, the weight loss rates of hemicellulose, cellulose and lignin components reach the highest value, at the temperature of 320, 349, and 488 °C, respectively.
- Minerals in actual PP have some catalytic effects on the devolatilization process.
- Ash in actual biomass raises decomposing rate of MC/PP blends during co-firing process compared with that of MC/mPP blends.
- Ash matter in actual PP also decreases the ignition temperature and peak temperature of actual PP.
- Ash in actual PP may have a catalytic effect on the combustion process which makes the ignition of blends with higher biomass blending level take place easily at lower temperatures.
- There is no obvious difference in terms of peak temperatures regardless of the type and percentage of the biomass in the blends.
- Burnout temperature is not affected by the PP blending at low blending level which is very much helpful to co-firing application.
- In main combustion during 370–625 °C, blends with PP have lower E than blends with mPP at same blending level. Co-combustion of blends with actual PP takes place more easily than blends with mPP since catalytic effect of ash in PP lowers the E of combustion of MC/PP blends.

Acknowledgment Ministry of Science and Technology of China (Grant No. 2008DFA61600), Bureau of Science and Technology of Ningbo City (Grant No. 2008B10048) and Ningbo Municipal Innovation Team on WEEE Recycling Technologies (Grant No. 2012B82011) are acknowledged for the financial support to this study. The University of Nottingham Ningbo China is also appreciated for providing Scholarship to Ph.D. students involved in this work.

Nomenclature

A Pre-exponential factor (min^{-1})
A Remaining quota of residuals (%)
E Activation energy (kJ/mol)
K Decomposition rate (%/min)
R Universal gas constant (8.314 kJ/K/mol)
T Absolute temperature (K)

References

1. Varol M, Atimtay AT, Bay B, Olgun H (2010) Investigation of co-combustion characteristics of low quality lignite coals and biomass with thermogravimetric analysis. Thermochim Acta 510(1–2):195–201
2. Loo SV, Koppejan J (2008) The hand book of biomass combustion and co-firing. Earthscan, London, pp 203–206
3. Gil MV, Casal D, Pevida D, Pis JJ, Rubiera F (2010) Thermal behaviour and kinetics of coal/biomass blends during co-combustion. Bioresour Technol 101(14):5601–5608
4. Yuzbasi NS, Selçuk N (2011) Air and oxy-fuel combustion characteristics of biomass/lignite blends in TGA-FTIR. Fuel Process Tech 92(5):1101–1108
5. Wang CP, Wang FY, Yang QR, Liang RG (2009) Thermogravimetric studies of the behavior of wheat straw with added coal during combustion. Biomass Bioenerg 33(1):50–56
6. Song ZL, Zhao XQ, Ma CY, Wang T, Li LZ (2009) Kinetics of pyrolysis of straw bales by microwave heating. 2009 Asia-Pacific Power and Energy Engineering Conference, Ieee, New York, p 469–473
7. Muthuraman M, Namioka T, Yoshikawa K (2010) Characteristics of co-combustion and kinetic study on hydrothermally treated municipal solid waste with different rank coals: a thermogravimetric analysis. Appl Energ 87(1):141–148
8. Vamvuka D, Pitharoulis M, Alevizos G, Repouskou E, Pentari D (2009) Ash effects during combustion of lignite/biomass blends in fluidized bed. Renew Energy 34(12):2662–2671
9. Li XG, Lv Y, Ma BG, Jian SW, Tan HB (2011) Thermogravimetric investigation on co-combustion characteristics of tobacco residue and high-ash anthracite coal. Bioresour Technol 102(20):9783–9787
10. Sahu SG, Sarkar P, Chakraborty N, Adak AK (2010) Thermogravimetric assessment of combustion characteristics of blends of a coal with different biomass chars. Fuel Process Tech 91(3):369–378
11. Li XG, Ma BG, Xu L, Hu ZW, Wang XG (2006) Thermogravimetric analysis of the co-combustion of the blends with high ash coal and waste tyres. Thermochim Acta 441 (1):79–83

12. Muthuraman M, Namioka T, Yoshikawa K (2010) A comparative study on co-combustion performance of municipal solid waste and Indonesian coal with high ash Indian coal: a thermogravimetric analysis. Fuel Process Tech 91(5):550–558
13. Steenari BM, Lindqvist O (1999) Fly ash characteristics in co-combustion of wood with coal, oil or peat. Fuel 78(4):479–488
14. Hanaoka T, Inoue S, Uno S, Ogi T, Minowa T (2005) Effect of woody biomass components on air-steam gasification. Biomass Bioenerg 28(1):69–76
15. CEN/TS 15443 (2006) Solid recovered fuels: methods for the preparation of the laboratory sample. CEN, Brussels, Belgium
16. BS ISO 17246 (2010) Coal: proximate analysis, 2nd edn. BSi, London, UK
17. Omar R, Idris A, Yunus R, Khalid K, Aida Isma MI (2011) Characterization of empty fruit bunch for microwave-assisted pyrolysis. Fuel 90(4):1536–1544
18. Lester E, Cloke M (1999) The characterisation of coals and their respective chars formed at 1300 °C in a drop tube furnace. Fuel 78(14):1645–1658
19. Fierer N, Schimel JP, Cates RG, Zou J (2001) Influence of balsam poplar tannin fractions on carbon and nitrogen dynamics in Alaskan taiga floodplain soils. Soil Biol Biochem 33(12–13):1827–1839
20. Sun RC, Sun XF, Wang SQ, Zhu W, Wang XY (2002) Ester and ether linkages between hydroxycinnamic acids and lignins from wheat, rice, rye, and barley straws, maize stems, and fast-growing poplar wood. Ind Crop Prod 15(3):179–188
21. Biagini E, Cioni M, Tognotti L (2005) Development and characterization of a lab-scale entrained flow reactor for testing biomass fuels. Fuel 84(12–13):1524–1534
22. Hurt R, Sun JK, Lunden M (1998) A kinetic model of carbon burnout in pulverized coal combustion. Combust Flame 113(1–2):181–197

Chapter 34
High-Performance Recycling System for Waste Plastics Using Raman Identification

Hirofumi Kawazumi, Akihiro Tsuchida, Tomoya Yoshida, and Yasuo Tsuchida

Abstract Raman spectroscopy has potential for application to waste plastic recycling when large-scale, accurate sorting processes are required. We developed a high-speed Raman identifier with a 3-ms measuring time. This identifier was successfully integrated with an on-line sorting system in a shredded plastic recycling plant. A practical-scale (200–600 kg/h) demonstration facility was constructed with 50 Raman apparatuses on a 30-cm-wide conveyor (speed: 100 m/min). This facility included preprocessing using specific gravity classification and putty removal. The Raman identification system was used to control air jets to sort polypropylene, polystyrene and acrylonitrile-butadiene-styrene copolymer with high accuracy from shredded plastics from post-consumer electrical appliances. Raman plastic identification can also provide solutions to problems at recycling sites such as the detection of brominated flame-retardants and the identification of black plastics.

Keywords Waste plastic sorting • Raman spectroscopy • Closed loop recycling

34.1 Introduction

Globally, plastic recycling is an important issue because the basic resource for most plastics is petroleum. Recycling can save oil resources and reduce emissions of carbon dioxide. There are several approaches to plastic recycling, e.g., thermal, chemical and mechanical. Among these, mechanical recycling is the most effective in reducing the environmental burden [1]. Mechanical recycling is categorized into two processes: open- and closed-loop recycling. Open-loop recycling is currently

H. Kawazumi (✉)
School of Industrial Technology, Kinki University, Iizuka, Fukuoka 820-8555, Japan
e-mail: kawazumi@fuk.kindai.ac.jp

A. Tsuchida • T. Yoshida • Y. Tsuchida
Saimu Corporation, Keisen, Fukuoka 820-0609, Japan
e-mail: akihiro@saimu-net.ne.jp; t.yoshida@saimu-net.ne.jp; yasuo@saimu-net.ne.jp

I. Dincer et al. (eds.), *Progress in Sustainable Energy Technologies Vol II: Creating Sustainable Development*, DOI 10.1007/978-3-319-07977-6_34

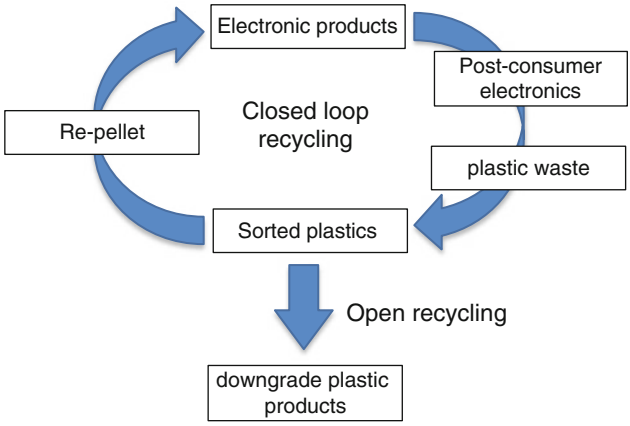

Fig. 34.1 Mechanical recycling of plastics in home electric appliances

the most commonly applied and produces low-grade plastic commodities from low-purity and mixed plastic pellets. Closed-loop recycling is an innovative recycling procedure that has recently been developed. Highly purified post-consumer plastic pieces are transformed into regenerated products related to the original products by using well-designed collection schemes and state-of-the-art sorting and refining technology, as shown in Fig. 34.1. In Japan, the law encourages the recycling of resources from post-consumer electrical appliances and states that air-conditioners, refrigerators, TVs and washing machines must be collected by their distributors and sent to recycling plants operated by electronics companies. In total, 0.64 million tons of appliances were collected in 2009. In such legally mandated recycling, the types of waste plastics involved are relatively few and their chemical composition is relatively uniform [2, 3]. Therefore, there is a high demand for closed-loop recycling.

Currently, a major sorting technique is float–sink and/or pneumatic classification based on density differences. However, these approaches do not offer adequate performance for closed-loop recycling. The homogeneity of the collected plastics should be more than 95 % to maintain the characteristics of virgin plastics. To increase the purity of sorted plastic waste, some optical identification techniques are required. In this paper, we demonstrate the applicability of Raman spectroscopy to industrial-scale waste plastic recycling that requires high-speed, on-line technology. We developed a compact, rapid and viable Raman identifier with specifications suitable for post-consumer plastics recycling sites. This identifier also has potential to solve the problems of detecting brominated flame retardants and identifying black plastics. These are serious problems at plastic recycling sites because some brominated compounds are regulated pollutants as defined in the Restriction of the Use of Certain Hazardous Substances in Electrical and Electronic Equipment (RoHS) directive of the European Union, and no practical identification technique exists for sorting black or deeply colored plastics. The Raman technique,

which is based on vibrational spectroscopy, can identify the components in plastics and can therefore detect brominated compounds at the time of sorting. Our compact apparatus was able to obtain Raman spectra from black plastics to facilitate plastic sorting.

34.2 Raman Spectroscopy for Plastic Recycling

The currently available optical techniques for automatic plastic identification are summarized in Table 34.1. Vibrational spectroscopy, including infrared absorption (IR), near-infrared diffuse reflectance (NIR) and Raman scattering measurements, is one of the most sophisticated candidates in terms of reliability because it provides molecular structural information. Laser-induced plasma spectroscopy has recently been announced as a key technology in a portable identifier [4]. X-ray fluorescence analysis is commonly used to detect metal pieces in the food industry and halogenated compounds in plastics recycling.

The spectra of polystyrene (PS) obtained using the standard measuring instruments of the three vibrational spectroscopy methods are compared in Fig. 34.2. In laboratories, IR measurement is a standard method for analyzing molecular structures and to identify various kinds of plastics. Raman scattering measurement provides similar information about molecular structures. Although the sensitivity and sample handling are improved by using Fourier-transform infrared spectroscopy (FT-IR), the severe limitations of IR outlined in Table 34.1 are evident when it is used for large-scale waste plastic sorting. NIR is used in sorting systems in both large [5] and portable identification apparatuses [6] because light near the visible region can be rapidly detected with great sensitivity and at reasonable cost.

Table 34.1 Comparison of optical plastic identification techniques

Technique	Features	Limitations
Raman	Reliable identification for a wide range of plastics with sharp peak appearances	Weak Raman scattering intensity. Less popularity and know-how for the plastic sorting
IR	Reliable identification for a wide range of plastics with accumulated database and know-how	Difficulties of non-contact measurements for solid polymers Necessity of reference signal Sensitive to roughness and wetness of the surface
NIR	Fast identification for major plastics. Time-tested performance to massive sorting for plastics and paper	Low accuracy due to broad spectra. Not able to identify dark color plastics
LIPS	Rapid characterization for the components of the plastics including halogen elements	No performance and accuracy test in practical applications Necessity of pulsed high-power laser
XRF	Commonly used to detect bromine in any plastics	Only for bromine detection, not for plastic identification

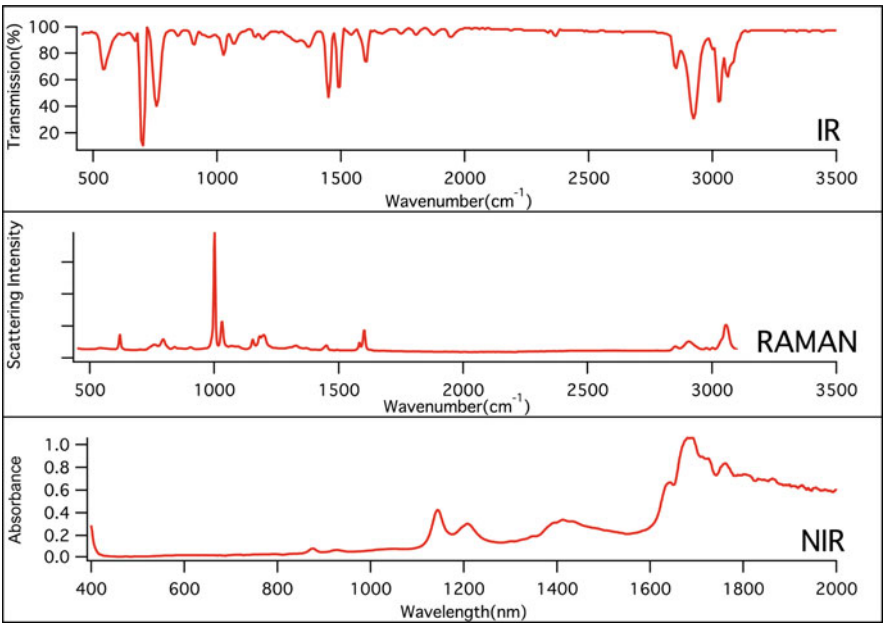

Fig. 34.2 Spectra of PS in various spectroscopies. IR; Shimadzu IRPrestige-21 with Ge ATR prism. RAMAN; Thermo Scientific DXR Smart Raman. NIR; Jasco UV–VIS-NIR spectrophotometer V-670

However, NIR identification is less accurate because of its broad spectrum, as shown in Fig. 34.2. Furthermore, strong water absorption at 1.4 and 1.9 μm obscures the NIR spectrum.

Raman spectroscopy is used with microscopes for local analysis in biological and materials research because of the high spatial resolution of laser excitation compared with IR spectroscopy. In addition, Raman spectroscopy has other advantages for practical application in the sorting of post-consumer plastics. These advantages are:

1. Raman spectra present sharp peaks, making identification more accurate, easier and faster.
2. Signal intensity is proportional to the excitation light intensity. Although Raman scattering is known as a small probability phenomenon, high-power-laser irradiation provides adequate signal intensity even with short measuring times.
3. The Raman scattering phenomenon is less sensitive to the direction of the detector and to the sample surface condition such as its roughness.
4. Even black plastics provide a scattering signal that can be used for identification. Non-contact measurement is practicable for plastic chips moving on a conveyor. In contrast, tight contact measurement using the attenuated total reflection (ATR) method is essential in FT-IR, and no reflectance signal occurs from black surfaces in NIR.

5. The Raman technique requires no reference signal.
6. Raman spectra are not disturbed by water or CO_2 absorption.

A few papers and patents were found that discuss the application of Raman spectroscopy to plastic identification [7, 8]. However, Raman identification is currently less popular than NIR for plastic sorting. Recently, compact, low-cost Raman apparatuses have been commercialized as a result of improvements in optical communication devices such as solid-state lasers and optical filters. These improvements encouraged us to develop a Raman-based plastic identification and sorting system for industrial use.

34.3 Raman Plastic Identifier

We developed two types of specialized Raman identifier for application to waste plastic recycling. One is a thin box unit (32 cm × 55 cm × 4 cm) for fast, on-line identification. Its thin shape makes it possible to set up a battery of Raman spectrometers above a conveyer to improve the throughput. The other unit is a portable apparatus (23 cm × 35 cm × 12 cm) for precise identification in off-line use. The basic optical configuration is the same for the two types of identifier. The excitation laser is focused on the surface of the plastics and the scattered light is collected coaxially by the same lens (focal length: 30 mm, N.A.: 0.22). A sufficient Raman signal was obtained even at a distance of 10–50 mm from the plastic surface.

The Raman identifier consists of a 785-nm high-power diode laser operated at 2 W and a back-thinned FFT-CCD detector (Hamamatsu Photonics S7030, Hamamatsu, Japan) with 1,024 pixels corresponding to a Raman shift of 200–2,500/cm. The accumulated charges produced by photons in the 58 longitudinal pixels are binned further into the last pixel line to improve sensitivity. The optical system was designed to achieve high optical throughput at the appropriate resolution of 20/cm. The laser focusing can detect shredded plastic pieces of less than 1 cm in diameter. A data analysis system is embedded in a field programmable gate array circuit (FPGA) that is used instead of a CPU to reduce the signal processing time. Consequently, the Raman shift in the spectrum shows in the pixel number of the CCD detector.

34.4 Results and Discussion

34.4.1 Industrial-Scale Plastic Sorting

Over 3 years, Saimu Corporation constructed a demonstration facility in Osaka, Japan, featuring an automatic identification and sorting system for shredded plastics

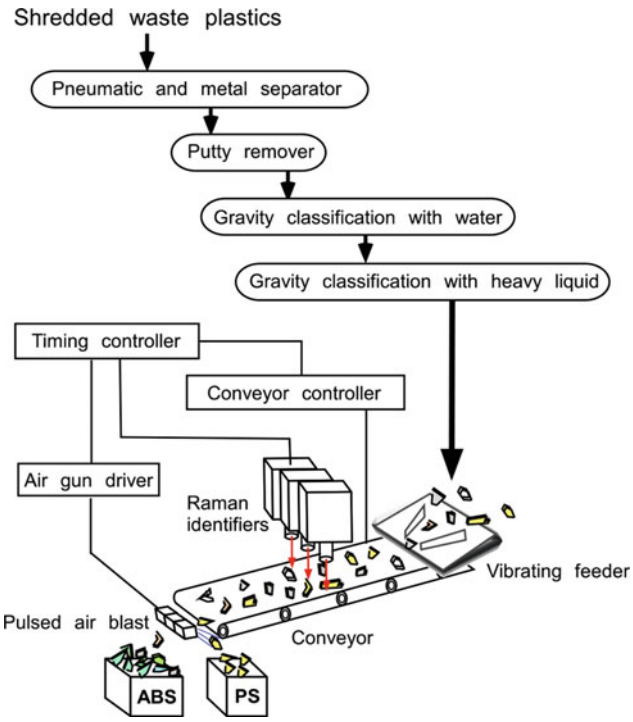

Fig. 34.3 Schematic diagram of massive plastic sorting system

from post-consumer electric appliances. The shredded plastics are produced within a recycling facility where large plastic and metal components are dismantled and collected. The shredded plastic pieces from refrigerators, washing machines and air-conditioners are mostly white and consist of three major plastics, polypropylene (PP), polystyrene (PS) and acrylonitrile–butadiene–styrene copolymer (ABS), and other plastics such as polyvinylchloride (PVC), styrene foam, wiring, rubber and putty. For closed-loop recycling, plastic compound companies require the sorted plastics to have greater than 95 % homogeneity.

Figure 34.3 shows the schematic of the large-scale plastic sorting system including 50 on-line Raman apparatuses above a 30-cm-wide conveyor (speed; 100 m/min); in Fig. 34.3, only three Raman units are shown. The overall sorting process is as follows: styrene foam, dust and wiring are removed using a pneumatic separator; ferromagnetic metal is removed using a magnetic separator; and putty is removed using our proprietary remover equipped with needles. Then, the plastic mixture is roughly classified into PP and PS/ABS fractions in a water tank based on the differences in specific gravity. Next, PVC and other heavy plastics are separated from PS/ABS. Finally, the plastic pieces are fed to the system that uses the Raman identifiers to improve the purity of PP or to classify PS and ABS. At the end of the conveyor an array of pulsed air blasts directs the selected plastics into

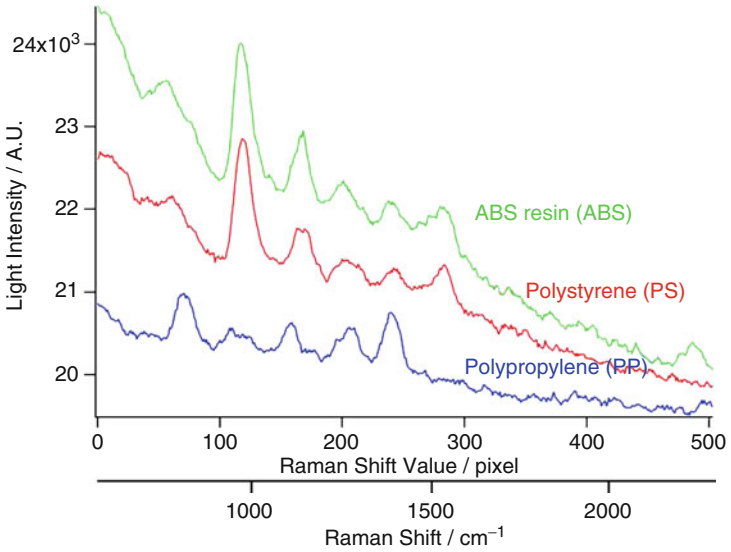

Fig. 34.4 Raman spectra of plastics in 3-ms measurement; the sample is moving on conveyer at 100 m/min

the appropriate container. The 50 Raman identifiers work in parallel on one conveyor lane for shredded plastic pieces 5–20 mm in diameter and can process 200–600 kg/h.

This large-scale, accurate sorting system requires the acquisition of Raman spectra with adequate signal-to-noise ratios in a short measuring time, as shown in Fig. 34.4. The spectra of the three major plastics exhibit distinctive peaks in the 3-ms measurement. The plastic pieces are moving on the conveyer at a speed of 100 m/min. The peak at 2,200/cm differentiates ABS from PS; these two plastics have similar spectra and are in the same specific gravity fraction, and so are difficult to separate.

Figure 34.5 shows an example of the performance of our shredded plastic sorting system. The upper charts show the breakdown percentages before and after sorting for the suspended plastic fraction in the specific-gravity-separation water tank, and the lower charts show the same for the settled fraction. A final plastic purity of 98 % was obtained, and the main cause of the 2 % debasement was the air blasts missing their targets. The collected ABS was tested for its mechanical strength. Table 34.2 shows the physical properties of the collected (recycled) and virgin ABS test specimens. Strength deteriorates appreciably if new components are fabricated using waste plastics alone. However, the formability of recycled ABS as adequate to regenerate parts for electrical appliances, as shown in Fig. 34.6. Currently, two plastic compound companies add our sorted plastics to virgin material to reduce their raw material costs.

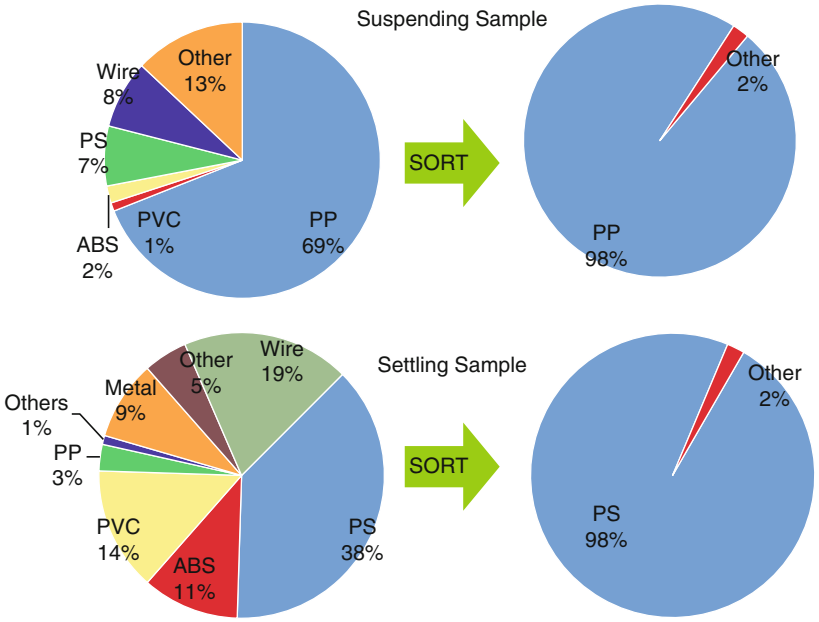

Fig. 34.5 Performance of the waste plastic sorting system based on Raman spectroscopy; samples from the specific gravity classification with water

Table 34.2 Physical properties of ABS test specimens

	Collected ABS	Virgin ABS
Dynstat impact test (Kg cm/cm^2)	10.3	65.6
Tensile strength (MPa)	37.40	49.14
Deformation at break (%)	58.4	141.8
Flexural strength (Mpa)	59.08	73.12

Fig. 34.6 Formability of the recycled plastics

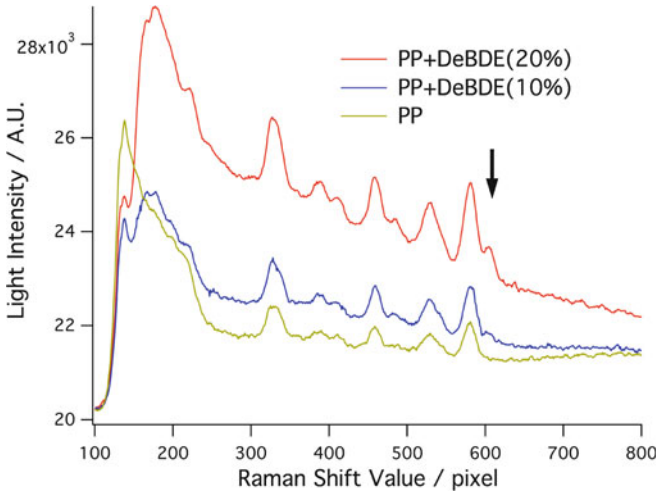

Fig. 34.7 Raman spectra of PP containing DeBDE; the *arrow* indicates a peak assigned bromine compound

34.4.2 Precise Identification

The large-scale sorting system that we have developed can currently be applied to white shredded plastics. However, the recycling sites of post-consumer plastics need more precise identification of a broader range of plastics. The most pressing requirement is the detection of plastics containing brominated flame retardants because of the RoHS directive. A sorting technology based on X-ray absorption is being developed for the detection of bromine in plastics [9]. Our portable Raman identifier can distinguish the components of the plastics and so can detect brominated compounds at the same time. Figure 34.7 shows the Raman spectra of PP containing decabromodiphenyl ether (DeBDE) with a measurement time of 100 ms. A clear peak of DeBDE appears among the peaks of PP. More than 3 wt% of DeBDE was detected. This level of sensitivity is sufficient for plastic sorting because brominated flame retardants are added to products at up to about 10 wt% to resist heat and fire.

This Raman technique might be useful for the identification of black plastics. The only other available technique of ATR infrared spectroscopy is not appropriate for plastic sorting because of the large laboratory-oriented equipment and the necessity of close contact to the ATR prism. Figure 34.8 shows the Raman spectra of black PP, PS and ABS with a measurement time of 0.5 s. These plastics contained 0.5 % carbon black. The background in the spectra increases in the whole region with decreasing scattering intensity, and a broad peak at around 500 pixels appears from the amorphous carbon black. However, we were able to distinguish some characteristic peaks for plastic identification, and we successfully developed a smart identification algorithm for use with the portable Raman apparatus.

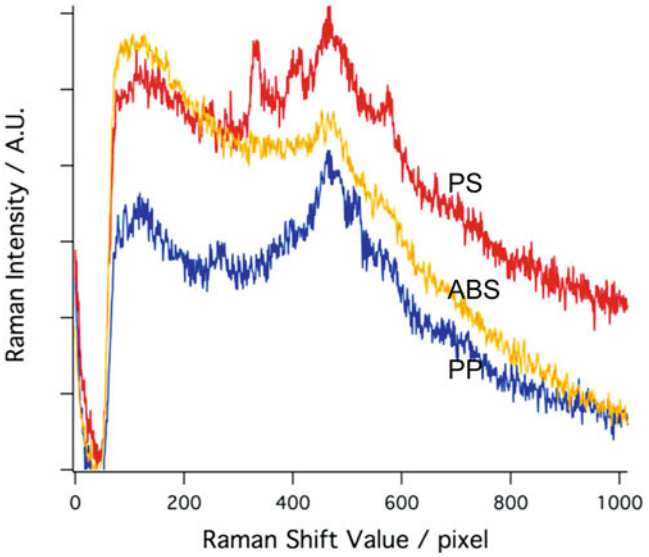

Fig. 34.8 Raman spectra of black-colored plastics included 0.5 % carbon black

34.5 Conclusions

In this paper we successfully demonstrated the applicability of Raman spectroscopy to industrial-scale post-consumer plastic sorting with acceptable performance for commercial application. The demonstration facility was operated stably for 1 year. We perform suitable pre-treatments for the Raman identification system for any standard of waste plastics and have accumulated much practical knowledge for application to waste plastic sorting. This identification technique based on Raman scattering could be applied to waste plastics not only from electrical appliances but also from Information and Communication Technology equipment and automobiles. Large-scale recycling of these plastics will save vast amounts of resources and energy.

Acknowledgements This work was supported by Grant-in-Aid for Scientific Research (B) 22510092. The authors have received financial support from The Ministry of Economy, Trade and Industry of Japan.

References

1. Lazarevica D, Aoustin E, Buclet N, Brandt N (2010) Plastic waste management in the context of a European recycling society: comparing results and uncertainties in a life cycle perspective. Resour Conservat Recycl 55:246–259
2. Dodbiba G, Takahashi K, Sadaki J, Fujita T (2006) The recycling of plastic wastes from discarded TV sets: comparing energy recovery with mechanical recycling in the context of life cycle assessment. J Clean Prod 16:458–470

3. Qu X, Stuart Williams JA, Grant ER (2006) Viable plastics recycling from end-of-life electronics. IEEE Trans Electron Packag Manuf 29:25–31
4. Anzano J, Casanova ME, Bermúdez MS, Lasheras RJ (2006) Rapid characterization of plastics using laser-induced plasma spectroscopy. Polymer Test 25:623–627
5. http://www.pellencst.com/en/21/les-systemes-de-detection. Accessed 25 Jun 2012
6. http://www.iosys-seidel.de/en/mirogun.html. Accessed 25 Jun 2012
7. Allen V, Kalivas JH, Rodriguez R (1999) Post-consumer plastic identification using Raman spectroscopy. Appl Spectrosc 53:672–681
8. Sommer EJ, Rich JT (2001) Application of Raman spectroscopy to identification and sorting of post-consumer plastics for recycling. US Patent 6,313,423
9. Naka J, Tanimura J, Hirano N, Kinugawa M, Sirouzu T (2008) Detection method of Br in polymers and sorting apparatus. Japan Patent JP-A-2008-126892

Chapter 35
Clean Combustion of Low Quality Fuel in Fluidized Bed Combustor

Rami S. El-Emam, Farouk M. Okasha, and Salah H. El-Emam

Abstract Combustion characteristics for rice straw and mazut in a fluidized bed combustor have been investigated. Rice straw has been prepared as pellets in order to increase its bulk density and control feeding flow rate. Rice straw pellets have been burnt in bubbling fluidized combustor operating at atmospheric pressure. Over-bed fuel feeding of fuel is applied to provide steady condition of performance. Mazut combustion in the fluidized bed has been also investigated. In-situ desulfurization is considered for the case of mazut combustion. It is concluded that post-combustion of volatiles in the fluidized bed combustor results in a peak temperature values in the freeboard zone. The peak temperature value and position shifts based on the operating condition of the fluidized bed. Carbon monoxide and nitrogen oxides emissions are measured for the presented cases of fuel combustion. Nitrogen oxides emission measurements are reported as 175–270 ppm which is considered relatively low. The effect of fluidization velocity, static bed height and excess air on emissions of carbon monoxide and nitrogen oxides is also investigated. Improvement in combustion of mazut is achieved with the increase in bed temperature, static bed height, and with excess air. Adding limestone particles to the fuel caused sulfur retention up to 90 %.

Keywords Fluidized bed • Biomass • Rice straw • Mazut • Emissions

35.1 Introduction

Abundance of agriculture waste and residues are burnt haphazardly in Egypt, without energy recovery, causing severe pollution levels in the environment, especially after rice harvesting season which is the second most cultivated crop in Egypt.

R.S. El-Emam (✉)
Faculty of Engineering and Applied Science, University of Ontario Institute of Technology, Oshawa, Canada

Department of Mechanical Power Engineering, Mansoura University, Mansoura, Egypt
e-mail: Rami.Elemam@uoit.ca

F.M. Okasha • S.H. El-Emam
Department of Mechanical Power Engineering, Mansoura University, Mansoura, Egypt

I. Dincer et al. (eds.), *Progress in Sustainable Energy Technologies Vol II: Creating Sustainable Development*, DOI 10.1007/978-3-319-07977-6_35

Alternatively, utilizing agriculture waste as biomass driven fuel preserves the diminishing conventional fossil fuels and alleviates the growing waste disposal problem and results in a remarkable reduction in the emissions that have negative impact on the environment. According to the Egyptian Agriculture Engineering Researches Institute, the annual potential of agriculture wastes in Egypt is about 22.5 million ton. About 35 % of them are utilized as animal feeding and fertilizer and 65 % are available for energy production which is 7 million ton oil equivalent (TOE).

Due to their simplicity, fuel flexibility and higher efficiency, fluidized bed combustors are good candidates for handling agricultural residues and biomass driven fuel into useful energy. It is also a good candidate for heavy liquid fuel. Fluidized bed combustors operate at relatively low temperature values, compared with other combustion (FBC) technologies, which helps in minimizing the emissions for nitrogen oxides. A detailed case study provides insights to the technical specifications of the various equipment, systems and cost economics of fluidized bed combustion technology for cogeneration systems have been reported [1]. Co-generation through fluidized bed combustion boiler using biomass is considered a renewable clean technology which can also help in mitigation of greenhouse gas emissions.

Under similar operating condition, combustion process of rice straw is not experiencing different emissions and operating issues compared with wheat straw and rice husk. Pretreatment of biomass fuel is utilized to enhance the fuel properties. The two fundamental properties of rice straw analyzed by Kargbo et al. [2] are calorific and density values. They tested sizing and compression as utilized as pretreatment technologies. Results show that both physical and chemical properties of rice straw are improved significantly by the pretreatment technologies.

Srinath et al. [3] studied the combustion characteristics of rice husk in a rectangular fluidized bed and reported that maximum carbon monoxide concentration occurs at active combustion zone. Based on CO emission and unburned carbon content in fly ash, the combustion efficiency of the fluidized bed combustor was calculated for the rice husk fired under different operating conditions. The maximum combustion efficiency of the rice husk is found to be 95 %. Effect of adding rice straw to wood fuel on the combustion and emission characteristics is investigated by Thy et al. [4]. They reported that there is experimental evidence that the addition of straw to conventional biomass boiler fuels in some instances may reduce potassium fouling. Naik et al. [5] carried out an investigation to highlight the common biomass available in Canada such as wheat straw, barley straw, flax straw, timothy grass and pinewood. They studied the calorific values, ash, cellulose and hemicellulose contents in the studied samples. Their analyses showed that pinewood, wheat and flax have greater potential for bioenergy production.

Liquid biofuel combustion in fluidized bed is investigated experimentally by Miccio et al. [6]. They performed combustion of biodiesel and sunflower oil in a lab-scale internal circulating fluidized bed reactor (ICFB) for co-gasification of biomass and waste fuels or incineration of liquid wastes. The combustion of fuel vapors was managed to occur with a limited residence time by feeding the fuel the riser. They investigated the occurrence of the micro-explosive behaviour that was

observed in the combustion process. Combustion efficiency and carbon monoxide emissions were observed to be a little different between biodiesel and sunflower oil. A new possibility is envisaged for applications in which the released heat is directed at producing high temperature, high pressure fluid streams, taking advantage of the extremely high heat transfer coefficients in fluidized bed [7].

As rice straw represents a challenging issue of agriculture wastes in Egypt, the current study is concerned with investigating the combustion of rice straw in fluidized bed. It also presents combustion of mazut, as common heavy oil utilized in Egypt, in fluidized bed combustor. Mazut has relatively high sulfur content, as listed in Table 35.1, which causes negative environmental impact when combusted in conventional combustor. Hence, alternative combustion technologies should be implemented to limit the emissions level. The main objectives of this study are preparation of rice straw in adequate form of pellets, and assessment of FBC at different operating conditions with observation of the emissions of carbon monoxide and nitrogen oxides. Also sulfur retention is considered with adding calcium (limestone) when combustion of mazut is investigated.

35.2 Experimental Work

Atmospheric bubbling fluidized bed is considered in the proposed work. Figure 35.1 shows a schematic of the experimental test system. A detailed description of the test system, auxiliary components and pellets preparation can be found elsewhere [8, 9]. The combustor is a cylindrical column of 300 mm inner diameter and 3300 mm height. Primary air, which serves in fluidizing bed materials and burning fuel, provided through a nozzle type distributer. Continuous over-bed feeding is achieved using a paddle shaft which is driven by variable speed electric motor. A hopper on top of the combustor column is used for feeding the fluidized bed with sand particles. Flue gases pass through a cyclone to collect the entrained particulates. All parts of the fluidized bed column are insulated using blankets of thermal

Table 35.1 Fuel analysis and properties

	Rice straw	Mazut
Ultimate analysis (dry basis, %)		
Carbon	42.04	84.8
Hydrogen	6.26	11.59
Oxygen	39	–
Sulfur	0.64	3.21
Nitrogen	1.23	–
Ash	10.83	0.07
Properties		
Density, kg/m^3	0.9 (pellet)	946.1 (15.5 °C)
LHV, MJ/kg	19.441	40.820
Moisture	8.9 %	0.2 %

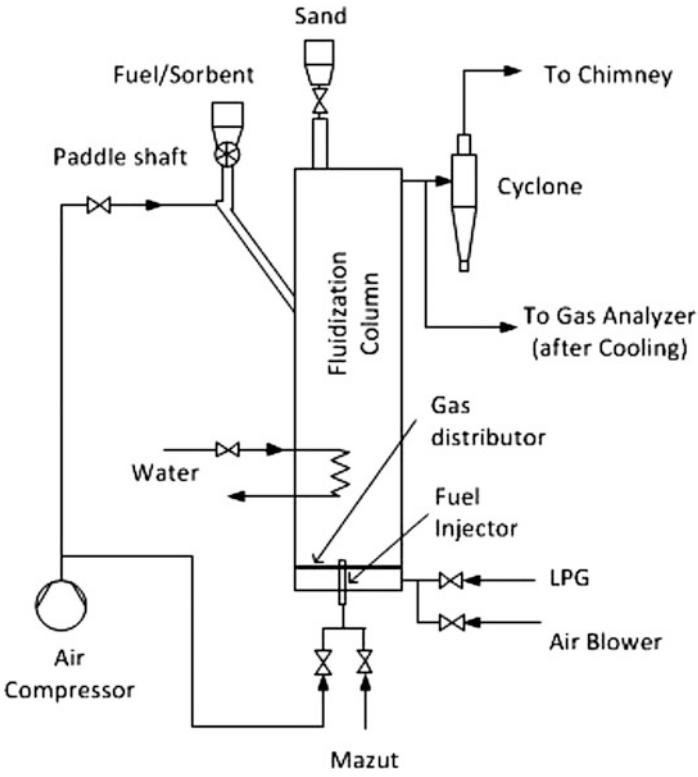

Fig. 35.1 Diagram of the test system equipped for pellets or mazut combustion

wool. Silica sand with of 0.25–0.5 mm is considered as bed material, which has minimum fluidization velocity of 5.6 cm/s at 850 °C. Pellets of rice straw are prepared by pressing chopped straw under 200 bar inside a die. The pellet are produced in 12 mm diameter and 10 mm length of cylindrical shape with bulk density of 0.9 g/cm^3 compared with 0.05 g/cm^3 as initial bulk density.

When liquid fuel is injected into a fluidized bed, residence time experienced with the fuel is short due to immediate evaporation. Consequently, rapid mixing of droplets and air is important. The fuel injector is fixed at the bottom of the combustor. It passes through the centerlines of the plenum chamber and the distributor plate to reach the fluidized bed. A detailed description of the mazut injector can be found elsewhere [10]. Analysis and properties of the used rice straw and mazut fuels are listed in Table 35.1. Calcium based sorbent is utilized with the combustion of mazut to facilitate the removal of sulfur dioxide from the combustion emissions. This is one of the advantages of using fluidized bed instead of conventional combustion technologies. Limestone particles with size of 0.5–0.8 mm are utilized in different molar ratios described by Ca/S ratio.

35.3 Results and Discussion

The experimental measurements and results of combustion of rice straw pellets and mazut are illustrated in this section. The temperature profiles through the fluidized bed height at different cases are also presented. Emissions and combustion efficiency are also presented. Effects of varying fluidization velocity, static bed height and excess air ratio on the combustion process are studied. A comparative analysis of combustion of both fuels is introduced based on the efficiency and emissions at different operating conditions.

35.3.1 Combustion of Rice Straw Pellets

The results representing the axial temperature profile show a uniform temperature through the bed zone. The temperature then starts increasing till a peak temperature is reaching in the freeboard zone. The position and degree of overheating is controlled by the operating parameters of the fluidized bed combustor. It is noticed that part of the volatile get into complete combustion in the freeboard zone where occurrence of flame is observed. This may have occurred because of lack of mixing with oxygen. In the following subsections, studies on effect of fluidized bed operating parameters are performed. When effect of one parameter is investigated, other parameters are kept as in the base case condition.

It is also noticed in the presented results that nitrogen oxides are relatively low. Through the combustion process, carbon monoxide reacts with the formed nitrogen monoxide forming elemental nitrogen. At the same time, with proceeding in the combustion process, the reduction of nitrogen oxide through reacting with char is getting lower [11, 12]. The results also report fixed carbon losses which is calculated as the rate of collected carbon, using the cyclone, to the total rate of fixed carbon feed in the fuel.

35.3.1.1 Effect of Fluidization Velocity

The effect of varying the fluidization velocity on temperature profile, emissions and combustion performance is presented in Figs. 35.2, 35.3, and 35.4. The results in Fig. 35.2 discuss the effect of fluidization velocity on the axial temperature profile of rice straw pellets combustion. It is noticed that at higher velocity, a more uniform temperature profile is achieved through bed and splashing zones. This is because of the higher rigorous bed particles mixing. The overheating is reported as 47.8, 68.9 and 87.12^{0}C at 0.3, 0.5, 0.7 m/s, respectively. From the temperature profiles, a shift in the peak temperature along freeboard zone height is noticed with increasing the velocity. The shorted gas residence time with higher velocity is probably responsible for this shift.

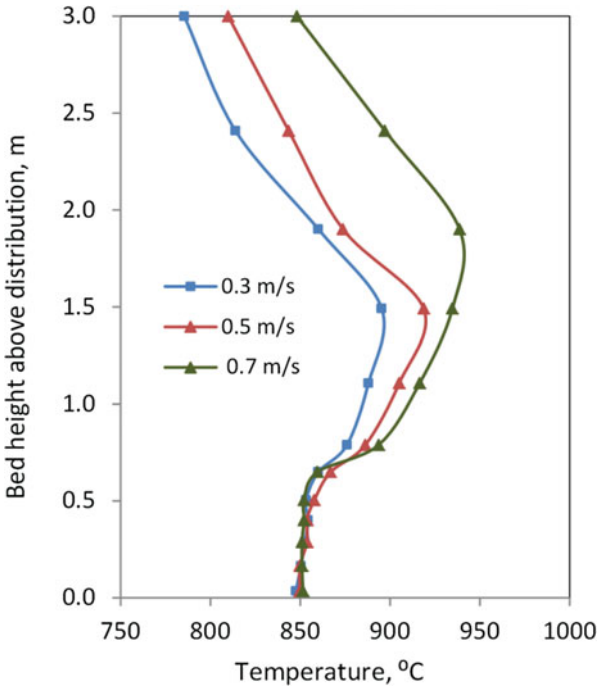

Fig. 35.2 Effect of fluidization velocity on the axial temperature profile for straw pellets combustion

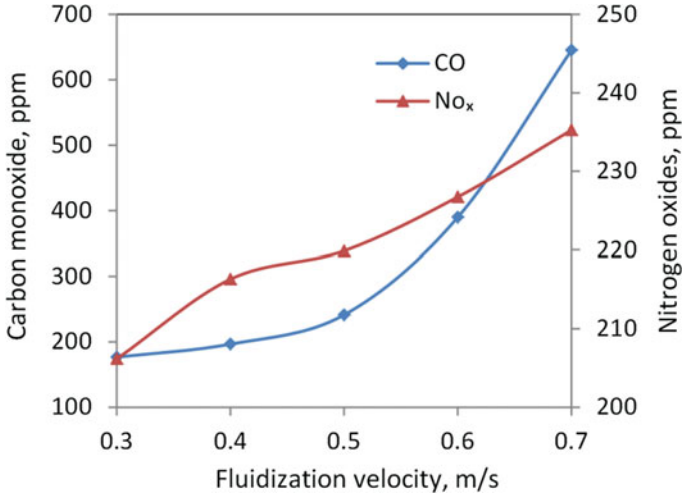

Fig. 35.3 Carbon monoxide and nitrogen oxides emissions of straw pellets combustion at different fluidization velocity values

Fluidization velocity has a noticeable effect on carbon monoxide emissions as seen in Fig. 35.3. At lower fluidization velocity, better combustion occurs where the mass transfer between the two phases, i.e.; bubble and emulsion, is enhanced with

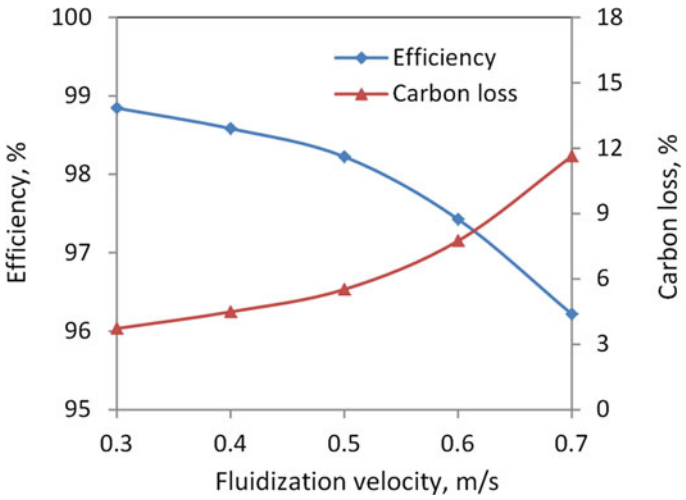

Fig. 35.4 Effect on fluidization velocity on straw pellets combustion efficiency and carbon loss percentage

the smaller bubbled produced at lower rising velocity. Also the residence time in bed and freeboard zone is longer with slower fluidization, this result in more reduction of carbon monoxide to form carbon dioxide. The results in Fig. 35.3 also show the change in nitrogen oxides with fluidization velocity. Nitrogen oxides are supposed to decrease with increasing the fluidization velocity as the more carbon monoxide formation, the more nitrogen oxides reduction. However, as a result of the less time available for the reduction reaction at high velocity, it appears that nitrogen oxides increase. Figure 35.4 shows the effect of fluidization velocity on the combustion efficiency and carbon loss. Efficiency values drop at higher velocity where more carbon loss is indicated where coarser particulates are dragged with the flue gases at higher velocity.

35.3.1.2 Effect of Excess Air Ratio

Results in Figs. 35.5, 35.6, and 35.7 show the influence of changing the excess air ratio over the combustion performance of rice straw pellets in the fluidized bed. Figure 35.5 illustrates the effect of excess air on the axial temperature profile. Three different excess air ratios are considered. Increasing the available oxygen with more excess air, results in a higher combustion reaction rate. This means that most of the combustion occurs inside the bed zone at higher excess air ratio. The results agree with this as peak temperature value is achieved closed to the bed zone with higher excess air. It can also be noticed that the lower the air, the hotter the gases at the end of the fluidized bed height. The reason for this is the combustion of volatiles that escape to the freeboard zone at low excess air ratio, causing more heat release along the combustor height by the extended flame of combustion.

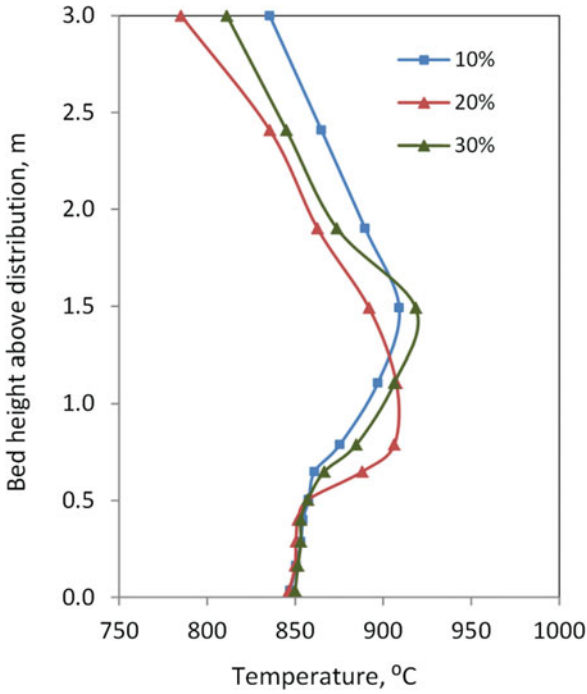

Fig. 35.5 Effect of excess air on the axial temperature profile for straw pellets combustion

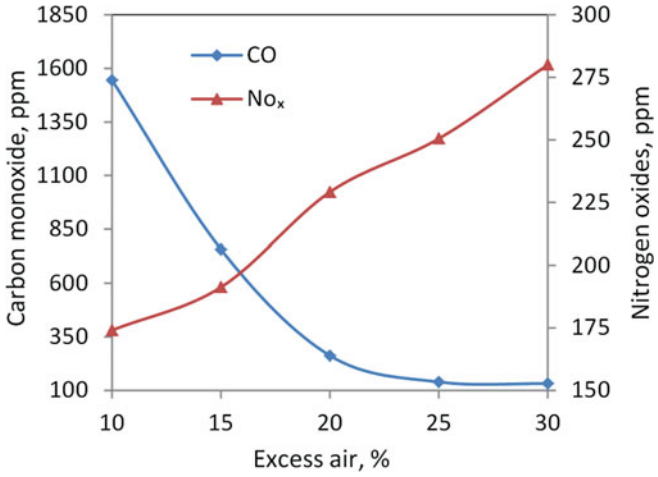

Fig. 35.6 Carbon monoxide and nitrogen oxides emissions of straw pellets combustion at different excess air ratios

Figure 35.6 elucidates that for excess air less that 20 %, carbon monoxide in the flue gases seems to be really high where it reaches 1,550 ppm at 10 % of excess air. It also shows that increase of excess air over 25 % doesn't produce more impact on carbon monoxide concentration reduction. With regards to nitrogen monoxide

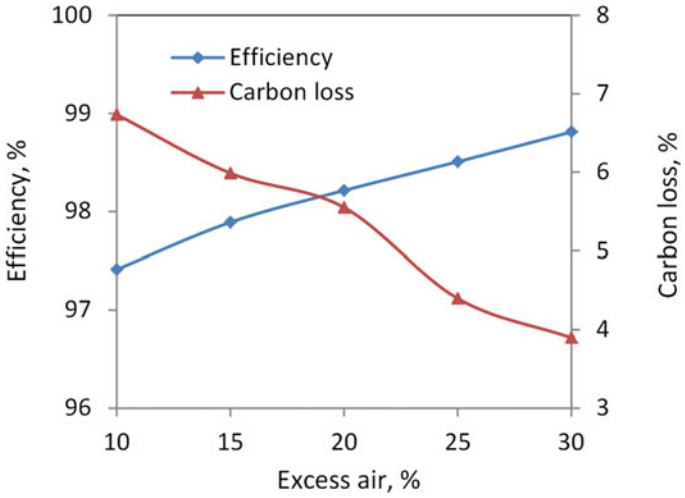

Fig. 35.7 Effect on excess air on straw pellets combustion efficiency and carbon loss percentage

concentration, excess air increases the chances of nitrogen oxides formation as it increases from 175 to 276 ppm with increase of excess air from 10 to 30 %. Also, the enhancement of combustion process with the increase of excess air, causes lower nitrogen oxides reduction reactions rates. Results in Fig. 35.7 show the increase of combustion efficiency and reduction of carbon loss with increasing excess air. This is a result of the lower carbon monoxide formation which means enhanced combustion.

35.3.1.3 Effect of Static Bed Height

Static bed height influences the fluidized bed combustor performance. Figure 35.8, 35.9, and 35.10 shows these effects on the axial temperature profile, carbon monoxide and nitrogen oxides emissions. Also changes in efficiency and carbon loss are investigated. The results presented in Fig. 35.8 show that at higher bed height, the peak temperature value shifts more into the freeboard zone where more volatiles escape the bed zone without combustion. It is also noticed that the freeboard zone temperature decreases with the bed height increase as overheating with changing the static bed height from 20, 30 to 40 cm is measured as 94.5, 71.7 and 47.1 °C, respectively.

Increasing static bed height results in a longer residence time in the bed zone. This cause a slightly enhancement in the combustion which appeases in the limited reduction in carbon monoxide in Fig. 35.9, which is accompanied by an increase in nitrogen oxides from 210 to 250 ppm. The improvement in combustion process can be seen in Fig. 35.10 as well as the efficiency slightly increase with the increase of static bed height.

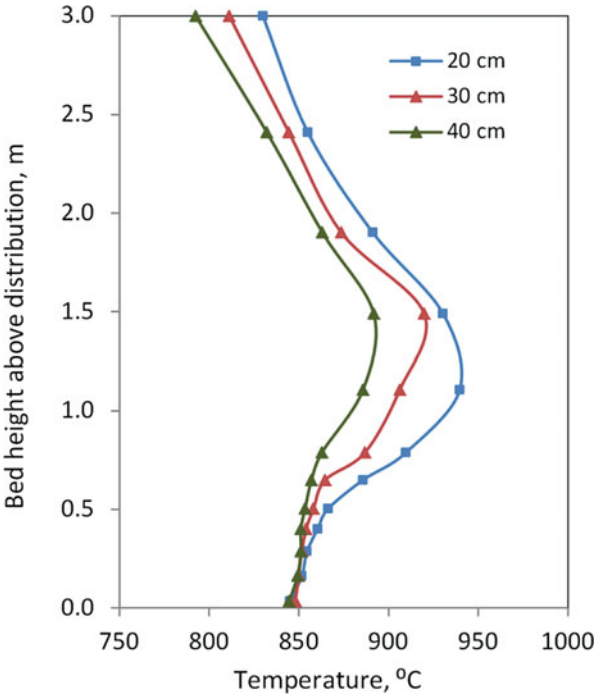

Fig. 35.8 Effect of static bed height on the axial temperature profile for straw pellets combustion

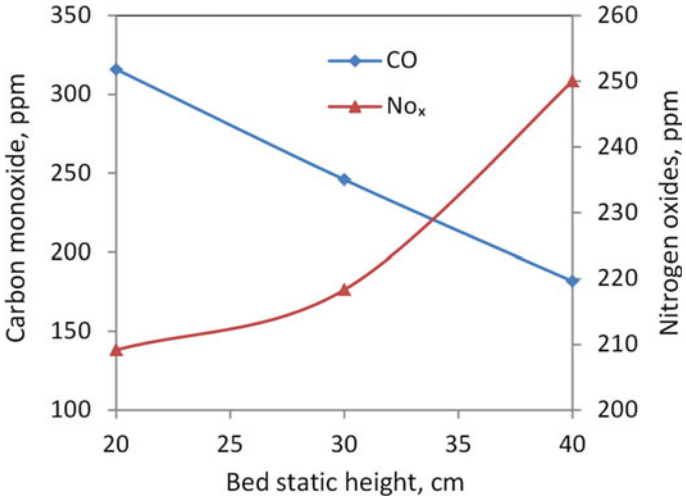

Fig. 35.9 Carbon monoxide and nitrogen oxides emissions of straw pellets combustion at different static bed height values

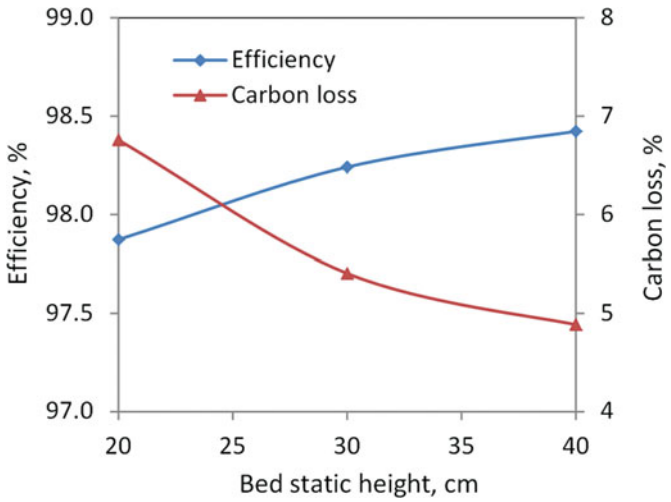

Fig. 35.10 Effect on static bed height on straw pellets combustion efficiency and carbon loss percentage

35.3.2 Combustion of Mazut

The performance of mazut combustion in fluidized bed combustor is presented in comparative form with rice straw pellets combustion. Mazut is utilized with preheated temperature of 100°C. Figure 35.11 shows a comparison of the temperature profile through the fluidized bed column with bed temperature of 850°C and static bed height of 50 cm. Mazut flow rate is 10 kg/h with fluidization velocity of 1 m/s is considered for the presented results. Occurrence of post combustion in the freeboard zone is observed with a peak temperature that is also reported to vary in value and position with the operating and fluidization conditions.

Carbon monoxide and nitrogen oxides of mazut combustion and rice straw are presented Table 35.2 and 35.3 considering the effect of static bed height and excess air ratio on the emission levels measured in ppm. Two static bed heights are considered and three different excess air ratios are tested. Also the calculated combustion efficiency values are presented for both fuels. Generally, bed height and excess air causes have a positive effect on reducing of carbon monoxide and nitrogen oxides emissions.

From the results presented in Fig. 35.12, it is clear that increasing the temperature cause a noticeable reduction in carbon monoxide formation as it is can be seen in Fig. 35.12a. This is because of the increase in reaction rate of combustion and the enhancement of gases diffusion at higher temperature values. However, for rice straw pellets, reduction in carbon monoxide from 850 to 900 °C is insignificant. These results are reflected on the nitrogen oxides formation and combustion efficiency as indicated in Fig. 35.12c and d, respectively. For combustion of mazut, generally, lower emissions are shown compared with combustion of rice

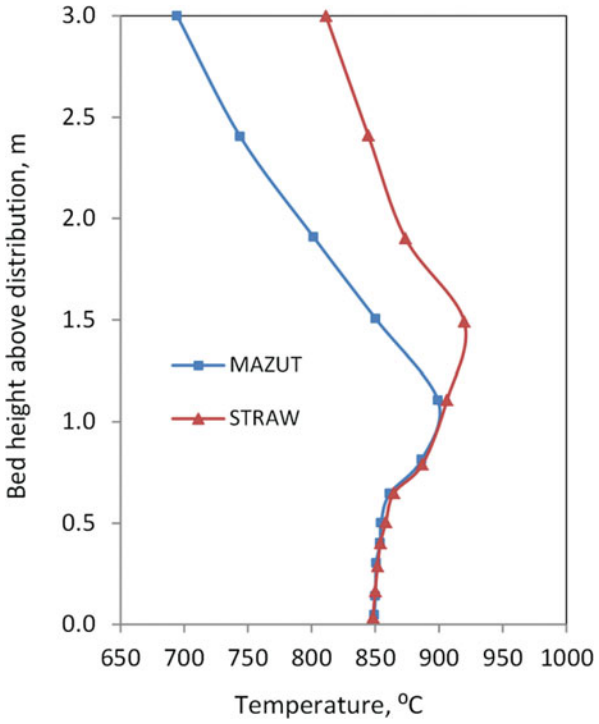

Fig. 35.11 Comparative analysis of axial temperature profile

Table 35.2 Effect of static bed height on combustion emissions and efficiency

	Straw pellets	Mazut
Static bed height = 40 cm		
Carbon monoxide	181.7 ppm	430.5 ppm
Nitrogen oxides	250.0 ppm	101.9 ppm
Combustion efficiency	98.4 %	99.0 %
Static bed height = 30 cm		
Carbon monoxide	245.8 ppm	1070 ppm
Nitrogen oxides	218.3 ppm	94.2 ppm
Combustion efficiency	98.2 %	97.8 %

straw. The performance enhancement with increasing the bed temperature is significant at with stepping up from 750 to 850°C. Limited improvement is achieved with increasing the temperature from 850 to 900°C.

The results in Fig. 35.13 show the concentration of sulfur dioxide in the emissions of mazut combustion case considering no attempt of sulfur retention with limestone addition. The effect of excess air on sulfur dioxide is shown. Excess air causes lower emissions of sulfur dioxide, It can be seen from this figure that sulfur dioxide in flue gases is reduced from 2017 ppm to 1686 ppm by increasing excess air from 10 % to 30 %. In Fig. 35.14 and 35.15, sulfur retention with limestone addition is presented. Five different mole ratios of calcium to sulfur are

Table 35.3 Effect of excess air ratio over the combustion emissions and efficiency

	Straw pellets	Mazut
10 % Excess air		
Carbon monoxide	1544.7 ppm	515.6 ppm
Nitrogen oxides	174.1 ppm	71.4 ppm
Combustion efficiency	97.4 %	98.3 %
20 % Excess air		
Carbon monoxide	262.1 ppm	419 ppm
Nitrogen oxides	229.1 ppm	87.0 ppm
Combustion efficiency	98.2 %	99.2 %
30 % Excess air		
Carbon monoxide	131.4 ppm	144.2 ppm
Nitrogen oxides	280.0 ppm	96.1 ppm
Combustion efficiency	98.8 %	99.7 %

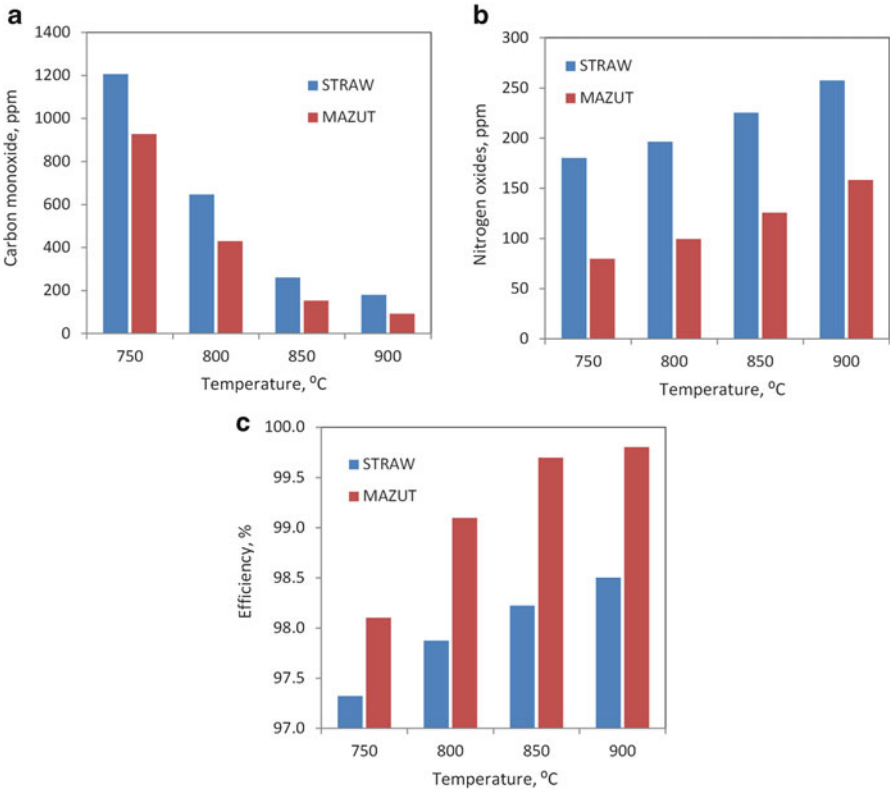

Fig. 35.12 Comparison between straw pellets and mazut combustion in fluidized bed (**a**) carbon monoxide emissions, (**b**) nitrogen oxides emissions, (**c**) combustion efficiency

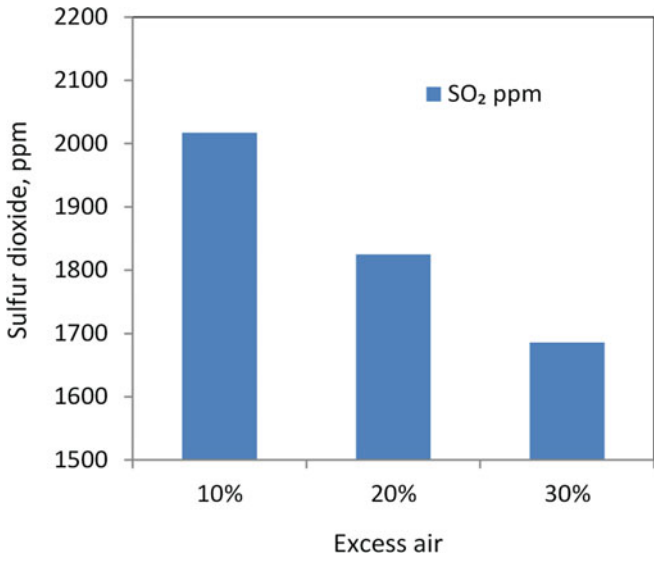

Fig. 35.13 Sulfur dioxide emissions of mazut combustion with no added calcium (limestone) at different excess air ratios

tested, presented in 5 steps from no limestone addition to 1, 2, 3, 4, and 5 of Ca/S molar ratios. Sulfur retention in Fig. 35.14 is presented as percentage of steps of Ca/S ratio, so it shows the enhancement achieved in sulfur retention by increasing Ca/S with respect to the previous step. Results in Fig. 35.15 show sulfur retention for each step of Ca/S as percentage of no limestone addition case. It can be noticed that the effect of step one results in about 40–48 % reduction in sulfur retention, where sulfur dioxide is reduced to 1210, 961 and 872 ppm for 10, 20 and 30 % excess air. The enhancement in retention decreases with higher Ca/S ratios. However, sulfur dioxide emission is reduced to 282, 202 and 151 ppm for 10, 20 and 30 % excess air when adding Ca/S of ratio 5. This gives around 87 to 91 % of sulfur retention as can be seen in Fig. 35.15. These results also show a better sulfur retention with higher excess air.

35.4 Conclusions

Rice straw and mazut are successfully burned in a bubbling fluidized bed. Different operating conditions are tested and their effect on the temperature profile and combustion emissions are investigated. Sulfur retention for the case of mazut combustion is also considered. The following conclusions of the presented work can be drawn:

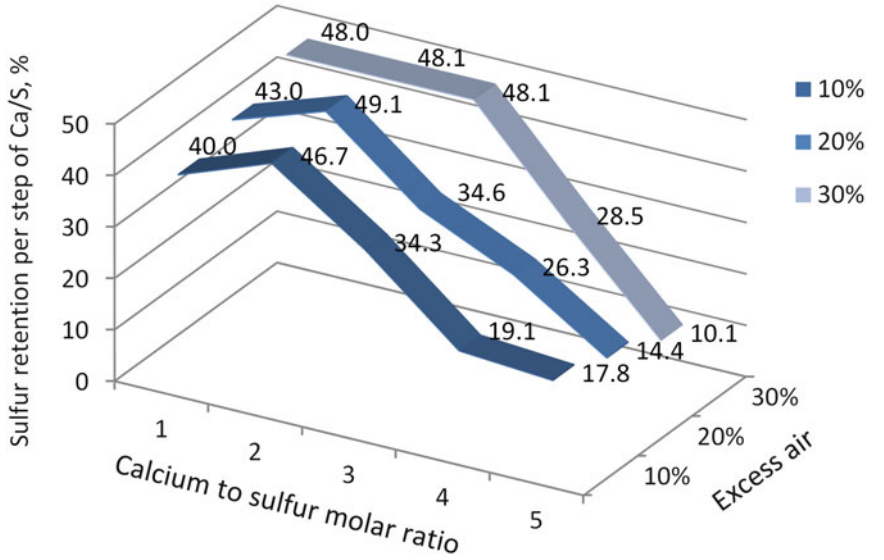

Fig. 35.14 Sulfur retention percentage calculated per step of calcium (limestone) ratio for mazut combustion at different excess air ratios

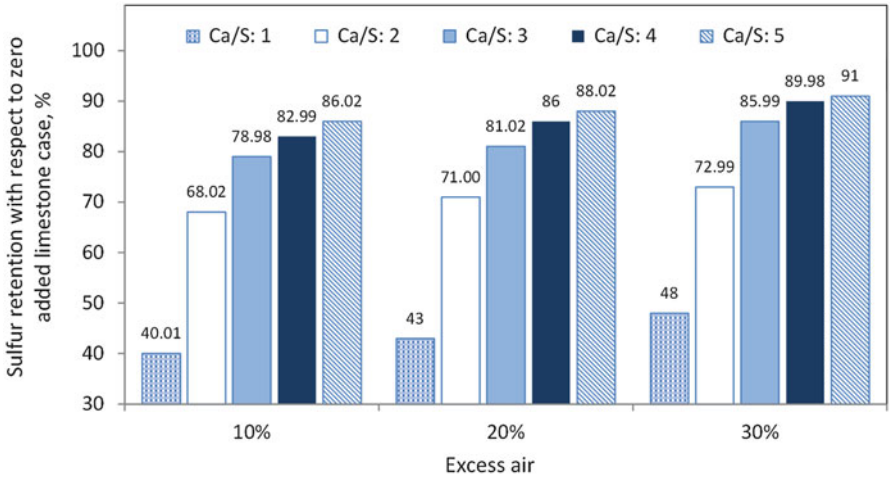

Fig. 35.15 Sulfur retention in mazut combustion, calculated as percentage of zero-added limestone case

- Post-combustion of volatiles is observed and it causes peak temperature values in the freeboard zone. The peak temperature value and location are dependent on operating and fluidization conditions.

- High combustion efficiency over a wide range of operating conditions is achieved. Combustion efficiency increase with increasing bed temperature, static bed height and excess air ratio.
- Increase of excess air and static bed height cause improvement in the efficiency of rice straw combustion with reduction in carbon loss, however, fluidization velocity has a negative impact on combustion efficiency.
- The Nitrogen oxides emissions from 175 to 270 ppm are measured for combustion of rice straw.
- Combustion of mazut achieved combustion efficiency of up to 99.8 %. Bed temperature, static bed height and excess air causes an increase in the combustion efficiency.
- Excess air helps in sulfur retention in mazut combustion.
- Sulphur retention is enhanced by adding limestone. Reduction of sulfur dioxide to 151 ppm at excess air of 30 % is achieved compared with 1667 ppm when no limestone is added.

References

1. UNEP-DT IE Energy Branch. Technical study report: biomass fired fluidized bed combustion boiler technology for cogeneration. http://www.unep.fr/energy
2. Kargbo FR, Xing J, Zang Y (2010) Property analysis and pretreatment of rice straw for energy in grain drying: a review. Agric Biol J N Am 1(3):195–200
3. Srinath S, Reddy GV (2011) Combustion and emission characteristics of rice husk in a rectangular fluidized bed combustor. 2nd international conference on environmental science and technology IPCBEE, vol.6**.**
4. Thy P, Jenkins BM, Williams RB, Lesher CE (2004) Slag formation and potassium volatilization from rice straw blended wood fuel. Am Chem Soc Div Fuel Chem 49(1):89
5. Naik S, Goud VV, Rout PK, Jacobson K, Dalai AK (2010) Characterization of Canadian biomass for alternative renewable biofuel. Renew Energy 35(8):1624–1631
6. Miccio F, Kalisz S, Baxter D, Svoboda K (2008) Combustion of liquid bio-fuels in an internal circulating fluidized bed. Chem Eng J 143:172–179
7. Miccio M, Miccio F (2010) Fluidized combustion of liquid fuels: pioneering works past applications, today's knowledge and opportunities. Proceedings of the 20th international conference on fluidized bed combustion, 71–82
8. Shaaban W (2010) Fluidized bed combustion of rice straw and bitumen pellets. MSc Thesis, Mansoura University, Egypt
9. Zaater G (2006) Utilization of agriculture waste in energy production using fluidized bed furnaces. MSc Thesis, Mansoura University, Egypt
10. Okasha FM, El-Emam SH, Mostafa HK (2003) The fluidized bed combustion of a heavy liquid fuel. Exp Therm Fluid Sci 27:473–480
11. Tillman DA (1991) The combustion of solid fuels and wastes. Academic, San Diego, CA
12. Looffler G, Andahazy D, Wartha C, Winter F, Hofbauer H (2001) NO_x and N_2O formation mechanisms—a detailed chemical kinetic modeling study on a single fuel particle in a stationary fluidized bed, 16th International FBC Conference, FBC01-0068, Reno Nevada

Chapter 36
Theoretical and Experimental Study of a Novel Film Evaporation Cooling System

Hooman Golchoobian, Mohamad Hasan Taheri, Majid Amidpour, and Omid Pourali

Abstract A novel cogeneration cooler is presented in this paper. The entered air cools in two streams. In the first stream, air goes into the channels and cooling happens without increasing humidity. The second stream is the air flow that goes out of the channels on the water film and cooling happens with increasing of humidity. Both of the two cooled air is useful, but for different places in one building. The film evaporation cogeneration cooler with its' two new idea can save considerable amount of energy. Production of cooled air with evaporation of water film from surface of aluminum channels and production of humid and non-humid cooled air in this cooler are two helpful ideas that theoretical and experimental calculations approve the practicability of ideas. The results show that this novel cooler has high COP and in the cases that both of its cooled air production can be useful, it has so high performance and can conserve much energy.

Keywords Film evaporation • Indirect cooling • Humid and non-humid air

36.1 Introduction

The liquid film evaporation in air exists in different industrial applications like chemical industries, distillation, cooling tower, air conditioning and drying. Evaporation of the pure liquid film has been extensively investigated.

A numerical analysis was carried out by Tsay et al. [1] to study the detailed heat transfer characteristics for a falling liquid ethanol film by solving the respective governing equations for the liquid film and the induced gas flow together. Yan and Lin [2] investigated laminar natural heat and mass transfer in a vertical plate and channel with pure liquid film evaporation. It is shown that the influence of the liquid is substantial near the interface. Yan [3] studied the pure liquid film evaporation by mixed convection of a humid air in a vertical channel. A numerical study of heat

H. Golchoobian (✉) • M.H. Taheri • M. Amidpour • O. Pourali
K.N. Toosi University of Technology, Tehran, Iran
e-mail: h.golchoobian@gmail.com; hasan.taheri@gmail.com; amidpour@kntu.ac.ir; o.pourali@kntu.ac.ir

I. Dincer et al. (eds.), *Progress in Sustainable Energy Technologies Vol II: Creating Sustainable Development*, DOI 10.1007/978-3-319-07977-6_36

and mass transfer from a falling pure liquid film on isothermal inclined plate was presented by Agunaoun et al. [4]. The water film cooling over the glass cover of a solar still including evaporation effects was studied by Bassam et al. [5]. It was shown that the presence of the cooling film neutralizes the effect of wind speed on still efficiency. Feddaoui et al. [6] provided a numerical study of the evaporative cooling of pure liquid film falling down along a vertical tube under mixed gas convection. An experimental study on an enhanced falling film evaporation air flow absorption and closed circulation solar still was presented by Zheng Hongfei [7].

36.2 System Description

A novel cogeneration cooler is presented in this paper. In this cooler, inlet air cools in two streams. In the first stream inlet air goes into the channels and cooling happens without increasing humidity. The second stream is the air flow that goes out of the channels on the water film and cooling happens with increasing of humidity. Both of the two cooled air is useful, but for different places in one building. The schematic of the cooler is presented in Fig. 36.1. It's clear in the Fig. 36.1 that 6 aluminium channels are used to drive air. The outside of channels are covered by water film and 2 fans are used to increase the evaporation rate. There is another fan for moving the inside air of channels. In the Table 36.1 the dimension of cooler and characteristics of fan are presented.

The test was done in a laboratory of the university. The ambient temperature was 28˚˜C and relative humidity was 30 %. Moreover, two power sources were used for running the axial fans.

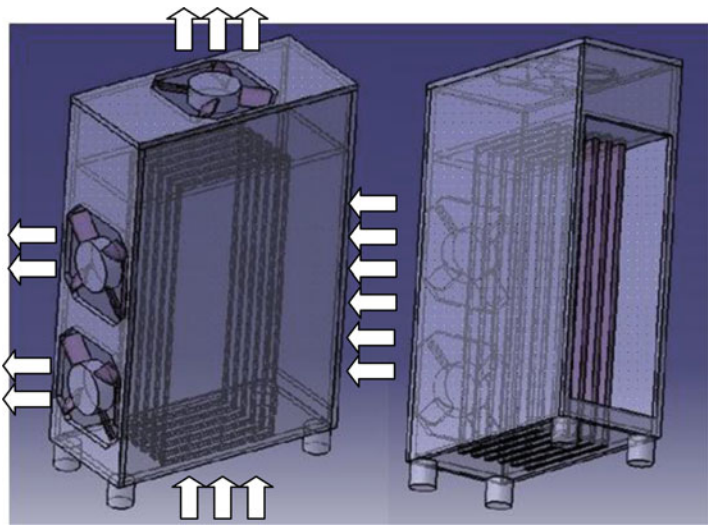

Fig. 36.1 Schematic of film evaporation cooler

Table 36.1 Cooler characteristics

Number of fans	3
Number of channels	6
Channel material	Aluminum
Flow rate of fans at 8,200 rpm	9.43 ft^3/min
Cooler dimensions	9 cm × 20 cm × 32 cm
Channel dimensions	0.5 cm × 10 cm × 23 cm

Table 36.2 Power supply characteristics

Input electricity	110/220 V AC and 6 Hz
Output current	0–5 V
Output voltage	0–30 V

Fig. 36.2 Schematic of water film on an insulated plate with air flow

36.3 Description of Experimental Apparatus

Two adjustable power supplies are used in the experiments that the characteristics of them in Table 36.2.

A prototype for the cooler is designed and manufactured. Two power sources are used for running the fans. One of the fans that is for the channel inside air runs in its' normal power. But the two other fans voltage change step by step. In each sequence the air temperature of fan outlets is measured. By this way the produced cooling rate and COP of the cooler is calculated by the Eqs. (36.18) and (36.19).

$$Q_c = \dot{m} C_p (T_{in} - T_{out}) \tag{36.1}$$

$$COP = \frac{Q_c}{Q_{fans}} \tag{36.2}$$

36.4 Mathematical Model

The calculation is done in three stages. In the first stage, we assume that the plate is insulated on the left side and an air flow is on the right side on the film of water as it's shown in the Fig. 36.2.

For the first stage, heat and mass processes in the water film and gas flow can be described in detail by the appropriate governing equations and interfacial conditions.

Governing equations and interfacial conditions of the first stage are described blow. It's the same as Tsay et al. Work [1].

Boundary and interfacial conditions are presented in Eqs. (36.3)–(36.6).

At x = 0:

$$T_L = T_{L,in'} \quad T_G = T_{\infty'} \quad u_G = v_G = 0 \quad w_v = w_{v,\infty} \tag{36.3}$$

At y = 0:

$$u_L = 0 \qquad \frac{\partial T_L}{\partial y} = 0 \tag{36.4}$$

At y → ∞:

$$u_G = 0 \quad T_G = T_\infty \quad w_v = w_{v,\infty} \tag{36.5}$$

$$u_{L,i} = u_{G,i} \quad T_{L,i} = T_{G,i} \quad \left(\mu_L \frac{\partial u_L}{\partial y}\right)_i = \left(\mu_G \frac{\partial u_G}{\partial y}\right)_i \tag{36.6}$$

x-momentum equation for water film is defined as the following.

$$\frac{\partial}{\partial y}\left(\mu_L \frac{\partial u_L}{\partial y}\right) + \rho_L g = 0 \tag{36.7}$$

Energy equation for water film is defined as Eq. (36.8).

$$\rho_L C_{pL} u_L \frac{\partial T_L}{\partial x} = \frac{\partial}{\partial y}\left(\lambda_L \frac{\partial T_L}{\partial y}\right) \tag{36.8}$$

Continuity equation for gas flow can be written as Eq. (36.9).

$$\frac{\partial}{\partial x}(\rho_G u_G) + \frac{\partial}{\partial y}(\rho_G v_G) = 0 \tag{36.9}$$

X-momentum equation for gas flow is defined as the following.

$$\rho_G\left(u_G \frac{\partial u_G}{\partial x} + v_G \frac{\partial u_G}{\partial y}\right) = \frac{\partial}{\partial y}\left(\mu_G \frac{\partial u_G}{\partial y}\right) + (\rho_G - \rho_\infty) g \tag{36.10}$$

Energy equation for gas flow is defined as below.

$$\rho_G c_{pG}\left(u_G \frac{\partial T_G}{\partial x} + v_G \frac{\partial T_G}{\partial y}\right) = \frac{\partial}{\partial y}\left(\lambda_G \frac{\partial T_G}{\partial y}\right) + \rho_G D\left(c_{pv} - c_{pa}\right) \frac{\partial T_G}{\partial y} \frac{\partial w_v}{\partial y} \tag{36.11}$$

Species diffusion equation of water vapour is defined as Eq. (36.12).

$$\rho_G\left(u_G\frac{\partial w_v}{\partial x}+v_G\frac{\partial w_v}{\partial y}\right)=\frac{\partial}{\partial y}\left(\rho_G D\frac{\partial w_v}{\partial y}\right) \tag{36.12}$$

36.5 Interfacial Condition

Transverse velocity of gas is defined as below.

$$v_{G,i}=-\left(\frac{D}{1-w_v}\frac{\partial w_v}{\partial y}\right)i \tag{36.13}$$

Mass fraction of water vapour can be calculated by Eq. (36.14).

$$w_{v,i}=\frac{M_v P_{v,i}}{M_v(P_\infty-P_{v,i})+M_v P_{v,i}} \tag{36.14}$$

Energy balance at the interface is defined by Eq. (36.15).

$$-\left(\lambda_L\frac{\partial T_L}{\partial y}\right)i=\left(\lambda_G\frac{\partial T_G}{\partial y}\right)i+m_{v,i}h_{LG} \tag{36.15}$$

Evaporation rate can be written as Eq. (36.16).

$$m_{v,i}=\left(\frac{\rho_G D}{1-w_v}\frac{\partial w_v}{\partial y}\right)i \tag{36.16}$$

36.6 Numerical Method

A finite-difference method is used to solve the governing Eqs. (36.7)–(36.12). The axial convection terms are approximated by the backward difference and the transversal convection and diffusion terms are approximated by the central difference. The calculations presented here were obtained with a 100×35 grid in x and y directions.

In the second stage, heat transfer on the left side of the plate is considered too which is shown in Fig. 36.3. Convection coefficients of the two sides are calculated as the Eqs. (36.17) and (36.18).

Nusselt number for laminar flow:

$$Nu=0.664Re^{0.5}Pr^{1/3} \tag{36.17}$$

$$Nu=\frac{hl}{k} \tag{36.18}$$

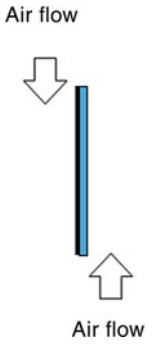

Fig. 36.3 Schematic of water film on a metal plate with air flow on its' both sides

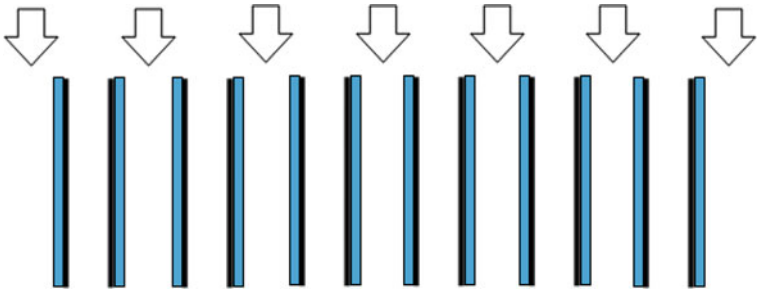

Fig. 36.4 Schematic of water films and air flow on the cooler channels

A coefficient is defined as the fraction of equivalent resistant of the left side to the right side. This coefficient describes distribution of heat transfer between two sides of each plate.

$$CF = \frac{R_{conv,r}}{R_{conv,l} + R_{cond,p} + R_{cond,f}} \xrightarrow{By\ neglecting\ R_{cond,p}\ and\ R_{cond,f}} CF = \frac{h_{left}}{h_{right}} \tag{36.19}$$

In the last stage, the cooler is considered completely. Calculation for all of 12 plates of the cooler which are shown in Fig. 36.4 is done.

36.7 Results and Discussion

It's concluded from the theoretical calculation that evaporation rate on the outside of channels increases with air flow rate. It's shown in Fig. 36.5. This water evaporation from outside of channels will cause air cooling both in outside and inside of channels.

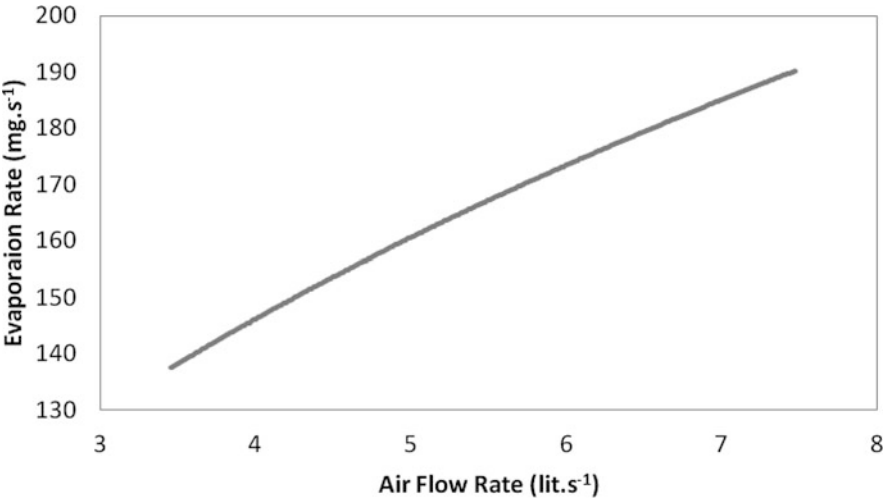

Fig. 36.5 Evaporation rate of water on the channels with air flow variation

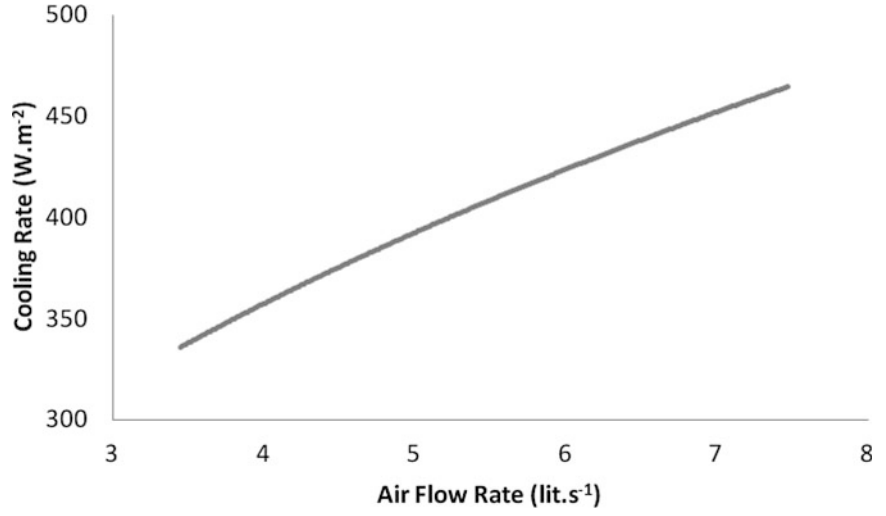

Fig. 36.6 Cooling rate of the cooler with air flow variation

In Fig. 36.6 the changes of produced cooling with air flow is shown. It's the result of theoretical calculation. Cooling rate.

Temperatures of air flow of inside (channel 2) and outside (channel 1) of channels are measured and the results are shown in Fig. 36.7. By increasing the flow rate of channel outside, the channel inside temperature increases and channel outside temperature decreases at first but for higher air flow, the temperature of outside channel increases.

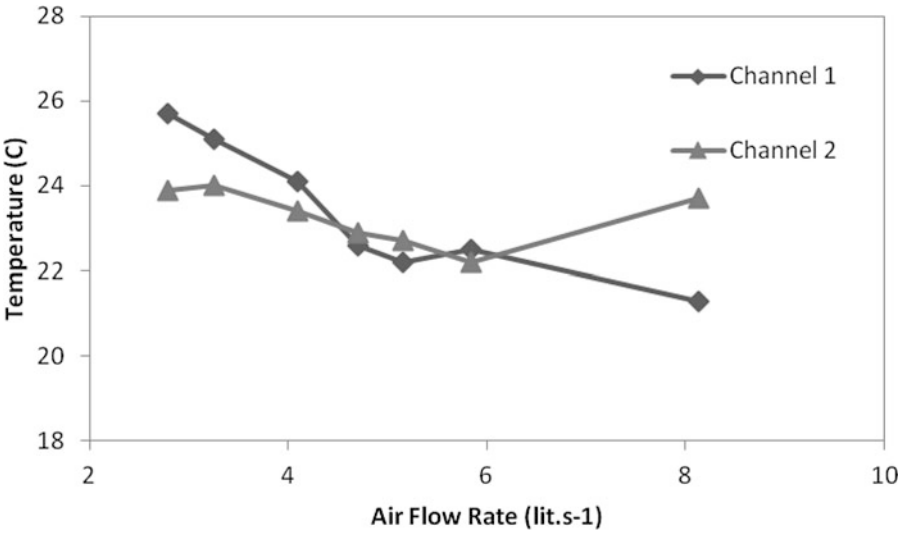

Fig. 36.7 Temperatures of air flow of inside and outside of channels (result of experiments)

36.8 Conclusion

The film evaporation cogeneration cooler with its' two new idea can save considerable amount of energy. Production of cooled air with evaporation of water film from surface of aluminum channels and production of humid and non-humid cooled air in this cooler are two helpful ideas that theoretical and experimental calculations approve the practicability of ideas. The results show that this novel cooler has high COP and in the cases that both of its cooled air production can be useful, it has so high performance and can conserve much energy.

Nomenclature

c_p Specific heat, J kg^{-1} °C^{-1}
D Mass diffusivity, m^2 s^{-1}
g Gravitational acceleration, m s^{-2}
h Heat transfer coefficient, W m^{-2} °C^{-1}
k Conduction coefficient
l Length, m
m Mass rate, kg s^{-1}
M_v Molecular weight, kg mol^{-1}
Nu Nusselt Number
$P_{v,i}$ Vapor pressure, Pa

Q External heat flux of wetted wall, W m^{-2}
Re Reynolds number
T Absolute temperature, K
u_G Axial velocity, m s^{-1}
v_G Transverse velocity, m s^{-1}
w Mass fraction

Greek Symbols

λ Thermal conductivity of the fluid, W m^{-1} K^{-1}
μ Dynamic viscosity of the fluid, kg m^{-1} s^{-1}

Subscripts

Cond Conduction
Conv Convection
f Surrounding fluid
G Gas flow
L Water film
v Vapor

References

1. Tsay YL, Lin TF, Yan WM (1990) Cooling of a falling liquid film through interfacial heat and mass transfer. Int J Multiphase Flow 16(5):853–865
2. Yan WM, Lin TF (1991) Evaporative cooling of liquid film through interfacial heat and mass transfer in a vertical channel numerical study. Int J Heat Mass Transfer 34:1124–1191
3. Yan WM (1992) Effects of film evaporation on laminar mixed heat and mass transfer in a vertical channel". Int J Heat Mass Transfer 12:3419–3429
4. Agunaoun A, Daif A, Barriol R, Daguenet M (1994) Evaporation en convection force d'un film mince s'écoulant en régime permanent laminaire et sans onde sur une surface plane incline. Int J Heat Mass Transfer 37:2947–2956
5. Abu-Hijleh BAK, Mousa HA (1997) Water film cooling over the glass cover of a solar still including evaporation effects. Energy 22:43–48
6. Feddaoui M, Belabmidi E, Mir A, Bendou A (2001) Numerical study of the evaporative cooling liquid film in laminar mixed convection tube flows". Int J Therm Sci 40:1011–1020
7. Hongfei Z (2001) Experimental study on an enhanced falling film evaporation air flow absorption and closed circulation solar still. Energy 26:401–412

Chapter 37
Environmental Friendly Food Smoking Technologies

Aydin Killic, Haydar Kucuk, and Adnan Midilli

Abstract This study deals with the development of the food smoking technologies for environmental friendly unit operations. Smoking process include some different unit operations such as salting, drying and smoking. In this regard, the last innovative studies on the smoking technologies first defined. Second, the main environmental characteristics of unit operations in smoking process are discussed. Third, some sustainable strategies for improving the smoking process and minimizing the environmental impact are developed. Finally, a case study, including the cold air assisted salting, drying and smoking of the food, is presented by considering some food quality and safety parameters. Finally, the results show that the best method reduced environmental impact is the low temperature assisted brining, drying and liquid smoking. In summary, the low temperature process assisted production techniques are potential techniques for food smoking industry in order to achieve better product quality, safety and reduced environmental impact.

Keywords Food • Salting • Drying • Smoking • Environment

37.1 Introduction

The impacts of food production systems are an important environmental problem in food industry. Some of the global issues launch the environmental changes and reduce the environmental sustainability. Particularly, in order to reduce the environmental effects in the food industry, the useful projects, plans, programs, policies, strategies and technologies should be taken into consideration [1]. In order to perform these targets, one of the best ways is to develop, first, an acceptable chain defining well the environmental pollution and its effects. The second way is

A. Killic (✉)
Department of Food Engineering, Faculty of Engineering, Recep Tayyip Erdoğan University, Rize 53100, Turkey
e-mail: aydin.kilic@erdogan.edu.tr

H. Kucuk • A. Midilli
Energy Division, Department of Mechanical Engineering, Faculty of Engineering, Recep Tayyip Erdoğan University, Rize 53100, Turkey
e-mail: haydar.kucuk@erdogan.edu.tr; adnan.midilli@erdogan.edu.tr

I. Dincer et al. (eds.), *Progress in Sustainable Energy Technologies Vol II: Creating Sustainable Development*, DOI 10.1007/978-3-319-07977-6_37

to expose an applicable strategic program indicating the most important steps to increase the food productivity, safety and quality. The researchers, scientists and manufacturers dealing with the food productivity, safety and quality should try to minimize the environmental effects in food industry and, in this regard, develop and expose some food production technologies to struggle the effects of the environmental change. The food industries require high quality standards for better contributing to the manufacturers, and improving the product quality. This industry also requires the environmentally friendly production technologies as well as food smoking technologies.

Smoking is used to the preservation and flavoring of perishable food. This food process technique is considered one of the oldest preservation methods in food industry. In order to increase the product quality and minimize the environmental, the optimal smoking technology and the high quality production method should be identified. Regarding smoking method, the low temperature process cycle is important to take into consideration for fighting the environmental impacts and decreasing the environmental pollution.

Food smoking method include common unite operations such as the *salting*, *drying* and *smoking*. The applications of these unit operations increase to the shelf-life of product as a result of the combine effect. The optimization of the individual unit operations involved in salting, drying, smoking with respect to increased processing yield is an important factor in food sector [2–4].

Salting: as a first unit operation of smoking process, salting is one of the oldest preservation method used to be in food industry. This process is important for the food safety and sensory characteristics. Biomaterial absorbs salt rapidly in case the higher temperature of salting process. However, a standard brining in low temperature give a results for product quality and safety. Salting in a cold store is also a good way to keep brines cool. Brining temperature may be a hazard critical control point if brining times are over 3–4 h [5, 25].

Drying: as another unit operation of smoking process, there are four primary methods used to be in food industry such as hot, cold, spray, vacuum and freeze [6]. Hot air drying can be applied for the solid foods like vegetables, fruit and muscle food; Spray drying can be used for liquids and semi-liquids like milk; cold drying can be used for semi drying process and the most sensitive foods; vacuum drying process can be used for the liquids and freeze drying process can be applied to a large variety of foods. It can be said that, during drying, moisture content is reduced until a safe level in which there is some biochemical, physical and microbiological quality lost by microorganism, enzymes and other agents. Drying processes can be conducted at high temperature and short time (HTST), Low temperature high velocity (LTHV) and at low temperature and long time (LTLT) [6–9]. In this regard, many types of dryer providing different air temperature and velocity can be used. In this study, cyclone type cold air dryer is used as a key study. In the thermal processes of perishable foods and cooling is employed as one of the preservation techniques to prevent their spoilage and maintain their quality [22]. Under all these considerations, it can be explained that food drying is a typical

process of heat and moisture transfer which induces changes in biological products undergoing drying [9, 10].

On the other hand, the *smoke* is produced by hard wood material burning that has environmental pollutants such as polycyclic aromatic hydrocarbons (PAH). An alternative method to smoking is the use of liquid smoke (L_S). Ls is a liquid form of smoke as a food additive. This smoking method is used as a flavorings agent that has not any environmental emission during food production. This process is made without any fire, smoke and dust. Soon there will be only one smoke flavor, artificially produced by a uniform condensation method in which fresh smoke is condensed in water and then purified. Because of the purification process, the use of smoke flavoring is considered less of a health concern than the traditional smoking process [11].

It was presumed that the liquid smoking process, that under controlled burning, decreases the emissions of pollutants to the environment. The LS system isn't producing any emission and tars to the environment. L_S process could replace the traditional hot and cold-smoking [11]. Computerized smoking chambers with external smoke generators, and emission and temperature control systems, have replaced direct flue gas smoke which used more traditional smoking kilns [11, 12]. From an environmental view point, smoking with pyrolytic flue gases is not very favorable as it produce polyaromatic hydrocarbon (PAH) emissions to the environment. PAH are commonly considered to be a risk of carcinoma and, as these also end up in the finished product after traditional food smoking [11, 13]. The content of PAH was lower in liquid-smoked fish at 4 °C than in traditionally smoked fish. The use of them has many advantages compared to traditional smoking techniques. The amount of toxic compounds contents deriving from burning of hard wood sawdust can be controlled in the smoke flavorings of food products. In order to produce safe food products, the European Regulation requests data on the composition and lays down, the maximum permitted concentrations for PAH. According to the new rules of EU Food Commission, the food flavorings process is imposed as a liquid smoke without fire [11, 14–16].

On the other hand, *the product quality and safety* of the smoked food is greatly influenced by smoking conditions. Low temperature process conditions have a positive influence on the quality of biological materials, which have harmful effects on quality. For example, cold air drying of fish minimizes fatty acid oxidation and reduces protein denaturizing because low-temperature drying process gives a lower nutrient degradation [8]. During low temperature drying, lipid oxidation and antioxidant losses in food material can be reduced by short drying times and low temperature. In this regard, this type of process aims at minimizing the chemical degradation reactions can be viewed as the decomposition of a particular chemical compound [9, 17].

Under these important considerations, the main targets of this chapter is to investigate the appropriate minimization ways to reduce the effects of the environmental impacts of food smoking process by applying low temperature assisted salting, drying and smoking process technique. Consequently, in order to minimize to the environmental impacts and quality lost, the best way is to encourage the use

of the food smoking techniques causing less environmental effects, and to apply the low temperature process with liquid smoking.

37.2 Environmental Aspects of Food Smoking

37.2.1 Food Smoking Cycle

Some smoked food products as below;

1. *Meat products,*
2. *Poultry products,*
3. *Seafood,*
4. *Dairy products,*
5. *Composite foods,*
6. *Bakery products,*
7. *Cereals products*

Ls is a liquid form of smoke as a food additive. This smoking method is used as a flavorings agent that has not any environmental emission during food production. Liquid smoke is produced by controlled thermal degradation of hard wood sawdust by the limited oxygen condition [15].

Smoke production cycle include tree step;

1. Pyrolysis of hard wood sawdust,
2. Condensation of wood smoke,
3. Refining of liquid smoke [15].

Every these steps have too many environmental impacts because of the complex chemicals mixtures [15].

Figure 37.1 presents common food smoking steps.

Figure 37.1 presents the common food smoking cycle that includes industrial environment. As shown in this figure, all production steps can produce environmental impacts. The emissions including greenhouse gases, liquid and solid pollutants can be produced during the processes. Thus, these emissions can pollute the land, air and water. After the environmental pollution, a global warming effect and public health risks can be produced on the industrial environment. Therefore, it is recommended that emission free unit operations such as low temperature process and liquid smoking should be utilized in the food smoking cycle in order to decrease the environmental [1].

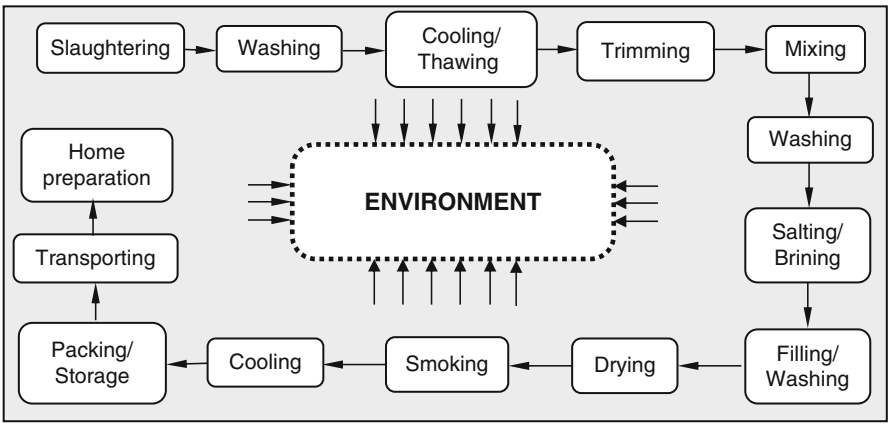

Fig. 37.1 Common food smoking life cycle (*modified from* [1])

37.2.2 The Food Smoking Process and Environmental Pollution

There are two common methods of smoking process such as *traditional* (Hot smoking and cold smoking) and *mechanical* method. *The traditional method* involves the food being practiced in smoke cabinet by the slowly smouldering of hard wood sawdust. *The traditional* smoking process has high environmental impacts such as heat and pollutant. On the other hand, *the mechanical smoking* process is generated through the use of a hard wood smoke concentrates by turning smoke into a solid or liquid form.

Wood sawdust contains some hazardous materials such as carbon monoxide, phenols, and polcyclicaromatic hydrocarbons. The environmental pollution level of a smoke kiln was investigated in an experimental study. According to this study, by the drying of 1,000 kg finished product emitted 0.3 kg CO, 0.15 kg inorganic particle and 0.2 kg carbon. Soot and tar compounds deposited on the chamber walls the smoking Peru is a strong alkaline funds from which follows a large consumption of water and high organic load of wastewater [18].

Figure 37.2 shows the environmental pollution impacts of food smoking process.

37.3 Environmental Friendly Fish Smoking: A Case Study

Smoking processes are the oldest process technique and common unit operations in food industry. Salting is a preliminary operation in some smoking, drying and marinating processes that have been mostly empirically developed. Optimization of the individual unit operations are important factor in the food industry [3, 19].

Fish muscle absorbs salt more rapidly at high process temperature. On the other hand, the standard Lt brining process has a preservative characteristic and

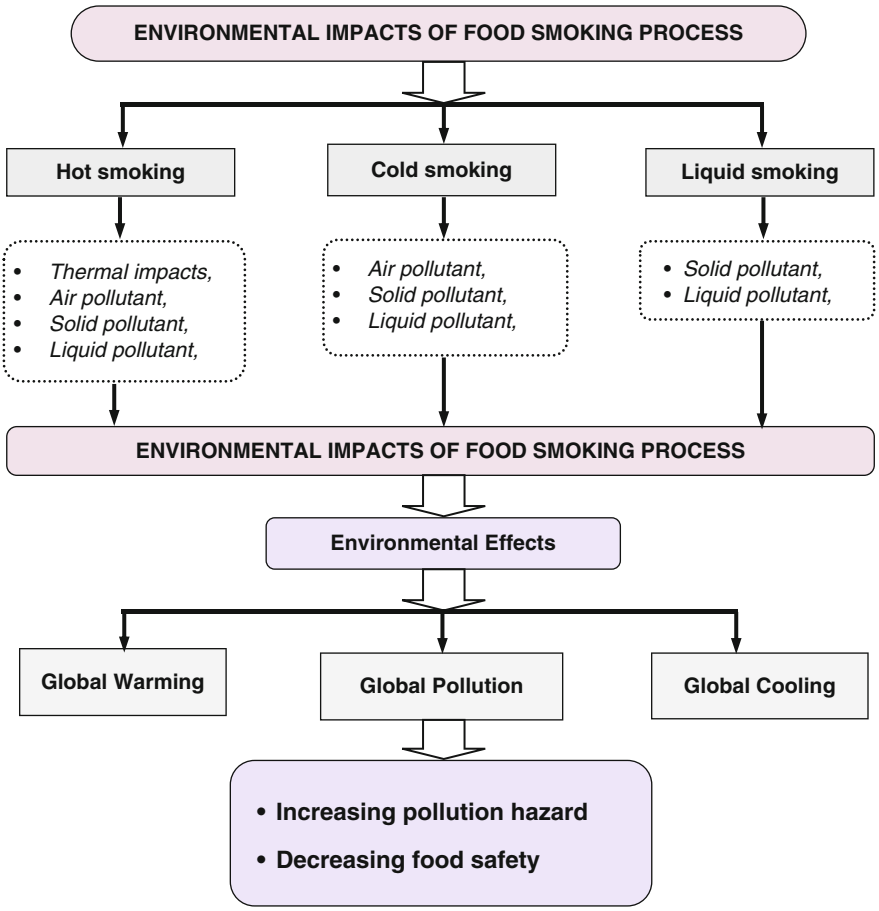

Fig. 37.2 Environmental pollution effects of food smoking process (*modified from* [1])

environmental impact technologically. The brining in a cold cabinet is also a good way to keep brines in a standard low temperature. In addition, a slowly salt transfer has a positive effect on food quality. In this regard, Lt brining process has tree positive effect including food quality, food safety and environmental benign [5]. During this study, a cold process cabinet was used for the salting process like as an environmental friendly unit operation.

On the other hand, drying is considered a common unit operation in many processes. The removal of moisture prevents the growth of microorganisms and minimizes many of the moisture mediated deteriorative reactions in food. There are four primary methods of drying [6, 9, 20, 21]. During the drying application, moisture content is decreased until a safe level in which there is a minimum spoilage caused by microorganism, enzymes and many other agents. Many types of the dryer providing cold air or hot air can be used for the practical applications.

In this study, a cyclone type cold air dryer is used as an environmental friendly process. In the thermal processes of perishable foods, cooling is employed as one of the preservation techniques to prevent their spoilage and maintain their quality as environmental benign technology [9, 10, 22].

37.3.1 Assumptions

- Firstly, it is expected that cold brining (4 °C) process will contribute to improve the total quality of biomaterial.
- Second, it is expected that cold drying (4 °C) process will contribute to improve the total quality of biomaterial and decrease environmental *thermal impact*.
- Third, it is expected that liquid smoking (4 °C) decrease environmental *solid pollutants*.
- Finally, it is expected that liquid smoking (4 °C) decrease environmental *air pollutants*.

37.3.2 Experimental Parameters

In order to investigate process conditions of liquid smoked fish samples and to find an appropriate practical solution to production parameters for fish quality, all production steps were performed at 4 °C. During the cold drying process, the constant drying air velocity was 7 m/s. When the each smoking experiment was performing, the following were measured at every half an hour for each control point (CP) [1].

1. Temperatures,
2. Air humidity,
3. Drying air velocity
4. Weight loses of the product.

As fish quality indicators, the fallowing parameters are selected;
Common physical and chemical parameters;

1. a_w
2. *pH*
3. *Total volatile basic nitrogen (TVB-N)*
4. *Thiobarbituric acid reactive substances (TBARS)*

Microbiological parameters;

1. *Total Viable Count (TVC)*
2. *Total Psychrophilic Count (TPC)*
3. *Total Yeast and Moluld (TYM)* [1].

37.3.3 Materials and Methods

37.3.3.1 Cold Brining (Cb) and Liquid Smoking (Ls) Procedure

Rainbow trout (*Oncorhynchus mykiss*) Horse Mackerel (*Trachurus trachurus*), Striped sea bream (*Lithognathus mormyrus*) were used as a raw material for Cold brining (Cb) and Low Temperature (LT) assisted Liquid smoking (Ls) process. The selected raw fish samples were slaughtered, gutted, trimmed and washed at 4 °C. Then the other fish samples were brined (100 g $NaCl^{-1}$) for ~8 h at 4 °C at a ratio 1:2 (fish:brine) before cold air assisted liquid smoking process. The final salt content of the fillets was average ~2 g/100 g. During the brining process, fish samples were individually weighed. The weight of fish fillet was identified to calculate yield at each hour of the brining process. On the other hand, the total weight changes (ΔM°), should be equal to the sum of the water and NaCl content as weight changes (ΔM^{w} and ΔM^{NaCl}). The total water and NaCl weight changes of brine (ΔM°, ΔM^{w} and ΔM^{NaCl}, respectively) were calculated. After the fish brining process, all samples were liquid smoked (Ls) (%3, 20 s.) [23–25]. Figure 37.3 presents Ls fish production flow diagram during the processes.

Experimental setup was constructed in a cold air cabinet. Figure 37.4 presents low temperature high velocity drying method (LTHV) assisted smoking unit: Cp: Control point, L: Layer (Modified from [9, 25]).

In order to investigate drying conditions of fish samples and to find an appropriate solution to drying problems for quality, Lt drying experiments were performed at 4 °C for constant drying air velocity (7 m/s). Figure 37.4 presents to the control diagram of Lt smoking process parameters.

The cold-air evaporator, which is one of the most important parts of the experimental set up, was used as a cooler in the liquid smoking production system. There were tree separated cupboard for every unit operation including Cb, Ls and Lt drying (LTHV). Before smoking production, the initial moisture contents of fish samples were determined as below: an average 10 g of the raw material was put down in an oven, and kept there at 105 °C throughout equilibrium moisture in percentage. a_w values (Water activity) were measured using an Aqua Lab Model cx2 (Sensitivity = ± 0.003) [9].

The experimental analyses were started and the following methods were repeated in each study. Fresh fish samples was carefully cleaned, trimmed and placed as 200 g samples into the middle tray as a 2.5 mm thin layer. The study was performed as single layer. In this regard, 1st and 2^{nd} trays were left empty so that air velocity could be homogeneously diffused to the product. In the experiments, temperature of the evaporator was controlled by a thermostatic sensor. The cold air was contributed by a radial fan that the air passing through the cooler evaporator. In the Lt assisted drying, temperature was monitored with a temperature controller [9]. During each drying experiment, the measured were parameters at every half an hour as below;

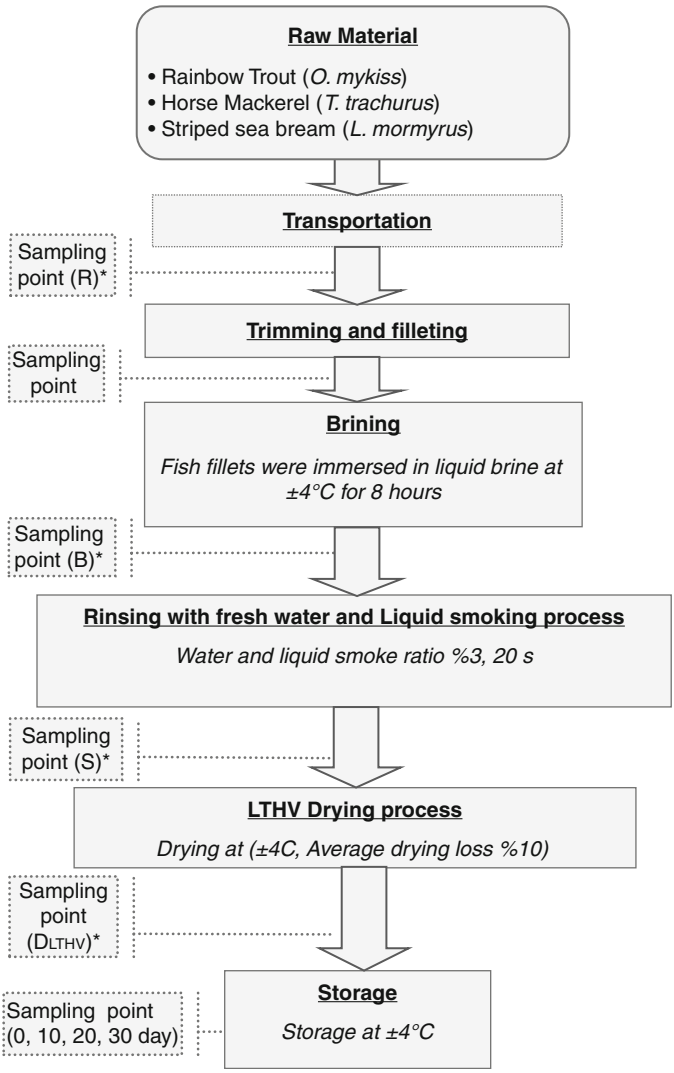

Fig. 37.3 Ls Fish production flow diagram: During the processes (*R: Raw material; B: Brined; Cb; cold brined Ls: Liquid Smoked: D_{LTHV}; LTHV dried) (*modified from* [25])

1. *Relative Humidity*: all values of humidity were measured with a METTLER model digital infrared humidity meter at various control points of the system, with reading accuracy of ±0.01 °C), which are cold store humidity (RHs), evaporator outlet humidity (RH1), dryer inlet humidity (RH2), tray inlet humidity (RH3), tray outlet (RH4) and dryer outlet humidity (RH6). Figure 37.5 shows the parameter control diagram of cold air assisted thin layer drying unit (Modified from [9, 25]) (Modified [1, 26]).

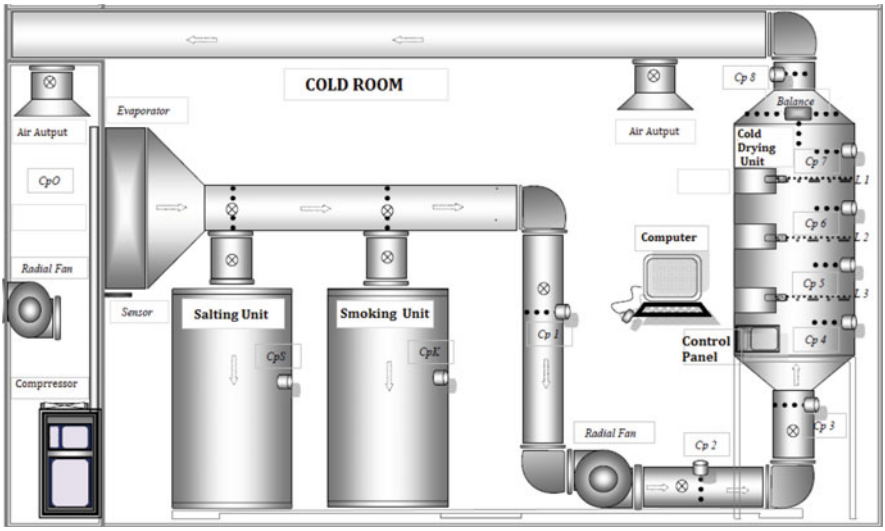

Fig. 37.4 Low temperature (Lt) assisted smoking unit: Cp: Control point, L: Layer (Modified from [9, 25])

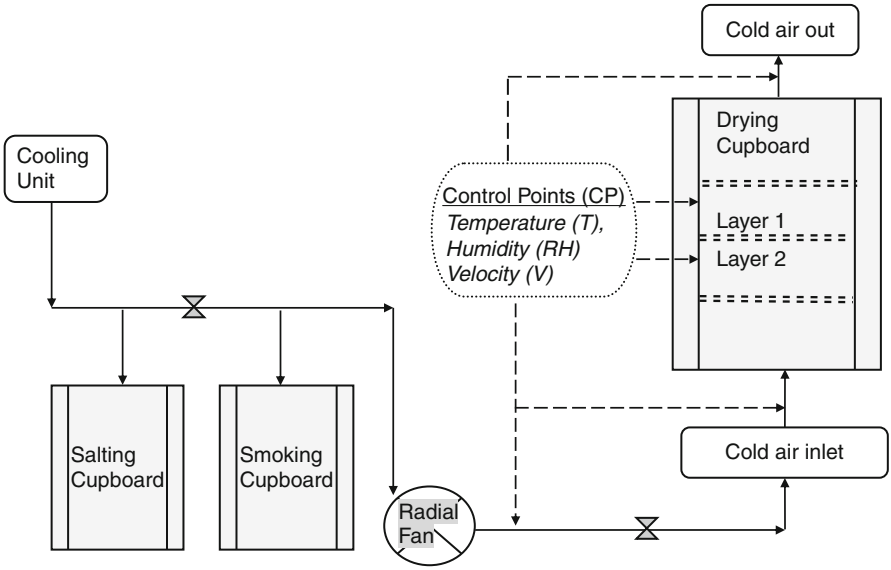

Fig. 37.5 Parameter control diagram of cold air assisted thin layer drying unit (*Modified from* [9, 25]) (*Modified* [1, 26])

2. *Cold Drying Temperatures*: The temperatures during drying process were identified with a METTLER model digital infrared thermometer such as;

   - *Cold store temperature (Ts),*
   - *Evaporator outlet temperature (T1),*
   - *Dryer inlet temperature (T2),*
   - *Tray inlet temperature (T3),*
   - *Tray outlet temperature (T4),*
   - *Dryer outlet temperature (T6).*

3. *Cold Air Velocity*: a TA-2 model automatic digital thermo anemometer was used to velocity identification at various control points of the drying system, with reading accuracy of ±0.01. The velocities are measured such as;

   - *Evaporator outlet (V1),*
   - *Dryer inlet (V2),*
   - *Tray inlet (V3),*
   - *Tray outlet (V4),*
   - *Dryer outlet (V6).*

4. *Samples Weight Loss*: this process parameter was carefully weighed by using two sensitive digital balance, with reading accuracy of ±0.01 °C [9].

37.3.3.2 Experimental Procedure

After Lt assisted Ls process, the produced Ls fillets were analyzed to determine the chemical, microbiological properties as well as quality indicators and shelf stability [9]. After production process of the product, all fish samples analyzed for the moisture, crude lipid, protein, ash, pH, salt, Water activity (a_w), condition factor, total volatile basic nitrogen (TVB-N), thiobarbituric acid reactive substance (TBARS) content, total viable count (TVC and mould (TYM) at the beginning of cold air drying process. LTHV assisted Cb and Ls samples were stored at 4 °C and analyzed at each 10 day of the storage time (0–10 to 20–30) [25].

37.4 Results and Discussion

37.4.1 Environmental Friendly Strategies Improving Food Quality and Safety

Food quality and safety are very important to the public health. Therefore, the negative effects on the raw food materials should be reduced by applying some environmental friendly food production strategies. Figure 37.6 shows the results of the increasing pollution and some sustainable strategies for the food quality and safety.

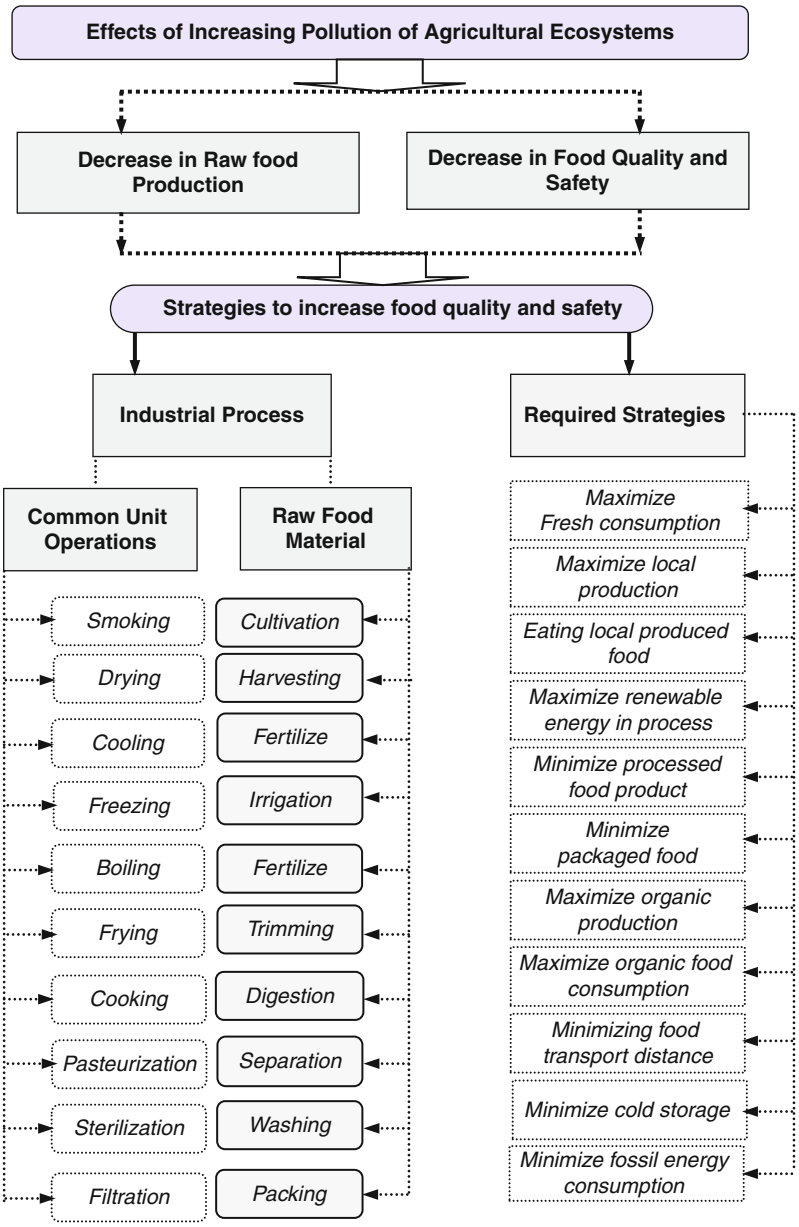

Fig. 37.6 Increasing pollution and practical sustainable strategies for food production, quality and safety (modified [27, 28, 29])

37.5 Results of the Case Study

Considering the main advantages of the unit operations of food processing systems, it can be said that Lt process technology can be assumed as one of the environmental friendly food processing technique. Applying this technology, the following results have been observed. Variation of temperature at 4 °C of cold air drying temperatures at 7 m/s was recorded during the experimental process. The values showed a good stability in the cold dryer. In order to determine the effects of thin layer cold drying on fish quality, the experimental applications were carried out by using the experimental set-up in the Biology laboratory of Nigde University. In this regard, before the properties indicating the fish quality were determined and discussed in detail, the parameters such as weight loss, dimensionless mass loss and moisture content of fish were identified [24, 25].

37.5.1 Cb Characteristics of Liquid Smoked Ls Fish

As shown in Fig. 37.7, the effect of fish species on the salt diffusion was not significant ($p > 0.05$). The salt content of fish fillets was average 2 % at 4 °C of 8 h (10 g^{-1} Na Cl). The differences in the salt contents weren't significant in fish species ($p > 0.05$) [24]. The NaCl content was 2,1 for trout, 2,2 g/g for mackerel and 2,2 g/g for bream at the end of the brining process. On the other hand, Gallart-Jornet et al. [23] found that, the NaCl content of cod and salmon was 0.152 w/w for cod

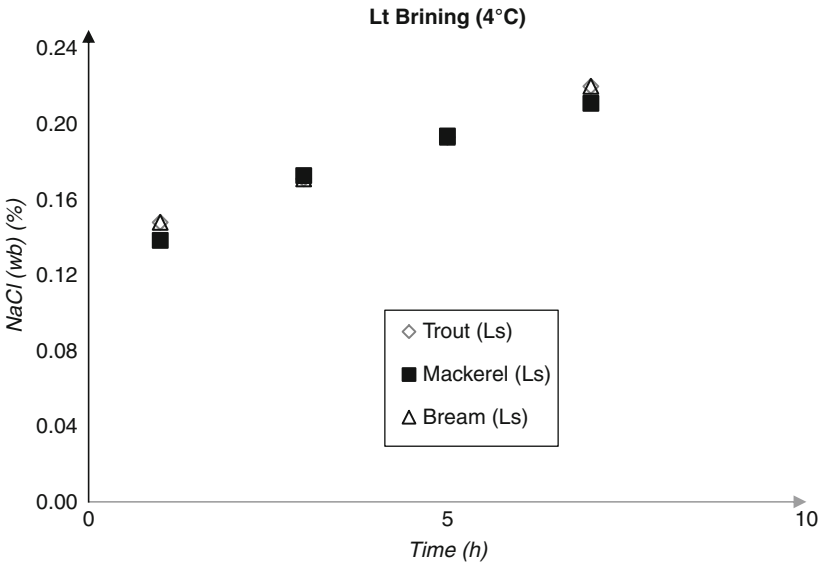

Fig. 37.7 NaCl content of fish fillets as a function at 4 °C (*modified from* [24, 25])

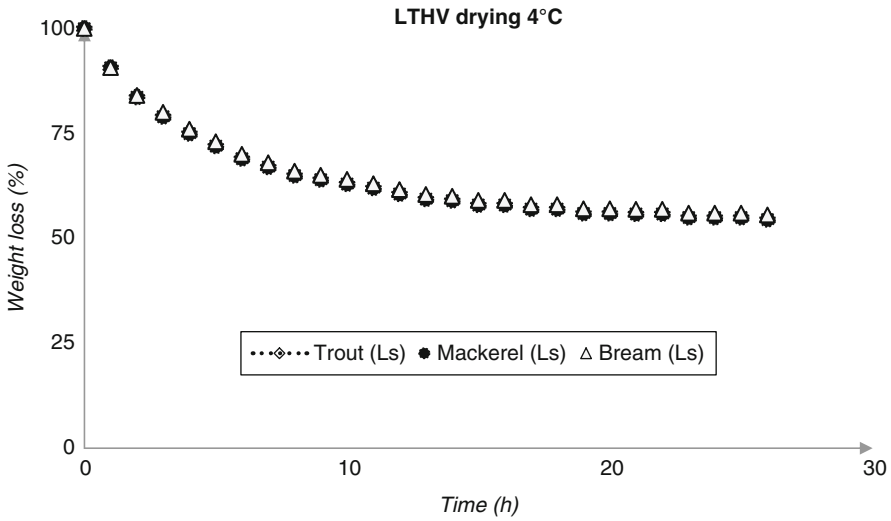

Fig. 37.8 The weight loss of fish samples versus drying time at 4 °C of cold air drying temperatures for Rainbow Trout, Horse Mackerel, Striped sea bream fillets at 7 m/s (*modified from* [24, 25])

and 0.106 w/w for salmon at the end of the brining process at 4 °C. A clear effect of brine concentration was found on the fish fillets during the brining [24, 25].

Figure 37.7 presents to the variations of NaCl in fish muscle as a function of brining time at 4 °C [24, 25].

37.5.2 Drying Characteristics of the Lt Assisted Ls Fish

Based on the experimental data, the single layer cold air drying curve equations for fish samples were found to be [24, 25]:

$$M(t) = 0.94\, exp(-0.15t) \text{ for Rainbow Trout } (O.\ mykiss) \text{ at } 4\ ^\circ\text{C} \quad (37.1)$$

$$M(t) = 0.95\, exp(-0.13t) \text{ for Horse Mackerel } (T.\ trachurus) \text{ at } 4\ ^\circ\text{C} \quad (37.2)$$

$$M(t) = 0.97\, exp(-0.15t) \text{ for Striped sea bream } (L.\ mormyrus) \text{ at } 4\ ^\circ\text{C}. \quad (37.3)$$

Figure 37.8 shows to the weight loss as a function of drying time for Rainbow Trout, Horse Mackerel, Striped sea bream based on drying air temperatures at 7 m/s. The corresponding exponential equation showed a good harmony with the experimental results in the cold air dryer. Consequently, it can be said that the drying curves follow the same trend and show a decrease by the increasing time [24, 25].

The weight of Lt dried samples decreased to ~ %50 at 4 °C in a drying time of 28 h. It was mean while observed that the fish fillets were slowly lost their weights

Table 37.1 Quality characteristics of Lt assisted Ls fish 4 °C (Modified from [24, 25]

Experimental groups		Quality parameters		
		TVB (mg/100 g)	TBA (mg MA/kg)	TVC (log $_{cfu}$/g)
Trout (*O. mykiss*)	R	19	0,7	1,2
	Cb	19	0,7	1,9
	Ls	19	0,7	1,4
	D	19	0,8	2,4
Horse Mackerel (*T. trachurus*)	R	18	0,3	1,7
	Cb	19	0,9	1,3
	Ls	18	0,5	1,5
	D	19	0,6	2,5
Striped sea Bream (*L. mormyrus*)	R	18	0,3	1,7
	Cb	19	0,8	1,3
	Ls	18	0,5	1,5
	D	19	0,6	2,5

R Raw, *Cb* cold brined, *Ls* liquid smoked, *D* dried (n = 10)

at drying temperature of 4 °C. The other fish species had the almost the same moisture content at the same drying velocity and drying temperature. A significant differences weren't observed for the other fish species ($p > 0.05$) [24, 25].

37.5.3 Ls Fish Quality and Safety

Total volatile basic nitrogen (TVB-N) is one of the common chemical quality parameter that is widely used for evaluation of the indicator of muscle food spoilage. TVB-N value as quantitative quality indicator of the dried fish samples was also determined for each experimental fish group. Based on the experimental data, it was identified that the TVB-N value had a significant results in all fish group. It was noticed that the fish samples cold smoked and dried at 4 °C had the lowest TVB-N value. The cold air drying process have a positive effect on the dried fish quality. Table 37.1 shows some quality aspects for Lt assisted Ls fish [24, 25].

Thiobarbituric acid reactive substances (TBARS) value showed significant differences between the experimental groups (Table 37.1.). Moreover, it was observed that the mackerel and bream had the least TBARS value while the TBARS was higher for trout dried at temperatures of 4 °C. Consequently, it can be said that cold air drying process have a positive effect on the lipid quality of Lt assisted Cb and Ls fish samples. As another quality indicator, t*otal viable counts (TVC)* remained stable in the experimental fish groups dried at 4 °C for 28 h [24, 25].

Figure 37.9 presents the variation of TVC (log cfu/g) content of Lt assisted Ls trout samples as a function of process steps and storage periods at 4 °C. As given in Fig. 37.9. TVC values of trout samples more stable at 4 °C. This differences were significant statistically ($p < 0.05$).

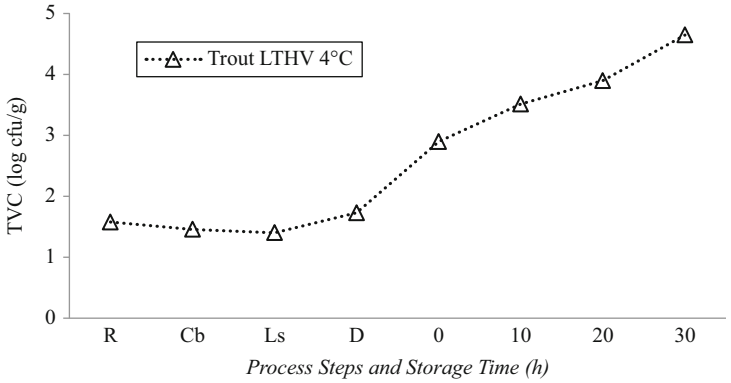

Fig. 37.9 TVC (log cfu/g) content of Lt assisted Ls trout samples as a function of process steps and storage periods at 4 °C (*modified from* [24, 25])

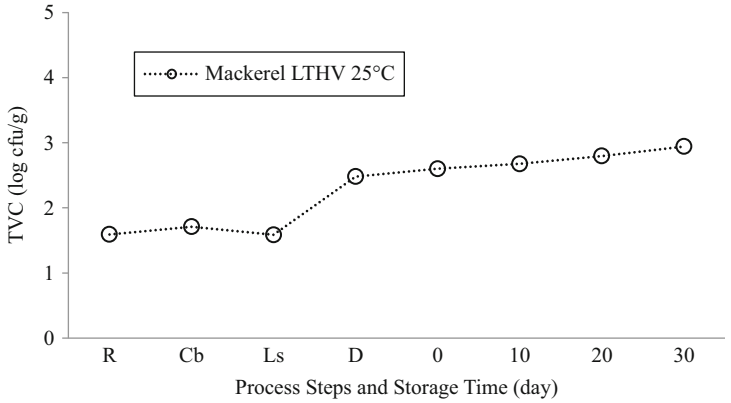

Fig. 37.10 TVC (log cfu/g) content of Lt assisted Ls mackerel samples as a function of process steps and storage periods at 4 °C (*modified from* [24, 25])

Figure 37.10 present the variation of variation of TVC (log cfu/g) content of LTHV assisted Cb and Ls mackerel samples as a function of process steps and brining time (day) at 25 °C [24]. As a shown in Fig. 37.10, TVC values of mackerel samples more stable at 4 °C like as trout. This differences were significant statistically ($p < 0.05$) [24, 25].

Thus, it is said that Lt assisted Ls technique applied at 4 °C contributes to improve the microbiological quality and shelf life of the smoked fish ($p < 0.05$) [24, 25]. Figure 37.11 shows TVC (log cfu/g) content of Lt assisted Ls bream samples as a function of process steps and storage periods (modified from [24, 25]).

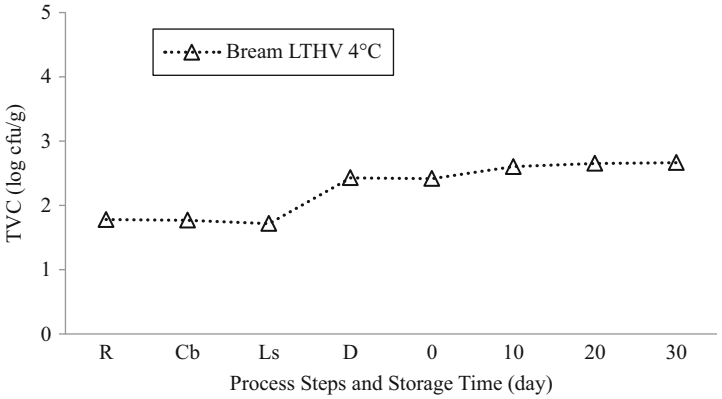

Fig. 37.11 TVC (log cfu/g) content of Lt assisted Ls bream samples as a function of process steps and storage periods at 4 °C (*modified from* [24, 25])

37.6 Conclusion

In this study, the required environmental benign low temperature drying, brining and liquid smoking applications for improving the food quality, safety and sustainability have been presented. In order to experience the advantage of the low temperature assisted brining, liquid smoking and drying process, a case study has been investigated. Based on the experimental results, the following conclusions are drawn;

- Considering the results, it can be said that one of the most appropriate technique for better food quality and sustainability is the Cold brining (Cb), low-temperature high-velocity (LTHV) drying and liquid smoking (Ls) method.
- In this regard, it is recommended that the Cb, LTHV and Ls process methods as common unit operations to be an environmental friendly food process technique for food quality, safety and sustainability in practical applications.
- As an important result of this technology, although the values of TVB-N, TBARS and of the fish fillets at 4 °C have the low values. Therefore, the better drying air temperature has been selected to be 4 °C because fish samples dried at this temperature had the lower values for the quality loss.
- Final moisture content of fish samples is average 27 % (wb) at 4 °C for constant drying velocity of 7 m/s during cold air drying process.
- According to the results of the case study, it can be said that one of the most appropriate technique for better food quality and sustainability is Cb and low-temperature high-velocity (LTHV) drying assisted Ls method with the least environmental impacts.

Finally, it is investigated that the application of cold salting, drying and liquid smoking can be applied to increase total quality of muscle foods. Accordingly, it is recommended that the Lt assisted Cb and Ls application should be used in food

industry due to food safety, food quality and environmental benign characteristics. Moreover, it is expected that the strategies and programs for the food processing systems will contribute to the food literature.

Acknowledgement The authors acknowledge the support provided by Nigde University in Turkey.

Nomenclature

LTHV	Low Temperature High Velocity
L_{LTHV}	Liquid smoke assisted LTHV
Ls	Liquid Smoking
Cb	Cold Brining
a_w	Water activity
CP	control point
M	weight loss, kg
M_t	weight of fish at t, kg
M_o	weight of fish at $t = 0$, kg
M_e	weight of fish in equilibrium state, kg
$M_{t+\Delta t}$	moisture content at $t + \Delta t$, kg water/kg dry matter, wb
t	time, h
W	moisture content, %
v	the constant of drying velocity, h^{-1}
F	*Fresh fish*
B	*Brined fish*
C	*Group control*
db	*Dry Basis*
wb	*Wet Basis*
TVC	*Total viable count*
TPC	*Total psychrophilic count*
TLC	*Total lactic acid bacteria*
TYM	*Total yeast and moluld*
TVB-N	*Total volatile bases nitrogen*
TBARS	*Thiobarbituric acid reactive substance*
WPS	*Water phase salt*
MA	*Malonaldehyde*
h	*hue*
db	*Dry bases*
Nd	*Not defined*
wb	*Wet bases*
C_h	*Chroma*

References

1. Kilic A, Midilli A, Dincer I (2008) A strategic program to reduce greenhouse gases emissions produced from food industry. Proceedings of the global conference on global warming (GCGW-08), Turkey, 648
2. Kilic A, Oztan A (2013) Effect of ascorbic acid utilization on cold smoked fish quality (oncorhynchus mykiss) during process and storage. Food Sci Technol Res 19(5):823–831
3. Birkeland S, Rora AM, Skara T, Bjerkeng B (2004) Effects of cold smoking procedures and raw material characteristics on product-yield and quality parameters of cold smoked Atlantic salmon. Food Res Int 27:273–286
4. Martinez O, Salmerón J, Guillen MD, Casas C (2011) Characteristics of dry- and brine-salted salmon later treated with liquid smoke flavoring. Agric Food Sci 20:217–227
5. Hilderbrand KS (2001) Fish smoking procedures for forced convection smokehouses. Seafood Processing Specialist Oregon State University Extension Sea Grant Program Hatfield Marine Science Center, Newport, Oregon, pp 97–365
6. Piga A, Del Caro A, Corda G (2003) Influence of drying parameters on polyphenols and antioxidant activity. J Agric Food Chem 51(12):3675–3681
7. Arason S (2003) The drying of fish and utilization of geothermal energy—the Icelandic experience, International Geothermal Conference, Reykjavík
8. Lewicki PP (2006) Design of hot air drying for beter foods. Trends Food Sci Technol 17:153–163
9. Kilic A (2009) Low temperature and high velocity (LTHV) application in drying: characteristics and effects on the fish quality. J Food Eng 91:173–182
10. Midilli A, Kucuk H (2003) Mathematical modeling of thin layer drying of pistachio by using solar energy. Energy Convers Manag 44:1111–1122
11. Hattula T, Elfving K, Mroueh UM, Luoma T (2001) Use of liquid smoke flavouring as an alternative to traditional flue gas smoking of rainbow trout fillets (*Oncorhynchus mykiss*). Lebensmittel-Wissenschaft und-Technologie 34(8):521–525
12. Karl H (1997) Influence of the smoking technology on the quality of smoked ish regarding undesirable compounds. In: Luten JB (ed) Seafood from producer to consumer, integrated approach to quality. Elsevier, Amsterdam, pp 633–639
13. Sikorski ZE (73) Smoking of fish and carcinogens. In: Burt JR (ed) Fish smoking and drying, the effect of smoking on the nutritional properties of fish. Elsevier Applied Science, London, pp 81–1988
14. Simon R, de la Calle B, Palme S, Meier D, Anklam E (2005) Composition and analysis of liquid moke flavouring primary products. J Sep Sci 28(9–10):871–82
15. Theobald A, Arcella D, Carere A, Croera C, Engel K-H, Gott D, Gurtler R, Meier D, Pratt I, Rietjens IMCM, Simon R, Walker R (2012) Safety assessment of smoke flavouring primary products by the European Food Safety Authority. Trends Food Sci Technol 27:97–108
16. EFSA (2007) Draft programme Scientific Forum. From safe food to healthy diets, EU risk assessment past, present and future. European Food Safety Authority, Scientific forum, p. 2
17. Van Loey AM, Smout CI, Hendrick ME (2005) Kinetic data for biochemical and microbiological processes during thermal processing (chap 13). In: Rao MA, Rizvi SSH, Datta AK (eds) Engineering properties of foods, 3rd edn. CRC Taylor & Francis, Boca Raton, FL, pp 611–643
18. Đukić VN, Okanović ĐG (2011) Application of best available techniques for environmental prevention in meat processing. Food Feed Res 38(2):87–93
19. Ismail N, Wootton M (1992) Fish salting and drying: a review. ASEAN Food J 7(4):175–183
20. Dincer I (1998) Moisture loss from wood products during drying-Part I: moisture diffusivities and moisture transfer coefficients. Energy Sour 20:67–75
21. Dincer I, Hussain MM, Sahin AZ, Yilbas BS (2002) Development of a new moisture transfer (Bi–Re) correlation for food drying applications. Int J Heat Mass Transf 45:1749–1755
22. Abbas KA, Ahmad MMHM, Sapuan SM, Wan MA, Jamilah B, Dincer I (2006) Numerical analysis of heat transfer in cooling of fish packages. Int Commun Heat Mass Transf 33:889–897

23. Gallart-Jornet L, Barat JM, Rustad T, Erikson U, Escriche I, Fito P (2007) A comparative study of brine salting of Atlantic cod *(Gadus morhua)* and Atlantic salmon *(Salmo salar)*. J Food Eng 79:261–270
24. Karakaya SG (2010) LTHV assisted liquid smoked fish quality and shelf life. M.sc., Thesis. Nigde University, Science Institute, Turkey
25. Kilic, A (2011) Low temperature high velocity drying (LTHV) applications in muscle foods (Ch 10). In: D.A. Medina, A.M. Laine (eds) Food quality: control, analysis and consumer concerns. ISBN: 978-1-61122-917-2
26. Midilli A, Dincer I (2007) Key strategies of hydrogen energy systems for sustainability. Int J Hydrogen Energy 32(5):511–524
27. Kilic A, Midilli A, Dincer I (2010) A strategic program to reduce greenhouse gases emissions produced from food industry (Chapter 10). In: Dincer I et al (eds) Global warming engineering solutions: green energy and technology. Springer, New York, pp 197–210
28. Kilic A, Midilli A, Dincer I (2009) An environmental-benign fish drying technique for better quality and sustainability. Proceedings of the global conference on global warming-2009 (GCGW-09), Turkey, 564
29. Kilic A, Midilli A, Dincer I (2010) A novel fish-drying technique for better environment, quality and sustainability. Int J Global Warming 2(3):262–278

Chapter 38
Impact of Shape, Occupation and External Parameters in the Overall Thermal Performance of Office Buildings in Santiago, Chile

Claudio Vásquez, Alejandro Prieto, and Carlos Aguirre

Abstract Office buildings in Santiago do not respond adequately to their climate context, which brings issues of discomfort at indoor spaces or high energy consumption in order to achieve comfortable conditions. The paper intends to establish certain relationships between several parameters registered on different office buildings in Santiago in order to address the issue about how different variables related to design and operation of the buildings impact on its overall performance. This is carried out via Principal Component Analysis of selected parameters registered inside several floors within representative office building types present in the city. Preliminary findings suggest that internal conditions hold no relation with external parameters due to the reliance on active air-conditioning systems; or with shape parameters registered on-site. On the other hand it is possible to identify occupation as a key parameter on workspace thermal performance and overheating as a relevant issue to consider at design stages.

Keywords Façade • Office building • Comfort

38.1 Introduction

Since the last decade of the 20th century, the development of office buildings in Santiago has been growing increasingly promoted by private investors. This issue has allowed the generation of important processes of technological transfer on construction methods followed by a consequent sophistication of building components. This becomes more apparent by looking the development of façade systems and solutions. The amount of office buildings that consider curtain-wall as its principal façade system reaches to 64 % on all the buildings constructed in the last decade (considering only high-standard office buildings) (Fig. 38.1).

C. Vásquez (✉) • A. Prieto • C. Aguirre
Pontificia Universidad Católica de Chile, 1916 El Comendador street, Santiago 7530091, Chile
e-mail: clvasque@uc.cl; alejandroprieto@uc.cl; caguirr@uc.cl

I. Dincer et al. (eds.), *Progress in Sustainable Energy Technologies Vol II: Creating Sustainable Development*, DOI 10.1007/978-3-319-07977-6_38

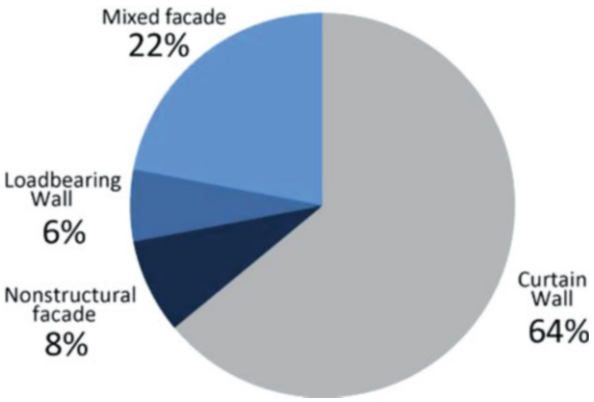

Fig. 38.1 Façade systems present on high-standard offices buildings constructed in Santiago from 2003 to 2011

Nevertheless, the high standards of technical aspects of construction in office buildings are not correlated with high standards on indoor environment conditions nor the amount of energy required for their operation under comfortable levels. Mainly, the buildings are characterized as slender shape prisms with high window-to-wall ratio, low thermal mass and very little use of solar protection on facades, which does not relate directly with the climate conditions of Santiago.

According to Köppen's climatic classification, Santiago has warm temperate climate with a dry summer, like California, North Africa, the Mediterranean zone and the Persian Gulf. This means a short period of winter rains and a long dry season. The thermal oscillation reaches to 13 °C between the warmest month (January) and coldest (July) and 14–16 °C between daily maximum and minimum. Moreover the levels of radiation in the horizontal plane are between 1.380 and 1.666 kWh/m^2 year, equivalent to Chile's northern desertic coastal zone.

It is established as a hypothesis for the present research that office buildings in Santiago do not respond adequately to their climate context, which brings issues of discomfort at indoor spaces or high energy consumption in order to achieve comfortable conditions. However, there is few information on how does the buildings operate in terms of indoor ambient quality and how the different variables related to the design and operation of the building impact on the overall performance.

The paper intends to establish certain relationships between several parameters registered on different office buildings in Santiago, in order to respond the questions formulated and therefore be able to contribute to a general knowledge associated with the design and operation of offices buildings in the city.

The analyzed parameters are characterized according to the following groups (Table 38.1):

- *External parameters*: The knowledge of the climate conditions of a specific region is basic to understand the phenomenon which should be taken care for in the design of any building, in order to generate comfortable indoor conditions. The preliminary analysis considers the study of the thermal environment so it

Table 38.1 Analyzed parameters by group

External	Internal	Int/Ext differential
External Temp (inst)	Internal Temp (instantaneous)	Temp differential (ext/int)
AVG External Temp last 8 h	AVG Internal Temp last 8 h	Rel. Humidity differential (ext/int)
Solar radiation (inst)	Internal Relative Humidity (inst)	Thermal comfort index (yes/no)
AVG Solar radiation last 8 h	Internal Rel.humidity last 8 h	
External rel.humidity (inst)		
External rel.humidity last 8 h		

Occupation	Shape	Months
Day type (workday/weekend)	Floor area (m^2)	October
Internal gains: Occupation (kWh)	Exposed facade area (m^2)	November
Internal gains: Lighting (kWh)	Floor height (m)	December
Internal gains: Equipment (kWh)	Floor volume (m^3)	January
Internal gains: total (kWh)	Floor Shape factor (m^2/m^3)	February
Internal gains: total/floor area (kWh/m^2)	Facade area/Floor volume (m^2/m^3)	March

comprehends the external parameters related directly with it, such as temperature, relative humidity and solar radiation.

- *Internal parameters*: For the analysis presented on this paper, only thermal characteristics of the indoor environment were considered. The measurement of temperature and relative humidity at offices is being carried accordingly to international measurement and verification protocols developed by several organizations such as EVO (Efficiency Valuation Organization) and NREL (National Renewable Energy Laboratory) [1, 5]. The importance of adequate thermal indoor conditions has been registered on standards [13, 14], and has been evaluated specifically on workspaces on several research projects via surveys, such as the BUS method and PROBE project [9], and the realization of on-site measurements like the ones conducted under the HOPE project [2] and other similar studies [4, 10].
- *External/internal differential parameters*: These set of data comprehend parameters constructed from the ones described above, to evaluate the difference between the internal and external conditions and comfort level of the indoor environment. To achieve this a "thermal comfort index" is included in the analysis as a dummy variable. This is a yes/no index that indicates if the instantaneous temperature and relative humidity are within comfort range.
- *Occupation parameters*: Occupation role in thermal indoor conditions has been researched on office buildings by several investigators, following the initial investigations led by Francis Duffy, distinguishing work patterns and their consequently comfort levels among employees [3, 7]. On the current stage of analysis of the study cases, internal occupation is considered via internal gains,

trying to relate it to the thermal performance of indoor space. It is distinguished between occupation, equipment and lighting gains via on-site registry of the conditions. Also, a dummy variable called "day type factor" is included on the analysis. It is a 0/1 value given to the day measured if it correspond to a weekend or a work day respectively, so it correlates directly to internal gains parameters.

- *Shape parameters*: The buildings were previously characterized as part of the selection process of the study cases. Some indicators well recognized on previous studies were utilized such as shape factor, window-to-wall ratio and floor plan proportion [6, 11, 12]. However, given that analyzed cases correspond to specific floors within several buildings, shape parameters included in the analysis refer to formal variables of the selected floors derived from the indicators described above. For the characterization of the study cases, some general shape parameters were utilized, such as floor area, volume and height. Also, two parameters were included, derived from shape factor: A floor shape factor, considering the relationship between surface area and indoor air volume (including floor and ceiling area, not exposed to external variables); and another one which relates exposed façade area and indoor air volume (thus considering only exposed surfaces).
- *Month related parameters*: Dummy variables that are included in the analysis to comprehend any variation or anomaly on the performance of the building due to external parameters not registered specifically.

38.2 Methodology

38.2.1 Methodology for the Measurement and Gathering of Data

This paper is part of a general research which main objective is to establish a baseline of post-occupancy energy consumption and indoor ambient quality of office buildings in Santiago, Chile.

The methodology considers the continuous monitoring of several floors in four office buildings for one year. The study cases analyzed were determined by an extensive study of the buildings in the city which have been used for more than two years, establishing their main characteristics in order to focus on representative examples of the typology (Fig. 38.2).

There are three types of data considered that allow an overall assessment of the performance of each one of the cases: Ambient parameters, energy consumption and comfort perception. The ambient parameters allow comparing the state of the exterior and interior space during occupied and unoccupied hours, in order to understand the conditions under which the building operates, while energy consumption readings and comfort surveys tell how much does this operation cost and how it is perceived, respectively (Fig. 38.3).

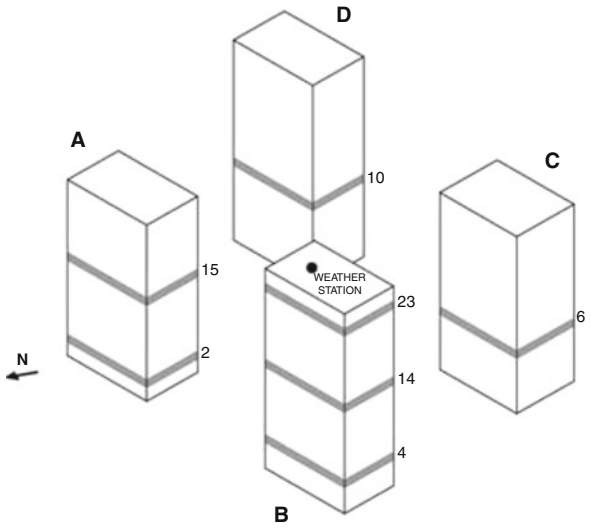

Fig. 38.2 Selected study cases: Several floors in four office buildings, considering the installation of a local weather station

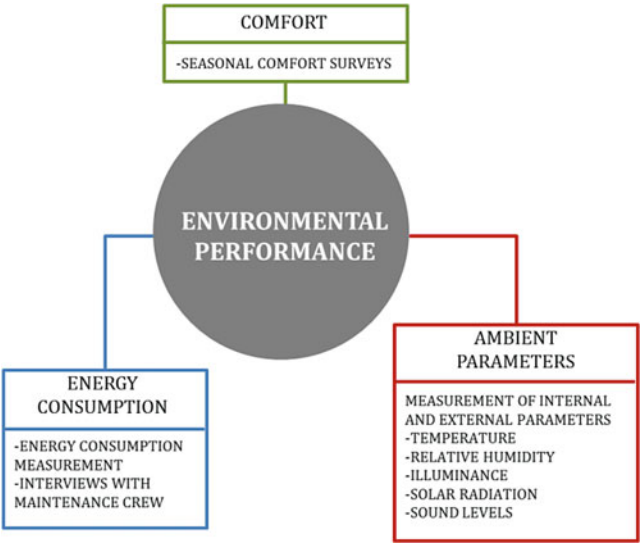

Fig. 38.3 Measurement protocol for the main research. Only ambient thermal parameters are considered on the first stage of analysis

This paper takes a particular aspect of the general research, showing the preliminary findings at a first stage of analysis of data registered during spring and summer seasons. The analyzed data consists in internal temperature and relative humidity readings, gathered since October, 2011 until March, 2012, at intervals of 10 min; and external temperature, relative humidity and solar radiation, measured by a local weather station mounted on-site, considering the same sampling rate.

38.2.2 Methodological Aspects of the Analysis

To be able to visualize the relationship between the physical factors measured at the interior environment of the offices, the external variables, and the operational and design parameters of the building, the data is analyzed via Principal Component Analysis. Besides the analytical aspects inherent to the method, it is also useful to check that measured variables don't repeat information and therefore, they settle in the dimensions identified in the theoretical framework.

The principal component analysis [8], sets the dimensions whose correlation is zero on a set of data. In conducting this analysis, it is possible that measured variables that are related with each other, are sorted and settle on different dimensions which are known as underlying factors. In that sense, the hypothesis is that the dimensions have a clear relationship between them, identifying the theoretical dimensions considered on the measurement of the variables (temperature, humidity, aspects related to internal gains, cyclical effects, etc.).

However, given the amount of data registered and the fact that it consisted on temporal successive series, it was difficult to apply the method to analyze the entire set. Therefore, as a first stage of results review, the analysis is carried out for cross-section sets of data (considering temperature lag), in order to establish certain relationships between the parameters under the same time constant and then compare the results to evaluate changes through the day.

The analyzed cross-sections were carried out at 9:00 and 18:00, for every day of spring and summer seasons (October to March). The election of the time frame for the analysis considers two relevant moments on a typical day, the estimated start and end of a work schedule. Besides, the conditions between those two moments are considered via the inclusion of a dummy variable, which illustrates the average internal temperature and relative humidity and the average values for the external parameters from the past 8 h. The inclusion of this variable allows the comparison between occupied and unoccupied moments of the day, as well as day and night variations, which is a relevant topic considering the climate specific conditions of Santiago, Chile.

The principal component analysis is conducted at the parameters registered at 9:00 and 18:00 separately, allowing an understanding of the resulting dimensions and the relationships between the parameters for each time frame, and then compare the results to evaluate possible changes through the day, in form of quantity and order of the encountered relationships. Besides, the analysis is conducted separately for each season in order to compare the results not only daily, but also considering seasonal variations on the measured parameters (Fig. 38.4)

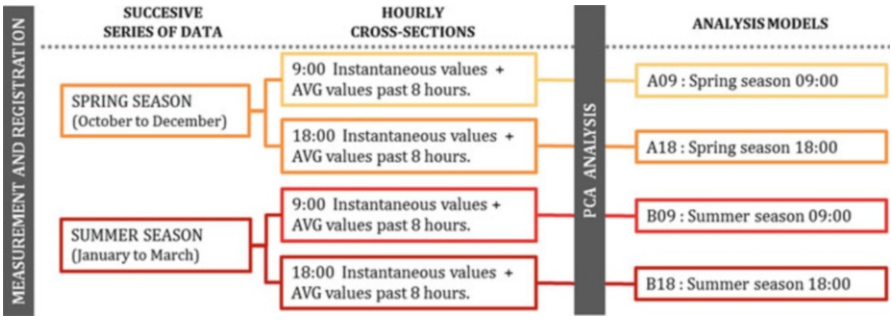

Fig. 38.4 Analysis methodology for the set of data

38.3 Results and Discussion

The Principal Component Analysis (PCA) conducted for the registered parameters, shows several issues worth mention, concerning the groups obtained in the process and the differences seen in the relationships between parameters when comparing the analysis for each season and time of day: Spring 9:00 (A09), Spring 18:00 (A18), Summer 9:00 (B09), Summer 18:00 (B18).

First, the PCA shows concordance between the groups obtained and the type of parameter, which means that the parameters are consistent to each other, so they were measured correctly. Table 38.2 shows the PCA for all four analyzed situations distinguishing the resulting groups (components) for each one, due to the presence of coefficients of correlation of 0.5 or higher. The lack of data in one or more columns means that such group doesn't exist for said situation. The analyzed parameters are classified according to their type for better understanding of the measured dimensions.

There are external parameters, measured on the meteorological station; internal temperature and humidity parameters, measured inside each of the study cases; parameters that describe the difference between inside and outside; occupation parameters, such as day type (labour/non-labour) and internal gains; shape parameters; and finally, the months on which the study took place, converted on factors in order to comprehend any variable associated with each month not directly measured.

The external parameters are distributed on two components (1 & 2). All the parameters are contained in the first group on spring season, but solar radiation shows no relevant relationship with the rest (temperature and relative humidity) on summer, at neither 9:00 nor 18:00, although it is highly related to January and March, which conforms the second group of external variables.

The third group includes all the occupation parameters; and the fourth and fifth all shape parameters, divided on two groups according to the different relationships between them. The sixth and seventh groups include internal temperatures and relative humidity parameters respectively, but they don't appear for all the analyzed

Table 38.2 PCA results for each model. Values over or below 0.5/−0.5 are marked

		1° COMPONENT (EXTERNAL)				2° COMPONENT (EXTERNAL 02)				3° COMPONENT (OCCUPATION)				4° COMPONENT (SHAPE)				5° COMPONENT (SHAPE 02)				6° COMPONENT (INT TEMPERATURE)				7° COMPONENT (INT HUMIDITY)				8° COMPONENT (MONTHS)			
	PARAMETERS	A09	A18	B09	B18	A09	A18	B09	B18	A09	A18	B09	B18	A09	A18	B09	B18	A09	A18	B09	B18	A09	A18	B09	B18	A09	A18	B09	B18	A09	A18	B09	B18
EXTERNAL	External Temp (inst)	0,9	1,0	0,9	-0,9			0,3	0,1	0,0	0,0	0,0	0,1	0,0	0,0	0,0	0,0	0,0	0,0	0,0	0,0	0,3		0,2		0,2	0,2	0,1		0,0	0,1	0,1	-0,1
	AVG External Temp last 8 hrs	0,8	0,9	0,9	-0,8			0,0	0,1	0,1	0,0	0,1	0,0	0,0	0,0	0,0	0,0	0,0	0,0	0,0	0,0	0,4		0,2		0,2	0,2	0,1		0,0	0,0	0,2	0,0
	Solar radiation (inst)	0,8	0,6	0,2	-0,1			0,9	0,9	-0,1	0,0	0,0	0,0	0,0	0,0	0,0	0,0	0,0	0,0	0,0	0,0	-0,1		0,1		0,1	0,2	0,0		0,3	0,3	0,0	-0,1
	AVG Solar radiation last 8 hrs	0,8	0,8	0,1	-0,2			1,0	0,9	0,0	-0,1	0,1	0,0	0,0	0,0	0,0	0,0	0,1	0,0	0,0	0,0	0,1		0,1		0,1	0,1	0,0		0,4	0,2	0,0	0,1
	External rel.humidity (inst)	-0,9	-0,8	0,1	0,9			-0,1	0,1	0,0	0,1	0,0	0,0	0,0	0,0	0,0	0,0	0,0	0,0	0,0	0,0	-0,1		0,0		0,4	0,5	0,8		0,1	0,0	-0,2	0,1
	External rel.humidity last 8 hrs	-0,7	-0,9	-0,9	0,9			0,3	0,1	-0,1	0,1	-0,1	0,0	0,0	0,0	0,0	0,0	0,0	0,0	0,0	0,0	-0,2		0,1		0,6	0,4	0,2		0,1	0,1	0,1	0,0
INTERNAL	Internal Temp (instantaneous)	0,3	0,1	-0,1	0,0			0,1	-0,1	-0,3	-0,9	-0,6	-0,9	-0,1	0,2	0,0	0,2	0,0	0,0	0,1	-0,1	0,8		0,7		-0,1	-0,1	-0,1		0,1	0,0	0,1	0,0
	AVG Internal Temp last 8 hrs	0,3	0,2	0,0	0,0			0,0	0,0	0,1	-0,8	0,0	-0,9	0,1	0,0	0,3	0,0	0,2	-0,1	0,3	-0,1	0,8		0,8		0,0	-0,1	-0,2		0,1	0,0	0,1	0,0
	Internal Relative Humidity (inst)	0,0	0,0	-0,5	0,5			0,3	0,3	0,1	0,5	0,1	0,6	0,0	-0,1	-0,1	-0,3	0,0	0,0	-0,1	0,1	-0,1		-0,2		1,0	0,8	0,5		0,0	0,0	0,3	0,1
	Internal Rel.humidity last 8 hrs	0,0	0,1	-0,5	0,6			0,3	0,3	0,0	0,5	0,0	0,5	-0,2	0,0	-0,3	-0,2	-0,1	0,1	-0,2	0,1	-0,1		-0,2		0,9	0,8	0,5		0,0	0,0	0,3	0,1
INT/ EXT	Temp differential (ext/int)	-0,9	-0,9	-0,9	0,6			-0,2	-0,1	-0,1	-0,3	-0,3	-0,7	0,0	0,1	0,0	0,1	0,0	0,0	0,0	-0,1	-0,1		0,2		-0,2	-0,2	-0,1		0,0	-0,1	-0,1	0,0
	Rel. Humidity differential (ext/int)	1,0	0,9	0,9	-0,7			0,0	0,1	0,0	0,2	0,2	0,4	-0,1	-0,1	0,0	-0,2	0,0	0,0	0,0	0,0	0,1		-0,2		-0,1	0,0	-0,1		-0,1	0,0	-0,1	0,0
	Thermal comfort index (yes/no)	0,0	-0,1	-0,1	0,0			-0,1	0,0	0,2	0,8	0,3	0,9	-0,1	0,0	0,0	0,1	0,0	0,0	0,0	0,0	-0,4		-0,7		0,0	0,1	0,0		0,0	0,0	0,1	0,0
OCCUPATION	Day type (workday/weekend)	0,1	0,0	0,1	-0,1			0,0	0,0	0,9	0,9	0,9	1,0	0,1	0,1	0,1	0,1	0,0	0,0	0,0	-0,1	-0,1		-0,2		0,0	0,1	0,0		0,0	0,0	0,0	0,0
	Internal gains: Occupation (kWh)	0,0	0,0	0,1	-0,1			0,0	0,0	1,0	0,9	1,0	0,9	0,0	0,0	-0,1	0,0	0,1	0,0	0,1	0,0	-0,1		-0,1		0,1	0,1	0,0		0,0	0,0	0,0	0,0
	Internal gains: Lighting (kWh)	0,0	0,0	0,1	-0,1			0,0	0,0	0,9	0,9	0,9	0,9	-0,2	-0,2	-0,2	-0,2	0,1	0,1	0,1	0,1	0,0		-0,1		0,0	0,1	0,0		0,0	0,0	0,0	0,0
	Internal gains: Equipment (kWh)	0,0	0,0	0,1	-0,1			0,0	0,0	1,0	0,9	0,9	0,9	-0,1	-0,1	-0,1	-0,1	-0,1	-0,1	-0,1	-0,1	-0,1		-0,1		0,0	0,1	0,0		0,0	0,0	0,0	0,0
	Internal gains: total (kWh)	0,0	0,0	0,1	-0,1			0,0	0,0	1,0	1,0	1,0	1,0	-0,1	-0,1	-0,2	-0,2	0,1	0,0	0,1	0,0	0,0		-0,1		0,0	0,1	0,0		0,0	0,0	0,0	0,0
	Int gains: total/floor area (kWh/m2)	0,0	0,0	0,1	-0,1			0,0	0,0	1,0	1,0	1,0	1,0	0,1	0,1	0,1	0,1	0,0	0,0	0,0	0,0	-0,1		-0,1		0,0	0,1	0,0		0,0	0,0	0,0	0,0
SHAPE VARIABLES	Floor area (m2)	0,0	0,0	0,0	0,0			0,0	0,0	0,1	0,1	0,1	0,1	-1,0	-1,0	-1,0	-1,0	0,1	0,1	0,1	0,1	0,0		-0,1		0,1	0,0	0,0		0,0	0,0	0,0	0,0
	Exposed facade area (m2)	-0,1	0,0	0,0	0,0			0,0	0,0	0,0	0,0	0,0	0,0	0,4	0,4	0,4	0,4	0,7	0,7	0,7	0,7	0,2		0,2		-0,1	0,0	0,0		0,0	0,0	0,0	0,0
	Floor height (m)	0,0	0,0	0,0	0,0			0,0	0,0	-0,1	-0,1	-0,1	-0,1	0,2	0,2	0,2	0,2	-0,9	-0,9	-0,9	-0,9	0,0		0,0		0,0	0,0	0,0		0,0	0,0	0,0	0,0
	Floor volume (m3)	0,0	0,0	0,0	0,0			0,0	0,0	0,0	0,0	0,0	0,0	0,0	0,0	0,0	0,0	1,0	1,0	1,0	1,0	0,0		0,0		0,0	0,0	-0,1		0,0	0,0	0,0	0,0
	Floor Shape factor (m2/m3)	0,0	0,0	0,0	0,0			0,0	0,0	-0,1	-0,1	-0,1	-0,1	0,9	0,9	0,9	0,9	0,4	0,4	0,4	0,4	0,1		0,1		-0,1	0,0	0,0		0,0	0,0	0,0	0,0
	Facade area / Floor vol (m2/m3)	0,0	0,0	0,0	0,0			0,0	0,0	-0,1	-0,1	-0,1	-0,1	1,0	1,0	1,0	1,0	-0,1	-0,1	-0,1	-0,1	0,0		0,1		-0,1	0,0	0,0		0,0	0,0	0,0	0,0
MONTHS	October	-0,4	-0,5							-0,1	0,0			0,0	0,0			0,0	0,0			-0,3				-0,4	-0,4			-0,6	-0,7		
	November	0,0	0,1							0,1	0,1			0,0	0,0			0,0	0,0			0,0				-0,3	-0,4			0,9	0,9		
	December	0,4	0,4							0,0	-0,1			0,0	0,0			0,0	0,0			0,4				0,6	0,8			-0,3	-0,2		
	January			-0,2	0,3			0,9	0,7			0,0	0,0			0,0	0,0			0,0	0,0			-0,1				0,0				-0,3	0,6
	February			0,1	-0,1			-0,2	0,2			0,0	0,0			0,0	0,0			0,0	0,0			0,1				-0,1				0,9	-1,0
	March			0,1	-0,2			-0,7	-0,9			0,0	0,0			0,0	0,0			0,0	0,0			0,0				0,1				-0,6	0,4

A09 Spring season 09:00 h, *A18* Spring season 18:00 h, *B09* Summer season 09:00 h, *B18*Summer season 18:00 h

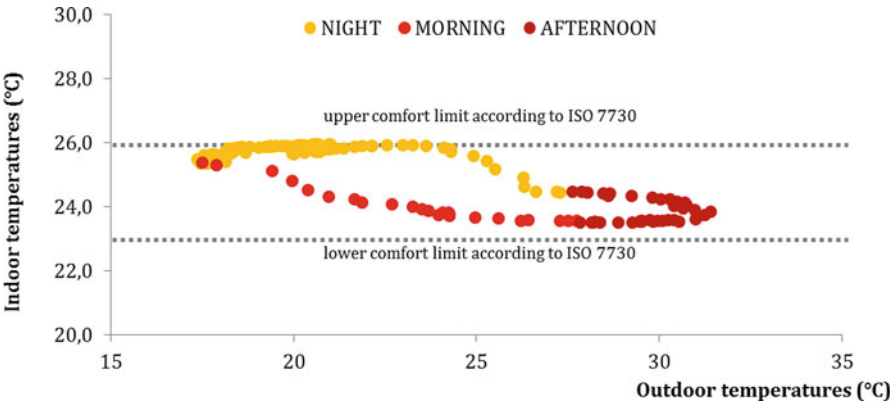

Fig. 38.5 Graph comparing indoor air temperature and outdoor air temperature on a typical workday for one of the study cases

cases. While internal relative humidity appears to be a phenomenon that doesn't relate clearly to other parameters (thus, being in its own independent group), in the case of internal temperature this is true only at 09:00 for both spring and summer, meaning that air temperature of the offices relates to other parameters as the day goes by. Finally, the last group includes the type of month previously explained.

Besides the composition of the components, which as it was previously stated, shows high consistency on the measuring, it seems relevant to discuss a few conclusions related to the relationships encountered between certain parameters:

(a) Interior/exterior differential holds no relation with internal conditions.
As it was predicted, the difference between internal and external conditions shows no relationship with the ambient parameters measured inside the buildings, particularly in the case of air temperature. In buildings like the ones being analyzed at the current research (buildings with high window-to-wall ratio, low thermal mass and high internal gains) the achievement of acceptable indoor conditions relies on the use of HVAC systems. In the analyzed cases, this proves to be especially true at warm months, showing high energy consumption for the extensive use of AC units.

These characteristics, documented via energy consumption bills and interviews with the maintenance managers of each building, are reflected directly on the results obtained on the PCA. Observing the results, it is confirmed that indoor temperatures hold minimum relation with external temperatures, and also the differential between interior and exterior is not related to the indoor measurements. These results show the presence of temperature controlled interior spaces, in opposition with a high thermal amplitude, characteristic of the climatic context of Santiago (Fig. 38.5).

The autonomy of indoor temperature becomes more apparent on summer data, reaching factors as low as −0,07 and −0,03 for 9:00 and 18:00 respectively for the correlation between internal temperatures and the "external"

component. The fact that there are values closer to zero at 18:00 also proves the artificial conditions under which the indoor environment operates at work hours, however, analyzing the minor difference between them, it could be stated that conditions over night show few variation in terms of temperature (the air-tightness of the façade system prevent the use of night ventilation or other strategies that could reduce the heat stored during the day).

The fact that relative humidity appears to be indirectly related to external factors only on summer season responds to no apparent reason, so it should be further analyzed on future inquiries.

(b) Shape factors do not relate directly with internal ambient parameters.
At the office buildings analyzed under the present research were found no relationships between the measured ambient parameters and variables related to the shape and design of the workspaces. Common shape indicators as floor area, volume and height, and specific variables such as façade area, shape factor and façade area per floor volume were included in order to understand its influence on the interior thermal environment, but there were no relevant correlation found.

The analysis suggests that these issues hold relatively minor importance in office buildings with the characteristics mentioned before (high window-to-wall ratio, low thermal mass, high internal gains), if it is compared with occupation issues, climatic context or technical specifications of façade systems. Nevertheless, the similarity of the cases studied at the present research suggests the necessity of further investigation on a larger amount of more heterogeneous office buildings in order to address this issue in more conclusive ways.

(c) Overheating and occupation: Key issues in office building design and maintenance
The necessity of lowering the internal temperatures to achieve comfort is shown in the PCA analysis. The results show high correlation (−0,74) for the thermal comfort index (TCI) at the "internal temperature component" at 9:00 on summer season and almost reaches −0,5 on spring (−0,44). The observed values suggest that the presence of thermal comfort is related indirectly to the internal temperature measured, or in other words, as the indoor temperature goes higher, thermal comfort descends, which describes the issue of overheating as a major design factor to consider in order to achieve indoor comfort.

The correlations addressed are shown only at 9:00 cases, because as it was said before, at that time internal temperatures are less influenced by the operation of AC units. On the other hand, comfort issues at 18:00 appears related to Occupation parameters, which make sense given that 18:00 model considers the effect of occupation during work hours.

It is noted that "Occupation" component comprehends not only parameters related to use and occupation of the office space, but also indoor temperature and relative humidity values registered during work hours. The fact that internal ambient conditions appear related to occupation instead of being isolated on its own component (as may be noticed on 9:00 models), suggest that operation and use of the workspace has a relevant impact in the indoor conditions and thermal comfort.

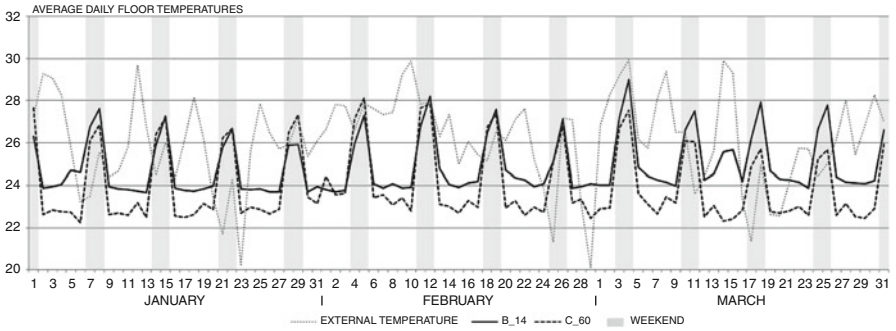

Fig. 38.6 AVG daily floor temperatures for summer season

In fact, results show that the "thermal comfort index (TCI)" is directly related to internal gains parameters and day type factor. The fact that TCI is directly related to day type suggests that there are better levels of comfort on work days than on weekends, which proves to be logical by looking the complete data series (Fig. 38.6), which show higher temperatures on weekends due to overheating and lack of ventilation measures.

TCI appears indirectly related to indoor temperature at 18:00 models also, which confirms the issue of overheating addressed previously. However, if higher temperatures equal low comfort levels, the resulting relationship between internal gains and comfort levels apparently should not exist, as occupation and equipment gains should rise indoor temperatures. The fact that it does appears on the PCA indicates the distortion produced as a result of the use of AC units, showing an apparent correlation via an external variable not analyzed in the present document: energy consumption. By analyzing the results, it is possible to suggest that as internal gains increase, also increases the stress of the AC system to generate comfortable thermal conditions, and therefore lower indoor temperatures. Given that all correlations between these parameters seem to be stronger on summer (period of greatest demand for the AC units due to external conditions), it is plausible to defend the stated hypothesis. However, there is need for further detailed analysis in order to quantify and measure the correlations visualized in more precise ways, including energy consumption as another input to evaluate the performance of AC system.

38.4 Conclusions

The present document shows preliminary findings from the first stage of analysis of an on-going investigation, therefore the issues mentioned on this paper are not presented as conclusive matters. However, the preliminary analysis presented raise

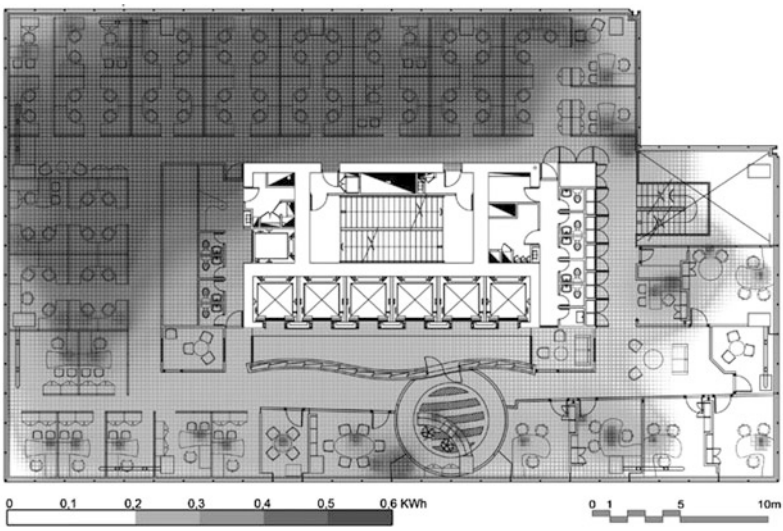

Fig. 38.7 Internal gains distribution in one of the analyzed floors

certain concerns worth mention about the design and operation of office buildings in Santiago, Chile, which should be addressed in more detail on further analysis and investigations.

In regard of indoor environment conditions, it shows the presence of overheating problems inherent on the design of these kinds of buildings, due to high window-to-wall ratio and low thermal mass. Besides, this issue becomes more relevant considering high internal gains, characteristic of the occupation of office buildings.

Also, regarding operation of the workspace there are no measures being taken to reduce the heat stored inside the building, like the use of nocturnal ventilation due to air-tight facades. Another issue worth mention relates to workstations distribution on the floor plan. Not only there is high occupation on the study cases, but also is observed an uneven distribution of it, which may cause discomfort on local zones given that AC units are mainly controlled centrally (only closed offices have AC controls attached to the wall) (Fig. 38.7).

The issues exposed on the present document show part of the complexity associated with indoor conditions actively controlled on several offices buildings in Santiago, without taking the advantages of a more natural relationship with external environment, which could improve thermal comfort levels for the occupants, reducing the stress of AC system and energy consumption associated with it.

Acknowledgment This work was done with the support of CONICYT (National Council of Scientific and Technological Research), Chile, through the project No. 11100143. It has also had the support of the Center for Sustainable Urban Development (CEDEUS), CONICYT/FONDAP Project 15110020.

References

1. Barley D et al. (2005) Procedure for measuring and reporting commercial building energy performance/technical report NREL/TP-550-38601. EE.UU: National Renewable Energy Laboratory (NREL)
2. Bluyssen P, Aries M, Van Dommelen P (2011) Comfort of workers in office buildings: the European HOPE Project. Build Environ 46:280–288
3. Bodin C (2008) Office type in relation to health, well-being, and job satisfaction among employees. Environ Behav 40(5):636–668
4. Choi J-H, Loftness V, Aziz A (2012) Post-occupancy evaluation of 20 office buildings as basis for future IEQ standards and guidelines. Energy Buildings 46:167–175
5. Cowan J, et al (2002) International performance measurement and verification protocol (IPMVP) vol II: concepts and practices for improved indoor environmental quality 2nd ed (2000). Canada: EVO (Efficiency Valuation Organization)
6. Depecker P (2001) Design of buildings shape and energetic consumption. Build Environ 36:627–635
7. Duffy F (1998) New environments for working: The re-design of offices and environmental systems for new ways of working. Construction Research Communications Ltd., UK
8. Hair J, Anderson R (2005) Análisis multivariante. McGraw Hill, España
9. Leaman A (2010) BUS occupant survey method: details for licensees. In: http://www.usablebuildings.co.uk. Accessed on 25 Jan 2012
10. Nicol F, McCartney K (2000) Smart controls and thermal comfort project. Final report
11. Ourghi R et al (2007) A simplified analysis method to predict the impact of shape on annual energy use for office buildings. Energy Convers Manag 48:300–305
12. Rivard H et al (2006) Floor shape optimization for green building design. Adv Eng Inform 20:363–378
13. VV.AA (2004) ANSI/ASHRAE Standard 55-2004. Thermal environmental conditions for human occupancy. EE.UU: ASHRAE
14. VV.AA (2006) ISO 7730:2005: ergonomics of the thermal environment—analytical determination and interpretation of thermal comfort using calculation of the PMV and PPD indices and local thermal comfort criteria. Switzerland: ISO (International Organization for Standarization)

Chapter 39
Multisource Heat Pump System: The Case Study of a New School Building

Marco Noro, Renato Lazzarin, and Filippo Busato

Abstract The concept of a low energy building in the temperate climate (according to the Koppen climate classification) is based on the reduction of heat losses through a better insulation, the heat recovery on mechanical ventilation and the use of high efficiency heating/cooling systems integrated with renewables. It is very difficult to achieve good results in terms of global energy efficiency if one of these elements is missing. In 2009 a new school building, integrating those three elements, started its operation in Agordo town, northern Italy. Its main features concern a well insulated envelope and a space heating and ventilation system driven by an innovative multisource heat pump system concept. Outdoor air is a common heat source, whose limits are well known. Heat pump features can take advantage of better sources than air, as for instance the ground heat, solar heat, and heat recovery. These sources are those used by the analyzed system. A multisource system aims to enhance the performances of the heat pump, both in terms of heating capacity and of efficiency, of the heat pump. The present work shows data monitoring and analysis for a real working application, for a period of about two heating seasons, during which the behavior of the system can be analysed and the eventual malfunctioning of the plant can be identified. The energy balance indicates that the integration of different sources not only increases the thermal performance of the system as a whole but also optimizes the use of each source, thus leading to a lower stress on the ground and to a higher utilization of the solar system. The results are then compared to those could have been obtained with the use of a single source system, i.e. the ground, taking no advantage from the heat recovery and the solar system.

Keywords Gas absorption heat pump • Solar heating • Multisource heat pump • School building

M. Noro (✉) • R. Lazzarin
Department of Management and Engineering, University of Padua,
Stradella San Nicola, 3, 36100 Vicenza, Italy
e-mail: marco.noro@unipd.it; renato@gest.unipd.it

F. Busato
3F Engineering, via del Giglio 40/A, 35133 Padova
e-mail: filippo.busato@gmail.com

I. Dincer et al. (eds.), *Progress in Sustainable Energy Technologies Vol II: Creating Sustainable Development*, DOI 10.1007/978-3-319-07977-6_39

39.1 Introduction

To reduce the energy need of the building and the heating and cooling installed capacity in the temperate climate (according to Koppen climate classification), good options are:

- to design a low energy building envelope with good thermal insulation;
- to choose energy effective technologies based on high efficiency generation system, such as heat pumps;
- to integrate them as much as possible with heat recovery devices and renewable energy sources.

Designed in 2006–07, the new High School Building of Agordo (province of Belluno, northern Italy) – enclosing the three features above mentioned – started its operations in autumn 2009. The building is operated by the Belluno Province Administration, appointed for the public education service.

The town of Agordo lays in the geographic area of the Dolomiti mountains in a valley at 611 m a.s.l., where the climate is severe during wintertime (3,376 degree-days). The building has a total floor area of 5,680 m^2, the outward surface of 13,608 m^2 encloses a gross heated volume of 19,644 m^3; the envelope is well insulated, the outer walls and the roof allowing for an average thermal transmittance of about 0.16 W/(m^2 K), the floor having a thermal transmittance to the ground [1] of 0.4 W/(m^2 K), the glazing system having a thermal transmission of 1.38 W/(m^2 K).

From the architectural and functional point of view, the building is made of two main wings and a central belt: the south-east wing is on three storeys and houses teaching rooms, used mainly (but not only) in the morning; the west wing is on two storeys and houses the laboratories, used mainly (but not only) in the afternoon; finally the central belt, on three storeys houses the administrative offices manned all the day and the auditorium, used occasionally.

The school is closed from the middle of June to the end of August, so the climatization system does not provide summer cooling, but only ventilation and space heating.

Through dynamic simulation in the TRNSYS environment different solutions were evaluated with respect to the heating system [2, 3]. A multisource absorption heat pump system has been designed to fulfil the needs of the building: the sources are ground, sun, recovery on ventilation. The design of the system in order to optimize the size of the borehole ground exchangers field and the solar system was carried out to find the most viable mix [4]. The ratio between the thermal input from the source and the thermal output is much lower for an absorption heat pump than for a compression one, that would need a much larger (and much more expensive) borehole field. This consideration applies only to the heating mode of course.

39.2 Description of the HVAC Plant

The HVAC system in teaching rooms, laboratories and offices provides space heating by means of radiant floor and ventilation by means of three independent AHUs each of those serving a single-duct [5] system. The auditorium is served by an all-air system. From the design calculations, performed according to the UNI EN 12831:2006 standard, the space heating requires a maximum power of 146 kW and the ventilation system requires 122 kW of sensible heat, being the design indoor conditions set to 20 °C of air temperature and the ventilation being neutral (air supplied at 20 °C).

Under the ground floor of the south-east wing lays the central heating plant. For sake of simplicity a reduced functional diagram of the plant is shown in Fig. 39.1; hydraulic streams and therefore energy flows within the plant can be easily understood, while many hydraulic attachments (hydraulic separators, filters, valves, pumps) were hidden as well as the secondary circuits of the radiant floor. Table 39.1 reports the main characteristics of the heating generators; the heat pumps were designed to cover the base load, the condensing boiler to supplement the peak load as well as to backup an eventual fault of one or more heat pumps.

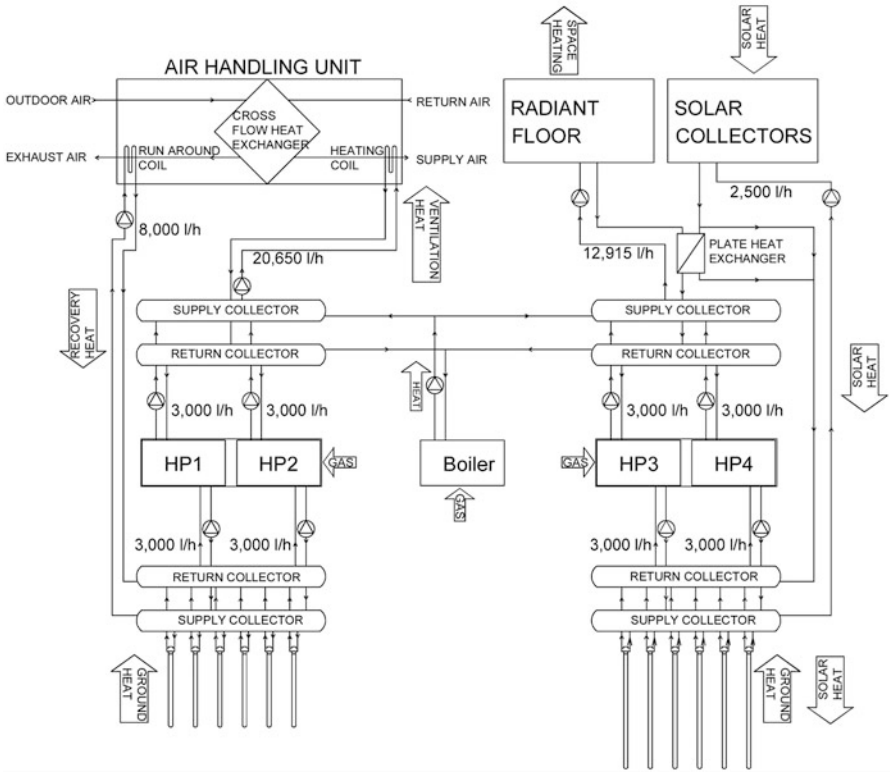

Fig. 39.1 Simplified functional diagram of the HVAC plant

Table 39.1 Heating generators of the central HVAC plant

Component	Rated electric consumption (kW)	Rated capacity (kW)	Rated efficiency
HP1 + HP2	0.15	74 (B0W60)	1.25 (GUE [6])
HP3 + HP4	0.15	76 (B0W40)	1.40 (GUE [6])
Boiler	0.18	114.4	1.02 (condensing)

Table 39.2 Electric consumption of the auxiliaries

Auxiliary	Electric power (kW)
Primary pumps space heating	0.42
Primary pumps ventilation	0.42
Evaporator pumps space heating	0.42
Evaporator pumps ventilation	0.42
Ground borehole pumps heating	0.44
Ground boreholes pumps ventilation	0.42
Solar circuit pump	0.47
Run around coils pumps	0.37
Secondary pumps space heating	1.10
Secondary pumps ventilation	0.80
AHU fans	1.31

The AHUs are equipped with sensible heat recuperators made of cross flow heat exchangers; they were sized with an efficiency limited to 50 % in order to avoid frosting problems.

The thermal source for the ventilation heat pumps can be either the ground (750 m, 6 × 125 m in a row, of vertical tube heat exchangers) or the exhaust airflow [7]. By means of a run-around coil (visible in Fig. 39.1, downstream the cross flow recuperator on the exhaust flow) a total recovery is then produced at the absorption heat pump evaporator level.

The thermal source for the space heating heat pumps can be either the ground (960 m, 6 × 160 in a row, of vertical tube heat exchangers) or a solar section of 50 m^2 of flat plate solar collectors (four arrays in parallel, each of those made of five modules in series) that can also serve directly the radiant floor, by means of the plate heat exchanger (Fig. 39.1, top right side). In summer the solar system can re-generate the ground.

Boreholes heat exchangers were designed with double-U pipes with an outer diameter of 32 mm and a thickness of 2.9 mm.

In the simplified scheme special attention shall be paid to the AHUs since only two out of four of them (for a global volume flow of 20,600 m^3/h out of 25,000 m^3/h) are equipped with the run around coil, while the two left (4,400 m^3/h) save energy only from the cross flow recuperator.

In Table 39.2 the rated electric consumption of the auxiliaries is shown. It is not worth to list all the pumps in the paper, but it is more straightforward to group them according to their function.

39.3 Operation of the HVAC Plant: Monitoring

Now the control strategy is explained.

The need for sensible heating of the AHUs depends directly on the outdoor air temperature and on the volume flow, which is constant for every AHU. The teaching rooms AHUs are scheduled to work from 6 am to 2 pm, that of the laboratories from 10 am to 6 pm, and that of the offices from 6 am to 6 pm. HP1, HP2 and the boiler are activated once the return temperature falls below given thresholds. The sequence of activation of the HPs is swapped every 2 weeks. The run around coil is activated when the temperature of the exhaust flow downstream the cross flow recuperator rises above 10 °C that is considered as an upper bound for the highest temperature that ground could offer.

The need for space heating is determined by the number of active circuits (each room has its own thermostatic on-off control, according to Italian regulations). The same scheduling of the AHUs applies to the heating system. HP3, HP4 and the boiler are activated once the return temperature falls below given thresholds, and the sequence of activation of the HPs is swapped every 2 weeks. The solar system is activated according to measured solar radiation I_β (W/m^2).

The efficiency of the solar field can be roughly defined with a first order model (the reason is explained a few lines below) as

$$\eta = \eta_0 - a_1 \frac{T_m - T_{oa}}{I_\beta} \tag{39.1}$$

where η_0 is the zero-loss solar system efficiency, a_1 the heat loss coefficient, T_m the mean temperature of the fluid, T_{oa} the outside air temperature. η_0 and a_1 can be calculated from the respective values referred to the single collector, i.e. 0.75 and 4.14 W/(m^2 K), multiplied by CF5 which is the series correction factor [8], equal to 0.881 (for the five collectors in series).

Let the threshold radiation I_T be defined as follows (the reason to adopt a first order model to describe the system is due to the need of having a first order equation between radiation and temperatures):

$$I_T = \frac{a_1 (T_m - T_{oa})}{\eta_0 - \eta_{\min}} \tag{39.2}$$

thus being the radiation that provides the minimum acceptable efficiency η_{min} given the solar field characteristics, the minimum average temperature desired T_m and the outdoor temperature T_{oa}. The desired T_m was set at 5 °C and η_{min} to 0.01. Whenever solar radiation on the field I_β exceeds I_T the solar loop pump is activated. If the solar circuit outlet temperature exceeds 38 °C (i.e. the radiant floor supply temperature increased by 3 °C) the solar outlet goes into the plate heat exchanger, otherwise the exchanger is bypassed. Then the solar outlet feeds the evaporator collectors thus increasing the evaporation temperature. When there's no need for space heating, the solar outlet is directed to the borehole heat exchangers.

The monitoring of the plant was set-up with the cooperation of the building's and the plant's controller designer. The interface of the monitoring systems, running on the PC that controls the plant, has been accessible from any remote terminal via a virtual private network (VPN, after authentication), from the end of October 2009 to the end of March 2011. During this first phase the remote access was open to allow the designer to make small adjustments on the control variables of the plant, after that the access to the control PC was discontinued, as well as the data logging, and the control of the plant is allowed from inside the building only.

In the period indicated above the following cumulative energy flows (mass flow times the temperature difference between inlet and outlet, via simple thermal energy meters) were logged monthly:

- Condenser and evaporator of each heat pump (at the collectors);
- Ground circuits, the one for ventilation and that for space heating;
- Primary circuit of AHU heating coils and run-around coils;
- Solar circuit;
- Primary circuit of the radiant floor.

All the energy meters are located in the central heating plant, therefore the energy delivered to each circuit is the gross value including distribution losses.

The previous listed ones and other significant parameters, as for instance inlet-outlet temperatures for hydraulic circuits and supply-return temperatures in air ducts, room temperatures, mixing valve positions, on-off state of the heat pumps, were logged hourly, but presumably due to malfunctions in the monitoring software the sequence is often broken, so it was necessary to post process the data in order to fill the gaps. However the hourly data were of a great help to reveal some improper use in the control of internal temperatures, which will be detailed in a following paragraph.

The gas consumption was given from the natural gas bills (being the heating/ventilation plant the only gas consumer in the building) of the season 2009–2010 and 2010–2011, respectively 20,832 Sm^3 and 22,033 Sm^3. The LHV is assumed to be 9.55 kWh/Sm^3 (34.38 MJ/Sm^3), since the gas provider only gives the HHV equal to 38.32 MJ/Sm^3.

39.4 Energy Performances 2009–2011

Once the energy flows of the plant described above are available few assumptions need to be made in order to complete the analysis.

With respect to the heat pump, the GUE is defined as follows [6]:

$$GUE = \frac{E_{AC}}{E_{in}} \tag{39.3}$$

where E_{AC} is the energy delivered to the primary circuit from the heat pump condenser-absorber, and E_{in} is the input energy (gas) to the heat pump. E_{in} is not measured directly, but since the first law for an absorption heat pumps offers:

$$E_G + E_E = E_{AC} \tag{39.4}$$

with E_E the energy supplied to the evaporator from the heat source; the generator is fired by natural gas, therefore $E_G = E_{in} \cdot \eta_G$, then GUE becomes:

$$GUE = \frac{E_{AC}}{E_{AC} - E_E} \cdot \eta_G \tag{39.5}$$

where E_{AC} and E_E are known.

The same rationale applies to the backup condensing boiler. Italian national regulations sets the minimum required efficiency for a boiler as 90 % + 2log$_{10}$ (P_n) where P_n [kW] is the rated capacity of the burner. For a conservative approach it has been decided to set the annual average efficiency of the burners (those of the heat pumps, having a rated efficiency of 97.5 % and that of the condensing boiler, having a rated efficiency exceeding 100 %) equally to 85 %, in order to account for part load operation and the several duty cycles.

The electricity consumption of the auxiliaries (pumps, fans) was not measured, however it has been estimated considering the rated electric consumption of each and the scheduling of the building described in Sect. 39.3 for primary and secondary circuit pumps, and from the on/off time of each with respect to ground, solar, recovery circuit logged data.

Figure 39.2 illustrates the central heating plant energy distribution between heat pump, direct solar and boiler. When the balance is made on the whole year 2010, the solar direct contribution is 8.2 %, exceeding the backup boiler that contributes for 6.1 %. PER is calculated as the ratio between the thermal energy produced and the primary energy input, including electric auxiliaries of primary, secondary, source circuits (ground solar circulation pump) and the electric consumption of heat pumps; the conversion factor from primary to electricity is 0.46, according to Italian regulation [9]. PER** is the ratio between thermal energy produced and primary energy input, considering the natural gas consumption only. It is interesting to see how the PER** rises above PER values in mild months, when the direct solar heating contribution is a significant fraction of the total delivered energy, since the pumping energy becomes more relevant compared to the gas demand in the warmer season.

Figure 39.3 depicts the share of solar energy between direct space heating, the evaporator or the regeneration of the ground. With the exception of few months the utilization of the solar system exceeds 50 %, even in the coldest months. Figure 39.4 shows the space heating heat pumps efficiency GUE, working on the two different sources. The solar source influence is really appreciable, since it raises the GUE from around 1.46–1.53. Hereinafter the seasonal GUE values will be discussed. In the whole 2010, the solar energy delivered to the evaporator is equal to the 13 % of the total energy required at the evaporator level.

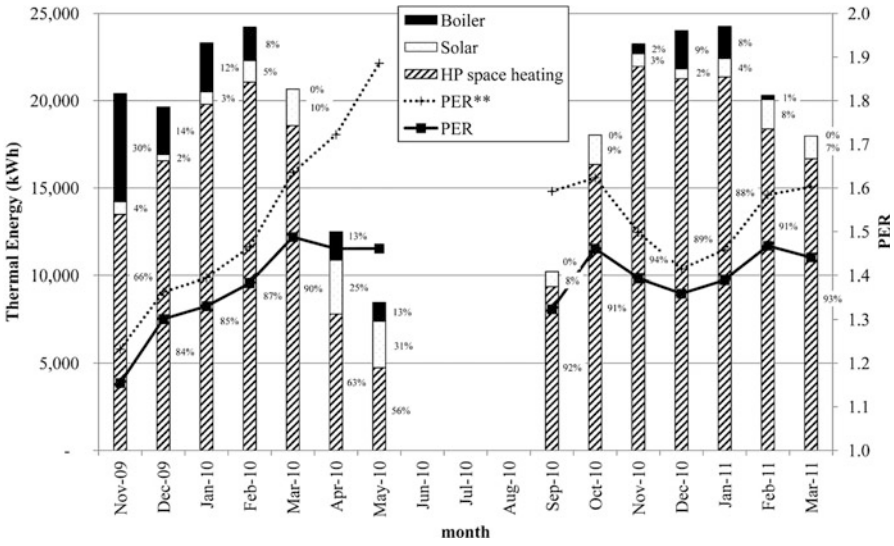

Fig. 39.2 Monthly space heating share of thermal energy, from boiler, solar direct and heat pumps (percentage on the *right* of the stacks). The primary energy ratio for the space heating requirements is also shown (to be read against the *right* Y axis). PER** is the ratio between thermal energy produced and primary energy input, considering the natural gas consumption only

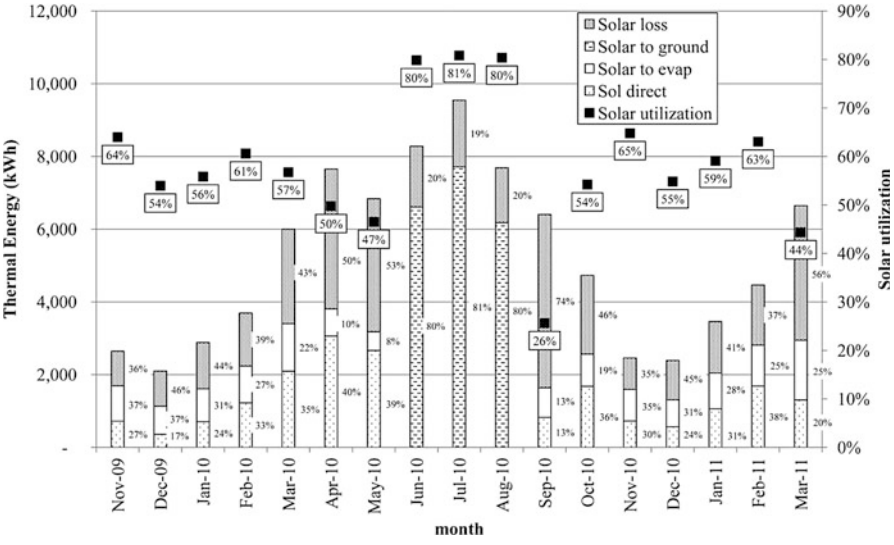

Fig. 39.3 Solar collectors measured energy flows, including collector losses, energy discharged to the ground, to the evaporator and to direct heating of the radiant floor (percentage on the *right* of the stacks). The percentage of solar utilization is shown (to be read against the *right* Y axis)

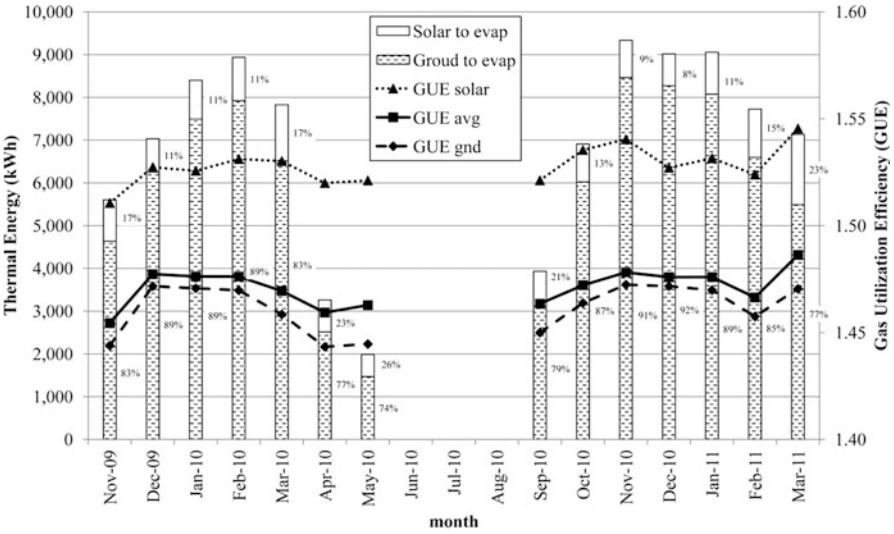

Fig. 39.4 Monthly representation of the source used by the heat pump for space heating (ground or solar, percentage on the *right* of the stacks), with GUE values associated to each source (to be read against the *right* Y axis)

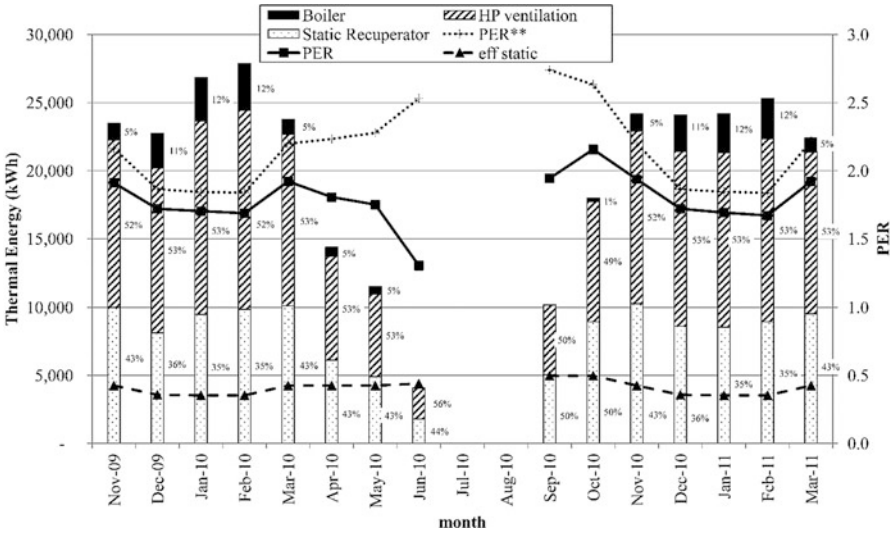

Fig. 39.5 Monthly ventilation share of thermal energy, from boiler, heat pumps and the static recuperators (percentage on the *right* of the stacks). The primary energy ratio for the ventilation purpose and the static recuperator efficiencies are also shown (to be read against the *right* Y axis)

Figure 39.5 illustrates the energy shares in the ventilation section. Considered that only return temperature was available to the data logger, the ventilation demand has been calculated as a first law balance between outlet and return conditions.

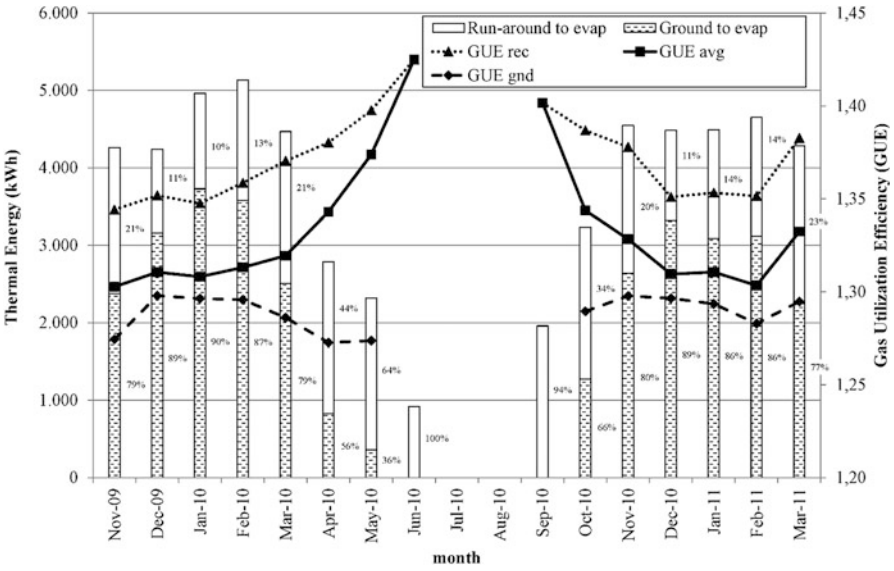

Fig. 39.6 GUE of ventilation heat pumps by source (percentage on the *right* of the stacks), with GUE value associated to each source

The difference between sensible energy demand for ventilation and energy supplied to the AHU from the central heating plant is the amount of recovered energy on the static recuperator. Being the ventilation balances (same volume flow supplied and returned) it was also possible to calculate the efficiency of the recuperator, pictured in Fig. 39.5 as well. Indeed after that of the heat pumps, the most relevant contribution is given from the static recuperator, with monthly efficiency ranging from 35 to 50 %. The same rationale for PER and PER** explained for space heating applies to ventilation (electricity consumption includes the fans).

As it can be seen in Fig. 39.6, ventilation heat pumps' GUE is lower than that of space heating. This is due to the fact that ventilation dedicated heat pumps produce higher set point temperature water (at a temperature level ranging from 55 to 60 °C). Again the effect of the heat recovery by means of the run-around coils is significant, as in warm months (from April to October) the evaporator is fed mostly by the run-around coils circuit.

The shape for the GUE ground monthly efficiency trend is quite similar for space heating and ventilation, since it is basically depending on the on-off duty cycles of the HPs' (higher in milder months); the slight decrease in ventilation HPs' GUE with respect to space heating is due to the fact that the borehole field of space heating is regenerated in summer.

For the year 2010 it is then possible to look into the Table 39.3 for a detailed energy balance of the heating plant. The quantity GUE* is the Gas Utilization Efficiency as it should be calculated according to thermodynamics; as per [6] the GUE only account for gas consumption, while GUE* includes the electric consumption of the Heat Pump (converted to primary).

Table 39.3 Summary of the energy performance of the plant

Space heating			Ventilation			Global		
Quantity	Energy/ performance	Unit	Quantity	Energy/ performance	Unit	Quantity	Energy/ performance	Unit
Space heating	164,657	kWh_t	Ventilation	184,931	kWh_t	Total energy delivered	349,588	kWh_t
Solar direct	13,553	kWh_t	Static recuperator	75,222	kWh_t	Total gas consumption	196,141	kWh_t
HP3 + 4	140,951	kWh_t	HP1 + 2	96,557	kWh_t			
Gas to HP	95,702	kWh_t	Gas to HP	73,020	kWh_t			
Boiler	10,154	kWh_t	Boiler	13,152	kWh_t			
Gas to boiler	11,946	kWh_t	Gas to boiler	15,473	kWh_t			
El cons HP	495	kWh_{el}	El cons HP	408	kWh_{el}	HP el consumption	903	kWh_{el}
			Vent UTA	1,447	kWh_{el}	AHU fan consumption	1,447	kWh_{el}
Ground pumps	307	kWh_{el}	Recovery pumps	576	kWh_{el}	Source pump consumption	3,869	kWh_{el}
Solar pumps	2,922	kWh_{el}	Ground pumps	65	kWh_{el}			
Evaporator pumps	511	kWh_{el}	Evaporator pumps	1,142	kWh_{el}	Evaporator pumps	1,653	kWh_{el}
Primary pumps	685	kWh_{el}	Primary pumps	1,142	kWh_{el}	Primary pumps	1,827	kWh_{el}
Secondary pumps	1,060	kWh_{el}	Secondary pumps	1,305	kWh_{el}	Secondary pumps	2,365	kWh_{el}
GUE HP3 + 4	1.473		GUE HP1 + 2	1.322				
GUE* HP3 + 4	1.456		GUE* HP1 + 2	1.306				
PER space heating	1.365		PER ventilation	1.834		PER	1.57	
PER CP	1.404		PER CP	1.976		PER CP	1.63	
PER w/o electricity	1.530		PER w/o electricity	2.090		PER w/o electricity	1.78	

The PER CP is the Primary Energy Ratio calculated at the Central Heating Plant excluding the secondary distribution pumps and/or fans, and the PER w/o electricity is the ratio of the delivered thermal energy over the thermal energy consumption. If compared to the PER that is the most important parameter with respect to primary energy conservation, these figures offer some interesting information about the weight of the auxiliaries (distribution system) on the global energy consumption for climatization.

The calculated specific primary energy demand EP [kWh/(m^2 year)] is then equal to 39.1 for 2010. The target value for the building (according to Italian standards, so allowing standard coefficients for distribution, emission, control efficiency) in the design phase was 30 kWh/(m^2 year). The reasons were then investigated for such a difference. The analysis on the monitored set-point in the different building wings and the supply-return temperatures of the AHUs revealed that in the whole building the air temperature most of the time was set between 23 and 24 °C.

Trial calculations have been performed to estimate the EP in standard conditions, so with 20 °C internal temperature. The behaviour of the solar system has been considered equal to that of the real operating conditions, as well as the efficiency of the sensible recuperator on the AHUs, the need of space heating and that of ventilation was considered as proportional to the heating degree hours HDH, according to the procedure described in [10]. Therefore it was assumed:

$$\left(\frac{E_{sh}}{HDH}\right)_{23.5\ ^\circ C} = \left(\frac{E_{sh}}{HDH}\right)_{20\ ^\circ C} \tag{39.6}$$

the same applying for ventilation as well. The HDH were calculated (with respect to the "on" period of the plant) by means of the hourly weather data provided by the Regional Agency for Environment ARPAV, for the weather station in Agordo (BL). The GUE of the heat pumps and the boiler efficiency considered equal to those in real operating conditions. By means of this rough but effective procedure, the EP in standard conditions is estimated to equal 31.5 kWh/(m^2 year), so only 5 % far from the design value. This method keeps this evaluation on the safe side, since it doesn't account for solar gains that becomes more and more relevant while decreasing the temperature difference between inside and outside.

Strong recommendations were then reported to the Belluno Province Administration in order to survey the air temperature set-point for the times to come.

39.5 Scenarios Without Multisource

It is now interesting to investigate on how the concept of multisource system increases the performances of a single source system. Being the HVAC plant based on water-to-water heat pumps, the main heat source on which the system relies is the ground; then the ventilation system is supplemented also by the heat

recovery source, and the space heating by the solar source. To determine what happens if one of the supplementary source is missing, calculations were made to assess different scenarios.

With respect to ventilation the scenarios are: no run-around coils recovery, no static recuperator. In this last case two subcases were defined, in the first the heat pump replaces the heat recovery as well, in the second the boiler replaces the recovery (the first case cannot be a real option since the capacity of the heat pumps is insufficient, and it would require further heating capacity). The fan power has been adjusted to different AHUs configurations.

With respect to space heating two scenarios were evaluated: once the solar is missing, in the first scenario the HP replaces the solar system, in the second the boiler replaces the solar system. In both cases the solar is replaced only to heating purposes, neither ground regeneration is provided in summer.

The GUE of the heat pump was extrapolated by means of a ten parameter polynomial function (ARI standard) of the ground loop average temperature (peak load) and supply temperature in the real operating conditions. Then for each scenario the monthly average ground loop temperatures were estimated by means of EED software (it was also used during the design phase), finally the balance illustrated in Table 39.3 was produced.

For sake of brevity the complete balance of each scenario is omitted, though the synthetic indicators are reported in the following Table 39.4.

The two indicators are important to different considerations. GUE always decreases in case of single source systems, since the ground is heavily solicited, both in the ventilation section and in the space heating. The solar system contribution to the evaporator is less important than that of run-around coil recovery, however solar system allows summer ground regeneration. From the calculations performed in EED however it seems that summer regeneration produces less benefits that those of a lower extraction during wintertime.

The overall PER indicates that the supplementary source gives a greater effect on the space heating than in the ventilation system. This is of course due to the fact that solar system also provides for "almost free" heating effect, while run-around coils recovery only increases the GUE of the heat pumps with a reasonable cost in terms of higher fan and pumping consumptions. Moreover, the space heating heat pumps work at a lower condensation temperature than the ventilation ones. According to the following [11]:

$$\frac{\left(\frac{\partial GUE_{CA,h}}{\partial \Delta T}\right)_{T_c}}{GUE_{CA,h}} = -\frac{1}{\Delta T} \tag{39.7}$$

the sensitivity of the GUE to the evaporation temperature increases while temperature lift decreases (ΔT is the difference between condensation and evaporation temperature). Therefore, since the heating system works at lower condensation temperature than ventilation, the heating section benefits from the multisource concept more than the ventilation one.

Table 39.4 Performance indicators in the different scenarios

Ventilation					Space heating			
	Reference	No run-around coils	HP replaces static recuperator	Boiler replaces static recuperator		Reference	HP replaces solar	Boiler replaces solar
GUE HP 1 + 2	1.322	1.285	1.287	1.285	GUE HP 3 + 4	1.473	1.460	1.461
PER	1.834	1.832	1.126	0.962	PER	1.365	1.320	1.256

Table 39.5 Comparison between the old and the new buildings

	Gross volume (m^3)	Fuel consumption	LHV	Specific primary energy consumption (kWh/m^3)
Old	17,715	64,160 l	10.48 kWh/l	37.98
New	19,644	21,432 Sm^3	9.55 kWh/Sm^3	10.42

39.6 Conclusions

From the calculations reported in Table 39.3 the natural gas consumption in 2010 is equal to 20,532 Sm^3. The average of the two heating seasons 2009–10 and 2010–11 is from the natural gas bill equal to 21,432 Sm^3/year. The difference (4.2 %) from the calculated consumption could be ascribed mainly to:

- inaccuracy of the energy meters that equipped the hydraulic circuits;
- the incorrect evaluation of the yearly average burners' efficiency

However the estimation is quite good considered that no gas consumption measurement was allowed on the single units.

It is interesting to underline that the previous building that housed the same high school in Agordo enclosed a gross volume of 17,715 m^3 and burned Diesel oil for an amount of 64,160 l in 2006–07.

Table 39.5 finally shows the comparison between the new and the old buildings serving the same purpose.

As it can be seen the new building specific primary energy consumption is almost a fourth of the old one.

Acknowledgement Special thanks are paid to Areatecnica Studio Vigne & partners (designers of the plant) represented by Gianluca Vigne (C.E.O.), and to Luigino Tonus, head of the General Service Dept of the Belluno Province Administration.

Nomenclature

E	Energy (kWh)
EP	Specific primary energy demand for heating (kWh/(m^2 y))
GUE	Gas utilization efficiency
P	Power (kW)
PER	Primary energy ratio
T	Temperature (°C)

Greek Symbols

β	Slope of the solar system
η	Efficiency of solar system

Subscript

avg	Average
CA	Condenser-absorber
E	Evaporator
G	Generator
gnd	Ground
in	Input
p	Peak
sh	Space heating
th	Thermal
vent	Ventilation

Acronyms

AHU	Air handling unit
CF5	Correction factor for a series of 5 solar collectors
CP	Central heating plant
HDH	Heating degree hours
HHV	Higher heating value
HP	Heat pump
HVAC	Heating, ventilation, air conditioning
LHV	Lower heating value
VPN	Virtual private network

References

1. UNI EN ISO 13370 (2008) Thermal performance of buildings – heat transfer via the ground – calculation methods. UNI (IT)
2. Busato F, Lazzarin R, Noro M, Vigne G (2008) Energetic and environmental analysis of an integrated multi-source heat pump system for a school building. Proceedings of 46th international conference AiCARR, Milano, 2008. pp 879–895, ISBN 9788895620046
3. Minchio F (2006) Pompe di calore termiche nella climatizzazione (thermal heat pumps for climatization). Ph.D. dissertation in energy systems, supervisor prof. Lazzarin R, University of Padova, Italy
4. Busato F, Lazzarin R, Noro M (2010) Ground or solar source for space heating which is better? Energetic assessment based on a case history. Proceedings of the Clima 2010 REHVA conference, Antalya, TK
5. ASHRAE (2008) Air distribution, Ch. 4.10, Ashrae handbook – HVAC systems and equipment, ASHRAE Inc., Atlanta, GA
6. UNI EN 12309-1 (2002) Gas-fired absorption and adsorption air-conditioning and/or heat pump appliances with a net heat input not exceeding 70 kW. UNI (IT)
7. Lazzarin R (2012) Dual source heat pump systems: operation and performance. Energ Build 52: 77-85, http://dx.doi.org/10.1016/j.enbuild.2012.05.026

8. Oonk RL et al (1979) Calculation of performance on N collectors in series from test data on a single collector. Solar Energy 23:535–536
9. AA VV (2008) Delibera EEN 3/08. Italian Authority for Electric Energy & Gas, Milan
10. Busato F, Lazzarin R, Noro M (2011) Ten years history of a real gas driven heat pump plant: energetic, economic and maintenance issues based on a case study. Appl Therm Eng 31 (10):1648–1654
11. Lazzarin R, Busato F, Minchio F, Noro M (2011) Le sorgenti termiche delle pompe di calore. Collana AiCARR vol 18, Delfino, Italy. ISBN 9788897323167

Chapter 40
Application of Heat Pipe System in Data Center Cooling

Xiaodong Qian, Zhen Li, and Hao Tian

Abstract With the development of global information industry, the scale of data centers become larger, meanwhile the energy consumption and running cost are grown rapidly. The energy saving problem of data center has been more and more concerned around the world. The energy consumption of data centers in Beijing was studied in this paper. The results show that the energy utilization problem of cooling systems is especially prominent, and their average energy consumptions account for 47 % in these data centers. With the proposal of energy saving in cooling system, heat pipe cooling system is introduced in this paper. As free cooling utilization device, when the outdoor temperature is lower than the environment set temperature, the data center can be cooled by the outdoor cold environment through this system, and the energy consumption of cooling system will be reduced significantly. At present, this system has been applied in dozens of data centers and communication base stations in China and the energy saving effects are obvious. Case studies show that after using the heat pipe cooling systems, the cooling systems of data center and the communication base station can separately achieve the energy saving of 38.9 and 55.7 %.

Keywords Data center • Free cooling • Heat pipe cooling system • Energy saving

40.1 Introduction

Data center is a building densely placed a lot of IT equipment, such as servers, storage devices, network equipment and so on. It is a service platform of data processing, storage, transmission and exchange. Data center is a typical kind of high energy buildings. With the uninterrupted operation mode, the using time of data centers are

X. Qian • Z. Li (✉)
Key Laboratory of Thermal Science and Power Engineering of Ministry of Education, School of Aerospace, Tsinghua University, Beijing 100084, China
e-mail: qxd08@mails.tsinghua.edu.cn; lizh@tsinghua.edu.cn

H. Tian
Department of Building Science, Building Energy Research Center, Tsinghua University, Beijing 100084, China
e-mail: 16011657@qq.com

I. Dincer et al. (eds.), *Progress in Sustainable Energy Technologies Vol II: Creating Sustainable Development*, DOI 10.1007/978-3-319-07977-6_40

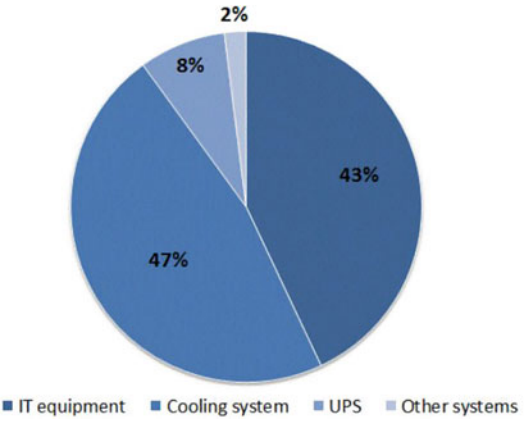

Fig. 40.1 Energy consumption constitution of data centers in the survey

three times of commercial buildings. Moreover, because of the IT equipment's dense display mode, the power density of data centers can reach 200–3,000 W/m^2 and is 100 times of commercial buildings [1]. With the development of global information industry, the demand for data center is further increased and the energy consumption is grown rapidly. A statistical report from Lawrence Berkeley National Laboratory in 2007 showed that the data center energy consumption doubled every 5 years [2]. In recent years, China data center market is also entering a high speed development period. From 2007 to 2009, the data center investment growth rate is more than 15 %, and energy consumption will achieve 100 billion kWh in 2015 [3].

To understand the data center energy consumption features in China and find the breakthrough point of energy saving, a survey of data center energy consumption was carried out in Beijing. The 2011 energy consumption of data center in Beijing is nearly eight billion kWh and accounts for 5 % of Beijing's total electricity consumption. Data center consumes energy in the IT equipment, cooling system, UPS and other systems. Figure 40.1 shows the analysis result of energy consumption constitution of these data centers. Cooling system and IT equipment are the biggest two parts of energy consumption in data centers. The average energy consumption of cooling system occupied 47 % and is 4 % more than IT equipment. The average PUE of data centers in the survey is about 2.3 and has a wide gap with data centers in developed countries. According to the field survey, it is found that raised-floor and cold and hot aisles are not commonly used in these data centers. Air conditionings are all running on cooling mode in the whole year and none of the energy saving equipment is applied in these data centers. High energy consumption of cooling system is the common problem of global data centers and is especially serious in China. Therefore, cooling system energy conservation plays an important role in high-efficiency energy utilization and energy saving in data centers.

In this paper, free cooling utilization is introduced for the energy saving of data center cooling system. Based on this idea, heat pipe cooling system (HPCS) is proposed and the energy saving effect of HPCS energy saving renovations was analyzed in the case studies.

40.2 Free Cooling Utilization of Data Center Cooling System

Data center is usually a sealed room because of the temperature, humidity and cleanliness requirements by the IT equipment. Meanwhile, the high heat density makes it need to be cooled all through the year. The uninterrupted operation mode of cooling system is the main reason for the high energy consumption of data center. In most parts of the world, especially high latitudes areas contain huge free cooling resources. When the outdoor temperature is lower than the environment set temperature, the data center can be cooled by the outdoor cold environment instead of the air conditionings and the energy consumption of cooling system will be reduced significantly. This energy saving idea is called free cooling utilization of data center cooling system.

Cooling system's free cooling utilization is considered as the most effective way of data center energy saving. Choosing a suitable technology and developing efficient and reliable equipment is the key to the free cooling utilization. Many researches have been performed in recent years [4–6]. Free cooling utilization can be divided into two categories, direct free cooling utilization and indirect free cooling utilization. Direct free cooling utilization is a convenient way to use outdoor environment. The low temperature outdoor air is directly transported into the data center and cools the IT equipment. With the contribution of outdoor air, the operation time of air conditionings is greatly reduced and the energy consumption of cooling system will be also lower. The main defect of this method is that outdoor air will change the data center's humidity and bring the dust. Humidity and cleanliness have great impacts on the performance and service life of IT equipment. So the extra cost needs to be consumed to control the humidity and filter the outdoor air. Indirect free cooling utilization is a method by using heat exchange equipment to remove heat from data center to outdoor environment. Because the inside and outside air will not directly contact with each other, this method can keep the humidity and cleanliness of data center. The key of indirect free cooling utilization is to find a high efficient heat exchange technology.

The characteristics of direct and indirect free cooling utilization technologies are shown in Table 40.1 [6–9]. The energy saving effect of direct free cooling

Table 40.1 Comparison of free cooling utilization technologies

Technology	Ventilation (humidity and dust control)	Air to air heat exchanger	Heat pipe heat exchanger
Free cooling utilization method	Direct	Indirect	Indirect
Environmental adaptation	Poor	Good	Good
Cooling effect	Good	Poor	Good
Structure	Compact	Bulky	Compact
Initial investment	Low	High	High
Maintenance cost	High	Middle	Low

utilization is bound by the cost of humidity and dust control. Indirect free cooling utilization is more popular in practical applications because of the good environment adaptation. The two main technologies of indirect free cooling utilization are air to air heat exchanger and heat pipe heat exchanger. Because of the low heat transfer coefficient, the air to air heat exchanger is usually bulky. While Heat pipe is a highly efficient and reliable heat transfer component. The heat pipe heat exchanger is compact and the maintenance cost is low. It is a good choice for free cooling utilization.

40.3 Heat Pipe Cooling System (HPCS)

40.3.1 Working Principle of HPCS

Grover [10] from Los Alamos National Laboratory first invented a heat pipe and completed the experiment. According to the structure, heat pipe can be divided into two types: integrated and separated heat pipes. In addition to the high heat transfer capability, separated heat pipe also has the features of long distance and multi-fluid heat transfer ability, good adaptability and sealing performance, and flexible area adjustable between evaporator and condenser [11].

Based on the separate heat pipe, HPCS is proposed in this paper and shown in Fig. 40.2. This system composed of evaporator, condenser, gas pipe and liquid pipe. Part inside the data center is the evaporator and its task is absorbing heat and cooing IT equipment. For ease of installation, evaporator of HPCS has many styles, such as cabinet type and ceiling type and their photos are shown in Fig. 40.3. Part outside

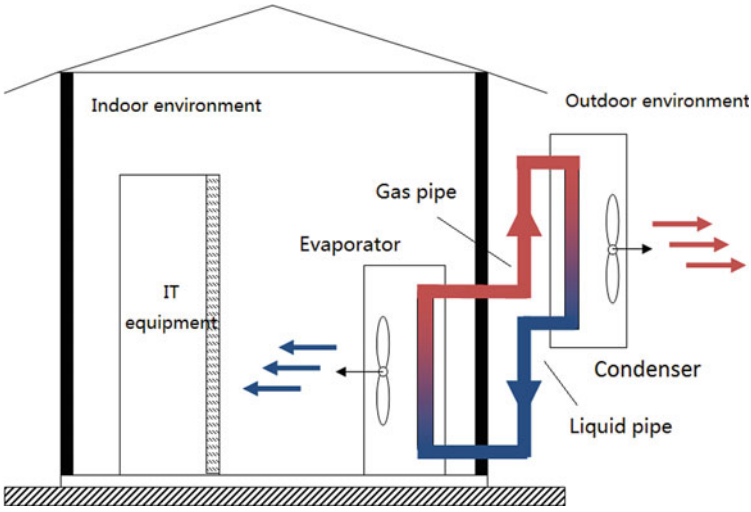

Fig. 40.2 Schematic of HPCS

Fig. 40.3 Cabinet type and ceiling type evaporators of HPCS

the data center is the condenser and is responsible for providing the cold source and transport heat to outdoor environment. Evaporator and condenser are connected by gas pipes and liquid pipes. In the evaporator, the working fluid absorbs heat from data center and evaporates from liquid state to gaseous state. Then the gaseous working fluid flows upward into the condenser through the gas pipe. The working fluid releases heat into outside environment and condenses to the liquid state in the condenser. Under the action of gravity, the working fluid flows down back to the evaporator. Through the circulation happening in the HPCS, the heat generated by IT equipment can efficiently transports from data center to outside environment. In addition, data center is isolated from the outdoor environment during the heat transfer process and avoids the impacts of outdoor air's humidity and dust.

HPCS has the good features of high heat transfer capability and low energy consumption. It belongs to the passive heat transfer device and the temperature difference between inside and outside of data center is the heat transfer driving force. The fans of evaporator and condenser are the only energy consumption component and the power is less than 20 % of the air conditionings. Experimental result in Fig. 40.4 shows that when the temperature difference is 5 °C, the EER of HPCS is 6. As the temperature difference increasing to 10 °C, the EER can reach 15. While the EER of air conditionings used in data center is usually less than 3. By combined operating with air conditionings, HPCS can be used to cool the data center instead of the air conditioning when the outdoor temperature is lower than the set temperature. Because the HPCS's power is much smaller than the air conditioning, the combined operation mode can significantly reduce the energy consumption of data center cooling system. In addition, the air conditioning's running time will greatly reduced and maintenance period and service life will be largely extended.

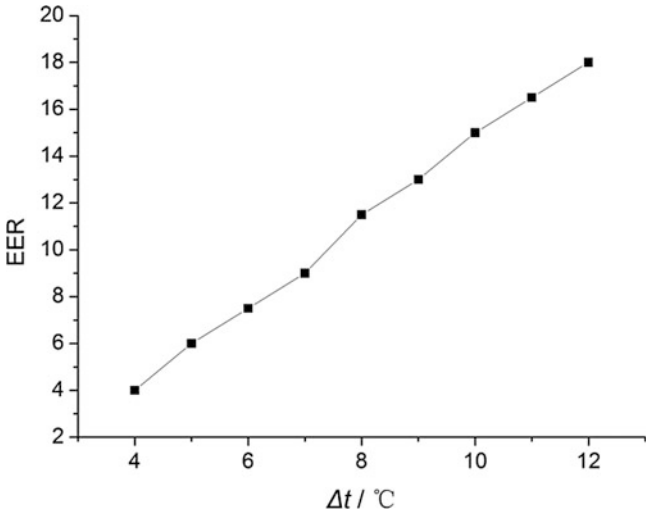

Fig. 40.4 EER of HPCS

40.3.2 Energy Saving Solution of HPCS

In data centers, HPCSs and air conditionings are installed independently and work dependently. The start working temperature difference of HPCS is 3–5 °C. By monitoring the temperatures inside and outside of data center, HPCSs and air conditionings can be automatically controlled. When the temperature difference satisfies the working requirement of HPCS, like in winter and most time in spring and autumn, the HPCSs are open and air conditions are turned off. While if the outside environment temperature is high, like in summer, the data center is cooled by air conditionings and the HPCSs are turned off.

The average energy consumption of HPCS is less than 20 % of air conditioning, so this energy saving solution's effect depends on the length of HPCS's working time. According to the working principle of HPCS, the working hours is mainly affected by the data center set temperature and its location's climatic condition. The set temperature of data center is usually 23–25 °C. Telecommunication base station is a special type of small data center and its environment requirement is a little lower than conventional data center. The temperature of telecommunication base station usually maintained at 26–28 °C. If the start temperature difference of HPCS is 5 °C, the HPCSs can replace the air conditions when the outside environment temperature is lower than 18 °C for data center and lower than 21 °C for telecommunication base station. Statistical data in Fig. 40.5 gives the hours of China's ten major cities which dry bulb temperatures are lower than 18 and 21 °C. Latitude and altitude are the two main influence factors of the dry bulb temperature. Higher latitude and altitude of the place, longer the HPCS can be used throughout the year. The latitude is increased from south to north in China. Guangzhou is a typical

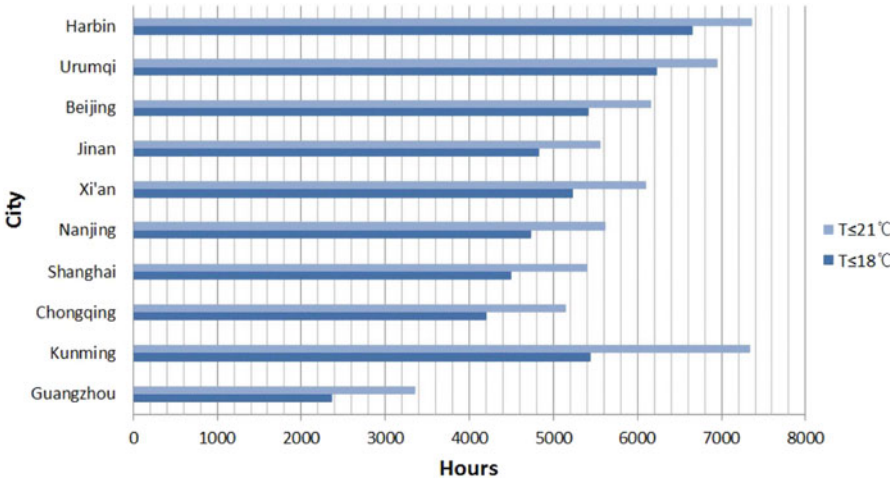

Fig. 40.5 Annual meteorological statistics of ten major cities in China

Table 40.2 Theoretical energy saving rate

City	Altitude (m)	Geographic coordinates	Data centers (%)	Telecommunication base stations (%)
Guangzhou	41.0	23.17°N 113.33°E	21.6	30.6
Kunming	1,892.4	25.02°N 102.68°E	49.7	67.1
Chongqing	259.1	29.58°N 106.47°E	38.4	47.0
Shanghai	5.5	31.40°N 121.45°E	41.1	49.4
Nanjing	7.1	32.00°N 118.80°E	43.2	51.3
Xi'an	397.5	34.30°N 108.93°E	47.8	55.8
Jinan	170.3	36.60°N 117.05°E	44.1	50.8
Beijing	31.3	39.80°N 116.47°E	49.4	56.3
Urumqi	935.0	43.78°N 87.65°E	56.9	63.5
Harbin	142.3	45.75°N 126.77°E	60.8	67.2

southern city and its HPCS's working hours is about 30 % of the year. In Harbin, a typical northern city, the HPCS's working hours is more than 75 % of the year. Kunming is also a northern city but its altitude is much higher than Guangzhou. So HPCS's working hours in Kunming is more than twice in Guangzhou. Assume that HPCS's power is 20 % of air conditioning. Table 40.2 gives the theoretical energy saving rates of data center and telecommunication base station in these ten cities after adopting the energy saving solution of HPCS.

40.4 Energy Saving Applications of HPCS

A Telecommunication base station in Luoyang was implemented the HPCS energy saving renovation in 2009. The floor plan is shown in Fig. 40.6. The area of the telecommunication base station is 27 m^2 and the environment set temperature is 28 °C. There are seven data racks and the total power of the IT equipment is 4.3 kW. The telecommunication base station was originally cooled by an air conditioning and the rated cooling capacity is 7.3 kW. In the energy saving renovation, a HPCS was installed and displayed in Fig. 40.7. Energy consumption test was conducted from November 2009 to April 2010 and test results were listed in Table 40.3. The cooling system energy consumption was decreased from 31.3 kWh per day to 7.8 kWh per day in the test. According to the climatic condition of Luoyang, the HPCS working hours is 6,505 h per year. By accounting, after adopting the energy saving solution of HPCS, the full year energy saving rate can reach 55.7 %.

A Beijing's data center, which shown in Fig. 40.8, was conducted the HPCS energy saving renovation in the end of 2009. The area of the data center is 138 m^2 and the environment set temperature is 25 °C. There are 29 data racks and the total power of the IT equipment is 30 kW. The data center adopted the underfloor air supply system and was originally cooled by two air conditionings. The total rated cooling capacity of them is 45 kW. During the energy saving renovation, three

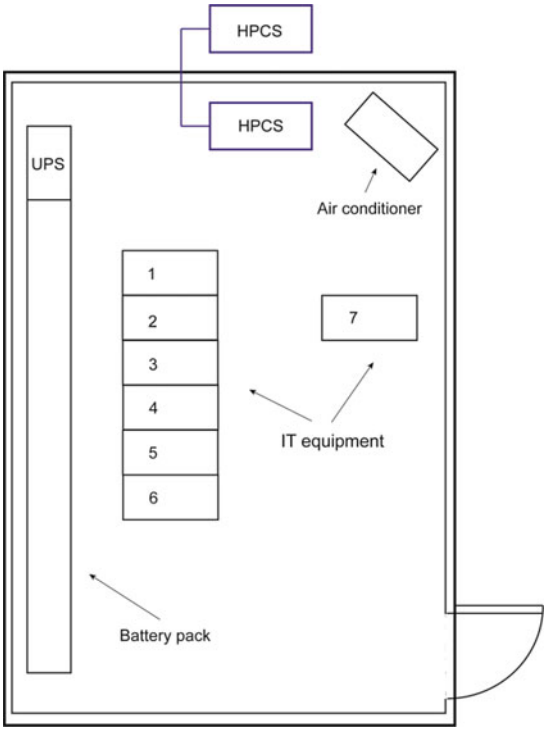

Fig. 40.6 Floor plan of a telecommunication base station in Luoyang

Fig. 40.7 HPCS of the telecommunication base station in Luoyang

Table 40.3 Test result of the telecommunication base station in Luoyang

Data	Air conditioning cooling(kWh/day)	HPCS cooling (kWh/day)	Energy saving rate (%)
2009.11	36.3	7.9	78
2009.12	23.5	6.25	73
2010.01	24.3	7.5	69
2010.02	29.3	6.6	77
2010.03	33.6	6.6	80
2010.04	40.9	11.8	71
Average	31.3	7.8	75

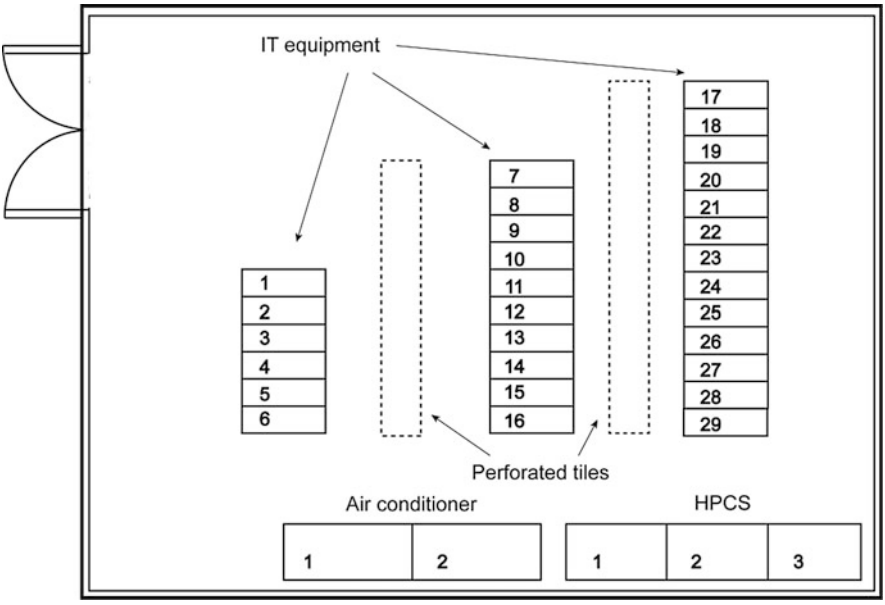

Fig. 40.8 Floor plan of a data center in Beijing

Fig. 40.9 HPCS of the data center in Beijing

HPCSs were installed and combined worked with the air conditionings. The evaporators and condensers of HPCSs are shown in Fig. 40.9. Energy consumption was tested from December 2009 to April 2010. In the test, HPCSs were running normally and cooling system energy consumption was reduced from 461 kWh per day to 164 kWh per day. Based on the climatic condition of Beijing, the HPCS working hour length is 5,414 h per year and the full year energy saving rate can achieve 38.9 % by using the energy saving solution of HPCS.

HPCS is a kind of excellent free cooling utilization device and its energy saving solution is a simple and effective way to solve the high energy consumption problem of cooling system. HPCS's free cooling utilization efficiency is high and the energy consumption is low. In practical applications, HPCSs are easy to install in the data centers or telecommunication base stations. It is independent with the air conditionings on structure. Thus, IT equipment and air conditionings do not need to turn off during the installation of HPCSs. So far, our team has completed dozens of HPCS energy saving renovations in China and part of them are list in Table 40.4.

40.5 Conclusions

High energy consumption of cooling system is the common problems of global data centers and is particularly serious in China. Minimizing the air conditioning's working time by free cooling utilization is one of the most effective ways to reduce the energy consumption of cooling system. Direct free cooling utilization and

Table 40.4 HPCS energy saving renovations

Number	Date	City	Type	Area/m2	IT equipment power/kW	Energy saving rate (%)
1	2009.04	Beijing	DC	30	6	37
2	2009.09	Guangzhou	TBS	25	3.5	25
3	2009.09	Luoyang	TBS	17	4.3	56
4	2009.09	Kunming	TBS	15	5.2	39
5	2009.11	Beijing	DC	138	40	39
6	2009.12	Hohhot	DC	50	10	58
7	2010.01	Beijing	DC	40	30	42
8	2010.02	Panjin	TBS	24	1.9	36
9	2010.04	Nanchang	TBS	28	3.2	57
10	2010.12	Beijing	DC	140	60	42
11	2011.04	Hangzhou	DC	100	60	40
12	2011.12	Beijing	DC	200	90	48

indirection free cooling utilization are compared and the later one is more popular in practical applications owing to the good environment adaptation. In indirect free cooling utilization technologies, heat pipe heat exchanger is a good choice because of the high heat transfer capability and the low maintenance cost.

Based on the separate heat pipe, HPCS is proposed in this paper. It has the feature of high heat transfer capability, low energy consumption and easy to install. As free cooling utilization device, when the outdoor temperature is lower than the set temperature, the data center can be cooled by the outdoor cold environment through HPCS, and the energy consumption of cooling system will be reduced significantly. So far, our team has completed dozens of HPCS energy saving renovations in China and the energy saving effects are obvious. A telecommunication base station in Luoyang and a data center in Beijing were studied in this paper, and the full year energy saving rates can respectively achieve 55.7 and 38.9 % by using the energy saving solution of HPCS.

Acknowledgement The work was supported by the National Natural Science Foundation of China (51138005, 51376097).

Nomenclature

DC Data center
EER Energy efficiency rate
PUE Power usage effectiveness
TBS Telecommunication base station
Δt Temperature difference(°C)

References

1. ASHRAE TC 9.9 (2010) Best practices for datacom facility energy efficiency, 2nd edn. Beijing: China Architecture and Building Press
2. Koomey JG (2007) Estimating total power consumption by servers in the US and the World. Technical report, Lawrence Berkeley National Laboratory
3. CCID Consulting (2010) 2009–2010 IDC business market research annual report. Beijing
4. Anubhax K, Yogendra J (2008) Use of airside economizer for data center thermal management. Second international conference on thermal issues in emerging technologies theory and application. pp 115–124
5. Ellis G, Guiles JR (2007) Airside economizers: are they doing what we want them to do? Contracting Business 5:62–65
6. Wang JG, Kang LG, Liu J, Bao LL (2009) Practicability analysis of using natural cold source for cooling an IDC plant. Heating Ventilating & Air Conditioning 39(2):128–132
7. Li QH, Huang H, Zhang ZB (2010) Performance experiment of heat pipe type air conditioning units for computer and data processing rooms. Heating Ventilating & Air Conditioning 40 (4):145–148
8. Udagawa Y, Waragai S, Yanagi M, Fukumitsu W (2010) Study on free cooling system for data centers in Japan. 32nd international telecommunications energy conference. pp 1–5
9. Lui YY (2010) Waterside and airside economizers design considerations for data center facilities. ASHRAE Transact 116(1):98–108
10. Grover GM, Cotter TP, Erikson GF (1964) Structure of very high thermal conductance. J Appl Phys 35(6):1990–1991
11. Zhuang J (1989) Heat pipe and heat pipe exchanger. Shanghai Jiao Tong University Press, Shanghai

Chapter 41
Energy and Exergy Analysis of a Trigeneration Facility with Natural Gas Engine

Emin Acikkalp, Ozgur Balli, Hasan Yamik, and Haydar Aras

Abstract Natural gas engine (Wartsila 18VSG) having meanly 5,993 kW electrical power output and used in a Trigeneration system located in Ankara was analyzed in terms of energy and exergy. Analysis, which is used actual data, was made to natural gas engine, heat recovery boiler and absorption chiller, while trigeneration system on full load operation conditions. Energy loss, energy efficiency, exergy destruction and exergy efficiencies of the trigeneration system was calculated. The energy and exergy efficiencies of system were determined as 64 and 39 % respectively. FESR (fuel energy saving ratio) and FESxR (fuel exergy saving ratio) were calculated as 27, 28 % respectively for Trigeneration facility.

Keywords Trigeneration • Energy analysis • Exergy analysis • Exergy destruction • Energy efficiency • Exergy efficiency

41.1 Introduction

CHP systems can be defined as systems produce electric and heat together. Simple kind of these technologies can be shown in early twentieth century. However, this method gave up in the cheap fuel period and it was started to use again after fuel crisis between 1973 and 1979. When it is used a simple cycle like, gas turbine or engine, 30 or 40 % energy convert to electrical power, but 70 or 90 % of inner

E. Acikkalp • H. Yamik
Engineering Faculty, Department of Mechanical and Manufacturing Engineering, Bilecik University, Bilecik, Turkey
e-mail: eacikkalp@gmail.com; hasan.yamik@bilecik.edu.tr

O. Balli
First Air Supply and Maintenances Center, TUAF, Eskisehir, Turkey
e-mail: balli07balli@yahoo.com

H. Aras (✉)
Engineering and Architecture Faculty, Department of Mechanical Engineering, Eskisehir Osmangazi University, Eskisehir, Turkey
e-mail: haras@ogu.edu.tr

I. Dincer et al. (eds.), *Progress in Sustainable Energy Technologies Vol II: Creating Sustainable Development*, DOI 10.1007/978-3-319-07977-6_41

energy can be utilized, by using cogeneration system because of using discharge heat [1]. In this days not only electrical power and heating energy using in process produce at CHP systems, but also it is utilized at cooling purposes and it is called trigeneration. In Turkey CHP systems are tries to become widespread.

An energy system's thermodynamic performance is determined, by analyzing energy and exergy terms. Energy amount is interpreted with energy analysis and energy quality with exergy analysis.

In this study a trigeneration system used Wartsila 18VSG with 8.2 MW capacity natural gas engine is analyzed in terms of energy and exergy and a method is shown to determine engine's actual power analyze. Meanly mechanic power and electrical power of system are respectively 6,020 kW and 5,993 kW determined by the firm.

41.2 Thermodynamic Analysis

In this section energy and exergy terms was obtained for the trigeneration system and subsystems.

41.2.1 System Definition and Assumptions

Illustration of system is shown at Fig. 41.1. There, HT is closed loop that cools engine's area at high temperatures such as, engine cylinders, turbocharge and cylinder heads. LT closed loop cools turbocharge air and engine oil with a heat exchanger. HT and LT water is cooled through radiator and sent to engine again. At waste heat boiler, domestic hot water or process water is provided by utilizing exhaust gas. A portion of hot water produced at waste heat boiler is sent to absorption chiller to chill climate water.

Assumptions done in this study is listed as follows [1];

- Trigeneration system operates at steady state condition.
- Air and combustion gasses are ideal gasses.
- Combustion is complete.
- Kinetic and potential terms in energy and exergy analyze are neglected.
- Pressure and temperature of environment are 100 kPa and 298.15 K respectively.

Specific heats of oil are 1,97 $kJ(kgK)^{-1}{}_{@\,298.15K}$, 2,03 $kJ(kgK)^{-1}{}_{@\,336.15K}$, 2,08 $kJ(kgK)^{-1}{}_{@\,347.15K}$ and 2,08 $kJ(kgK)^{-1}{}_{@\,347.42K}$ [2].

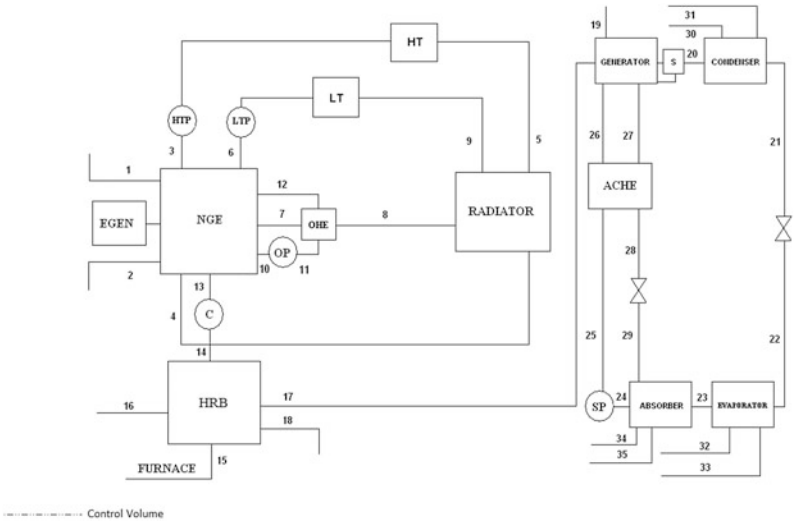

Fig. 41.1 The schematic of trigeneration system

41.2.2 Energy Analysis of System

Energy analysis for the control volume can describe as following [3];

$$\dot{Q} + \dot{W} = \dot{E}_Q + \dot{E}_W = \sum_o \dot{E}_o - \sum_i \dot{E}_i \tag{41.1}$$

As neglecting magnetic, electrical, nuclear and surface tension energy balance can be expressed as [4, 5] (Cengel and Boles 2008);

$$\dot{E} = \dot{E}_{ph} + \dot{E}_{ch} \tag{41.2}$$

Physical energy for air, combustion gas, water and oil is [4, 5];

$$\dot{E}_{ph} = \dot{m}\left(c_{P(T)}T - c_{P(T_o)}T_o\right) = \dot{m}\left(h_{(T)} - h_o\right) \tag{41.3}$$

Energy of fuel is [6];

$$\dot{E}_{ch} = \dot{m}_f LHV \tag{41.4}$$

Composition of natural gas is given in Table 41.1 and its low heat value is $H_u = 44661$ kJ/kg.

Table 41.1 Composition of natural gas [7, 8]

Composition	Volume (%)	Mass (%)	Low heat value (kJ/kg)
CH_4	93.3401	88.8320	50,000
C_2H_4	0.2109	0.3760	47,525
C_3H_8	0.0290	0.1000	46,390
C_4H_{10}	0.0124	0.0430	45,775
N_2	6.4076	10.6490	–
Total	100.00	100.00	44,661

Combustion formula is shown as following;

$$0,9334CH_4 + 0,0002109C_2H_4 + 0,00029C_3H_8 + 0,000125C_4H_{10} + 0,064077N_2 + 4,3590(0_2 + 3,76N_2) \rightarrow 0,9351918CO_2 + 1,8690108H_2O + 2,48923028\ O_2 + 16,453917\ N_2 \tag{41.5}$$

Air fuel mixture is 40. Before combustion process, working fluid is a mixture of air and natural gas. Molecular weight of this mixture is $M_m = 28{,}28$ kmol/kg and gas constant is $R_m = 0{,}294$ kJ/kgK. After combustion period, gas' mass composition are as 6.7 % CO_2, 5.3 % H_2O, 13 % O_2, 75 % N_2. Molecular weight of combustion gasses was $M_g = 28.29$ kmol/kg and gas constant is $R_g = 0{,}294$ kJ/kgK. Air fuel mixture's specific heat at constant pressure was calculated by using Eq. (41.5) below [6]

And calculated from Eq. (41.5);

$$c_{vm} = 0,7910 - \frac{0,65284T}{10^3} + \frac{1,8321T^2}{10^6} - \frac{14,1170T^3}{10^{10}} + \frac{3,8709T^4}{10^{13}} \tag{41.6}$$

Specific heat constant volume of combustion gas is;

$$c_{vg} = 0,4734 + \frac{0,7516T}{10^3} - \frac{0,3840T^2}{10^6} + \frac{0,9829T^3}{10^{10}} - \frac{0,0995T^4}{10^{13}} \tag{41.7}$$

41.2.3 Energy Efficiencies

Energy efficiency is rate energy output to energy input. Efficiencies for heat exchangers and chillers [9];

$$\eta = \frac{\dot{E}_{cold,o} - \dot{E}_{cold,i}}{\dot{E}_{hot,i} - \dot{E}_{hot,o}} \tag{41.8}$$

Efficiency for pump [3];

$$\eta = \frac{\dot{E}_o - \dot{E}_i}{\dot{W}_{Pump}} \tag{41.9}$$

Efficiency of any component of trigeneration system is, [5];

$$\eta_j = \frac{\dot{E}_{o,j}}{\dot{E}_{i,j}} \tag{41.10}$$

Finally efficiency of trigeneration system [10];

$$\eta_{TRIGEN} = \frac{\dot{E}_{products}}{\dot{E}_F} = \frac{\dot{W}_{el,net} + \dot{E}_{heating,net} + \dot{E}_{cooling,net}}{\dot{E}_{F,NG}} \tag{41.11}$$

41.2.4 Exergy Terms

Exergy analysis for the control volume can describe as following [3];

$$\sum \left(1 - \frac{T_o}{T_k}\right)\dot{Q}_k + \dot{E}x_W + \sum_i \dot{E}x_i - \sum_o \dot{E}x_o = \dot{E}x_D \tag{41.12}$$

As neglecting magnetic, electrical, nuclear and surface tension energy balance can be expressed as [4, 5];

$$\dot{E}x = \dot{E}x_{ph} + \dot{E}x_{ch} \tag{41.13}$$

Physical exergy for air, combustion gas [11, 12];

$$\dot{E}x_{ph} = \dot{m}\left[c_{P(T)}\left[T - T_o - T_o \ln\left(\frac{T}{T_o}\right)\right] + RT_o\left(\frac{P}{P_o}\right)\right] \tag{41.14}$$

Physical exergy of solids and liquids exergy at constant specific heat [13];

$$\dot{E}x_{ph} = \dot{m}\left[Cp_{(T)}\left[T - T_0 - T_0 \ln\left(\frac{T_0}{T}\right)\right] - \nu(P - P_0)\right] \tag{41.15}$$

Physical energy for water [14];

$$\dot{E}x_{ph} = \dot{m}[(h - h_o) - T_o(s - s_o)] \tag{41.16}$$

Gas hydrocarbon whose formula is C_aH_b exergy [15];

$$\frac{\dot{E}x_{ch,NG}}{\dot{m}_{NG} LHV_{NG}} = \gamma_{NG} \cong 1.033 + 0.0169\frac{b}{a} - \frac{0.0698}{a} \tag{41.17}$$

γ denote exergy grade function. γ_{NG} is equal to 1.0308 for natural gas.

41.2.5 Exergy Efficiencies

Exergy efficiency is rate energy output to energy input. Exergy efficiencies for heat exchangers and coolers [9];

$$\psi = \frac{\dot{E}x_{cold,o} - \dot{E}x_{cold,i}}{\dot{E}x_{hot,i} - \dot{E}x_{hot,o}} \tag{41.18}$$

Exergy efficiency for pump [3];

$$\psi = \frac{\dot{E}x_o - \dot{E}x_i}{\dot{W}_{Pump}} \tag{41.19}$$

Exergy efficiency of any component of trigeneration system is [5];

$$\psi_j = \frac{\dot{E}x_{o,j}}{\dot{E}x_{i,j}} \tag{41.20}$$

Finally exergy efficiency of trigeneration system [9];

$$\psi_{TRIGEN} = \frac{\dot{E}x_{products}}{\dot{E}x_F} = \frac{\dot{W}_{el,net} + \dot{E}x_{heating,net} + \dot{E}x_{cooling,net}}{\dot{E}x_{F,NG}} \tag{41.21}$$

41.2.6 Other Thermodynamic Performance Parameters

One of the most important parameter is Power to heat ratio (PHR_e)[16]. It can be defined as;

$$PHR_e == \frac{\dot{W}_{net}}{\dot{E}_Q + \dot{E}_{CW}} \tag{41.22}$$

Another parameter is equivalent electrical efficiency (EEE) [17];

$$\eta_{EEE} == \frac{\dot{W}_{net}}{\dot{E}_{TF} - \frac{\dot{E}_Q + \dot{E}_{CW}}{\eta_{be}}} \tag{41.23}$$

A parameter called PURPA (The Public Utility Regulatory Policies Act) can defined as a scale of recognizing the quality of electrical output to thermal outputs [18].

$$\eta_{PURPA} == \frac{\dot{W}_{net} + 0.5\left(\dot{E}_Q + \dot{E}_{CW}\right)}{\dot{E}_{TF}} \tag{41.24}$$

For the trigeneration system fuel energy saving ratio FESR (Fuel energy saving ratio) can be defined as [13, 17–19].

$$FESR = \frac{\left(\dot{E}_{F,W} + \frac{\dot{E}_Q + \dot{E}_{CW}}{\eta_{be}}\right) - \left(\dot{E}_F\right)_{TRIGEN}}{\left(\dot{E}_{F,W} + \frac{\dot{E}_Q + \dot{E}_{CW}}{\eta_{be}}\right)} \tag{41.25}$$

Fuel exergy depletion ratio can be defined as [20];

$$\alpha_k = \frac{\dot{E}x_{C,k}}{\dot{E}x_{TF}} \tag{41.26}$$

Relative exergy consumption ratio is calculated from [20];

$$\beta_k = \frac{\dot{E}x_{C,k}}{\dot{E}\,x_{TF}} \tag{41.27}$$

The productivity lack ratio for the exergy is [20];

$$\chi_k = \frac{\dot{E}x_{C,k}}{\dot{E}x_{UP}} \tag{41.28}$$

The exergetic improvement potential can be expressed following [21];

$$ExIP_k = (1 - \psi)Ex_{C,k} \tag{41.29}$$

Similar parameters can be defined for energy terms. Fuel energy depletion ratio can be defined as [8, 22];

$$\phi_k = \frac{\dot{E}_{L,k}}{\dot{E}_{TF}} \tag{41.30}$$

Relative energy loss ratio [8, 22];

$$\Theta_k = \frac{\dot{E}_{L,k}}{\dot{E}_{TL}} \tag{41.31}$$

Productivity lack ratio [8, 22];

$$\Omega_k = \frac{\dot{E}_{L,k}}{\dot{E}_{UP}} \tag{41.32}$$

Energetic improvement potential [8, 22];

$$EIP_k = (1 - \eta)E_{L,k} \tag{41.33}$$

Finally, power to heat ratio, equivalent electrical efficiency (EEE) and fuel saving ratio can be written by the exergy terms as follows [13];

$$PHR_{ex} = \frac{\dot{W}_{net}}{\dot{E}x_Q + \dot{E}x_{CW}} \tag{41.34}$$

$$\psi_{EEE} = \frac{\dot{E}x_Q + \dot{E}x_{CW}}{\psi_{be}} \tag{41.35}$$

$$FExSR = \frac{\left(\dot{E}x_{F,W} + \frac{\dot{E}x_Q + \dot{E}x_{CW}}{\psi_{be}}\right) - \left(\dot{E}x_F\right)_{TRIGEN}}{\left(\dot{E}x_{F,W} + \frac{\dot{E}x_Q + \dot{E}x_{CW}}{\psi_{be}}\right)} \tag{41.36}$$

41.3 Results

In this study a trigeneration system with natural gas engine (Wartsila 18VSG) was investigated about energy and exergy. Values calculated for engine is shown in Table 41.2. Pressure, temperature, mass flow, energy and exergy rates are indicated in Table 41.2.

41.3.1 Energy Analysis Results for Trigeneration Subsystem

Energy input, energy output, energy losses and energy efficiencies for each component of trigeneration system is listed in Table 41.3. Energy efficiencies of engine, waste heat boiler, absorption chiller and radiator are 96, 94, 73, 86 % respectively, energy efficiencies of HT pump, LT pump, oil pump, compressor and solution pump are 79, 80, 87, 97, 74 % respectively, energy efficiencies of oil heat exchanger, generator, absorber, evaporator, condenser, ACH heat exchanger are 77, 70, 87, 89, 37, 89 % respectively.

Maximum energy loss is at radiator (2,774.16 kW). Others are engine, absorption chiller and waste heat boiler respectively.

41.3.2 Exergy Analysis Results for Trigeneration Subsystem

Exergy input, exergy output, exergy losses and exergy efficiencies for each component of trigeneration system is listed in Table 41.4. Exergy efficiencies of engine, waste heat boiler, absorption chiller, radiator, HT pump, LT pump, oil pump, compressor, oil heat exchanger, generator, absorber, evaporator, condenser, ACH

Table 41.2 Trigeneration system pressure, temperature, energy rate and exergy rate

Point	Fluid	Temperature (K)	Pressure (kPa)	Mass flow (kg/s)	Energy rate (kW)	Exergy rate (kW)
0	Air	298.15	100			
1	Air	298.15	100	16.385	0	0
2	Natural gas	298.15	300	0.415	18,534.32	19,105.17
0’	Water	298.15	100			
3	Water	358.15	450	63.06	15,828.70	1,409.95
4	Water	364.15	320	63.06	17,419.57	1,690.37
5	Water	358.08	150	63.06	15,828.70	1,409.95
6	Water	311.15	450	25.65	1,393.41	31.89
7	Water	314.15	350	25.65	1,716.4	46.62
8	Water	321.95	320	25.65	2,551.41	241.93
9	Water	311.08	150	25.65	1,386.9	30.21
0’’	Oil	298.15	100			
10	Oil	347.15	350	36.68	4,944.09	7,188.64
11	Oil	347.42	455	36.68	4,967.71	7,204.62
12	Oil	336.15	450	36.68	4,104.4	5,477.26
13	Gas	662.15	285	16.8	7,872.31	3,915.14
14	Gas	748.78	450	16.8	9,875.14	5,616.78
15	Gas	515	428	16.8	4,588.14	3,100.8
16	Water	373.15	450	34.73	10,912.51	1,184.21
17	Water	393.15	200	25.06	9,995.93	1,327.23
18	Water	393.15	200	9.67	4,871.84	5,12.18
19	Water	373.15	150	25.06	7,874.1	854.49
20	Water	372.15	83	0.67	1,728.65	21.86
21	Water	342.15	83	0.67	126.02	13.92
22	Water	277.65	0.73	0.67	126.02	66.81
23	Water	277.65	0.73	0.67	1,513.56	1,453.85
0’’’[a]	Water-LiBr (64 %)	298.15	100			
24[a]	Water-LiBr (64 %)	321.35	83	9.53	435.95	158.46
25[a]	Water-LiBr (64 %)	323.35	83	9.53	473.75	161.20
26[a]	Water-LiBr (64 %)	362.15	83	9.53	1,064.64	183.82
0[iv, a]	Water-LiBr (59.5 %)	298.15	100			
27[a]	Water-LiBr (59.5 %)	341.15	83	8.86	440.35	96.94
28[a]	Water-LiBr (59.5 %)	314.55	83	8.86	286.08	21.92
29[a]	Water-LiBr (59.5 %)	310.55	0.73	8.86	286.08	130.23

(continued)

Table 41.2 (continued)

Point	Fluid	Temperature (K)	Pressure (kPa)	Mass flow (kg/s)	Energy rate (kW)	Exergy rate (kW)
30	Water	312.55	120	54.9	3,723.192	90.85
31	Water	317.65	80	54.9	4,475.28	142.88
32	Water	285.35	250	54.35	−2,608.26	1,692.38
33	Water	279.85	180	54.35	−4,168.65	1,187.05
34	Water	302.55	250	72.23	1,323.25	−3.35
35	Water	308.15	120	72.23	3,022.83	59.53

[a]Li-Br enthalpy and entropy values were taken from [23, 24]
[iv]represents to forth environment conditions that belong to 59.5 % Li/Br mixture

heat exchanger, solution pump are 74, 73, 39, 75, 54, 17, 59, 11, 98, 14, 7, 1, 20, 30, 6 respectively. Maximum exergy loss is at engine (6,823.2 kW) because of irreversibilities in chemical reactions. Others are absorption chiller.

41.3.3 Energy and Exergy Analysis Results of Trigeneration System

In the study energy and exergy efficiencies were calculated as 64 and 39 % respectively. Results for overall system can be shown in Tables 41.5 and 41.6. Total energy and exergy losses of system are 8,113.27, 12,996.72 kW respectively.

41.4 Conclusions

In this study a trigeneration system with Wartsila 18VSGD natural gas engine was investigated in terms of energy and exergy. Some specific results were listed following;

- Calculated energy and exergy efficiencies of trigeneration system are 64 and 39 %.
- Maximum energy loss at a component is at radiator (2,774.16 kW).
- Maximum energy loss to environment is 4,588.14 kW.
- Maximum exergy consumption is at engine (6,823.2 kW).
- Maximum energetic improvement potential in absorber (839.12 kW) and maximum exergetic improvement potential is in engine (1,774.03 kW).

According to these results plant owner has an opinion about recovery will be done. In addition, it is determined how actual power can produce from engine under certain or mean environment condition and according to this several solutions can

Table 41.3 Parameters interested with energy for components

Component	Energy input (kW)	Energy output (kW)	Energy loss (kW)	η (%)	Φ (%)	Θ (%)	Ω (%)	EIP (kW)
Engine (NGE)	39,860.8	38,312.7	1,548.13	96	8	23	15	61.93
Heat recovery boiler (HRB)	20,787.7	19,455.9	133.74	94	0.7	2	1.3	8.02
Absorption chiller (AC)	2,121.83	1,560.39	561.44	73	3	8.5	5.4	151.6
Radiator	19,974.6	17,200.5	2,774.16	86	1.5	41	26	388.38
HT pump (HTP)	24	18.91	5.09	79	0.03	0.08	0.05	1.07
LT pump (LTP)	10	7.95	2.05	80	0.01	0.03	0.02	0.41
Oil pump (OP)	27	23.62	3.38	87	0.02	0.05	0.03	0.44
Oil heat exchanger (OHE)	863.31	835.01	28.3	97	0.15	0.4	0.3	0.85
Compressor (C)	2,600	2,002.83	597.17	77	3	9	6	137.35
Generator	2,121.83	1,475.54	646.29	70	1.02	10	5.4	193.88
Condenser	1,835.63	1,604.14	231.49	87	1.25	3.5	2	30.09
Evaporator	1,560.39	1,387.54	172.85	89	0.9	2.6	1.5	19.01
Absorber	2,110.5	778.56	1,331.94	37	7.2	20	11	839.12
Absorption chiller heat exchanger (ACHE)	590.89	525.45	65.44	89	0.35	0.1	0.5	7.2
Solution pump (SP)	50	37.8	11.8	74	0.07	0.2	0.1	3.39

Table 41.4 Parameters interested with exergy for components

Component	Exergy input (kW)	Exergy output (kW)	Exergy consumption (kW)	ψ (%)	α (%)	β (%)	χ (%)	ExIP (kW)
Engine (NGE)	26,024.3	19,201.1	6,823.2	74	36	59	90	1,774.03
Heat recovery boiler (HRB)	6,800.99	4,940.21	1,860.78	73	9.7	16	25	502.41
Absorption chiller (AC)	1,305.37	505.33	800.04	39	4.2	7	10	488.02
Radiator	1,936.18	1,456.96	479.22	75	2.5	4.1	6.4	119.81
HT pump (HTP)	24	13.05	10.95	54	0.05	0.09	0.15	5.04
LT pump (LTP)	10	1.68	8.32	17	0.04	0.07	0.11	6.91
Oil pump (OP)	27	15.98	11.02	59	0.06	0.1	0.15	4.52
Oil heat exchanger (OHE)	1,727.36	195.31	1,532.05	11	8	13	20	1,363.52
Compressor (C)	2,600	2,515.98	84.02	98	0.4	0.7	1.1	1.68
Generator	472.74	65.02	407.72	14	2.13	3.6	5.5	350.64
Condenser	284.68	20.04	264.64	7	1.4	2.3	3.5	246.12
Evaporator	505.23	4.24	500.99	1	2.6	4.3	6.7	495.98
Absorber	142.27	28.23	114.04	20	0.6	1	1.5	91.23
Absorption chiller heat exchanger (ACHE)	75.09	22.62	52.47	30	0.3	0.5	0.7	36.73
Solution pump (SP)	50	2.74	47.26	6	0.2	0.4	0.6	44.11

Table 41.5 Parameters interested in energy for overall trigeneration system

System data			Performance parameters		
Data	Unit	Value	Parameter	Unit	Value
$\dot{E}_F$	kW	18,534.3	η	%	64
$\dot{E}_{W.net}$	kW	6,360.33	η_W	%	34
$\dot{E}_Q$	kW	3,955.26	η_{HEAT}	%	21
$\dot{E}_{Q.ACH}$	kW	1,560.39	η_{COOL}	%	8
$\dot{E}_{TL}$	kW	6,658.32	η_{PURPA}	%	49
$\dot{E}_{F.SHP}$	kW	6,894.56	η_{EEE}	%	55
η_{be}	%	80	PHR_e	%	1.15
			FESR	%	27
			Φ	%	36
			Ω	%	64
			EIP	kW	2,397

Table 41.6 Parameters interested in exergy for overall trigeneration system

System data			Performance parameters		
Data	Unit	Value	Parameter	Unit	Value
$\dot{E}x_F$	kW	19,105.17	ψ	%	39
$\dot{E}x_{W.net}$	kW	6,360.33	ψ_W	%	33
$\dot{E}x_Q$	kW	655.2	ψ_{HEAT}	%	3.4
$\dot{E}x_{Q.ACH}$	kW	505.33	ψ_{CW}	%	2.6
$\dot{E}x_C$	kW	11,584.31	ψ_{EEE}	%	55
$\dot{E}x_{F.SHP}$	kW	7,600	PHR_{ex}	%	5.5
ψ_{be}	%	15.27	FExSR	%	28
			α	%	60
			χ	%	39
			ExIP	kW	7,066.43

be thought. First solution advice is that it can be utilized from the waste heat of HT and LT loops, by installing heat exchangers to them.

Exergy and energy methodology submitted at this study might be useful, while designed and improved similar trigeneration systems.

Nomenclature

c_P Specific heat capacity at constant pressure ($kJkg^{-1}$)
c_v Specific heat capacity at constant volume ($kJkg^{-1}$)
$\dot{E}$ Energy rate (kW)
$\dot{E}x$ Exergy rate (kW)
$\dot{E}xIP$ Exergetic improvement potential rate (kW)

FESR	Fuel energy saving ratio (%)
FExSR	Fuel exergy saving ratio (%)
h	Enthalpy (kJkg^{-1} K^{-1})
LHV	Lower heating value of fuel (kJkg^{-1})
$\dot{m}$	Mass rate (kgs^{-1})
P	Pressure (kPa)
$\dot{Q}$	Heat (kW)
PHR	Power-to-heat ratio (%)
R	Universal gas constant
s	Entropy (kJkg^{-1} K^{-1})
T	Temperature (K)
u	Specific internal energy (kJkg^{-1})
U	Internal energy (kJ)
$\dot{W}$	Work (kW)

Abbreviations

ACH	Absorption chiller
ACHE	Absorption chiller heat exchanger
C	Compressor
CHP	Combined heat and power
EEE	Equivalent electrical efficiency
EGEN	Electric generator
HRB	Heat recovery boiler
HT	High temperature loop
HTP	High temperature loop pump
LT	Low temperature loop
LTP	Low temperature loop pump
NGE	Natural gas engine
OHE	Oil heat exchanger
OP	Oil pump
PURPA	Public Utility Regulatory Policies Acts
S	Separator
SP	Solution pump

Subscripts

be	Boiler efficiency
C	Consumption
ch	Chemical
cw	Chilled water
cold	Cold side
COOL	Cooling

D	Destruction
e	Energitic
E	Engine
ex	Exergitic
F	Fuel
hot	Hot side
i	Inputs
j	j'th component
k	Boundary of system
L	Loss
m	Mixture of natural gas and air
NG	Natural gas
o	Outputs
ph	Physical
$\dot{Q}$	Heat
T	Temperature
UP	Useful products
$TRIGEN$	Trigeneration
$\dot{W}$	Work

Greek letters

α	Fuel exergy depletion ratio (%)
β	Relative exergy loss ratio (%)
χ	Productivity lack ratio based on exergy (%)
γ	Fuel exergy grade function (%)
η	First law (energy) efficiency (%)
ψ	Second law (exergy) efficiency (%)
ϕ	Fuel energy depletion ratio (%)
Θ	Relative energy loss ratio (%)
Ω	Productivity lack ratio based on energy (%)

References

1. Balli O, Aras H, Hepbasli A (2010) Thermodynamic and thermoeconomic analyses of a trigeneration TRIGEN system with a gas–diesel engine: part II – an application. Energy Conserv Manage 51:2252–2259
2. Lockwood FE, Zhang ZG, Cho SUS, Wang JC (2008) Thermal characteristics of new and used diesel engine oils. www.oetg.at/website/wtc2001cd/html/M-21-27-729-LOCWOOD.pdf. Accessed on May 2011
3. Bejan A, Tsatsaronis G, Moran M (1996) Thermal design and optimization. Wiley, NewYork, NY

4. Moran MJ, Shapiro HN (1995) Fundamentals of engineering thermodynamics. Wiley, New York, NY
5. Cengel YA, Boles MA (2008) Thermodynamics: an engineering approach, 6th edn. McGraw-Hill, NewYork, NY
6. Kreith F (2000) The CRC handbook of thermal engineering. Boca Raton, FL, CRC, p 1131
7. Balli O, Aras H (2007) Energetic analysis of a combined heat and power system CHP in Turkey. Energy Explore Exploit 25:39–62
8. Balli O, Aras H (2007) Energetic and exergetic performance evaluation of a combined heat and power system with the micro gas turbine MGTCHP. Int J Energy Res 37:1425–1440
9. Wark KJ (1995) Advanced Thermodynamics of engineers. McGraw-Hill, New York, NY
10. Rosen MA, Le MN, Dincer I (2005) Efficiency analysis of a cogeneration and district energy system. Appl Therm Eng 25:147–159
11. Kotas TJ (1995) The exergy method of thermal plant analysis. Krieger, Malabar, FL, Reprint edn
12. Ebadi MJ, Gorji-Bandpy M (2005) Exergetics analysis of gas turbine plants. Int J Exerg 2:285–290
13. Balli O, Aras H, Hepbasli A (2010) Thermodynamic and thermoeconomic analyses of a trigeneration TRIGEN system with a gas–diesel engine: part I – methodology. Energy Conserv Manage 51:2260–2271
14. Moran MJ, Sciubba E (1994) Exergy analysis: principles and practice. J Eng Gas Turbine Power 116:285–290
15. Moran MJ (1989) Availability analysis: a guide to efficient energy use. ASME, New York, NY
16. Huang FF (1996) Performance assessment parameters of a cogeneration system. In: Proceedings of ECOS'96, Stockholm, Sweden
17. Horlock JH (1997) Cogeneration – combined heat and power CHP, 2nd edn. Krieger, Malabar, FL
18. US EPA. United States Environmental Production Agency. Catalogue of CHP technologies. http://www.epa.gov/chp/technologies.html. Accessed on May 2011
19. Feng X, Cali M, Qian L-L (1998) A new performance criterion for cogeneration system. Energy Convers Manag 39:1607–1609
20. Xiang JY, Cali M, Santarelli M (2004) Calculation for physical and chemical exergy of flows in system elaborating mixed-phase flows and a case study in a study in IRSOFC plant. Int J Energy Res 28:101–115
21. Van Gool W (1997) Energy policy: fairly tales and factualities. In: Soares D, da Cruz M, Pereira C, Soares IMRT, Reis AJPS (eds) Innovation and technology-strategies and policies. Kluwer, Dordrecht, The Netherlands, pp 93–105
22. Dıncer I, Cengel YA (2001) Energy, entropy and exergy concepts and their roles in thermal engineering. Entropy 3:116–149
23. Florides GA, Kalogirou SA, Tassou SA, Wrobel LC (2003) Design and construction of a LiBr–water absorption machine. Energy Convers Manag 44:2483–2508
24. Chua HT, Toh HK, Malek A, Ng KC, Srinivasan K (2000) Improved thermodynamic property fields of LiBr ± H2O solution. Int J Refrig 23:412–429

Chapter 42
Numerical Study of Solidification in Triplex Tube Heat Exchanger

Abduljalil A. Al-Abidi, Sohif Mat, K. Sopian, M.Y. Sulaiman, and AbdulrahmanTh. Mohammad

Abstract Thermal energy storage is very important to eradicate the discrepancy between energy supply and energy demand and to improve the energy efficiency of solar-energy systems. The latent heat thermal energy storage systems have gained greater attention recently due to their reliability and high storage density at nearly constant thermal energy. The present work explores numerically the solidification process of a phase change material (PCM) in a triplex tube heat exchanger (TTHX) equipped with internal and external fins to enhance the heat transfer during the charging and discharging of the PCM. A two-dimension (2D) numerical model is developed using the Fluent 6.3.26 software program; the pure conduction and natural convection are considered for the simulation. Experimental and numerical data were adopted to validate the model from the literature; a good agreement has been found. Predicted results indicated that the solidification rate time of the TTHX with internal and external fins was about 50 % of the solidification time of the TTHX without fins.

Keywords Solidification • Triplex tube heat exchanger • Phase change material • Fluent

42.1 Introduction

Phase change material (PCM) thermal energy storage is a technique that has been gotten a greater consideration recently due to their high thermal energy density per unit volume/mass and their availability for different engineering fields with a wide temperature range. Since solar energy is considered as an intermittent energy source that leads to low efficiency of most thermal solar energy applications (TSEA). Thermal energy storage is very important to eradicate the discrepancy between energy supply and energy demand and to improve the energy efficiency of solar

A.A. Al-Abidi (✉) • S. Mat • K. Sopian • M.Y. Sulaiman • A.T. Mohammad
Solar Energy Research Institute, National University of Malaysia, Bangi, Selangor, Malaysia
e-mail: abo_anas4@yahoo.com; Sohif@kum.my; k_sopian@eng.ukm.my; sulaiman_yusof@yahoo.com; abd20091976@gmail.com

I. Dincer et al. (eds.), *Progress in Sustainable Energy Technologies Vol II: Creating Sustainable Development*, DOI 10.1007/978-3-319-07977-6_42

energy systems. In addition, most of the TSEA need a constant or near constant temperature to work with high efficiency strategies: the using of latent heat thermal energy storage (LHTES) as thermal energy storage can deliver this constant temperature, which meets the melting temperature of the PCM.

The using of PCM can be found in different engineering fields such as thermal storage of a building structure and equipment (roof, wall, ceiling, domestic hot water, heating and cooling systems), electronic products, drying technology, waste heat recovery, refrigeration and cold storage, and solar cookers. Most of the PCMs are known as low thermal conductivity substances that limit the using of these materials as thermal energy storage, and that lead to a long time for the melting and solidification process; the heat transfer enhancement technique is the subject of many researchers to overcome this poor characteristic of PCM. Several researchers have studied the heat transfer enhancement in PCMs including finned tubes, insertion of a metal matrix to the PCM, using multi-tubes, using bubble agitation in PCMs, using PCM dispersed with high conductivity particles, and employing multiple families of PCMs in LHTES.

Most researchers reported that the increase of the heat transfer area will lead to improve the heat transfer between the heat transfer fluid and the PCM. The majority of the heat enhancement techniques have been based on the application of fins embedded in the PCM; this is probably due to their simplicity, ease in fabrication, and low cost of construction [1]. There are different fin configurations applied to the PCM, including external fins, and internal fins (circular, longitudinal, rectangular). The designing parameters of the thermal energy storage, such as the geometry of the thermal storage, the fins attached to the heat transfer tubes either internally or externally, the fin length, the fin thickness and the high thermal conductivity of metals that are immersed in the PCM, play a key role in the enhancement of the solidification process of the PCM. Moreover, the effect of the operation parameters, such as the heat transfer fluid (HTF) inlet temperature and mass flow rate were found to affect the solidification of the PCM, but the majority of researchers reported that there is a big influence of the designing parameters in time to complete the solidification process in contrast to the operation parameters.

Bauer [2] developed an analytical model to investigate the effective utilization of fins in LHTES; they studied the solidification times of PCM using two geometries; the first geometry is a finned plane wall and the second geometry is a tube surrounded by the PCM-fin arrangement. Mosaffa et al. [3] presented a two-dimensional analytical model to study the solidification process of a PCM in a shell and tube heat exchanger with radial fins; they reported the PCM solidified more quickly in the cylindrical shell storage than in the rectangular storage, In addition, the solid fraction of the PCM increases more quickly when the cell aspect ratio is small. Ismail et al. [4] investigated numerically and experimentally the effect of fin design parameters such as the fin length, fin thickness, number of fins, and the aspect ratio of the annular space on the complete solidification, solidified mass fraction, and the total stored energy of the PCM.

Stritih et al. [5] used a rectangular external fin to enhance the heat transfer during melting and solidification of a latent heat storage for thermal application in building

purposes; they concluded that heat storage (melting) was not a problem during thermal storage applications, and that the extraction of heat (solidification) can be effectively enhanced with fins. Bilen et al. [6] investigated experimentally the melting and solidification characteristics of ($CaCl_2.6H_2O$)as a PCM in a vertical double-concentric pipe energy storage system; different design and operation parameters were studied such as the numbers of fins inside the PCM, mass flow rate, and the inlet HTF temperature; they reported that the effect of the designing parameters are much more than the effect of the operation parameters.

Ismail et al. [7] conducted an experimental and numerical investigation of the solidification of PCM around a curved cold tube; different operation parameters such as the Dean number, cooling fluid flow rate and its temperature on the interface velocity, were studied to determine the effect of these parameters on the time for complete solidification and the solidified mass. Lipnicki and Weigand [8] studied experimentally and theoretically the natural convection and solidification of a vertical annular enclosure; the inner cylinder was cooled down below the solidification temperature of the HTF (water), whereas the outer cylinder was kept at a constant temperature above 0 °C. The thermal resistance of the contact layer between the cooled inner wall and the solidified layer was investigated; they reported that the influence of the contact layer between the frozen layer and the cold surface is of significant importance for the solidification process. Sanusi et al. [9] examined experimentally the effect of graphite nanofibers (GNFs) on both the thermal storage and solidification time of a PCM that is embedded between two sets of aluminum fins. They performed the influences of the aspect ratio and power density of the PCM solidification. The time required for the finished melting and solidification of PCM is very important to absorb/release energy as much as possible from solar energy; moreover, the charging process depends on the HTF mass flow rate and inlet temperature. The inlet HTF temperature fluctuations would affect the charging process, especially when the charging source depends on solar energy. Ismail and Moraes [10] studied numerically and experimentally the effect of the PCM container materials, configuration, and dimensions on the solidification of various PCMs to obtain the time required for complete solidification.

In the present work, the effects of longitudinal external and internal fins on the solidification process in Triplex tube heat exchanger (TTHX) are investigated numerically; the number of fins, fin length, and fin thickness were studied to improve the performance of the PCM thermal energy storage.

42.2 Physical and Numerical Models

42.2.1 Physical Model

Figure 42.1 shows the physical configuration of the TTHX, the inner tube radius r_i is 25.4 mm with 1.2 mm thickness, the middle tube radius r_m is 75 mm and the outer tube radius r_o is 100 mm; with 2 mm thickness, all pipes are made from copper to

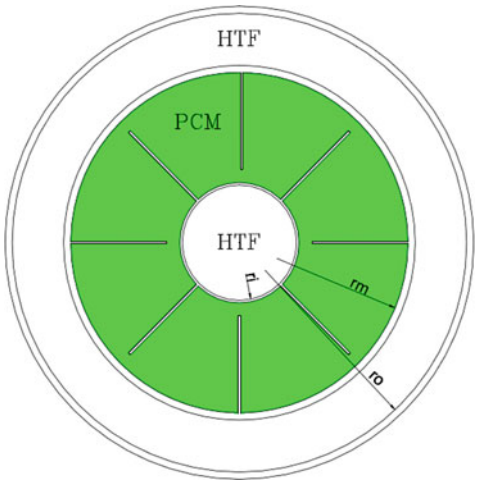

Fig. 42.1 Schematic diagram of triplex tubes heat exchanger unit

Table 42.1 Thermo-physical properties of the PCM

Property	Unit	Value
Density of PCM, solid, ρ_s	kg/m^3	990
Density of PCM, liquid, ρ_l	kg/m^3	770
Specific heat of PCM, liquid, Cp_l, Cp_s	J/kg K	2,000
Latent heat of fusion, L	J/kg	176,000
Melting temperature, Tm	K	355.15
Thermal conductivity, k	W/m K	0.2
Thermal expansion coefficient	1/K	0.001
Dynamic viscosity, μ	Kg/m.s	0.03499

ensure high thermal conductivity, which enhances the heat transfer phenomena between the PCM and the HTF. There have been different numerical experiments that were done for different fin lengths of 30, 35, and 42 mm, respectively, fin thickness of 1,1.5, and 2 mm, and the number of fins (4, 6, 8).

The outer tube and the inner tube are for the HTF, whereas the middle tube is for the PCM, where the PCM is based on commercially available materials, RT82 (Rubitherm GmbH), with the thermo-physical properties listed in Table 42.1. This thermal energy storage will be used to deliver the required thermal energy to a liquid desiccant air-conditioning system and the HTF will be water, so the minimum temperature required to operate the liquid desiccant air conditioning is about 65 °C.

42.2.2 Governing Equation

For the mathematical equations of the solidification process of the PCM inside the middle tube of the TTHX, the flow is consider as laminar, unsteady, and

incompressible. The thermal resistances of the inner and middle tube are negligible, and the viscous dissipation is considered negligible. The effect of natural convection during solidification is considered, whereas the thermo-physical properties of the HTF and PCMs are independent of the temperature; the viscous incompressible flow and the temperature distribution are solved using the Navier-Stokes and thermal energy equation, respectively, the continuity, momentum, and thermal energy equations can be written as [11]:

Continuity:

$$\partial_t(\rho) + \partial_i.(\rho u_i) = 0 \tag{42.1}$$

Momentum:

$$\partial_t(\rho u_i) + \partial_i\left(\rho u_i u_j\right) = \mu\partial_{jj}u_i - \partial_i p + \rho g_i + S_i \tag{42.2}$$

The energy equation:

$$\partial_t(\rho h) + \partial_t(\rho\Delta H) + \partial_i(\rho u_i h) = \partial_i(k\partial_i T) \tag{42.3}$$

Where ρ is the density of PCM (RT82), u_i is the fluid velocity μ, is the dynamic viscosity, p is the pressure, g is the gravity acceleration, k is the thermal conductivity, and h is the sensible enthalpy. The sensible enthalpy can be expressed as:

$$h = h_{ref} + \int_{T_{ref}}^{T} cp\Delta T \tag{42.4}$$

H, can be defined as:

$$H = h + \Delta H \tag{42.5}$$

Where h_{ref} is the reference enthalpy at the reference temperature T_{ref}, cp is the specific heat, ΔH is the latent heat content that may change between zero (solid) and L (liquid), the latent heat of the PCM, and β is the liquid fraction that happens during the phase change between the solid and liquid state when the temperature is $T_l > T > T_s$, so it can be written as:

$$\beta = \Delta H/L \tag{42.6}$$

$$\beta = \begin{cases} 0 & \text{if} \quad T < T_s \\ 1 & \text{if} \quad T > T_l \\ (T - T_s)/(T_l - T_s) & \text{if} \quad T_l > T > T_s \end{cases} \tag{42.7}$$

The source term S_i in the momentum equation, Eq. (42.2), is defined as:

$$S_i = C(1-\beta)^2 \frac{u_i}{\beta^3} \tag{42.8}$$

C is a constant reflect of the mushy zone, it is between 10^4 and 10^7, so 10^5 is considered for this work [12].

42.2.3 Initial and Boundary Conditioning

At the initial time, the PCM was considered in a liquid state, and the initial temperature of the PCM is about 363.15 K whereas a constant temperature of the tube wall represented the HTF temperature, which was about 338.15 K, which reflects the minimum temperature required for liquid desiccant air conditioning system operation. The boundary conditions of the TTHX can be written as below;

$$\text{at } r = r_i, \rightarrow T = T_{HTF} \tag{42.9}$$

$$\text{at } r = r_m \rightarrow T = T_{HTF} \tag{42.10}$$

The initial temperature for the three models will be

$$\text{at } t = 0 \rightarrow T = T_{ini} \tag{42.11}$$

42.2.4 Numerical Modeling

Using the commercial computational program (Fluent 6.3.26), a solidification and melting model is used to simulate the solidification process of the PCM, two dimensions(r, θ) of the TTHX are drawn and meshed in a geometric modeling and mesh generation software, Gambit, which is part of the Fluent software; the boundary layers and zone types are defined, then the mesh is exported to the Fluent software. Different computational grids are adopted for the different cases to reduce the time required for simulation. A half-section grid is used for cases with eight fins and four fins, whereas the full section is used for the six-fin type. The Fluent software employs the finite volume method as described by [13] and uses the enthalpy–porosity formulation to solve the mass, velocity and energy equations. The PRESTO scheme is used for the pressure correction equation, and a well-known Semi-Implicit Pressure-Linked Equation (SIMPLE) algorithm is used for the pressure–velocity coupling, the under-relaxation value factors for pressure, velocity, energy, and liquid fraction are 0.3, 0.2, 1, and 0.9, respectively. Different grid meshing and time steps for the cases have been tested carefully at the primary calculation for the melt fraction of the TTHX; different time steps; 1 (chosen), 0.5, and 0.6 were examined for the simulation; also, to check the independency of the grid size for the numerical solution, three grid sizes were examined: 16,889 cells (chosen), 19,924 cells, and 25,136 cells. The 16,889-cells grid with a 1 s time step

was found enough to achieve the predetermined convergence of the energy equation (10^{-5}), and 10^{-3} for the velocities.

42.2.5 Validation of the Model

The validation of the numerical method has been done by comparing the experimental and numerical data reported by [14] for the solidification process of paraffin (RT60) inside a vertical cylinder with internal longitudinal fins, the outside diameter of the tube is 60 mm and the inner tube diameter is 54 mm, with a cross-shaped cross-section fin with dimensions of 1.5 mm thickness and 27 mm height welded from the top and bottom of the tube. The same meshing method and time step were applied for the model, which led to 1,593 cell grid generation and time step of 1 s, the boundary conditions of the model were applied for a temperature of 328.15 K, and a convection heat transfer coefficient of 400 W m^2 K^{-1}. The verification of this model work was based on a comparison of four temperature points inside the PCM, which were plotted as functions of time in Fig. 42.2. It is obvious that the results obtained by the present model are in good agreement with the experimental and numerical data reported by [14].

42.3 Results and Discussion

Figure 42.3 shows the melting fraction versus time of the PCM during the discharging period (solidification) with different numbers of fins (4, 6, 8) and without fins for comparison; the fin length and thickness are 42 mm and 1 mm, respectively. One can observe that an increase in the presence of the fins leads to reducing the solidification time. The time for the complete solidification for eight fins was about half of that of the configuration without fins, indicating a strong reduction in time required for releasing their energy to the load.

It can be seen that the solid fraction was increased at the primary time of the energy being released because the thermal resistance between the inner tube surface and the PCM was small; as the time progressed, the thermal resistance increased due to the increase of the solid fraction in the PCM, consequently, the heat-transfer decreased and the PCM slightly increased to the solid state. The effect of the fin length on the solidification rate time for eight fins is shown in Fig. 42.4, in which the melting fraction was plotted versus time. It is clear that the solidification rate time decreases when the fin length increases, but after a specific length the effect is close together as shown for a length of 35 and 42 mm. There is not a big difference in the time for the complete solidification according to the fin length.

Figure 42.5 shows the influence of the fin thickness on the solidification rate of PCM with a fin length 42 mm and the time required to complete melting; it can be said that there is little effect from the thickness on the solidification process; their

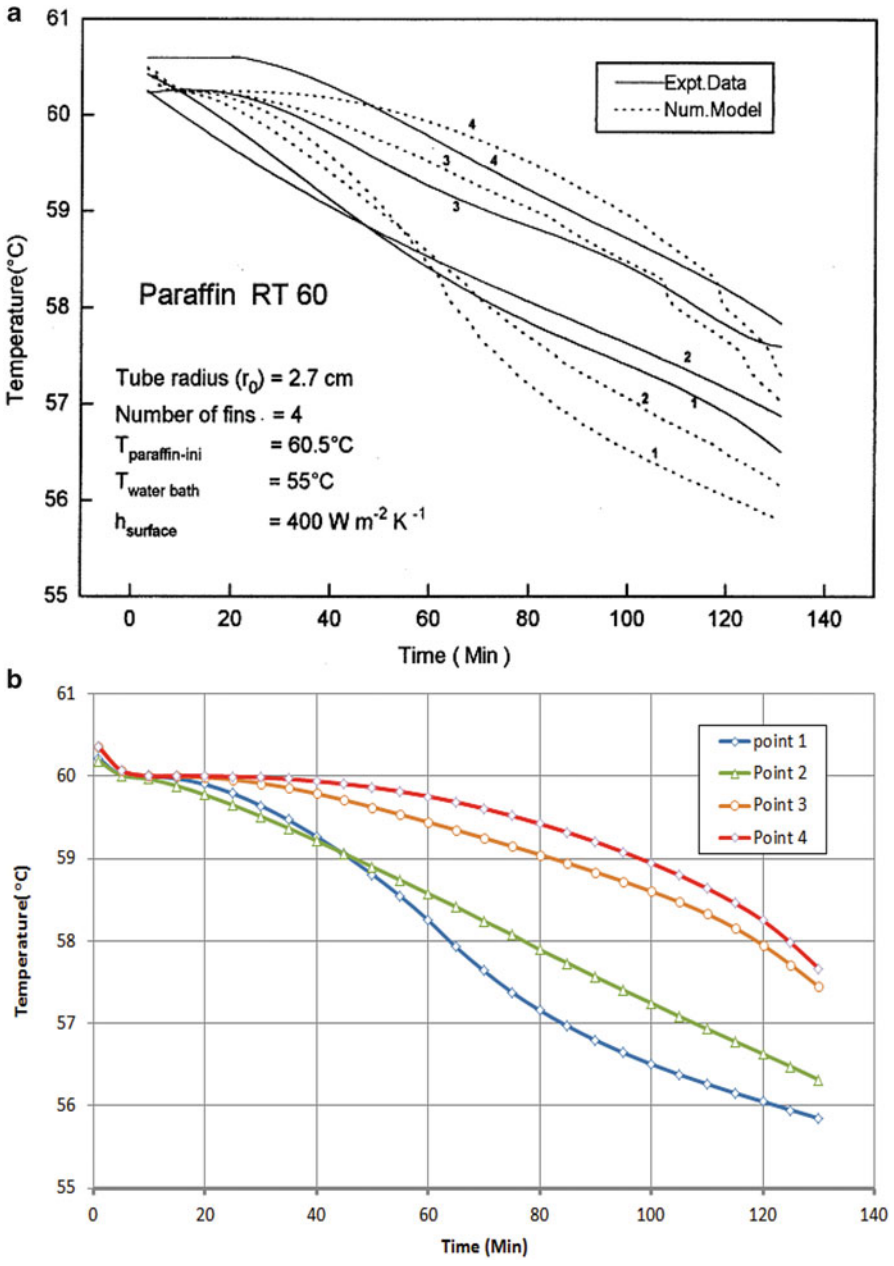

Fig. 42.2 Comparison results of four temperature points (**a**) the experimental and numerical works, (**b**) present model

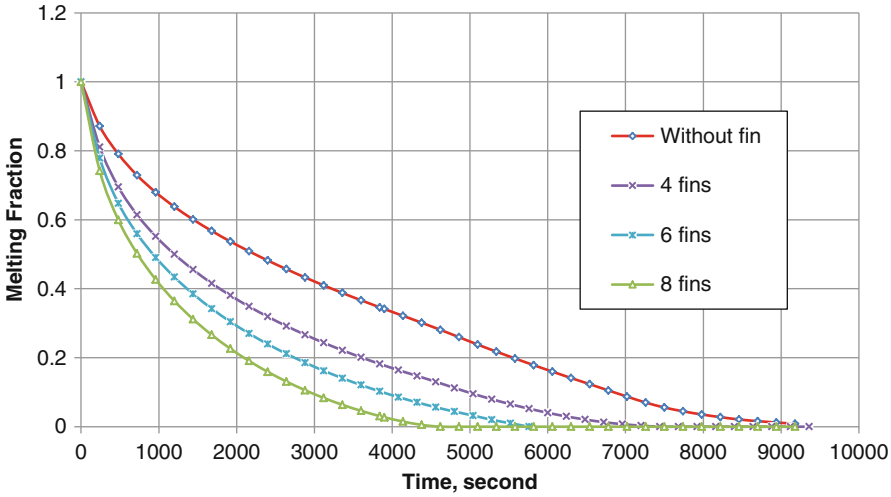

Fig. 42.3 Number of fins effect to the solidification rate of the PCM

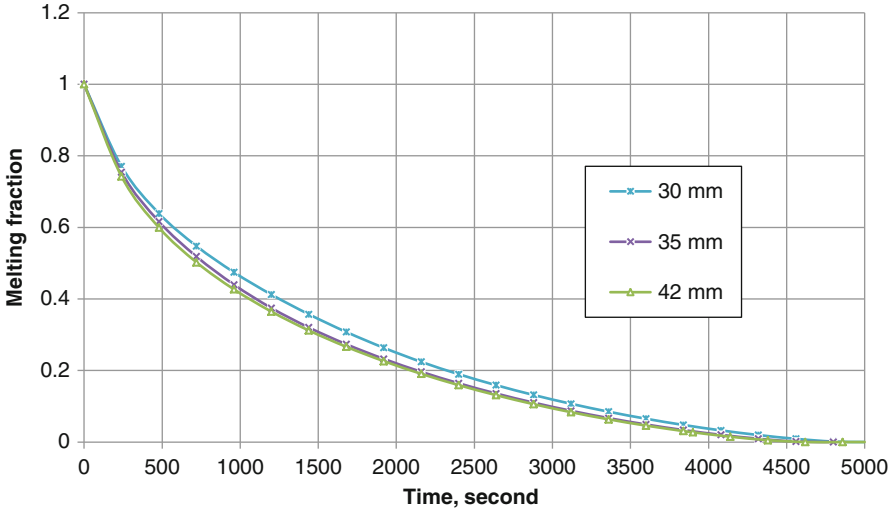

Fig. 42.4 Fin length effect to the solidification rate of the PCM

effect was totally close together when the thickness increased. This is because the fin content decreases appreciably, while there is a small increase in the heat transfer area when thin fins are used. Therefore, it is desirable to have thin fins for better performance in LHTES as reported by [15]. In general it can be conclude that the solid fraction is significantly accelerated by adding internal and external fins to the TTHX, this is because the fin extent the heat transfer area and conducted directly to the PCM surfaces.

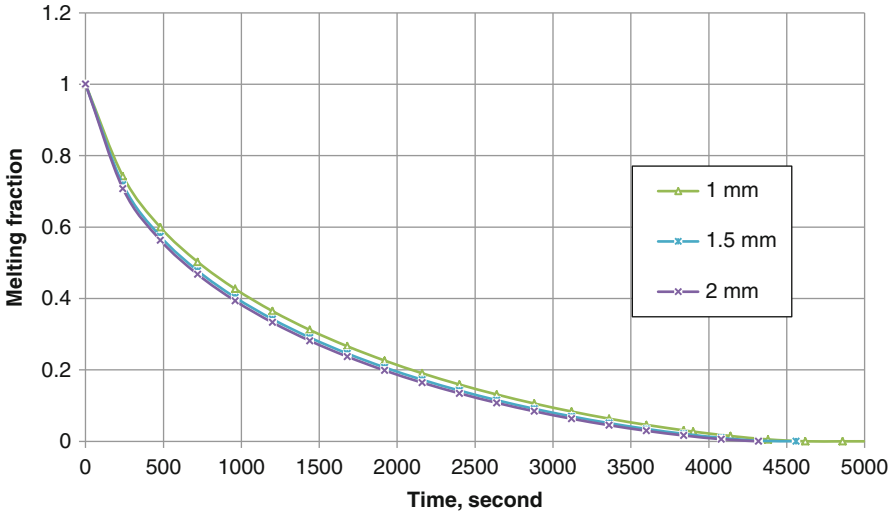

Fig. 42.5 Fin thickness effect to the solidification rate of the PCM

42.4 Conclusion

The using of internal and external fins to accelerate the solidification rate of RT82 as a PCM in triplex tube heat exchangers were investigated numerically; different design parameters such as the fin length, fin thickness, and number of fins were analyzed. Based on the simulation results, these parameters have a significant influence on the time for complete freezing of the PCM; the effect of fin thickness, and fin length are small compared to the number of fins, which have a strong effect on the solidification rate time. According to the results, the eight-fin configuration achieved the complete solidification earlier with respect to other cases. The simulation was validated by adopting experimental and numerical works from the literature; there was good agreement between the present simulations and previous works.

Nomenclature

C Mushy zone constant (kg/m^3.s)
Cp Specific heat of PCM (J/kg)
Gi Gravity acceleration in the i-direction (m/s^2)
h Sensible enthalpy (J/kg)
H Enthalpy (J/kg)
k Thermal conductivity (W/m.K)
L Latent heat fusion (J/kg)

Si Momentum source term in the i-direction (Pa/m)
T Temperature (°C or K)
ui Velocity component (m/s)

Greek Letters

μ Dynamic Viscosity (kg/m.s)
β Liquid fraction
P Fluid density(kg/m^3)

Subscripts

HTF Heat transfer fluid
i, j Components
ini Initial
L Liquidus of the phase change material
M Melting
Ref Reference
S Solidus of the phase change material
T Time

References

1. Agyenim F, Hewitt N, Eames P, Smyth M (2005) A review of materials, heat transfer and phase change problem formulation for latent heat thermal energy storage systems (LHTESS). Renew Sustain Energ Rev 14:615–628
2. Bauer T (2012) Approximate analytical solutions for the solidification of PCMs in fin geometries using effective thermophysical properties. Int J Heat Mass Transf 54:4923–4930
3. Mosaffa AH, Talati F, Basirat Tabrizi H, Rosen MA (2012) Analytical modeling of PCM solidification in a shell and tube finned thermal storage for air conditioning systems. Energ Build 49:356–361
4. Ismail KAR, Alves CLF, Modesto MS (2001) Numerical and experimental study on the solidification of PCM around a vertical axially finned isothermal cylinder. Appl Therm Eng 2001(21):53–77
5. Stritih U (2004) An experimental study of enhanced heat transfer in rectangular PCM storage. Int J Heat Mass Transf 47:2841–2847
6. Blen K, Takgil F, Kaygusuz K (2008) Thermal energy storage behavior of CaCl2.6H2O during melting and solidification. Energy Source Part A 30:775–787
7. Ismail KAR, Filho LMS, Lino FAM (2012) Solidification of PCM around a curved tube. Int J Heat Mass Transf 55:1823–1835
8. Lipnicki Z, Weigand B (2012) An experimental and theoretical study of solidification in a free-convection flow inside a vertical annular enclosure. Int J Heat Mass Transf 55:655–664
9. Sanusi O, Warzoha R, Fleischer AS (2011) Energy storage and solidification of paraffin phase change material embedded with graphite nanofibers. Int J Heat Mass Transf 54:4429–4436

10. Ismail KAR, Moraes RIR (2009) A numerical and experimental investigation of different containers and PCM options for cold storage modular units for domestic applications. Int J Heat Mass Transf 52:4195–4202
11. Darzi AR, Farhadi M, Sedighi K (2012) Numerical study of melting inside concentric and eccentric horizontal annulus. Appl Math Model 36:4080–4086
12. Brent AD, Voller VR, Reid KJ (1988) Enthalpy-porosity technique for melting convection-diffusion phase change: application to the melting of a pure metal. Numer Heat Tran 13:297–318
13. Patankar SV (1980) Numerical heat transfer and fluid flow, 1st edn. Hemisphere-McGraw-Hill, Washington, DC
14. Velraj R, Seeniraj RV, Hafner B, Faber C, Schwarzer K (1999) Heat transfer enhancement in a latent heat storage system. Sol Energy 65:171–180
15. Padmanabhan PV, Murthy MVK (1986) Outward phase change in a cylindrical annulus with axial fins on the inner tube. Int J Heat Mass Transf 29:1855–1868

Chapter 43
Computer Simulation of Heat and Mass Transfer in a Cross Flow Parallel-Plate Liquid Desiccant-Air Dehumidifier

Abdulrahman Th. Mohammad, Sohif Bin Mat, M.Y. Sulaiman, Kamaruzzaman Sopian, and Abduljalil A. Al-abidi

Abstract A MATLAB program using finite difference technique is investigated to predict the distribution of air stream parameters as well as desiccantsolution parameters inside the parallel plate absorber. The present absorber consists of 14 parallel plates with a surface area per unit volume ratio of 80 m^2/m^3. Calcium chloride as a liquid desiccant flows through the top of the plates to the bottom while the air flows through the gap between the plates making it a cross flow configuration. The model results show the effect of desiccant mass flow rate on the performance of the dehumidifier (moisture removal rateand the effectiveness). The results show that the maximum temperature and humidity ratio differences of the air are 2.56 °C and 11 g/Kg with a maximum solution mass flow rate of 160 g/s. The maximum temperature and minimum concentration differences of solution in the direction flow of solution are 3.185 °C and 0.34 % with a maximum solution mass flow rate of 160 g/s. The moisture removal rate increases rapidly with solution flow rate from 1.41 to 2.196 g s^{-1}, but the moisture removal stagnates at high desiccant solution mass flow rates. The effectiveness achieves an increase of 0.39–0.66 when the solution mass flow rate increases from 30 to 160 g s^{-1}.

Keywords Finite difference • Liquid desiccant • Moisture removal • Effectiveness

A.T. Mohammad (✉)
Department of Mechanical Engineering, Baqubah Technical Institute, Foundation of Technical Education, Baghdad, Iraq
e-mail: abd20091976@gmail.com

S.B. Mat • M.Y. Sulaiman • K. Sopian • A.A. Al-abidi
Solar Energy Research Institute, University Kebangsaan Malaysia, 43600 Bangi, Selangor, Malaysia
e-mail: sohif@ukm.my; sulaiman_yusof@yahoo.com; k_sopian@yahoo.com; abo_anas4@yahoo.com

I. Dincer et al. (eds.), *Progress in Sustainable Energy Technologies Vol II: Creating Sustainable Development*, DOI 10.1007/978-3-319-07977-6_43

43.1 Introduction

Many researchers have performed theoretical analysis and computer simulations of the heat and mass transfer performance of the liquid desiccant dehumidifier, such as Liu et al. [1], who used a theoretical model to predict the air and solution parameters inside a cross flow liquid desiccant dehumidifier/regenerator as well as the outlet parameters; the model used NTU as the input parameter. Xiao-HuaLiu et al. [2] investigated an analytical solution to give air and desiccant parameters as well as enthalpy and moisture efficiency in a cross flow dehumidifier. Yin and Zhang [3] developed an NTU-Le model to determine the characteristics of liquid desiccant dehumidification. Dai and Zhang [4] built up a mathematical model to predict the performance of a liquid desiccant air dehumidifier with honeycomb as a packed bed. Liu et al. [5] estimated the hour-hour performance of the dehumidifier using a simplified method with empirical correlations.Mohammad et al. [6] proposed an artificial neural network model (ANN) for predicting the performance of a liquid desiccant dehumidifier in terms of moisture removal rate and the effectiveness. The results show that 6-3-3-1 ANN structure was the best model for predicting the watercondensation rate, where as the 6-6-6-1 was the best model for predicting the dehumidifier effectiveness. Local volumetric average approach wasusedby-PengandPan [7] to investigate the transient heat and mass transfer in liquid desiccant air-conditioning process at low flow conditions.

From the literature, most of researchers have investigated experiments on the counter flow liquid desiccant dehumidifiers because their performance tends to be better than the cross flow dehumidifiers. But, very limited experimental performance data is available on this type of dehumidifiers' arrangements. Therefore, in this study, finite difference technique wasused to show the distribution of the air and the solution parameters: air and solution temperature, humidity ratio of air, and solution concentration inside a parallel plate liquid desiccant dehumidifier under the effect of the solution mass flow rate.The moisture removal rate and the dehumidifier effectiveness were investigated under the effect of solution flow rate.

43.2 Dehumidifier Design

A parallel plate dehumidifier consists of a number of vertical parallel plates with polypropylene material. The distance between each two adjacent plates is1 cm. Its geometry is presented in Fig. 43.1. All parameters in the design of the dehumidifier and its specifications are summarized in Table 43.1.

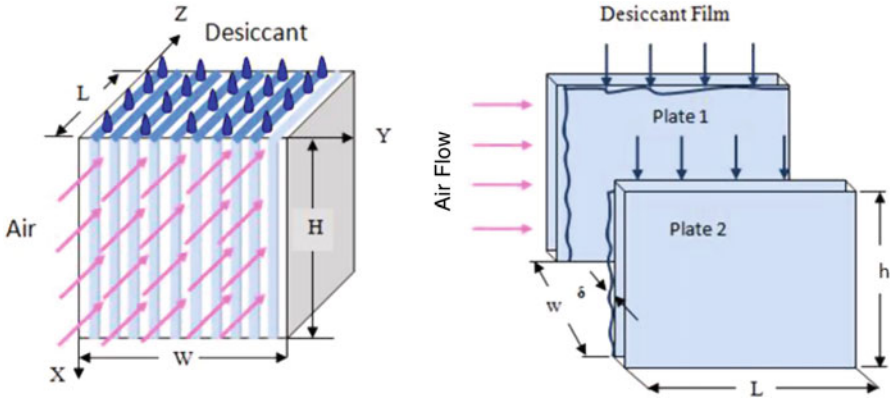

Fig. 43.1 Schematic of the cross flow parallel plate dehumidifier

Table 43.1 Dehumidifier parameter design

	Dehumidifier dimensions			
Type	Length (H) (cm)	Width (W) (cm)	Depth (L) (cm)	Process
Parallel plate with a cross flow	75	25	30	Adiabatic
Plate dimensions				
Number of plates	Length (y) (cm)	Width (L) (cm)	Thickness (t) (cm)	Distance between two plates (w) (cm)
14	60	30	0.4	1

43.3 Mathematical Models

The *Z*-axis denotes the direction of air flow while the *X*-axis is the direction of the solution perpendicular to the air flow, which is in a cross flow configuration. A theoretical two-dimensional analysis of an adiabatic process was developed based on the following assumptions: (1) Steady state (2) Two-dimensional flows (3) No heat transfer from the solution to the plates (4) The interfacial area of heat and mass transfer are equal (5) No heat and mass transfer to or from the surroundings (6) Laminar and fully-developed flow (7) The heat and mass transfer coefficients are uniform throughout the module.

43.3.1 Basic Equation of Heat and Mass Transfer Coefficients

The rates of heat and mass transfer between the air and solution can be expressed as overall coefficients, heat transfer coefficient, and mass transfer coefficient; these coefficients must be known to find the existing conditions for the air and the solution in a liquid desiccant dehumidifier. Appendix 1 represents the set equations of all the parameters for calculating heat and mass transfer coefficients, NTU, and Lewis number.

43.3.2 Energy and Mass Balance Equations

The heat and mass transfer process which takes place in liquid desiccant dehumidifier is the same process in cooling tower. There is little difference between them, while the cooling tower uses the water as the working liquid, the process only humidifies, but in liquid desiccant chamber uses a salt-water solution can humidify or dehumidify the air depending on the operation conditions. The liquid desiccant chamber is filled with packing material, the solution drips from the top, wetting the packing material, while air is blows through from the bottom in a counter, parallel, and cross current arrangement. The heat transfer process occurs because of temperature difference between the air and the solution, while the mass transfer is driven by a difference between the partial pressure of the water vapor in the air and the vapor pressure of a liquid.

The schematic for a differential element of a cross-flow liquid desiccant dehumidifier is shown in Fig. 43.2. Energy and mass balance equations for differential element may be written as in Eqs. (43.1–43.3):

$$\frac{\dot{m}_a}{H}\frac{\partial h_a}{\partial z}+\frac{1}{L}\frac{\partial(\dot{m}_s h_s)}{\partial x}=0 \tag{43.1}$$

$$\frac{\dot{m}_a}{H}\frac{\partial w_a}{\partial z}+\frac{1}{L}\frac{\partial \dot{m}_s}{\partial x}=0 \tag{43.2}$$

$$d(\dot{m}_s \xi)=0 \tag{43.3}$$

AccordingtoArshad [8] and Stevens et al. [9] the overall heat and mass transfer and moisture transfer between the air and solution are represented by Eqs. (43.4–43.6):

$$\frac{\partial h_a}{\partial z}=\frac{NTU * Le}{L}\left[(h_e-h_a)+\lambda_{Ts}\left(\frac{1}{L_e}-1\right)*(w_e-w_a)\right] \tag{43.4}$$

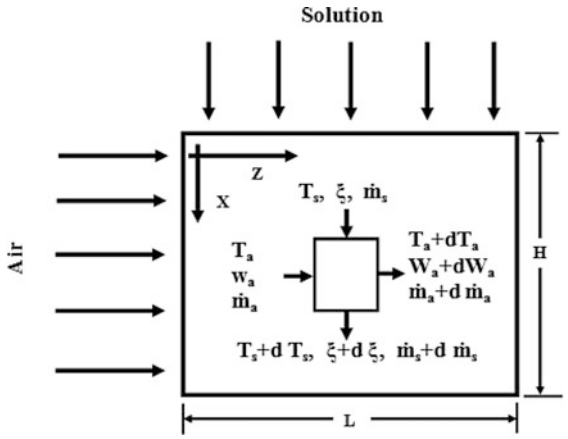

Fig. 43.2 Schematic of the differential element of the dehumidifier

Where λ_{Ts} the vaporization latent heat, L_e and NTU are the Lewis number and number of transfer unitsrepresent in Eqs. (43.23) and (43.24).Gandhidasan et al. [10], Jain et al. [11] and Chung and Wu [12] predicted that the Lewis number is equal one. Then Eq. (43.4) becomes:

$$\frac{\partial h_a}{\partial z} = \frac{NTU}{L}(h_e - h_a) \tag{43.5}$$

The equation of moisture transfer can be written as:

$$\frac{\partial w_a}{\partial z} = \frac{NTU}{L}(w_e - w_a) \tag{43.6}$$

Where w_e and h_e are the humidity ratio and enthalpy of air in equilibrium with $CaCL_2$, respectively (Appendix 2)

43.3.3 Boundary Conditions

The inlet boundary conditions of air and solution are:

$$T_s = T_{s,in}, \quad \xi = \xi_{in} \text{ at } \quad x = 0 \tag{43.7}$$

$$T_a = T_{a,in}, \quad w_a = w_{a,in} \text{ at } \quad z = 0 \tag{43.8}$$

Solving the above equations of heat and mass transfer processes between the air and liquid desiccant with the boundary conditions in Eqs. (43.7) and (43.8) can give the distribution of the air and solution parameters inside the dehumidifier, as well as the air and solution parameters outlet of the dehumidifier.

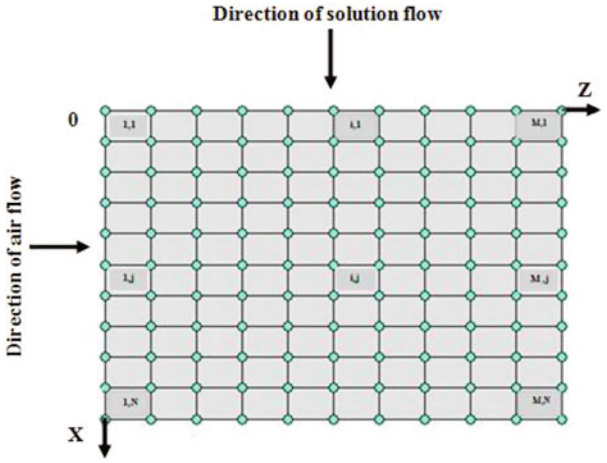

Fig. 43.3 Meshes in two dimensions

The phenomena can be represented by M × N meshes in a 2-D domain in the x-z plane as shown in Fig. 43.3. Equations (43.1–43.6), then become as follows in terms of an (i, j) mesh.

$$\dot{m}_a\left(h_{a,i+1,j} - h_{a,i,j}\right) = \frac{N}{M}\left(\dot{m}_{s,i,j}h_{s,i,j} - \dot{m}_{s,i,j+1}h_{s,i,j+1}\right) \tag{43.9}$$

$$\dot{m}_a\left(w_{a,i,j} - w_{a,i+1,j}\right) = \frac{N}{M}\left(\dot{m}_{s,i,j+1} - \dot{m}_{s,i,j}\right) \tag{43.10}$$

$$\dot{m}_{s,i,j+1}.\xi_{i.j+1} = \dot{m}_{s,i,j+1}.\xi_{i.j} \tag{43.11}$$

$$h_{a,i+1,j} - h_{a,i,j} = \frac{NTU}{M}\left(h_{e,i,j} - h_{a,i,j}\right) \tag{43.12}$$

$$w_{a,i+1,j} - w_{a,i,j} = \frac{NTU}{M}\left(w_{e,i,j} - w_{a,i,j}\right) \tag{43.13}$$

43.3.4 The Dehumidification Effectiveness and Moisture Removal

The rate of water transfer from the air to the liquid desiccant is defined as moisture removal (dehumidification mass rate), and is given by Yin et al. [13].

$$M_{de} = \dot{m}_a(w_{a,in} - w_{a,out}) \tag{43.14}$$

which can also be described as:

$$M_{de} = \dot{m}_s\left(\frac{\xi_{in}}{\xi_{out}} - 1\right) \tag{43.15}$$

The performance of the dehumidifier is described in terms of dehumidification effectiveness by Moon et al. [14]

$$\varepsilon = \frac{w_{a,in} - w_{a,out}}{w_{a,out} - w_e} \tag{43.16}$$

where $w_{a,in} - w_{a,out}$ is the actual change of the humidity ratio, and $w_{a,out} - w_e$ is the maximum possible change of the humidity ratio.

43.3.5 SolvingProcedures

The steps for solving the air and desiccant states inside and outside the dehumidifier using a finite difference technique are:

1. Calculate the heat transfer and mass transfer coefficients using Eqs. (43.17–43.22).
2. Calculate the number of transfer units using Eq. (43.24).
3. Assume the Lewis number is equal to one (the Lewis number is the ratio between the thermal diffusivity to mass diffusivity and in gasmixturesboth-PrandtlandSchmididtnumbers are of the order of magnitude of unity) as in Eq. (43.25).
4. Guess the liquid desiccant outlet concentration (40 %).
5. Guess the liquid desiccant outlettemperature (20 °C).
6. Calculate the enthalpy and humidity ratio of humid air in equilibrium withthe liquid desiccant using Eqs. (43.26) and (43.27).
7. From Eqs. (43.12) and (43.13) calculate the enthalpy and humidity ratio of air in the next mesh (i + 1).
8. Known enthalpy and humidity ratio of air in step 5 and by using air physical property, calculate the temperature of air in the same mesh (i + 1).
9. Calculate the desiccant outlet mass flow rate and concentration in (j + 1) mesh using Eqs. (43.10) and (43.11), if the difference between the old and new values of concentration is less than assumed convergence (1×10^{-3}), go to the step 12, otherwise go to the step 4.
10. From known of steps 5 and 7 can calculate the outlet enthalpy of desiccant in mesh (j + 1).
11. Using desiccant physical property, calculate the desiccant temperature in (j + 1), since the desiccant enthalpy and concentration are known, if the difference between the old and new values of temperature is less than assumed convergence (1×10^{-1}), go to the step 12, otherwise go to the step 5.
12. Repeat the steps from 4 to 11 on the all meshes till (M, N).

The data which used in simulation is summarized in Table 43.2. The constant properties of air and calcium chloride that used in program are listed in Table 43.3. For more explaining of the program, a detailed flow chart is shown as figure in Appendix 3).

Table 43.2 Data of simulation

Parameter	y (m)	w (m)	A_s (m^2m^{-3})	M	N	Ts (suggested) (°C)	ξ (suggested) (%)	Le
Value	0.6	0.01	80	10	15	20	40	1

Table 43.3 Constant properties of air and calcium chloride [15]

Properties	Air	Calcium chloride
ρ (Kg/m^3)	1.11	1394
μ (Kg/m.s)	1.9×10^{-5}	1.19×10^{-2}
Cp (J/Kg.K)	990	2,330
K (W/m.K)	0.0275	0.525
D (m^2/s)	2.65×10^{-5}	2.5×10^{-5}

43.4 Results and Discussion

The dehumidification performance depends on six input parameters of the air and liquid desiccant, including air and solution temperature, air and solution mass flow rate, air humidity ratio and solution concentration. The finite difference technique model can give the distribution of air temperature and humidity ratio as well as solution temperature and concentration insidethe liquid desiccant dehumidifier module. The outlet parameters (moisture removal rate and the effectiveness) can investigate, which are important for studying the improvement of the heat and mass transfer in the dehumidifier. The air and desiccant inlet parameters are set as in Table 43.4.

43.4.1 Effect of Desiccant flow Rate on Air Temperature and Humidity Ratio Distribution

Figure 43.4 gives the distribution of air temperature and air humidity ratio inside the dehumidifier under the effect of solution flow rate with the above inlet parameters in Table 43.3. In this case, the air is heated and dehumidified along its flow direction. At the air outlet (Z = L), the air at the top has the highest temperature and lowest humidity ratio, the maximum temperature and humidity ratio differences of the air are 2.56 °C and 11 g/Kg with a maximum solution mass flow rate of 160 g/s, while the minimum ratio differences are 1.98 °C and 8.86 g/Kg with a minimum solution flow rate of 30 g/s. This may be explained as follows, increasing solution flow rate ensures well contact between the air and the solution and also increases the heat and mass transfer coefficients. Therefore, the moisture removed increases rapidly with solution flow rate, but it stagnates at high desiccant solution flow rate.

Table 43.4 Air and desiccant inlet parameters

	$\dot{m}_a$ (Kg s^{-1})	T_a (°C)	w_a (Kg_{H2O}/Kg_{dry})	$\dot{m}_a/\dot{m}_s$	T_s (°C)	ξ (%)
Input parameters	0.16	30	0.021	0.18–1	34	40

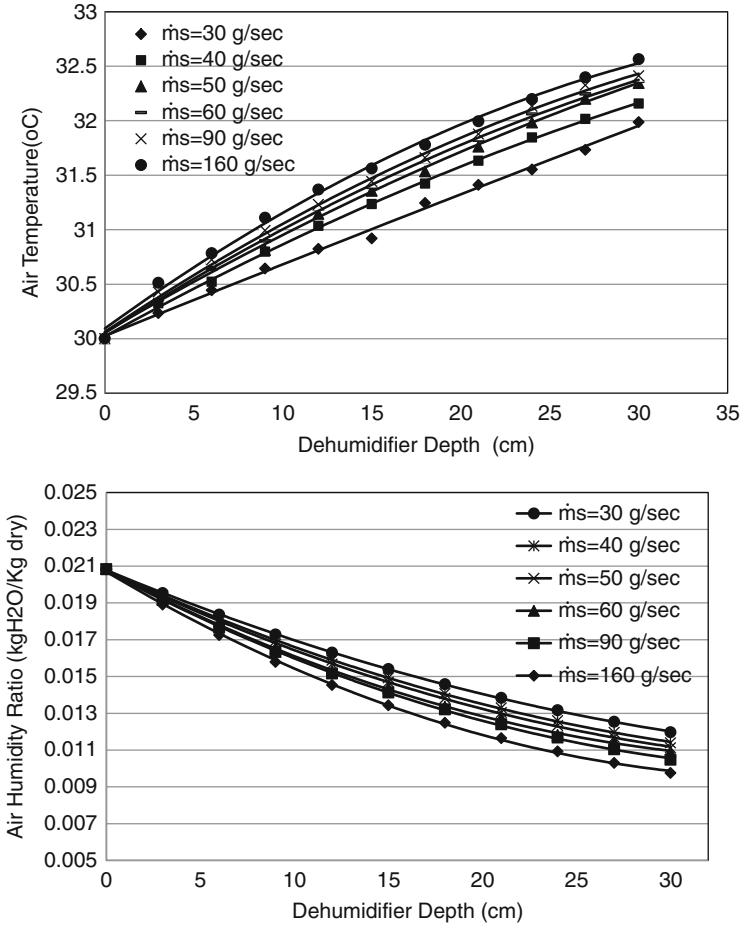

Fig. 43.4 The effect of solution mass flow rate on the air temperature and humidity ratio

43.4.2 Effect of Desiccant Flow Rate on the Desiccant Temperature and Concentration Distribution

At the desiccant outlet (X = H) as shown in Fig. 43.5, the maximum temperature and minimumconcentration differences of solution in the direction flow of solution are 3.185 °C and 0.34 % with a maximum solution mass flow rate of 160 g/s, and the minimum temperature and maximum concentration differences are 0.924 °C and

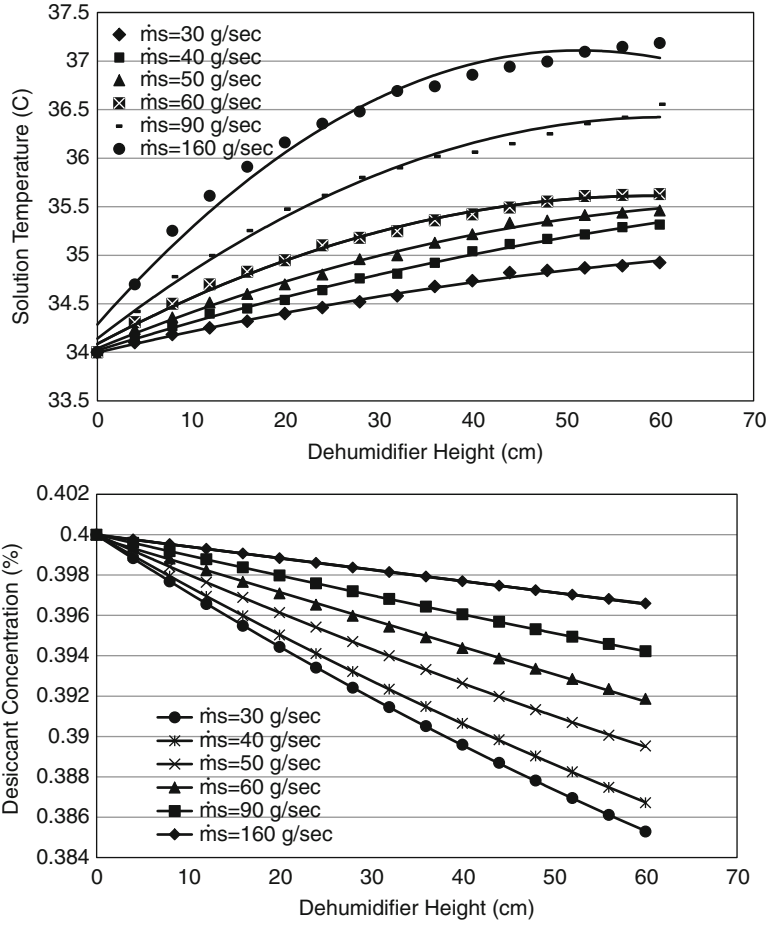

Fig. 43.5 The effect of solution mass flow rate on the solution temperature and concentration

1.14 % with a minimum solution mass flow of 30 g/s. The reason may be explained as follows. The desiccant contacted the humid air, and more moisture was transferred from the air to the solution since the mass transfer potential was large there. Therefore, desiccant temperature increased most and the solution concentration reduces slightly with the increasing desiccant flow rate.According to the results, the desiccant concentration differences in the direction of desiccant flow can be neglected.

43.4.3 Effect of Desiccant Flow Rate on Dehumidifier Effectiveness and Moisture Removal

Figure 43.6 shows the effect of solution mass flow rate on the dehumidifier performance; according to the Fig. 43.6the moisture removal rate increases rapidly with solution flow rate from 1.41 to 2.196 g s^{-1}. But the moisture removal stagnates at high desiccant solution mass flow rates because of the increasing solution mass flow rate, which increases the mass transfer coefficient between the liquid desiccant and the air flow, but reduces the contact time. The dehumidifier effectiveness also shows similar trend as shown in Fig. 43.6. The figure indicates that the effectiveness achieves an increase of 0.39–0.66 when the solution mass flow rate increases from 30 to 160 g s^{-1}. This increase may beexplained as follows. Increasing solution flow rate enhances the heat and mass transfer coefficients. The average water vapor pressure difference between the desiccant and air increased due to the reduced variation of the surface vapor pressure of the desiccant in the dehumidifier which maintains a good mass transfer between the air and desiccant.

43.4.4 Validation of the Model Results

The performance of the cross-flow dehumidifier in terms of the moisture removal rate and the effectiveness in the present study is compared with the other experimentalstudybyBassuoni [16]. Figure 43.6 shows the trend of the effect of solution flow rate on the moisture removal rate and the effectiveness of the dehumidifier. The present work mentions an increasing trend of moisture removal rate with the solution flow rate. Good agreement between the simulation and experimental when the solution temperature increasedby 8 °C. This can be explained as follows.The vapor pressure of the solution rises with increasing the solution temperature, and it reduces the mass transfer potential between the solution and moisture in the air. The dehumidifier effectiveness increases as the solution flow rate increases and good agreement between the simulation and experimental at solution temperature is 42 °C. Table 43.5 shows the comparison of the operational conditions and outlet results between the present study and experiment in literature.

43.5 Conclusions

A MATLAB programusing finite difference is investigated to show the distribution of the air and the solution parameters inside a parallel plate cross-flow liquid desiccant-air dehumidifier. The dehumidifier effectiveness and moisture removal are used as the dehumidifier performance indicators. The results of the present model led to the following conclusions:

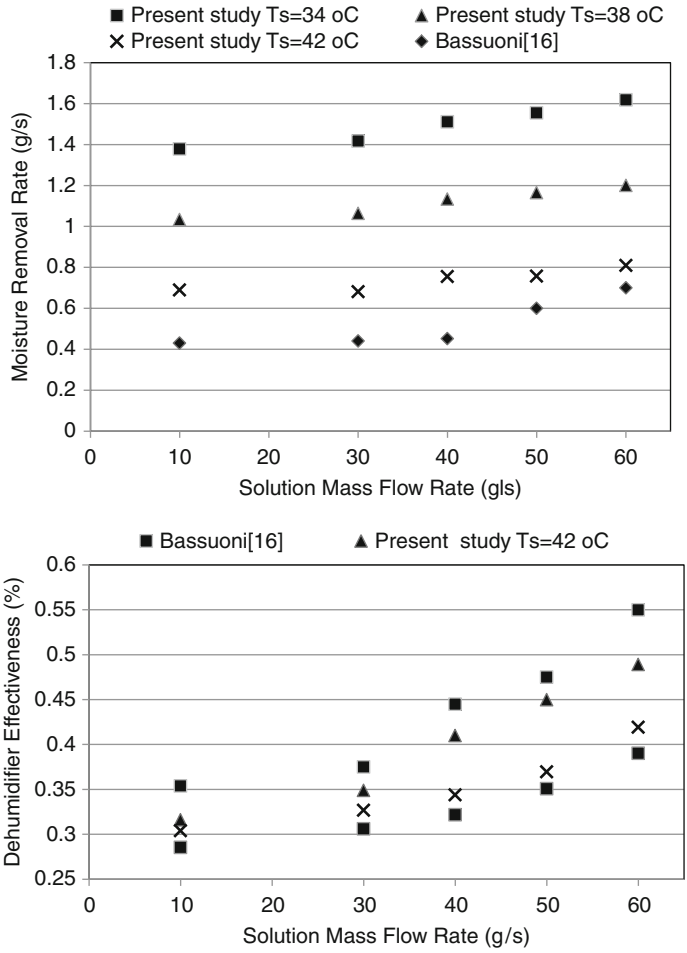

Fig. 43.6 The effect of solution mass flow rate on the dehumidifier effectiveness and moisture removal

- The maximum temperature and humidity ratio differences of the air are 2.56 °C and 11 g/Kg with a maximum solution mass flow rate of 160 g/s, while the minimum ratio differences are 1.98 °C and 8.86 g/Kg with a minimum solution flow rate of 30 g/s.
- The maximum temperature and minimum concentration differences of solution in the direction flow of solution are 3.185 °C and 0.34 % with a maximum solution mass flow rate of 160 g/s, and the minimum temperature and maximum concentration differences are 0.924 °C and 1.14 % with a minimum solution mass flow of 30 g/s.
- The moisture removal rate increases rapidly with solution flow rate from 1.41 to 2.196 g s^{-1}. But the moisture removal stagnates at high desiccant solution mass

Table 43.5 Comparison of the operational conditions and outlet results between the present study and experiment in literature

	Bassuoni [16]	Present study
Liquid desiccant	$CaCL_2$	$CaCL_2$
Specific area (m^2m^{-3})	390	80
Flow type	Cross flow	Cross flow
Packing type	Structured packing-corrugation angle of 60°	Polypropylene–parallel plate
Dimensions (m)	$0.35 \times 0.35 \times 0.2$	$0.75 \times 0.4 \times 0.30$
$\dot{m}_a$ (Kg s^{-1})	0.144	0.16
T_a (°C)	31	30
w_a (Kg_{H2O}/Kg_{dry})	0.018	0.021
$\dot{m}_s$ (g s^{-1})	10–60	10–60
ε (%)	0.354–0.55	0.285–0.48
M_{de} (g/s)	0.43–0.70	0.689–1.61

flow rates because of the increasing solution mass flow rate, which increases the mass transfer coefficient between the liquid desiccant and the air flow, but reduces the contact time.

- The dehumidifier effectiveness also shows similar trend as shown in Fig. 43.6. The figure indicates that the effectiveness achieves an increase of 0.39 to 0.66 when the solution mass flow rate increases from 30 to 160 g s^{-1}.

Nomenclature

A_C	A cross flow area between air and solution (m^2)
A_S	Specific area of the plates per unit volume,(m^2m^{-3})
c_p	Specific heat of air (kJ kg^{-1}/°C)
D	Mass diffusivity (m^2 s^{-1})
D_h	Hydraulic diameter (m)
H	Height of dehumidifier (m)
h_a	Air enthalpy (kJ kg^{-1})
h_e	Equilibrium enthalpy of air (kJ kg^{-1})
h_h	Heat transfer coefficient (w m^{-2}/K)
h_m	Mass transfer coefficient (m s^{-1})
h_s	Solution enthalpy (kJ kg^{-1})
K	Conductivity (W m^{-1}/K)
L	Thickness of dehumidifier (m)
Le	Lewis number
M	Number of point in solution direction
M_{de}	Moisture removal rate in dehumidifier (g s^{-1})

$\dot{m}_a$	Air mass flow rate (kg s^{-1})
$\dot{m}_s$	Solution mass flow rate (kg s^{-1})
N	Number of point in air direction
NTU	Number of transfer units
Nu	Nusseltnumber
P_{at}	Atmospheric pressure (bar)
P_w	Wetted parameter (m)
P_{ws}	Saturation pressure (bar)
P_{wz}	Partial pressure of water vapor in the solution (bar)
T_a	Airtemperature (°C)
T_a	Solution temperature (°C)
w	Width channel between two plates (m)
w_a	Humidity ratio of air (kg_{H2O}/kg_{dry})
w_e	Equilibrium humidity ratio of air (kg_{H2O}/kg_{dry})
y	Height of plate (m)

Greek Letters

ξ	Solution concentration (%)
δ_s	Solution thickness (m)
ε	Dehumidifier effectiveness (%)
α	Thermal diffusivity (m^2 s^{-1})
λ_{TS}	Vaporization latent heat (kJ kg^{-1})
μ	Viscosity (N s m^{-2})
ρ	Density (kg m^{-3})

Subscripts

a	Air
e	Equilibrium
in	Inlet
out	Outlet
s	Solution

Appendix 1: Summary of Calculations Steps of Heat and Mass Transfer Coefficients, NTU, and Lewis Number

In the following, a brief summary of the calculation heat and mass transfer coefficients, NTU, and Lewis number in a cross-flow liquid desiccant dehumidifier are presented.

TheNusseltnumberfor laminar air flow through a duct is 7.54 [17].

Cross flow area between the air and solution is given by

$$A_C = y * (w - 2 * \delta_s) \tag{43.17}$$

$$\delta_s = \left(\frac{4_s}{\rho_s g}\right)^{1/3} \tag{43.18}$$

Where y is the height of plate, δ_s is the solution film thickness, and w is the distance between two plates.

Wetted perimeter is represented by:

$$P_w = 2 * y \tag{43.19}$$

Therefore, the hydraulic diameter of air is represented as:

$$D_h = \frac{4 * A_c}{P_w} \tag{43.20}$$

The heat transfer coefficient is represented by:

$$h_h = \frac{N_u K_a}{D_h} \tag{43.21}$$

Thermal diffusivity of air is given by:

$$\propto_a = \frac{K_a}{\rho_a * C_{pa}} \tag{43.22}$$

Where K_a is the airconductivity.

Mass transfer coefficient is defined as, [17]

$$h_m = \frac{h_h}{C_{pa}} \left(\frac{\alpha_a}{D_a}\right)^{-\frac{2}{3}} \tag{43.23}$$

The number of transfer units, based on unit cross-sectional area of the plates is given by

$$NTU = \frac{h_m A_s L}{m_a} \tag{43.24}$$

Where A_s is the specific area of the plates per unit volume 80 $m^2 m^{-3}$.

Lewis number is given by:

$$Le = \frac{h_h}{h_m C_{pa}} \tag{43.25}$$

Appendix 2: Equilibrium Equations

The humidity ratio and enthalpy of air in equilibrium with $CaCL_2$ solution is calculate according to these equations

$$\log_{10} P_{ws} = -0.21254 + 3.13619 \times 10^{-2} \times T - 1.22512 \times 10^{-4} \times T^2 + 3.6384 \times 10^{-7} \times T^3 - 5.6707 \times 10^{-10} \times T^4 \quad (43.26)$$

Where P_{ws} is the saturation pressure and T is the solution temperature between (10 °C < T < 80 °C) Radhwan et al. [18].

The partial pressure of water vapor in the solution $CaCL_2$ is given by Esayed et al.[19].

$$P_{wz} = P_{ws}(1.146 - 1.76\xi) \quad (43.27)$$

Then the equilibrium humidity ratio of air is given by:

$$w_e = 0.62185 \frac{P_{wz}}{P_{at} - P_{wz}} \quad (43.28)$$

Where P_{at} is theatmosphericpressure, Kinsara et al.[20].

From property of air at w_s and the solution temperature can calculate the equilibrium enthalpy of air with the $CaCL_2$ solution.

Appendix 3: Program Algorithm

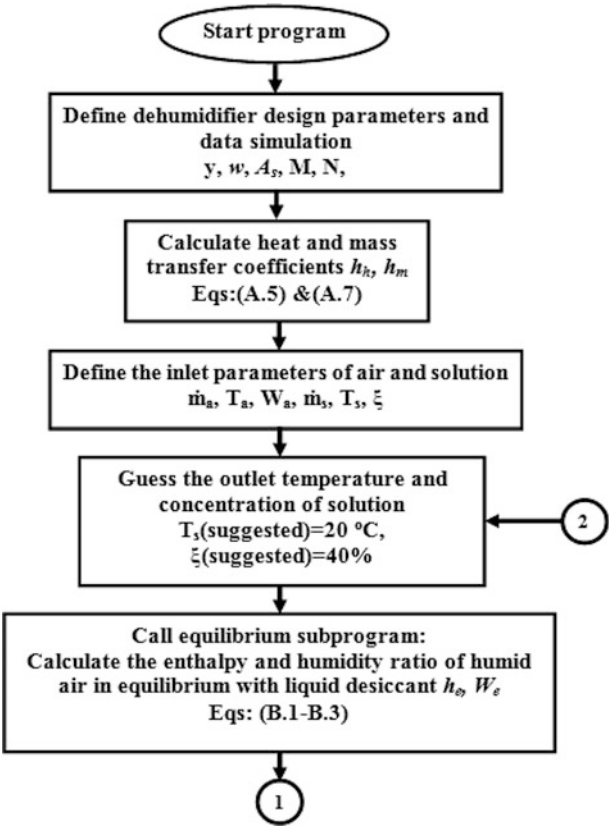

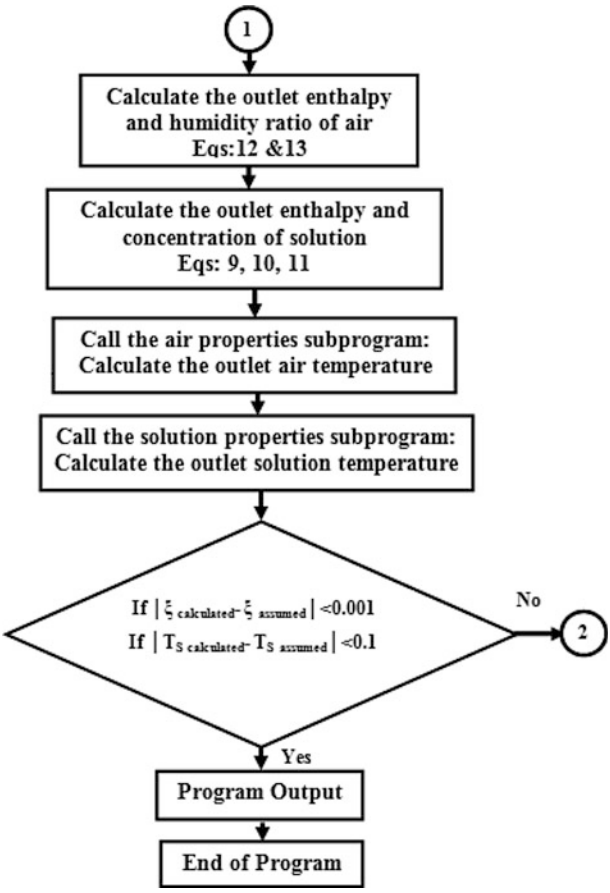

References

1. Liu XH, Jiang Y, QuK Y (2007) Heat and mass transfer model of cross flow liquid desiccant air dehumidifier regenerator. Energ Convers Manag 48:546–554
2. Liu X-H, Jiang Y, Kai-Yang Q (2008) Analytical solution of combined heat and mass transfer performance in a cross-flow packed bed liquid desiccant air dehumidifier. Heat Mass Transf 51:4563–4572
3. Yin Y, Zhang X (2008) A new method for determing coupled heat and mass transfer coefficients between air and liquid desiccant. Heat Mass Transf 51:3287–3297
4. Dai YJ, Zhang HF (2004) Numerical solution and theoretical analysis od heat and mass transer in a cross flow liquid desiccant air dehumidifier packed with honeycomb paper. Energ Convers Manag 45:1343–1356
5. Liu XH, Qu KY, Jiang Y (2006) Empirical correlations to predict the performance of the dehumidifier using liquid desiccant in heat and mass transfer. Renew Energy 31:1627–1639

6. Mohammad AT, Mat SB, Sulaiman MY, Sopian K, Al-abidi AA (2013) Implementationand-validation of an artificial neural network for predicting the performance of a liquid desiccant dehumidifier. Energ Convers Manag 67:240–250
7. Peng SW, Pan ZM (2009) Heat and mass transfer in liquid desiccant air-conditioning process at lowflowconditions. Commun Nonlinear Sci Numer Simul 14:3599–3607
8. Arshad YK (1994) Sensitivity analysis and component modeling of a packed- type liquid desiccant system at partial load operating conditions. Int J Energy Res 18:643–655
9. Stevens DI, Braun JE, Klein SA (1989) An effectiveness model of liquid desiccant system heat/mass exchangers. Sol Energy 42:449–455
10. Gandhidasan P, Kettleborough CF, Ullah MR (1986) Calculation of heat and mass transfer coefficients in a packed tower operating with a desiccant-air contact system. J Sol Energy Eng Trans ASME 1986:108
11. Jain S, Dhar PL, Kaushik SC (2000) Experimental studies on the dehumidifier and regenerator of a liquid desiccant cooling system. Appl Therm Eng 20:253–267
12. Chung TW, Wu H (2000) Comparison between spray towers with and without fin coils for air dehumidification using triethylene glycol solutions and development of the mass transfer correlations. Ind Eng Chem Res 39:2076–2084
13. Yin Y, Zhang X, Chen Z (2007) Experimental study on dehumidifier and regenerator of liquid desiccant cooling air conditioning system. Build Environ 42:2505–2511
14. Moon CG, Bansai PK, Jain S (2009) New mass transfer performance data of a cross-flow liquid desiccant dehumidification system. Int J Refrig 32:524–533
15. Mesquita LCS, Harrison SJ, Thomey D (2006) Modeling of heat and mass transfer in parallel plate liquid-desiccant dehumidifiers. Sol Energy 80:1475–1482
16. Bassuoni MM (2011) An experimental study of structured packing dehumidifier/regenerator operating with liquid desiccant. Energy 36:2628–2638
17. Hueffed AK (2007) A simplified model of heat and mass transfer between air and falling-film desiccant in parallel-plate dehumidifier. M.Sc. thesis, Mechanical engineering department, Facuility of Mississipi State University
18. Radhwan MM, Gari HN, Elsayed MM (1993) Parametric study of a packed bed dehumidifier/regenerator using $CaC1_2$ liquid desiccant. Renew Energy 13:49–60
19. Elsayed MM, Gari HN, Radhwan MM (1993) Effectiveness of heat and mass transfer in packed beds of liquid desiccant system. Renew Energy 3:661–668
20. Kinsara AA, Elsayed MM, AI-Rabghi OM (1996) Proposed energy-efficient air-conditioning system using liquid desiccant. Appl Therm Eng 16:791–806

Chapter 44
Experimental Study of the Heat Transfer Performance of PCMs Within Metal Finned Containers

Yongcai Li, Shuli Liu, and Yaqin Zhang

Abstract Latent heat thermal energy storages (LHTES) are particularly attractive methods owing to these factors: meet the time shift between energy supply and demand; provide a high energy storage capacity; store and release heat at a relatively constant temperature; provide constant comfort thermal environment without temperature swings when it is applied for space heating or cooling. Nevertheless, the efficiency of using the LHTES techniques is heavily affected by the low thermal conductivities of phase change materials (PCMs). This characteristic of PCMs prolongs the charging and discharging cycle and barriers the widely practical application of LHTES. Hence, researchers generated a lot of related technologies, such as metal fines, carbon fibres, metal honeycomb structure, etc, to overcome this issue and aimed to achieve reasonable thermal conductivities.

The objective of this paper is to study the heat performance of two kinds of PCMs within three different types of metal finned structures (straight fins, honeycomb and square finned structure) at the volume ratios of 1.8, 2.7, and 3.6 %, respectively. Two organic PCMs, paraffin wax RT 25 (phase transform at 25 °C) and RT 42 (phase transform at 42 °C) are employed as the heat storage media. The characteristics of them with the thermal conductivity enhancers (TCEs) during the melting and solidification process were investigated experimentally. The results indicate that the heat transfer improvements during the melting process are more efficiency than the solidification process for all of the three structures and both PCMs. To be specific, for paraffin RT 25, the heat transfer efficiencies were increased by 25, 33, and 37 %, in the finned, honeycomb and square cell structured container during the melting process, and increased by 8, 12, and 17.1 %, respectively for the solidification processes. The similar effect happened for paraffin RT 42, the heat transfer efficiencies were increased by 28, 33, and 40 % during melting process, and increased by 17, 28, and 35 %, respectively during freezing process. The performance of the TCEs on the RT 42 is slightly better than that of RT 25, especially during the solidification process due to its higher heat transfer rate between the PCM and TECs induced by a relative higher melting temperature.

Y. Li • S. Liu (✉) • Y. Zhang
Faculty of Engineering and Computing, Coventry University, JL 127, Coventry CV1 5FB, UK
e-mail: liy30@uni.coventry.ac.uk; aa6328@coventry.ac.uk; yaqin19851228@163.com

I. Dincer et al. (eds.), *Progress in Sustainable Energy Technologies Vol II: Creating Sustainable Development*, DOI 10.1007/978-3-319-07977-6_44

Meanwhile, the efficiencies of the volume ratios of the TECs were examined. The results show that straight fins have the best efficiency compared to others.

Keywords Phase change material (PCM) • Finned metal structures • Phase change • Heat transfer enhancement efficiency

44.1 Introduction

Phase change materials (PCMs) are known as excellent candidates for latent heat thermal energy storages (LHTES) and have been applied in many engineering applications, since they provide the following advantages: (1) PCMs possess high heat storage density to store large amounts of latent heat in a small PCM volume, thereby the heat losses from the system maintains in a reasonable level during the charging and discharging period [1]; (2) PCMs melt and solidify at a nearly constant temperature hence, constant comfort thermal environment without temperature swings could be achieved when they applied for space heating or cooling. Due to the importance of PCMs to the LHTES, a large number of researchers have been carried out working on PCMs. In 1983 Abhat [2] classified the available materials into organic, inorganic and eutectic materials. However, the low thermal conductivity of PCMs limits their application in LHTES. For low temperature LHTES (normally <200 °C), paraffin wax, hydrated salts and eutectics are often used as heat storage media, whereas the thermal conductivities of them are around 0.2–0.6 W/m K, which prolongs the charging and discharging period. The phase change time is the most important design parameter in LHTES applications [3], as the primary function of a PCM in application is to store as much thermal energy for as long as possible during the solid to liquid phase transition, and to release the stored thermal energy as much as possible before next charging-discharging cycle. As the low thermal conductivity of the PCM is detrimental to the system performance, studies about thermal conductivity enhancers have attracted more and more attention over last decade. Various methods for PCM thermal conductivity enhancement have been proposed and studied by a number of researchers. Heat transfer enhancement methods in LTHES can be summarised to the following categories:

- Microencapsulated PCM [1].
- Containing dispersed high metal conductivity particles or lessing rings [4].
- Graphite or concrete composite material [5].
- Extended surfaces such as finned structures or heat pipes [6–11].

The most common methods among others are the use of finned structures, dispersing metal particles or rings or carbon fibbers with high conductivity into PCM. Dispersing high conductivity materials into PCMs is less practical compared with inserting finned structures into PCMs because of that the substances dispersed in PCMs usually sink to the bottom or float to the top of the container due to their

different densities from PCMs. As finned metal structures are fixed, non-moving structures and offer extended surface area for heat transfer, they can maintain high performance after long period of charging–discharging cycles. The application of finned metal structures with different configurations has been reported by various researchers as an efficient method to improve heat transfer in PCMs.

Huang et al. [7] numerically and experimentally investigated the fin-enhanced PCM melting process to cool the photovoltaic devices. The research results indicate that the thermal performance was improved and heat transfer within the PCM was accelerated by the effect of natural convection within the molten PCM. However, superabundant of fins would limit the advection within the molten PCM, and decrease the beneficial effects of natural convection on reducing the thermal resistance between the hot wall and the PCM solid–liquid interface. It means that fluid motion in the molten PCM was suppressed for cases involving tightly-packed fins. Eftekhar et al. [12] investigated experimentally a different heat transfer enhancement method for melting of paraffin by constructing a model that consists of vertically arranged fins between two isothermal planes which not only provided additional conduction paths but also promoted natural convection within the molten PCM. Their photographs of the molten zone indicate that a buoyant flow induced in the neighbourhood of the vertical fin causes rapid melting of the solid wax.

The honeycomb structure is another type of fins that provides a more effective heat fin that maybe chose in various thicknesses. A PCM-based thermal container with a honeycomb structure was designed and investigated by Abhat [13]. De Jong and Hoogendoorn [14] utilized the aluminium honeycombs to improve the heat transfer in PCM system. Based on the experimental results, the aluminium honeycomb structure can apparently reduce the solidification times with a factor up to 7. Compared to the pure PCM, the thermal conductivity of the enhanced PCM was also apparently increased

The paper mainly focused on the heat transfer characteristics of PCMs with different TCEs subjected to constant heat flux during the melting process and natural cooling during the solidification process. In this study, two commercially available paraffin wax: paraffin RT 25 and paraffin RT 42 were used as PCMs, and three types of TCEs have been chosen for heat transfer enhancement in PCMs during charging and discharging period: metal fins, metal honeycomb structure and metal square cell structure. It is worth noting that introduction of TCEs into PCMs can enhance the heat transfer whilst has an adverse effect on the heat storage capacity of the LHESS. The heat storage capacity decreases with the increase of the volume of the TCEs, thus the enhancement efficiency for each TCE was evaluated herein.

44.2 Experimental Rig Setup and Test Procedures

44.2.1 Materials (PCMs and Metal Structures)

The phase change materials used in this study are paraffin RT 25 and paraffin RT 42, which are commercial organic PCMs. Organic PCMs have many advantages to be used for low temperature heat storage applications, such as good stability, no supercooling and anti-corrosion with a storage encapsulation. The commercial paraffin RT 25 and RT 42 do not have a "sharp" melting temperature, and their phase change take place within a temperature range around 25 °C and around 41 °C, respectively. The selection of these two PCMs is because that the two PCMs have similar physical properties and relatively large melting temperature difference, making them easy to be compared. The relevant thermo-physical properties of the paraffin RT 25 and RT 42 are listed in Table 44.1.

It is obvious in Table 44.1 that RT25 and RT 42 have low thermal conductivities which are detrimental to the performance of energy storage system. Particularly during the solid solidification process, conduction is the mainly heat transfer mechanism. PCM solidifies on the heat transfer surface and acts as a self-insulator which is dominated to the whole system performance. It is necessary to add material with high thermal conductivity into the PCM system to strengthen the heat conduction. The use of fins in PCM-based heat storage system is considered as one way to enhance the thermal conductivity of the PCM. Meanwhile a square cell metal structure which based on the fins structure and a honeycomb metal structure are employed in this study. Generally, the small percentage (usually <7 %) of heat storage loss is reasonable [16], in order to minimize the influence of adding TCEs on the heat storage capacity, the volume percentages of these three TCEs are within 5 % of the volume of PCM container. The volume percentages of fins, honeycomb structure and square structure are 1.8, 2.7, and 3.6 %, respectively. These three kind of metal structures made of steel with a thermal conductivity $k = 84$ kW/mK are showed in Fig. 44.1.

Table 44.1 Thermo-physical properties of RT25 and RT 42 [15]

Thermo-physical properties	Paraffin RT 25	Paraffin RT 42
Melting temperature (K)	273 + 26	273 + 41
Thermal conductivity (kW/mK)	Solid: 0.2	Solid: 0.2
	Liquid: 0.2	Liquid: 0.2
Heat of fusion (kJ/kg)	147	174
Density (ρ) (kJ/m^3)	Solid: 880	Solid: 880
	Liquid: 760	Liquid: 760
Heat capacity (kJ/kg K)	Solid: 2.9	Solid: 1.8
	Liquid: 2.11	Liquid: 2.4

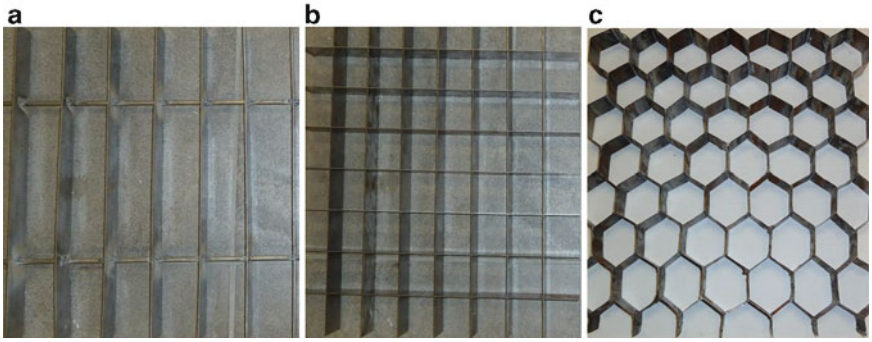

Fig. 44.1 Three metal structures for heat-transfer enhancement (**a**) finned structure, (**b**) square cell metal structure, and (**c**) honeycomb structure

44.2.2 Experimental Rig Set-Up

The experimental testing rig was set up in Environment laboratory G38 in Sir John Laing Building at Coventry University, as shown schematically in Fig. 44.2.

This testing rig consists of three major parts: heat storage unit, heat source system and data acquisition system. A rectangular container made of stainless steel with dimensions of $400 \times 400 \times 400$ mm, a matte black painted stainless steel is used as the heat absorber. Inner side walls of the PCM container covered with rubber strips to avoid ruinous mechanical stress on the storage containers at the same time maintaining thermal contact with the PCM-cum-heat absorber. The container filled with paraffin wax RT 25 and RT 42 from Rubitherm Technologies GmbH, Germany. The styrofoam board with a thermal conductivity of $k = 0.041$ kW/mK is applied as the thermal insulation material in this study. In this manner, the effect of lateral heat transfer from the sides can be negligible for this study and the melting process can be regarded as one dimensional problem. The temperatures of this system were measured by eleven K-type thermocouples with accuracy of ± 0.3 °C, three thermocouples were sticked on the absorber plate shielded by using the styrofoam board in a size of 20 mm $\times$ 20 mm to avoid being directly heated by the light source, and one thermocouple was used to measure the ambient air temperature. Along the vertical direction, seven thermocouples were used to measure the PCM temperatures at pre-selected locations. Three thermocouples were placed at the central part of the container, being 5, 20, and 40 mm deeply away from the absorber plate respectively, and four thermocouples are placed at different horizontal and vertical positions inside PCM to monitor the transient temperature variation as well (*see* Fig. 44.2).

All of the thermocouples were connected to the data acquisition (Labjack U3) that connected to a PC, and then the temperature variations were automatically recorded in the computer every 10s for the further data processing. For data analysis, only the data measured by the four thermocouples placed in the central

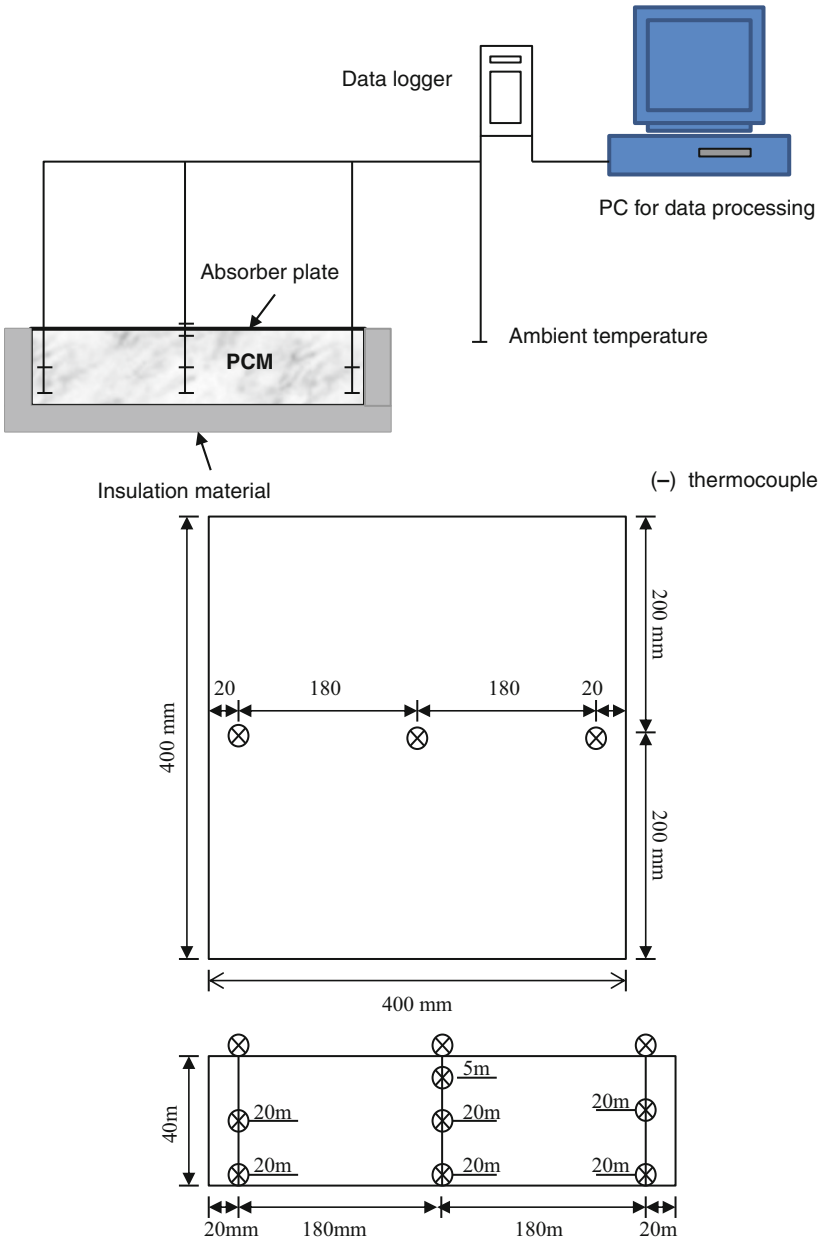

Fig. 44.2 Schematic diagram of the experimental testing rig and the positions of the thermocouples

part of test container had been used in an attempt to reduce the boundary effect. A simple small-scale solar simulator used as the heat source to provide a constant heat flux of 900 W/m^2 to melt the PCMs from solid phase to liquid phase, which is a multiple-lamp system consists of eight 120-W halogen lamps installed in a staggered form in an area of 500 mm by 500 mm.

44.2.3 Measurement Procedures

For melting process, all the experiments were carried out with the same initial temperature under the same constant heat flux. The melting and solidification characteristics of pure PCMs were firstly tested. The finned structure, square cell structure and honeycomb structure were put into the container, respectively. The heat transfer performances of them were measured under the same constant heat flux. For the cooling process, all the samples were cooled by natural convection at the same room temperature.

44.3 Results and Discussion

The aims of this research are to determine the following items:

- The temperature profiles during melting and solidification processes.
- The melting time and solidification time.
- The enhancement effects of the three TCEs on different PCMs during melting and solidification processes.

Heat transfer in PCM is a very complicated process, it is non-stationary, due to the phase changes during the charging and discharging processes, and it is non-homogeneous, because of the adding of TCEs. Therefore, the phase change process of the PCM inside the container during melting and solidification is a time-dependent process. The results are presented in two parts: charging and discharging process.

44.3.1 Melting Process

The melting of the RT 25 without and with fins were investigated firstly, the testing started at the room temperature 20 °C, and then, the solar simulator was turned on to heat up the PCM container. Figure 44.3, respectively displays the temperature variations with time of the absorber plate and three thermocouples inside paraffin RT 25 for pure PCM and PCM with the TCEs. For the pure PCM case, at the beginning the temperature of the absorber plate increased sharply until the paraffin

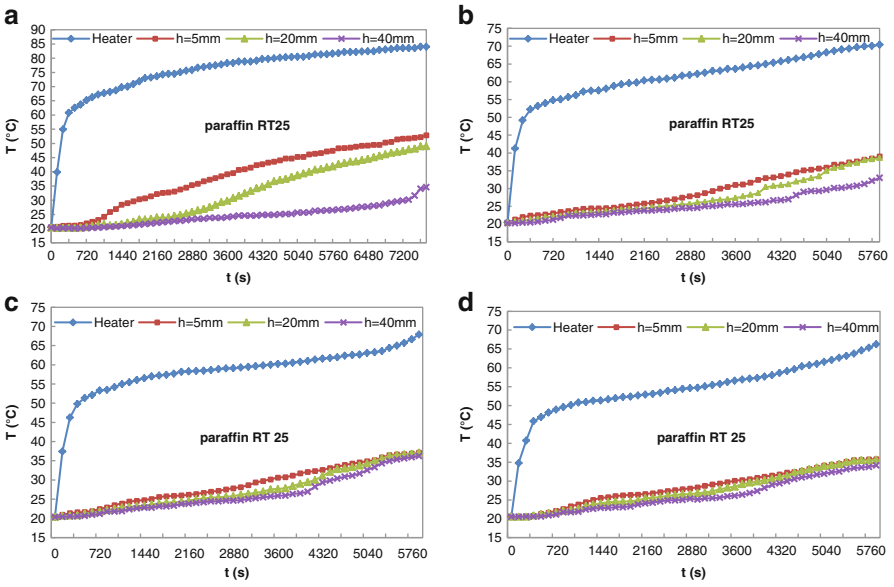

Fig. 44.3 Temperature variations with time for RT 25 without and with TCEs: (**a**) Pure PCM sample, (**b**) Straight fins sample, (**c**) Honeycomb structure sample and (**d**) Square cell structure sample

starts melting, and then turned into a moderate rise. During the melting process for the pure PCM sample, the temperature of PCM climbed slowly because of the low thermal conductivity of the solid paraffin, as the heat transfer was only dominated by conduction. When the temperature reached to a plateau, about 25 °C, indicating a phase change process occurred afterwards. Then, it is evident that the temperature increased suddenly occurd to all three thermocouples where the natural convection took place and afterward the combined conduction and convection determined the melting process. Another reason for abrupt transitions was that the input heat cannot be conducted to the solid paraffin quickly due to the low thermal conductivity, and most of energy was absorbed by the melted paraffin to a high temperature rather than transfer in the vertical direction. . However, for the testing with TCEs, the temperature inside paraffin climbed quickly at the beginning, indicating that the heat flux can be rapidly conducted to all paraffin with the assistance of the TCEs even at the solid state, due to the high heat conductivity of the TCEs. TCEs strengthened the heat transfer from the absorber to the inside of the PCM package and the temperature rise on the absorber surface is reduced. It can be seen clearly that with the volume fraction of the TCEs increase, the level of thermal stratification was reduced, leading to a more uniform temperature distribution in the PCM.

At the lowest test point (h = 40 mm), the temperature suddenly increased indicating that the phase change has completely finished the transition from solid to liquid. The melting times were estimated from the temperature-time curves of the test samples until the temperatures to reach 27 °C from the initial temperature

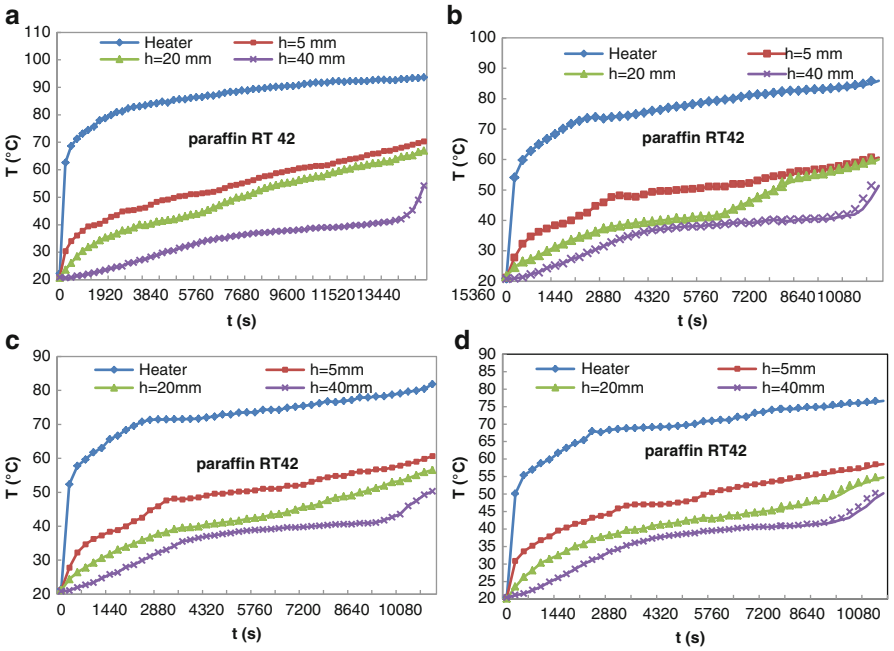

Fig. 44.4 Temperature variations with time for RT 42 without and with TCEs: (**a**) Pure PCM sample, (**b**) Straight fins sample, (**c**) Honeycomb structure sample and (**d**) Square cell structure sample

(20 °C). The whole melting processes for four samples last for about 102, 76, 68, and 64 min, respectively.

Figure 44.4 shows the temperature—time profiles of paraffin RT 42 without and with TCEs, for the test of pure RT 42, the RT 42 exhibited quit different heat transfer behaviour from RT 25. The temperature inside RT 42 increased quickly and then reached a plateau around the melting temperature of 38 °C. That is because the temperature of the absorber surface for RT 42 is much higher than that for RT 25, leading to the quicker heat transfer to the solid. The absorber surface temperatures for RT 42 samples are all higher than those corresponding to RT 25 samples. Another different behaviour from RT 25 is that RT 42 sample have more clear thermal stratification than RT 25 even applying TCEs into PCM. Similarly, adding TCEs into RT 42 can reduce the absorber surface temperature and the thermal stratification inside PCM, and consequently achieve more uniform temperature distribution. After the temperature at h = 40 mm reached 43 °C, the PCM pack temperature increased sharply, and then the phase change transition finished. The melting times for the samples are 240, 172, 160, and 144 min.

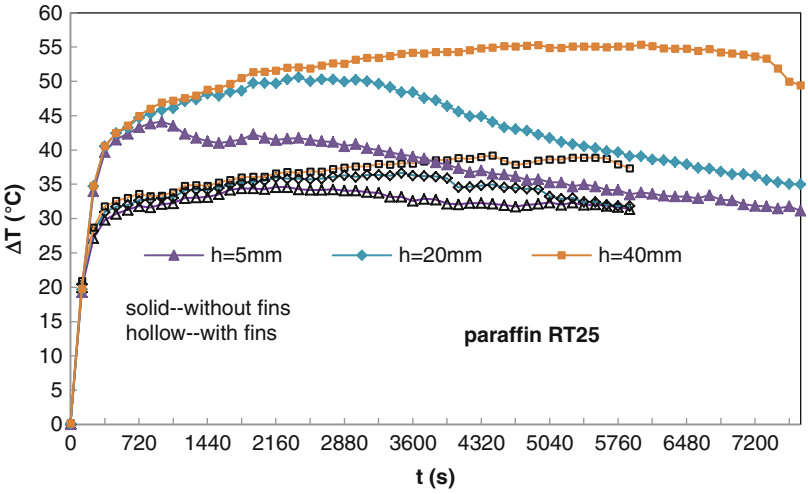

Fig. 44.5 Temperature differences with time between RT 25 and absorb plate

44.3.2 Effects of TCEs on Natural Convection

In order to facilitate the understanding of the heat transfer characteristics inside PCM with TCEs, the transient temperature differences between the heat absorber and PCM (RT 25) with fins at different locations (5, 20, 40 mm from the absorber plate, respectively) are investigated and displayed in Fig. 44.5.

It indicated that the transient temperature difference between the RT25 and absorb plate increased sharply in the solid zone. This can be attributed to the temperature of the heat absorber increased much quickly than that of PCM at the beginning of melting process. But it rises slowly when PCM stars melting. After the PCM completed the transition from the solid to liquid state, the temperature difference lines experience a drop for both of samples, due to the heat transfer enhancement caused by the natural convection effect. However, From Fig. 44.5, the temperature difference of the sample with fins is lower than that of without fins. Lower temperature difference indicates higher heat transfer capability, which is caused by the high thermal conductivity of metal finned structures embedded in PCMs. Compared to the results of the pure PCM without fins during charging process, fins can effectively enhance solid/liquid phase change heat transfer, particularly at solid zone of PCM. When the PCM starts melting, natural convection can improves the heat transfer performance, thereby reducing the temperature difference between the absorber and PCM. It can also be noticed that in liquid phase zone the sample without fins has a bigger drop than that one with fins, meaning they have high heat transfer rate than the sample with fins. This is because that the metal fins suppresses and impairs natural convection in the liquid phase zone whilst enhances heat conduction in the solid phase zone, but the loss in heat

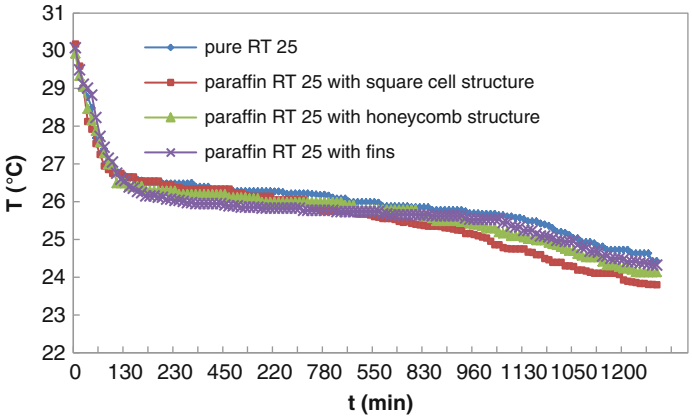

Fig. 44.6 Temperature variations of RT 25 samples during solidification process (h = 40 mm)

convection is not fully offset by the increase in heat conduction. Therefore, adding TCEs into PCMs leads to a different heat transfer performance in different regions (solid, solid/liquid and liquid regions). This phenomenon happened to other RT 25 and RT 42 samples. It can be concluded that embedding TCEs into PCMs does not always improve heat transfer in every phased stage. The optimal design should be achieved in the practical application for the best thermal performance.

44.3.3 Solidification Process

Most of studies focus on improving the heat transfer during melting stage but solidification period is equally important as the melting. Very a few published works were carried out on the effect of TCEs on solidification duration. Hence, the heat transfer performances of TCEs are investigated in this paper.

All of the solidification tests were cooled down by natural cooling in an environmental temperature around 20 °C. The initial temperatures for the RT 25 and RT 42 samples were 30 and 50 °C, respectively. Figures 44.6 and 44.7 present the temperature variations of these two samples with time at the lowest point (h = 40 mm). The reason for selecting those points just because when the PCMs completely finished the solidification indicates all the PCM inside container has been in solid state. It is obviously that the general trends of two samples are similar. The effect of the initial sensible heat diminished after 170 min for the RT 25 samples with whilst 70 min for RT 42 samples. The effect of natural convection decreased with the superheat became weaken. When the temperature reduced to around 26.6 °C and 44 °C for RT 25 and RT 42, the solidification process started. At the beginning of the freezing process, the heat transfer in PCM dominated by natural convection and conduction. After the phase change finished, the

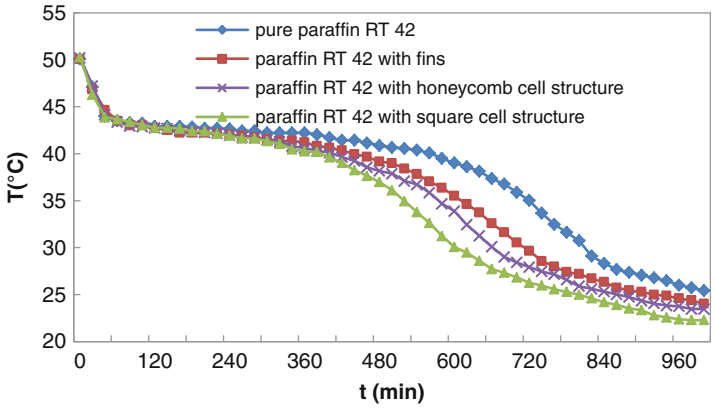

Fig. 44.7 Temperature variations of RT 42 samples during solidification process (h = 40 mm)

temperature of the samples with TCEs reduced faster than the pure PCM samples for both RT 25 and RT 42. The solidification times for RT 25 samples are 20 h 50 min, 19 h 10 min, 18 h 20 min and 17 h 20 min, and for RT 42 samples are 9 h 40 min, 8 h, 7 h and 6 h 20 min. This indicates that TCEs play an important role in improving heat transfer inside PCMs especially when natural convection does not take place.

44.3.4 Effects of TCEs on PCMs

The experimental results confirmed that TCEs are capable of influence on both of melting and freezing process by improving the thermal conductivity of PCM. The efficiency of the three TCEs on enhancing the heat transfer rate of paraffin RT 25 and RT 42 were studied by comparing the melting and freezing times of PCMs with enhancers with those without.

$$\eta = \frac{t_{Pure} - t_{TCE}}{t_{Pure}} \%$$

Where t_{Pure} is the melting/solidification time of PCM without TCEs, and t_{TCE} is the melting/solidification time of PCM with TCEs.

For RT 25 samples, the heat transfer inside PCM improved by 25, 33, and 37 %, respectively during the melting process, whilst the solidification times were shorten by 8 %, 12 % 17 % . For RT 42 samples, heat transfer enhancements were increased by 28, 33, and 40 % during the melting process, and increased by 17, 28, and 35 %, respectively during the freezing process. These figures can be defined as the efficiencies of the TCEs for two PCMs.

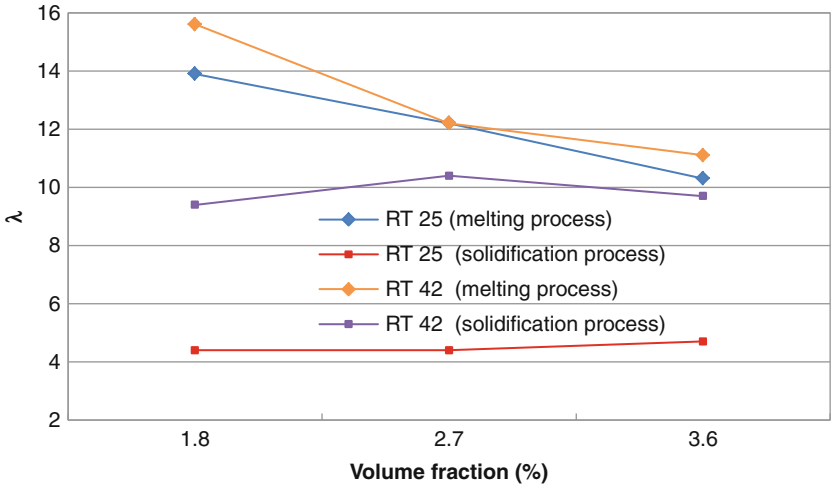

Fig. 44.8 Efficiency-volume ratios for RT 25 and RT 42

It must be noticed that use of metal heat transfer enhancers considerably increases the weight and decreases the volumetric heat of fusion of the LHTES system due to the high density and relative low heat storage capability of metal. Besides, adding TCEs into PCM does not improving the heat transfer rate of PCMs in the liquid region. For a heat storage system with a given volume, inserting metal structure into PCMs can enhance the heat transfer whilst influence the heat storage capabilities. Generally speaking, the heat transfer capacity of the PCM is getting better along with the increase in mass of metal structure whilst the heat storage capacity of PCM decreases with the increase of metal structure. In order to make a balance between the heat transfer enhancement and thermal energy storage capacity, a concept of measurement is presented herein, by introducing a simple equation: efficiency-volume ratio, λ which is defined as follow:

$$\lambda = \frac{\eta}{\text{volume fraction of the heat transfer enhancer}} = \frac{\eta}{\zeta}$$

$$\zeta = \frac{TCEs \quad volume}{\text{Total} \quad \text{volume} \quad of \quad volume}\%$$

Figure 44.8 shows the efficiency to volume ratios for RT 25 and RT 42 samples during the melting and solidification process. The efficiency to volume ratio is a direct indication of the effects of the heat transfer enhancers on the melting or freezing time. It can be seen clearly that for both of RT 25 and RT 42, these three TCEs have higher performance on PCMs during the melting process than solidification process. The heat transfer enhancement capacities of the TCEs decrease with the increase in volume fraction of the TCEs during melting process, whilst slightly

change with the volume fraction increase during solidification process. The performance of the TECs on the RT 42 is just slightly better than that of TCEs on RT 25 during melting process, whilst it is much higher than that of TCEs on RT 25 during solidification process. This due to the higher melting temperature of RT42, which induces higher heat transfer rate between the PCM and TECs, then consequently transferred heat to the ambient air.

44.4 Conclusions

Two different kinds of PCMs (paraffin 25 and paraffin 42) were selected to study the heat transfer performance of PCMs with different heat transfer enhancers under same conditions. The experimental results showed that all the heat transfer enhancers can improve the heat transfer performance on PCMs greatly during the melting and freezing process. To be specific, for paraffin RT 25, the heat transfer efficiencies were increased by 25, 33, and 37 %, respectively during melting process, when straight fins, honeycomb and square cell structure were applied to PCM. For solidification process, the heat transfer efficiencies were increased by 8, 12, 17 %, respectively. Regarding the paraffin RT 42 test samples, the heat transfer efficiencies were increased by 28, 33, and 40 % during melting process, and were increased by 17, 28, and 35 %, respectively during freezing process.

For a latent heat thermal energy storage system of a given volume, use of metal heat transfer enhancers does not always have positive effect on improving the heat transfer inside PCM. Since the TCEs increase the weight and decreases the volumetric heat of fusion of the LHTES system. A new quantity was used to describe the relationship between the heat transfer efficiencies improved by TCEs and the volume fractions of them, namely efficiency-volume ratio. The results showed that the heat transfer enhancement capacities of the TCEs on RT 25 and RT 42 decrease with the increase in volume fraction of the TCEs, and the capacities for RT 42 are slightly better than those for RT 42 during the melting process, but inconspicuously increase with the volume fraction increase during the solidification process. The performance of the TECs on the RT 42 is just slightly better than that of TCEs on RT 25 during the melting process. Meanwhile the heat transfer enhancement capacities for the two PCMs increase with the volume fraction increase, and the performances of TCEs on RT 42 are much higher than those on RT 25 during the solidification process. Hence, depending on the type of application, in where heat transfer might need to be enhanced either for charging, discharging or both, the optimal design of TCEs should be achieved to realize the best performance.

Nomenclature

t Time (s)

Greek Symbols

η Efficiency
λ Efficiency-volume ratio
ζ Volume fraction of the heat transfer enhancer

Subscript and Superscripts

pure PCM without TCEs
TCE PCM with TCEs

Acronyms

LHTES Latent heat thermal energy storages
PCM Phase change materials
TCEs Thermal conductivity enhancers

References

1. Sari A (2003) Thermal characteristics of a eutectic mixture of myristic and palmitic acids as phase change material for heating applications. Appl Therm Eng 23:1005–1017
2. Abhat A (1983) Low temperature latent heat thermal energy storage: heat storage materials. Sol Energ 30:313–332
3. Bugaje IM (1997) Enhancing the thermal response of latent heat storage systems. Int J Energ Res 21:759–766
4. Jegadheeswaran S, Pohekar SD (2010) Energy and exergy analysis of particle dispersed latent heat storage system. Int J Energ Environ 1(3):445–458
5. Sari A, Karaipekli A (2007) Thermal conductivity and latent heat thermal energy storage characteristics of paraffin/expanded graphite composite as phase change material. Appl Therm Eng 27:1271–1277
6. Akhilesh R, Narasimhan A, Balaji C (2005) Method to improve geometry for heat transfer enhancement in PCM composite heat sinks. Int J Heat Mass Tran 48(13):2759–2770
7. Huang MJ, Eames PC, Norton B (2005) Thermal regulation of building-integrated photovoltaics using phase change materials. Int J Heat Mass Tran 47(12–13):2715–2733
8. Robak CW, Bergman TL, Faghri A (2011) Enhancement of latent heat energy storage using embedded heat pipes. Int J Heat Mass Tran 54(15–16):3476–3484
9. Shabgard H, Bergman TL, Sharifi N, Faghri A (2010) High temperature latent heat thermal energy storage using heat pipes. Int J Heat Mass Tran 53(15–16):2979–2988

10. Lacroix M, Benmadda M (1997) Numerical simulation of natural convection dominated melting and solidification from a finned vertical wall. Numer Heat Trans Part A Appl 31 (1):71–86
11. Lacroix M, Benmadda M (1998) Analysis of natural convection melting from a heated wall with vertically oriented fins. Int J Numer Methods Heat Fluid Flow 8(4):465–478
12. Eftekhar J, Sheikh AH, Lou DYS (1984) Heat transfer enhancement in a paraffin wax thermal storage system. J Sol Energ Eng 106:299–306
13. Abhat A (1976) Experimental investigation and analysis of a honeycomb-packed phase change material device. In: AIAA 11th thermo-physics conference, p 9 (Paper AIAA-76-437)
14. De Jong AG, Hoogendoorn CJ (1981) Improvement of heat transport in paraffins for latent heat storage systems, in thermal storage of solar energy. In: Proceedings of an international TNO—symposium, Martinus Nijhoff Publishers, Amsterdam, The Netherlands, pp 123–33
15. Website: http://www.rubitherm.de/. Accessed June 2010, Rubitherm GmbH
16. Zhao CY, Lu W, Tian Y (2010) Heat transfer enhancement for thermal energy storage using metal foams embedded within phase change materials (PCMs). Sol Energ 84:1402–1412

Chapter 45
Simulation of Double Effect Absorption Refrigeration System

Ibrahim Atilgan and Cevdet Aygun

Abstract In this study the Double effect Absorption Refrigeration system (DAR) is developed and its thermodynamic analysis is performed using different working fluid pairs. The DAR consists of a high and low temperature generator, high and low temperature absorbers, condenser, evaporator, expansion valves, mixture and refrigerant heat exchangers and pumps and it is made up of two cycles.

In the DAR system, NH_3/H_2O is used as refrigerant/absorbent working pair at high temperature cycle and $NH_3/LiNO_3$ is used a refrigerant/absorbent working pair at low temperature cycle. This system is called as System I. In order to be able to compare the effects of using different fluid pairs in these two cycles, a new system is formed. In this new system, fluid pair at the high temperature cycle remained same as before (NH_3/H_2O), but NH_3/NaSCN is used at low temperature cycle and this new system is called as System II. While the selected results of calculations of both systems were presented in the figures, only the results of analysis of system II are tabulated in the study.

The analysis of the system is performed at various operation conditions and the coefficient of performance (COP) and the high temperature circulation ratios (f_H) were calculated and given graphically. Low temperature circulation ratios (f_L) were also calculated but not shown in the study. A computer program is developed in FORTRAN for the simulation of the DAR and results are given graphically. The results show that the performance of the $NH_3/LiNO_3$ working fluid pair has slightly better performance than NH_3/NaSCN, at low temperature cycle for the same working conditions. It is also observed that COP of the double effect system is greater than the COP of single effect system.

In this study, energy and exergy analyses of a two-stage heat pump-drying system are conducted, and the performance of the overall system is evaluated. The system has two cycles: a heat pump and a drying cycle. The working fluid of the heat pump and the drying cycles are R-134A and air, respectively.

Keywords Absorption refrigeration • Simulation • Double effect • Working fluid

I. Atilgan • C. Aygun (✉)
Department of Mechanical Engineering, Faculty of Engineering,
Gazi University, Ankara, Turkey
e-mail: atilgan@gazi.edu.tr; caygun@gazi.edu.tr

I. Dincer et al. (eds.), *Progress in Sustainable Energy Technologies Vol II: Creating Sustainable Development*, DOI 10.1007/978-3-319-07977-6_45

45.1 Introductıon

For the absorption refrigeration systems the selection of the working fluid pairs is important. The performance of the system and its working conditions depend upon the thermodynamic properties of the working fluid. In these systems, NH_3/H_2O and H_2O/LiBr are used frequently. The DAR, which is developed in this study, consists of two cycles. While one of them is working at high temperatures the other cycle works at low temperatures. The DAR consists of a condenser, evaporator, circulation pumps expansion valves, the high and low temperature absorbers, the high and low temperature generators and the heat exchangers. The schematic diagram of the DAR is shown in Fig. 45.1.

For the first system, NH_3/H_2O is used at high temperature cycle and $NH_3/LiNO_3$ is used at low temperature cycle as working fluid pairs and this system is called as System I. For the purpose of comparison, while same fluid pair (NH_3/H_2O) is used at high temperature cycle, NH_3/NaSCN is used at low temperature cycle and this second system is as called System II.

The working principle of the DAR is as follows: The refrigerant that comes from the HTG and LTG are mixed at Junction J and enters to the condenser as the superheated phase at the reference point of "16." The ammonia condenses in the condenser and leaves the condenser at the Reference point of "17" and enters to the HE4. The ammonia is cooled to the saturated vapor in the heat exchanger and enters to the evaporator at the reference point of "19." The saturated ammonia vapor leaves the evaporator at the reference point of "20" and it is heated up when it passes through HE4 and comes to the Junction K. The some of the working fluid flow through the reference point of "22" and enters to the LTA. The ammonia is absorbed by the NaSCN or $LiNO_3$ that comes from the LTG and the rich mixture of NH_3/NaSCN or $NH_3/LiNO_3$ leaves the LTA.

Then, the mixture is pumped to the high pressure through P2, it enters to the HE3 and it is heated up when it passes through HE3. The mixture enters to the LTG where it is heated. Heat is transferred to the LTG from the HTA by the heat pipes. The superheated ammonia vapor leaves the LTG at the reference point of "15" and returns to the Junction J and the low temperature cycle is completed.

The saturated ammonia vapor leaves the evaporator and flows into the Junction K at the high temperature cycle. Some of the refrigerant leaving Junction K enters to the HE2 and its temperature increase. The refrigerant that leaves the HE2 end enters to the HTA through "24." In the HTA the refrigerant and the weak mixture mix and the rich mixture leaves the HTA at the reference point of "1." The heat generated in the HTA is transferred to the LTG by means of heat pipes. The pressure of the rich mixture increases in the pump P1 and a flow through reference point "2" enters to the HE1. In the HE1 the mixture temperature increases and enters to the HTG. The mixture is heated externally and ammonia is separated from the absorbent and leaves the HTG at the reference point of "13." The ammonia enters to the HE2 and it is cooled down. The cooled ammonia goes into Junction J and the high temperature cycle is completed.

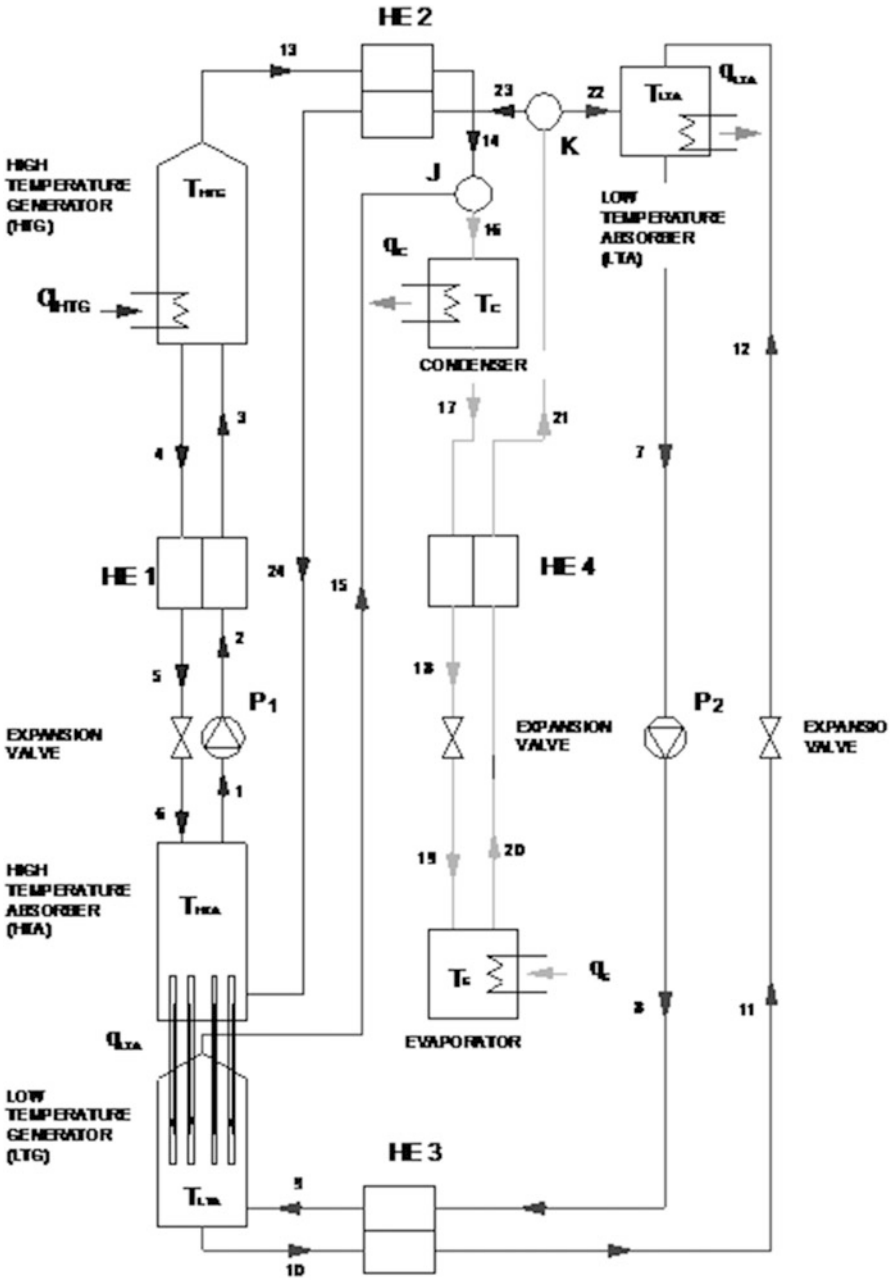

Fig. 45.1 Schematic diagram of the DAR

The irreversibilities of the components of absorption refrigeration system for NH_3/H_2O working pair was determined [1]. The dimensionless exergy loss of each component, the exergetic coefficient of performance, the coefficient of performance and the circulation ratio are given graphically for each different generator, evaporator, condenser and absorber temperature.

It was determined that for $T_{amb} - T_{ev} > 23$ °C the coefficient of performance of the NH_3-NaSCN system becomes higher than that of the NH_3-$LiNO_3$ system [2]. Thermodynamic analysis of single-stage and two stage ammonia-water absorption refrigeration systems at various working conditions using second law analysis is now possible to calculate.

Performance of single-stage absorption refrigeration systems at various working conditions using NH_3/H_2O, NH_3/NaSCN, and $NH_3/LiNO_3$ working pairs can be compared [3]. The performance of ammonia-sodium thiocyanate cycle is slightly better than that of the ammonia-lithium nitrate cycle. It is not necessary to use a rectifier with these two cycles. But the system with ammonia-sodium thiocyanate working pairs does not work under the −10 °C evaporator temperature.

It was showed that at the results of the study for the optimisation of water-lithium-bromide system is simpler than the ammonia-water systems and operates at a higher cooling ratio and smaller heat exchange surfaces for the same conditions [4]. Similarly, it was found that the performance of NH_3/NaSCN with solar energy is better than NH_3/H_2O absorption refrigeration system [5]. In addition, the NH_3/NaSCN offers lower equipment costs, as it does not require a rectifying column to prevent the absorbent from being carried over to the condenser.

The thermodynamic equations for the performance evaluation of the monomethylamine-water vapor absorption refrigeration system have been obtained, analysed and reported [6]. The equations have been derived from experimental data with a good agreement with the expected values and have been expressed in polynomial form. These equations were utilized on the energy and mass balances for obtaining the coefficient of performance (COP) with this pair and compared with the ammonia-water absorption system. It has been observed that this refrigerant-absorbent pair has a greater coefficient of performance at low generation temperatures and moderate condenser, absorber and evaporator temperatures.

The mixtures of lithium bromide and organic salts of sodium and potassium (formate, acetate and lactate) as alternative absorbents for absorption refrigeration machines was evaluated [7]. The main objective was to overpass the limitations of lithium bromide and improve the characteristics and the efficiency of the refrigeration cycle. In order to select the mixture that presents better properties for its employment in absorption refrigeration cycles, thermodynamic analysis have been done. The density, viscosity, enthalpies of dilution, solubility and vapor pressure data of the proposed mixtures have been measured. A simulation program has been developed to evaluate temperatures, heats exchanged in the different sections and the efficiency of the cycle.

The thermodynamic analysis of the water/lithium bromide absorption refrigeration cycle was performed [8]. The influences of operating temperature and effectiveness of heat exchanger on the thermal loads of components, coefficients of

performance (COP_c, COP) and efficiency ratio (η) were investigated. It was concluded that the COP_c and COP values increase with increasing generator and evaporator temperatures but decrease with increasing condenser and absorber temperatures. The η value varies with these temperatures. Also, the effects of solution and refrigerant heat exchangers on the performance, efficiency ratio of the system and fluid temperatures were compared. As a result, it was found that the solution heat exchanger (SHE) has more effect on the investigated parameters than the refrigerant heat exchanger (RHE). While the SHE increases the COP value up to a maximum 44 %, the RHE has an effect of only 2.8 %.

45.2 Thermal Properties of Working Fluids

Thermal properties of the working fluids are necessary for the simulation of the DAR. The equations of state based on those of Schulz has been developed previously [9]. The temperature range has been extended to 500 K and the pressure range to 50 bar. Values of specific volume, vapor pressure, enthalpies and equilibrium constants for mixtures were compared with the experimental data and the results are presented with enthalpy-concentration diagrams.

Thermodynamic relations for NH_3/NaSCN and $NH_3/LiNO_3$ mixtures was developed [10]. Optimum COP value was obtained at evaporator temperature of −10 °C, condenser temperature of 30 °C and generator temperature of 90 °C for the single stage absorption refrigeration system using $NH_3/LiNO_3$ mixture. In addition, for NH_3/NaSCN mixture optimum COP value was obtained at evaporator temperature of −10 °C, generator temperature of 100 °C. The system with NH_3/NaSCN mixture does not work under the evaporator temperature of −10 °C. For both systems COP is 10 % higher than the system with NH_3/H_2O mixture at the same working conditions.

Although the single effect absorption refrigeration system using NH3/H2O and NH3/NaSCN working fluids were simulated [11]. It is not easy to compare the results. At 30 °C condenser, and 110 °C generator and −10 °C evaporator temperatures the COP of the single effect system is 0.29 for NH_3/H_2O and 0.23 for NH_3/NaSCN working fluid pairs.

At the high temperature cycle of the system, NH_3/H_2O and at the low temperature cycle, NH_3/NaSCN and $NH_3/LiNO_3$ were used as refrigerant/absorbent working pairs for comparison.

Within the pressure limits of $0.369 < p < 112.98$ bar and the temperature interval of $221.42 < T < 405.16$ K the saturated pressure of ammonia vapor is given as [12].

$$\ln \hat{p} = D_1 + D_2\hat{T} + \frac{D_3}{\hat{T}} + D_4\hat{T}^2 + D_5\hat{T}^3 + D_6\frac{\left(1-\hat{T}\right)^{3/2}}{\hat{T}} \tag{45.1}$$

Table 45.1 The values of the coefficients in Eq. (45.1)

D_1	D_2	D_3	D_4	D_5	D_6
19.667984	−15.54993	−11.079219	9.114107	−2.152941	1.81269

where $\hat{p}$ and $\hat{T}$ are the dimensionless pressure and temperature respectively. Critical pressure and temperature are used to obtain these dimensionless parameters. The values of the coefficients in Eq. (45.1) are given in Table 45.1.

The Gibbs free energy function of the saturated liquid ammonia can be determined by:

$$\hat{g}_1 = a_1 - a_2\hat{T} + \int_{T_o}^{T} \frac{\hat{c}_{p1}}{\hat{T}} d\hat{T} + \left(a_3 + a_4\hat{T} + a_5\hat{T}^2\right)\left(\hat{p} - \hat{p}_0\right) + \frac{a_6\left(\hat{p}^2 - \hat{p}_0^2\right)}{2} \tag{45.2}$$

Constraints of the T and p of Eq. (45.2) are given as follows; $230 < T < 500$ K temperature range and $0.2 < p < 50$ bar pressure range [9]. At the liquid phase and constant pressure, dimensionless specific heat c_{p1} of the ammonia is formulated by

$$\hat{c}_{p1} = b_1 + b_2\hat{T} + b_3\hat{T}^2 \tag{45.3}$$

where the dimensionless parameters are given as:

$$\hat{p} = \frac{p}{p_B}, \quad \hat{T} = \frac{T}{T_B}, \quad \hat{c}_p = \frac{c_p}{R}, \quad \hat{g} = \frac{g}{RT_B} \tag{45.4}$$

where $T_B = 100$ K and $p_B = 10$ bar. The relation between specific Gibbs free energy function and specific enthalpy is given as:

$$h = -T^2\left(\frac{d(g/T)}{dT}\right)_p \tag{45.5}$$

Using Eqs. (45.2), (45.3) in Eq. (45.5) the expression for specific enthalpy in liquid phase may be obtained.

The relation between specific Gibbs free energy function and specific volume is given by [9]:

$$v = \left(\frac{dg}{dp}\right)_T \tag{45.6}$$

Using Eq. (45.2) in Eq. (45.6) the specific volume of the saturated liquid ammonia is written as

$$v = R\frac{T_B}{100p_B}\left(a_3 + a_4\hat{T} + a_5\hat{T}^2 + a_6\hat{p}\right) \tag{45.7}$$

The relations used for the enthalpy of ammonia within the temperature interval of at $213.15 < T < 333.15$ K saturation and same temperature interval over cooling and 393.15 K maximum heating condition was suggested in [12].

The specific enthalpy of the saturated liquid ammonia is calculated by:

$$h_1 = k_1 T_L + k_2 T_L^2 + k_3 T_L^3 \tag{45.8}$$

where $T_L = T_d - \Delta T_c$, T_d is the saturation temperature and ΔT_c, is the subcooled temperature difference. The specific enthalpy of saturated ammonia vapour is given as:

$$h_v = k_4 + k_5 T_d + k_6 T_d^2 + k_7 T_d^3 \tag{45.9}$$

and the specific enthalpy of superheated ammonia vapour is calculated by:

$$h_s = h_v \begin{pmatrix} 1 + k_8 \Delta T_s + k_9 \Delta T_s^2 + \\ k_{10} \Delta T_s T_d + k_{11} \Delta T_s^2 T_d + \\ k_{12} \Delta T_s T_d^2 + k_{13} \Delta T_s^2 T_d \end{pmatrix} \tag{45.10}$$

where ΔT_s is temperature difference between the superheated and saturated phases.

$$\Delta T_s = T - T_d \tag{45.11}$$

The unit of the specific enthalpy is J/kg and temperature is in terms of °C. The relation between saturation pressure and temperature of ammonia-water mixture is given as [11],

$$\log p = M - \frac{N}{T} \tag{45.12}$$

where p is in Pa and the temperature is in K. x is mass concentration. The values of M and N are given respectively, as;

$$M = 10,44 - 1,767x + 0,9823x^2 + 0,3627x^3 \tag{45.13}$$

$$N = 2013,8 - 2155,7x + 1540,9x^2 - 194,7x^3 \tag{45.14}$$

A relation for the Gibbs Free Energy Function in the liquid phase for ammonia-water mixture is proposed [9].

The saturation pressure of ammonia-sodium thiocyanate mixture is given as [7],

$$P = \exp\left(\begin{array}{l} 15,7266 - 0,298628X + \\ \left(-2548,65 - 2621,92(1-X)^3\right)\left(\dfrac{1}{t + 273,16}\right) \end{array} \right) \tag{45.15}$$

At the 0 °C reference temperature, enthalpy of ammonia-sodium thiocyanate mixture is given as [10],

$$h = \left(6464 - 80450,38X + 23972,57X^2\right)\left(\frac{1-X}{81,08}\right) + \int_0^T c_p dT \tag{45.16}$$

The mixture of specific heat is calculated by the following equation [10]:

$$\begin{aligned} c_p = {} & 2,4081 - 2,2814X + 7,9291X^2 - 3,5137X^3 \\ & + \left(0,0251X - 0,08X^2 + 0,0612X^3\right)T \\ & + \left(-0.0001X + 0,0003X^2 - 0,0001X^3\right)T^2 \end{aligned} \tag{45.17}$$

The saturation pressure of ammonia-lithium nitrate mixture is given as [10],

$$\begin{aligned} P = \exp\Bigg\{ & \left(16,29 + 3,59(1-X)^3\right) \\ & + \left(-2802 - 4192(1-X)^3\right)\left(\frac{1}{t + 273,16}\right)\Bigg\} \end{aligned} \tag{45.18}$$

At the 0 °C reference temperature, enthalpy of ammonia-lithium nitrate mixture is given as [10],

$$h = 689(X - 0.54)^{1,5} - 215 + \int_0^T c_p dT \tag{45.19}$$

The mixture of specific heat is calculated using the following equation [10]:

$$\begin{aligned} c_p = {} & 1,15125 + (3,382678X) \\ & + ((0,002198 + (0,004793X)T)) \\ & + \left(0,000118XT^2\right) \end{aligned} \tag{45.20}$$

45.3 Simulation of the System

In this study, a mathematical model was conceived and algorithm of this model used for developing a computer program in FORTRAN. Consequently, thermodynamic analysis of the DAR is performed in the various working conditions by using this computer program. The following assumptions are made in this analysis:

1. The ammonia vapour that leaves from the HTG and LTG is pure and at the generator temperature.
2. The weak solution that leaves the HTG and LTG is at the generator temperature. The solution that leaves the HTA and LTA is at the absorber temperature.
3. The ammonia that leaves the condenser is at saturated liquid phase and at the condenser temperature.

4. The ammonia that leaves evaporator is in saturated vapor phase and at the evaporator temperature.
5. The ammonia that leaves the generator is pure ammonia therefore rectifier and distillation column is not needed.
6. The temperature of LTG is 3 °C lower than the HTA temperature.
7. The ammonia vapor that leaves the HTA and LTA is superheated vapor.
8. There is no pressure loss at the components of the DAR.
9. The effectiveness of the heat exchangers of the DAR is taken as 0.8 in the analysis. The values of the working parameters used in the analysis are given in Table 45.2.

In the analysis, it is assumed that the pressure loss between the HTG and LTG is equal to [1].

$$\Delta p/p = 0.05 \tag{45.21}$$

In this relation p is exit pressure of fluid from pipe. The outlet pressure from the HTG and LTG is:

$$p_A = 1.05 p_Y \tag{45.22}$$

Similarly, it is assumed that the pressure loss is equal between evaporator with HTA and LTA.

$$\Delta p/p = 0.075 \tag{45.23}$$

Inlet pressures to the HTA and LTA are:

$$p_S = p_B/1,075 \tag{45.24}$$

The heat exchangers are assumed as counter flow heat exchangers and ε-NTU method is used in the analysis of the heat exchangers. The low and high pressure of DAR are:

$$p_L = p_{19} = p_{20} \tag{45.25}$$

$$p_H = p_{17} = p_{18} \tag{45.26}$$

Table 45.2 The values of the working parameters used in the analysis

Cooling load	q_E	2 kW
Evaporator temperature	T_E	−20–10 °C
Condenser temperature	T_C	24–28 °C
HTA temperature	T_{HTA}	50–100 °C
HTG temperature	T_{HTG}	56–200 °C
LTG temperature	T_{LTG}	47–97 °C
LTA temperature	T_{LTA}	24–28 °C

The heat load in the condenser is:

$$q_H = \dot{m}_{NH_3}(h_{16} - h_{17}) \tag{45.27}$$

The mass concentrations of the strong and weak solutions (NH_3/H_2O, NH_3/NaSCN and $NH_3/LiNO_3$) are calculated using Regula Falsi method. Mass concentration of mixture in the outlet HTA and mass flow rate is:

$$x_1 = x_2 = x_3 \tag{45.28}$$

$$\dot{m}_1 = \dot{m}_2 = \dot{m}_3 \tag{45.29}$$

The mass balance equations for the HTA are written as:

$$\dot{m}_6 + \dot{m}_{24} = \dot{m}_1 \tag{45.30}$$

and

$$\dot{m}_6 x_6 + \dot{m}_{24} = \dot{m}_1 x_1 \tag{45.31}$$

The energy balance equation for the HTA can be written as:

$$\dot{m}_6 h_6 + \dot{m}_{24} h_{24} = \dot{m}_1 h_1 + q_{HTA} \tag{45.32}$$

where q_{HTA} is the heat load that is transferred to LTG from HTA by heat pipes.

$$q_{HTA} = q_{LTG} \tag{45.33}$$

The mass balance equations for the LTA are written as,

$$\dot{m}_{12} + \dot{m}_{22} = \dot{m}_7 \tag{45.34}$$

$$\dot{m}_{12} x_{12} + \dot{m}_{22} = \dot{m}_7 x_7 \tag{45.35}$$

The energy balance equation for the LTA:

$$\dot{m}_{12} h_{12} + \dot{m}_{22} h_{22} = \dot{m}_7 h_7 + q_{LTA} \tag{45.36}$$

The energy balance equation for the HTG is written as

$$q_{HTG} + \dot{m}_3 h_3 = \dot{m}_4 h_4 + \dot{m}_{13} h_{13} \tag{45.37}$$

The energy balance equation for the LTG can be written as:

$$q_{LTG} + \dot{m}_9 h_9 = \dot{m}_{10} h_{10} + \dot{m}_{15} h_{15} \tag{45.38}$$

At the reference point "1" the mass flow rate of mixture is calculated using

$$\dot{m}_1 = \frac{1 - x_6}{x_1 - x_6}\dot{m}_{24} \tag{45.39}$$

At the reference point of "7" flow rate of mixture is calculated using Eqs. (45.34) and (45.35).

$$\dot{m}_9 = \frac{1 - x_{12}}{x_7 - x_{12}}\dot{m}_{22} \tag{45.40}$$

Similarly, at the reference point of "4" flow rate of mixture is calculated using

$$\dot{m}_4 = \frac{1 - x_3}{x_3 - x_4}\dot{m}_{13} \tag{45.41}$$

At the reference point of "10" flow rate of mixture is calculated using

$$\dot{m}_{10} = \frac{1 - x_9}{x_9 - x_{10}}\dot{m}_{15} \tag{45.42}$$

The mass and energy balance equations for the junction "J" are written as respectively:

$$\dot{m}_{14} + \dot{m}_{15} = \dot{m}_{16} \tag{45.43}$$

$$\dot{m}_{14}h_{14} + \dot{m}_{15}h_{15} = \dot{m}_{16}h_{16} \tag{45.44}$$

$$\dot{m}_{13} = \dot{m}_{14} \tag{45.45}$$

The mass balance for the junction "K" is written as:

$$\dot{m}_{21} = \dot{m}_{22} + \dot{m}_{23} \tag{45.46}$$

$$\dot{m}_{23} = \dot{m}_{24} \tag{45.47}$$

The expression for the mass flow rate at the reference point of "24" of is obtained as

$$\dot{m}_{24} = \frac{\left(\left(\frac{1-x_9}{x_9-x_{10}}\right)(h_{10} - h_9) + (h_{15} - h_9)\right)\dot{m}_{21}}{\left(\frac{1-x_1}{x_1-x_6}\right)(h_6 - h_1) + (h_{24} - h_1) + \left(\frac{1-x_9}{x_9-x_{10}}\right)(h_{10} - h_9) + (h_{15} - h_9)} \tag{45.48}$$

The coefficient of performance of the DAR can be written as

$$COP = \frac{q_E}{q_{HTG} + W_{p1} + W_{p2}} \tag{45.49}$$

The circulation ratio of the high temperature cycle:

$$f_H = \frac{\dot{m}_1}{\dot{m}_{13}} \tag{45.50}$$

Similarly the circulation ratio of the low temperature cycle:

$$f_L = \frac{\dot{m}_7}{\dot{m}_{15}} \tag{45.51}$$

45.4 Results and Discussion

In this work, NH_3/H_2O-$NH_3/LiNO_3$ (System I) and NH_3/H_2O-NH_3/NaSCN (System II) are used as refrigerant/absorbent working pairs for the simulation of the DAR. A computer program is developed for analysis of the DAR. The variation of the COP with generator, absorber, evaporator, and condenser temperatures are determined.

Figure 45.2 shows the variation of the COP with the temperature of the HTG, T_{HTG} for condenser temperature, $T_C = 24$ °C, temperature of HTA, $T_{HTA} = 80$ °C and evaporator temperatures, $T_E = 10$, 0 and −10 °C. It is observed that the System II (NH_3/H_2O-NH_3/NaSCN) has a lower COP than System I (NH_3/H_2O-NH_3/$LiNO_3$). The COP of the both systems are lower than 0.9. The COP at the smaller T_{HTG} is lower and increases with T_{HTG}. The COP increases exponentially and it stops at a certain value of T_{HTG}.

The COP of the DAR is high at the large T_E. The DAR doesn't work when T_{HTG} is less than 105 °C. The COP of DAR is almost constant above $T_{HTG} = 180$ °C.

As it is seen in Fig. 45.3 the COP of the DAR for System I and System II are similar at the $T_C = 28$ °C and at $T_{HTA} = 80$ °C and $T_E = -10$, 0, 10 °C. For both

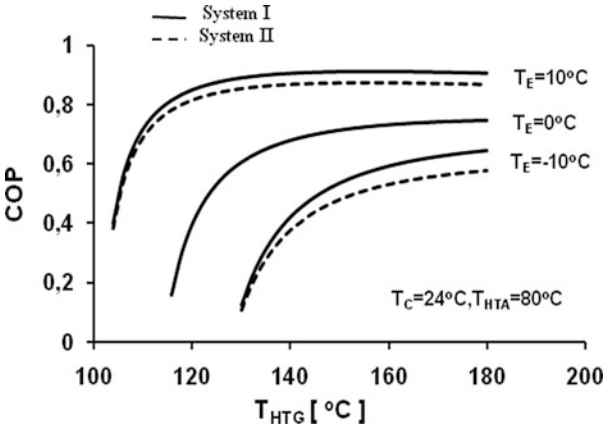

Fig. 45.2 Variation of the COP of the DAR with the HTG temperature at different evaporator temperatures and at $T_{HTA} = 80$ °C, $T_C = 24$ °C

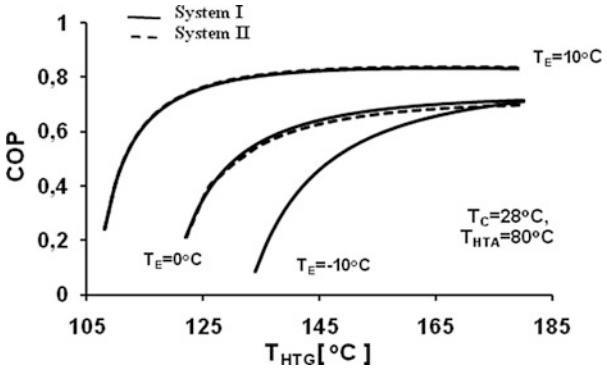

Fig. 45.3 Variation of the COP of the DAR with the HTG temperature at different evaporator temperatures and at $T_{HTA} = 80$ °C, $T_C = 28$ °C

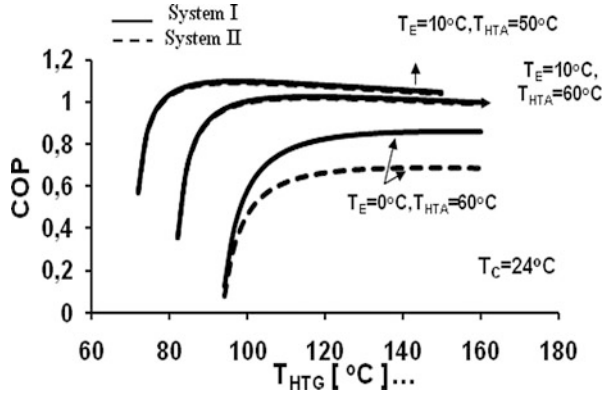

Fig. 45.4 Variation of the COP of the DAR with the HTG temperature at different evaporator temperatures and at $T_{HTA} = 50$ and 60 °C, $T_C = 24$ °C

systems the COP increases with the evaporator temperature. The System II works at $T_E > 0$ °C for $T_C = 28$ °C. It is observed that the maximum COP of System II is decreases 4.1 % and the maximum COP of System I decreases 7.9 % with the increase of condenser temperature from 24 to 28 °C. The DAR doesn't work when T_{HTG} is less than 105 °C. The COP of the DAR is almost constant above the $T_{HTG} = 180$ °C.

In Fig. 45.4, results are shown for $T_C = 24$ °C, $T_{HTA} = 50$ °C and 60 °C. The DAR can work over evaporator temperature of 0 °C and the maximum COP of the DAR rises up to 1.10.

The variation of the COP of the DAR with the temperature of the HTG is given in Fig. 45.5 at $T_{HTA} = 70$ °C, $T_C = 24$ °C and $T_{E=} -10$, 0, 10 °C. Both systems can work at evaporator temperature of −10 °C, but the COP of both systems can only rises up to 0.96.

Variation of the COP of the DAR with the HTG temperature at different evaporator temperatures of $T_E = -20$, −10, 0 and 10 °C, condenser temperature of $T_C = 24$ °C and $T_{HTA} = 90$ °C is given in Fig. 45.6. The maximum COP of System II is 0.86 and for System I it is 0.82. The systems start working above $T_{HTG} = 114$ °C and start decreasing beyond $T_{HTG} = 190$ °C.

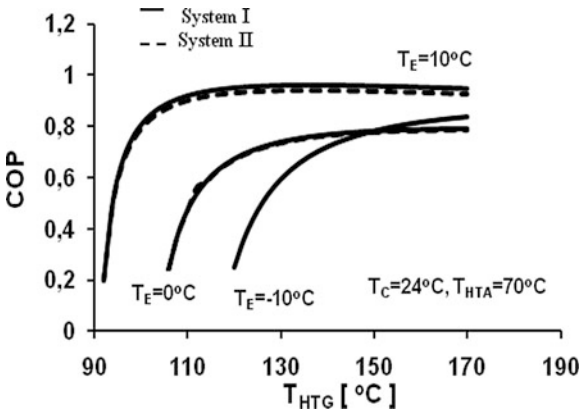

Fig. 45.5 Variation of the COP of the DAR with the HTG temperature at different evaporator temperatures and at $T_{HTA} = 70\ ^\circ C$, $T_C = 24\ ^\circ C$

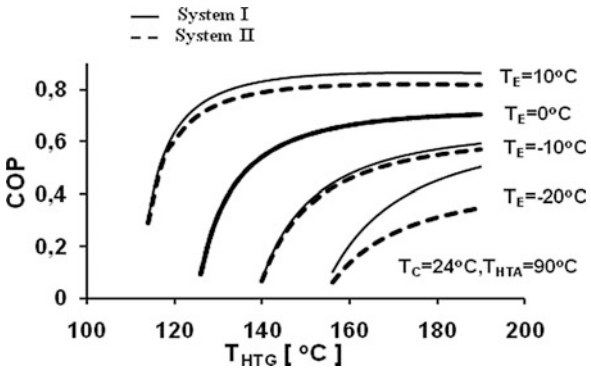

Fig. 45.6 Variation of the COP of the DAR with the HTG temperature at different evaporator temperatures and at $T_{HTA} = 90\ ^\circ C$, $T_C = 24\ ^\circ C$

Comparison of Figs. 45.5 and 45.6, show that the variation of COP of the DAR with increasing HTG temperature, tend to decrease as parametric value of T_{HTA} steps up from 70 to 90 °C for $T_E = -10, 0, 10\ ^\circ C$, but the systems start working at a lower evaporator temperature of $T_E = -20\ ^\circ C$.

For System I, variation of the circulation ratio of the high temperature cycle (f_H) with temperature of HTG is given in Fig. 45.7. It is shown that the f_H is 149.6 at $T_{HTG} = 130\ ^\circ C$ and f_H is 36.4 at $T_{HTG} = 134\ ^\circ C$, for $T_C = 24\ ^\circ C$, $T_{HTA} = 80\ ^\circ C$, and $T_E = -10\ ^\circ C$. The f_H of the DAR increases with a decrease of the evaporator temperature. The f_H is 6.088 at $T_C = 24\ ^\circ C$, $T_{HTA} = 80\ ^\circ C$, $T_{HTG} = 130\ ^\circ C$ and $T_E = 10\ ^\circ C$; but it rises up to 11.87 at $T_E = 0\ ^\circ C$. The trend in Fig. 45.7 also indicates that the f_H of the DAR decreases with an increase of the HTG temperature, for evaporator temperatures of $T_E = -10.0$ and $10\ ^\circ C$.

Variations of the COP with evaporator temperature for both systems are given in Fig. 45.8 for condenser temperature of 24 °C, HTA temperature of 80 °C, and HTG temperatures of 140 °C. As shown in the figure, the COP increases with evaporator

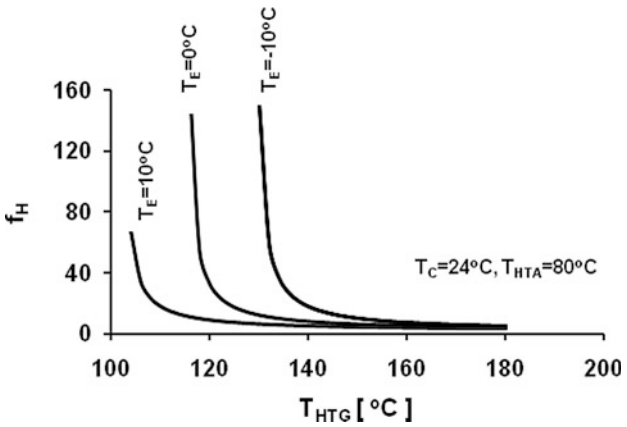

Fig. 45.7 Variation of the circulation ratio of the DAR at high temperature cycle with the HTG temperature at different evaporator temperatures and at $T_{HTA} = 80\ ^\circ C$, $T_C = 24\ ^\circ C$

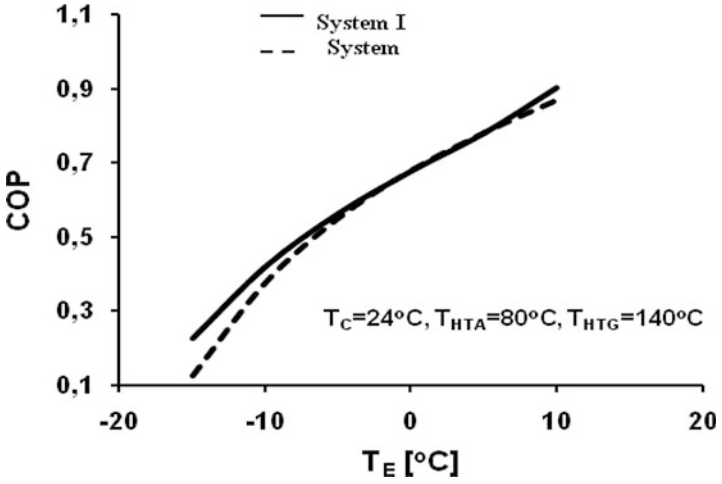

Fig. 45.8 Variation of the COP of the DAR with the evaporator temperatures at $T_{HTA} = 80\ ^\circ C$, $T_C = 24$ and $T_{HTG} = 140\ ^\circ C$

temperature. System II has better performance than System I at lower evaporator temperatures.

The results obtained from the simulation of the DAR are given in Table 45.3 for $T_c = 24\ ^\circ C$, $T_E = 0\ ^\circ C$, $T_{HTA} = 60\ ^\circ C$ for System II. The performance parameters of System II at the conditions given in Table 45.3 are given in Table 45.4.

Table 45.3 DAR's analysis results at $T_c = 24$ °C, $T_e = 0$ °C, $T_{HTA} = 60$ °C for system II

Reference point	T (°C)	h (kJ/kg)	X	P (bar)	$m \times 10^{+4}$ (kg/s)
1	60	30.21283	0.4047082	5.820903	65.004146
2	60.09095	31.20637	0.4047082	14.05266	65.004146
3	101.2763	123.6155	0.4047082	14.05266	65.004146
4	120	343.0018	0.2803915	14.05266	53.774291
5	72.67085	88.56872	0.2803915	14.05266	53.774291
6	72.67085	88.56872	0.2803915	5.820903	53.774291
7	24	−47.43581	0.2320188	5.820903	64.403161
8	24.29212	−46.74849	0.2320188	14.05266	64.403161
9	50.45771	17.85708	0.2320188	14.05266	64.403161
10	57	37.78723	0.2250139	14.05266	63.821033
11	31.12463	56.55319	0.2250139	14.05266	63.821033
12	31.12463	56.55319	0.2250139	5.820903	63.821033
13	120	1,715.708	1	14.05266	11.229857
14	46.31957	1,519.990	1	14.05266	11.229857
15	57	1,549.427	1	14.05266	5.8212620
16	51.495	1,530.040	1	14.05266	17.051119
17	24	113.0889	1	13.38348	17.051119
18	15.77061	75.29613	1	13.38348	17.051119
19	16.10164	75.29613	1	6.257471	17.051119
20	0	1,248.240	1	6.257471	17.051119
21	19.12741	1,487.872	1	6.257471	17.051119
22	19.12741	1,487.872	1	6.257471	5.8212620
23	19.12741	1,487.872	1	6.257471	11.229857
24	98.85603	1,677.352	1	6.257471	11.229857

Table 45.4 The performance parameters for working conditions given at the Table 45.3

Heat load at evaporator (kW), q_E	2.00
Heat load at condenser (kW), q_C	2.416060
Heat load at LTA (kW), q_{LTA}	7.530428
Heat load at HTA (kW), q_{HTA}	2.163518
Heat load at HTG (kW), q_{HTG}	2.967631
COP	0.6626126
Circulation ratio of high temperature cycle, f_H	5.788510
Circulation ratio of low temperature cycle, f_L	110.6344

45.5 Conclusions

The performance ranges of the double effect absorption refrigeration systems given in the literature are different than the DAR of this study. The following conclusions can be drawn from the simulation of the DAR:

The COP of the DAR grows with the increase of temperature of HTG up to a certain value of T_{HTG}, but afterwards it comes to a stop and it remains constant onward.

The COP of DAR also grows with the increase of the evaporator temperature T_E.

As the temperature of HTA increases, the DAR becomes capable of working at lower condenser temperatures, T_C. However this happens in return for decreasing COP values. At condenser temperature of 24 °C, System II is not capable of working below HTA temperatures of 80 °C. As for System I, it cannot work below HTA temperatures of 70 °C, for condenser temperature of 24 °C, when evaporator temperature T_E goes below 0 °C.

When the evaporator temperature decreases, the DAR can work at higher HTA temperatures. As the condenser temperature increases, the DAR can work only at higher HTG temperatures.

The DAR can work only at higher HTG temperatures as the evaporator temperatures decreases.

As the HTG temperature increases, the high temperature circulation ratio f_H becomes smaller and f_H grows as condenser temperature and HTA temperature increase or evaporator temperature decreases.

The COP of System II is less than the COP of the System I at the same operating conditions. The maximum COP of the DAR is obtained at condenser temperature of 24 °C, HTA temperature of 50 °C and evaporator temperature of 10 °C. The maximum COP of System I is 1.099 and for System II, it becomes 1.092.

System II has larger low temperature circulation ratio f_L than System I.

At condenser temperature of 24 °C, The DAR cannot work below the HTG temperature of 72 °C. At condenser temperature of 28 °C, it can work neither below the HTG temperature of 86 °C.

Nomenclature

C	Heat capacity per unit time (kW/K)
C	The heat capacity ratio
C_P	Specific heat at constant pressure (kJ/kmol K)
D	The values
f_H	The circulation ratio of the high temperature cycle
f_L	The circulation ratio of the low temperature cycle
h	The specific enthalpy (kJ/kg)
h_I	The specific enthalpy of the saturated liquid ammonia (kJ/kg)
h_S	The specific enthalpy of superheated ammonia vapour (kJ/kg)
h_V	The specific enthalpy of saturated ammonia vapour (kJ/kg)
g	The specific Gibbs free energy function (kJ/kmol)
m	Mass (kg)
$\dot{m}$	Mass flow rate (kg/s)
P	Pressure (kPa bar)

p_L Low pressure (kPa bar)
p_H High pressure (kPa bar)
T Temperature (°C)
T_E Evaporator temperature (°C)
T_C Condenser temperature (°C)
q Heat load (kW)
q_E Heat load at evaporator (kW)
q_C Heat load at condenser (kW)
W_P Pump energy supplied (kW)
X Mole fraction
x Mass concentration

Acronyms

COP Coefficient of performance
DAR Double effect absorption refrigeration system
HTA High temperature absorber
HTG High temperature generator
LTA Low temperature absorber
LTG Low temperature generator
HE Heat exchanger
EV Expansion valve
C Condenser
E Evaporator
P Pump

References

1. Ataer ÖE, Göğüş Y (1991) Comparative study of irreversibilities in an aqua-ammonia absorption refrigeration system. Int J Refrig 4:87–92
2. Rogdakis ED, Antonopoulos KA (1995) Thermodynamic cycle, correlation and nomograph for ammonia-sodium thiocyanate absorption refrigeration systems. Heat Recovery Syst CHP 15:591–599
3. Da-Wen S (1998) Comparison of the performances of NH_3-H_2O. NH_3-$LiNO_3$ and NH_3-NaSCN absorption refrigeration system. Energ Convers 39:357–368
4. Alizadeh S, Bahar F, Geoola F (1979) Design and optimisation of an absorption refrigeration system operated by solar energy. Sol Energ 22:149–154
5. Swartman RK, Ha V, Swaminathan C (1975) Comparison of ammonia-sodium thiocyanate as the refrigerant-absorbent in a solar refrigeration system. Sol Energ 17(2):123–127
6. Romero RJ, Guillen L, Pilatowsky I (2005) Monomethylamine-water vapor absorption refrigeration system. Appl Therm Eng 25:867–876
7. Donate M, Rodriguez L, Lucas A (2006) Thermodynamic evaluation of new absorbent mixtures of lithium bromide and organic salts for absorption refrigeration machines. Int J Refrig 29:30–35

8. Kaynaklı O, Kılıç M (2007) Theoretical study on the effect of operating conditions on performance of absorption refrigeration system. Energ Convers Manag 48:599–607
9. Ziegler B, Trepp C (1984) Equation of state for ammonia-water mixtures. Int J Refrig 7:101–106
10. Ferreira I (1984) Thermodynamic and physical property data equations for ammonia-lithium nitrate and ammonia-sodium thiocyanate solutions. Sol Energ 32:231–236
11. Bourseau P, Bugarel R (1986) Refrigeration par cycle a absorption-diffusion: comparison des performances des systemes NH_3-H_2O et NH_3-NaSCN. Int J Refrig 9:206–214
12. Cleland AC (1986) Computer subroutines for rapid evaluation of refrigerant thermodynamic properties. Int J Refrig 9:346–351

About the Authors

Ibrahim Dincer is a full professor of Mechanical Engineering and programs director in the faculty of Engineering and Applied Science at University of Ontario Institute of Technology. Renowned for his pioneering works, he has authored and co-authored many books and book chapters, over 800 refereed journal and conference papers, and numerous technical reports. He has chaired many national and international conferences, symposia, workshops, and technical meetings. He is the founding chair/co chair of various well-established international conferences, including the International Exergy, Energy, and Environment Symposium. He has delivered over 200 keynote and invited lectures. He is an active member of various international scientific organizations and societies, and serves as Editor-In-Chief for International Journal of Energy Research, International Journal of Exergy, and International Journal of Global Warming, as well as associate editor, regional editor, and editorial board member on various prestigious international journals. He is a recipient of several research, teaching, and service awards, including the Premier's Research Excellence award in Ontario, Canada, in 2004. He has made innovative contributions to the understanding and development of exergy analysis of advanced energy systems for his so-called five main pillars: (1) better efficiency, (2) better cost-effectiveness, (3) better environment, (4) better sustainability, and (5) better energy security. He was the chair of a new technical group in ASHRAE named Exergy Analysis for Sustainable Buildings.

Adnan Midilli is a full professor of Mechanical Engineering in Engineering Faculty of Recep Tayyip Erdoğan University, Rize, Turkey. He is an active member of various international scientific organizations and societies, and serves as editorial board member on various prestigious international journals. He is a recipient of several national research awards. He has been working to be researcher in the national and international research projects. His research interest includes sustainable energy technologies, sustainable development, thermodynamic design and modeling.

I. Dincer et al. (eds.), *Progress in Sustainable Energy Technologies Vol II: Creating Sustainable Development*, DOI 10.1007/978-3-319-07977-6

Haydar Kucuk is Associate Professor at Mechanical Engineering Department and Associate Dean of Engineering Faculty at the Recep Tayyip Erdoğan University. He teaches graduate and undergraduate courses in the fields of thermodynamics, fluid mechanics and heat transfer. His research interests involve numerical heat transfer and fluid flow, drying and drying models, energy and exergy analysis, economic analysis and sustainability and thermodynamics. He serves as referee for international prestigious journals. He has participated in national and international research projects as a researcher. He has contributed as technical chair in The Sixth International Exergy, Energy and Environment Symposium.

Index

I. Dincer et al. (eds.), *Progress in Sustainable Energy Technologies Vol II: Creating Sustainable Development*, DOI 10.1007/978-3-319-07977-6

R

T